GEOLOGICAL SURVEY OF CANADA
COMMISSION GÉOLOGIQUE DU CANADA

**PAPER/ÉTUDE
93-1D**

CURRENT RESEARCH, PART D
EASTERN CANADA AND NATIONAL AND GENERAL PROGRAMS

RECHERCHES EN COURS, PARTIE D
EST DU CANADA ET PROGRAMMES NATIONAUX ET GÉNÉRAUX

Energy, Mines and Resources Canada
Énergie, Mines et Ressources Canada

Canada

THE ENERGY OF OUR RESOURCES - THE POWER OF OUR IDEAS

L'ÉNERGIE DE NOS RESSOURCES - NOTRE FORCE CRÉATRICE

NOTICE TO LIBRARIANS AND INDEXERS

The Geological Survey's Current Research series contains many reports comparable in scope and subject matter to those appearing in scientific journals and other serials. Most contributions to Current Research include an abstract and bibliographic citation. It is hoped that these will assist you in cataloguing and indexing these reports and that this will result in a still wider dissemination of the results of the Geological Survey's research activities.

AVIS AUX BIBLIOTHÉCAIRES ET PRÉPARATEURS D'INDEX

La série Recherches en cours de la Commission géologique contient plusieurs rapports dont la portée et la nature sont comparables à ceux qui paraissent dans les revues scientifiques et autres périodiques. La plupart des articles publiés dans Recherches en cours sont accompagnés d'un résumé et d'une bibliographie, ce qui vous permettra, on l'espère, de cataloguer et d'indexer ces rapports, d'où une meilleure diffusion des résultats de recherche de la Commission géologique.

GEOLOGICAL SURVEY OF CANADA
COMMISSION GÉOLOGIQUE DU CANADA

PAPER / ÉTUDE
93-1D

CURRENT RESEARCH, PART D
EASTERN CANADA AND NATIONAL AND GENERAL PROGRAMS

RECHERCHES EN COURS, PARTIE D
EST DU CANADA ET PROGRAMMES NATIONAUX ET GÉNÉRAUX

1993

Available in Canada through authorized
bookstore agents and other bookstores

or by mail from

Canada Communication Group — Publishing
Ottawa, Canada K1A 0S9

and from

Geological Survey of Canada offices:

601 Booth Street
Ottawa, Canada K1A 0E8

3303-33rd Street N.W.,
Calgary, Alberta T2L 2A7

100 West Pender Street
Vancouver, B.C. V6B 1R8

A deposit copy of this publication is also available for
reference in public libraries across Canada

Cat. No. M44-93/1D
ISBN 0-660-57951-0

Price subject to change without notice

Cover description

Deformed sand volcanoes exposed on south-dipping bedding surface of Cambrian Goldenville Formation (15 m field of view). Tidmarsh Island, south of entrance to Ecum Secum Harbour, Nova Scotia. Photo by J.R. Henderson. GSC 203683-L

Description de la photo couverture

Injections de sable déformées sur une surface de stratification à pendage sud de la formation cambrienne de Goldenville (champ visuel de 15 m). Île Tidmarsh, au sud de l'entrée du havre Ecum Secum, en Nouvelle-Écosse. Photo : J.R. Henderson. GSC 203683-L

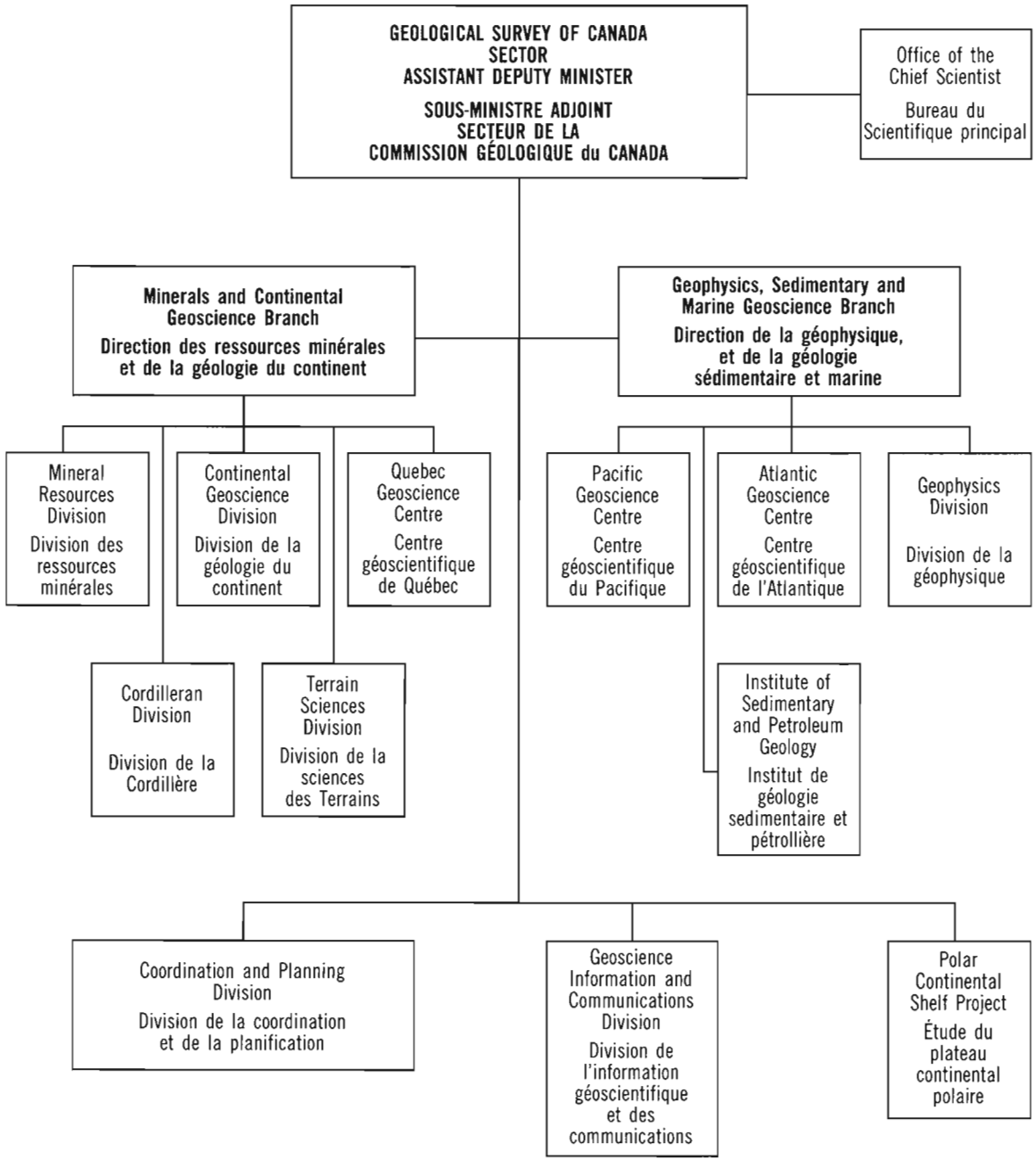
GEOLOGICAL SURVEY OF CANADA
SECTOR
ASSISTANT DEPUTY MINISTER
SOUS-MINISTRE ADJOINT
SECTEUR DE LA
COMMISSION GÉOLOGIQUE du CANADA
Office of the Chief Scientist
Bureau du Scientifique principal
Minerals and Continental Geoscience Branch
Direction des ressources minérales et de la géologie du continent
Geophysics, Sedimentary and Marine Geoscience Branch
Direction de la géophysique, et de la géologie sédimentaire et marine
Mineral Resources Division
Division des ressources minérales
Continental Geoscience Division
Division de la géologie du continent
Quebec Geoscience Centre
Centre géoscientifique de Québec
Pacific Geoscience Centre
Centre géoscientifique du Pacifique
Atlantic Geoscience Centre
Centre géoscientifique de l'Atlantique
Geophysics Division
Division de la géophysique
Cordilleran Division
Division de la Cordillère
Terrain Sciences Division
Division de la sciences des Terrains
Institute of Sedimentary and Petroleum Geology
Institut de géologie sedimentaire et pétrollière
Coordination and Planning Division
Division de la coordination et de la planification
Geoscience Information and Communications Division
Division de l'information géoscientifique et des communications
Polar Continental Shelf Project
Étude du plateau continental polaire

Separates

A limited number of separates of the papers that appear in this volume are available by direct request to the individual authors. The addresses of the Geological Survey of Canada offices follow:

601 Booth Street
OTTAWA, Ontario
K1A 0E8
(FAX: 613-996-9990)

Institute of Sedimentary and Petroleum Geology
3303-33rd Street N.W.
CALGARY, Alberta
T2L 2A7
(FAX: 403-292-5377)

Cordilleran Division
100 West Pender Street
VANCOUVER, B.C.
V6B 1R8
(FAX: 604-666-1124)

Pacific Geoscience Centre
P.O. Box 6000
9860 Saanich Road
SIDNEY, B.C.
V8L 4B2
(Fax: 604-363-6565)

Atlantic Geoscience Centre
Bedford Institute of Oceanography
P.O. Box 1006
DARTMOUTH, N.S.
B2Y 4A2
(FAX: 902-426-2256)

Québec Geoscience Centre
2700, rue Einstein
C.P. 7500
Ste-Foy (Québec)
G1V 4C7
(FAX: 418-654-2615)

When no location accompanies an author's name in the title of a paper, the Ottawa address should be used.

Tirés à part

On peut obtenir un nombre limité de «tirés à part» des articles qui paraissent dans cette publication en s'adressant directement à chaque auteur. Les adresses des différents bureaux de la Commission géologique du Canada sont les suivantes:

601, rue Booth
OTTAWA, Ontario
K1A 0E8
(facsimilé : 613-996-9990)

Institut de géologie sédimentaire et pétrolière
3303-33rd St. N.W.,
CALGARY, Alberta
T2L 2A7
(facsimilé : 403-292-5377)

Division de la Cordillère
100 West Pender Street
VANCOUVER, British Columbia
V6B 1R8
(facsimilé : 604-666-1124)

Centre géoscientifique du Pacifique
P.O. Box 6000
9860 Saanich Road
SIDNEY, British Columbia
V8L 4B2
(facsimilé : 604-363-6565)

Centre géoscientifique de l'Atlantique
Institut océanographique Bedford
B.P. 1006
DARTMOUTH, Nova Scotia
B2Y 4A2
(facsimilé : 902-426-2256)

Centre géoscientifique de Québec
2700, rue Einstein
C.P. 7500
Ste-Foy (Québec)
G1V 4C7
(facsimilé : 418-654-2615)

Lorsque l'adresse de l'auteur ne figure pas sous le titre d'un document, on doit alors utiliser l'adresse d'Ottawa.

CONTENTS

The Deer Cove deposit: an example of "thrust"-related breccia-vein type gold mineralization in the Baie Verte Peninsula, Newfoundland[1,2]

B. Dubé, K. Lauzière, and H.K. Poulsen[3]
Quebec Geoscience Centre, Sainte-Foy

Dubé, B., Lauzière, K., and Poulsen, H.K., 1993: The Deer Cove deposit: an example of "thrust"-related breccia-vein type gold mineralization in the Baie Verte Peninsula, Newfoundland; in Current Research, Part D; Geological Survey of Canada, Paper 93-1D, p. 1-10.

Abstract: The Deer Cove gold deposit is typical of a breccia-vein system. The mineralization is hosted by breccia-veins associated with the Deer Cove Sole "Thrust", one of the second order reverse faults that are common on the Baie Verte Peninsula. The along strike variation of orientation and movement of the Deer Cove Sole "Thrust" (DCST) from an east-west high-angle reverse fault to northwest and northeast oblique ramp with strike slip movement indicate variation in the strain rate along the length of the thrust. This strain rate variation resulted in extension subparallel to the strike of the thrust and allowed formation of the breccia-veins almost perpendicular to the orientation of the east-west segment of the thrust. The mineralized veins are genetically related to the Deer Cove Sole "Thrust", they were formed after the initiation of the reverse movement but before this progressive faulting event ended.

Résumé : Le gisement aurifère de Deer Cove est un système de veine bréchique typique. La minéralisation se localise dans des veines bréchiques associées au «chevauchement» sub-horizontal de Deer Cove, une des failles inverses de deuxième ordre fort répandues dans la péninsule de Baie Verte. La variation de l'orientation et de la direction de mouvement du chevauchement, soit d'une faille inverse est-ouest à des rampes obliques d'orientation nord-ouest et nord-est à mouvement de coulissage, témoigne d'une variation dans le taux de déformation le long du chevauchement. Cette variation du taux de déformation engendre une extension sub-parallèle à la direction du chevauchement et permet la formation des veines bréchiques presque perpendiculaires à l'orientation du segment est-ouest du chevauchement. Les veines minéralisées génétiquement reliées au «chevauchement» sub-horizontal de Deer Cove ont été formées après le début du mouvement inverse mais avant que ce mouvement de faille progressif ne prenne fin.

[1] Published with the authorization of Noranda Exploration Co. Ltd.
[2] Contribution to Canada-Newfoundland Cooperation Agreement on Mineral Development 1990-1994, a subsidiary agreement under the Economic and Regional Development Agreement. Project funded by the Geological Survey of Canada.
[3] Mineral Resources Division

INTRODUCTION

The Deer Cove gold deposit is located on the Pointe Rousse Peninsula, approximately 13 km north of the town of Baie Verte (Fig. 1). It is a mesothermal vein-type gold deposit (Dubé, 1990; Patey and Wilton, 1990) and as for most gold deposits, it is spatially associated with a major fault; the Baie Verte-Brompton Line (BBL). This fault is a suture zone between early Paleozoic continental and oceanic domains (Williams and St-Julien, 1982). The Deer Cove deposit differs from other gold occurrences in the area, in that the gold mineralization is located within breccia-veins (Dubé, 1990; Dubé et al., 1992). The Deer Cove prospect is a joint venture between Noranda Exploration Company Limited and Galveston Resources.

A total of nine visible gold occurrences were discovered in this area and were investigated to various degrees by geologists of Noranda Exploration. Previous work done in the area include regional studies by Norman and Strong (1975) and by Hibbard (1983), property-scale work by Gower et al. (1988, 1990) and metallogenic studies by Tuach et al. (1988); Lydon et al. (1988); Dubé (1990); Lydon et al. (1990); Patey (1990); Patey and Wilton (1990); and Dubé et al. (1992).

The objectives of this paper are to describe the structural setting of the mineralized veins and to document the style and intensity of deformation within the Deer Cove Sole "Thrust" from observations on surface outcrops and in the exploration ramp.

REGIONAL GEOLOGY

The Deer Cove deposit is located within the Deer Cove block of the ophiolitic rocks of the Pointe Rousse Complex (Norman and Strong, 1975). The area is characterized by numerous thrust faults that dissect the complex into a series of imbricated lithological blocks bounded by south-verging reverse faults and thrusts. Norman and Strong (1975) have recognized five structural blocks, bounded by major sole thrusts. The Deer Cove Sole "Thrust" (Fig. 2), the most prominent fault, juxtaposes mafic volcanic rocks from the stratigraphic top of an overturned south-facing ophiolite in the north against ultramafic rocks forming the stratigraphic base of another ophiolite sequence to the south (Gower et al., 1988, 1990). The general trend of the fault is east-northeast with dips of 50° to 60° north-northwest. A penetrative fabric associated with the thrusting is well developed within, and adjacent to, the fault zones but is poorly developed in rocks within the fault blocks.

The Deer Cove block is underlain by mafic volcanic rocks, diabase dykes and gabbro which represent the upper part of an ophiolite sequence (Gower et al., 1988, 1990). According to Gower et al. (1988, 1990), the mafic volcanics located within the hanging wall comprise interlayered pillowed and massive flows, hyaloclastites, volcaniclastites, and minor jasper iron-formation, all of which are cut by diabase dykes and sills. The mafic volcanic sequence is structurally overlain by a poorly developed, a unit of sheeted diabase dykes which consists predominantly of massive, fine grained, subvolcanic

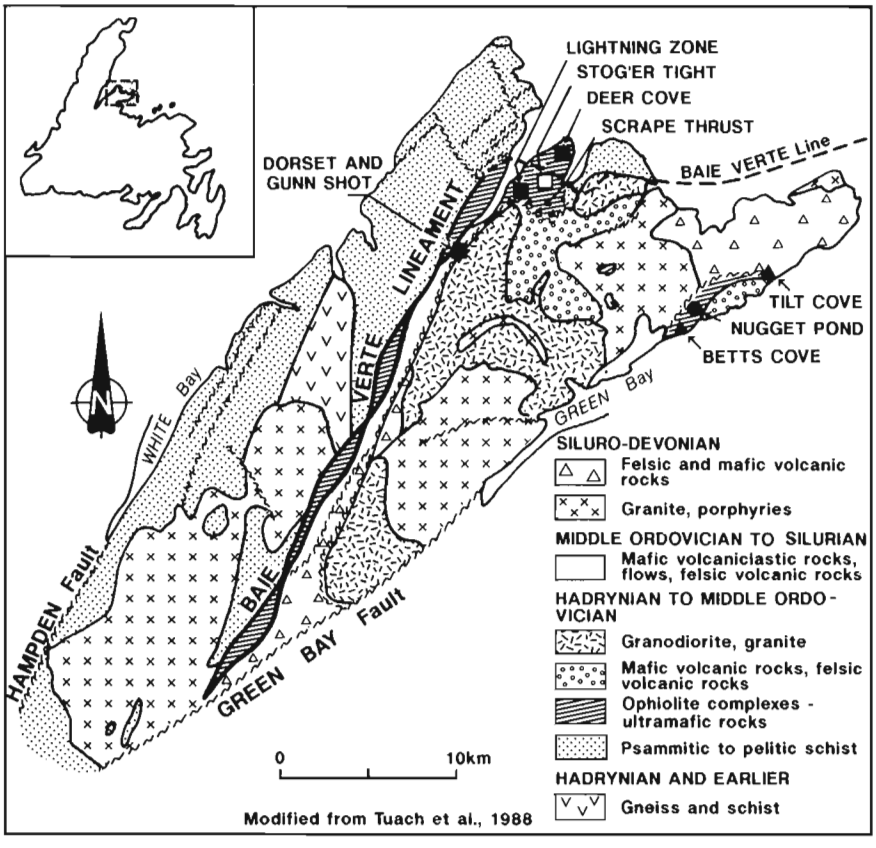

Figure 1.

Geographical and geological localization of the Deer Cove gold deposit and other mesothermal gold showings along the Baie Verte-Brompton Line. (Modified from Tuach et al., 1988). The open and solid squares locate altered wallrock- and vein-type gold mineralization respectively (Dubé, 1990).

mafic rocks which may be large sills. The northern part of the block is underlain by massive, fine- to medium-grained gabbro. All these rocks have been chloritized and veined with abundant epidote as a result of regional greenschist metamorphism.

STRUCTURE OF THE DEPOSIT

Deformation is heterogeneously distributed throughout the mafic volcanic sequence, and is most intense in and next to ductile faults. The most important fault is the Deer Cove Sole "Thrust" (Fig. 2). Detailed structural mapping indicates that the Deer Cove Sole "Thrust" is a ductile-brittle zone marked by a sharp millimetre-wide gouge developed between strongly deformed and altered (chloritized and carbonatized) metabasalt with jasper fragments in the hanging wall and serpentinized ultramafic rocks in the footwall (Fig. 3). The fault contact is east-west-oriented and dips moderately to the north (58-70°). Both the angular relationship between the fault plane and the schistosity (N310/79°) developed on both sides of the fault plane, and dragging of the foliation, indicate that the Deer Cove Sole "Thrust" is a high angle reverse fault, as the dip of the fault is steeper than 45°. Down-dip, east-northeast-trending stretching lineations and slickenlines developed on the foliation planes adjacent to the gouge are consistent with this interpretation (Fig. 4A). Local subhorizontal striations on foliation and slip planes adjacent to the fault are also observed and could suggest a later reactivation. In the footwall, non-coaxial fabrics are developed in a wide zone of serpentinite, and millimetre-scale synthetic and anthitetic shear bands are consistent with a reverse movement along the Deer Cove Sole "Thrust". In the hanging wall, a strong planar fabric is developed up to 15 m north of the fault contact. The fabric is penetrative and the dip is shallower than the fault plane (N30-50°) (Fig. 4B). Many kink bands oriented at 120/50° and 080°/55°, and showing reverse, south-directed vergence are present in this high strain zone (Fig. 4B). We believe that they are related to the strong anisotropy of the foliated hanging wall. Thrust planes oriented at 270/40° with down-dip stretching lineations are developed within this zone. Farther away in the hanging wall, the dip of the foliation

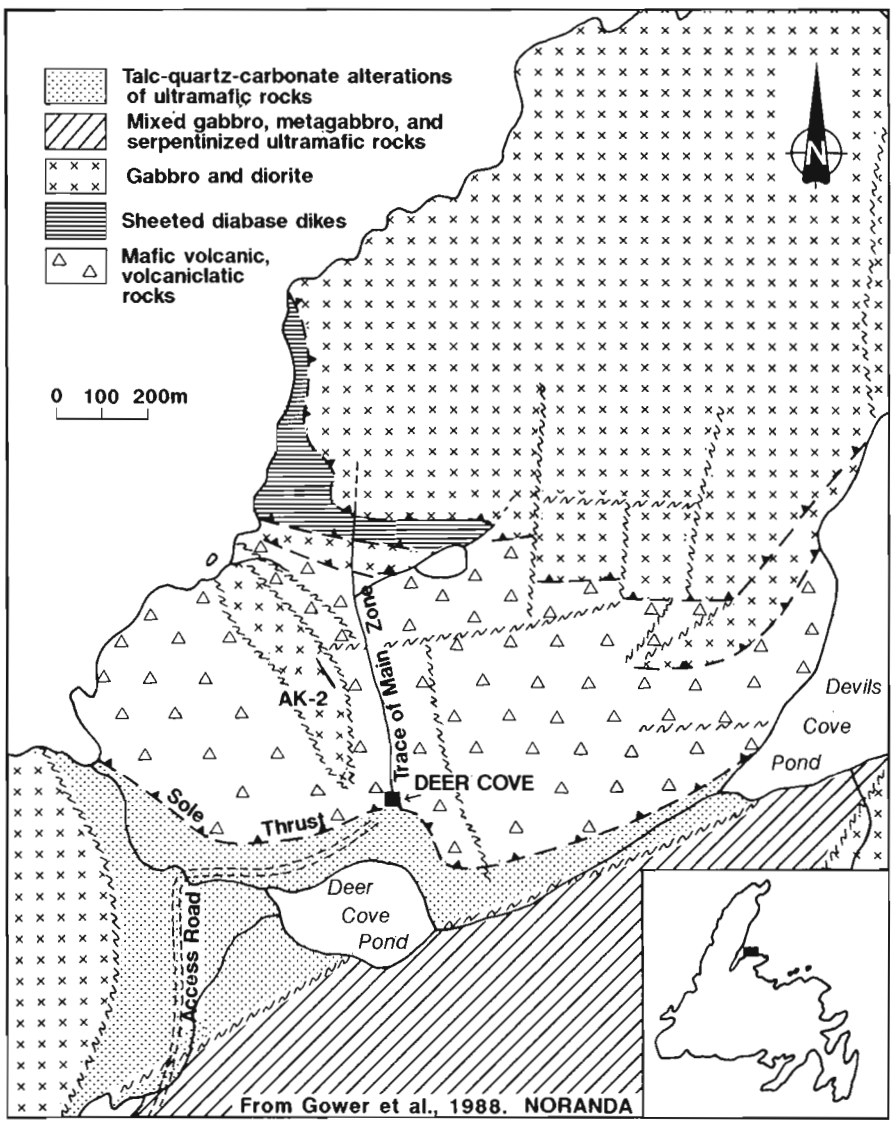

Figure 2.

Geological map of the Deer Cove area (Modified from Gower et al., 1990).

Figure 3. Cross-section view of the Deer Cove Sole "Thrust".

is steeper (45°-60°). Farther north, the deformation grades into a strongly developed cleavage oriented on average at N265/50° with a down-dip to slightly oblique stretching lineation. The stretching lineation is defined by elongate clasts, fragments, and chlorite grains or locally by rodding of quartz and calcite veins (Fig. 5). Locally developed C-S fabric are compatible with the reverse sense of motion. As well, en echelon sigmoidal extensional quartz veins oriented at N100/65° confined within the gabbroic dykes are well consistent with the kinematic interpretation (Fig. 4C).

A number of steep northwest and north oriented faults are common in the area. The northwest set contains an oblique, moderately- to shallow-plunging stretching lineation, compatible with a south-directed "thrust". Faults of this set were seen to progressively change orientation, becoming more or less east-west with a down-dip stretching lineation. This northwest set could represent an oblique ramp system related to the thrusting. Underground, northwest oriented faults displaced the mineralized vein with a sinistral sense of motion, over 2 m (Fig. 4D). Locally, the northwest faults are injected by ribboned quartz shear veins containing traces of pyrite. An example of the steep north-south set outcrops near the main zone to the east. It exhibits subhorizontal to shallow plunging stretching lineations, striations and quartz fibres related to sinistral strike-slip movement (Fig. 6). As suggested by Gower et al. (1988, 1990), we believe that these faults represent tear faults developed during the thrusting event. Quartz-chlorite veins are commonly found in these fault zones.

MINERALIZATION

The two most significant gold occurrences from this area are the Main zone and the AK2 zone (Gower et al., 1988, 1990) (Fig. 2). These two zones are exposed on surface as well as underground in the exploration ramp. Other less significant gold-bearing structures occur elsewhere on the property.

Main zone

The Main zone (Fig. 2) consists of discontinuous lenses of brecciated quartz hosted by a south-trending (170-175°) and 45-55° west-dipping structure developed in mafic volcanic rocks, sheeted dykes and gabbro (Fig. 7, 8). The hosting structure is at high angle to the east oriented fabric dipping to the north, containing a down-dip stretching lineation and developed in the hanging wall of the "thrust" zone. This main mineralized structure has been traced for a strike length of over 500 m, from the Deer Cove Sole "Thrust" to the south and is open to the north (Gower et al., 1988, 1990).

The mineralized zones consist of lenses of breccia-type quartz veins, from less than 1 m wide up to 3 m (Fig. 9). They enclose 30 to 50% angular altered wallrock fragments (up to 60 cm) and chlorite patches. Up to 3% sulphides, mostly pyrite with minor chalcopyrite and arsenopyrite, occur for the most part in both adjacent wallrock and wallrock fragments incorporated in the breccia veins, along fractures and, less commonly, as disseminations. Gower et al. (1990) reported that gold mineralization is found both in quartz veins and in altered wallrock, either as free gold or associated with the sulphides, and that the highest gold grades strongly correlate with high pyrite concentrations.

Aside from pyritization of wallrock up to 30 cm away from the vein, sericitization is the best developed alteration; some fuchsite was locally observed. Gower et al. (1990) report a broad carbonate alteration halo which is best developed in the most intensely deformed rocks as it is the case for the chlorite schists in the vicinity of the Deer Cove Sole "Thrust".

In several localities a fabric is found in the brecciated quartz veins thus suggesting that they were emplaced prior to, or during the thrust-related deformation. The crinkled aspect of the ore zone in the vicinity of the Deer Cove Sole "Thrust" in the southernmost 30 m of its length both in surface and underground exposures (Fig. 7) supports such an interpretation. There, as reported by Gower et al. (1988, 1990), the cleavage related to the Deer Cove Sole "Thrust" is axial-planar to sharp folds that plunge abruptly toward the north-northwest. Transposed ribboned breccia veins were locally observed both on surface and underground. This most deformed segment of the Main zone is more highly mineralized, averaging 14.25 g/t Au over a width of 2.9 m for the southernmost 32 m (Gower et al., 1988, 1990).

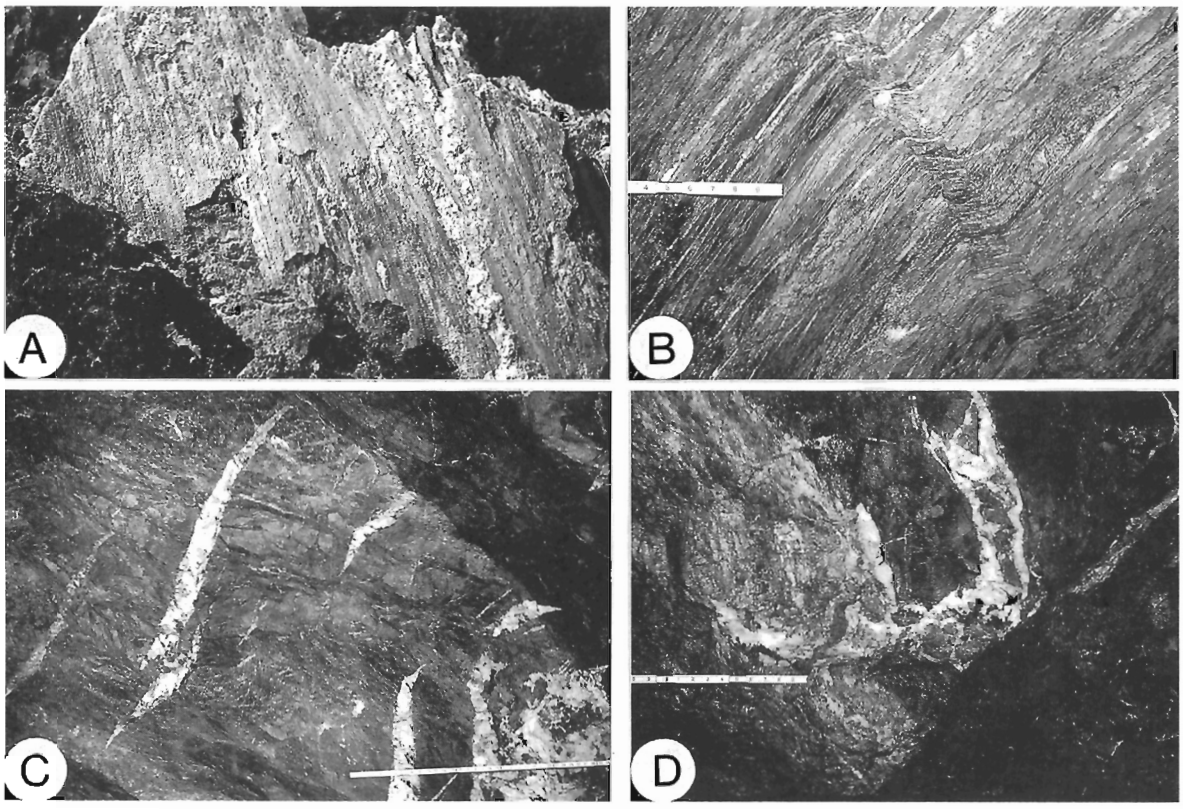

Figure 4. **A**) Longitudinal view showing down-dip slickenlines on the Deer Cove Sole "Thrust" plane. **B**) Cross-section view showing the high strain hanging wall and the kinks (scale bar equals 18 cm). **C**) Cross-section view of the "en echelon" sigmoidal extension quartz veins confined within the gabbroic dyke and indicating a reverse sense of motion (scale bar equals 75 cm). **D**) Oblique view of an northwest oriented brittle sinistral fault crosscutting the main mineralized breccia vein (scale bar equals 35 cm).

Figure 5. Vertical section view showing the down-dip stretching lineation defined by elongated clasts.

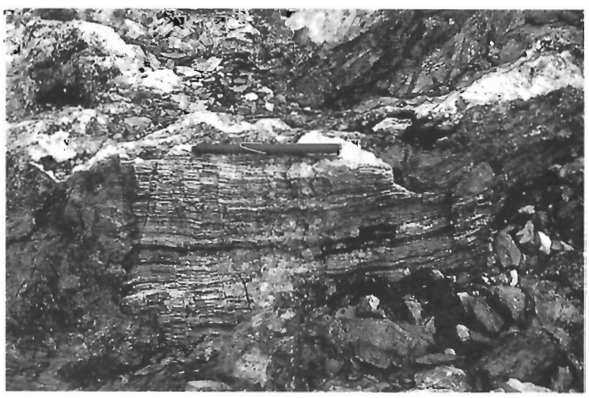

Figure 6. Longitudinal view showing subhorizontal quartz fibres along an extension quartz vein located within a north-south oriented tear fault.

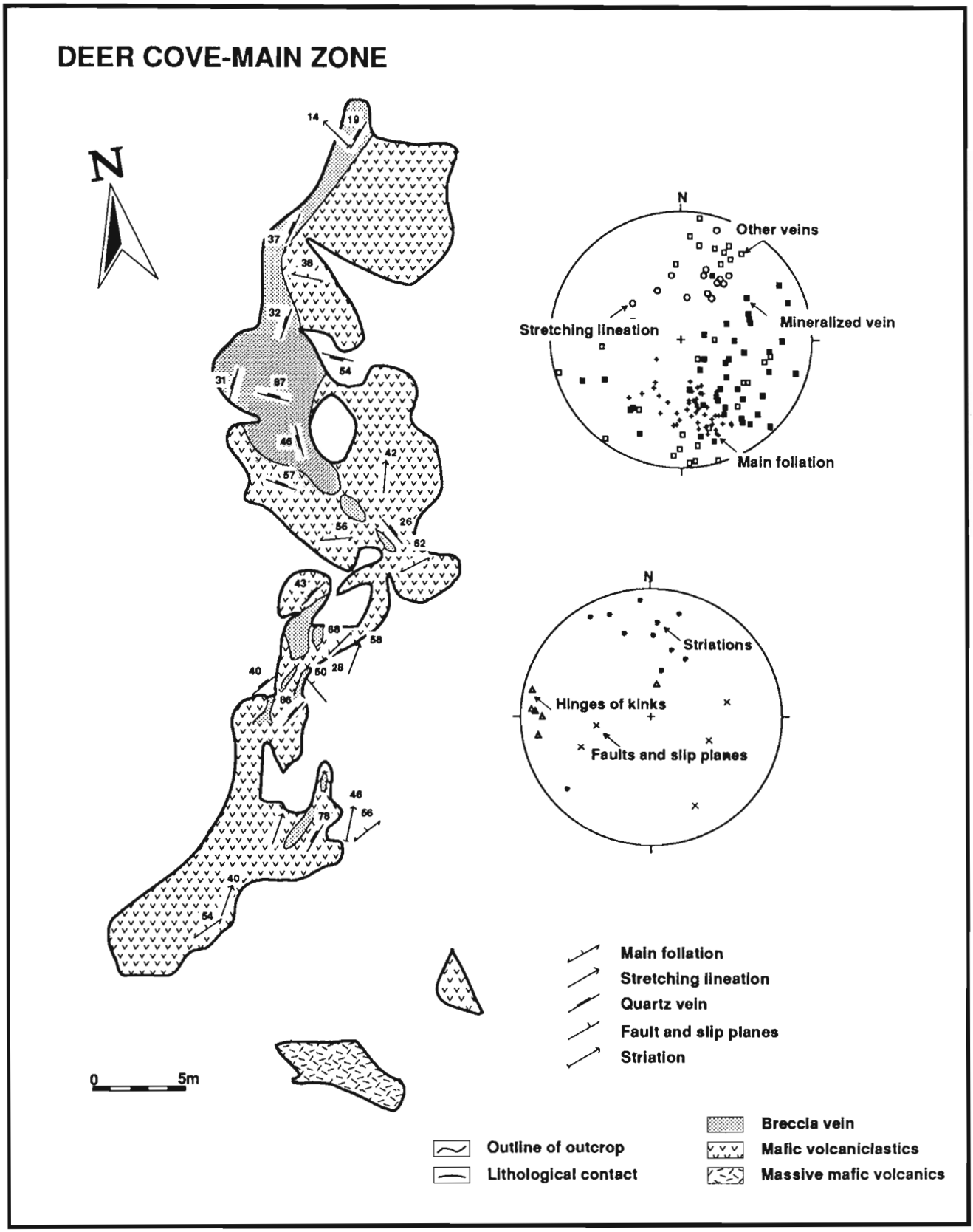

Figure 7. Detailed map of the Main zone near the portal, showing the main structural elements, vein distributions, and equal area projections of structural data (lower hemisphere).

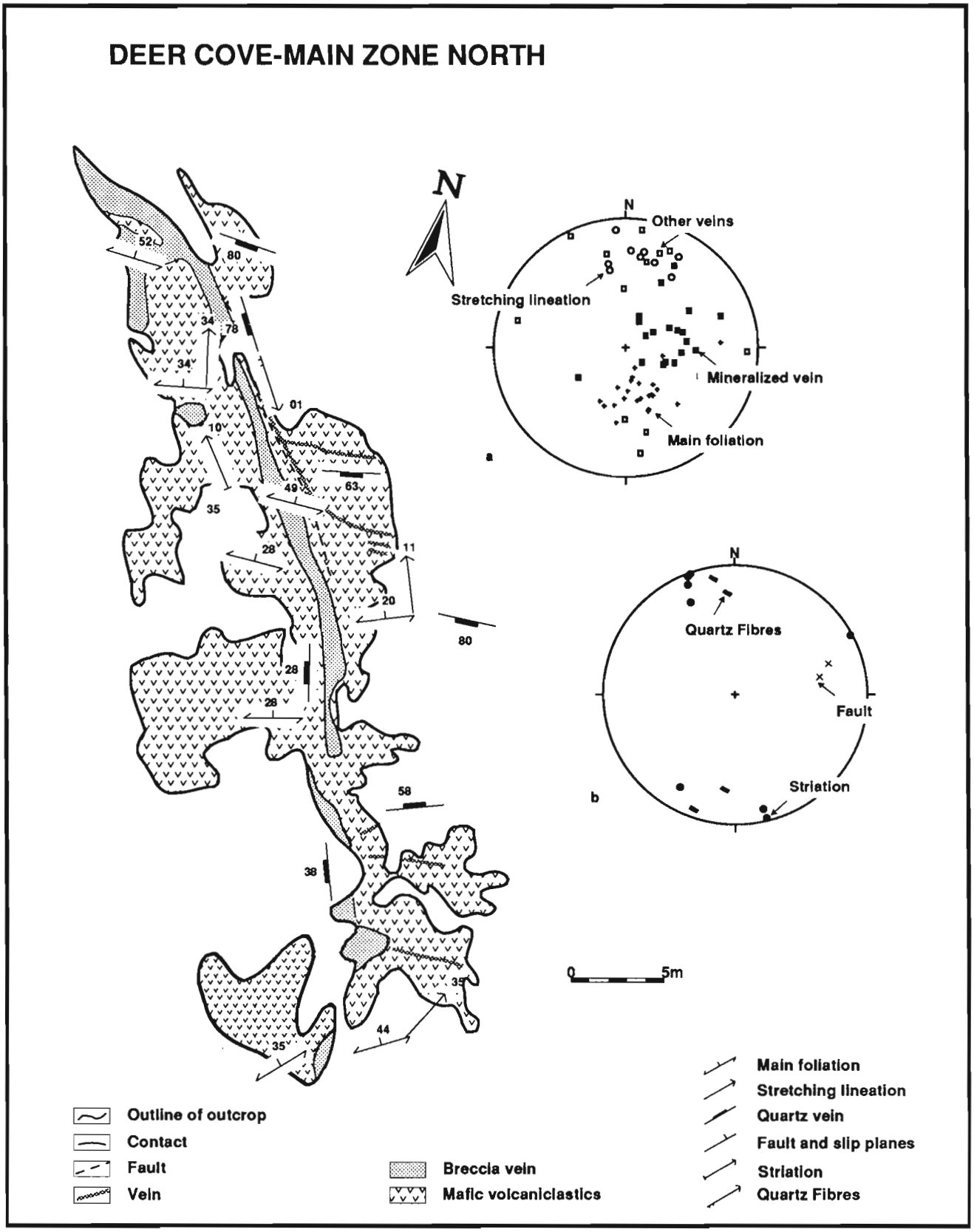

Figure 8. Detailed map of the Main zone away from the portal, showing the main structural elements, vein distributions, and equal area projections of structural data (lower hemisphere).

However, the mineralized vein is seen to locally cut lithological and "thrust" contacts. This observation, also recognized by Gower et al., (1990), suggests that the vein development was initiated after the beginning of the thrusting event. A number of late faults oriented at N005/55°-N345/40° displace the ore zone over 1-2 m with a sinistral sense of motion.

AK2 zone

The mineralization at the AK2 zone (Fig. 2) is hosted by a quartz vein located within a 2 m wide shear zone within a gabbro. The mineralized quartz vein is locally controlled by a sheared contact between the gabbro and adjacent volcanic rocks probably related to the layer anisotropy induced by the gabbro. The gold is found in a breccia-type vein that contains up to 40% fragments of chloritic material. Unlike the main zone, the AK2 zone is relatively undeformed and contains little pyrite.

Figure 9. Plan view of the main mineralized breccia vein as seen underground (scale bar equals 45 cm).

The shear zone hosting the AK2 mineralization strikes N318/50° (Fig. 2). Within it and making a small angle with the shear zone boundary, there is a well developed foliation trending on average N298/47°. This planar fabric contains an oblique, shallow- to moderately-plunging, stretching lineation. The angular relationship between the shear zone boundary and the foliation, combined with the stretching lineation suggests a dextral reverse movement along this shear zone. Structures, similar to shear bands and produced by a fracture cleavage (N320/40°) cutting and dextrally dragging the main fabric, support this hypothesis. The vein is clearly discordant to the main fabric in the shear zone (N335/30°) but is parallel to the fracture cleavage producing the shear band structures.

Towards the northern extremity of the outcrop, the shear zone and the vein progressively change their orientation. The main fabric in the shear zone becomes more or less east-west (N254/31°) whereas the stretching lineation is down-dip.

DISCUSSION AND CONCLUSION

We agree with Gower et al., (1988, 1990), that the Main zone mineralization occurred during the deformation that produced the south-verging thrusting. The zone is folded near the "thrust" and the strong cleavage associated with it, is axial planar to these folds. However, the mineralized zone crosscuts and therefore postdates the "thrust" contact between the mafic volcanic rocks and sheeted dykes as well as the "thrust" contact between the sheeted dykes and gabbro. Gower at al., (1988, 1990) proposed a preliminary genetic model (Fig. 10) similar to the listwaenite model of Buisson

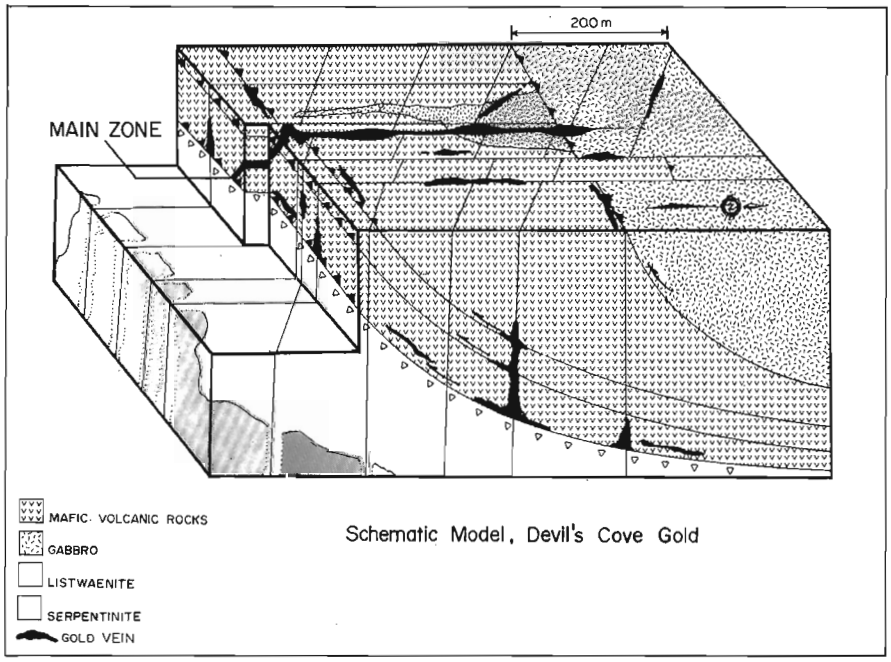

Figure 10.

Schematic genetic model for the Deer Cove deposit proposed by Gower et al., (1988, 1990).

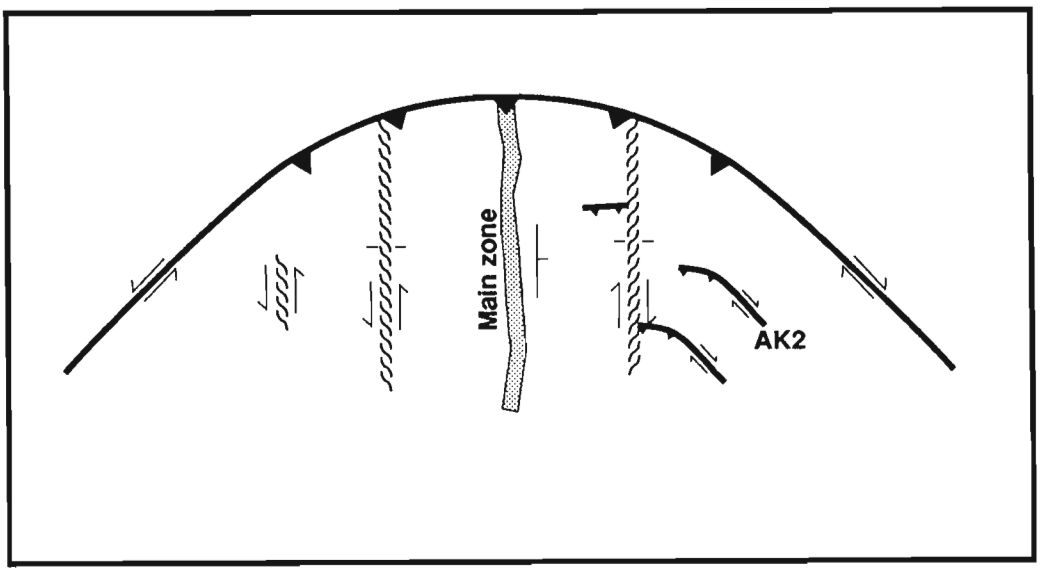

Figure 11. Schematic structural model showing the lateral variation of orientation and related movement of the Deer Cove Sole "Thrust" from east-west with reverse movement to NW and NE oblique ramps with strike slip movement. This variation induced differences in the strain rate along the length of the Deer Cove Sole "Thrust" which resulted in extension subparallel to the strike of the Deer Cove Sole "Thrust" and formation of the breccia-vein almost perpendicular to the orientation of the east-west segment of the Deer Cove Sole "Thrust". Arrows point to overthrusted block.

and Leblanc (1985, 1986) in which gold is associated with carbonatized ultramafic rocks in ophiolites. According to that model, gold mineralization at Deer Cove was deposited after that the Deer Cove Block had been imbricated, but before the end of movement along the Deer Cove Sole "Thrust". Gold was liberated from the serpentinized ultramafic rocks marking the footwall of the Deer Cove Sole "Thrust", possibly by the dehydration of a large volume of serpentine caused by its alteration to talc and magnesite.

Based on our structural study, we propose that the Deer Cove gold deposit is a typical stockwork breccia vein system, and is similar to the San Antonio stockwork in the Archean Rice Lake greenstone belt of the Superior Province (Poulsen et al., 1986; Lau, 1988). The gold mineralization at Deer Cove is hosted by breccia-veins associated with one of the second order reverse faults (Deer Cove Sole "Thrust") that are common on the Baie Verte Peninsula. The mean orientation of the Main zone is N170/50°, whereas that of the AK2 zone is N318/50°, and both are discordant to the regional foliation and to the Deer Cove Sole "Thrust". As indicated at the AK2 zone, the orientation of the deformation zone controlled the slip direction. The major "thrust" strikes east and has a south-directed vergence with associated down-dip stretching lineations whereas the AK2 structure strikes northwest with subhorizontal to oblique stretching lineations thus suggesting strike slip movement. Both structures indicate however an overall south-directed tectonic transport. This south-directed tectonic transport, despite variation in orientation of the structures, is a critical structural aspect which controlled the development of the breccia-vein hosting the mineralization. Along strike variation of orientation and related movement of the Deer Cove Sole "Thrust" from an east-west high-angle reverse fault to northwest and northeast oblique ramp with strike slip movement imply that there was variation in the strain rate along the length of the Deer Cove Sole "Thrust". This variation in the strain rate produced extension subparallel to the strike of the Deer Cove Sole "Thrust", mainly located within the middle part of the Deer Cove block. This extension allowed formation of the breccia-vein almost perpendicular to the orientation of the east-west segment of the Deer Cove Sole "Thrust" (Fig. 11). Shear related veins within the northwest strike-slip segment of the Deer Cove Sole "Thrust" (AK2 zone) and in north-south tear faults (small quartz-chlorite veinlets) (Fig. 11), are also consistent with this interpretation. In such a model, the mineralized breccia-vein of the Main zone is genetically related to normal faulting in weakly deformed blocks, explaining the absence of penetrative deformation associated with the veining. Lydon et al. (1988) proposed a model of sudden devolatization of H_2O/CO_2 fault-zone fluids by hydrofracturing of the hanging wall which is compatible with this structural interpretation. The sudden decompression of fluids, channellized within the extension zone, resulted in the precipitation of the gold mineralization and explains the hydrobrecciation which characterizes the mineralized zones.

The mineralized veins at Deer Cove are genetically related to the Deer Cove Sole "Thrust". As proposed by Gower et al. (1988, 1990), crosscutting relationships indicate that they were formed after initiation of the reverse movement but before this progressive faulting event ended suggesting that the thrusting sequence progressed towards the foreland.

ACKNOWLEDGMENTS

The authors express their sincere thanks to Ian Perry, A. Huard, V. Arseneault, and D. MacInnis of Noranda Exploration for their great scientific collaboration, access to unpublished information and material, logistic support, and permission to publish. Logistic support by Corona Corporation has also been greatly appreciated. M. Bélanger, G. Gosselin, and D. Watanabe provided dedicated and excellent field assistance. Thanks are also due to Yvon Houde for drafting some of the diagrams. The manuscript has benefited from the constructive criticism of S. Swinden and A. Tremblay.

REFERENCES

Buisson, G. and Leblanc, M.
1985: Gold in carbonatized ultramafic rocks from ophiolite complexes; Economic Geology, v. 80, p. 2028-2029.
1986: Gold-bearing listwaenites (carbonatized ultramafic rocks) from ophiolite complexes; in Metallogeny of Basic and Ultrabasic Rocks, (ed.) M.J. Gallagher, R.A. Ixer, C.R. Neary, and H.M. Prichard; Institute of Mineralogy and Metallogeny, London, p. 121-132.

Dubé, B.
1990: A preliminary report on contrasting structural styles of gold-only deposits in western Newfoundland; in Current Research, Part B; Geological Survey of Canada, Paper 90-1B, p. 77-90.

Dubé, B., Lauzière, K., and Poulsen, K.H.
1992: Thrust-related breccia-vein type gold mineralization: the Deer Cove deposit, Baie Verte Peninsula, Newfoundland; in Gold mineralization in Western Newfoundland, (ed.) B. Dubé, K. Lauzière, S. Swinden, and M. Wilson; Geological Association of Canada-Mineralogical Association of Canada, Wolfville, 1992, Field trip guide book, p. 25-36.

Gower, D., Graves, G., Walker, S., and MacInnis, D.
1988: Lode gold mineralization at Deer Cove, Point Rousse Complex, Baie Verte Peninsula; in The Volcanogenic Sulphide Districts of Central Newfoundland, (ed.) H.S. Swinden and B.F. Kean: Geological Association of Canada, Mineral Development Division, St. John's, Newfoundland, p. 43-48.

Gower, D., Graves, G., Walker, S., and MacInnis, D.
1990: Lode gold mineralization at Deer Cove, Point Rousse Complex, Baie Verte Peninsula; in Metallogenic framework of base and precious metal deposits, Central and Western Newfoundland, (ed.) H.S. Swinden, D.T.W. Evans, and B.F. Kean; 8th IAGOD Symposium Field Trip Guidebook; Geological Survey of Canada, Open File 2156, p. 165-172.

Hibbard, J.
1983: Geology of the Baie Verte Peninsula, Newfoundland; Newfoundland Department of Mines and Energy, Mineral Development Division, Memoir 2, 279 p.

Lau, M.H.S.
1988: Structural geology of the vein system in the San Antonio gold mine, Bisset, Manitoba, Canada; M.Sc. thesis, University of Manitoba, Winnipeg, Manitoba, 154 p.

Lydon, J.W., Al, T., Richardson, D.G., and Lancaster, R.D.
1988: Magmatic and hydrothermal processes of precious metal enrichment in Newfoundland ophiolites; Geological Survey of Canada, Program with abstracts, p. 24.

Lydon, J.W., Lavigne, J.G., and Roddick, J.C.M.
1990: The relationships of gold mineralization to the thermal and tectonic history of the Baie Verte Peninsula, Newfoundland (abstract); Geological Survey of Canada, Minerals Colloquium, January, 1990, Program with Abstract, p. 26.

Norman, R.E. and Strong, D.F.
1975: The geology and geochemistry of ophiolitic rocks exposed at Ming's Bight, Newfoundland; Canadian Journal of Earth Sciences, v. 12, p. 777-787.

Patey, K.S.
1990: Lode gold mineralization at Deer Cove, Baie Verte Peninsula, Newfoundland; B.Sc. thesis, Memorial University of Newfoundland, St. John's, Newfoundland, 97 p.

Patey, K.S. and Wilton, D.H.C.
1990: The Deer Cove mesothermal lode gold deposit, Baie Verte Peninsula, Newfoundland - A Mother Lode Analogue; Geological Association of Canada-Mineralogical Association of Canada, Annual Meeting, Vancouver, Program with abstracts, v. 15, p. 102.

Poulsen, K.H., Ames, D.E., Lau, S., and Brisbin, W.C.
1986: Preliminary report on the structural setting of gold in the Rice Lake area, Uchi subprovince, Southeastern Manitoba; in Current Research, Part B; Geological Survey of Canada, Paper 86-1B, p. 213-221.

Tuach, J., Dean, P.L., Swinden, H.S., O'Driscoll, C.F., Kean, B.F., and Evans, D.T.W.
1988: Gold mineralization in Newfoundland: a 1988 review, in Current Research, Newfoundland Department of Mines, Mineral Development Division, Report 88-1, p. 279-306.

Williams, H. and St-Julien, P.
1982: The Baie Verte-Brompton Line: Early Paleozoic continent ocean interface in the Canadian Appalachians; in Major structural zones and faults of the northern Appalachians; (ed.) P. St-Julien and J. Béland; Geological Association of Canada, Special Paper 24, p. 177-208.

Geological Survey of Canada Project 890026 AJ

Ordovician-Silurian stratigraphy between Gander Bay and Birchy Bay, Newfoundland

K.L. Currie
Continental Geoscience Division

Currie, K.L., 1993: Ordovician-Silurian stratigraphy between Gander Bay and Birchy Bay, Newfoundland; in Current Research, Part D; Geological Survey of Canada, Paper 93-1D, p. 11-18.

Abstract: The Dog Bay fault, locally a north-trending zone of dextral movement, separates different Ordovician-Silurian sequences. To the east, Ordovician shale, greywacke, and conglomerate of the Hamilton Sound group disconformably underlie Silurian Indian Islands Group. Rocks exhibit doubly plunging folds, locally complexly refolded. To the west, mélange and volcanics of the Ordovician(?) Duder group underlie Stoneville formation and Silurian Botwood Group. All are thrown into west-verging folds. No stratigraphic links are known across the Dog Bay fault, which is ductile within mélange and Stoneville formation, but a brittle feature in Silurian rocks to the south. Since the fault separates diverse Silurian strata, it is a terrane boundary. Several gold prospects occur along this boundary. Small east-over-west thrusts abound east of the Dog Bay fault. To the west, the Reach fault, a young feature, exhibits brittle left-hand displacement of up to 15 km.

Résumé : La faille de Dog Bay, qui est par endroits une zone de mouvement dextre orientée vers le nord, sépare différentes séquences ordoviciennes et siluriennes. À l'est, un shale, une grauwacke et un conglomérat ordoviciens du groupe de Hamilton Sound sont recouverts en discordance par le Groupe silurien d'Indian Islands. Les roches présentent des plis de plongement double, replissés par endroits de manière complexe. À l'ouest, le mélange et les roches volcaniques du groupe ordovicien(?) de Duder sont sous-jacents à la formation de Stoneville et au Groupe silurien de Botwood. Toutes ces roches sont déformées en plis de vergence ouest. Aucuns liens stratigraphiques n'ont été établis de part et d'autre de la faille de Dog Bay, ductile à l'intérieur du mélange et de la formation de Stoneville, mais constituant une structure cassante dans les roches siluriennes situées au sud. Étant donné que la faille sépare diverses strates siluriennes, elle constitue la limite d'un terrane. Il existe plusieurs gîtes aurifères possibles le long de cette limite. De petits chevauchements est sur ouest abondent à l'est de la faille de Dog Bay. À l'ouest, la faille de Reach, structure récente, montre un déplacement horizontal sénestre de type cassant pouvant atteindre 15 km.

INTRODUCTION

The Exploits Subzone of Newfoundland (Williams et al., 1988) records evolution of the eastern margin of the Iapetus Ocean in Ordovician and Silurian strata. The ophiolitic substrate of the subzone was obducted onto the Gander Zone prior to 475 Ma (Colman-Sadd et al., 1992). Late Arenig to mid-Silurian stratified rocks form a cover sequence which locally extends onto the Gander Zone (Wonderley and Neuman, 1984). In the northeastern Exploits Subzone, this sequence was previously divided into Ordovician deep-water turbidites of the Davidsville Group, assumed to pass gradationally upward into shallow water deposits, then to terrestrial strata of the Silurian Botwood Group (O'Neill, 1991), although fossils with Ashgillian ages have not been found in the supposed transition zone. This simple model can be applied in modified form in the Bay of Exploits area where strata of the Exploits Group, approximately coeval with the Davidsville Group, contain abundant volcanic rocks, and deep marine turbiditic sedimentation continued through Ashgill time (O'Brien, 1991), ending with the distinctive Sansom-Goldson greywacke-conglomerate sequence which underlies the Botwood Group. Difficulties with this model, as applied to the northeast Exploits Subzone, have been apparent for several years. Currie et al. (1980) pointed out that contrasts in sedimentary environment between Davidsville and Botwood groups implied major unconformity. The Davidsville Group appears to be composite (Currie, 1992). Juxtaposition of Indian Islands Group with contemporary Botwood Group implied a tectonic boundary, but the nature of this boundary was not understood. In order to solve these problems, the Comfort Cove map area (2E/7) was remapped.

PREVIOUS WORK

The Comfort Cove map area was mapped at 1:50 000 scale by Patrick (1956), but regional mapping by Williams (1964, 1972) established fundamental stratigraphic relations in the area. Extensive work has been undertaken west of the Reach fault, dating back to Twenhofel and Shrock (1937), but much less work has been done east of the Reach fault, although studies were undertaken by McCann (1973), Wu (1979), and Karlstrom et al. (1982). The present contribution concentrates on this relatively poorly known region, where new roads have vastly increased amount and quality of exposure.

DESCRIPTION OF UNITS

General statement

Rocks between Gander Bay and Birchy Bay (Fig. 1) fall into two main packages, separated by a major feature trending north-northeast through Dog Bay, here named the Dog Bay fault. East of the Dog Bay fault, the Hamilton Sound group consists of Barrys Ponds conglomerate, which rests unconformably on ophiolitic Gander River complex and grades into chloritic shale-siltstone rhythmites containing intervals of greywacke and conglomerate (Round Pond shale). The Round Pond shale is facies equivalent to coticule-bearing Woody Island siltstone. Both are overlain by Caradocian sulphidic black shale with calcareous beds and local chert lenses (Main Point shale). All units contains olistostromal horizons. Limestone breccia, siltstone, greywacke, and grey shale of the Silurian Indian Islands Group disconformably overlie the Hamilton Sound group. West of the Dog Bay fault, the oldest exposed rocks, the Ordovician(?) Duder group, consist predominantly of shale, siltstone, and volcanic rocks, including tuffs, basaltic pillow breccia, and conglomerate. Much of the Duder group is disrupted to locally chaotic. The upper shale-dominated portion (Sawmill shale) contains numerous blocks of both local and exotic lithologies. The Botwood Group, disconformably above the Stoneville formation, consists of basal subaerial volcanics (Port Albert volcanics) overlain by fine grained, green tuffaceous sandstone (Dog Bay formation). An upper unit of red sandstone and shale (Ten Mile sandstone) may lie unconformably on the lower part of the group. Strata on both sides of the Dog Bay fault host posttectonic biotite granodiorite (Loon Bay and Tims Harbour plutons) with numerous dykes and Jurassic lamprophyre dykes.

East of Dog Bay fault

Kennedy and McGonigal (1972) introduced the term Davidsville Group to designate green to black shale/siltstone rhythmites characteristic of the Hamilton Sound-Gander River-Glenwood region. Rocks around Davidsville do not belong to this group (Currie, 1992) and the stratigraphy proposed by O'Neill and Blackwood (1989) south of the mapped area does not apply around Gander Bay. The proposed Hamilton Sound group (Currie, 1992) consists (from the base upward) of Barrys Ponds conglomerate, Round Pond shale, Woody Island siltstone (in part facies equivalent to the Round Pond shale), and Main Point shale. It differs from the Davidsville Group in lacking the Weirs Pond Formation (O'Neill and Blackwood, 1989), upon which much of the tectonic interpretation of the group has been based (O'Neill and Blackwood, 1989; Colman-Sadd et al., 1992).

Barrys Ponds conglomerate does not outcrop in the map area, but rests unconformably on gabbro of the Gander River complex just south of the map area. It consists of unsorted, commonly coarse, debris of ultramafic, volcanic, and trondhjemitic rocks of the Gander River complex set in a chloritic matrix. This unit fines upward into chloritic shale with local conglomerate lenses (Round Pond shale).

The Round Pond shale typically consists of alternating beds of greenish-black shale and grey, fine greywacke on a scale of 5-20 mm. Toward the top of the unit the proportion of shale increases markedly. Single or composite lenses of conglomerate and greywacke from 10 cm to 4 m in thickness occur throughout the Round Pond shale at apparently random intervals, forming an estimated 5% of the volume of the unit. Conglomerate is of two types. Type 1, derived directly from the Gander River Complex exhibits sparse, subrounded cobbles to boulders of siltstone, trondhjemite, and volcanic rocks in a chlorite-rich, dark matrix and appears to be most

common in the lower part of the section. Type 2, possibly derived from the Gander Zone, consists of graded, granule- to pebble-sized siltstone, shale, quartz, and feldspar clasts set in a grey-green, chlorite-feldspar-quartz matrix. Both types occur close together in roadcuts (gridref 835593, 823675[1]) and lie within shale sequences. The thickness of the Round Pond shale is uncertain, but unfolding of numerous upright tight folds suggests a thickness less than 2 km. Pickerill et al. (1979) interpreted the Round Pond shale as extreme distal turbidites or contourites deposited in deep water.

Woody Island siltstone (Currie, 1992) outcrops north of Charles Cove, and is interpreted to be equivalent to the Round Pond shale, some parts of which it strongly resembles. Woody Island siltstone consists of thin-bedded siltstone-shale rhythmites in which the lower siltstone portion grades upward to black shale. Thin, contorted coticules are ubiquitous and highly characteristic. The unit has been moderately to strongly hornfelsed north of Charles Cove, making distinction from the overlying Charles Cove clastics very difficult.

The Main Point shale, which overlies the Round Pond shale, consists largely of black, pyritic shale. Stringers of pyrite up to 5 mm thick occur. Black marly layers up to 3 cm thick locally form up to 25% of the rock and contorted, blue-black, thin manganiferous layers (coticules) occur in the basal part of the unit. Black chert lenses up to 10 cm thick are common east of Gander Bay, but rare to the west. At Tippes Point an olistolith of pillow lavas in black shale exceeds 10 by 20 m. Several other thin mélange horizons occur in the same region. A fossil collection from Main Point suggested a mid-Caradoc age (Williams, 1972).

The Dog Bay Point mélange of sparse, large gabbro and pillow lava blocks in black siltstone to shale matrix was described by Williams (1992). The matrix probably consists of disrupted Woody Island siltstone. Mélange occurs in all units of the Hamilton Sound group, and sampled the underlying Gander River Complex. Mélange does not occur in the overlying Indian Islands Group.

Patrick (1956) assigned Silurian siltstones and limy argillites which outcrop around Dog Bay Point to the Indian Islands Group. Williams (1972) retained the name because the rocks overlapped in age with the Botwood Group, but differed in stratigraphy. This year's mapping shows that the Indian Island Group extends much further south than previously thought. The group is here divided into three informal units, namely the basal Charles Cove formation, the Horwood formation, and the Centennial formation. Relations between these units are commonly obscured by small-scale thrusts. The base of the Charles Cove formation locally consists of spectacular limestone breccia with blocks of crinoid coquina in a carbonate matrix. The best exposure is on a small island (gridref 839739). South of the map area along the east side of Rocky Pond similar limestones breccias are exposed, and limestone cobbles occur in conglomerate at Burnt Lake. Between Burnt Lake and Rocky Pond conglomerate grades upward to coarse greywacke with rare large cobbles, and then to buff siltstone with fossiliferous limestone lenses, locally with convolute bedding, flute casts, and other sedimentary structures. North of Highway 331, much of the siltstone is hornfelsed to greenish black, highly fractured massive rock. Brecciation is widespread, locally in east-west vein-like masses, but is commonly pervasive. Williams (1972) reported the coral *Favosites* cf. *favosus* from the base of the Charles Cove formation at Tims Harbour, implying that all of the Indian Islands Group is Silurian in age. Wu (1979) reported the brachiopod *Pentamerus* cf. *oblongus* from a loose block of calcareous siltstone (gridref 812732) implying that the upper part of the unit could be upper Llandovery to Wenlock in age.

The Horwood formation consists of thin bedded, grey to black shale with 1 to 5 mm beds of buff siltstone. Calcareous beds locally comprise up to 20% of the unit. Continuous sections from shale into siltstone can be observed on the coast north of Horwood (gridref 807826) and at Rodgers Cove (gridref 817722). At the former locality, facing directions show that shale is younger.

Centennial formation forms a single fold core consisting of red to purple, thin bedded shale and sandstone with dewatering structures, shale flake conglomerate, and other evidence of shallow water to terrestrial deposition. It appear to grade downward to Horwood shale. The Indian Islands Group as a whole represents overwhelming of carbonate reefs by upward-fining clastic deposition presumably due to uplift of a hinterland.

West of the Dog Bay fault

Rocks between the Dog Bay and Reach faults comprise the Duder group of volcanics, sedimentary rocks and mélange; the Stoneville formation of conglomerate and shale, and the Botwood Group.

Duder group

The name Duder group is proposed for a belt of rocks extending from Dog Bay southwest to the region of Long Pond, and into Gander River map area. Excellent exposures occur in trenches on the Clutha gold prospect. The group consists of dark shale, salic tuffs and flows, mafic pillow breccia and gabbro sills, siltstone grading from white through dark green to blue-black, and minor conglomerate with well rounded cobbles of chert, siltstone, volcanics, and minor granite set in a tuffaceous matrix. Volcanics consist of salic crystal tuffs with quartz and feldspar crystals, and mafic pillow breccia, locally containing interstitial limestone. Abundant dykes and sills occur in the volcanic interval, in particular thick salic and mafic dykes with composite and/or comingled textures. Variably silicified and cherty siltstone and shale grade from green through white to black (manganiferous). The Duder group is cyclic with conglomerate or agglomerate at the base, a volcanic interval,

[1] All grid references to UTM grid zone 21U, square XE (2E/7 and 8)

and an overlying sedimentary interval. The cycles vary from 50 to 150 m thick. Between Duder Lake and Horwood the Duder group forms a mélange of elongate boudins of gabbro and tuff up to 150x20 m within a dark siltstone-shale matrix (tectonic mélange). The upper part of the group at Stoneville, and between Rocky Pond and Duder Lake, consists of dark grey shale with disrupted tuff beds and some foreign blocks (Sawmill shale).

Churchill and Evans (1992) described thick (>50 m), coarse gabbro masses within the Duder group as dykes, and interpreted them to cut the Botwood Group. However, the masses appear concordant to surrounding strata, grade into massive to pillowed material, and display complex internal contacts suggesting that the gabbro formed cogenetic subvolcanic sills. North of Duder Lake, vertical Duder group with a gabbro sill contacts gently dipping (<30°) red sandstone of the Botwood Group (gridref 698688) along an apparent fault-modified unconformity.

The age of the Duder group is unknown, except that it is older than the Llandovery or younger Stoneville formation. The group does not resemble any major stratigraphic unit in this region, but the assemblage of volcanic and sedimentary rocks with numerous thick gabbro dykes, and limestone associated with pillowed basalt has a counterpart in the New Bay Formation of the Exploits Group (O'Brien, 1991).

The Botwood Group as defined by Williams (1972) included a basal conglomerate-greywacke (Sansom-Goldson), a volcanic unit (Lawrenceton), and a micaceous sandstone unit (Wigwam). The turbiditic greywacke-conglomerate sequences have been shown to be of late Ordovician age to

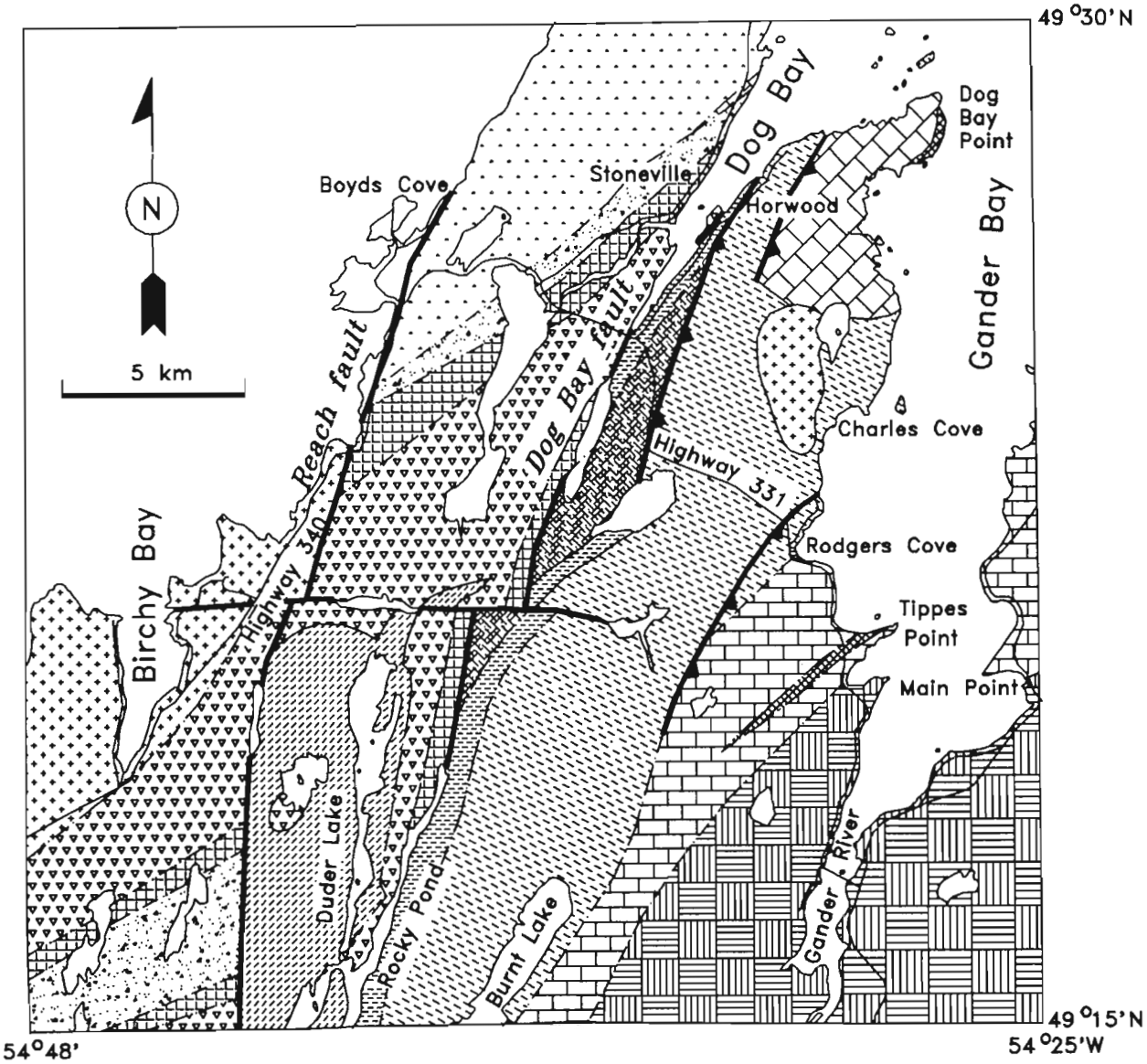

Figure 1. Geological map of the Gander Bay-Birchy Bay area, northeast Newfoundland (NTS areas 2E/7 and 2E/8).

the southwest of the map area (O'Brien, 1991), and are now excluded from the Botwood Group (Williams, 1993). The volcanic unit north of Stoneville differs from that at Lawrenceton, and there are at least two sandstone units of formational status. This report therefore uses local names.

Matrix supported conglomerate with rather sparse, well rounded clasts of chert, siltstone, epidotized volcanic rocks and porphyry, and granite (some deformed) in increasing order of abundance, together with intercalated greywacke and shale occurs on both sides of the Port Albert peninsula, but the conglomerate fines and thins to the southeast, where it splits into two or more intervals enveloped by black shale and turbidites. McCann and Kennedy (1974) gave different names on opposite sides of the peninsula, but the rocks are clearly correlative, and the name Stoneville formation (McCann, 1973) is adopted for the whole. At Beaver Cove, just north of the mapped area fossiliferous limestone cobbles contain a poorly preserved Llandovery C6 fauna (Williams, 1972). These cobbles bear witness to a Llandovery carbonate reef complex which has not been found in outcrop.

Abundant conglomerate in the southwest corner of the map area. resembles the Stoneville formation in clast provenance and size, and occurs at a similar stratigraphic position. It may be correlative to the Stoneville forming a pin across the Reach fault, and indicating about 15 km of sinistral offset.

Mafic and salic tuff and agglomerate of the Port Albert formation (McCann, 1973) outcrop on a short stretch of shoreline northeast of Stoneville, but Williams (1993) has shown that the unit can be traced more than 30 km to the northeast. At Port Albert (8 km northwest of Stoneville) the rocks comprise basalt with a vesicular base overlain by salic tuffs, and the total thickness of volcanics is estimated to be 300 m. The unit is thinner to the southeast, and is absent southwest of Stoneville. A welded disconformable contact between Port Albert volcanics and Stoneville formation is spectacularly displayed on the coast just north of Port Albert (Williams, 1993).

A broad belt of fine grained greenish sandstone (Dog Bay formation of McCann and Kennedy, 1974) extends from Stoneville to the Reach fault. The rocks typically form graded beds 10 to 50 cm thick. Much of the upper part of the unit is

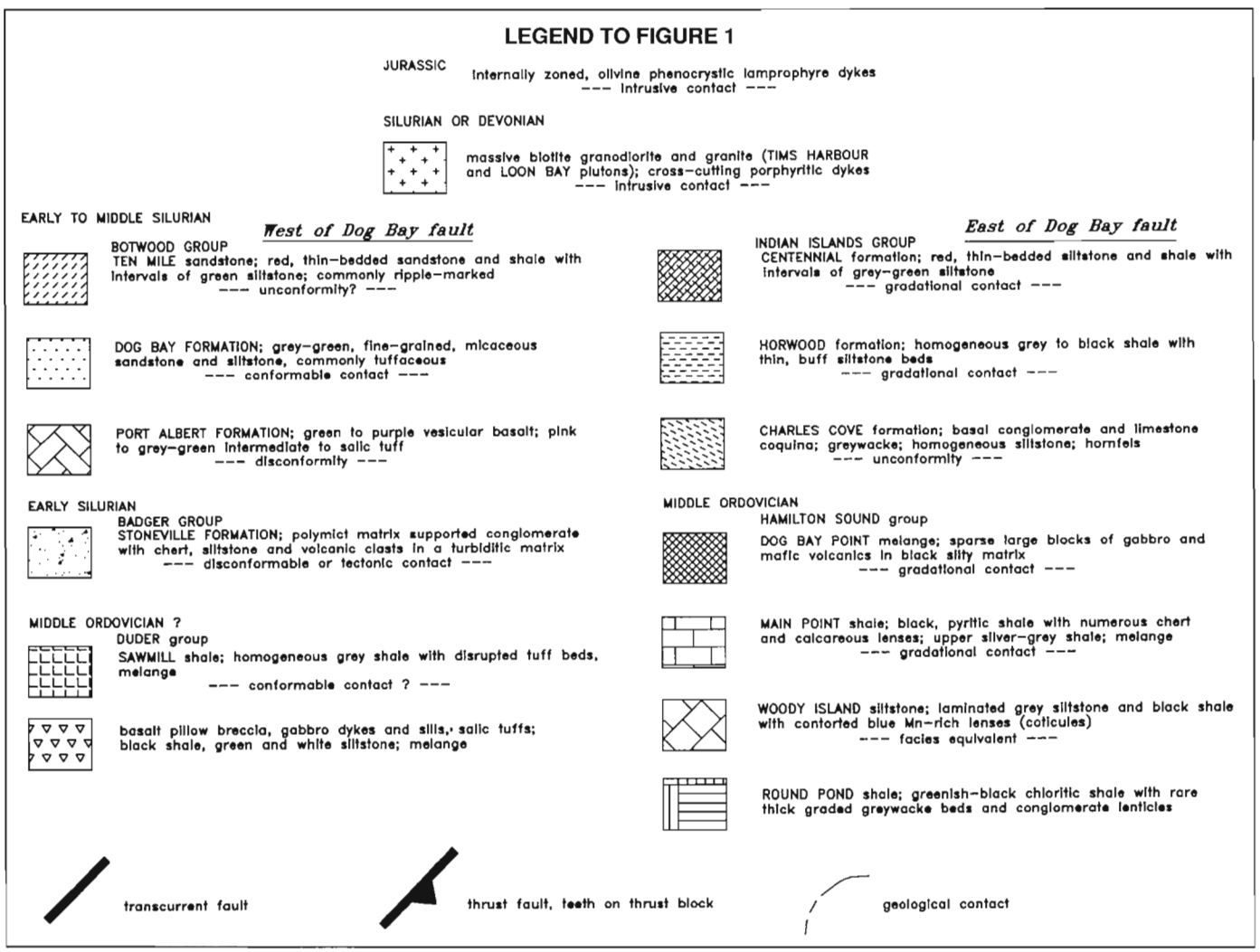

tuffaceous with salic or chloritic fragments up to 5 cm across. The sandstone is typically micaceous and ripple-marked, but displays little evidence of littoral or subaerial deposition. This unit can be traced a further 20 km northeast of the map area to Change Islands and Fogo Island (Williams, 1993).

A red sandstone-shale sequence outcrops around Duder Lake. This unit, termed Ten Mile sandstone, resembles Wigwam Formation of the type area, which is thinly laminated pink to purple sandstone with abundant red to purple shale interbeds. Dewatering structures and desiccation cracks testify to shallow water to subaerial deposition. Dips in the Ten Mile sandstone are commonly low (<40°) except within a few tens of metres of faults. The unit forms multitudes of large slabby boulders. The age of the Ten Mile sandstone is uncertain. Well-known fossiliferous rocks on Salmon Pond Brook and nearby Trans-Canada Highway, formerly assigned to the Botwood Group, are now reassigned to the Indian Islands Group (Williams, 1993).

Intrusive rocks

Biotite granodiorite of the Loon Bay and Tims Harbour plutons, several small plutons, and a host of related dykes, cut supracrustal rocks on both sides of the Dog Bay fault. The Loon Bay pluton exhibits two phases, one with large anhedral quartz, and the other with large euhedral plagioclase. The pluton has virtually no chilled margin, and has a hornfels aureole only a few tens of metres wide. Screens and inclusions of country rocks are rare, and enclaves are restricted to small, rounded dioritic types with plagioclase phenocrysts. The Tims Harbour pluton resembles the plagioclase-porphritic phase of the Loon Bay, but is finer grained. The Tims Harbour pluton has a very extensive suite of plagioclase porphyry dykes, and a hornfels aureole encompassing much of central Horwood Peninsula. Small plutons similar to Tims Harbour, and with extensive dyke swarms, occur near gridref 784630 and 798851.

The Loon Bay pluton is cut by two black, olivine-porphyritic lamprophyres. One lies posttectonically in the Reach fault near gridref 693754. These dykes form part of the Jurassic alkaline lamprophyre swarm of Notre Dame Bay (Strong and Harris, 1974). Similar dykes occur along the west shore of Gander Bay north of Rodgers Cove.

STRUCTURAL GEOLOGY

Faults

The Dog Bay fault follows Rocky Pond and Dog Bay, bisecting the map area from north to south. In Dog Bay a zone of transpressive dextral and east-over-west ductile motion at least 2 km wide is underlain by mélange. Related metre-scale zones of dextral and east-over-west movement occur throughout Horwood peninsula and up to a kilometre west of Dog Bay. On Rocky Pond the fault zone is no more than 100 m wide, and ductile deformation appears to be minimal. The displacement across the Dog Bay fault is unknown, but believed to be large.

The Reach fault, on the west side of the region mapped this year, is a regionally important feature. The work of Williams (1993) combined with the mapping reported here give several correlations across the fault suggesting sinistral motion of up to 15 km. The shatter zone associated with this fault outcrops on Highway 340 just south of Boyds Cove, where it is cut by a Jurassic lamprophyre dyke.

Steep east-over-west thrusts either observed or inferred from juxtaposition of strata are common along the west shore of Gander Bay. None of the individual faults appears to have major displacement, but the cumulative effect is probably large.

Folds

West of the Dog Bay fault, disposition of rocks is controlled by large tight to isoclinal, northwest-verging folds with wavelengths of several kilometres and shallow plunges whose axes can be traced for tens of kilometres (Williams, 1993). East of Dog Bay fault minor folds in the Hamilton Sound group have steep plunges, suggestive of large-scale sheath-like folding, but probably mainly due to intense east-west compression as described by Piasecki (1992). Many minor folds in the Indian Island Group are upright and have low plunges. This region is also affected by complex interference patterns whose effects are incompletely understood.

Despite the diversity of fold styles, the dominant cleavage is reasonably continuous across the region, trending northeast and dipping steeply. The dip noticeably steepens from west to east across the Dog Bay fault. East of Gander Bay the prevailing dip is to the west, while west of the bay it is to the east. Two generations of late, small-scale kink folds, one plunging steeply and the other gently, affect the main axial plane cleavage, but do not control outcrop pattern. They appear to be a result of local collapse and accommodation, probably due to emplacement of plutons and late east-over-west thrusting.

Pre-cleavage folds, some downward facing, have been known in this region for many years. Karlstrom et al. (1982) suggested that they were due to early major thrusting. Current mapping has refuted an inferred thrust between the Stoneville formation and the Port Albert formation, and supports the contention of earlier workers that pre-cleavage folds are slump structures.

All major fold axes and the Dog Bay fault gradually change trend from about of 025 on the south edge of the map to about 075 northeast of the map area. The Reach fault is unaffected by this flexure. The cause of this clockwise deflection is unknown. In scale and style it resembles the Hermitage flexure of southern Newfoundland.

DISCUSSION

The Dog Bay fault, the first boundary found in Newfoundland which separates Silurian rather than Ordovician terranes, has been traced from the Indian Islands to the Trans-Canada

Highway, a distance of more than 100 km, and is clearly a major boundary. Such a major regional feature requires major revision of post-Arenig models for the northeast Exploits Subzone. Strata west of the fault are suspect relative to the Gander River complex and related substrates. Gold mineralization at the Clutha prospect and the Duder Lake area (Churchill and Evans, 1992) appears to be associated with this feature. Relations of Silurian terranes to major Silurian deformation and plutonism are presently essentially unknown.

This report proposes the term Hamilton Sound group for the sequence Barry's Pond formation-Round Pond shale-Main Point shale which lies east of the Dog Bay Fault. These strata were previously assigned to the Davidsville Group, a term which has been loosely applied to a variety of middle Ordovician shale-dominated sequences which cannot all be directly correlated. Blackwood (1972) and O'Neill (1991) assumed the Davidsville Group graded into redbeds of the Botwood Group. Our mapping demonstrates that these groups lie in different terranes. The gold-bearing strata around Duder Lake cannot belong to the Davidsville Group, as supposed by Churchill and Evans (1992), for the same reason. Many other similar examples extending southward into central Newfoundland could be quoted.

Even in the "type" area east of Gander Bay, rocks previously assigned to the Davidsville Group probably belong to several units. The base of the Hamilton Sound group is conglomerate of Gander River Complex debris in a chloritic matrix, a unit of uncertain, but pre-Caradoc, possibly Arenig or Llanvirn-Landeilo age. Basal Davidsville Group, according to O'Neill (1991), consists of limy shale and limestone (Weirs Pond Formation) of Llanvirn-Llandeilo age (Stouge, 1980) which rests on serpentinite of the Gander River Complex. This unit is overlain by multicoloured limy shales and siltstones, which contain Caradoc fossils on Weirs Pond (Williams, 1972). The top of this limy sequence is faulted against Gander River Complex and Hamilton Sound strata. The Weirs Pond slice exhibits a different Ordovician stratigraphy than the Hamilton Sound group. Confusion arose because both rest on Gander River Complex, assumed to form a single, geographically-restricted unit. An ophiolitic substrate is assumed to underlie all of the Dunnage Zone. Units resting on different, but adjacent, fault slices of this substrate could have originated tens or even hundreds of kilometres apart. The same reasoning applies to mélange units. They may have been laterally extensive and approximately coeval, but at present there exists no firm basis for correlating different mélanges.

The Botwood Group as originally defined included three distinct sequences, The basal conglomerate-greywacke sequence has been redefined as Badger Group (Williams, 1993). Shallow water to terrestrial redbeds at the top of the group (Ten Mile sandstone) cross folds associated with underlying volcanics and tuffaceous sandstone at a high angle. Presence of an unconformity is probable. In the Comfort Cove area, all three packages may be of Silurian age, but further southwest O'Brien (1991) has demonstrated a late Ordovician age for part of the Badger Group.

The proposed revisions of stratigraphy are based on remapping aided by new exposure and increased access. This work emphasizes conclusions of O'Brien (1991) that each panel of geology must be examined and assessed on its own merits. Terms like Davidsville Group and Botwood Group are vague and so poorly defined that they have become essentially meaningless. Remapping of much of the northeast Exploits Subzone is required to understand its post accretionary history.

ACKNOWLEDGMENTS

The mapping reported here is a collaborative project with Hank Williams and Mark Piasecki. I am greatly indebted to them for logistical help, for innumerable discussions, and above all for fruitful ideas.

REFERENCES

Blackwood, R.F.
1982: Geology of the Gander Lake (2D/15) and Gander River (2E/2) area; Newfoundland Mineral Development Division Report 82-4, 56 p.

Churchill, R.A. and Evans, D.T.W.
1992: Geology and gold mineralization of the Duder Lake gold showing, eastern Nortre Dame Bay, Newfoundland; Newfoundland Geological Surveys Branch Report 92-1, p. 211-220.

Colman-Sadd, S.P., Dunning, G.R., and Dec, T.
1992: Dunnage-Gander relationships and Ordovician orogeny in central Newfoundland: a sediment provenance and U/Pb age study; American Journal of Science, v. 292, p. 317-355.

Currie, K.L.
1992: A new look at Gander-Dunnage relations in Carmanville map area, Newfoundland; in Current Researach, Part D; Geological Survey of Canada, Paper 92-1D, p. 27-33.

Currie, K.L., Pajari, G.E., and Pickerill, R.K.
1980: Carmanville map-area, Newfoundland (2E/8); Geological Survey of Canada, Open File 776.

Karlstrom, K.E., van der Pluijm, B.A., and Williams, P.F.
1982: Structural interpretation of the eastern Notre Dame Bay area, Newfoundland: regional post Middle Silurian thrusting and asymmetrical folding; Canadian Journal of Earth Sciences, v. 19, p. 2325-2341

Kennedy, M.J. and McGonigal, M.H.
1972: The Gander Lake and Davidsville Groups, northeastern Newfoundland: new data and geotectonic implications; Canadian Journal of Earth Sciences, v. 9, p. 53-459.

McCann, A.M.
1973: Structural and stratigraphic relationships in Silurian rocks of the Port Albert-Horwood area, Twillingate-Fogo districts, Newfoundland; M.Sc. thesis, Memorial University of Newfoundland, Saint John's, Newfoundland, 84 p.

McCann, A.M. and Kennedy, M.J.
1974: A probable glacio-marine deposit of Late Ordovician-Early Silurian age from the north central Newfoundland Appalachian Belt; Geological Magazine, v. 111, p. 549-564.

O'Brien, B.H.
1991: Geological development of the Exploits and Notre Dame subzones in the New Bay area, (parts of 2E/6 and 2E/11), Notre Dame Bay, Newfoundland; Newfoundland Geological Surveys Branch, Report 91-1, p. 155-166.

O'Neill, P.P.
1991: Geology of the Weir's Pond area, Newfoundland (NTS 2E/1); Newfoundland Geological Surveys Branch, Report 91-3, 144 p.

O'Neill, P.P. and Blackwood, R.F.
1989: A proposal for revised stratigraphic nomenclature of Gander and Davidsville Groups and the Gander River Ultrabasic Belt of northeastern Newfoundland; Newfoundland Geological Surveys Branch, Report 80-1, p. 127-130.

Patrick, T.O.H.
1956: Comfort Cove, Newfoundland; Geological Survey of Canada, Paper 55-31.
Piasecki, M.A.J.
1992: Tectonics across the Gander-Dunnage boundary in northeastern Newfoundland; in Current Research, Part E; Geological Survey of Canada, Paper 92-1E, p. 259-268.
Pickerill, R.K., Pajari, G.E., and Currie, K.L.
1979: Evidence of Caradocian glaciation in the Davidsville Group of northeastern Newfoundland; in Current Research, Part C; Geological Survey of Canada, Paper 79-1C, p. 67-72.
Stouge, S.
1980: Conodonts from the Davidsville Group, northeastern Newfoundland; Canadian Journal of Earth Sciences, v. 17, p. 268-272.
Strong, D.F. and Harris, A.H.
1974: The petrology of Mesozoic alkaline intrusives of central Newfoundland; Canadian Journal of Earth Sciences, v. 11, p. 1208-1219.
Twenhofel, W.H. and Schrock, R.R.
1937: Silurian strata of Notre Dame Bay and Exploits Valley, Newfoundland; Geological Society of America Bulletin, v. 48, p. 1743-1772.
Williams, H.
1964: Botwood, Newfoundland; Geological Survey of Canada, Map 60-1963.
Williams, H. (cont.)
1972: Stratigraphy of Botwood map-area, northeast Newfoundland; Geological Survey of Canada, Open File 113, 103 p.
1992: Mélanges and coticule occurrences in the northeast Exploits Subzone, Newfoundland; in Current Research, Part D; Geological Survey of Canada, Paper 92-1D, p. 121-128.
1993: The Dog Bay Line – a new tectonic feature in central Newfoundland; in Current Research, Part D; Geological Survey of Canada, Paper 93-1D.
Williams, H., Colman-Sadd, S.P., and Swinden, H.S.
1988: Tectono-stratigraphic subdivisions of central Newfoundland; Geological Survey of Canada, Paper 88-1B, p. 91-98.
Wonderley, P.F. and Neuman, R.B.
1984: The Indian Bay Formation: fossiliferous Early Ordovician volcanogenic rocks in the northern Gander terrane, Newfoundland, and their regional significance; Canadian Journal of Earth Sciences, v. 21, p. 525-532.
Wu, T.W.
1979: Structural, stratigraphic and geochemical studies of the Horwood Peninsula-Gander Bay area, northeast Newfoundland; M.Sc. thesis, Brock University, Saint Catherines, Ontario, 185 p.

Geological Survey of Canada Project 730044

Stratigraphy and structure of the Botwood Belt and definition of the Dog Bay Line in northeastern Newfoundland

Harold Williams[1]
Continental Geoscience Division

Williams, H., 1993: Stratigraphy and structure of the Botwood Belt and definition of the Dog Bay Line in northeastern Newfoundland; in Current Research, Part D; Geological Survey of Canada, Paper 93-1D, p. 19-27.

Abstract: The Botwood belt of middle Paleozoic strata extends from Fogo Island halfway across Newfoundland. In Comfort Cove (2E/7) area. Upper Ordovician-Silurian rocks are exposed in major northeast-trending folds. The Dog Bay Line is a tectonic boundary that separates contrasting Silurian rocks and structures. To the northwest, a terrestrial volcanic-sedimentary sequence (Botwood Group) overlies an upper Ordovician-Silurian marine greywacke-conglomerate sequence (informal Badger group) with sharp stratigraphic relations. To the southeast, a silty, limy Silurian sequence, the Indian Islands Group, directly overlies Ordovician shales and mélange.

Along the coast, the Dog Bay Line is marked by a mélange of volcanic rocks and gabbros in sheared dark shales, all presumably Ordovician. Inland, the line extends 70 km to Glenwood and beyond. Dextral offset is probably many tens of kilometres.

Gold mineralization at Duder Lake occurs in rocks and structures like those along the Dog Bay Line.

Résumé : La zone de Botwood (Paléozoïque moyen) commence à l'île Fogo et traverse la moitié de Terre-Neuve. Dans la région de Comfort Cove (2E/7), des roches de l'Ordovicien inférieur au Silurien affleurent dans de grands plis d'orientation nord-est. La ligne de Dog Bay est une limite tectonique qui sépare des roches et structures siluriennes contrastées. Au nord-ouest, une séquence terrestre volcano-sédimentaire (Groupe de Botwood) recouvre une séquence marine de grauwacke et conglomérat correspondant à la partie supérieure de l'Ordovicien au Silurien (groupe de Badger, informel), et caractérisée par des relations stratigraphiques nettement définies. Au sud-est, une séquence silurienne silteuse et calcaire, le Groupe d'Indian Islands, recouvre directement les shales et mélanges ophiolitiques ordoviciens.

Le long du littoral, la ligne de Dog Bay se caractérise par la présence d'un mélange de roches volcaniques et de gabbros dans des shales sombres cisaillés, le tout correspondant probablement à l'Ordovicien. À l'intérieur des terres, la ligne se prolonge sur 70 km jusqu'à Glenwood et au-delà. Le déplacement horizontal dextre atteint probablement plusieurs dizaines de kilomètres.

La minéralisation aurifère observée au lac Duder se manifeste dans des roches et structures comme celles bordant la ligne de Dog Bay.

[1] Department of Earth Sciences, Memorial University of Newfoundland, St. John's, Newfoundland A1B 3X5

INTRODUCTION

The Botwood Belt (Williams, 1967; Williams et al., in press a) is the area of middle Paleozoic rocks that extends from the northeast coast of Newfoundland more than half way across the island toward the southwest. Along the northeast coast, the belt extends from the Reach Fault to Gander Bay and offshore to Change Islands, Fogo Island, and Indian Islands (Fig. 1). The area was mapped several times before but subdivisions, nomenclature, and relationships between rock groups were always problematic. Parts of the area were mapped by Patrick (1956), Baird (1958), Williams (1963), Eastler (1969, 1971), McCann (1973), and Wu (1979). The entire area is covered by the reconnaissance maps of Williams (1964) and Karlstrom et al. (1982). The present study is part of a larger project to map the Carmanville and Comfort Cove areas at 1:50:000 scale and eventually update the Botwood (2E, east-half) map area for publication at 1:100 000 scale (see also Currie, 1993).

The Botwood Belt is unique among middle Paleozoic belts in Newfoundland as it contains an upper Ordovician-Silurian turbidite sequence, overlain by a Silurian terrestrial volcanic-sedimentary sequence. It also contains a Silurian shallow marine siltstone-shale-limestone sequence capped by redbeds.

The name Dog Bay Line is introduced for the major tectonic boundary that separates upper Ordovician-Silurian turbidites and overlying Silurian terrestrial rocks to the northwest from Silurian shallow marine sedimentary rocks to the southeast. From Dog Bay to Indian Islands Tickle, the line is marked by mélange that was first depicted by Karlstrom et al. (1982). The line is also a broad shear zone in coastal regions, the Indian Islands Fault Zone of Williams et al. (1988). Inland, the most intense shearing is expressed in the upper Ordovician-Silurian turbidite sequence that trends southwest and diverges from the southerly course of the Dog Bay Line (Fig. 2). Rocks and structures adjacent to the Dog Bay Line between Horwood and Duder Lake are host to gold mineralization (Churchill and Evans, 1992).

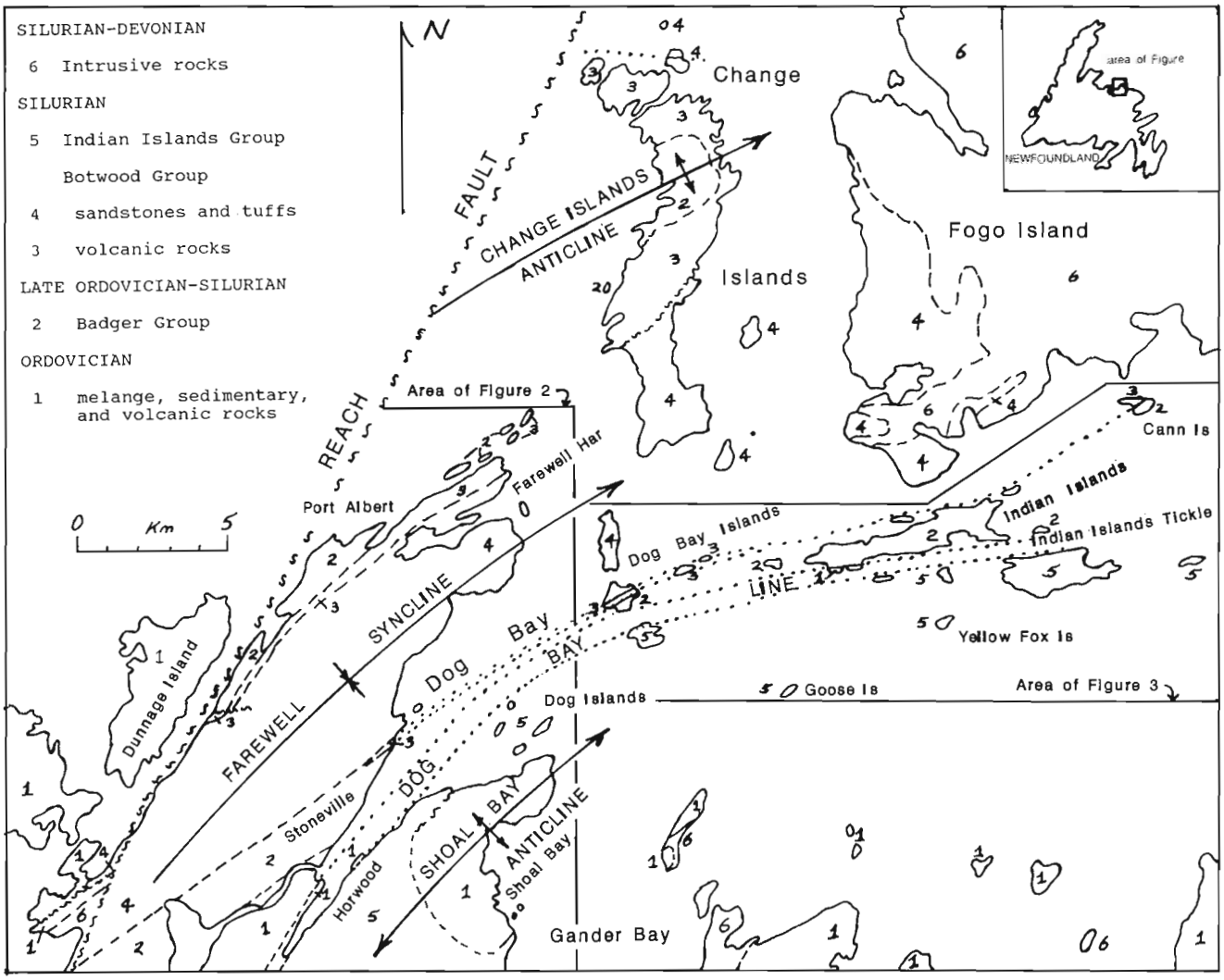

Figure 1. Regional structures and lithic divisions of the northeast Botwood Belt.

Previous work in the northeast Botwood Belt that led to the liveliest tectonic discussions centred on interpretations that (1) the Silurian terrestrial rocks are allochthonous upon the underlying marine turbidite sequence (Karlstrom et al., 1982, 1983; Currie et al., 1983), and (2) the Reach Fault is a major tectonostratigraphic boundary (Williams et al., 1972, 1974) or Iapetus Suture (McKerrow and Cocks, 1977, 1978). Both interpretations are now known to be erroneous. What was the best example of an inferred structural boundary at Port Albert between terrestrial Silurian rocks and underlying marine turbiditic rocks is now the type area for an observable stratigraphic contact, and the Reach Fault is a late rectilinear feature with the marine turbidite sequence coextensive across it.

STRATIGRAPHY

Northwest of the Dog Bay Line, the upper Ordovician-Silurian marine turbidite sequence of greywackes and conglomerates is referred to the informal Badger group, a name proposed for all the upper Ordovician-Silurian greywacke-conglomerate sequences of the Badger and Botwood belts of northeast Newfoundland (Williams et al., in press a, b). Rocks of the Badger group in the study area are also known as the Beaver Cove and Stoneville formations (McCann, 1973; McCann and Kennedy, 1974). They were previously assigned to the Indian Islands Group (Patrick, 1956; Baird, 1958; Williams, 1964, 1967, 1972), Farewell Group (Patrick, 1956;

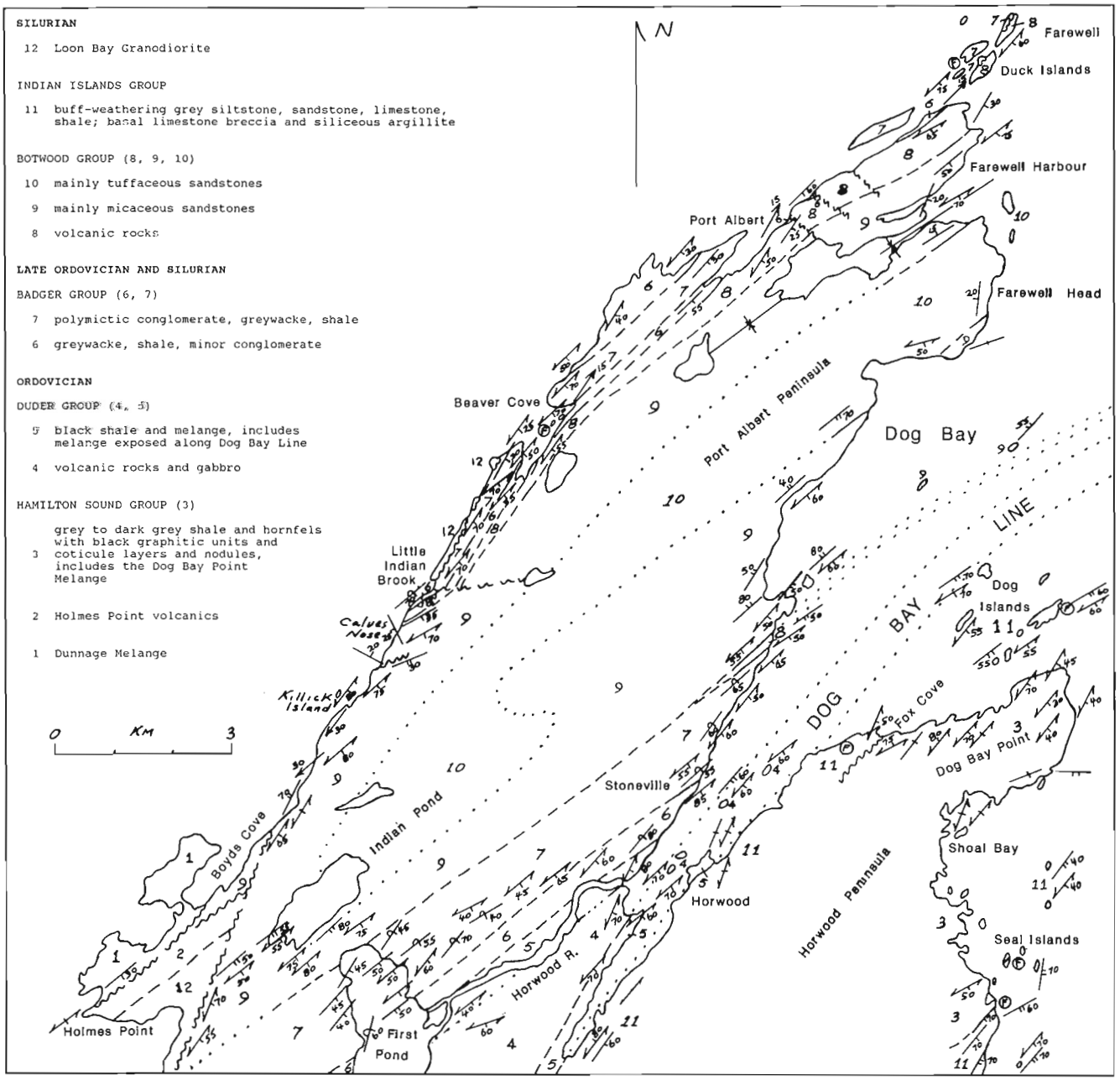

Figure 2. Stratigraphy and structure of the Port Albert and Horwood peninsulas.

Baird, 1958), Fogo Group (Baird, 1958), Botwood Group (Williams, 1963, 1964, 1967, 1972; McCann, 1973), and Change Islands Formation (Eastler, 1969, 1971). The Silurian terrestrial volcanic-sandstone sequence above the marine turbidites is the Botwood Group as originally defined in the Botwood area of Bay of Exploits (Williams, 1962). The terrestrial rocks were previously assigned to the Farewell Group, Indian Islands Group, Fogo Group (Patrick, 1956; Baird, 1958) and Botwood Group (Williams, 1963, 1964; McCann, 1973). The marine turbidite sequence and overlying terrestrial volcanic-sandstone sequence are sufficiently different to warrant separate names; thus the Badger-Botwood distinction.

Southeast of the Dog Bay Line, Silurian siltstones, shales, limestones, and sandstones are assigned to the Indian Islands Group (Patrick, 1956; Baird, 1958; Wu, 1979). It is redefined to exclude all rocks northwest of the Dog Bay Line that are a natural part of the Badger group. The Ordovician rocks at Dog Bay Point are also excluded (Williams, 1992).

The Badger group overlies black shale and mélange at Stoneville (Fig. 2) and it is separated from the Dunnage Mélange to the west by the Reach Fault. The contact between the Badger and Botwood groups is conformable, although it may be an erosional disconformity. Indian Islands Group overlies black shales, sandstones, and mélange at Gander Bay with a conformable contact that may also represent an erosional break.

Badger group

Greywackes and conglomerates of the Badger group are present on both limbs of the Farewell Syncline and in the core of the Change Islands Anticline (Fig. 1). The group is about a kilometre thick on opposite limbs of the Farewell Syncline. Two mappable formations are recognized in the Badger group throughout most of Badger Belt west of Reach Fault; a lower predominantly greywacke formation (Sansom) and an upper mainly conglomerate formation (Goldson). Equivalent formations are possible at Stoneville (Fig. 2) and Western Indian Island (Fig. 3) but at Port Albert, greywackes both overlie and underlie the conglomerate unit (Fig. 2) and the conglomerate unit is absent at Change Islands and Cann Island.

Greywackes of the Badger group are thin- to medium-bedded with siltstone and conglomerate interbeds. They exhibit sole marks, convolute bedding, and grading. These features are well preserved at Change Islands. Conglomerates are thick-bedded with some beds exceeding a metre in thickness. Clasts are mainly chert, siltstone, siliceous volcanic rocks, quartz-feldspar porphyry, granite, jasper, mafic volcanic rocks, quartz, and limestone. Where deformation is intense along the southeast limb of Farewell Syncline clasts are discoid or elongate in the plane of cleavage. The rocks are less deformed on the northwest limb of the Farewell Syncline. Outsize equidimensional clasts of porphyry and granite at Stoneville have been interpreted as glacial dropstones (McCann and Kennedy, 1974). An absence of glacio-marine features elsewhere, coupled with occurrences of warm-water corals and brachiopods, refute the glacial model.

The base of the Badger group is exposed at the shoreline opposite the Pentecostal Church in Stoneville. There, dark shales and greywackes in beds from a few centimetres to 10 cm thick are steeply-dipping, northwest-facing and in apparent stratigraphic contact with black shales that contain pebbles and cobbles of tonalite. Farther southwest toward the mouth of Horwood River, the black shales contain a 1 m

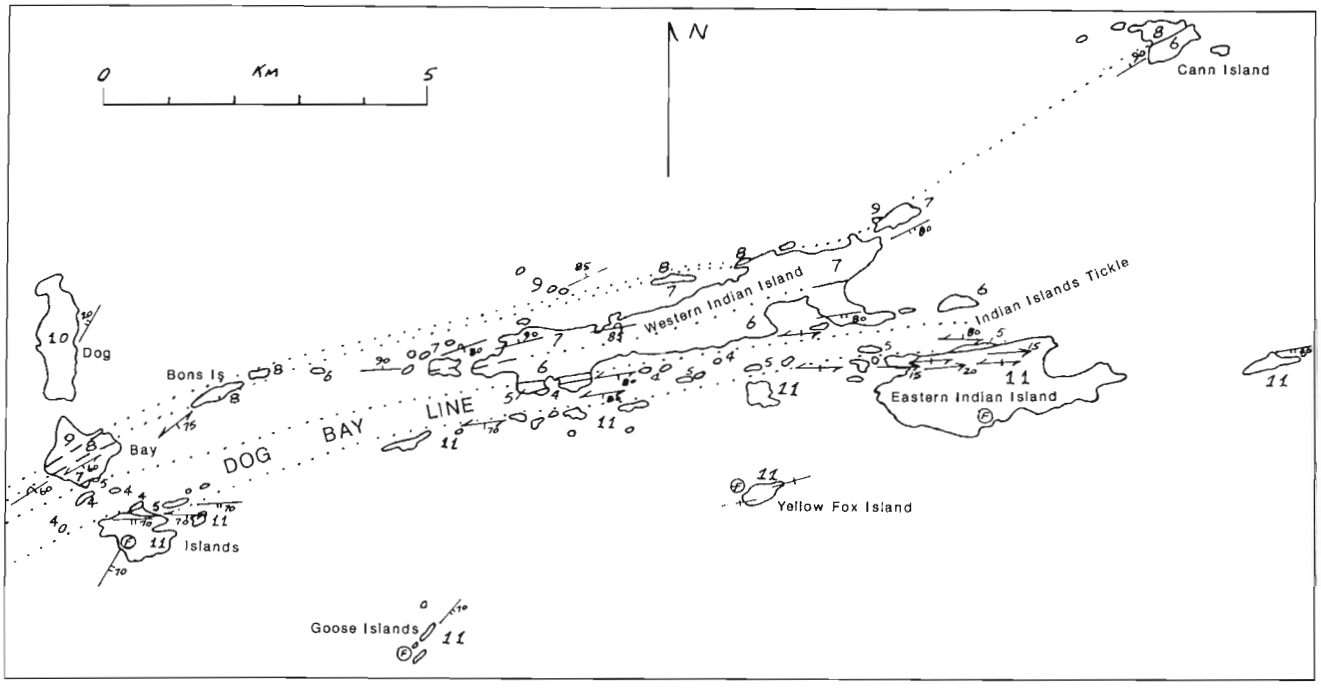

Figure 3. Stratigraphy and structure of Dog Bay Islands and Indian Islands; legend as in Figure 2.

boulder of buff-weathering limestone and a much larger flattened block of vesicular fragmental volcanic rock. These shaley rocks presumably overlie volcanic rocks to the southeast. All are assigned to the informal Duder group (Currie, 1993).

Conglomerates of the Badger group contain fossiliferous limestone boulders at Beaver Cove, Farewell Duck Islands, and Change Islands. These are dated generally as late Ordovician-early Silurian (Williams, 1972) and a Llandovery age is reported for the Change Islands occurrence (Eastler, 1969). The Sansom Formation of eastern New World Island contains a Llandovery fauna at its top and it overlies Caradoc shales. The overlying Goldson Formation has interlayered shales of Llandovery age (Williams, 1972).

Botwood Group

The Botwood Group of the northeast Botwood Belt consists of a lower volcanic unit, the Port Albert Formation, and overlying sandstones of the Dog Bay Formation (McCann, 1973; McCann and Kennedy, 1974). These divisions correspond to the Lawrenceton and Wigwam formations in the type area (Williams, 1972).

The lower volcanic unit consists of flows and coarse, unsorted volcaniclastic rocks, in roughly equal proportions, that are purplish green to purple, red, and green. Mafic volcanic rocks are predominant. Vesicules and calcite amygdules are common and some flows are porphyritic. Purple to dark red varieties, best seen at Change Islands, are distinctive with both calcite amygdules and feldspar phenocrysts. Red sandstone is interbedded with the volcanic rocks at Change Islands.

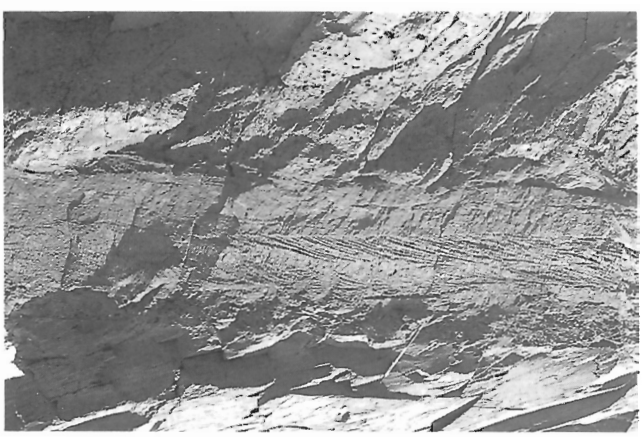

Figure 4. Contact between the Badger and Botwood groups displayed in a large talus boulder 1 km northeast of Port Albert. Dark grey band with cross-bedding in centre of photo is the 25-40 cm coarse sandstone at the base of the Botwood Group. It overlies turbidites of the Badger group and is overlain by vesicular volcanics of the Port Albert Formation, Botwood Group.

Figure 5. Volcanic breccia within the upper Badger group at Cann Island.

The volcanic rocks are thicker northeastward along the northwest limb of the Farewell Syncline and they are more extensive at Change Islands. They are thin or absent on the southeast limb of the Farewell Syncline (Fig. 2).

Three divisions were mapped in the overlying sandstones on the Port Albert Peninsula (McCann, 1973); crossbedded grey micaceous sandstone, thin-bedded grey sandstone with ripple-drift lamination, and massive tuffaceous sandstone with obvious volcanic clasts. Micaceous sandstones occur above the Port Albert volcanics near Farewell Harbour and along strike at Change Islands (unit 9 of Fig. 2). Tuffaceous sandstones occur higher in the section (unit 10 of Fig. 2). These are most extensive at Farewell Head and offshore. Thick volcanic units occur above micacous sandstones at Brimstone Head on Fogo Island and at Little Fogo Islands (Baird, 1958: Williams, 1964, 1972). Buff-weathering thin- to medium-bedded grey sandstones with numerous small shale chips and larger buff sandy clasts occur along the east side of the Reach Fault and are well exposed on the shoreline south of Holmes Point behind the Causeway Motel. Subdivision of the Botwood sandstone unit is possible in the northeast (Fig. 2), but all four lithic varieties, locally alternating, are recognized in a 1 km roadcut between Reach Fault and Indian Pond. Abundant red felsic and dark mafic dykes are associated with the tuffaceous sandstones at Farewell Head.

The contact between Botwood and Badger groups is stratigraphic, although commonly modified by faults, such as at Little Indian Brook and Farewell Duck Islands (Fig. 2). The sharpest stratigraphic contact is exposed on the shoreline 1 km northeast of Port Albert. There, a resistant 25-40 cm coarse sandy bed with a conglomeratic base overlies grey to purplish turbidites of the Badger group. The resistant sandy bed is graded at its base and crossbedded toward its top. Vesicular green lava overlies the sandy bed. The base of the Botwood Group is defined as the base of the resistant sandy bed. Numerous large talus boulders at the shoreline display the entire contact (Fig. 4). At Cann Island, a 1 m unit of coarse green volcanic breccia occurs within greywackes below the volcanic contact (Fig. 5). At Change Islands, greywackes

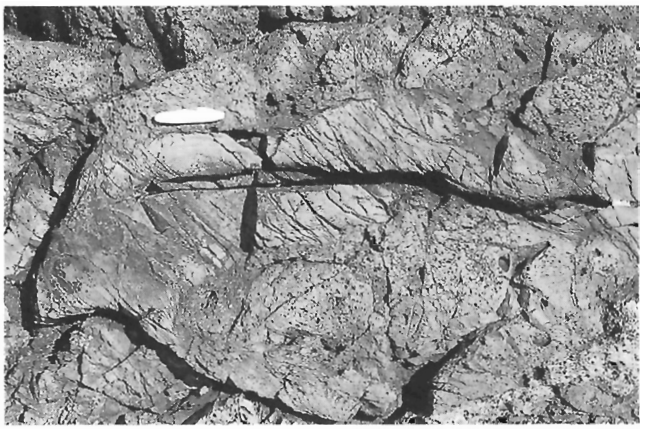

Figure 6. Greywacke inclusion in volcanic rocks of the Botwood Group, Change Islands.

near the contact contain volcanic boulders, and overlying volcanic rocks contain greywacke inclusions (Fig. 6). These local relations indicate a temporal overlap of volcanism and turbidite deposition.

Stratigraphic contacts between the volcanic and sandstone units of the Botwood Group are well exposed at Farewell Harbour and Change Islands, and along the southeast limb of the Farewell Syncline at Dog Bay Islands and Western Indian Island. At Farewell Harbour and Change Islands, conglomerate at the base of the sandstone unit contains clasts of underlying volcanic rocks. In other places, volcanic rocks occur as thin interlayers near the base of the sandstone unit.

No fossils are known in the Botwood Group of the study area. The rocks are assigned to the Silurian because they overlie the Badger group and a dyke that cuts Botwood sandstones at Port Albert Peninsula is dated isotopically at 422 ± 2 Ma (Elliott et al., 1991).

Indian Islands Group

The base of the Indian Islands Group is defined by a fossiliferous coarse limestone breccia with interlayered limestone and shale at Seal Islands and on the nearby shoreline (Fig. 2). Underlying rocks are mainly dark grey to black shales with coticule nodules and interbeds, and local mélange – Hamilton Sound group (Currie, 1993). A similar relationship occurs at Rodgers Cove 7 km to the south. There, a coarse limestone breccia with associated buff-weathering shales and limestones overlies dark grey sandstones and shales, that are followed southward to Victoria Cove by locally chaotic dark shales. The contact between the Indian Islands Group and Ordovician rocks on the west side of the Shoal Bay Anticline at Fox Cove is faulted.

Three informal formations are recognized in the Indian Islands Group at Horwood Peninsula (Currie, 1993): (1) Charles Cove formation of buff-weathering grey siltstone, shale, and sandstone including the basal breccia unit at Seal Islands and Rodgers Cove, (2) Horwood formation of grey to dark grey shale, with thin siltstone and sandstone beds along the east side of Dog Bay, and (3) Centennial formation of red sandstones and shales east of the Horwood formation. The redbeds are gradational with grey rocks of the Horwood formation and presumably occur at the top of the group. At Dog Islands, thin bedded buff-weathering shales, siltstones, and limestones predominate. Sandstones and siltstones with limestone beds occur at Eastern Indian Island, Yellow Fox Island, and Goose Islands.

Silurian fossils occur in limestones at the base of the Indian Islands Group at Seal Islands and they occur in limestone interbeds among siltstones and shales at Eastern Indian Island, Dog Islands, southern Dog Bay Island, Yellow Fox Island, and Goose Islands. These are mainly Llandovery. A Wenlock fauna occurs in limey sandstone and limestone at Glenwood (Williams, 1972).

STRUCTURE

The Change Islands Anticline, Farewell Syncline, and Shoal Bay Anticline, from north to south (Fig. 1) are the dominant structures that control outcrop patterns in the area. An early interpretation of a northeast-trending syncline coincident with Dog Bay (Patrick, 1956; Baird, 1958) was refuted by Williams (1964, 1972) as the rocks on the northwest side of the bay face northwest and away from the synclinal axis. The Badger-Botwood contact on the northwest side of Dog Bay (Fig. 2) was interpreted as a fault (Williams, 1964) and extended offshore as the Indian Islands Thrust (Eastler, 1969). Correlation of greywackes and conglomerates on opposite sides of the Farewell Peninsula led to the definition of Farewell Syncline (McCann, 1973). This was supported by the subsequent structural studies of Karlstrom et al. (1982). Correlation of units across Change Islands (Eastler, 1969) led to the definition of Change Islands Anticline. An anticline at Shoal Bay was first depicted by Karlstrom et al. (1982) and this is supported by assigning mélange, black shales, and coticules at Dog Bay Point to the Ordovician (Williams, 1992) and defining the base of the Silurian Indian Islands Group at Seal Islands. Mélange along the Dog Bay Line was depicted previously as exposed in a sharp anticlinal core (Karlstrom et al., 1982).

Northwest of Dog Bay Line, the Change Islands Anticline and Farewell Syncline are complementary structures with northeast axes and gentle plunges toward the northeast. They are truncated by the Reach Fault to the west and the Fogo Batholith to the east. Sandstones of the Botwood Group are steep to overturned at the northern limb of the Change Islands Anticline and conglomerates and greywackes of the Badger group are steep and overturned on the southeast limb of the Farewell Syncline. A regional southeast-dipping cleavage is most intense along the southeast limb of Farewell Syncline with isoclinal folds and extreme flattening of conglomerate clasts in Badger group. Deformation is mild along the axis of the syncline at Farewell Harbour where micaceous sandstones of Botwood Group are locally subhorizontal.

Southeast of Dog Bay Line, the Shoal Bay Anticline is a complex structure with a northeast-trending axis. It is defined by Silurian rocks that surround Ordovician rocks. Smaller folds at Dog Bay Line on the north shore of Eastern Indian Island (Fig. 7) and along the road at Horwood are upright and open with mainly gentle plunges. Examples are well-exposed in the large roadcut just east of the Horwood turnoff.

The major folds northwest of Dog Bay Line are overturned to the northwest and the intensity of deformation increases southeast toward the line. Folds on the southeast side of the line are more upright and open, and there is no wide zone of intense deformation comparable to that on its northwest side.

Dog Bay Line is the most important structural feature in the area. The mélange that marks its course from Dog Bay to Indian Islands Tickle has a morphological expression of small islands, sunkers, and shoals like the Dunnage Mélange and other coastal mélanges in northeast Newfoundland (Fig. 8). Black shales of the mélange matrix are in tectonic contact with conglomerates of the Badger group at middle Dog Bay Island and they are in tectonic contact with buff-weathering sandstones of Indian Islands Group at southern Dog Bay Island and along the north shore of Eastern Indian Island. Quartz veining is common at these contacts. Gabbroic and volcanic blocks in the mélange are similar to gabbros and volcanics of Duder group. The blocks are attenuated with local intense shearing at their peripheries. The gabbros are gradational with adjacent or surrounding volcanic rocks through a decrease in grain size, suggesting comagmatic relations. The gabbros nowhere cut surrounding shales. Shearing in the mélange, the kinds of blocks and matrix, and the absence of exotic blocks suggest that it represents a tectonized equivalent and northeast continuation of Duder group (Fig. 2). Shear bands and minor folds indicate a dextral sense of transcurrent displacement and dip-slip movement (Williams et al., 1988; M.A.J. Piasecki, pers. comm., 1992). Similar kinematics are displayed in the adjacent Badger group. The asymmetry and northwest-overturning of Farewell Syncline and Change Islands Anticline imply northwest compression.

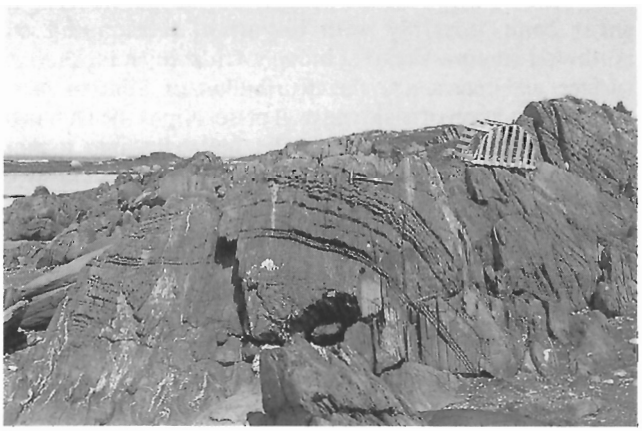

Figure 7. Upright open fold with steep cleavage in the Indian Islands Group, north shore of Eastern Indian Island.

Figure 8. Gabbro block in sheared black shales at Indian Islands Tickle.

Dog Bay Line continues inland to Rocky Pond (Fig. 9) where it separates Silurian buff-weathering siltstones and sandstones of the Indian Islands Group on its east side from the Ordovician Duder group to the west (Currie, 1993). At the eastern embayment of Rocky Pond (Hatchet Pond), fossiliferous limestone boulder conglomerates and grey chert pebble conglomerates are assigned to Indian Islands Group. Farther south, Dog Bay Line is placed between rocks typical of Indian Islands Group and red and grey micaceous sandstones and shales of Botwood Group. Between Salmon Pond and Gander River, fossiliferous sandstones and limestones are reassigned from Botwood Group to Indian

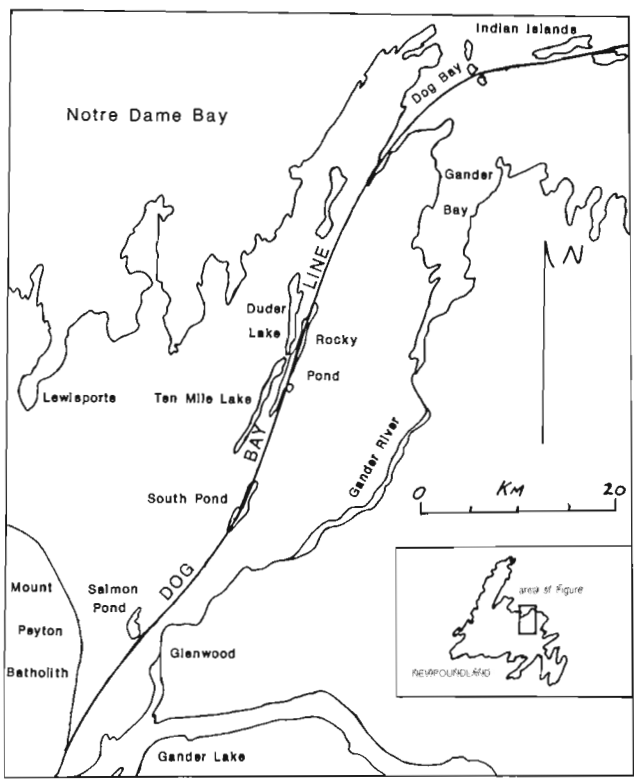

Figure 9. Interpreted inland course of the Dog Bay Line.

Islands Group. At the waterfalls of Salmon Pond Brook, grey siltstones with folded cleavage are typical of Indian Islands Group in Gander Bay, and Dog Bay Line is postulated to lie between the deformed grey siltstones and red micaceous sandstones of Botwood Group farther west. South of Glenwood, the line is truncated by the Mount Peyton Batholith. On the opposite side of the batholith at Miguels Lake, a narrow belt of sheared Ordovician mafic volcanic rocks and altered pyritic ultramafic rocks occurs among Silurian sedimentary rocks (Colman-Sadd and Russell, 1988). This implies a structural situation like that at Dog Bay.

Reach Fault at the western coastal boundary of the northeast Botwood Belt extends at least 10 km southward. Where exposed, the fault is marked by a narrow zone of brecciation and shearing. Sheared granodiorite occurs along the fault north of Little Indian Brook (Fig. 2) and a wider zone of brecciated rocks occurs at Boyds Cove. The latter were referred to the Holmes Point Complex (Kay, 1976) that consists mainly of sedimentary rocks of Botwood Group and siliceous volcanic rocks like those at Holmes Point. The fault zone is also exposed on the highway 2 km south of Holmes Point. There the fault separates crushed and broken Loon Bay granodiorite on its western side from buff-weathering siltstones of Botwood Group to the east. Black pebbly mudstones, typical of Dunnage Mélange, are structurally wedged within crushed granodiorite. The Loon Bay granodiorite, dated isotopically at 408 ± 2 Ma (Elliott et al., 1991), is the youngest rock affected by the fault. A brownish-weathering lamprophyre dyke of the Mesozoic Notre Dame Swarm (Strong and Harris, 1974) cuts brecciated granodiorite in the fault zone.

Comparisons of rocks and structures on opposite sides of the Reach Fault indicate a left lateral offset of 5 to 15 km as follow: (1) the nearest match for Botwood Group sandstone and associated volcanic rock west of the fault at Boyds Cove is found 5 km northward near Little Indian Brook, (2) broken siliceous rocks along the fault at Killick Island, Calves Nose, and farther north resemble siliceous volcanic rocks at Holmes Point, (3) sheared granodiorite between Little Indian Brook and Beaver Cove is correlated with the Loon Bay granodiorite more than 5 km southward, and (4) the Badger group of Farewell Syncline reappears on the west side of the fault where displaced about 15 km southward (Currie, 1993). Shear bands and minor folds also indicate left-lateral displacement (Williams et al., 1988; M.A.J. Piasecki, pers. comm., 1992). The presence of pebbly mudstone in the fault zone south of Holmes Point implies that Dunnage Mélange occurs on the east side of the fault at Beaver Cove or northward.

Dog Bay Line is curvilinear, it is parallel to lithic belts and major fold axes, and it predates the intrusion of nearby plutons. Reach Fault is rectilinear, it truncates the major curvilinear structures, and it cuts plutonic rocks.

ECONOMIC GEOLOGY

Several gold prospects are known in gabbros and volcanic rocks of Duder group south of Dog Bay (Churchill and Evans, 1992). The mineralization occurs in veins within gabbros. Continuity of Duder lithologies along Dog Bay Line and the likelihood of hydrothermal activity along this major structure make Dog Bay Line an interesting target for gold exploration.

DISCUSSION

Contrasts between Silurian rocks on opposite sides of Dog Bay Line and its inland continuity highlight its importance as a tectonic junction. It may be a terrane boundary, but comparisons among Ordovician rocks and faunas on opposite sides of the line do not support this suggestion (Williams, 1992).

Most features of mélange along Dog Bay Line suggest a tectonic origin by disruption of the Ordovician Duder group. Similar kinematics of shearing in the mélange and the adjacent Badger group suggest synchronous mélange formation and intense deformation of Badger group. In this case, the Dog Bay Line is a Silurian or younger transcurrent shear zone, possibly with important telescoping and northwest compression that brought Ordovician rocks to the surface and rearranged the distribution of Silurian facies belts. Restoration of major dextral offset aligns the Dunnage, Dog Bay Point, and Carmanville mélanges into a more conventional northeast belt. Other scenarios remain to be explored.

Mélange beneath Badger group at Stoneville appears olistostromal and relationships there are similar to those of southeastern New World Island where the Badger group overlies Caradoc black shales, that in turn overlie Dunnage Mélange.

The Badger group of Botwood Belt is equivalent to upper Ordovician-Silurian greywackes and conglomerates at New World Island. There, Ordovician and Silurian rocks occur in northeast-trending repeated sections with steep to overturned northwest-facing beds. Silurian olistostromal mélanges locally occur between the repeated sections. The model for Silurian olistostromal mélange and repeated sections at New World Island is synsedimentary southeastward thrusting (Reusch, 1987; Williams et al., 1988). East of Reach Fault, polarity of penetrative structures is to the northwest. This implies a local synsedimentary first deformation of southeast polarity followed by a penetrative northwest compressional event that affected the entire area.

The absence of terrestrial rocks of Botwood Group on the west side of Reach Fault is another concern. If the model for Silurian mélange formation at New World Island is correct, synsedimentary southeast thrusting there preceded or was synchronous with terrestrial volcanism and sedimentation in the nearby Botwood Belt.

Recognition of Dog Bay Line and its tectonic implications may lead to a subdivision of Botwood Belt, but this is presently premature. Tracing the full extent of Dog Bay Line, comparing Silurian faunas on its opposite sides, and paleomagnetic and other thematic studies are obvious follow-ups to its stratigraphic and structural definition in northeast Newfoundland.

ACKNOWLEDGMENTS

Any worthwhile contributions or ideas contained herein result from the many discussions held during the field season with co-workers K.L. Currie and M.A.J. Piasecki. The Department of Energy, Mines and Resources Canada is thanked for supporting this work through a contract with the author. Thanks also to K.L. Currie and Dennis Johnston for reviews of the manuscript.

REFERENCES

Baird, D.M.
1958: Fogo Island map-area, Newfoundland; Geological Survey of Canada, Memoir 301, 62 p.

Churchill, R.A. and Evans, D.T.W.
1992: Geology and gold mineralization of the Duder Lake gold showings, eastern Notre Dame Bay, Newfoundland; in Current Research (1992) Newfoundland Department of Mines and Energy, Geological Survey Branch, Report 92-1, p. 211-220.

Colman-Sadd, S.P. and Russell, H.A.J.
1988: Miguels Lake (2D/12), Newfoundland; Newfoundland Department of Mines, Geological Survey Branch, Open File Map 88-50.

Currie, K.L.
1993: Ordovician-Silurian stratigraphy between Gander Bay and Birchy Bay, Newfoundland; in Current Research, Part D; Geological Survey of Canada, Paper 93-1A.

Currie, K.L., Pickerill, R.K., and Pajari, G.E. jr.
1983: Structural interpretation of the eastern Notre Dame Bay area, Newfoundland: regional post-Middle Silurian thrusting and asymmetrical folding: Discussion; Canadian Journal of Earth Sciences, v. 20, p. 1351-1352.

Eastler, T.E.
1969: Silurian geology of Change Islands and eastern Notre Dame Bay, Newfoundland; in North Atlantic-Geology and Continental Drift, (ed.) M. Kay; American Association of Petroleum Geologists, Memoir 12, p. 425-432.
1971: Geology of Silurian rocks, Change Islands and easternmost Notre Dame Bay, Newfoundland; Ph.D. thesis, Columbia University, New York, 143 p.

Elliott, C.G., Dunning, G.R., and Williams, P.F.
1991: New U-Pb zircon age constraints on the timing of deformation in north-central Newfoundland and implications for early Paleozoic Appalachian orogenesis; Geological Society of America, Bulletin, v. 103, p. 125-135.

Karlstrom, K.E., van der Pluijm, B.A., and Williams, P.F.
1982: Structural interpretation of the eastern Notre Dame Bay area, Newfoundland: regional post-Middle Silurian thrusting and asymmetrical folding; Canadian Journal of Earth Sciences, v. 19, p. 2325-2341.
1983: Structural interpretation of the eastern Notre Dame Bay area, Newfoundland: regional post-Middle Silurian thrusting and asymmetrical folding: Reply; Canadian Journal of Earth Sciences, v. 20, p. 1353-1354.

Kay, M.
1976: Dunnage Mélange and subduction of the Protoacadic Ocean, northeast Newfoundland; Geological Society of America, Special Paper 175, 49 p.

McCann, A.M.
1973: Structural and stratigraphic relationships in Silurian rocks of the Port Albert-Horwood area, Twillingate-Fogo districts, Newfoundland; M.Sc. thesis, Memorial University of Newfoundland, St. John's, 84 p.

McCann, A.M. and Kennedy, M.J.
1974: A probable glacio-marine deposit of Late Ordovician-Early Silurian age from the north central Newfoundland Appalachian Belt; Geological Magazine, v. 111, p. 549-564.

McKerrow, W.S. and Cocks, L.R.M.
1977: The location of the Iapetus Ocean suture in Newfoundland; Canadian Journal of Earth Sciences, v. 14, p. 488-495.
1978: A lower Paleozoic trench-fill sequence, New World Island, Newfoundland; Geological Society of America, Bulletin, v. 89, p. 1121-1132.

Patrick, T.O.H.
1956: Comfort Cove, Newfoundland; Geological Survey of Canada, Paper 55-31.

Reusch, D.N.
1987: Silurian stratigraphy and melanges, New World Island, north central Newfoundland; in Northeastern Section of the Geological Society of America, (ed.) D.C. Roy; Geological Society of America, Centennial Field Guide, v. 5, p. 463-466.

Strong, D.F. and Harris, A.
1974: The petrology of Mesozoic alkaline intrusives of central Newfoundland; Canadian Journal of Earth Sciences, v. 11, p. 1208-1219.

Williams, H.
1962: Botwood (west-half) map-area, Newfoundland; Geological Survey of Canada, Paper 62-9, 16 p.
1963: Twillingate map-area, Newfoundland; Geological Survey of Canada, Paper 63-36, 30 p.
1964: Botwood, Newfoundland; Geological Survey of Canada, Map 60-1963.
1967: Silurian Rocks of Newfoundland; in Geology of the Atlantic Region, (ed.) E.R.W. Neale and H. Williams; Geological Association of Canada, Special Paper 4, p. 93-137.
1972: Stratigraphy of Botwood map-area, northeastern Newfoundland; Geological Survey of Canada, Open File 113, 117 p.
1992: Mélanges and coticule occurrences in the northeast Exploits Subzone, Newfoundland; in Current Research, Part D; Geological Survey of Canada, Paper 92-1D, p. 121-127.

Williams, H., Dean, P.L., and Pickering, K.T.
in press a: Botwood Belt; in Chapter 4 of Geology of the Appalachian-Caledonian Orogen in Canada and Greenland, (ed.) H. Williams; Geological Survey of Canada, Geology of Canada, no. 6 (also Geological Society of America, The Geology of North America, v. F-1).

Williams, H., Kennedy, M.J., and Neale, E.R.W.
1972: The Appalachian Structural Province; in Variations in Tectonic Styles in Canada, (ed.) R.A. Price and R.J.W. Douglas; Geological Association of Canada, Special Paper, no. 11, p. 181-261.
1974: The northeastward termination of the Appalachian Orogen; in The Ocean Basins and Margins, v. 2: the North Atlantic, (ed.) A.E.M. Nairn and F.G. Stehli; Plenum Press, New York, p. 79-123.

Williams, H., Lafrance, Bruno, Dean, P.L., Williams, P.F., Pickering, K.T., and van der Pluijm, B.A.
in press b: Badger Belt; in Chapter 4 of Geology of the Appalachian-Caledonian Orogen in Canada and Greenland, (ed.) H. Williams; Geological Survey of Canada, Geology of Canada, no. 6 (also Geological Society of America, The Geology of North America, v. F-1).

Williams, P.F., Elliott, C.G., and Lafrance, B.
1988: Structural geology and mélanges of eastern Notre Dame Bay, Newfoundland; Geological Association of Canada, Field Trip Guidebook, Trip B2, 60 p.

Wu, T.W.
1979: Structural, stratigraphic and geochemical studies of the Horwood Peninsula-Gander Bay area, northeast Newfoundland; M.Sc. thesis, Brock University, St. Catherines, Ontario, 185 p.

Geological Survey of Canada Project 730044

Stratigraphic and structural relations within the western Dunnage Zone, Glover Island region, western Newfoundland[1]

Peter A. Cawood[2] and Jeroen A.M. van Gool[2]
Continental Geoscience Division

Cawood, P.A. and van Gool, J.A.M., 1993: Stratigraphic and structural relations within the western Dunnage Zone, Glover Island region, western Newfoundland; in Current Research, Part D; Geological Survey of Canada, Paper 93-1D, p. 29-37.

Abstract: The Glover Island region straddles the boundary between the Humber and Dunnage zones. Lithostratigraphic units comprise: gneissic basement (Cobble Cove gneiss); unconformably overlying cover sequence (Keystone schist); ophiolitic rocks of the Grand Lake complex; volcanic and high level intrusive rocks of the Glover Formation; the Glover Island granodiorite; and siliciclastics of the Carboniferous Anguille and Deer Lake groups. The Keystone shear zone, developed within the basal mafic greenschist and ultramafic lithologies of the Grand Lake complex, marks the boundary of the Humber and Dunnage zones. The Kettle Pond shear zone separates the Grand Lake complex from Glover Formation, and marks a site of quartz-sericite alteration and mineralization. Major penetrative deformation and associated greenschist facies metamorphism is probably of mid-Paleozoic age. Brittle fracturing and faulting of Carboniferous, and possibly older age, follows the Cabot Fault system.

Résumé : La région de Glover Island chevauche la limite des zones de Humber et de Dunnage. Les unités lithostratigraphiques comprennent; le socle gneissique du gneiss de Cobble Cove; la séquence de couverture, sus-jacente en discordance, du schiste de Keystone; les roches ophiolitiques du complexe de Grand Lake; les roches volcaniques et les roches intrusives de haut niveau de la Formation de Glover; la granodiorite de Glover Island; et les roches silicoclastiques des groupes d'Anguille et de Deer Lake, d'âge carbonifère. La zone de cisaillement de Keystone, qui s'est formée dans les roches mafiques basales appartenant au faciès des schistes verts et dans les roches ultramafiques du complexe de Grand Lake, marquent la limite entre les zones de Humber et de Dunnage. La zone de cisaillement de Kettle Pond sépare le complexe de Grand Lake de la Formation de Glover, et marque un site d'altération en quartz et séricite et de minéralisation. Une importante déformation pénétrative et le métamorphisme associé dans le faciès des schistes verts, datent probablement du Paléozoïque moyen. Les ruptures cassantes et les failles d'âge carbonifère, et peut-être plus ancien, suivent le réseau de failles de Cabot.

[1] Contribution to Canada-Newfoundland Cooperation Agreement on Mineral Development 1990-1994, a subsidiary agreement under the Economic and Regional Development Agreement. Project funded by the Geological Survey of Canada.

[2] Centre for Earth Resources Research, Memorial University of Newfoundland, St. John's, Newfoundland A1B 3X5

INTRODUCTION

The Glover Island region lies along the Baie Verte-Brompton Line (Williams and St. Julian, 1978, 1982), a fundamental structure in the northern Appalachians separating ancient continental margin of the North American miogeocline to the west from accreted structural terranes to the east. West of the line, the Humber Zone (Fig. 1; Williams, 1978) in the vicinity of Glover Island consists of siliciclastic and carbonate rocks, unconformably overlying gneissic basement, with the whole sequence polydeformed and metamorphosed up to amphibolite-facies during mid-Paleozoic orogenesis (Kennedy, 1982; Cawood and van Gool, 1992). East of the line, within the Dunnage Zone, a sequence of ultramafic to silicic igneous rocks and minor epiclastic rocks is locally intruded by granite (Knapp et al., 1979; Knapp, 1980, 1983).

Riley (1957) first noted the presence of psammites and pelites on the west side of Glover Island and volcanic rocks on the east, separated by ultramafic and mafic plutonic intrusions. Williams and St. Julian (1978, 1982) noted that the plutonic rocks represent an ophiolitic fragment, and the structural contact with the metasedimentary rocks to the west marked the trace of the Baie Verte-Brompton Line in this region. Knapp (1983) carried out detailed mapping of Glover Island, concentrating on its southern and central portions. He divided the western sequence into basement gneiss and structurally overlying metaclastics, and interpreted the volcanic rocks on the east side of the island to be nonconformable on the ophiolitic sequence. Carboniferous strata outcrop on the northern end of Glover Island and around the shore of Grand Lake north of the island (Hyde, 1982). This paper describes the central and northern segments of Glover Island and equivalent units on the adjoining mainland.

GEOLOGY

The geology of Glover Island and environs is shown in Figure 2. This region lies within Corner Brook map sheet (12A/13) and the northern segment of Little Grand Lake map sheet (12A/12). Six lithostratigraphic units are recognized: gneissic basement (Cobble Cove gneiss); unconformably overlying cover sequence (Keystone schist); plutonic ophiolitic rocks (Grand Lake complex); volcanic and high level intrusive rocks (Glover Formation); the Glover Island granodiorite; and red to olive green siliciclastics of the Carboniferous Anguille and Deer Lake groups. Fault bounded blocks of mafic igneous rock intruded by younger granitoids, probably representing broad correlatives of Glover Formation and Glover Island granodiorite, occur along the Cabot Fault system.

The terms Cobble Cove gneiss, Keystone schist, and Grand Lake complex were introduced by Knapp (1983). The Cobble Cove and Keystone units represent a thin isolated sliver of Humber zone lithologies preserved east of the Cabot Fault, the main strand of which runs down Grand Lake west of Glover Island. The name Glover Formation was introduced by Riley (1957) for the volcanic rocks east of the granite gneiss and metaclastic schist. Knapp (1983) raised the Glover Formation to group status and redefined it to include the Kettle Pond and Tuckamore formations. The Kettle Pond formation was restricted to a sequence of predominantly quartz-sericite schists stratigraphically overlying the Grand Lake complex whereas the Tuckamore formation corresponds largely with the original character of the unit as established by Riley (1957). Our mapping has shown that the rocks mapped by Knapp (1983) as the Kettle Pond formation, as well as immediately adjoining segments in the Tuckamore formation and Grand Lake complex, lie within a complex shear zone and that the contact with the Grand Lake complex is structural rather than stratigraphic. We therefore discontinue use of the Kettle Pond and Tuckamore formations as stratigraphic units and revert to the term Glover Formation for igneous rocks east of the Grand Lake complex. The Grand Lake complex and Glover Formation constitute elements of the Dunnage Zone. We propose the term Glover Island granodiorite for a previously unnamed pluton, first mapped by Riley (1957), on the northeast side of the island. Nomenclature of Carboniferous units follows Hyde (1982).

DESCRIPTION OF LITHOSTRATIGRAPHIC UNITS

The Cobble Cove gneiss (Knapp, 1983) forms a sequence of quartzofeldspathic orthogneisses along the west-central side of Glover Island. The gneiss, well exposed in the lower reaches of Keystone Brook, immediately east of Cobble Cove and along the shore north of the cove (Fig. 2), has an across-strike width of approximately 500 m and is unconformably overlain by the Keystone schist. The base of the sequence is not exposed but is presumably truncated by the Cabot Fault system.

These gneisses consist of varying proportions of quartz, plagioclase, K-feldspar, biotite, and minor muscovite giving a compositional range from diorite to granodiorite. They are layered on centimetre-scale due to variations in proportions of leucocratic and melanocratic minerals. Minor quartzite and mafic schist layers are also present, as well as little deformed, pink aplitic to pegmatitic, crosscutting granite dykes.

The Keystone schist (Knapp, 1983), comprises interbanded psammite, quartz pebble conglomerate, and pelite, along with minor amphibolite, marble, quartzite, biotite schist, and graphitic schist. The schist is well exposed in Keystone Brook and along the west coast of the island north of the Cobble Cove gneiss. Siliciclastic units of the schist consist of varying proportions of quartz, feldspar, and muscovite, with some porphyroblastic biotite developed in the lower parts of the formation. Amphibolite, consisting of plagioclase and hornblende, plus epidote, chlorite, and porphyroblastic biotite, occurs in layers up to a few metres thick, parallel to bedding and restricted to the lower half of the unit. One band 70 m thick outcrops in Keystone Brook. Marble and calc-schist occur in beds up to 2 m thick in the upper part of the unit, associated with biotite and graphitic schists. Distribution of amphibolites and marbles formed the basis for Knapp's (1983) informal division of the formation into lower and upper members.

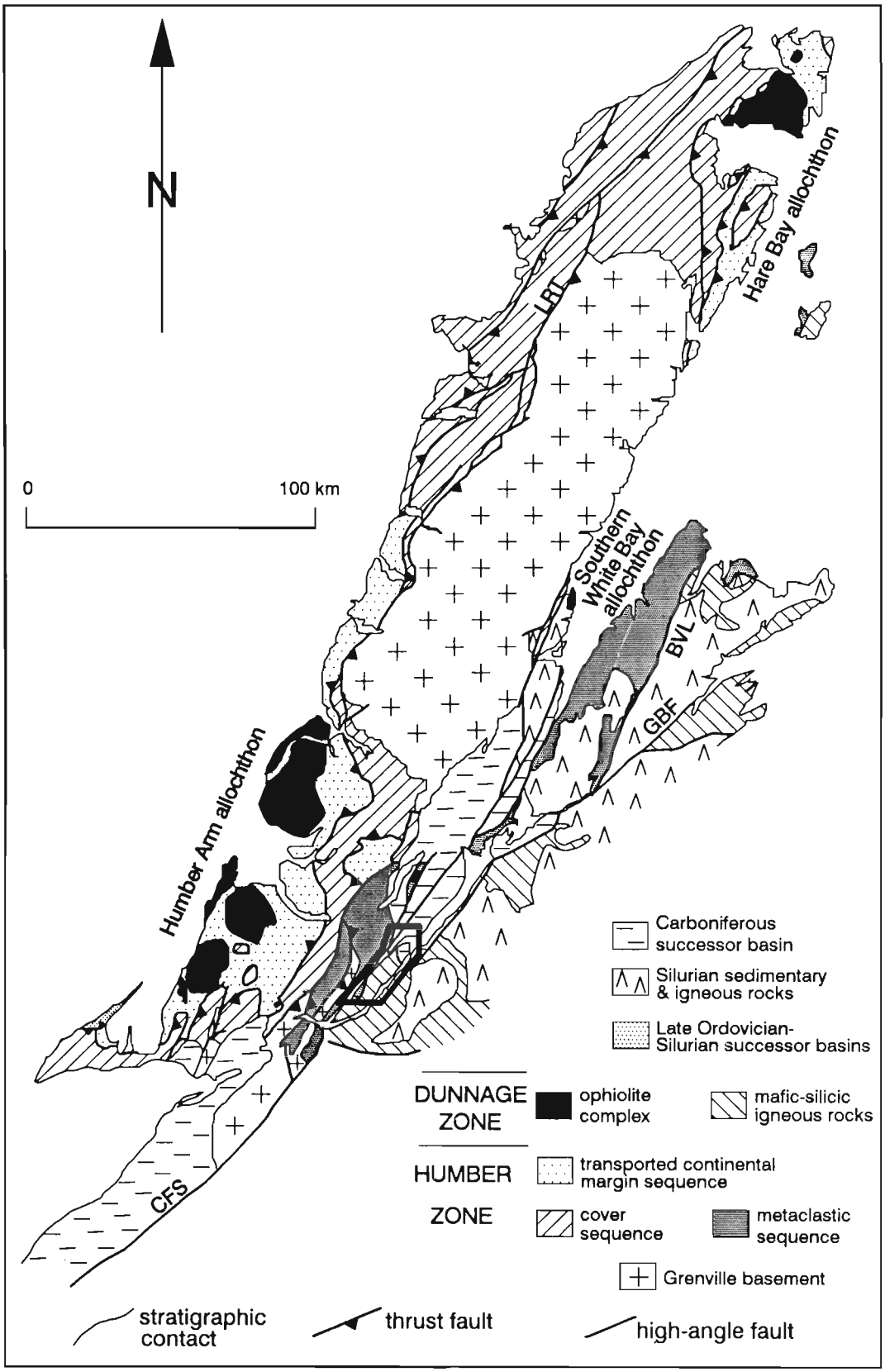

Figure 1. Simplified geological map of west Newfoundland. Box outlines location of Figure 2. Abbreviations: LRT - Long Range Thrust; BVL - Baie Verte Line; GBF - Green Bay Fault; CFS - Cabot Fault System.

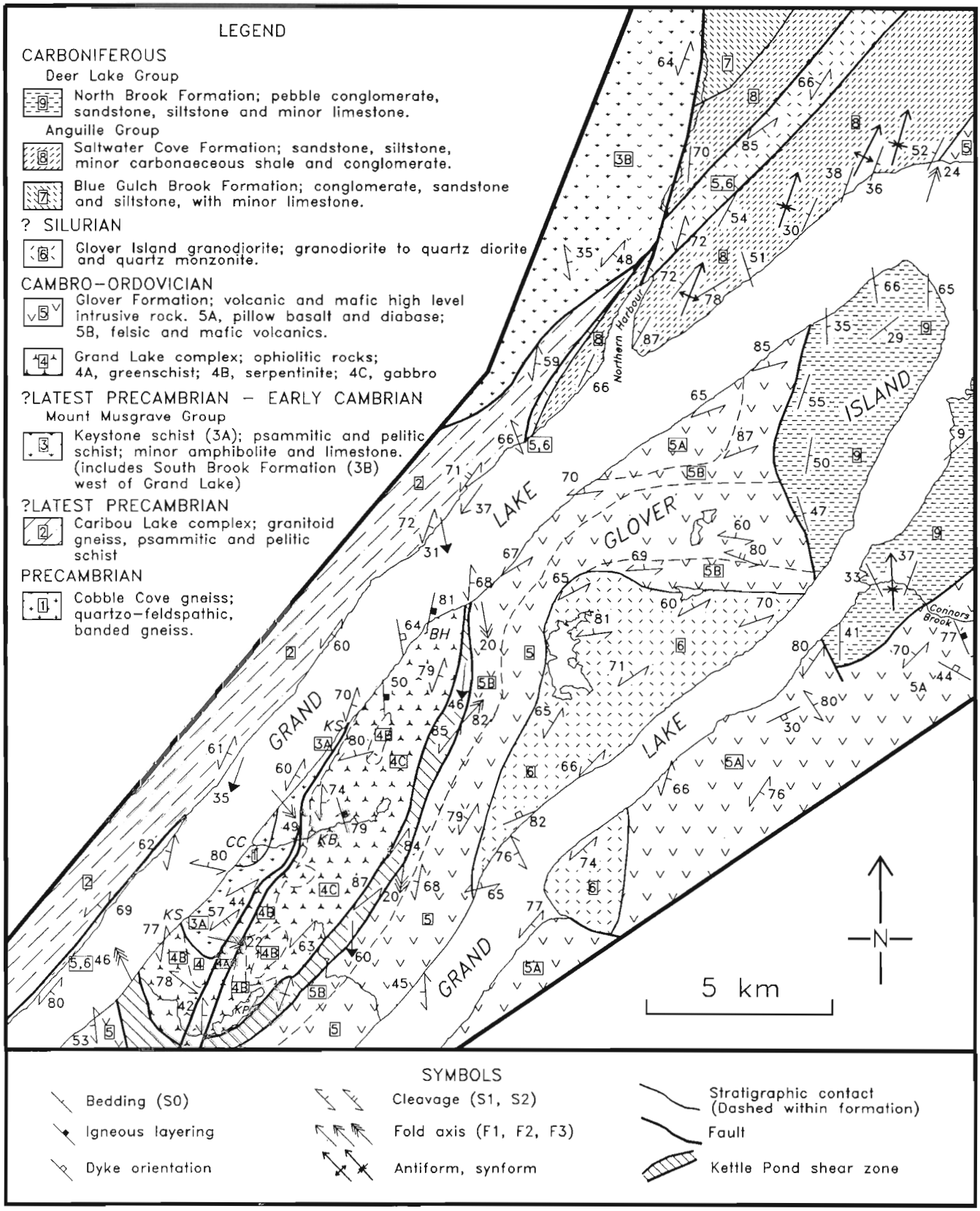

Figure 2. Geological map of the Glover Island region. Abbreviations: BH - Bluff Head; KB - Keystone Brook; CC - Cobble Cove; KS - Keystone shear zone.

The Keystone schist has an across-strike width of approximately 800 m. The upper contact is faulted against serpentinite and greenschist of the Grand Lake complex. The basal unconformity on the Cobble Cove gneiss is exposed in Keystone Brook at grid reference 434004 and on the shore at grid reference 436015, where psammites and quartz granule to quartz pebble conglomerates overlie granitoid gneiss.

The Grand Lake complex (Knapp, 1983), well exposed on the shore of the island, on hills south of Bluff Head, and along Keystone Brook, (Fig. 2) consists predominantly of gabbro but includes ultramafic rocks, greenschist, trondhjemite, and crosscutting mafic dykes. The across-strike width is approximately 2000 m and both western and eastern contacts are major shear zones. The western contact is characterized by variably serpentinized and metasomatized ultramafic rock abruptly structurally overlying the metaclastics of the Keystone schist. In Keystone Brook and south, the serpentinite is separated from the schist by up to 30-40 m of greenschist. The greenschists occur in both green to purple banded and massive varieties, and contain a chlorite, epidote, plagioclase, carbonate, and oxide minerals. They probably represent metamorphosed and metasomatized mafic igneous rocks. Alteration is presumably related to tectonic emplacement. Orange-brown-weathering talc-carbonate rocks, which overlie greenschists in Keystone Brook and elsewhere mark the base of the Grand Lake complex, consist of talc, iron carbonate, serpentinite, oxide minerals, and rare fuchsite. White to orange weathering massive serpentinized peridotite, up to several hundred metres thick in Keystone Brook, directly overlies talc-carbonate rocks. Serpentinized ultramafic rocks outcrop in kilometre-size discontinuous lenses within lower segments of the gabbro sequence (Fig. 2).

Gabbros of the Grand Lake complex contain a hornblende, clinopyroxene, and plagioclase. They are divisible into a lower, layered cumulate sequence with alternating melanocratic and leucocratic layers, and an upper massive, mainly leucocratic section. Trondhjemite east of Keystone Brook consists of blue quartz, albitized plagioclase, and primary ferromagnesian minerals replaced by chlorite. Some, and possibly all, of the trondhjemite occurs as lenses within the Kettle Pond shear zone, rather than as intrusions into the Grand Lake complex as proposed by Knapp (1983). Shear zones occur west of the main trondhjemite outcrops but outcrop was insufficient to trace them into the main shear zone east of the complex.

Mafic dykes ranging in thickness from 30 cm to 2 m, with well developed chilled margins, intrude ultramafic and gabbroic segments of the Grand Lake complex. The dykes are generally aphyric but locally plagioclase-phyric segments occur in the cores. Dykes consistently strike northeast and dip steeply (Fig. 3).

The Glover Formation (Riley, 1957), which consists of mafic to silicic volcanic and high level intrusive igneous rocks and minor volcaniclastic rocks, underlies the northern and eastern segments of Glover Island as well as the area east of Grand Lake. Exposure along the shores of the lake, particularly the northwest coast of Glover Island is excellent, but outcrop in the interior of the island and east of the lake is poor.

Pillow lavas, tuffs, massive flows, and high level intrusive diabase and microgabbro occur throughout the formation but extrusive phases dominate in the eastern half of the island and east of Grand Lake. Pillows range in diameter from 20 cm to over 1 m with most averaging between 30 cm to 60 cm. Silicic igneous rocks, ranging from dacitic to rhyolitic volcanic rocks and tuffs occur interstratified with the mafic rocks in the western parts of the formation, and are well exposed along the northwest shore of the island. Thin bands of extensive pyrite alteration, locally up to several metres wide occur within the mafic volcanic rocks and silicic tuffs of the formation.

Structural disruption within the Glover Formation, and lack of younging directions make it difficult to estimate original thickness of the unit. A thickness of several thousand metres is suggested by regional distribution of lithologies.

On the east side of Glover Island, the Glover Formation is intruded by a quartz dioritic and quartz monzonitic pluton (Riley, 1957; Knapp, 1983) herein termed the Glover Island granodiorite (Fig. 2). Satellite plutons outcrop on the east shore of Grand Lake and in Connors Brook. Principal mineral phases are plagioclase, quartz, potassium feldspar, and biotite, locally altered to chlorite and hematite. The pluton is cut by co-genetic pegmatitic and aplitic dykes, and contains dioritic xenoliths. It contains marginal rafts of the surrounding Glover Formation.

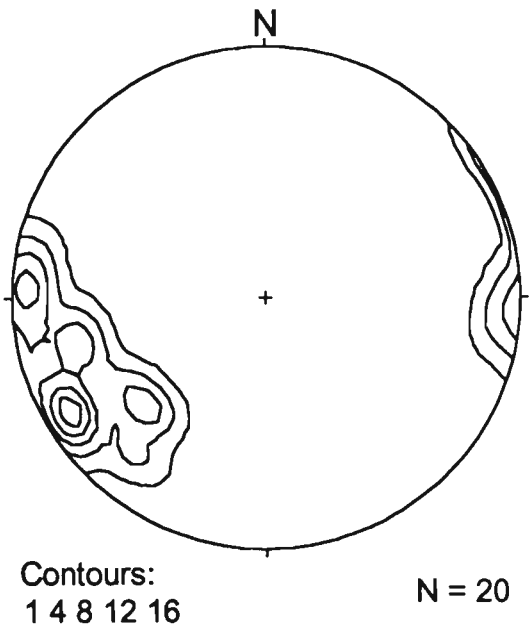

Figure 3. Plot of poles to mafic diabase dykes in the Grand Lake complex north of Keystone Brook. Plotted in lower hemisphere equal-area projection.

Granitoid rocks, intrusive into sequences of Dunnage Zone mafic igneous rocks ranging from pillow lavas to gabbro, occur along the west side of Grand Lake as far north as Northern Harbour (Fig. 2). They are restricted to long, narrow, fault bounded blocks associated with the Carboniferous Cabot Fault system,

Carboniferous rocks of the Anguille and Deer Lake groups outcrop in some shore and stream sections at the northern end of the map area (Fig. 2; Hyde, 1982). Grey siliciclastics with minor limestone (Blue Gulch Brook Formation and Saltwater Cove Formation of the Anguille Group) outcrop around and north of Northern Harbour (Fig. 2), while red-brown pebble conglomerates with interstratified sandstone, siltstone, and minor limestone (North Brook Formation of the Deer Lake Group) are exposed on and east of Glover Island. Carboniferous strata unconformably overlie Dunnage Zone rocks west and northeast of Northern Harbour, but elsewhere the contact with basement is faulted.

CORRELATION OF ROCK UNITS

The Cobble Cove gneiss and Keystone schist represent a basement/cover sequence. The granitoid gneissic composition of the Cobble Cove unit suggests that it could

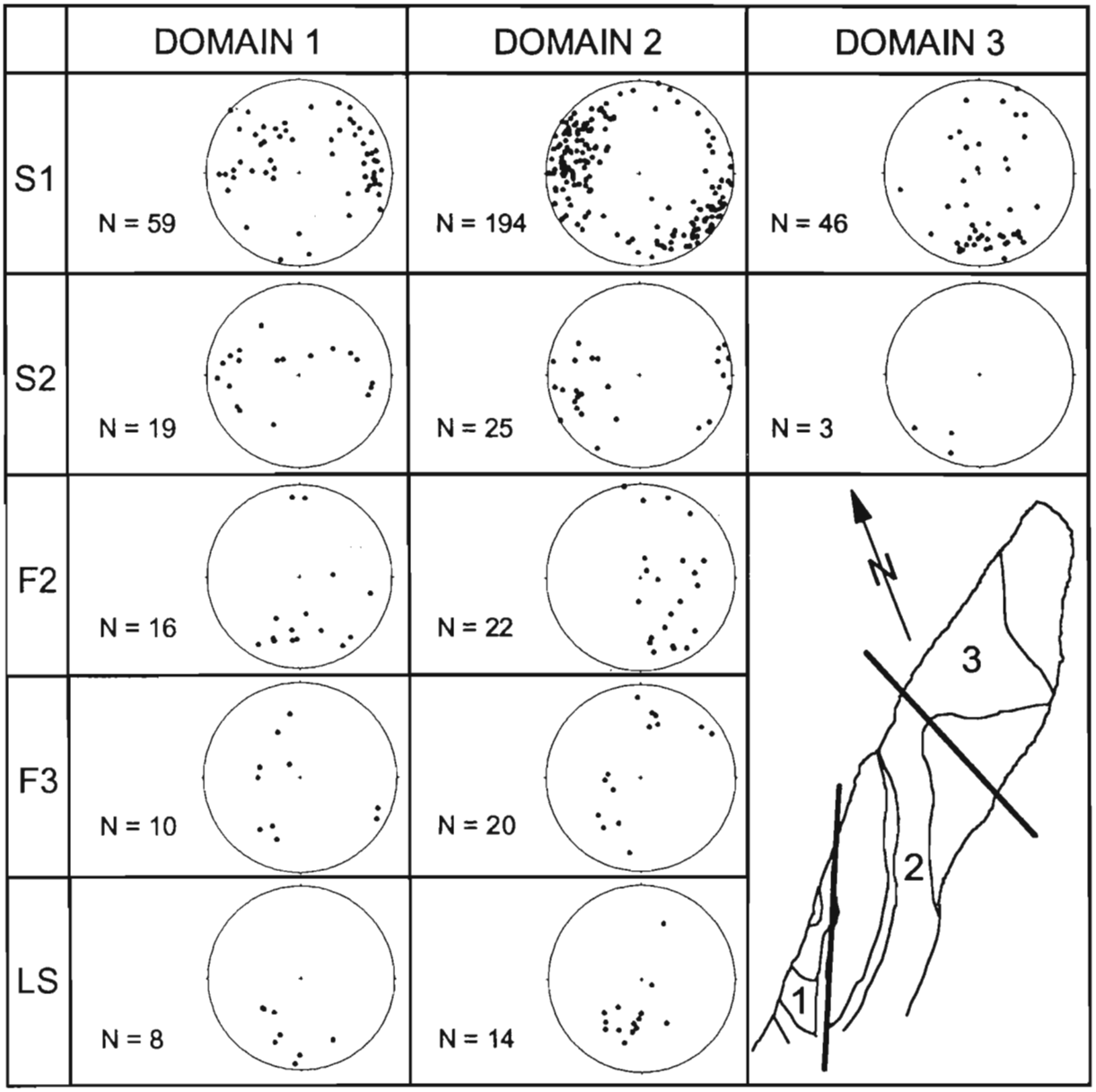

Figure 4. Structural orientation data for lower and middle Paleozoic rock units on Glover Island. Poles to planes (S_0, S_1) and linear structures (F_2, F_3, L_s) are plotted in lower hemisphere, equal-area projection. Ls - elongation lineation.

constitute part of the Grenville basement to the Appalachian Orogen with the interbanded amphibolites possibly representing mafic igneous activity related to initiation of the Appalachian cycle (cf. Knapp, 1983). In Cobble Cove, and along the coast to the north, dioritic phases of the gneiss are cut by granitoid phases showing weak fracture cleavage. The relatively mild deformational state of this lithology and its restriction to basement may indicate correlation with ca. 620 Ma silicic igneous activity noted in the Hare Hill region to the southwest (van Berkel and Currie, 1988) and the Round Pond region to the northwest (Williams et al., 1985). The arkosic composition of the metaclastic rocks of the Keystone schist as well as the presence of interbanded amphibolites, supports earlier correlation of this unit with the Fleur de Lys Supergroup on the Baie Verte Peninsula and the Mount Musgrave Group around Corner Brook Lake (Williams and St. Julian, 1978; Kennedy, 1982; Knapp, 1983; Cawood and van Gool, 1992).

Williams and St. Julian (1982) and Knapp (1983) have compared the Dunnage Zone rock units on Glover Island (Grand Lake complex and Glover Formation) with similar sequences on the Baie Verte Peninsula. The Grand Lake complex was correlated with the Advocate Complex on the basis of its deformed and disrupted ophiolitic character, and the inferred similar structural position immediately east of the Baie Verte Line. The interpreted unconformable contact between the complex and the overlying Glover Formation, and the recognition of conglomerate along the contact led to correlation of the conglomerate with conglomerates of the Flatwater Pond Group. Recognition of a structural, rather than stratigraphic, contact between the Grand Lake complex and Glover Formation destroys the basis for these correlations.

STRUCTURE

The bulk of Dunnage zone rocks on Glover Island are low strain, although several high strain zones cut the sequence. The relatively low strain contrasts with the high strain rocks in the adjacent Humber Zone (Cawood and van Gool, 1992). A regionally developed foliation is present in most mid-Paleozoic and older rock units on Glover Island and locally multiple generations of foliations, folds, and faults are observed. Overprinting relationships between the various structural elements show that the rocks have experienced a complex deformation history.

Structural elements are plotted on Figures 2, 4, and 5. The lower to middle Paleozoic rocks on Glover Island were subdivided into three domains, which are shown in the inset map in Figure 4. The central domain 2 is separated from domain 1 to the west by the Keystone shear zone. Domain 3 to the east contains rocks with a predominant easterly strike. Structural data for the Carboniferous rock units postdate domain formation and are shown separately (Fig. 5).

Main foliation – S_1

The dominant foliation is the oldest structure recognized in most rocks, although layering in Cobble Cove gneiss and flow banding in intrusive rocks existed prior to D_1 deformation. S_1 varies in style in different rock types (cf. Knapp, 1983), but the continuity of orientation throughout most of the area (Fig. 2) suggests that the main foliation in all units is approximately equivalent and related to assembly of the various units during D_2.

The gneissic layering in the Cobble Cove gneiss has orientation similar to S_1 in the overlying metasediments, but is interpreted to be older (Grenvillian?). The overlying Keystone schist is intensely foliated by S_1, a penetrative schistosity defined by fine grained micas, and in conglomerate by elongated quartz and feldspar clasts.

Greenschist and serpentinite of the Grand Lake complex are highly foliated, reflecting movement of the complex over Humber Zone lithologies along the Keystone shear zone. Gabbros in the complex show a weak mineral alignment of primary origin, but are locally cut by narrow shear zones, probably related to the bounding shear zones, in which minerals are flattened to form a mylonitic foliation, with slight alteration to greenschist mineralogy.

Regional S_1 foliation in the Glover Formation is variably developed but shows an overall decrease in intensity away from the Kettle Pond shear zone. The foliation is not penetrative in all parts of the formation, but where penetrative

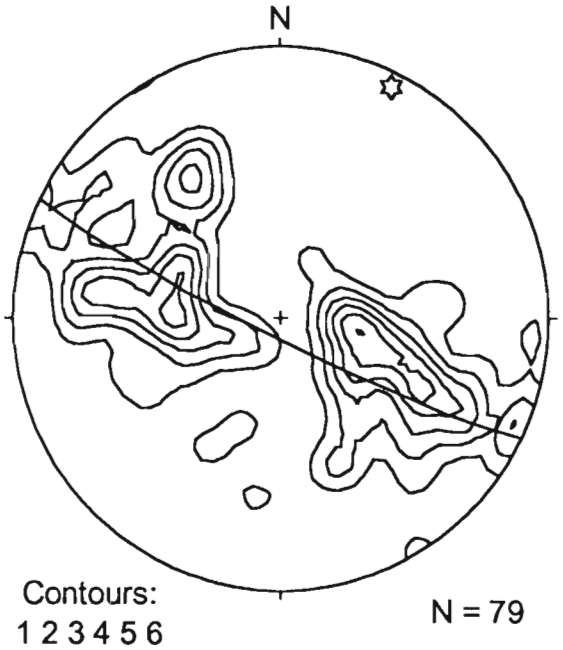

Figure 5. Poles to bedding in Carboniferous rocks of Deer Lake Basin, plotted in lower hemisphere, equal-area projection. The great circle represents the calculated p-girdle. The star is the calculated fold axis, which is orientated at 06° to 026°.

S_1 cleavage is lacking, flattening of pillows shows that the rocks are deformed. Fine grained volcanic and volcaniclastic rocks usually have a foliation that is parallel to original layering.

In the Glover Island granodiorite, S_1 consists of a preferred orientation of elongated quartz and feldspar grains and isolated biotites, with local fracture cleavage. The fabric is quite weak in the coarse grained lithologies and better developed in the medium grained parts of the pluton. Although the S_1 foliation in the granodiorite is parallel to, and assumed to be continuous with the dominant foliation in surrounding rocks of the Glover Formation, some xenoliths of inferred Glover Formation contain a foliation which is truncated by, and at an angle to, the foliation in the engulfing granitoid.

Figure 4 shows the dominant north-northeast striking orientation of the S_1 foliation in the central part (domain 2) of Glover Island, with fanning of the foliation reflected in both northwest and southeast dip directions. Orientations in domains 1 and 3, in the southwest and northeast respectively, are significantly different as a result of large scale, late-stage folding.

Shear Zones

The Keystone and Kettle Pond shear zones are major ductile dislocations, juxtaposing contrasting lithotectonic assemblages. The Keystone shear zone, developed within basal Dunnage Zone rocks, marks the trace of the Baie Verte-Brompton Line in this region. It is developed within the western segments of the Grand Lake complex and is best exposed in Keystone Brook, where strongly foliated greenschist and ultramafic rock abruptly overlie Keystone schist. North of Keystone Brook where the greenschists are absent, the shear zone is developed entirely within variably sheared and metasomatized ultramafic rock. Near the southwestern end of the map the shear zone is folded into a north-northwest striking orientation. Where the shear zone strikes into the Grand Lake, there is minor interbanding of ultramafic rock and psammite along the contact zone. To the east and northeast, however, lithologies from the Keystone schist are notably absent from the shear zone and the abrupt contact between the schist and Grand Lake complex (e.g., Keystone Brook) may indicate late-stage brittle reactivation of the contact (Fig. 2).

The Kettle Pond shear zone is a zone of up to several hundred meters wide, consisting of highly strained and interleaved lithologies from the adjoining Grand Lake complex to the west and the Glover Formation to the east. All rocks in the shear zone are retrogressed to either greenschists, sericite schists, quartz-porphyroclastic mica schists and serpentinites or talc-carbonate schists, representing deformed and retrogressed mafic rocks, felsic volcanics, trondhjemite, and ultramafic rocks, respectively. The S_1 foliation in the shear zone is very steep and has a north-northeast strike. Elongation lineations plunge shallowly to moderately to the south (L_s in Fig. 4), suggesting a predominant component of strike-slip movement. Towards its southern end the shear zone is folded about a steep axis, interpreted to be related to movement on younger strike-slip faults south of Keystone Brook. Kinematic indicators on outcrop scale are uncommon, but generally indicate dextral strike-slip movement in the main eastern part of the zone, whereas along Grand Lake, asymmetric quartz lenses indicate a component of reverse movement. Extensive quartz-sericite alteration within the shear zone is associated with widespread disseminated pyrite and chalcopyrite mineralization. Gold mineralization south of the map area on Glover Island occurs in or near the Kettle Pond shear zone.

Folding

Folds related to S_1 foliation were observed only in the Keystone schist, commonly in marbles, forming asymmetric, isoclinal F_1 folds with strong axial planar cleavage (S_1).

S_1 foliation is folded by at least one generation of folds. F_2 folds have no axial planar cleavage and form generally parallel folds. Fold axial planes have a wide range of orientations, but generally dip fairly steeply and have orientations at small angles to S_1 (Fig. 4), resulting in strongly asymmetric folds. F_2 folds are rare and occur predominantly in, and west of, the Kettle Pond shear zone. In sheared volcanic rocks south of Cobble Cove, F_2 crenulations and an S_2 crenulation cleavage locally overprint the S_1 foliation.

A set of open crenulations (F_3), which lack a well developed crenulation cleavage, has shallow to moderate, north or south plunging axes (Fig. 4). The axial planes are often at a high angle to the S_1 foliation. In interbanded mafic and felsic volcanics south of Cobble Cove, overprinting of F_2 and F_3 folds was observed. Here the orientations of both sets of fold axes was variable. The fold sets have identical styles and where overprinting relationships are absent F_2 and F_3 folds cannot be distinguished. In such cases folding was attributed to F_2.

Two large scale folds occur on Glover Island. One is outlined by the orientation of the boundary between the Glover granodiorite and the Glover Formation rocks, and by the S_1 foliation. The lack of small scale parasitic folds prevents estimation of relative timing of this fold. A second fold exists south of Cobble Cove, where both the Keystone and the Kettle Pond shear zones and other lithological boundaries are folded in a steeply south-dipping antiform, which is interpreted to be a result of movement on faults of the Cabot Fault system.

The Cabot Fault system

The western arm of Grand Lake contains a major strand of the Cabot Fault system. Apart from the sliver of Cobble Cove gneiss and Keystone schist, the fault corresponds with the Humber/Dunnage boundary and metamorphic grade changes from amphibolite grade in the west to greenschist grade in the east. The Cabot Fault system forms a complex network of faults, which locally splay from the main zone, as in Northern Harbour and south of Bluff Head, where the Baie Verte-Brompton Line on Glover Island is reactivated. Rocks along the western arm of Grand Lake are locally intensely

fractured. Pseudotachylites occur in the granitoid rocks on the west shore of Grand Lake in the southwestern corner of the map (Fig. 2).

Contrasting metamorphic grades between mid-Paleozoic and older rock units across the Cabot Fault, combined with relatively minor sinistral offset of the Carboniferous boundary between Northern Harbour and the northern end of the Glover Island suggest a complex movement history on the fault.

Brittle faults separate Carboniferous rocks from Dunnage Zone rocks. West and north of Northern Harbour several other late faults bound a sliver of Dunnage Zone mafic to silicic volcanic rocks cut by granitoid (Fig. 2). Knapp (1983) suggested that several east-striking faults cut the rocks of Glover Island. No evidence for such faults was found.

Structure in Carboniferous rocks

The Carboniferous rocks of the Deer Lake basin generally show no sign of penetrative deformation on outcrop scale. However older Anguille Group rocks are folded in a set of shallowly north-northeast-plunging folds with amplitudes of tens to hundreds of metres. Folding within the Carboniferous sequence is well exposed along the northwestern shore of Grand Lake. Figure 5 is a plot of poles to bedding planes, which outline the shallowly north-northeast-plunging fold axes. Outcrop-scale folds are rare and were only observed in thinly bedded sequences. A foliation at a small angle to bedding was locally observed in the shales. Younging directions in the Carboniferous sedimentary rocks indicate that the folds are facing upwards. Both reverse and normal faults with offsets on the scale of several metres to several tens of metres cut the rocks.

Timing of deformation

Timing of deformation within the Glover Island region is poorly constrained. The continuity, and uniform orientation, of the principal foliation across stratigraphic and structural boundaries suggests that deformation and assembly of the disparate rock units was consanguineous. On the basis of this assumption, deformation postdates the Glover Island granodiorite, the youngest deformed unit within the Glover Island region, but regional penetrative deformation must predate deposition of the little deformed Carboniferous strata, which unconformably overlie deformed units in both the Humber and Dunnage zones. Dunning et al. (1990) have demonstrated that the principal mid-Paleozoic orogeny, at least in southwest Newfoundland, corresponds with the Silurian Salinian orogeny. The limited constraints from the Glover Island region are consistent with this event being responsible for the bulk of the deformation and metamorphism observed on the island. In addition, the continuity of the tectonic fabric across the Keystone and Kettle Pond shear zones suggests that formation of these structures as well as the juxtaposition of main lithological assemblages within the area, including the Humber/Dunnage boundary are also of mid-Paleozoic age. This contrasts with previous studies which have assumed that assembly of the lithotectonic units was related to the Ordovician Taconian orogeny (e.g. Williams and St. Julian, 1982; Knapp, 1983).

ACKNOWLEDGMENTS

We thank Jim Ryan and Rob Taylor for assistance with field work and Greg Dunning and Steve Colman-Sadd for stimulating discussion in the field area. Stuart Cochrane of the Newfoundland Department of Mines allowed access to the Pasadena core storage facilities.

REFERENCES

Cawood, P.A. and van Gool, J.A.M.
1992: Stratigraphic, structural, and metamorphic relations along the eastern margin of the Humber Zone, Corner Brook map area, western Newfoundland; in Current Research, Part E; Geological Survey of Canada, Paper 92-1E, p. 239-247.

Dunning, G.R., O'Brien, S.J., Colman-Sadd, S.P., Dickson, W.L., O'Neill, P.P., and Krogh, T.E.
1990: Silurian Orogeny in the Newfoundland Appalachians; Journal of Geology, v. 98, p. 895-913.

Hyde, R.S.
1982: Geology of the Carboniferous Deer Lake Basin; Mineral Development Division, Newfoundland Department of Mines and Energy, Map 82-7, scale 1:100 000.

Kennedy, D.P.S.
1982: Geology of the Corner Brook Lake area, western Newfoundland; M.Sc. thesis, Memorial University of Newfoundland, St. John's, Newfoundland, 370 p.

Knapp, D.A.
1980: The stratigraphy, structure and metamorphism of central Glover Island, western Newfoundland; Geological Survey of Canada, Paper 80-1B, p. 89-96.
1983: Ophiolite emplacement along the Baie Verte-Brompton Line at Glover Island, western Newfoundland; Ph.D. thesis, Memorial University of Newfoundland, St. John's, Newfoundland, 338 p.

Knapp, D., Kennedy, D., and Martineau, Y.
1979: Stratigraphy, structure and regional correlation of rocks at Grand Lake, western Newfoundland; Geological Survey of Canada, Paper 79-1A, p. 317-325.

Riley, G.C.
1957: Red Indian Lake (west half), Newfoundland; Geological Survey of Canada, Map 8-1957.

van Berkel, J.T. and Currie, K.L.
1988: Geology of the Puddle Pond (12A/5) and Little Grand Lake map areas, southwestern Newfoundland; Newfoundland Department of Mines, Mineral Development Division, Report 88-1, p. 99-107.

Williams, H.
1978: Tectonic lithofacies map of the Appalachian Orogen; Memorial University of Newfoundland, Map no. 1, scale 1:1 000 000.

Williams, H. and St. Julian, P.
1978: The Baie Verte-Brompton Line in Newfoundland and regional correlations in the Canadian Appalachians; in Current Research, Part A; Geological Survey of Canada, Paper 78-1A, p. 225-229.
1982: The Baie Verte-Brompton Line: Continent-Ocean interface in the Northern Appalachians; in Major Structural Zones and Faults of the Northern Appalachians; (ed.) P. St. Julian and J. Bernard; Geological Association of Canada, Special Paper 24, p. 177-207.

Williams, H., Gillespie, R.T., and van Breemen, O.
1985: A late Precambrian rift-related igneous suite in western Newfoundland; Canadian Journal of Earth Sciences, v. 22, p. 1727-1735.

Geological Survey of Canada Project 730044

The Isle aux Morts metabasalt, southwest Newfoundland[1]

David I. Schofield[2], John A. Winchester[2], and Cees R. van Staal
Continental Geoscience Division

Schofield, D.I., Winchester, J.A., and van Staal, C.R., 1993: The Isle aux Morts metabasalt, southwest Newfoundland; in Current Research, Part D; Geological Survey of Canada, Paper 93-1D, p. 39-46.

Abstract: Preserved pillowed metabasalts in the Port aux Basques gneisses of southwestern Newfoundland are important for understanding the tectonic setting of the surrounding gneisses. The Isle aux Morts metabasalt (IAMM) occur as tectonic lenses in the Isle aux Morts Fault Zone, which separates the Port aux Basques Complex with Gander affinities from the Harbour le Cou Group of the Dunnage Zone. Chemical analyses show that the Isle aux Morts metabasalt represent a suite of evolved tholeiitic basalts with MORB affinities, unlike any of the mafic rocks in the Harbour le Cou Group. This relationship suggest that the Isle aux Morts metabasalt are exotic with respect to the rocks of the Harbour le Cou Group. The structural position of the Isle aux Morts metabasalt is similar to that of the GRUB belt in central and northeastern Newfoundland if the Gander affinities of the Port aux Basques Complex are confirmed.

Résumé : L'étude des métabasaltes en coussins conservés dans les gneiss de Port aux Basques dans le sud-ouest de Terre-Neuve est importante à une meilleure compréhension du cadre tectonique des gneiss environnants. Les métabasaltes de l'Isle aux Morts (IAMM) se présentent sous forme de lentilles tectoniques dans la zone de failles d'Isle aux Morts, qui sépare le complexe de Port aux Basques, lequel présente des affinités avec le terrane de Gander, du Groupe de Harbour le Cou situé dans la zone de Dunnage. Les analyses chimiques montrent que le les IAMM représentent une série de basaltes tholéiitiques évolués présentant des affinités avec les basaltes de la dorsale médio-atlantique (MORB), contrairement à tous les types de roches mafiques du Groupe de Harbour le Cou. Cette relation porte à croire que les IAMM sont des éléments allochtones par rapport aux roches du Groupe de Harbour le Cou. La situation structurale des IAMM est semblable à celle de la zone GRUB dans le centre et le nord-est de Terre-Neuve, si les affinités du Complexe de Port aux Basques avec le terrane de Gander sont confirmées.

[1] Contribution to Canada-Newfoundland Cooperation Agreement on Mineral Development 1990-1994, a subsidiary agreement under the Economic and Regional Development Agreement. Project funded by the Geological Survey of Canada.
[2] Department of Geology, University of Keele, Keele, Staffordshire ST5 5BG, England

INTRODUCTION

The Port aux Basques gneiss in southwestern Newfoundland (Brown, 1976, 1977) has been problematic with respect to tectonostratigraphic correlations and tectonic modelling of the northern Appalachians. It was generally considered to represent a monotonous sequence of upper amphibolite facies gneisses and amphibolites, possibly of Precambrian age (e.g. Brown, 1976). Van Staal et al. (1992) showed that the Port aux Basques gneisses contain lithologically distinct units, although each is dominantly made up of psammitc and pelitic rocks. These units from west to east are: the Grand Bay Complex; the Port aux Basques Complex; and the Harbour le Cou Group (van Staal et al., in press). Furthermore, highly strained pillow basalts were observed in the Isle aux Morts Fault Zone (IMFZ; van Staal et al., 1992), associated with sedimentary rocks that have been grouped with the Harbour Le Cou Group. This association supports the Cambro-Ordovician age and Dunnage affinity proposed by Colman-Sadd et al. (1990) of the Harbour Le Cou Group and hints at the possibility that the IMFZ coincides with a tectonostratigraphic boundary, like the GRUB line between the Gander and Dunnage zones in central and northeastern Newfoundland (Williams et al., 1988). The lithological similarities between the rocks of the Port aux Basques Complex to the west of the IMFZ and the Gander Zone rocks in general further strengthens this analogue. The discovery of well preserved pillow basalts in the Harbour Le Cou Group near the village of Burnt Island by C. Lee and results of fieldwork (Lin et al., 1993) investigating the relationships between the Harbour le Cou and Bay du Nord groups, supported the earlier proposed correlation between these two groups made by Brown (1976).

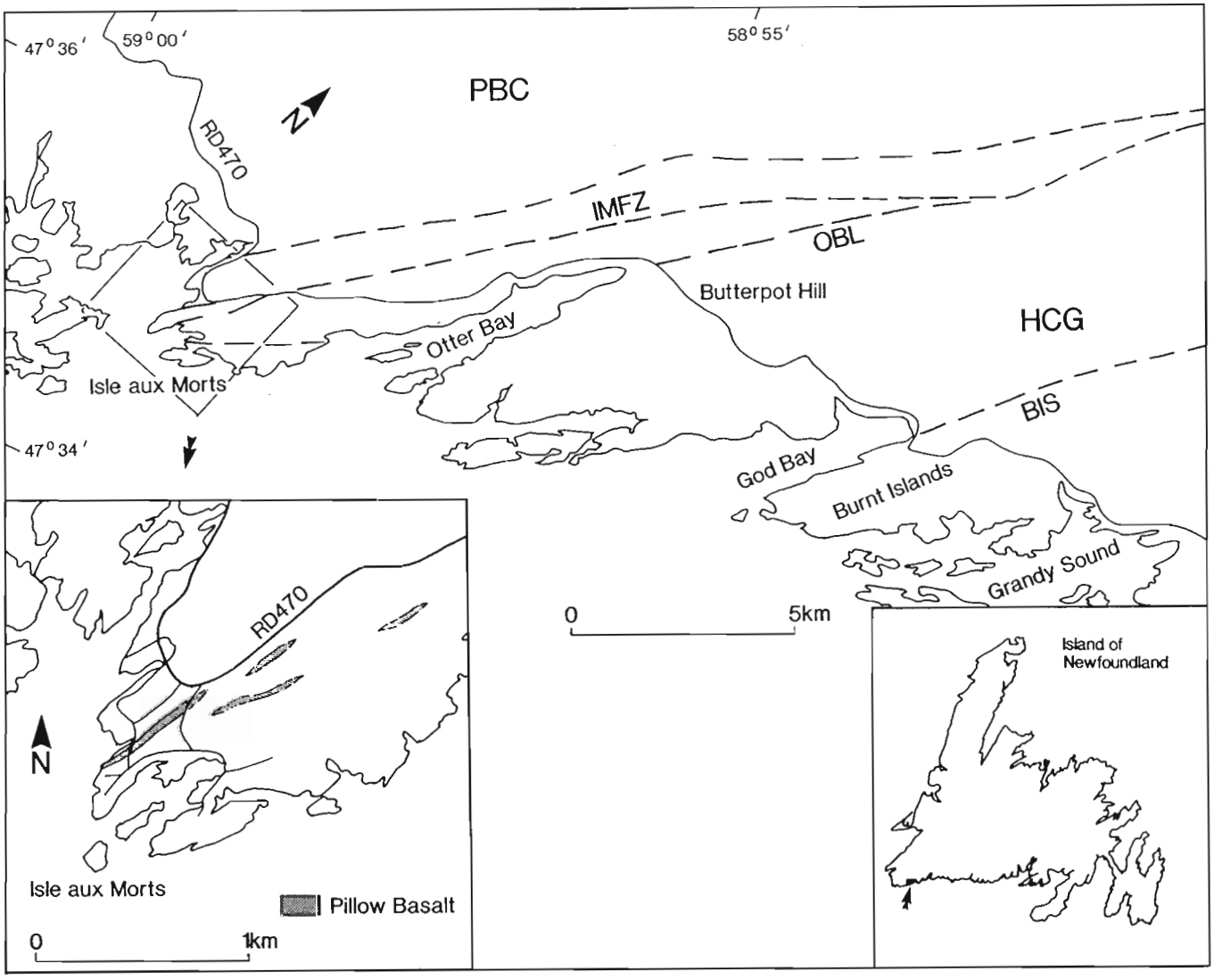

Figure 1. Map of Isle aux Morts area with inset showing the distribution of pillow basalts. BIS, Burnt Islands Shear; HCG, Harbour le Cou Group; IMFZ, Isle aux Morts Fault Zone; OBL, Otter Bay Lineament; PBC, Port aux Basques Complex.

Table 1a. Analyses of the Isle aux Morts metabasalt (IAMM) and Burnt Islands amphibolite

SAMPLE	WS945	WS946	WS947	WS948	WS949	WS960	WS961	WS962	WS963	WS964	WS965	WS993	WS1008	WS1010	WS1011	WS1014
	Isle aux Morts metabasalt											Burnt Islands amphibolite				
SiO2	45.71	47.90	50.89	50.61	54.97	49.49	50.71	49.83	58.75	49.06	55.06	49.03	54.65	57.30	55.75	43.21
TiO2	2.74	3.43	3.22	2.96	2.86	2.99	3.12	2.61	2.53	2.81	3.04	1.32	1.11	1.16	1.36	1.44
Al2O3	14.06	15.90	13.93	13.75	14.15	13.67	13.26	15.45	13.05	13.16	13.04	17.21	17.29	18.28	16.07	19.92
Fe2O3t	17.23	16.41	16.04	14.67	13.82	16.15	15.83	13.68	11.86	16.00	12.45	12.54	9.02	6.73	9.30	14.34
MnO	0.28	0.48	0.28	0.39	0.26	0.26	0.30	0.23	0.24	0.47	0.39	0.34	0.20	0.16	0.25	0.34
MgO	7.58	4.34	4.71	4.94	3.74	5.65	4.52	6.00	5.49	6.60	4.00	6.12	3.00	1.77	4.27	2.87
CaO	7.84	8.23	5.98	6.40	6.51	6.62	7.82	6.00	3.57	8.80	6.31	10.01	7.62	8.16	8.42	14.21
Na2O	3.87	2.50	4.77	5.57	1.71	4.20	4.08	5.25	4.47	0.84	5.13	2.93	4.03	5.59	4.14	1.65
K2O	0.19	0.48	0.20	0.24	1.43	0.54	0.35	0.13	0.09	0.86	0.28	0.38	2.52	0.79	0.24	1.15
P2O5	0.32	0.45	0.30	0.38	0.39	0.24	0.37	0.21	0.27	0.27	0.30	0.03	0.16	0.11	0.15	0.14
S	0.01	0.02	0.08	0.03	0.01	0.01	0.01	0.01	0.01	0.05	0.01	0.01	0.01	0.02	0.01	0.02
Ba	47	44	127	207	138	137	97	24	34	75	107	711	466	326	189	128
Cl	1	5	27	30	8	6	19	4	99	65	12	59	118	89	95	29
Cr	106	81	79	73	22	118	33	91	34	80	54	162	201	173	124	245
Cu	20	31	47	47	16	36	20	20	15	32	14	41	11	30	13	70
Ga	26	28	24	24	24	24	22	25	18	25	22	19	19	19	18	21
Nb	9	15	11	10	12	10	11	9	10	11	10	10	8	7	7	11
Ni	49	43	33	36	14	41	30	31	28	31	28	46	26	18	19	43
Pb	9	11	11	11	13	10	11	13	8	9	11	19	13	13	13	12
Rb	6	14	5	6	67	19	6	6	4	8	6	101	83	24	9	29
Sr	109	171	112	214	184	154	227	138	77	98	155	130	101	157	112	213
Th	3	2	1	1	2	3	3	3	4	2	1	5	5	6	3	5
V	641	497	540	534	498	583	578	435	462	574	491	202	201	215	291	281
Y	58	86	71	65	64	60	65	56	53	65	59	45	27	26	36	33
Zn	137	144	137	130	119	130	138	99	102	124	111	84	63	57	79	143
Zr	202	267	242	214	218	194	206	192	217	231	229	212	121	133	116	148
La	9	50	12	12	25	1	20	9	15	12	14	20	6	10	5	5
Ce	29	91	33	48	57	32	40	34	47	46	51	63	27	24	27	40
Nd	16	49	22	42	36	29	26	23	16	28	33	28	14	20	21	21

An investigation of the Isle aux Morts metabasalt (IAMM) was made to determine their tectonic setting and to test whether they are chemically related to metabasites of the Harbour Le Cou Group or represent the remnants of an exotic fragment. This paper reports on our preliminary results.

GEOLOGICAL SETTING

The Isle aux Morts metabasalt crop out in the township of Isle aux Morts, southwest Newfoundland, within a region of high strain described as the Isle aux Morts Fault Zone (IMFZ) (van Staal et al. 1992) (Fig. 1). They occur as highly deformed and metamorphosed pillow basalts, exposed on the foreshore approximately 100 m east of the fish cannery in the town and extending discontinuously inland to form several narrow (5-15 m thick) lenses elongate parallel to the main schistosity and shallowly northeasterly-plunging extension lineation. They are associated with variably migmatized psammitic to semipelitic schists in which porphyroblasts of both kyanite and sillimanite are locally developed. Sheets of gneissic granitoid rock are also elongated parallel to the main schistosity and are crosscut by a later northwest-trending porphyritic felsite dyke. To the west this package of rocks is faulted against contrasting highly strained psammites, which toward the west tend to weather rusty brown and become phyllonitic. The psammites contain rare calc-silicate lenses and lack granitoid sheets and metabasites. To the east they become extremely rodded and are separated from the Harbour le Cou Group by the Otter Bay Lineament (OBL).

The pillow basalts and associated basic sheets have been metamorphosed to amphibolites, commonly with garnet-iferous and biotite-rich rims. The metabasites are associated with pale grey rocks, either as interpillow material or discrete beds. Initially thought to be of cherty origin, these rocks have been shown by chemical analysis to be not particularly siliceous and they may instead have protoliths of chemically modified sediments or volcanics. Subsequent shearing has imparted a "pillowed" appearance to some of the associated metabasic sheets due to the distribution of strain into discrete anastomosing shear zones; no distinct shear fabric was observed at the margins of true pillows.

PETROGRAPHY

The Isle aux Morts metabasalt are medium grained amphibolites composed of green-brown pleochroic hornblende (11-72%), variably sericitized and hematite-stained plagioclase (An 25-40%) (5-35%), and quartz (3-25%). Most samples

Table 1b. Analyses of Otter Bay, Butterpot Hill, and Grandy Sound metabasite dykes

SAMPLE	WS838	WS934	WS935	WS936	WS972	WS973	WS974	WS988	WS858	WS859	WS861	WS862	WS863	WS978	WS987	WS991	WS1025
	Otter Bay west metabasite dykes								Otter Bay east metabasite dykes							Butter-pot	Grandy
SiO2	54.94	52.48	56.37	50.06	54.36	52.44	55.69	50.33	46.21	47.45	49.44	43.34	43.42	47.18	46.76	47.81	57.94
TiO2	1.27	1.15	1.28	0.93	1.08	1.08	1.20	0.82	1.22	0.97	1.04	1.14	1.16	1.07	0.85	4.10	1.86
Al2O3	15.36	16.72	15.41	17.01	15.62	16.04	15.64	17.73	18.59	17.07	17.59	18.12	18.59	18.42	17.81	13.34	15.17
Fe2O3t	9.70	9.51	9.46	9.60	8.88	9.06	9.36	8.26	11.31	12.02	11.01	12.94	12.37	11.50	10.59	17.00	10.47
MnO	0.22	0.19	0.18	0.15	0.16	0.18	0.16	0.19	0.65	0.61	0.40	0.69	0.61	0.28	0.19	0.28	0.23
MgO	5.97	9.19	5.09	8.54	6.36	6.95	5.40	7.88	7.64	8.71	8.33	8.59	7.66	9.00	9.37	5.02	3.84
CaO	6.43	3.36	6.31	9.67	7.07	7.63	6.76	10.51	11.98	10.06	8.63	12.59	10.94	6.20	10.09	7.93	5.82
Na2O	4.48	3.36	4.73	2.50	3.90	3.61	3.31	3.02	1.26	2.32	0.90	1.15	1.31	2.95	1.69	2.04	1.14
K2O	1.21	3.09	1.02	1.01	2.12	2.11	1.49	0.68	0.61	0.26	2.60	1.02	1.92	3.30	1.23	1.21	2.39
P2O5	0.10	0.13	0.15	0.09	0.11	0.13	0.12	0.10	0.39	0.17	0.03	0.15	0.09	0.09	0.09	0.63	0.28
S	0.01	0.01	0.01	0.01	0.01	0.01	0.01	0.01	0.01	0.01	0.01	0.01	0.01	0.01	0.01	0.04	0.01
Ba	435	432	289	222	482	529	274	140	47	160	240	104	104	1346	66	933	696
Cl	77	50	55	26	43	144	38	171	1	1	13	10	13	30	18	37	41
Cr	105	203	89	236	194	215	115	260	358	286	425	389	384	301	318	21	92
Cu	17	10	33	35	46	41	40	16	14	16	15	17	12	54	12	38	16
Ga	19	22	17	20	19	17	18	17	21	19	18	19	18	23	18	26	21
Nb	7	7	8	5	7	7	7	5	6	4	6	5	5	4	3	38	11
Ni	24	46	22	111	47	50	26	100	130	149	165	154	161	137	147	20	16
Pb	12	15	14	12	18	14	16	15	14	10	10	13	11	13	14	9	13
Rb	40	97	32	37	57	65	60	24	16	5	80	25	106	88	32	48	106
Sr	185	96	196	183	398	454	210	186	141	222	113	120	105	137	187	501	235
Th	6	3	2	1	1	1	3	1	1	1	1	1	1	2	1	1	6
V	268	242	276	208	250	253	274	234	262	292	257	236	238	286	268	480	214
Y	33	34	35	25	31	29	34	23	29	23	35	36	29	28	22	59	57
Zn	79	89	76	74	71	72	79	62	182	48	133	151	107	90	89	147	99
Zr	137	119	145	92	110	105	133	74	68	59	64	64	63	46	32	310	239
La	10	3	9	7	7	7	12	1	5	3	5	8	1	1	1	39	21
Ce	35	20	45	27	30	16	39	3	19	8	7	34	24	1	13	72	44
Nd	23	9	21	24	19	10	19	7	11	21	7	18	19	7	12	42	34

contain accessory apatite (0-2%) and magnetite (0-5%). In addition, some samples contain biotite (up to 50%) and porphyroblasts of garnet (1-6 mm across) (0-11%). Hornblende or hornblende/biotite laths define a variably developed schistosity. Garnet porphyroblasts are syntectonic with quartz- and biotite-rich strain shadows. Garnets usually have rims of quartz and display minor replacement by chlorite along fractures. They also have abundant quartz and hornblende inclusions which occasionally form trails subparallel to the schistosity. The mineralogy thus defines amphibolite facies metamorphism.

The intrusive basic rocks from the Otter Bay division occur as layer parallel amphibolites, amphibolite dykes with clear crosscutting relationships, or isolated pods surrounded by metasedimentary gneiss. They are in general medium grained, compositionally layered rocks composed of green-brown pleochroic hornblende (30-65%), intermediate plagioclase (11-31%) and quartz (5-20%). Some samples contain biotite (0-24%), while apatite (0-2%), magnetite (0-2%), and garnet (0-9%) occur as accessory minerals. Rare clinopyroxene porphyroblasts were observed in two samples (3-5%).

In these rocks the mineralogy also suggests amphibolite facies metamorphism, while a variably developed schistosity is defined principally by the preferred dimensional orientation of hornblende.

Amphibolite pods show little internal deformation, with randomly oriented biotite laths (0-38%) inserted into coarse blue-green hornblende (30-75%). Chlorite associated with the hornblende forms discrete blades and is not evidently derived from it. Oligoclase (13-19%) poikilitically encloses minor quartz grains (1-12%) and is patchily sericitized, while aggregates of epidote (0-10%) are also present. Accessory magnetite, sphene, and apatite are present, but no garnet was observed.

GEOCHEMISTRY

Full chemical analyses of 11 Isle aux Morts metabasalt and 22 other amphibolites collected from the Harbour le Cou Group in 1991 were undertaken at Keele University, England, using an ARL 8420 X-Ray Fluorescence spectrometer, calibrated against both international and internal Keele standards of appropriate composition (Table 1a, b).

Because amphibolite facies metamorphism has affected all the rocks in the Isle aux Morts area, selective element mobility is likely to have occurred. This is confirmed on a CaO-Na_2O binary diagram (Stillman and Williams, 1979) which shows that the metabasic rocks scatter outside the rectangle delimiting the field of "normal" unaltered basalts. This diagram also shows that most of the Isle aux Morts metabasalt are Na_2O enriched and plot within the spilitic field

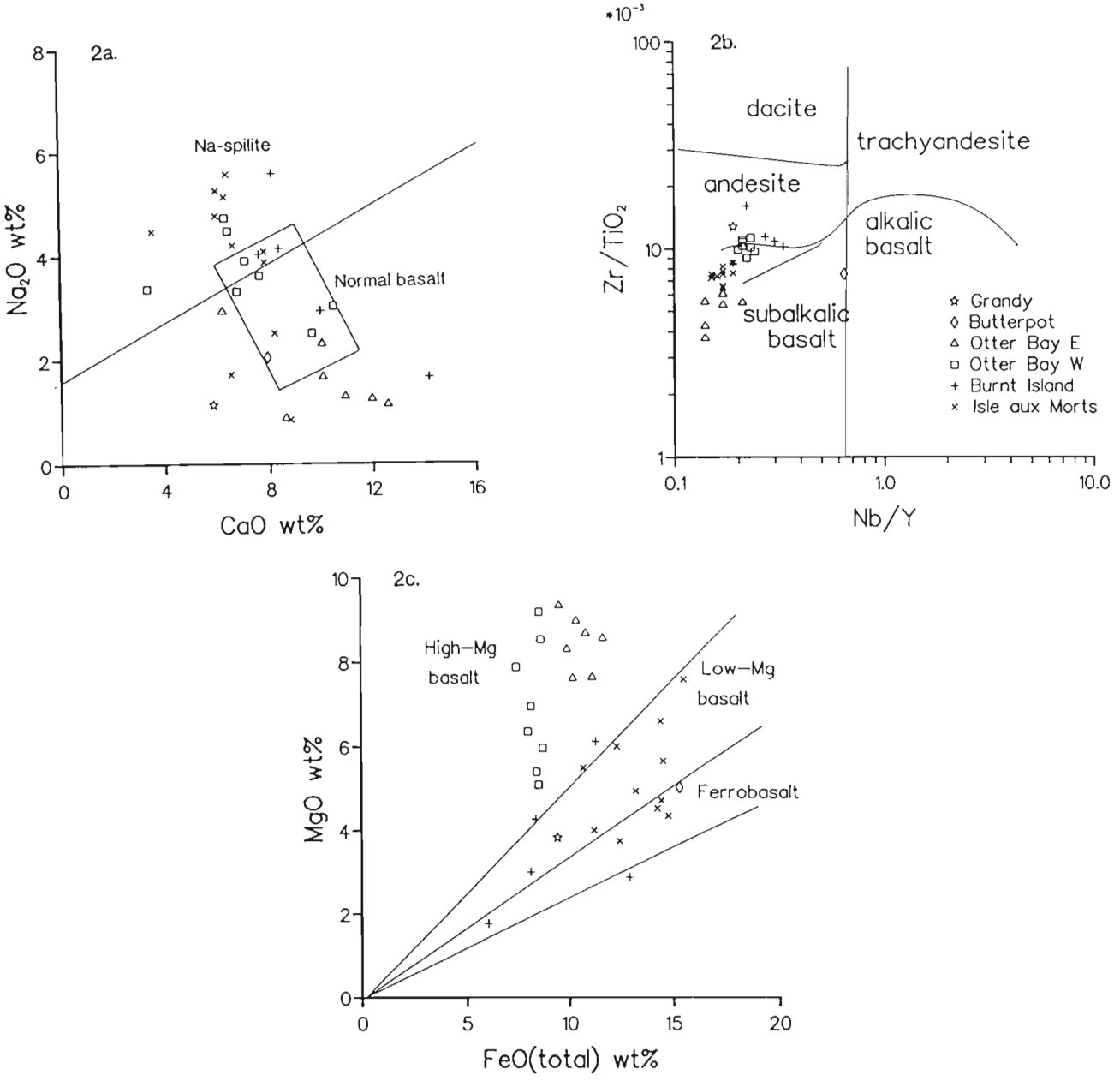

Figure 2. Major and trace element diagrams illustrating lithological characteristics of the data set. **a)** CaO-Na_2O binary plot. The diagonal line divides spillites from other basalts (Graham, 1976), and the rectangle outlines the field of normal unmodified basalt (Stillman and Williams, 1979). **b)** Nb/Y-Zr/TiO_2 classification diagram (Winchester and Floyd, 1977). **c)** FeO(total)-MgO diagram, discriminating groupings on the basis of composition, after Wood (1978).

(Graham, 1976; Fig. 2a). Most of the following chemical assessments therefore rely primarily on the high field strength group of trace elements (HFSE) which tend to be less mobile.

The metabasic rocks can be divided into six separate suites on basis of geographic distribution and chemistry (Fig. 2b, 2c, 3a, etc.). Besides the Isle aux Morts metabasalt, the Harbour le Cou Group contains two suites of intrusive amphibolites (Otter Bay amphibolites), localized respectively to the east and west of the Otter Bay lineament (OBL in Fig. 1). At the head of God Bay, near Burnt Islands is an extensive suite of pillowed metabasalts, while isolated metabasites from Butterpot Hill and Grandy Sound are different from all other metabasalts (Fig. 1). On a Nb/Y-Zr/TiO_2 classification diagram (Winchester and Floyd, 1977) almost all the metabasic rocks plot as subalkalic basalt (Fig. 2b). On this diagram and many succeeding diagrams both the Isle aux Morts metabasalt and other amphibolite suites plot in compact groupings. On a FeO(total)-MgO diagram (Wood, 1978) the Isle aux Morts metabasalt plot as low-Mg basalts and ferrobasalts, while most other amphibolites in the Harbour Le Cou Group plot as high-Mg basalts (Fig. 2c).

The high concentrations of HFSE serve to distinguish the Isle aux Morts metabasalt from all the amphibolites west of the Otter Bay lineament (Fig. 3a). Only two metabasites, collected near Butterpot Hill and north of Grandy Sound

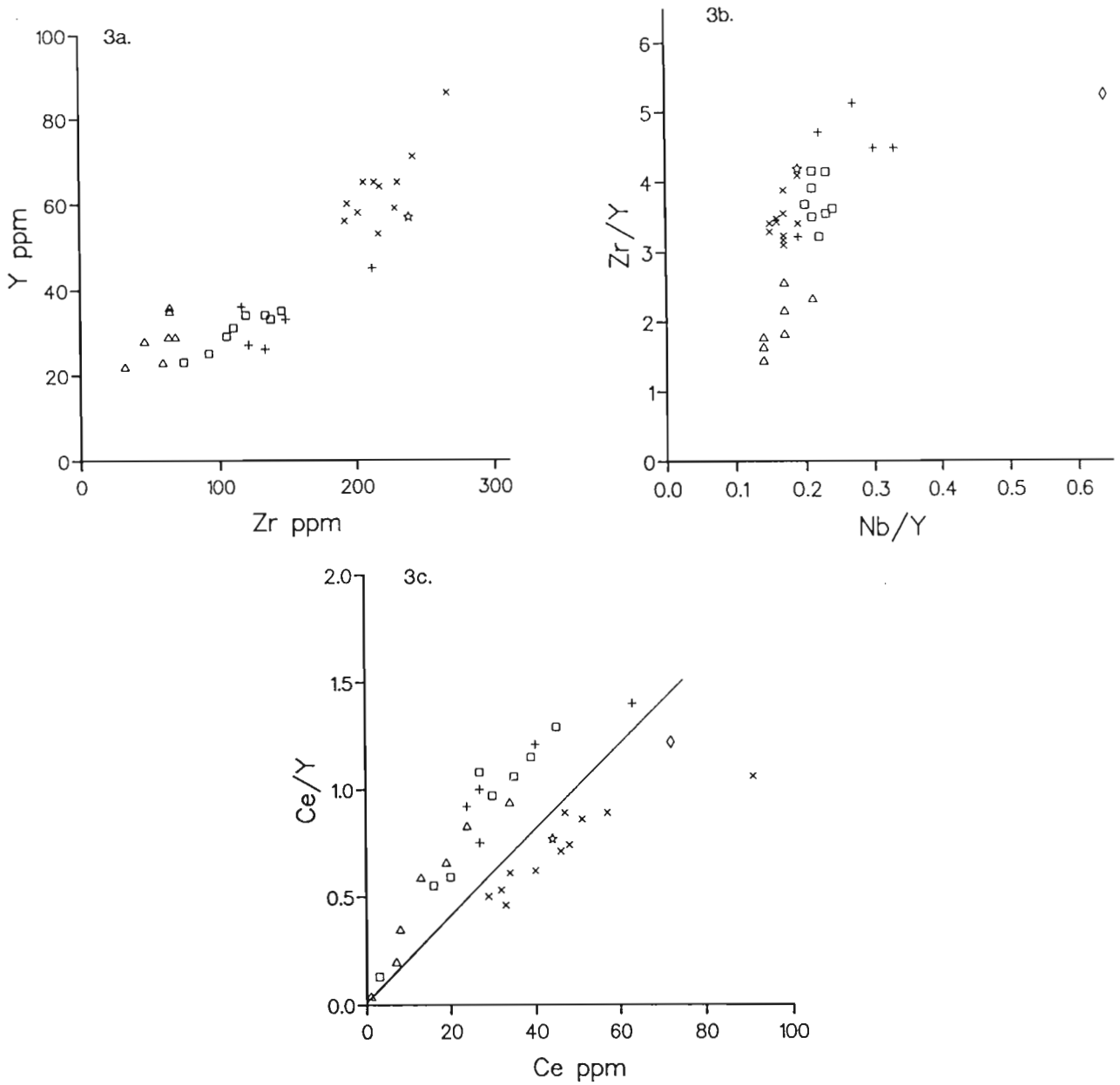

Figure 3. Binary trace element discriminant diagrams ditinguishing metabasic suites. **a)** Zr-Y; **b)** Nb/Y-Zr/Y; **c)** Ce-Ce/Y. Ornament as in Figure 2b.

(Fig. 1) have comparable HFSE contents to the Isle aux Morts metabasalt. As these samples were collected well to the east of the other Otter Bay amphibolites and have different Ti, Zr, and V concentrations (Table 1b), they probably represent unrelated metabasite suites. On a Zr-Y diagram the Otter Bay amphibolites show a bimodal distribution: those with Zr/Y ratios comparable to the Isle aux Morts metabasalt were collected between the Isle aux Morts fault zone and Otter Bay lineament, whereas those with a lower Zr/Y ratio were obtained to the east of the Otter Bay lineament. A Nb/Y-Zr/Y diagram (Fig. 3b) clearly separates the Otter Bay east amphibolites and Butterpot Hill amphibolite from the other amphibolite suites, while a Ce-Ce/Y diagram shows that the Isle aux Morts metabasalt are distinct from the Otter Bay and Burnt Island amphibolites (Fig. 3c). Further support is given by a plot on a Y-Cr diagram of Pearce (1982) (Fig. 4b), which shows that the Isle aux Morts metabasalt defines a trend separate from both suites of amphibolite intrusions in the Harbour le Cou Group. The Isle aux Morts metabasalt could be derived by 5% fusion of a plagioclase lherzolite source, whereas the other suites are characterised by lower Y contents, indicating a higher degree of partial melting. Confirmation of the tholeiitic nature of the magmatism is provided by a Ti-V discriminant diagram (Shervais, 1982) (Fig. 4c).

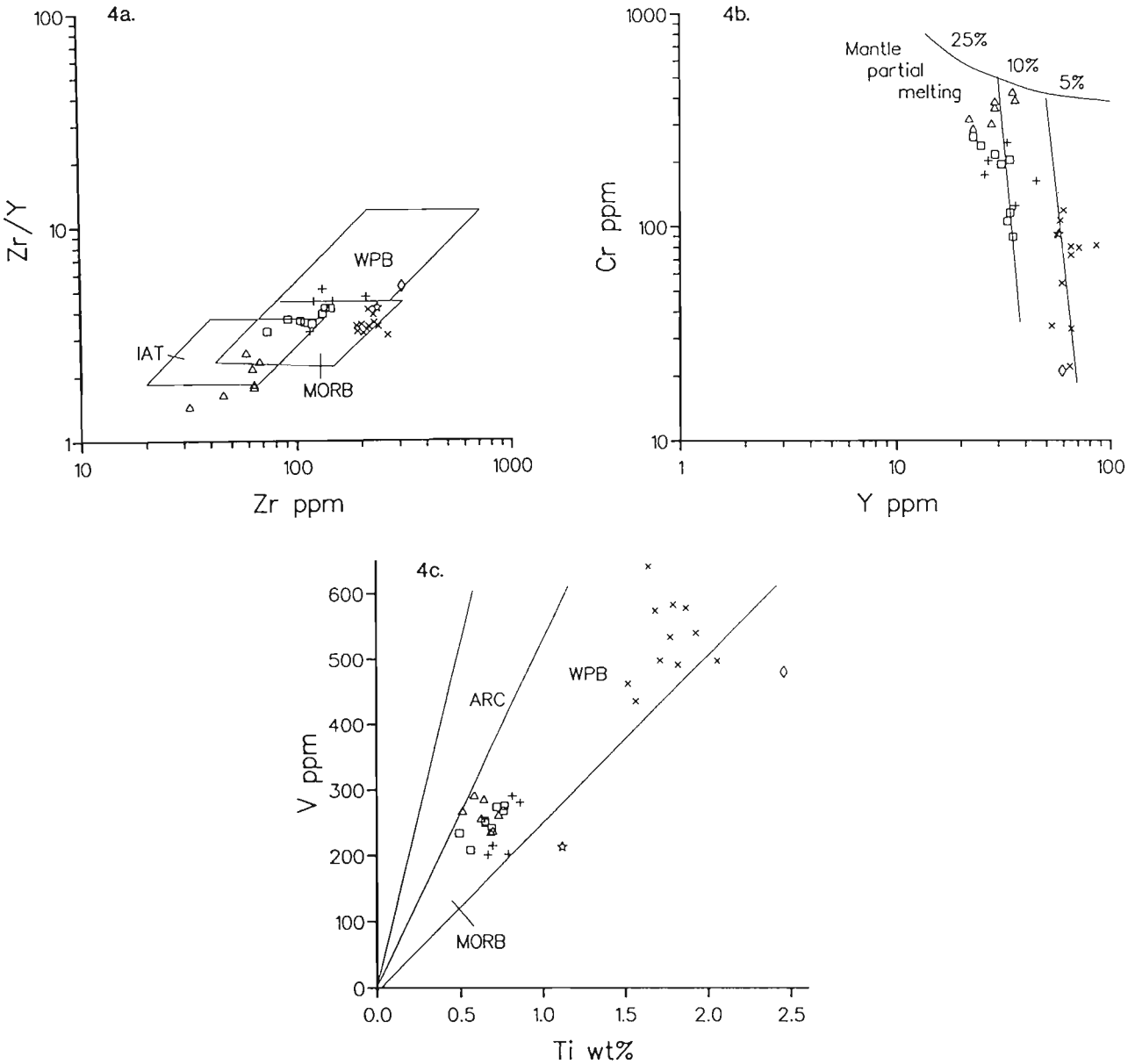

Figure 4. Binary diagrams suggesting tectonic setting. **a)** Zr-Zr/Y diagram after Pearce and Norry (1979); **b)** Y-Cr diagram after Pearce (1982); **c)** Ti-V diagram after Shervais (1982). Ornament as in Figure 2b.

TECTONIC SETTING OF THE ISLE AUX MORTS METABASALT

Element ratios plotted on a Zr-Zr/Y discriminant diagram (Pearce and Norry, 1979) place the Isle aux Morts metabasalt within the MORB field (Fig. 4a). Such a classification is consistent with a model in which the Isle aux Morts metabasalt represents a fault bounded sliver of evolved oceanic volcanic rocks. This model requires that the relationships between the Isle aux Morts metabasalt and the underlying metasediments is not stratigraphic. This latter requirement of the model cannot be tested adequately since the state of strain of the rocks does not allow us to discriminate between tectonically modified stratigraphic or completely allochtonous contacts. Alternatively the Isle aux Morts metabasalt represents the product of uncontaminated continental tholeiitic magmatism initiated during the formation of an extended continental margin prior to the magmatism responsible for the metabasites in the Harbour le Cou Group.

CONCLUSIONS

The Isle aux Morts metabasalt are a previously undescribed suite of evolved tholeiitic pillow basalts, in faulted contact with the Harbour le Cou Group metasediments. Their chemistry shows that they are not related to any of the above-described amphibolite suites in the Harbour le Cou Group, suggesting they are exotic. More work is necessary to test whether the Isle aux Morts metabasalt are related to a phase of continental tholeiitic magmatism or represent a tectonic sliver of exotic oceanic crust.

REFERENCES

Brown, P.A.
1976: Geology of the Rose Blanche map-area (110/11); Newfoundland Department of Mines and Energy, Mineral Development Division, Report 76-5, 16 p.
1977: Geology of the Port aux Basques map-area (110/10), Newfoundland; Newfoundland Department of Mines and Energy, Mineral Development Division, Report 77-2, 11 p.

Colman-Sadd, S.P., Hayes, J.P., and Knight, I.
1990: Geology of the Island of Newfoundland; Map 90-01, Geological Survey Branch, Department of Mines and Energy, Government of Newfoundland and Labrador.

Graham, C.M.
1976: Petrochemistry and tectonic significance of Dalradian metabasaltic rocks of the SW Scottish Highlands; Journal of the Geological Society, London, v. 132, p. 61-84.

Lin S., van Staal, C.R., and Lee, C.
1993: The Harbour le Cou Group and its correlation with the Bay du Nord Group, southwestern Newfoundland; in Current Research, Part D; Geological Survey of Canada, Paper 93-1D.

Pearce, J.A.
1982: Trace element characteristics of lavas from destructive plate boundaries; in Andesites: orogenic andesites and related rocks; (ed.) R.S. Thorpe; John Wiley & Sons, Chichester, United Kingdom, p. 525-548.

Pearce, J.A. and Norry, M.G.
1979: Petrogenetic implications of Ti, Zr, Y, and Nb variations in volcanic rocks; Contribution to Mineralogy and Petrology, v. 69, p. 241-254.

Shervais, J.W.
1982: Ti-V plots and the petrogenesis of modern and ophiolitic lavas; Earth and Planetry Science Letters, v. 59, p. 101-118.

Stillman, C.J. and Williams, C.T.
1979: Geochemistry and tectonic setting of some volcanic rocks in east and southeast Ireland; Earth and Planetary Science Letters, v. 41, p.288-310.

van Staal, C.R., Burgess, J.L., Hall, L., Lee, C., Lin, S., and Schofield, D.I.
in press: Geology of the Port aux Basques-Rose Blanche area (NTS 11-0/10 & 11-0/11); in Report of Activities 1992, Newfoundland Department of Mines and Energy, Geological Survey Branch.

van Staal, C.R., Winchester, J.A., Brown, M., and Burgess, J.L.
1992: A reconnaissance geotraverse through southwestern Newfoundland; in Current Research, Part D; Geological Survey of Canada, Paper 92-1D, p.133-143.

Williams, H., Colman-Sadd, S.P., and Swinden, H.S.
1988 Tectonic-stratigraphic subdivisions of central Newfoundland; in Current Research, Part B; Geological Survey of Canada, Paper 88-1B, p.91-98.

Winchester, J.A. and Floyd, P.A.
1977: Geochemical discrimination of different magma series and their differentiation products using immobile elements; Chemical Geology, v. 20, p. 325-343.

Wood, D.A.
1978: Major and trace element variations in the Tertiary lavas of eastern Iceland and their significance with respect to the Iceland Geochemical Anomaly; Journal of Petrology, v. 19, p. 393-436.

Geological Survey of Canada Project 730044

Pressure-temperature conditions and a P-T path for the Port aux Basques area, southwest Newfoundland[1]

Jerry L. Burgess[2], Michael Brown[2], and Cees R. van Staal
Continental Geoscience Division

Burgess, J.L., Brown, M., and van Staal, C.R., 1993: Pressure-temperature conditions and a P-T path for the Port aux Basques area, southwest Newfoundland; in Current Research, Part D; Geological Survey of Canada, Paper 93-1D, p. 47-55.

Abstract: Polyphase (D_1-D_3) deformed psammitic and pelitic gneisses of the Port aux Basques area in southwestern Newfoundland experienced amphibolite facies metamorphism during D_1 and D_2. Metamorphism and D_1-D_2 deformation are attributed to a Silurian crustal thickening event.

Microstructural relationships show that D_1-D_2 kyanite is replaced by late syn-D_2 sillimanite. Several mineral zones have been mapped. They include a kyanite zone, a lower sillimanite zone, and an upper sillimanite zone. The sillimanite-in and staurolite-out isograds define the boundaries between the kyanite and lower sillimanite zones, and lower and upper sillimanite zones respectively. Kyanite locally persists metastably in the lower sillimanite zone. Isograd surfaces related to syn-D_2 metamorphism were folded by F_3 into antiforms and synforms, and initially were probably subhorizontal. Pressure-temperature paths for rocks of the Port aux Basques area are clockwise in pressure-temperature space with peak temperatures of 650 ± 50°C at pressures in the range of 6-9 kbar.

Résumé : Les gneiss psammitiques et pélitiques qui ont subi une déformation polyphasée (D_1-D_3), et sont situés dans la région de Port aux Basques dans le sud-ouest de Terre-Neuve, ont été métamorphisés dans le faciès des amphibolites au cours de D_1 et D_2. Le métamorphisme et la déformation D_1-D_2 sont attribués à un épisode silurien d'épaississement de la croûte.

Les relations microstructurales montrent que la cyanite D_1-D_2 a été remplacée par de la sillimanite tardive à l'époque de D_2. Plusieurs zones minérales ont été cartographiées. Elles comprennent une zone de la cyanite, une zone inférieure de la sillimanite et une zone supérieure de la sillimanite. Les isogrades de l'apparition de la sillimanite et de la disparition de la staurolite définissent, respectivement, les limites, d'une part de la zone de la cyanite et de la zone inférieure de la sillimanite et, d'autre part des zones inférieure et supérieure de la sillimanite. La cyanite persiste par endroits à l'état métastable dans la zone inférieure de la sillimanite. Les surfaces isogrades associées au métamorphisme contemporain de D_2 ont été plissées par F_3, en donnant des antiformes et des synformes, et étaient sans doute initialement subhorizontales. Les cheminements pressions-températures des roches de la région de Port aux Basques sont dirigés dextrorsum dans l'espace pressions-températures, les températures maximales étant de 650 ± 50°C aux pressions de l'ordre de 6 à 9 kbar.

[1] Contribution to Canada-Newfoundland Cooperation Agreement on Mineral Development 1990-1994, subsidiary agreement under the Economic and Regional Development Agreement. Project funded by the Geological Survey of Canada.

[2] Department of Geology, University of Maryland at College Park, MD 20742 USA

INTRODUCTION

The geology of southwestern Newfoundland is characterized by orthogneiss of the Cape Ray Igneous Complex (CRIC), volcanic and sedimentary rocks of the Windsor Point Group, and amphibolite facies metasedimentary and meta-igneous rocks in the area between Grand Bay and east of Harbour le Cou. Tectonostratigraphic characterization and regional correlation of these high-grade rocks has become increasingly important because of the recognition of Silurian orogenesis in the Northern Appalachians. A multi-disciplinary geological investigation is being undertaken to better characterize the structural and metamorphic history of the Central Mobile Belt in southwestern Newfoundland. This report focuses on the relationship between staurolite- and kyanite-bearing rocks near Grand Bay and the sillimanite-bearing rocks to the east near Port aux Basques.

REGIONAL SETTING

The metamorphic rocks that occur between Grand Bay and Rose Blanche were informally called the Port aux Basques complex (van Staal et al., 1992a). This name and its subdivisions have been abandoned and a more formal and geologically meaningful nomenclature has been introduced (van Staal et al., 1992b) The Grand Bay Complex (GBC) includes those rocks that lie between the Cape Ray Fault Zone and the Grand Bay Thrust. The Port aux Basques Complex (PaBC) comprises rocks east of the Grand Bay Thrust to the Isle aux Morts Fault Zone. All supracrustal rocks between the Isle aux Morts Fault Zone and the Bay le Moine Fault have been combined into the Harbour le Cou Group (HlCG; Lin et al., 1993) (see Fig. 1).

Three episodes of penetrative deformation are present within each of the Grand Bay Complex, Port aux Basques Complex and Harbour le Cou Group. Isoclinal folds (F_1) and an axial planar schistosity (S_1) are overprinted by D_2 tight to isoclinal folds (F_2) and a differentiated crenulation cleavage (S_2), which is generally a penetrative schistosity as a result of advanced transposition of S_1. Therefore, the dominant schistosity is generally a composite foliation of S_1 and S_2 in orthogneisses and S_0, S_1, and S_2 in metasedimentary rocks. Unless otherwise specified, S_2 in the rest of the paper refers to this composite foliation. The northeast structural grain of the area is caused by D_3 structures, which have folded recumbent D_2 structures into a series of decametre to kilometre scale, upright to steeply inclined, commonly gently plunging open to tight noncylindrical folds (F_3). The intensity of D_3 varies throughout the area. In zones of lower D_3 strain, F_3 folds are open to tight and generally no penetrative S_3 foliation is developed. In other areas, particularly where D_3 strain is relatively high, F_3 is accompanied by a well developed S_3 crenulation cleavage and F_2 and F_3 folds cannot be separated on the basis of style alone. Voluminous syn-D_2 granitoid bodies permeate the area (van Staal et al., 1992b).

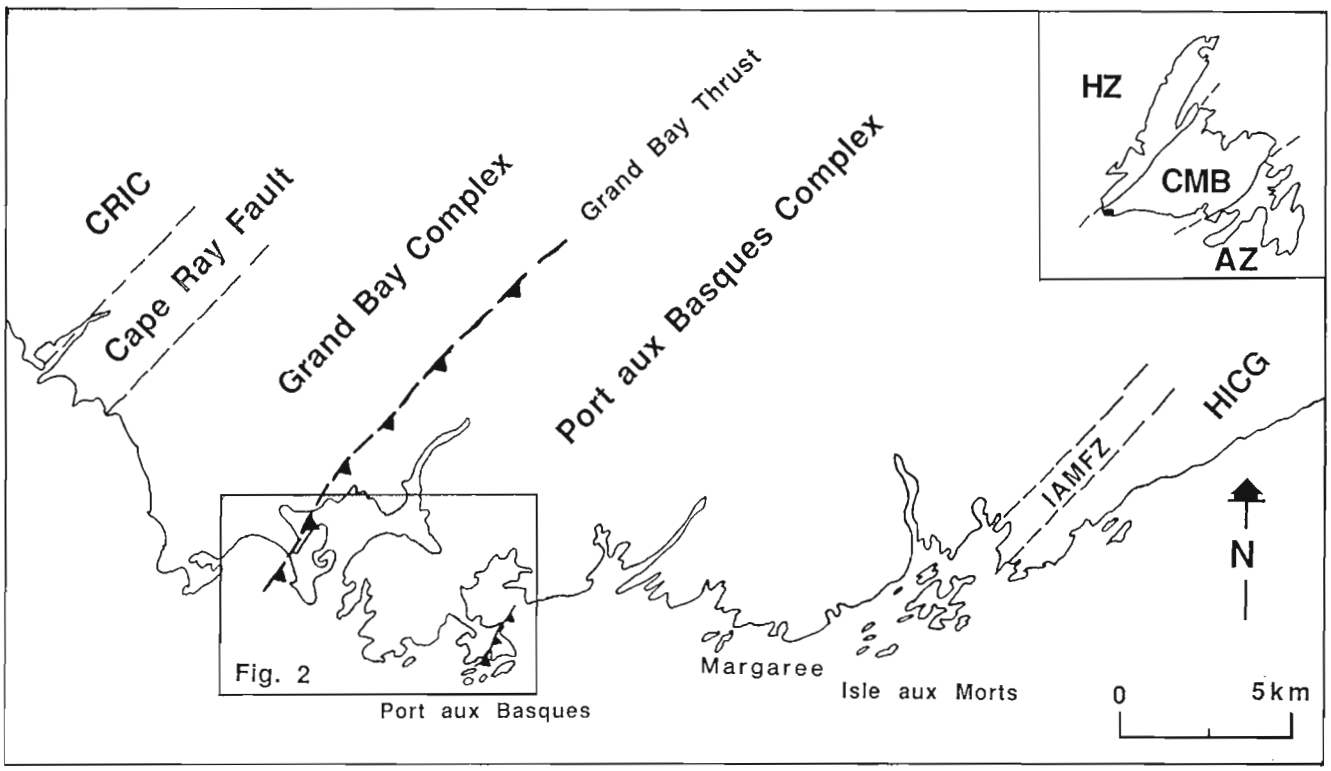

Figure 1. Index map of the Port aux Basques area, Newfoundland. HZ, Humber Zone; CMB, Central Mobile Belt; AZ, Avalon Zone; CRIC, Cape Ray Igneous Complex; IAMFZ, Isle aux Morts Fault Zone; HICG, Harbour le Cou Group.

Metamorphic conditions in the area increase from kyanite-bearing assemblages in the Grand Bay Complex to sillimanite-bearing assemblages in the Port aux Basques Complex and the Harbour le Cou Group. An assemblage that includes sillimanite and alkali-feldspar occurs around the village of Margaree. Evidence presented in this report and elsewhere (Burgess et al., 1992) demonstrates that peak conditions were reached during D_2. Where D_3 strain was relatively high, marked retrogression generally occurred.

ISOGRAD DISTRIBUTION

Systematic mapping of mineral assemblages at several hundred localities during the summer of 1992 resulted in the refinement of isograds mapped during 1991 (Fig. 2). Kyanite and staurolite are present throughout the Grand Bay Complex and no isograd for the first appearance of these minerals can be drawn (cf. Burgess et al., 1992). Identified isograds and assemblage zones are restricted to the Port aux Basques Complex. Isograds include the kyanite to sillimanite polymorphic reaction, a staurolite-out isograd and the first appearance of clinopyroxene in metabasic rocks (Fig. 2). Existence of the latter isograd was not noted before. Mineral zones comprise a kyanite zone, a lower sillimanite zone and an upper sillimanite zone. In the kyanite zone, pelitic rocks contain the assemblage kyanite+staurolite+garnet+biotite+muscovite+quartz+plagioclase. In the lower sillimanite zone, pelites consist of sillimanite (±metastable kyanite)+staurolite+garnet+biotite+muscovite+quartz+plagioclase. The upper sillimanite zone differs from the lower sillimanite zone in that kyanite and staurolite are absent. The staurolite-out isograd thus defines the boundary between the lower and upper sillimanite zones.

Staurolite- and kyanite-bearing assemblages are ubiquitous for rocks of pelitic composition in the Grand Bay Complex; sillimanite- and garnet-bearing assemblages characterize most of the Harbour le Cou Group. The distribution of these mineral assemblages and the isograd distribution thus indicates a regional increase in metamorphic grade to the east.

Isograds were previously regarded as lying parallel to the regional gneissic layering (Brown, 1973, Burgess et al., 1992). However, the geometry of the isograds, as mapped by

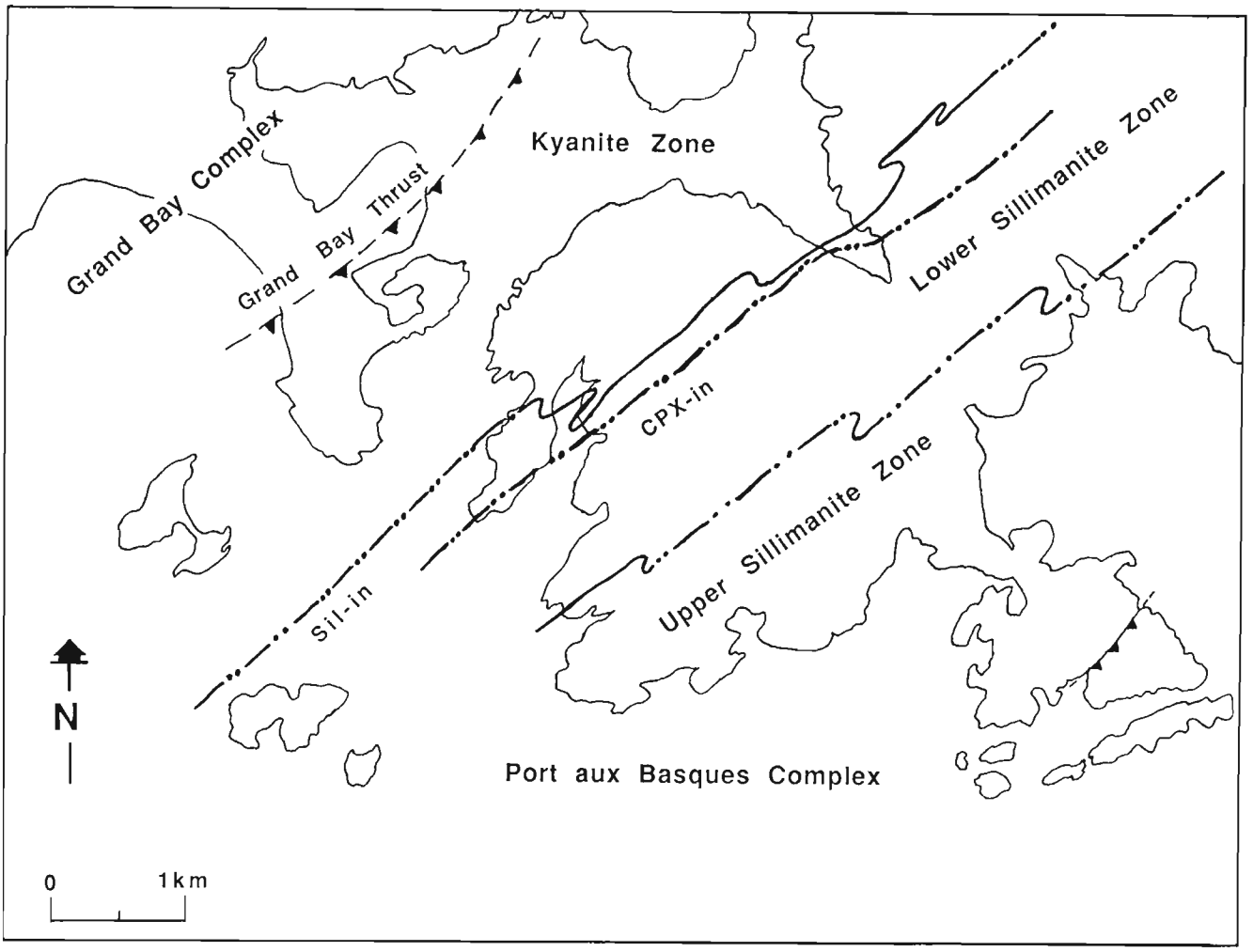

Figure 2. Map of the region surrounding the town of Port aux Basques, showing major lithotectonical units, isograds, and mineral zones.

us this summer (Fig. 2), indicates that they are probably folded. Peak metamorphism occurred late during D_2 (see below) and isograd surfaces are related to syn-D_2 metamorphism.

MICROSTRUCTURES AND TEXTURES

A major part of this study involves the relationship between porphyroblast growth and deformation. Garnet-staurolite-kyanite-bearing metapelites are present in the Grand Bay Complex and western Port aux Basques Complex; metapelites in the eastern Port aux Basques Complex and the Harbour le Cou Group are dominated by garnet-sillimanite-bearing assemblages. The dominant S_2 foliation in the metapelites is defined mainly by biotite and muscovite laths. It is generally accompanied by a mineral lineation defined by the long dimensions of kyanite and sillimanite. The metamorphism is of an intermediate pressure type with a sequence of mineral assemblages similar to the high-grade zones of Barrovian sequences. Porphyroblasts in pelites record several growth stages (Burgess et al., 1992).

The cores of garnet porphyroblasts locally preserve sinuous inclusion trails (S_1) that are oblique to the S_2 foliation in the matrix. These garnets may also display an inclusion-poor rim that separates the core with the inclusion trails from the matrix with the discordant external S_2 fabric. The age of growth of small idioblastic garnets that occur in the matrix are difficult to ascertain, although garnets of comparable size, shape, and composition occur in early- syn-D_2 kyanite or staurolite porphyroblasts, suggesting that they grew before D_2. Therefore, garnet porphyroblasts probably grew syn-D_1 and/or between D_1 and D_2, and possibly during the D_2 event (see also Burgess et al., 1992). The age relationships between staurolite or kyanite grains is locally difficult to ascertain; they are locally intergrown with each other, but elsewhere each includes the other, suggesting that both grew at the same time. Both minerals are wrapped by the S_2 schistosity and kyanite is folded by F_3 (Fig. 3). Kyanite contains quartz inclusion trails (S_1) which curve at the end into the S_2 fabric, which combined with the presence of kyanite inclusions inside early syn-D_2 staurolite (Burgess et al., 1992), suggests early syn-D_2 growth of at least some of the kyanite. Kyanite in one outcrop is folded by F_2, suggesting that some kyanite grew late during D_1 or in the interval between D_1 and D_2.

Anastomosing folia of sillimanite are commonly a major constituent of the S_2 fabric. Sillimanite also occurs as undeformed radiating aggregates that partially pseudomorph kyanite. In addition, sillimanite is present as inclusions in large, late muscovites that crosscut the S_2 fabric (Fig. 4). These different modes of occurrence of sillimanite occur

Figure 3. Kyanite folded by small-scale F_3 folds, Port aux Basques Complex.

Figure 4. Photomicrograph showing sillimanite inclusions in large muscovites that crosscut the S_2 fabric. Long dimension of field of view is 3 mm.

locally in the same rock. Rather than inferring separate growth stages for sillimanite in these rocks, we interpret the sillimanite to be syndeformational. If correct, it implies that the deformation is partitioned into high and low strain zones on the scale of an individual thin section, as suggested by Vernon (1975, 1987). Sillimanite is folded by F_3 (Fig. 5 and 6) and yet also defines a mineral lineation parallel to L_3 (Fig. 7) within S_3 (Fig. 8) This sillimanite curves into the S_3 orientation and is interpreted to have been rotated into the S_3 plane by fibre sliding. This rotation may have been accompanied by some recrystallization, implying that sillimanite was still stable during early D_3. The syn-D_1 sillimanite identified by Burgess et al. (1992) is now regarded as syn-D_2. The evidence for D_1 sillimanite was based on the assumption that the matrix foliation of the sample (see Fig. 12 of Burgess et al., 1992) was S_2; it is now known to be S_3. Therefore, sillimanite probably grew syn- to post-D_2 and probably early syn-D_3.

A preferred dimensional orientation of hornblende defines S_2 and L_2 in the amphibolites. A second generation of hornblende obliquely crosscuts the L_2,S_2 fabric and defines L_3. Garnet and clinopyroxene porphyroblasts are wrapped by the S_2 fabric, while some garnets contain inclusion trails of the earlier S_1 fabric. Garnet and clinopyroxene are therefore interpreted to have grown before the end of D_2. Blue-green hornblende occurs in amphibolites of the Grand Bay Complex. In general, hornblende becomes more greenish brown to the east and hornblende from rare amphibolites of the Harbour le Cou Group west of Burnt Island is brown.

A penetrative S_3 foliation (Fig. 5 and 8) is present in zones of relatively high-D_3 strain. Such zones are generally characterised by marked effects of retrogression. Porphyroblasts of garnet display embayed grain boundaries and partial replacement by chlorite indicating that metamorphic conditions during D_3 were in general lower compared to those accompanying D_2. Nevertheless, conditions appear to have remained in the sillimanite stability field during the early stages of D_3.

Microstructural evidence indicates that most porphyroblasts characteristic of peak conditions grew during D_2. Some kyanite may have grown during D_1. Therefore, D_2 and probably the bulk of D_1 structures were accompanied by syntectonic amphibolite facies metamorphism. The highest temperature condition appears to have been reached late during D_2. These general microstructural relations hold for the Grand Bay Complex and Harbour le Cou Group as well.

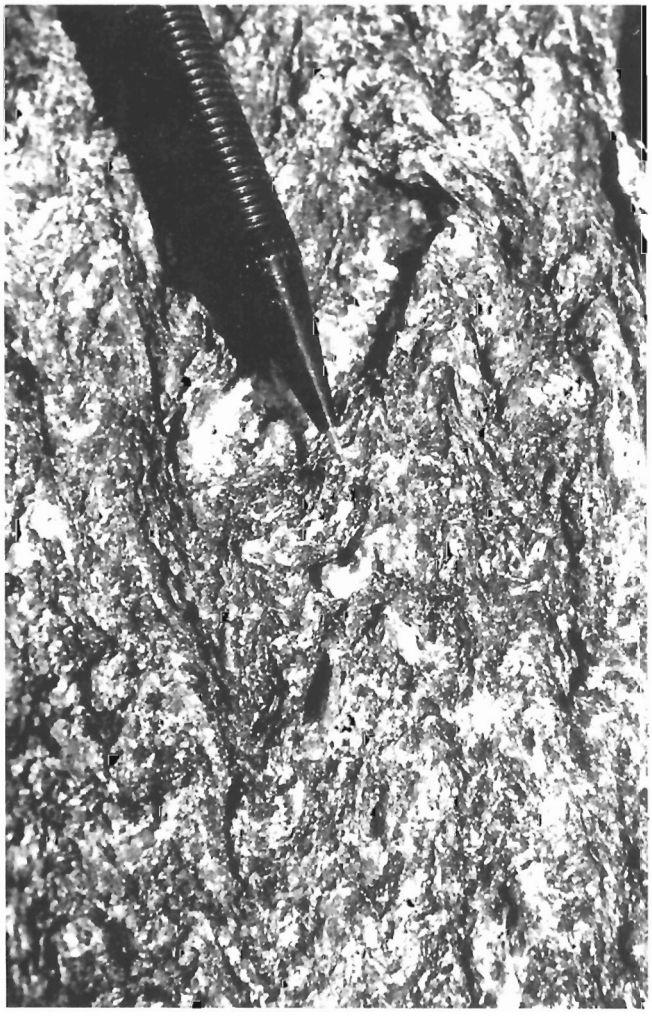

Figure 5. Syn-D_2 sillimanite overprinted by S_3 crenulation cleavage.

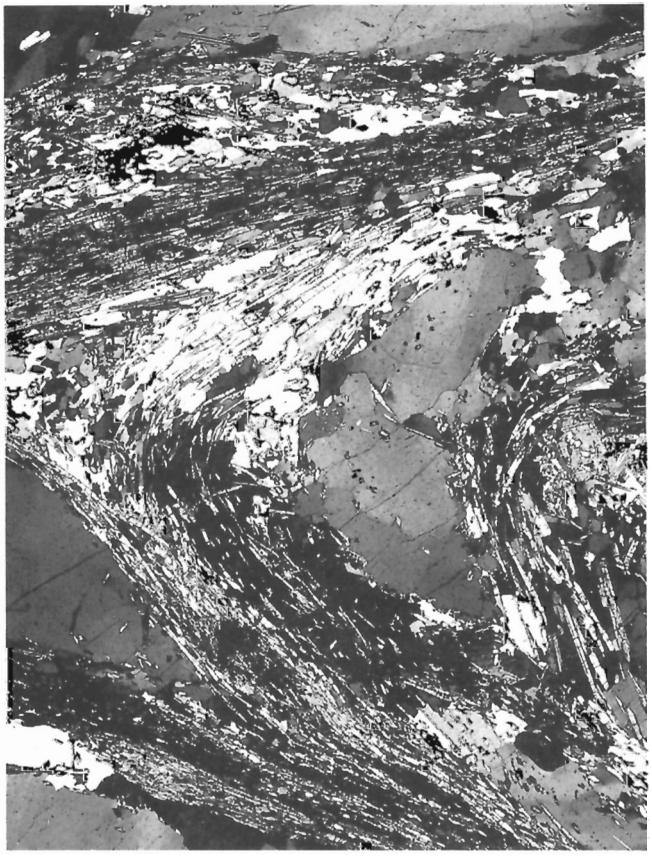

Figure 6. Photomicrograph showing S_2 sillimanite folded by F_3, Port aux Basques Complex. Long dimension of field of view is 7 mm.

Kyanite growth always predated F_3 and sillimanite was always syn- to post-D_2 and folded by F_3. Since the deformational sequence and microstructural relationships are the same in each of the rock units described above and it seems likely that their metamorphic histories are related to the same orogenic event.

PHASE ASSEMBLAGES AND MINERAL REACTIONS

Pelitic rocks of the Port aux Basques Complex are characterized by the following mineral assemblages (mineral abbreviations from Kretz, 1983): Grt+Ky+Ms+Bt; Grt+St+Ms+Bt; Grt+St+Ky+Ms+Bt; Sil+Ky+St+Grt+Ms+Bt; Sil+Ky+Grt+Ms+Bt; Sil+Grt+Ms+Bt; Sil+Grt+Kfs+Bt. All assemblages include plagioclase and quartz.

As the sillimanite isograd is approached, staurolite becomes gradually less abundant and decreases in grain size. The following two model reactions are inferred to relate the kyanite zone with the lower sillimanite zone: Ky = Sil (1) and St+Ms+Qtz = Sil+Grt+Bt (2). In the lower sillimanite zone a more marked decrease in grain size of staurolite is apparent, further indicating that staurolite is being reacted out. Close to the staurolite-out isograd, staurolite becomes less abundant and at the isograd only occurs as inclusions or armoured relics surrounded by plagioclase or muscovite.

Figure 9 represents the lower sillimanite zone, where the staurolite composition of sample PaB91-PRBE plots in the Sil-Bt-Grt field and reacts via reaction 2. This reaction is discontinuous in the end member KFMASH system and persistence of staurolite may be due to the effects of non-KFMASH components (Rumble, 1978). The upper sillimanite zone starts where reaction 2 has gone to completion.

The highest grade assemblage (Sil+Grt+Kfs) occurs in migmatitic rocks near the village of Margaree (Fig. 1). Muscovite is rare or absent in these rocks, probably because it was used up in the K-feldspar-producing reaction: Ms+Qtz = Sil+Kfs+Melt (3).

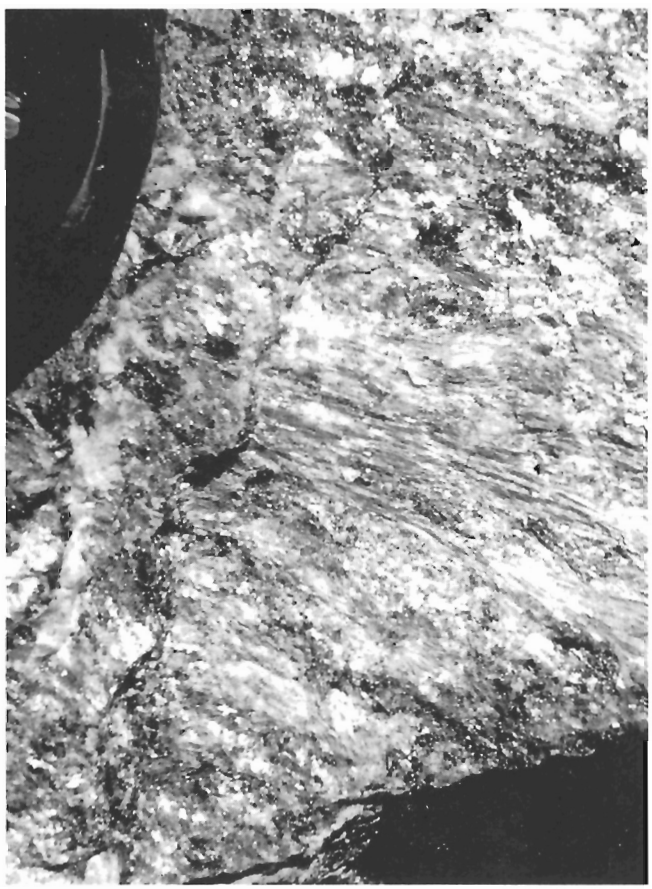

Figure 7. Sillimanite prisms defining L_3 lineation.

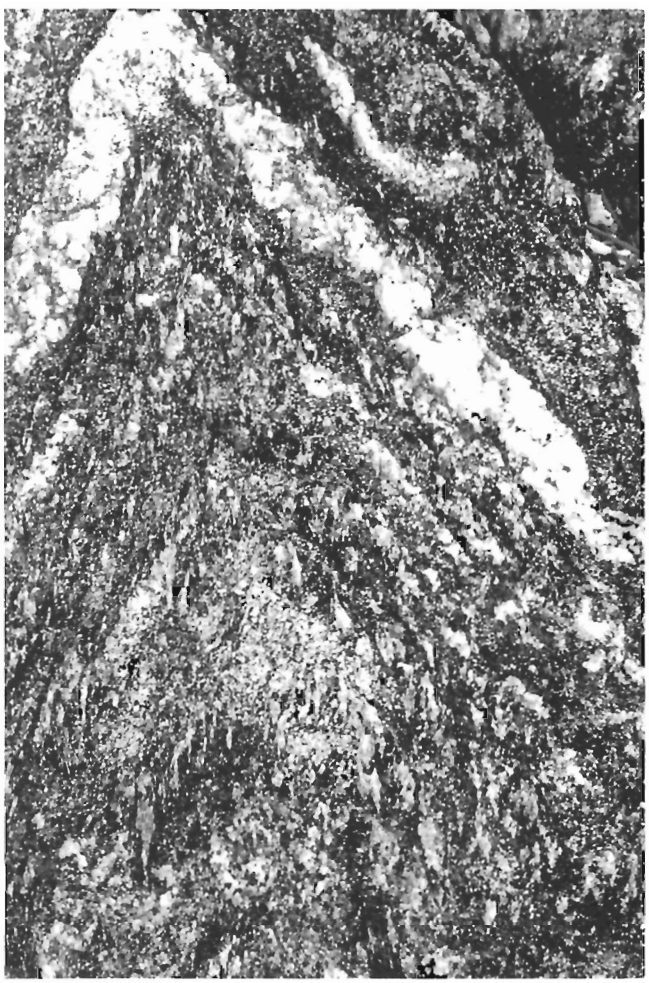

Figure 8. S_2 sillimanite and migmatitic layering tightly folded by F_3 such that the long dimension of sillimanite is approximately parallel to the S_3 axial plane cleavage to F_3 folds. Short dimension of field of view is 20 cm.

CONDITIONS OF METAMORPHISM

Variation of temperatures and pressures across the present erosional surface have been estimated by one of, or a combination of, phase assemblages, geothermobarometric data, and field evidence such as the development of migmatites.

Pelites of the Grand Bay Complex are relatively sparse but usually contain the AFM (Ms) assemblage Grt+St+Ky+Bt, which places the rocks in bathozone 4 of Carmichael (1978). Using the key univariant curves of Spear and Cheney (1989), Thompson (1982), and the aluminum silicate triple point of Bohlen et al. (1991) (see Fig. 11), the metamorphic pressure is constrained between 4.2 and 8.2 kbar. Relatively high pressures of 6 to 8 kbar are indicated by the assemblage Ky+Hbl+St+Bt+Qtz+Pl with chlorite and white mica (Selverstone et al., 1984; Thompson and Leclair, 1987), which has been observed in a distinctive, but rare calc-pelite rock in the Grand Bay Complex. Prograde chloritoid or chlorite does not occur in the pelites, indicating temperatures above the stability field of these minerals. At the other extreme, migmatites are absent in the Grand Bay Complex so that if a hydrous vapor phase was present the rocks did not reach the wet granite solidus. Using the petrogenetic grid of Spear and Cheney (1989) to evaluate temperatures for the breakdown of chloritoid and chlorite we obtain temperatures in the range of 550-650°C at the pressures inferred above.

Kyanite is present throughout the Grand Bay Complex and in the eastern part of the Port aux Basques Complex, suggesting no large metamorphic discontinuity across the Grand Bay Thrust. In contrast to the Grand Bay Complex, evidence for partial melting is present throughout the Port aux Basques Complex in the form of migmatites characterized by leucosomes with thin biotite selvages (Burgess et al., 1992).

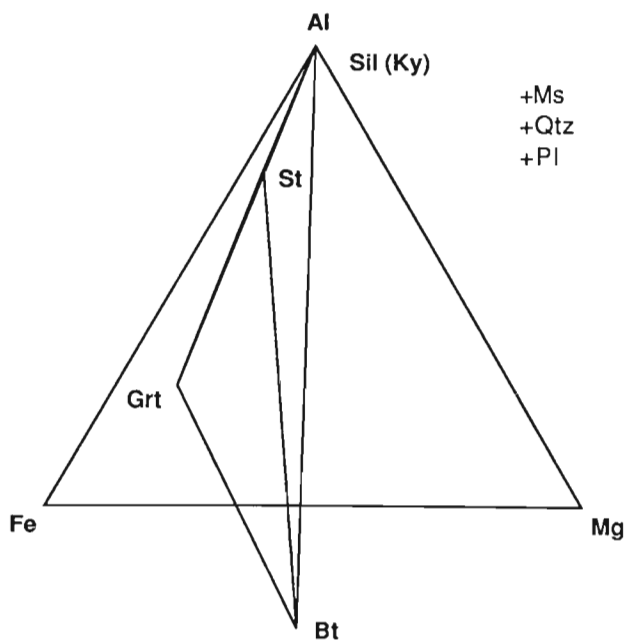

Figure 9. Thompson (1957) AFM diagram for sample PaB91-80, lower sillimanite zone.

However, this contrast does not necessarily reflect a major difference in metamorphic conditions across the Grand Bay Thrust, since it is possibly controlled by the availability of water.

The beginning of melting may have been initiated according to the model reaction: Or+Ab+Qtz+V = Melt (4). However, the leucosomes of some migmatites contain kyanite and garnet porphyroblasts in an assemblage with quartz and feldspar (Fig. 10). Kyanite porphyroblasts in the leucosome are relatively large compared with those in the matrix, whereas the garnet is skeletal. A more realistic melting reaction of the form: Ms+Bt+Qtz+V = Ky+Melt (5) probably is involved in the production of these migmatites. This model reaction in the KFMASH system was discussed by Vielzeuf and Holloway (1988); it has a steep positive slope with a minimum temperature in the kyanite field of around 730°C. The addition of an albitic component will shift this curve towards lower temperatures by approximately 100°C

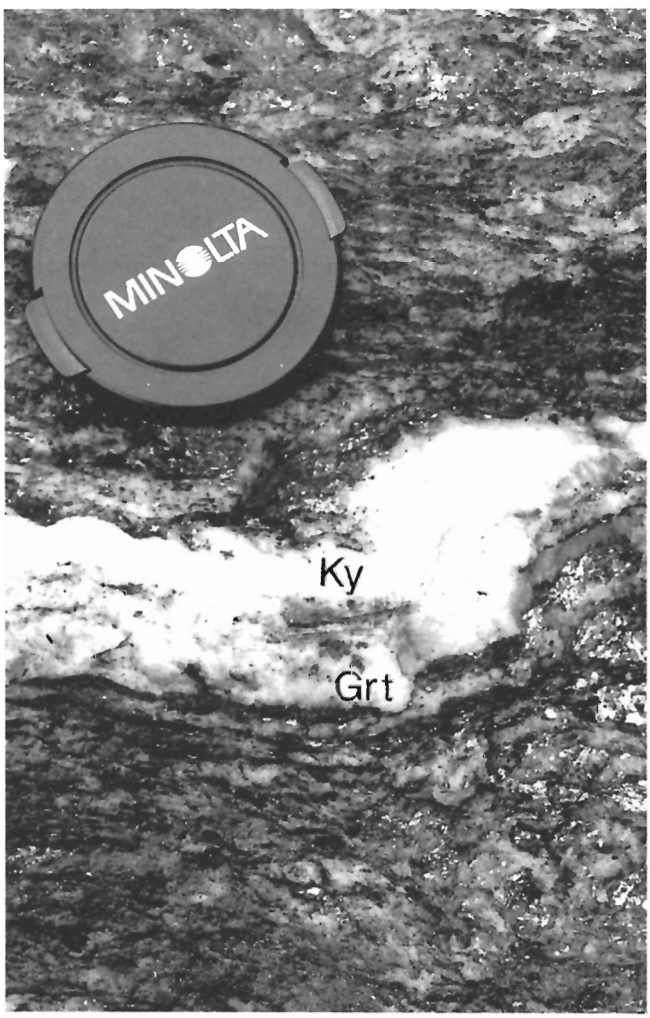

Figure 10. Kyanite prism (Ky – below and right of lens cap in leucosome) and skeletal garnet (Grt – below kyanite) within quartzo-feldspathic leucosome.

(Vielzeuf and Holloway, 1988), although this effect is moderated by the addition of an anorthite component (Thompson and Tracy, 1979).

Qualitative estimates of pressure and temperature for the Port aux Basques Complex may be obtained from the observation that the western part contains kyanite and staurolite, whereas sillimanite instead of kyanite occurs in the lower sillimanite zone. Therefore these rocks lie in bathozone 4 of Carmichael (1978), respectively in the kyanite and sillimanite fields, both beyond the granite minimum melting curve. Rocks of the upper sillimanite zone have reached or exceeded the staurolite breakdown reaction (3) and lie within bathozone 5 (P=8.2-9.5 kbar). Such conditions are consistent with the relatively high pressure assemblage Grt+Cpx+Qtz+Pl+Hbl (Bégin, 1992; Yardley, 1989) locally present in metabasic rocks of the lower and upper sillimanite zones.

Limited success has been obtained from geothermobarometry applied to mineral assemblages in pelites of the Port aux Basques Complex. This is probably due to post-peak diffusional processes and D_3 retrogression. However, the P-T estimates obtained from sample PRBE within the kyanite zone using the garnet-biotite thermometer of Ferry and Spear (1978) and the garnet-plagioclase-aluminum silicate-quartz baromometer of Hodges and Crowley (1985) are in the range of 625-690°C at 7-9 kbar, which are compatible with those deduced from the petrogenetic grid.

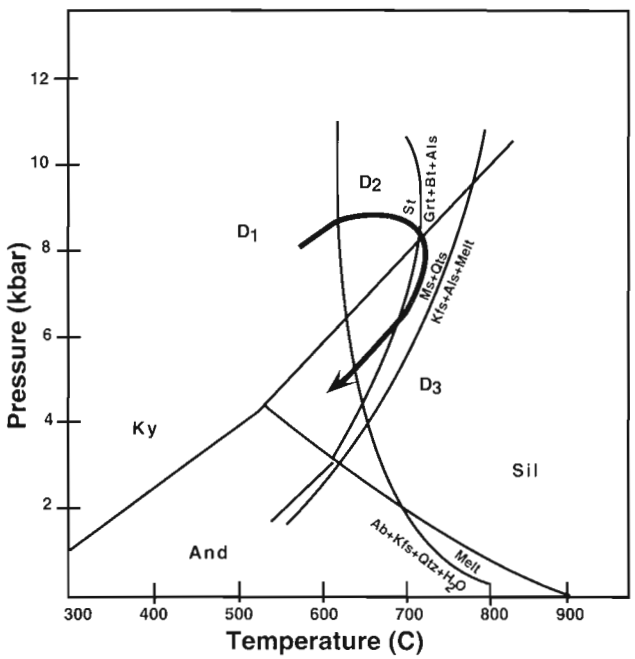

Figure 11. P-T diagram showing postulated P-T trajectory for the Port aux Basques Complex. The path is generalized and in reality consists of a nested family of P-T paths. The reaction St+Ms+Qtz = Grt+Bt+Als is from Spear and Cheney (1989). The reaction Ms+Qtz = Kfs+Als+Melt is from Thompson (1982). The reaction Ab+Kfs+Qtz+H2O = Melt is from Luth et al. (1964). The aluminum silicate (Als) triple point is from Bohlen et al. (1991).

Rocks of the Harbour le Cou Group have not been studied extensively, but the presence of sillimanite and garnet in pelites and brown hornblende in amphibolites indicates temperatures of at least 650°C at moderate pressures.

PRESSURE-TEMPERATURE DEFORMATION HISTORY

The D_1-D_2 kyanite to D_2 sillimanite transition suggests a clockwise trajectory in pressure-temperature space (Fig. 11). The present erosional surface reveals a partial Barrovian sequence typical of overthickened terranes. Such a metamorphic history is consistent with the style of deformation present in the rocks, since F_2 folds were probably recumbent prior to F3 folding (van Staal et al., 1992a) and at least locally were accompanied by thrusting (van Staal et al., 1992b). The clockwise path is therefore interpreted to be the result of a crustal thickening event, which took place in the Silurian (Dunning et al., 1990). Peak pressures and temperatures in the area were probably 650 ± 50°C in the range of 6-9 kbar. Retrogression accompanies D_3, which is thought to be related to transpression (van Staal et al., 1992a).

ACKNOWLEDGMENTS

John Percival and Shoufa Lin are thanked for critically reading this manuscript. Aletha Buschman, Nathalie Giroux, Lindsay Hall, Chris Lee, Shoufa Lin, Claudia Riveros, David Schofield, Katherine Venance, and John Winchester are thanked for their assistance and fruitful discussions in the field.

REFERENCES

Bégin, N.J.
1992: Contrasting mineral isograd sequences in metabasites of the Cape Smith Belt, northern Québec, Canada: three new bathograds for mafic rocks; Journal of Metamorphic Geology, v. 10, p. 685-704.

Bohlen, S.R., Montana, A., and Kerrick, D.M.
1991: Precise determinations of the equilibria kyanite = sillimanite and kyanite = andalusite and a revised triple point for Al_2SiO_5 polymorphs; American Mineralogist, v. 76, p. 677-680.

Brown, P.A.
1973: The structural and metamorphic history of the Port aux Basques region, Newfoundland; M.Sc. thesis, Department of Geology, Memorial University of Newfoundland, St. John's, Newfoundland.

Burgess, J.L., Brown, M., and van Staal, C.R.
1992: Preliminary report on the metamorphic geology of the Port aux Basques Complex, southwestern Newfoundland; in Current Research, Part D; Geological Survey of Canada, Paper 92-1D, p. 145-154.

Carmichael, D.M.
1978: Metamorphic bathozones and bathograds: a measure of the depth of post-metamorphic uplift and erosion on the regional scale; American Journal of Science, v. 278, p. 769-797.
1990: Metamorphism and geodynamics of the southwestern Grenville Province, Ontario, in International Geological Coorelation Program, Project 235-304, Field Trip 1 Guidebook, p. 27.

Dunning, G.R., O'Brian, S.J., Coleman-Sadd, S.P., Blackwood, R.F., Dickson, W.L., O'Neill, P.P., and Krogh, T.E.
1990: Silurian orogeny in the Newfoundland Appalachians; Journal of Geology, v. 98, p. 895-913.

Ferry, J.M. and Spear, F.S.
1978: Experimental calibration of the partitioning if Fe and Mg between biotite and garnet; Contributions to Mineralogy and Petrology, v. 66, p. 113-117.

Hodges, K.V. and Crowley, D.H.
1985: Error estimation and empirical geothermobarometry for pelitic systems; American Mineralogist, v. 70, p. 702-709.

Kretz, R.
1983: Symbols for rock-forming minerals; American Mineralogist, v. 68, p. 277-279.

Lin S., van Staal, C.R., and Lee, C.
1993: The Harbour Le Cou Group and its correlation with the Bay du Nord Group, southwestern Newfoundland; in Current Research, Part D; Geological Survey of Canada, Paper 93-1D.

Luth, W.D., Jahns, R.H., and Tuttle, O.F.
1964: The granite system at pressures of 4 to 10 kilobars; Journal of Geophysical Research, v. 69, p. 659-773.

Rumble, D.
1978: Mineralogy, petrology, and oxygen isotope geochemistry of the Clough Formation, Black Mountain, western New Hampshire, USA; Journal of Petrology, v. 19, p. 317-340.

Selverstone, J., Spear, F.S., Franz, G., and Morteani, G.
1984: High-pressure metamorphism in the SW Tauern Window, Austria: P-T paths from hornblende-kyanite-staurolite schists; Journal of Petrology, v. 25, p. 501-531.

Spear, F.S. and Cheney, J.T.
1989: A petrogenetic grid for pelitic schists in the system SiO_2-Al_2O_3-FeO-MgO-K_2O-H_2O; Contributions to Mineralogy and Petrology, v. 101, p. 149-164.

Thompson, A.B.
1982: Dehydration melting of pelitic rocks and the generation of H_2O-undersaturated granitic liquids; American Journal of Science, v. 282, p. 1567-95.

Thompson, A.B. and Tracy, R.J.
1979: Model systems for anatexis of pelitic rocks. II. Facies series melting and reactions in the system CaO-$KAlO_2$-$NaAlO_2$-Al_2O_3-SiO_2-H_2O; Contributions to Mineralogy and Petrology, v. 70, p. 429-438.

Thompson, J.B.
1957: The graphical analysis of mineral assemblages in pelitic schists; American Mineralogist, v. 42, p. 842-858.

Thompson, P.H. and Leclair, A.D.
1987: Chloritoid-hornblende assemblages in quartz-muscovite pelitic rocks of the Central Metasedimentary Belt, Grenville Province, Canada; Journal of Metamorphic Geology, v. 5, p. 415-436.

van Staal, C.R., Winchester, J.A., Brown, M., and Burgess, J.L. 1992a: Reconnaissance geotraverse through southwestern Newfoundland; in Current Research, Part D; Geological Survey of Canada, Paper 92-1D, p. 133-143.

van Staal, C.R, Burgess J.L., Hall, L., Lee, C., Lin, S., and Schofield, D.
1992b: Geology of the Port aux Basques-Rose Blanche area (NTS 11-0/10 & 11-0/11); in Report of Activities 1992, Newfoundland Department of Mines and Energy, Geological Survey Branch.

Vernon, R.H.
1975: Microstructures of high-grade metamorphic rocks at Broken Hill, Australia; Journal of Petrology, v. 9, p. 1-22.
1987: Growth and concentration of fibrous sillimanite related heterogeneous deformation in K-feldspar-sillimanite metapelites; Journal of Metamorphic Geology, v. 5, p. 51-68.

Vielzeuf, D. and Holloway, J.R.
1988: Experimental determination of the fluid-absent melting relations in the pelitic system; Contributions to Mineralogy and Petrology, v. 98, p. 257-276.

Yardley, B.W.D.
1989: An introduction to metamorphic petrology; Longman Scientific and Technical, Essex, England.

Geological Survey of Canada Project 730044

The Harbour le Cou Group and its correlation with the Bay du Nord Group, southwestern Newfoundland[1]

Shoufa Lin, Cees R. van Staal, and Christopher Lee[2]
Continental Geoscience Division

Lin, S., van Staal, C.R., and Lee, C., 1993: The Harbour le Cou Group and its correlation with the Bay du Nord Group, southwestern Newfoundland; in Current Research, Part D; Geological Survey of Canada, Paper 93-1D, p. 57-64.

Abstract: The lithologies and deformation histories of the "Otter Bay division", the Harbour le Cou Group, and the Bay du Nord Group are described. The "Otter Bay division" is lithologically and structurally indistinguishable from Harbour le Cou Group, and Harbour le Cou Group is expanded to include both units. The expanded Harbour le Cou Group is correlated with Bay du Nord Group. The difference in metamorphic grade between the two units can be explained by the movement along the Bay le Moine shear zone, which shows evidence for a component of dextral horizontal movement and a component of east-side-down vertical movement. This correlation indicates that the eastern part of the Port aux Basques gneiss is part of the Exploits Subzone of the Dunnage Zone; a correlation that is supported by the presence of tholeiitic pillow basalts in the expanded Harbour le Cou Group.

Résumé : On décrit, dans le présent article, les lithologies et les épisodes de déformation de la «division d'Otter Bay», le Groupe de Harbour le Cou et le Groupe de Bay du Nord. La «division d'Otter Bay» ne se laisse pas lithologiquement et structuralement distinguer du Groupe de Harbour le Cou, lequel a été élargi de façon à inclure les deux unités. Le Groupe de Harbour le Cou ainsi élargi est corrélé avec le Groupe de Bay du Nord. La différence entre les degrés de métamorphisme des deux unités peut s'expliquer par le mouvement survenu le long de la zone de cisaillement de Bay le Moine, qui fait preuve d'une composante de mouvement horizontal dextre et d'une composante de mouvement vertical avec affaissement du compartiment est. Cette corrélation indique que la portion orientale du gneiss de Port aux Basques fait partie de la sous-zone d'Exploits qui se situe dans la zone de Dunnage; cette corrélation est appuyée par la présence de basaltes tholéiitiques en coussins dans le Groupe élargi de Harbour le Cou.

[1] Contribution to Canada-Newfoundland Cooperation Agreement on Mineral Development 1990-1994, a subsidiary agreement under the Economic and Regional Development Agreement. Project funded by the Geological Survey of Canada.

[2] Department of Earth Sciences, Memorial University of Newfoundland, St. John's, Newfoundland A1B 3X5

INTRODUCTION

Southwestern Newfoundland is of special interest to the understanding of the Canadian Appalachians, since the Humber, Dunnage, and Gander zones of Newfoundland converge in this region. Crucial to the understanding of this region is the understanding of the Port aux Basques gneiss (Brown, 1976, 1977) and its relationships with the surrounding rocks.

The Port aux Basques gneiss was first defined by Brown (1976, 1977) as a unit of psammitic gneisses and pelitic schists with variable amounts of amphibolite. It extends from Cape Ray Fault Zone east to Harbour le Cou (Fig. 1). Brown (1976) also mapped a Harbour le Cou Group in the Rose Blanche-Harbour le Cou area. The Port aux Basques gneiss and Harbour le Cou Group are separated from the Bay du Nord Group to the east by the Bay le Moine shear zone (Fig. 1). According to Brown (1976), the Harbour le Cou Group is a higher-grade equivalent of Bay du Nord Group and Port aux Basques gneiss is the basement underlying them.

A reconnaissance geotraverse through southwestern Newfoundland led van Staal et al. (1992a) to divide the Port aux Basques gneiss into three informal divisions with distinct lithologies separated by shear zones. From the west to the east, these are the Grand Bay, Port aux Basques, and Otter Bay divisions (Fig. 1). The Grand Bay division mainly consists of thin-bedded shale-siltstone rhythmites, interlayered with numerous sheets of amphibolite, and ultramafic and granitoid rocks. The Port aux Basques division is a sequence of sandstones and shales intruded by abundant diabase dikes and sills; and "Otter Bay division" consists of feldspathic psammites, semipelites, and tholeiitic pillow basalts. This three-fold division of Port aux Basques gneiss has been corroborated by detailed field mapping during the 1992 field season, and Grand Bay and Port aux Basques divisions have been renamed the Grand Bay Complex and Port aux Basques Complex, respectively (van Staal et al., 1992b). Our present work shows, in contrast to previous interpretations (Brown, 1976; van Staal et al., 1992a), that "Otter Bay division" is indistinguishable from Harbour le Cou Group.

In this report, the lithologies and deformation histories of the "Otter Bay division", Harbour le Cou Group, and Bay du Nord Group are described. The Harbour le Cou Group is expanded to include the "Otter Bay division". The correlation proposed by Brown (1976) of this group with Bay du Nord Group is confirmed. The kinematics of Bay le Moine shear zone are also described to help understand this correlation.

"OTTER BAY DIVISION"

The "Otter Bay division" of van Staal et al. (1992a) includes the metamorphic rocks of the Port aux Basques gneiss of Brown (1976, 1977) to the east of the Isle aux Morts Fault Zone, including the "reworked gneiss" of Brown (1976). It is intruded by the Rose Blanche Granite to the east (Fig. 1). The rocks in this division were metamorphosed under amphibolite-facies conditions. The main lithologies in the division are described below.

1. Thin-bedded semipsammitic to semipelitic schist with abundant thin quartz-garnet layers. The schist is generally composed of sillimanite+muscovite+quartz+garnet. The quartz-garnet layers are different from the coticule layers described later in that the garnet in the former is light brown, possibly almandine, whereas that in the latter is pink, supposedly spessartite. This lithology occurs in the eastern part of "Otter Bay division" and is the most extensive rock type in the division.
2. Graded psammite to semipelite. Quartzite to feldspathic quartzite grades to muscovite-biotite-garnet-quartz± sillimanite schist. Individual beds are 10 to 30 cm thick, and graded bedding is easily recognizable.
3. Garnetiferous psammites with thin coticule (Mn-garnet+quartz) layers and purplish sillimanite-garnet-bearing pelites. This lithology occurs to the east of the Burnt Islands Shear (Fig. 2).

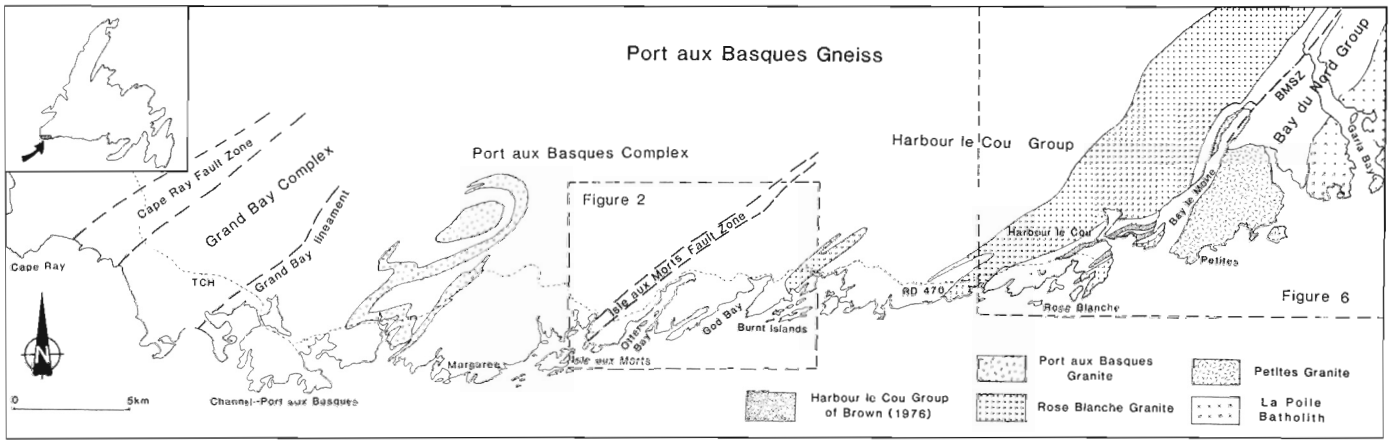

Figure 1. Map of southwestern Newfoundland with the distribution of the main rock units. The Harbour le Cou Group includes both the Otter Bay division of van Staal et al. (1992a) and the Harbour le Cou Group of Brown (1976). The locations of Figure 2 and Figure 6 are shown. BMSZ: Bay le Moine shear zone.

4. Thick-bedded feldspathic psammite with subordinate sillimanite-bearing pelites and calc-silicate layers, pods, and lenses. The psammite mainly consists of quartz and feldspar with minor amounts of biotite, muscovite, and garnet. Sillimanite occurs locally in the pressure shadows of garnet porphyroblasts. Variation in the amount of micas gives the rock a gneissic character. Graded bedding is recognized locally. The calc-silicate pods and lenses generally contain carbonate+garnet+clinopyroxene+anorthite+clinoamphibole. This lithology occurs mainly between the Isle aux Morts Fault Zone and the village of Burnt Islands (Fig. 2).

5. Pillow basalts are found at two localities, one in the village of Isle aux Morts, the other immediately to the west of Burnt Islands Shear (Fig. 2). The former has been described by van Staal et al. (1992a). It is entirely surrounded by minor shear zones of the Isle aux Morts Fault Zone and is locally up to 150 m thick. The latter occurs around the nose of a large F3 fold at the head of God Bay. It was described as plagioclase-hornblende gneisses with calc-silicate pods and was tentatively interpreted as para-amphibolite by van Staal et al. (1992a). During this summer's detailed field mapping, we found well-preserved pillow structures in the amphibolites in sections cut perpendicular to the stretching lineation (Fig. 3), and thus conclude that they are pillow basalts.

Three major generations of ductile deformation are recognized in the "Otter Bay division". F_1 folds are rare and their existence is mainly indicated by the S_1 foliation which is folded by F_2 (Fig. 4). F_2 folds are generally tight to isoclinal, and are recumbent or reclined in the hinges of F_3 folds. The S_2 foliation, which is axial planar to the F_2 folds, is the dominant foliation in rocks of the division. F_3 folds are open to tight and overprint F_2 folds (Fig. 4). In pelitic and semipelitic rocks, a crenulation cleavage is locally developed axial planar to the F_3 folds. Near Bay le Moine shear zone, F_3 folds consistently have a "Z" asymmetry, probably as a result of dextral movement along the shear zone.

HARBOUR LE COU AREA

Brown (1976) confined his Harbour le Cou Group to two narrow lenses around the Harbour le Cou and Rose Blanche area. This study found no distinction between these rocks and the surrounding rocks mapped by Brown as Port aux Basques

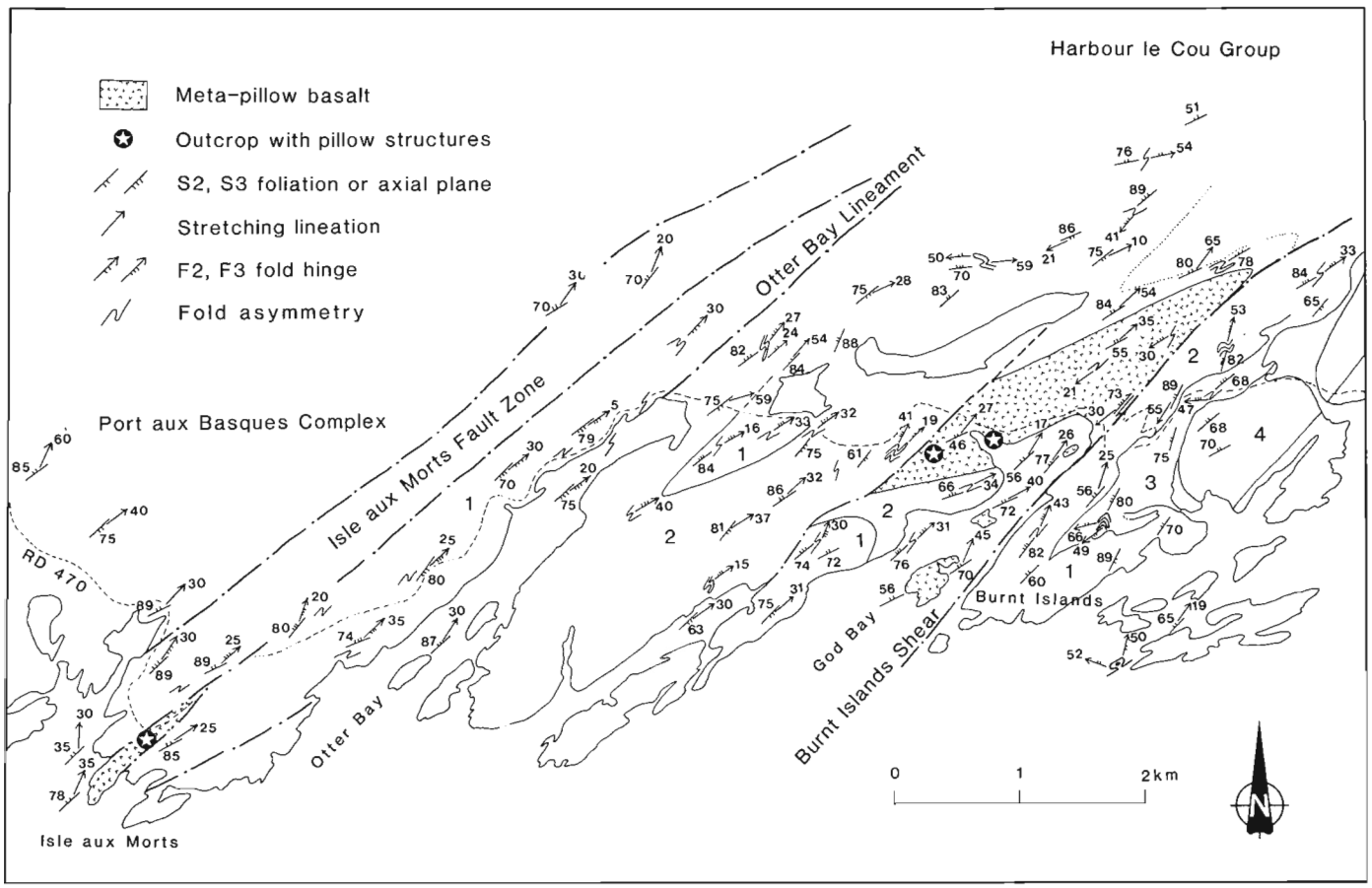

Figure 2. Structural geology map of the Isle aux Morts-Burnt Islands area. 1: thick-bedded feldspathic psammite with calc-silicate layers, pods and lenses; 2: thin-bedded psammite to semipelite; 3: Garnetiferous psammites with thin coticule layers; 4: Rose Blanche Granite. (Structural data of van Staal et al., 1992a are incorporated).

gneiss (i.e. the "Otter Bay division" described above). We here describe the rocks mapped by Brown (1976) as Harbour le Cou Group (Fig. 1). They are described for the convenience of later discussion.

These rocks were also metamorphosed to amphibolite-facies conditions; garnet is widespread and sillimanite is locally developed. They are pelitic to semipelitic schists with subordinate thick-bedded feldspathic psammite. Marble and calc-silicate layers were observed at one outcrop on the peninsula across Harbour le Cou. The schists locally contain sulphides and appear rusty where weathered.

These rocks also experienced a complicated deformation history and show evidence for F_1, F_2, and F_3 folding. Both the F_1 and the F_2 folds are very tight to isoclinal. The F_3 folds are open to very tight and consistently have a "Z" asymmetry. Overprinting relationship between F_2 and F_1 and between F_3 and F_2 are well exposed at the outcrop on the peninsula across Harbour le Cou (Fig. 5A, B).

The granite dike in Figure 5B is related to the two-mica Rose Blanche Granite. It is folded by F_2 and F_3. At a nearby outcrop, a pegmatite dike related to the same granite is controlled by the axial plane of an F_2 fold. These relationships indicate that the intrusion of the Rose Blanche Granite was syn-D_2.

BAY DU NORD GROUP

The Bay du Nord Group outcrops to the east of the Bay le Moine shear zone, which separates it from the "Otter Bay division" and the "Harbour le Cou Group" to the west (Fig. 1 and 6). The Bay du Nord Group is intruded by the La Poile Batholith to the east and the Petites Granite to the south. The rocks in the group were metamorphosed only to greenschist facies, and sedimentary structures are commonly well preserved. The lithologies of the group are described below, from west to east.

1. Thin-bedded, phyllitic siltstone and mudstone. Some of the rocks are tuffaceous. A rhyolite sill or flow is associated with the tuffaceous siltstone. It is concordant

Figure 3. Well-preserved pillow structures in the Otter Bay division. Section cut perpendicular to the stretching lineation. GSC 1992-281A. North shore of God Bay.

Figure 4. F_3-F_2 overprinting relationship in the Otter Bay division. Note that the F_2 fold involves an earlier foliation (S_1). GSC 1992-281B. The village of Rose Blanche.

with the bedding in the siltstone and experienced the same deformation history as the siltstone. This rock type occurs immediately to the east of the Bay le Moine shear zone.

2. Graded, thin- to thick-bedded immature sandstone to siltstone with conglomerate. The sandstone contains abundant fragments of feldspar and blue quartz. Graded bedding is well developed, especially in the medium- to thick-bedded sequence (Fig. 7A). Many beds show almost complete Bouma sequences from layers A to D, although layer E is usually lacking. The fine-grained rock in layer D is siltstone to mudstone, which is contact-metamorphosed to cordierite and/or andalusite grade near its contact with La Poile Batholith or Petites Granite.

Associated with this sandstone and siltstone is a conglomerate in the form of several layers from 10 cm to over 1 m thick, interbedded with immature sandstone (Fig. 7B). Laterally, two conglomerate layers may merge to form a single layer. Pebbles in the conglomerate range from less than 1 cm to over 10 cm, with the dominant size between 2 and 4 cm. The composition of the well-rounded pebbles include granite-diorite, quartz, and gneiss. The gneiss pebbles contain a predepositional foliation. Angular sandstone and shale clasts are also present. Both the clast-matrix ratio and the relative proportion of pebble types vary laterally. The conglomerate layer, a good marker in the Bay du Nord Group, is repeated several times in the map area, as a result of D_2 deformation. The structural repetition is consistent with the recorded changes in younging directions (Fig. 6).

3. Thick-bedded immature sandstone. The sandstone contains abundant lithic or feldspar fragments. This rock type lies to the east of lithology 2 and is intruded by the La Poile Batholith to the east.

The Bay du Nord Group also experienced a complex deformation history. The dominant foliation in the group is S_2. It formed by the transposition of an earlier foliation S_1. F_2 folds are very tight to isoclinal in finer grained rocks such as phyllitic siltstone to mudstone (Fig. 8A). They are less tight in thick-bedded, coarser grained sandstone. F_3 folds are open to very tight. They are strongly asymmetrical with consistent "Z" asymmetry (Fig. 8B). F_3 folds consistently overprint F_2 folds and S_2 foliation. They are tighter near the Bay le Moine shear zone and are interpreted to be related to the dextral movement along the shear zone. F_4(?) folds are "S" kinks (Fig. 8C). Their development appears to be related to movement along the Bay le Moine shear zone, since F_4(?) folds are only locally developed away from the shear zone and are more strongly developed, locally penetrative close to the shear zone. The kinematic implications of the F_4(?) folds has yet to be determined. Their orientation appears conjugate to F_3, and the F_4(?) folds may also be related to the D_3 dextral shear.

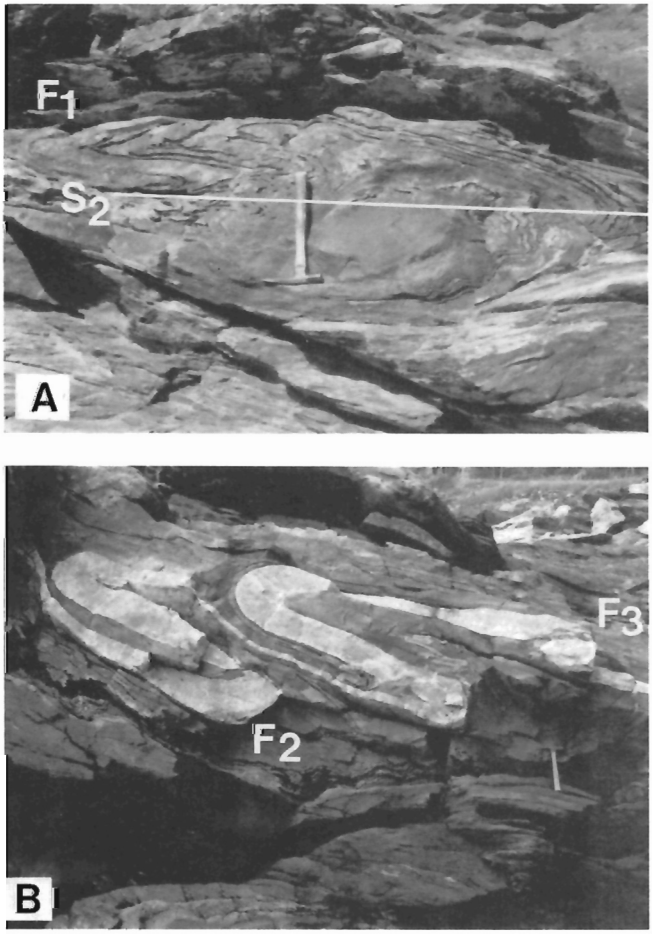

Figure 5. Structures in the Harbour le Cou Group of Brown (1976). **(A)** F_2-F_1 overprinting relationship. GSC 1992-281M. **(B)** F_3-F_2 overprinting relationship. The granite dike is related to the syn-D_2 Rose Blanche Granite. GSC 1992-281A. The peninsula across Harbour le Cou.

BAY LE MOINE SHEAR ZONE

The Bay le Moine shear zone is a large-scale structure, extending in a northeasterly direction for over 15 km from Bay le Moine, through northeast Garia Bay, to beyond the present map area. Topographically, it is a strong lineament, clearly evident on aerial photographs. The shear zone separates the "Otter Bay division" and the Harbour le Cou Group, both with amphibolite-facies mineral assemblages, to the west, from the Bay du Nord Group with greenschist-facies mineral assemblages to the east (Fig. 1 and 6). Elucidating the movement history along the shear zone is important for the understanding of the geology of this area.

The Bay le Moine shear zone has a complicated movement history, involving both ductile and brittle deformation. The earliest shear zone related structures in the Rose Blanche-Garia Bay area are local sinistral shear bands. However, there is no convincing evidence that this sinistral shearing was concentrated in the Bay le Moine shear zone. The most significant movement along the shear zone is oblique dextral. The zone of strong dextral shear is about 1 km wide, although the zone involved in the dextral movement is much wider. The F_3 folding described above is interpreted to be kinematically related to the dextral movement.

In the Bay le Moine shear zone, the "Otter Bay division", "Harbour le Cou Group", Bay du Nord Group, and Rose Blanche Granite are all strongly sheared, and mylonites are

well developed. The mylonitic foliation strikes northeasterly and is subvertical. The stretching lineation is subhorizontal near the shear zone centre and pitches moderately to the southwest away from the centre (Fig. 6). Abundant kinematic indicators, including S-C structure, shear bands, asymmetry of F_3 folds, boudinaged quartz veins and the sense of rotation of curvilinear fold axes, consistently indicate dextral shear with east-side-down vertical component (Fig. 9A, B). This vertical movement component is at least partly responsible for the difference in metamorphic grade across the shear zone.

The ductile deformation structures in the Bay le Moine shear zone are intruded by the Petites Granite. The granite is not involved in the ductile deformation, but is dextrally offset by about 2.8 km due to brittle movement along the shear zone. From Bay le Moine to Garia Bay, where the fault zone is exposed, the breccia zone is over 300 m wide. A large number of quartz veins, many of which are over 1 m wide, are associated with the breccia zone. The master quartz veins strike about 075°, at a low angle to the shear zone, indicating significant zone-normal extension during the brittle dextral movement. We suggest that this extension also aided the downward movement of the Bay du Nord Group relative to the rocks to the west of the shear zone.

CORRELATIONS

The "Otter Bay division" is lithologically distinct from the Port aux Basques Complex. As described above, the former is dominantly a dirty thick-bedded psammite, graded psammite to semipelite, thin-bedded semipelite and meta-pillow basalts. The latter is characterized by relatively clean psammite and pelite with abundant metadiabase dikes and sills, which on average form 20-25% of the complex (van Staal et al., 1992a, b). This indicates that the "Otter Bay division", which includes the "reworked gneiss" of Brown

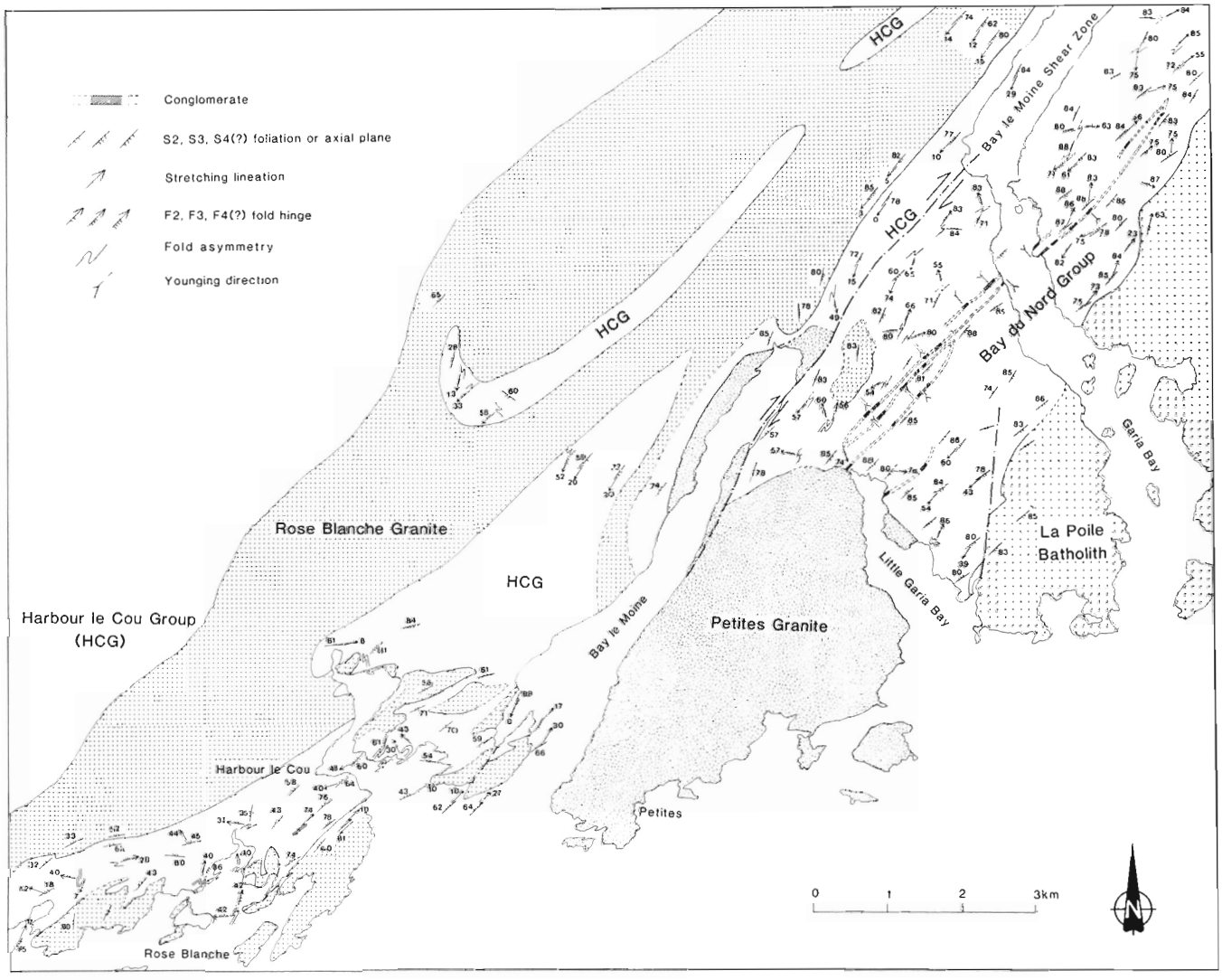

Figure 6. Structural geology map of the Rose Blanche-Garia Bay area. The Harbour le Cou Group includes the Otter Bay division of van Staal et al. (1992a). (The boundary of the Rose Blanche Granite is partly after Brown 1976)

(1976), is not the reworked Port aux Basques Complex, but belongs to a separate lithological unit (van Staal et al., 1992a). Instead, the present study shows that the "Otter Bay division" has similar lithologies to, and experienced the same deformation history as, the Harbour le Cou Group of Brown (1976). Consequently, we agree with Piasecki (unpublished GSC contract report) and expand the Harbour le Cou Group to include the "Otter Bay division". This study also confirms that the expanded Harbour le Cou Group and the Bay du Nord Group can be correlated, as suggested by Colman-Sadd et al. (1990). The Bay du Nord Group mainly consists of dirty thick-bedded sandstone, graded sandstone to siltstone, and thin-bedded siltstone to mudstone. Contrary to the suggestion by Brown (1976) that at least one generation of deformation found in his "reworked gneiss" is lacking in his Harbour le Cou Group and the Bay du Nord Group, all the structures recognized in the expanded Harbour le Cou Group are also recognized in the Bay du Nord Group. The only significant difference we observed between the Harbour le Cou Group and the Bay du Nord group is the contrast in metamorphic grade. The former mainly has amphibolite-facies mineral assemblages, whereas the latter has greenschist-facies assemblages. This difference in grade is at least in part the result of movement along the Bay le Moine shear zone.

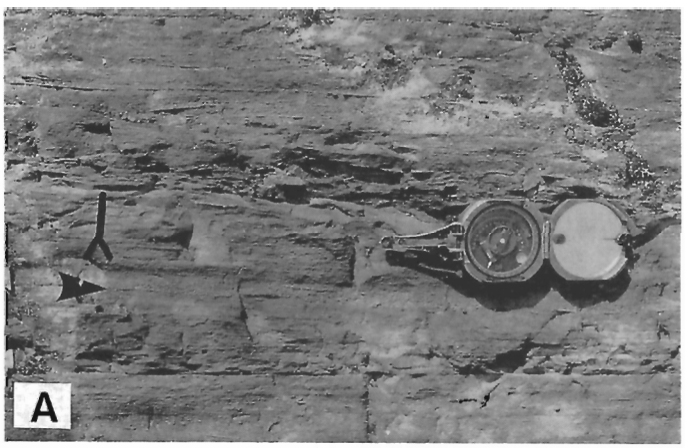

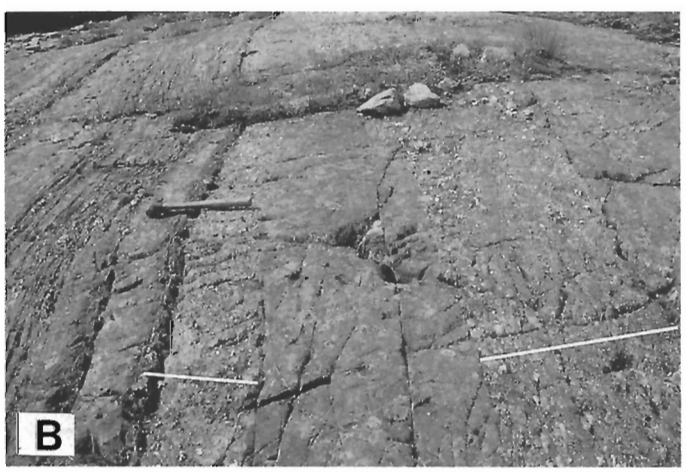

Figure 7. Lithologies of the Bay du Nord Group. (**A**) Graded sandstone. The base and the younging direction of a bed are indicated. GSC 1992-281E. (**B**) Conglomerate interbedded with sandstone. Conglomerate layers are indicated by the white lines. GSC 1992-281I. Between Little Garia Bay and Garia Bay.

Figure 8. Structures in the Bay du Nord Group. (**A**) Very tight F_2 folds. Note that the fold hinge indicated by the arrow involves an earlier foliation. GSC 1992-281C. Garia Bay. (**B**) F_3 "Z" folds. GSC 1992-281D. East of Garia Bay. (**C**) F_4(?) "S" folds. GSC 1992-281H. East of Garia Bay.

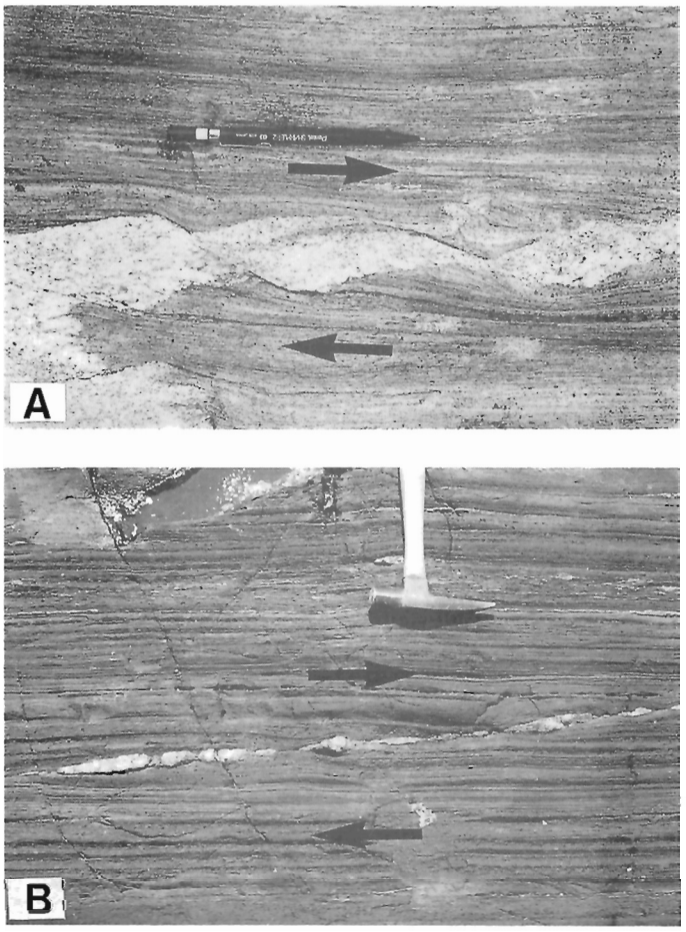

Figure 9. Shear sense indicators in the Bay le Moine shear zone, indicating dextral sense of shear. (**A**) Shear bands. GSC 1992-281K. The peninsula across Harbour le Coup. (**B**) Boudinaged quartz veins. GSC 1992-281F. Garia Bay.

SUMMARY AND DISCUSSION

The three-fold division of the Port aux Basques gneiss proposed by van Staal et al. (1992a) is supported during this summer's field mapping. The "Otter Bay division" is lithologically distinct from the Port aux Basques Complex and thus cannot be the "reworked gneiss". Instead, it is lithologically and structurally indistinguishable from the Harbour le Cou Group (Brown, 1976). The Harbour le Cou Group is expanded to include both the units. The expanded Harbour le Cou Group is correlated with the Bay du Nord Group, and the difference in metamorphic grade between the two units is explained in terms of the ductile and brittle movement along the Bay le Moine shear zone.

The above correlation implies that the Harbour le Cou Group is part of the Exploits Subzone of the Dunnage Zone (Williams et al., 1988). This contrasts with Piasecki (unpublished GSC contract report), who suggested that this part of the Port aux Basque gneiss is best correlated with the Meelpaeg Subzone of the Gander Zone. Our interpretation is supported by the presence of tholeiitic pillow basalts in the Harbour le Cou Group. Our mapping has suggested that the Grand Bay Complex is also part of the Exploits Subzone and the Port aux Basques Complex is part of the Gander Zone (van Staal et al., 1992b). If these interpretations are correct, parts of the Port aux Basques gneiss as defined by Brown (1976, 1977) in southwestern Newfoundland belong to both the Gander and the Dunnage zones of the Canadian Appalachians.

ACKNOWLEDGMENTS

We are grateful to Dr. Ken Currie for critically reading the manuscript, and to Drs. Keith Benn, Steve Colman-Sadd, and Hank Williams for discussions.

REFERENCES

Brown, P.A.
1976: Geology of the Rose Blanche map-area (11O/10), Newfoundland; Newfoundland Department of Mines and Energy, Mineral Development Division, Report 76-5, 16 p.
1977: Geology of the Port aux Basques map-area (11O/11), Newfoundland; Newfoundland Department of Mines and Energy, Mineral Development Division, Report 77-2, 11 p.

Colman-Sadd, S.P., Hayes, J.P., and Knight, I.
1990: Geology of the island of Newfoundland; Geological Survey Branch, Department of Mines and Energy; Government of Newfoundland and Labrador.

van Staal, C.R., Winchester, M., Brown, M., and Burgess, J.L.
1992a: Reconnaissance geotraverse through southwestern Newfoundland; in Current Research, Part D; Geological Survey of Canada, Paper 92-1D.

van Staal, C.R., Burgess, J.L., Hall, L., Lee, C., Lin, S., and Schofield, D.
1992b: Geology of the Port aux Basques-Rose Blanche Area (NTS 11O/10 & 11O/11); Report of Activities, Geological Survey Branch, Department of Mines and Energy, Government of Newfoundland and Labrador.

Williams, H., Colman-Sadd, S.P., and Swinden, H.S.
1988: Tectonic-stratigraphic subdivisions of central Newfoundland; in Current Research, Part B; Geological Survey of Canada, Paper 88-1B, p. 91-98.

Geological Survey of Canada Project 730044

A re-examination of relations between Dunnage subzones in southwest Newfoundland[1]

J.B. Whalen, K.L. Currie and M.A.J. Piasecki[2]
Continental Geoscience Division

Whalen, J.B., Currie, K.L., and Piasecki, M.A.J., 1993: A re-examination of relations between Dunnage subzones in southwest Newfoundland; in Current Research, Part D; Geological Survey of Canada, Paper 93-1D, p. 65-72.

Abstract: The Little Grand Lake Fault, which separates low-grade igneous rocks of the Notre Dame Subzone from granulite facies metamorphic rocks and granitoid gneisses of the Dashwoods Subzone, does not form a single discrete break or zone at surface. Older south-over-north movement on numerous steep, small, ductile mylonite zones up to 3 m wide was followed by small-scale, brittle-ductile, north-over-south thrusting. Near Little Grand Lake movement surfaces occur in a zone about 5 km wide, but further east the zone is more than 20 km wide. The older movement may correlate with similar motions west of the Long Range (Cabot) Fault. The main faults in the zone of older movement may be buried by younger movements, or destroyed by emplacement of younger intrusive suites. The Red Indian Line, the eastern boundary of both the Notre Dame and Dashwoods subzones, contains mylonitic Topsails granite, demonstrating post-Early Silurian sinistral movement.

Résumé : La faille de Little Grand Lake, qui sépare les roches ignées faiblement métamorphisées de la sous-zone de Notre Dame des roches métamorphiques du faciès des granulites et des gneiss granitoïdes de la sous-zone de Dashwoods ne constitue pas une seule cassure ou zone discrètes en surface. Un mouvement plus ancien, de direction sud sur nord, qui a eu lieu au-dessus de nombreuses petites zones mylonitiques ductiles et à fort pendage pouvant atteindre 3 m de large, a été suivi d'un chevauchement nord sur sud de petite échelle, de type casant-ductile. Près de Little Grand Lake, des surfaces de failles apparaissent dans une zone d'environ 5 km de large, mais plus à l'est, cette zone dépasse 20 km de large. Le mouvement plus ancien est peut-être corrélatif de mouvements similaires survenus à l'ouest de la faille de Long Range (Cabot). Les principales failles existant dans la zone de mouvement plus ancien sont peut-être dissimulées par des déplacements plus récents, ou ont été effacées par la mise en place de séries intrusives plus récentes. La ligne de Red Indian, limite orientale des sous-zones de Notre Dame et de Dashwoods, contient le granite mylonitique de Topsails, et prouve l'existence d'un mouvement sénestre plus récent que le Silurien précoce.

[1] Contribution to Canada-Newfoundland Cooperation Agreement on Mineral Development 1990-1994, a subsidiary agreement under the Economic and Regional Development Agreement. Project funded by the Geological Survey of Canada.

[2] Department of Geology, University of Keele, Keele, Staffordshire ST5 5BG, England

INTRODUCTION

The Appalachian orogen in Newfoundland can be broadly divided into a western hinterland (Humber Zone), an eastern hinterland (Avalon Zone), and a Central Mobile Belt (Williams, 1964). The Central Mobile Belt or Dunnage Zone was subdivided by Williams et al. (1988) into Notre Dame and Exploits subzones, interpreted as oceanic suspect terranes juxtaposed along the Red Indian Line (Fig. 1). The southern portion of Notre Dame Subzone, a region underlain mainly by high grade ortho- and para-gneisses, was redefined as the Dashwoods Subzone by Piasecki et al. (1990), who considered it to be bounded on the northern side by the Little Grand Lake Fault (Fig. 1). We here present field observations bearing on the nature of the Little Grand Lake Fault and the Red Indian Line.

Most subzone boundaries trend northeast, parallel to the trend of the Appalachian orogen as a whole. In southwestern Newfoundland, however, some major boundaries trend approximately east-west. O'Brien et al. (1991) documented a major boundary along the southwest coast marked by south-over-north thrusting. Whalen and Currie (1983) and van Berkel and Currie (1988) noted an east-west boundary through Little Grand Lake (Fig. 2), termed the Little Grand Lake Fault, separating low-grade Ordovician volcanic rocks and high-level Silurian granite and rhyolite to the north from foliated gabbroic to granitic plutons and granulite-facies supracrustals to the south. Whalen and Currie (1983) noted small-scale, low-angle, north-over-south thrusting of the Silurian Topsails Intrusive Suite along the Little Grand Lake Fault. This sense of thrust motion is unusual for a separator of Ordovician terranes.

The Red Indian Line, the northwest boundary of the Exploits Subzone (Williams et al., 1988) is a steep brittle fault in Notre Dame Bay (O'Brien, 1991). North of Red Indian Lake the line is poorly exposed, but it bends around the Hodges Hill batholith, and lies southeast of Silurian red sandstones along Red Indian Lake (Williams et al., 1988). In the Lloyds River valley it follows a mylonite zone separating volcanic rocks of the Victoria Lake Group from the Annieopsquotch ophiolite complex. The Exploits Subzone ends where the Red Indian Line merges with Noel Pauls Line, the boundary between the Dunnage and Gander zones.

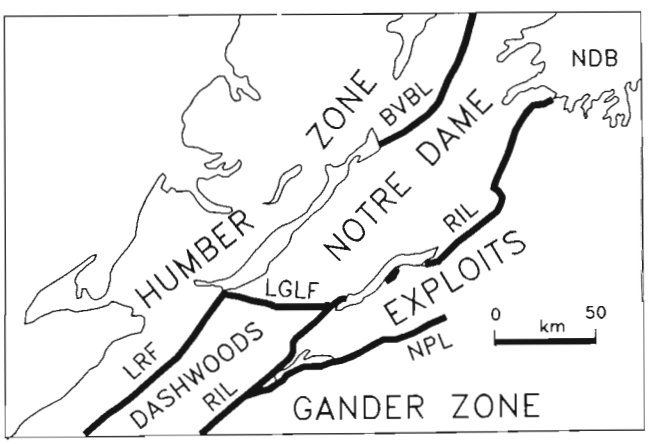

Figure 1. Tectonostratigraphic subdivision of central Newfoundland (modified after Williams et al. (1988) and Piasecki et al. (1990)). Abbreviations are as follows: LRF-Long Range Fault; RIL-Red Indian Line; LGLF-Little Grand Lake Fault; BVBL-Baie Verte-Brompton Line; NPL-Noel Pauls Line; NDB-Notre Dame Bay.

REGIONAL GEOLOGY

Southern Notre Dame Subzone

The southern part of the Notre Dame Subzone (Fig. 2) consists of an Ordovician ophiolite suite, volcanic and sedimentary rocks of the Glover Group (Knapp, 1979; Nowlan and Thurlow, 1984), Ordovician granitoid plutons, and Silurian granites of the Topsails Intrusive Suite (Whalen and Currie, 1983).

The Glover Group contains large amounts of basaltic pillow lavas structurally overlain by bimodal volcanic rocks with intercalated sedimentary rocks. Metamorphic grade is generally subgreenschist, but a wedge-shaped block, presumably fault bounded, along the north shore of Little Grand Lake exhibits higher grade rocks, up to amphibolite facies with minor anatexis in the salic portions. The most easterly exposures of the Glover Group, at about 57°30'W, are low grade pillow lavas.

Plutonic rocks of presumed Ordovician age form a significant, but poorly exposed component of this region (Whalen and Currie, 1988; Whalen et al., 1987). The plutons generally underlie low, swampy areas between ridges and hills of the Silurian Topsails Intrusive Suite, a diverse suite of leucocratic, metaluminous to peralkaline granites. Peralkaline portions contain a distinctive steel blue (arfvedsonitic) amphibole. The bulk of the Topsails Intrusive Suite shows little or no strain (Whalen and Currie, 1988).

Northwestern Dashwoods Subzone

Rocks in the northern portion of the Dashwoods Subzone (Fig. 2), can be divided into four units, namely granulite-grade metasedimentary rocks, migmatitic rocks, granitoid plutons, and basic intrusions. Rocks of sedimentary origin were detected by persistent thin compositional layering, local clots of sillimanite, rare layers of calc-silicate, quartzite, and thicker amphibolite layers (Currie and van Berkel, 1992). These rocks typically contain abundant small equant porphyroblasts of potassium feldspar, and thin lenticular leucosomes (sweats). The persistent presence of relict orthopyroxene shows that the unit underwent granulite facies metamorphism, although much of it is now retrograded to upper amphibolite facies. These high-grade metasedimentary rocks grade into migmatite characterized by a higher proportion of leucosome and contorted, discontinuous layers. Migmatite typically displays complex small-scale structures with contorted inclusions cut by a variety of small-scale mafic and salic dykes. The migmatites are sharply cut by younger, well-defined tonalitic to granitic plutons. All three units were

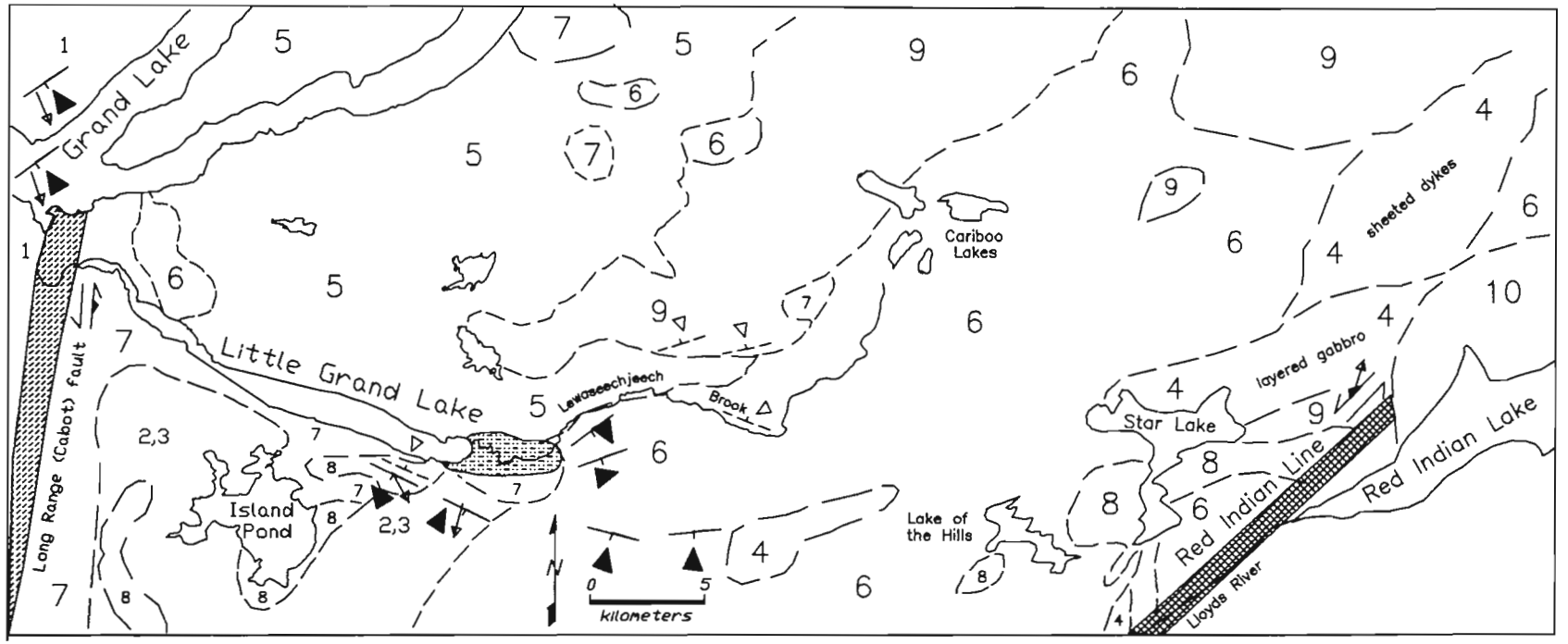

CARBONIFEROUS

10 red sandstone and conglomerate

mylonite, cataclasite

SILURIAN

9 Topsails Igneous Suite, metaluminous to peralkaline granites

stretching lineation

ductile zone showing dip. Arrow shows relative direction of motion of upper block

8 foliated metaluminous to peraluminous granites

7 gabbro, minor ultramafics

ORDOVICIAN

6 diorite, granodiorite, tonalite

5 GLOVER GROUP: pillow basalt, felsic volcanics, siltstone

brittle–ductile zone showing dip. Arrow indicates relative direction of motion of upper block

4 rocks of the ophiolite suite; gabbro, sheeted dykes

3 migmatite of granitoid, meta–sedimentary rocks and amphibolite

2 granulite–grade meta–sedimentary rocks

LATE PRECAMBRIAN

1 FLEUR DE LYS SUPERGROUP; metasedimentary rocks

transcurrent fault, sense of movement as shown; tooth on uplifted block

Figure 2. Geological sketch of the Little Grand Lake-Star Lake region, southwest Newfoundland (modified from Currie and van Berkel, 1992 and Whalen, unpub. data). (Hatched area at the mouth of Lewaseechjeech Brook is drift-covered.)

considered to be of Ordovician age because several of the plutons gave mid-Ordovician (~455 Ma, Currie and van Berkel, 1992) radiometric ages, and no Precambrian basement has been detected in this region (Currie et al., 1992), However slightly foliated biotite±muscovite granitic intrusions around Island Pond resemble metaluminous portions of the Topsails Intrusive Suite and could be Silurian in age. U-Pb dating in progress will test this hypothesis. Mafic intrusive rocks exposed along much of the south slope of Little Grand Lake are probably of Silurian age (Currie and van Berkel, 1989), but on Island Pond this unit is a heterogeneous mixture of gabbroic, dioritic, and diabasic lithologies, some of which could be Ordovician in age.

Northeastern Dashwoods Subzone

The triangular region bounded by the east end of Little Grand Lake, Lewaseechjeech Brook, and the south end of Red Indian Lake (Fig. 2) forms a generally low-lying area of poor exposure in which both Notre Dame and Dashwoods-type lithologies appear in a complex pattern, in contrast to the well exposed, sharply defined, narrow (<2 km) zone within and bordering Little Grand Lake along which contrasting high grade and low grade rocks are juxtaposed. Whalen and Currie (1988) outlined a number of intrusive units of presumed Ordovician age, which have been further subdivided by current mapping. Quantity and quality of exposure in this generally swampy area proved to be better than expected. The Ordovician(?) plutonic rocks include a diverse suite of gabbro, diorite, quartz diorite, tonalite, granodiorite and granite, which contains very large (up to 10 by 4 km) pendants or screens of mafic to ultramafic rocks. Northeast of Star Lake a well preserved body of layered pyroxene gabbro and sheeted dykes resembles part of an ophiolite suite, as suggested by Dunning et al. (1982). These mafic rocks are generally undeformed, but they are cut by veins and dykes of the younger granitoid suite. Near Cariboo Lakes, the Ordovician(?) units preserve primary igneous mineralogy, but to the south igneous mineralogy is progressively replaced by metamorphic mineralogy across a zone 10 to 15 km wide.

Migmatitic para- and orthogneisses near Cariboo Lakes and southeast of Star Lake exhibit steep north-trending compositional banding overprinted by a steep east-west tectonic foliation. These gneisses are interpreted to be older than the foliated but nongneissic igneous suites.

Between Lake of the Hills and Red Indian Lake ovoid bodies of granite (*senso stricto*) intrude Ordovician(?) plutonic units. These granites range from alkaline to peraluminous and include amphibole-, biotite-, biotite-muscovite-, and muscovite-garnet-bearing phases. Alkaline to metaluminous phases are lithologically identical to components of the Topsails Intrusive Suite, but all phases are slightly to strongly ductilely deformed.

STRUCTURAL OBSERVATIONS

Northwestern boundary zone

Piasecki et al. (1990) suggested that the topographic lineament in Little Grand Lake and Lewaseechjeech Brook represents a subzone boundary. If correct, evidence of the nature of this boundary should be preserved in the rocks on both sides of this lineament. We have examined localities along the lake and brook to search for such evidence.

Along the cliff-tops above the southern shore of Little Grand Lake (near grid references 426786 and 399789 on NTS sheet 12A/12, Little Grand Lake) granitoid rocks and migmatites with steep to vertical, east- to southeast-trending foliation contain zones of protomylonite, mylonite, and rare ultramylonite from 1 to 20 m wide, aligned parallel to foliation in adjacent rocks. Mylonite zones are separated by tens of metres of nonmylonitic rocks, and comprise <5% of the outcrop. Within the mylonitic rocks, the stretching lineation together with S-C fabric, shear bands, and deformed and rotated porphyroclasts indicate reverse dip-slip movements (south-over-north) and oblique reversed dip-slip (southeast-over-north-west) movement. Numerous smaller shear zones, including a 5 m ultramylonite exposed in a creek bed (at gridref 399789) indicate minor sinistral strike slip motion.

At gridref 426786, a sheet of steeply foliated Silurian(?) meta-gabbro contains thin (1-5 cm wide) brittle-ductile shears discordantly transecting foliation along surfaces dipping 20° toward 340°. Along these shear surfaces the metagabbro is rotated and stretched indicating small-scale north-over-south movements within the mafic sheet, and probably also of the sheet over the granitoid rocks to the south. Geometrically similar but less intense and more brittle deformation occurs in the Topsails Intrusive Suite near gridrefs 589835 and 616849 where steep joint surfaces are deformed and offset by low angle north-over-south motion.

East of Little Grand Lake, a prominent hill at gridref 513795 is capped by unfoliated, pink Topsails granite with steel blue amphibole. The occurrence of Topsails Intrusive Suite, the most southerly so far discovered, appears to be a slice less than 50 m thick, structurally emplaced by the late north-over-south thrusting. The underlying Dashwoods Subzone rocks, weakly to moderately foliated metagabbro, tonalite, granodiorite, and local migmatite, trend northeast and dip steeply southeast. Widely separated, minor zones of migmatite 10 to 30 cm wide are aligned parallel to foliation, and indicate dip-slip (southeast-side-down) to oblique dip-slip (south-southeast-side-down). The geometry of these small mylonitic zones appears compatible with that of antithetic conjugate minor shears related to the wider shears displacing south-over-north (cf. Twiss and Moores, 1992, p. 174; McClay, 1987, Fig. 6, 16a). Thin mylonites exposed on horizontal rock surfaces rarely exhibit dextral movements which may represent either the horizontal component of oblique slip, or distinct minor strike-slip movements. Significantly, the mylonitic fabrics occur in granitic sheets

that cut unfoliated to little foliated metagabbro and tonalite, indicating late synplutonic timing for the ductile shearing movements.

Lewaseechjeech Brook flows through almost continuous outcrop. However a sand plain obscures exposure at its mouth. We examined numerous outcrops in the brook and several tributaries, but found no evidence of ductile deformation in the dominantly granitoid rocks.

Our observations of kinematic patterns along the cliffs south of Little Grand Lake shows that two distinct phases of shearing have affected the region, namely (1) an earlier phase of ductile south-over-north movements of the Dashwoods Subzone over the Notre Dame Subzone, complicated by strike-slip movements suggestive of a partially transpressive shear regime, and (2) a later phase of substantially more brittle north-over-south thrusting of the Notre Dame Subzone over the Dashwoods Subzone. The evidence for south-over-north movements appears to be confined south of Lewaseechjeech Brook and evidence for north-over-south motion is mainly, but not entirely, north of the brook. Lewaseechjeech Brook does not follow a zone of movement.

Eastern boundary zone

About 10 km north of Star Lake, along the course of the Little Grand Lake Fault as shown by Currie and van Berkel (1992), an isolated hill of coarse grained peralkaline Topsails granite is surrounded by foliated granodioritic to tonalitic Ordovician(?) units (Whalen and Currie, 1988). This exposure of peralkaline granite grades from weakly foliated on the northwest side to a very strong foliation trending 030° and dipping vertically on the southeast side. Some ductile deformation on the Little Grand Lake Fault clearly postdates the Early Silurian Topsails Intrusive Suite.

On the hill at the northeast corner of Star Lake, one-feldspar (hypersolvus) peralkaline granite, a distinctive rock type of the Topsails Intrusive Suite (Whalen and Currie, 1988), intrudes Ordovician(?) banded pyroxene gabbro. On the southeast side of that hill this granite becomes strongly foliated and grades eastward into a 0.5 km wide mylonite zone dipping 75° toward 325°. This zone is also well exposed where the road along the west side of Red Indian Lake crosses the stream running out of Star Lake. An extension lineation plunging about 40° toward 010° combined with S-C fabrics, shear bands, and rotated, deformed porphyroclasts indicate sinistral movements with significant northwest-over-southeast thrusting. This mylonite zone, the largest so far discovered along the Red Indian Line, truncates all intrusive units in this area. To the southeast, Kean (1979) mapped Middle Ordovician and younger mafic volcanic rocks (his Unit 5). He considered the mylonitic equivalents of Ordovician(?) granodiorite (his unit 9) to be older than their less deformed equivalents (his unit 11b). To the southwest, the ductile deformation zone disappears beneath swamp, and to the northeast it disappears beneath Carboniferous rocks around Red Indian Lake.

Plutonic lithologies in the northeast Dashwoods Subzone form elongate foliated bodies which are discontinuous along strike. The trend of foliation swings from about 075° west of Lake of the Hills to about 045° east of Star Lake while maintaining steep northwest dips. Concordant alignment of primary amphibole and feldspar with secondary biotite suggests that this foliation results from a combination of syntectonic intrusion and posttectonic deformation. On both macro- and micro-scales diverse lithologies of pre-Silurian igneous units are abruptly juxtaposed. Igneous and/or tectonic juxtaposition on this scale has not been recognized further south in the Dashwoods Subzone or within the Notre Dame Subzone.

DISCUSSION

The results of our work, added to those of previous mappers, make it clear that a major movement zone associated with the Little Grand Lake Fault cannot be precisely located on the ground. The abrupt juxtaposition of metamorphic grades used to locate the fault near Little Grand Lake does not exist further to the northeast.

The Little Grand Lake Fault was originally proposed to separate low-grade Ordovician volcanic and high-level Silurian granitic rocks from high-grade Ordovician(?) metamorphic rocks and plutons (Whalen and Currie, 1983). When this proposal was made, it was known that tonalitic rocks typical of the Dashwoods Zone occurred in small volumes in and north of Lewaseechjeech Brook, particularly in the Hungry Mountain complex. However the Hungry Mountain complex was known to be allochthonous (Thurlow, 1981). Neither Silurian peralkaline granite of the Topsails type nor basaltic pillow lavas, the major lithologies north of the proposed fault, have been found south of the fault.

Along Little Grand Lake, the boundary juxtaposes subgreenschist with granulite-grade rocks, and must therefore exhibit a significant displacement. The simplest movement sense consistent with these observations is south-side-up. The widespread kinematic indicators of high-angle south-over-north thrusting observed by us are compatible with such a scheme, but we saw no indication that the scale of the movement was sufficient to explain the metamorphic contrast. The sense of motion broadly coincides with that observed west of the Long Range (Cabot) Fault (Currie, 1986), where discrete slices of rock moved north-northwest. The source of these slices clearly lay to the east of the present Long Range Fault, but our observations are the first clear indication of similar movements east of the Long Range Fault, and therefore potentially provide an important linkage. However, the scale and style of motions differ on opposite sides of the Long Range Fault. To the east, no discrete slices have been identified, and the observed movement zones appear to be relatively minor. A major south-over-north break could lie under Little Grand Lake and the drift-covered lower Lewaseechjeech Brook, but not higher in the brook where outcrop is abundant.

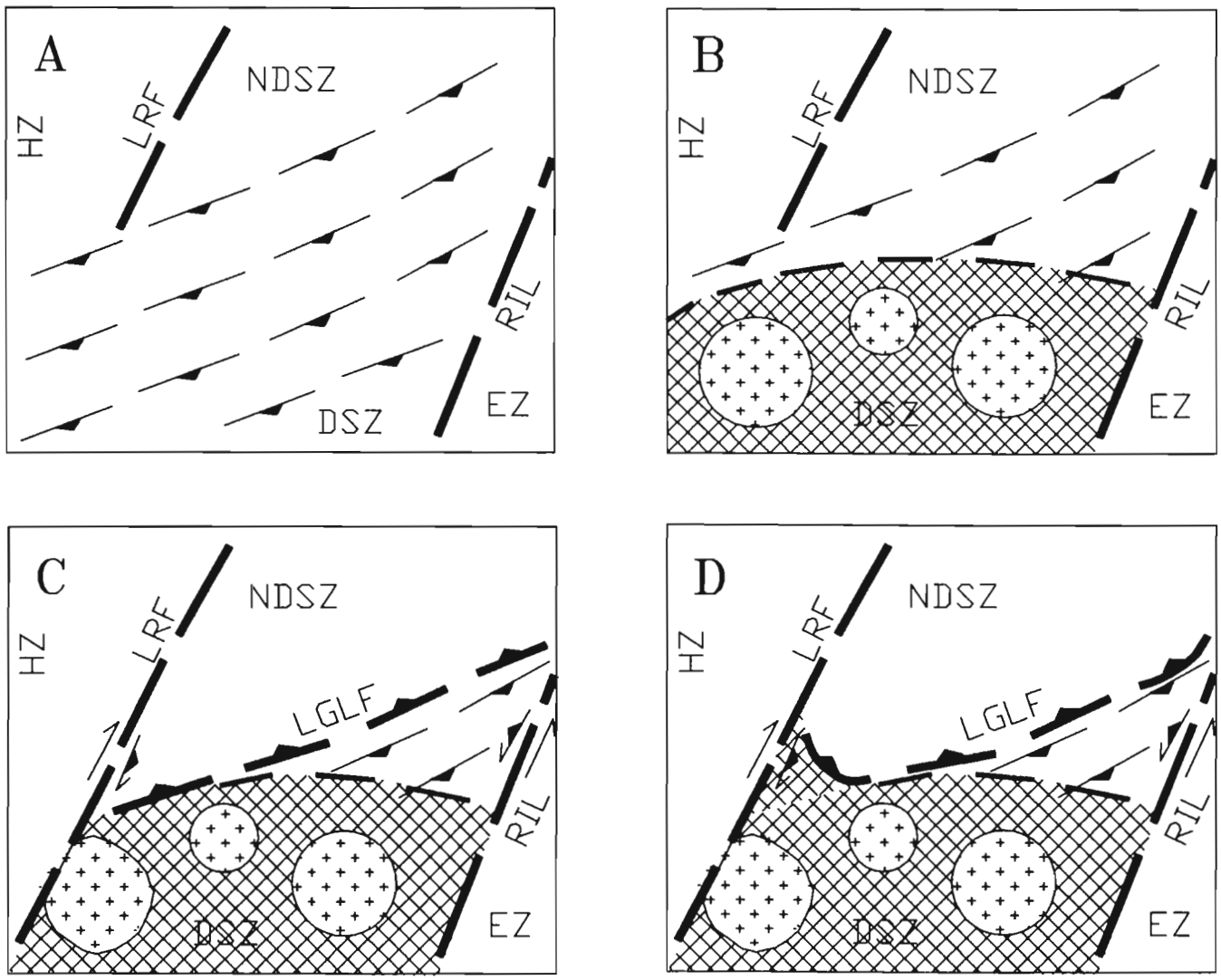

A. Mid-Ordovician(?) thrusting of the Dashwoods Subzone over the Notre Dame Subzone. The zone of imbrication is assumed to cross the (inactive) Long Range Fault.

B. Syn- and postthrusting metamorphism and plutonism in the thrust stack, obliterating much of the evidence of thrusting in the high-grade metamorphic rocks.

C. Post-Early Silurian reactivation of the Long Range Fault as a dextral feature, and the Red Indian Line as a sinistral feature, resulting in southward translation of the Notre Dame Subzone and development of the Little Grand Lake Fault. The fault is assumed to be marked by abrupt truncation of a thrust slice of Notre Dame lithologies at the west end, and by a zone of imbrication of Notre Dame and Dashwoods lithologies at the east end.

D. Present configuration after further movement on the Long Range Fault and Red Indian Line, resulting in warping of the Little Grand Lake Fault.

Figure 3. Cartoon of the possible development of the Little Grand Lake Fault and related structures. Abbreviations are as in Figure 1, with the following additions; HZ-Humber Zone; NDSZ-Notre Dame Subzone; DSZ-Dashwoods Subzone; EZ-Exploits Subzone. The hachured area represents high grade metamorphic rocks, the pattern of crosses represents plutons emplaced during this event.

We conclude that the Little Grand Lake lineament marks a complex boundary zone between the Notre Dame and Dashwoods subzones within which deep level crustal rocks of the Dashwoods Subzone were tectonically uplifted into juxtaposition with high level rocks of the Notre Dame Subzone by south-over-north movements distributed over numerous zones of ductile shearing. If discrete major zones of movement existed, they were buried beneath the Topsails Intrusive Suite by later north-over-south thrusting, or obliterated by syntectonic plutonism and static annealing such that evidence for dynamic recrystallization was destroyed. These north-over-south movements coincided with a late phase of Ordovician(?) plutonism and metamorphism in the Dashwoods Subzone. Subsequently the Notre Dame Subzone was thrust southward over the Dashwoods Subzone by post-Topsails Intrusive Suite movements along a zone of low angle brittle-ductile motion. The emplacement age of the Topsails Intrusive Suite has been precisely dated at 429 ± 3 Ma (Whalen et al., 1987).

Between Little Grand Lake and Red Indian Lake, interleaving of Dashwoods and Notre Dame lithologies may be due to multiple faults or thrusts. The apparent repetition of lithologies across strike is compatible with a thrust sequence. Mylonite zones along the Red Indian Line and northeastern Little Grand Lake Fault which cut the Topsails Intrusive Suite (Fig. 1 and 2) demonstrate ductile movement in post-Early Silurian time. Early Silurian intrusive rocks in Notre Dame Subzone remote from the Notre Dame-Dashwoods boundary are undeformed whereas plutons of equivalent age in the broad boundary zone have been ductilely deformed. This post-Early Silurian deformation is assumed to be equivalent to the brittle-ductile north-over-south motions observed further west. These movements appear to have been complex and extensive.

Our work has identified both metaluminous and peraluminous granites of probable Silurian age in the northeast Dashwoods Subzone. In the Notre Dame Subzone the Topsails Intrusive Suite is entirely metaluminous to peralkaline. A contrast in contemporaneous granite magmas must reflect differences in sources. Peraluminous granites require significant involvement of supracrustal components whereas the Topsails suite was derived mainly from infracrustal or I-type sources. No such geochemical contrasts exist between Ordovician intrusions (Whalen, unpub. data) or pre-Topsails Early Silurian mafic intrusive rocks in the two subzones (Currie and van Berkel, 1989). These observations suggest that the Notre Dame-Dashwoods boundary separates differing crustal lithologies, an interpretation supported by preliminary isotopic data (Whalen and Jenner, unpub. data). In this model, Ordovician plutons, and Early Silurian mafic plutons would be derived from subcrustal sources, which do not differ between subzones. The Topsails Intrusive Suite and contemporary granitoid rocks of the Dashwoods Subzone are assumed to be derived from higher-level sources, which differ between subzones.

Our observations can be summarized as follows. (1) Along Little Grand Lake there is an abrupt juxtaposition of granulite and subgreenschist facies rocks, accompanied by evidence for older synplutonic south-over-north motion, and younger north-over-south motion. (2) Between Little Grand Lake and Red Indian Lake, Notre Dame and Dashwoods lithologies are repeatedly juxtaposed in a geometry which suggests thrust imbrication. (3) Petrographic observations suggest both synplutonic and postplutonic deformation. (4) Latest movements on both the Little Grand Lake Fault and Red Indian Line post-date emplacement of the Early Silurian Topsails Intrusive suite (429 ± 3 Ma). (5) Primary igneous mineralogy is preserved in the northeastern corner of the Dashwoods Subzone, but is progressively metamorphically overprinted to the south and southwest. (6) Field, geochemical, and isotopic data demonstrate that Silurian granite plutons had differing crustal sources in the Dashwoods and Notre Dame subzones, but Ordovician and Silurian plutonic rocks of subcrustal derivation are similar or identical in the two subzones.

These observations can be explained by a synthetic model presented in cartoon form in Figure 3. South-over-north thrusting of the Dashwoods Subzone over the Notre Dame Subzone (Fig. 3A) is assumed to be the earliest detectable event, probably of mid-Ordovician age and connected with closure of the Iapetus Ocean. Thrusting is assumed to be followed or accompanied by mid- to late Ordovician metamorphism and emplacement of plutons (Fig. 3B). We assume metamorphic isograds cut obliquely across the north-verging imbrication, so that evidence of imbrication is destroyed in the high-grade rocks south of Little Grand Lake but preserved in the lower grade rocks further east. Since thrusting and metamorphism cross the Long Range Fault, this fault, the boundary between the Humber and Dunnage zones, is assumed to have been inactive at this time. We have no evidence that the Red Indian Line was active or inactive. In post-Topsails (Lower Silurian) time the Notre Dame Subzone was thrust south over the Dashwoods Subzone (Fig. 3C), producing abrupt juxtaposition of high- and low-grade rocks around Little Grand Lake, where a slice of low-grade rocks is assumed to lie on the high-grade rocks, but exposing an imbricate zone further east. The model implies that the sole of this imbricate stack must lie south of the southernmost exposure of Notre Dame lithology. In the region east of Little Grand Lake this is substantially further south than the position of the Little Grand Lake Fault shown by Currie and van Berkel (1992), and follows approximately the marked topographic break extending east-southeast from Little Grand Lake. Continued north- over-south thrusting could produce the pronouncedly curved trace of the Little Grand Lake Fault (Fig. 3D).

ACKNOWLEDGMENTS

Our field investigations were guided by manuscript maps prepared by J.T. van Berkel. J. Whalen benefitted from the able mapping assistance of M. O'Keefe.

REFERENCES

Currie, K.L.
1986: Geology of parts of Harry's River (12B/9) and Little Grand Lake (12A/12) map-areas, Newfoundland; Geological Survey of Canada, Open File Report 1409, scale 1:50 000; map with marginal notes.

Currie, K.L. and van Berkel, J.T.
1989: Geochemistry of post-tectonic mafic intrusions in the Central Gneiss Terrane of southwestern Newfoundland; Atlantic Geology, v. 25, p. 181-190.
1992: Notes to accompany a geological map of the southern Long Range, southwestern Newfoundland; Geological Survey of Canada, Paper 91-10, 10 p.

Currie, K.L., van Breemen, O, Hunt, P.A., and van Berkel, J.T.
1992: The age of granulitic gneisses south of Grand Lake, Newfoundland; Atlantic Geology, v. 28, p. 172-181.

Dunning, G.R., Carter, P.J., and Best, M.A.
1982: Geology of the Star Lake (west half), southwest Newfoundland; in Current Research, Part B; Geological Survey of Canada, Paper 82-1B, p. 21-26.

Kean, B.F.
1979: Geology of the Star Lake map area (12A/11) (east half), Newfoundland; Newfoundland Department of Mines and Energy, Mineral Development Division Map 79-1.

Knapp, D.A.
1979: Ophiolite emplacement along the Baie Verte-Brompton line at Glover Island, western Newfoundland; Ph.D. thesis, Memorial University of Newfoundland, St. John's, Newfoundland, 338 p.

McClay, K.R.
1987: The Mapping of Geological Structures; John Wiley and Sons, Toronto, Ontario, 312 p.

Nowlan, G.S. and Thurlow, J.G.
1984: Middle Ordovician conodonts from the Buchans Group, central Newfoundland, and their significance for regional stratigraphy of the Central Mobile Belt; Canadian Journal of Earth Sciences, v. 21, p. 284-286.

O'Brien, B.H.
1991: Geological development of the Exploits and Notre Dame subzones in the New Bay area (parts of NTS 2E/6,11), Notre Dame Bay, Newfoundland; in Newfoundland Department of Mines and Energy Report 91-1, p. 155-166.

O'Brien, B.H., O'Brien, S.J., and Dunning, G.R.
1991: Silurian cover, late Precambrian-Early Ordovician basement, and the chronology of Silurian orogenesis in the Hermitage flexure (Newfoundland Appalachians); American Journal of Science, v. 291, p. 760-799.

Piasecki, M.A.J., Williams, H., and Colman-Sadd, S.P.
1990: Tectonic relationships along the Meelpaeg, Burgeo and Burlington LITHOPROBE transects in Newfoundland; in Current Research, Newfoundland Department of Mines and Energy, Geological Survey Branch, Report 90-1, p. 327-339.

Thurlow, J.G.
1981: The Buchans Group: its stratigraphic and structural setting; in The Buchans Orebodies: Fifty Years of Geology and Mining, (ed.) E.A. Swanson, D.F. Strong and J.G. Thurlow, Geological Association of Canada, Special Paper 22, p. 79-91.

Twiss, R.J. and Moores, E.M.
1992: Structural Geology; Freeman and Company, New York, New York, 367 p.

van Berkel, J.T. and Currie, K.L.
1988: Geology of the Puddle Pond (12A/5) and Little Grand Lake (12A/12) map-areas, southwestern Newfoundland; Newfoundland Department of Mines, Mineral Development Division, Report 88-1, p. 97-107.

Whalen, J.B. and Currie, K.L.
1983: The Topsails igneous terrane of western Newfoundland; in Current Research, Part A; Geological Survey of Canada, Paper 83-1A, p. 15-23.
1988: Geology, Topsails Igenous Terrane, Newfoundland; Geological Survey of Canada, Map 1680A, scale 1:200 000.

Whalen, J.B., Currie, K.L., and van Breemen, O.
1987: Episodic Ordovician-Silurian plutonism in the Topsails Igneous Terrane, western Newfoundland; Transactions of the Royal Society of Edinburgh, v. 78, p. 17-28.

Williams, H.
1964: The Appalachians in northeastern Newfoundland - a two-sided symmetrical system; American Journal of Science, v. 262, p. 1137-1158

Williams, H., Colman-Sadd, S.P, and Swinden, H.S.
1988: Tectonic-stratigraphic subdivision of central Newfoundland; in Current Research, Part B; Geological Survey of Canada Paper 88-1B, p. 91-98.

Geological Survey of Canada Project 900037

Structure and anisotropy of magnetic susceptibility of the Rose Blanche Granite, southwestern Newfoundland: kinematics and relative timing of emplacement[1]

K. Benn[2], M. Genkin[2], C.R. van Staal, and S. Lin
Continental Geoscience Division

Benn, K., Genkin, M., van Staal, C.R., and Lin, S., 1993: Structure and anisotropy of magnetic susceptibility of the Rose Blanche Granite, southwestern Newfoundland: kinematics and relative timing of emplacement; in Current Research, Part D; Geological Survey of Canada, Paper 93-1D, p. 73-82.

Abstract: A preliminary structural and anisotropy of magnetic susceptibility (AMS) study of the syntectonic Rose Blanche Granite (RBG) is presented. This study shows that the Rose Blanche pluton was probably emplaced during the latest stages of D_2 and deformed during early-D_3, as weak but pervasive north-northeast-trending stretching lineations, recording high temperature deformation of the pluton, are compatible with D_3 regional transpression. Ductile and brittle-ductile shearing within the Rose Blanche pluton resulted from progressive D_3 deformation as the pluton cooled. It is suggested that the Rose Blanche pluton would serve as an ideal marker to constrain the timing of the onset of D_3 in the area.

Résumé : Une étude préliminaire de la structure et de l'anisotropie de la susceptibilité magnétique (ASM) du granite syntectonique de Rose Blanche (RBG) est présentée. Cette étude démontre que le pluton de Rose Blanche aurait été mis en place durant les stades finals de D_2 et aurait été déformé au cours de la phase initiale de transpression régionale D_3. On remarque la présence de linéations d'étirement de direction nord-nord-est à nord-est, de faible intensité mais très pénétratives, dans le pluton de Rose Blanche. Ces linéations, aussi montrées par des fabriques d'ASM, enregistrent une déformation D_3 de haute température. Ceci indique que le pluton de Rose Blanche aurait été mis en place durant les stades finals de D_2 ou au début de D_3. Des cisaillements ductiles et fragile-ductiles à l'intérieur du pluton de Rose Blanche témoignent d'une déformation D_3 progressive, lors du refroidissement du pluton. Les auteurs proposent que des datations isotopiques précises du pluton de Rose Blanche pourraient déterminer l'époque à laquelle a débuté la transpression D_3 dans cette région.

[1] Contribution to Canada-Newfoundland Cooperation Agreement on Mineral Development 1990-1994, a subsidiary agreement under the Economic and Regional Development Agreement. Project funded by the Geological Survey of Canada.

[2] Ottawa-Carleton Geoscience Centre, Department of Geology, University of Ottawa, Ottawa, Ontario K1N 6N5

INTRODUCTION

The structural study of syntectonic plutons provides useful information regarding the kinematics of crustal deformation related to, and synchronous with, their emplacement and subsequent cooling. Once the timing of magma emplacement relative to regional deformation events has been established through structural study within plutons and their wall rocks, the absolute age of the plutonic body may be obtained by isotopic methods, thus bracketing the ages of kinematic periods in the regional deformation history (Paterson and Tobisch, 1988). Furthermore, structures may be preserved within plutonic bodies which are overprinted in more ductile wall rocks during later deformation.

In granites, pervasive mineral *shape preferred orientations* (SPO) due to magmatic flow or to small degrees of *high temperature* (HT) solid state strain provide much of the information relating to magma emplacement and kinematics of deformation. These shape preferred orientation fabrics tend to be of low intensity. In general, foliations can be measured in the field, but mineral lineations may be difficult to determine directly, especially in rocks where they are defined by minerals which are weakly elongate (e.g. biotite or K-feldspar), or where outcrop conditions are poor. Anisotropy of magnetic susceptibility (AMS) can be used to indirectly determine the weak bulk shape preferred orientation of magnetic minerals in granitoids (Bouchez et al., 1990; Benn et al., in press). Where possible, anisotropy of magnetic susceptibility fabric orientations should be compared with field measurements of fabric elements, as inverse or intermediate anisotropy of magnetic susceptibility fabrics may result from the interference of structural fabrics or noncoaxiality of shape preferred orientation subfabrics corresponding to different mineral species (Rochette et al., in press; Benn et al., in press).

Field and anisotropy of magnetic susceptibility studies of pervasive mesoscopic fabric anisotropies in plutonic bodies must be complemented by detailed microstructural observations in order to determine whether the fabrics are related to emplacement or have been modified by later deformation (Paterson et al., 1989; Bouchez et al., 1990). Absence of textures or microstructures related to solid state deformation and/or recrystallization indicates that the rock fabric has been acquired during magmatic flow. The magmatic fabric may be modified to varying degrees by pervasive high temperature deformation (>550°C; Gapais, 1989) before cooling of the pluton; this deformation is recorded by intracrystalline substructures, elongate quartz and recrystallization. More discrete shear zones, with associated lower temperature metamorphic mineral assemblages, develop after cooling of the pluton.

In this paper we will present preliminary results of a structural and anisotropy of magnetic susceptibility study of the Rose Blanche granites, located within the Appalachians of southwestern Newfoundland. The goals of this paper are twofold: 1) to demonstrate how the study of structures within granite bodies, including weak deformational fabrics, can complement a classical structural study to unravel a regional kinematic picture; and 2) to provide new constraints on the relative timing of emplacement, with respect to the various phases of regional deformation, of the Rose Blanche granites.

REGIONAL GEOLOGY AND STRUCTURE

Geology

The Rose Blanche area is located within the Dunnage Zone of the Newfoundland Appalachians (Fig. 1). The geology of the area was first studied in detail by Brown (1976). Van Staal et al. (1992a) included the area in a reconnaissance geotraverse of southwestern Newfoundland between Cape Ray and the village of Rose Blanche. The following brief summary of the geology and structure of the Rose Blanche area is based on these previous works and on our field work carried out in 1992.

Supracrustal rocks of the Rose Blanche area are amphibolite grade pelitic schists and lesser feldspathic psammites of the Harbour le Cou Group (HLCG) (Lin et al., 1993; van Staal et al., 1992b). The Harbour le Cou Group is tightly infolded and intruded by abundant peraluminous and locally garnetiferous two-mica granites, collectively referred to as the Rose Blanche Granite. The Rose Blanche Granite resembles granites commonly found in collision zones (Maniar and Piccoli, 1989), generally considered to have been derived from melting of tectonically thickened crust, and emplaced near the end of large-scale overthrusting. Examples include leucogranites of the Himalaya (LeFort, 1981) and the Massif Central, France (Jover and Bouchez, 1986), the Eocene Ladybird suite in the Omineca Belt, Canadian Cordillera (Carr, 1992), and the Décelles Batholith, Pontiac Subprovince, Quebec (K.B., work in progress).

Structure

Regional D_1 folding is not observed in the Rose Blanche area where it is entirely overprinted by D_2 structures which have themselves been locally reworked by D_3. D_2 resulted in the development of isoclinal and inclined F_2 folds in the Harbour le Cou Group, and a differentiated S_2 crenulation cleavage generally dipping moderately to the west (Fig. 2a). Based on observations of structural relationships, van Staal et al. (1992a) suggested that sheets of Rose Blanche Granite were emplaced syn-D_2. L_2 stretching lineations generally plunge to the west (Fig. 2a). L^1_2 intersection lineations and axes of intrafolial F_2 folds of quartz veins are subparallel to parallel to L_2. Within the study area, D_3 regional transpression has resulted in northeast-southwest tight to isoclinal refolding of D_2 fabrics. Small scale F_3 folds and dextral D_3 chevrons and kink bands are abundant. S_3 crenulation cleavage is well developed in the Harbour le Cou shear zone (HLCSZ). F_3 axis orientations (Fig. 2b) vary from steeply NW-plunging where D_3 is less intense, to shallowly northeast-plunging in the Harbour le Cou shear zone where they appear to have been rotated into parallelism with the movement vector within the shear zone.

STRUCURE OF THE ROSE BLANCHE GRANITE

The Rose Blanche Granite is present both as sill-like sheets and as larger discrete plutons. This work concentrated on an area around the village of Rose Blanche, where a homogeneous medium grained granite pluton outcrops over about 5 km^2 along the coast (Fig. 1). The pluton will herein be referred to as the Rose Blanche pluton.Several generations of structures are identified within the Rose Blanche Granite, recording deformation at different stages in its emplacement and cooling history. This allows determination of the relative time of emplacement of the granite with respect to deformation. These generations of structures will be discussed from oldest to youngest.

D_2

Thin sheets of Rose Blanche Granite are characterized by the presence of a magmatic interlayering of pegmatite and medium grained granite. An S_2 foliation and a west-plunging L_2 stretching lineation, concordant with those in the host metasediments, are superimposed on magmatic grain-size layering in the sheets to the west of the Rose Blanche pluton. L_2 in the sheets is defined by stretched quartz and mica aggregates in the medium grained rock. These D_2 fabrics are affected by north-northeast-trending F_3 folds, and a steeply west-dipping S_3 axial planar foliation defined by micas is locally well developed. These structures and others indicate that the granite intruded late syn-D_2 (van Staal et al., 1992; Lin et al., 1993)

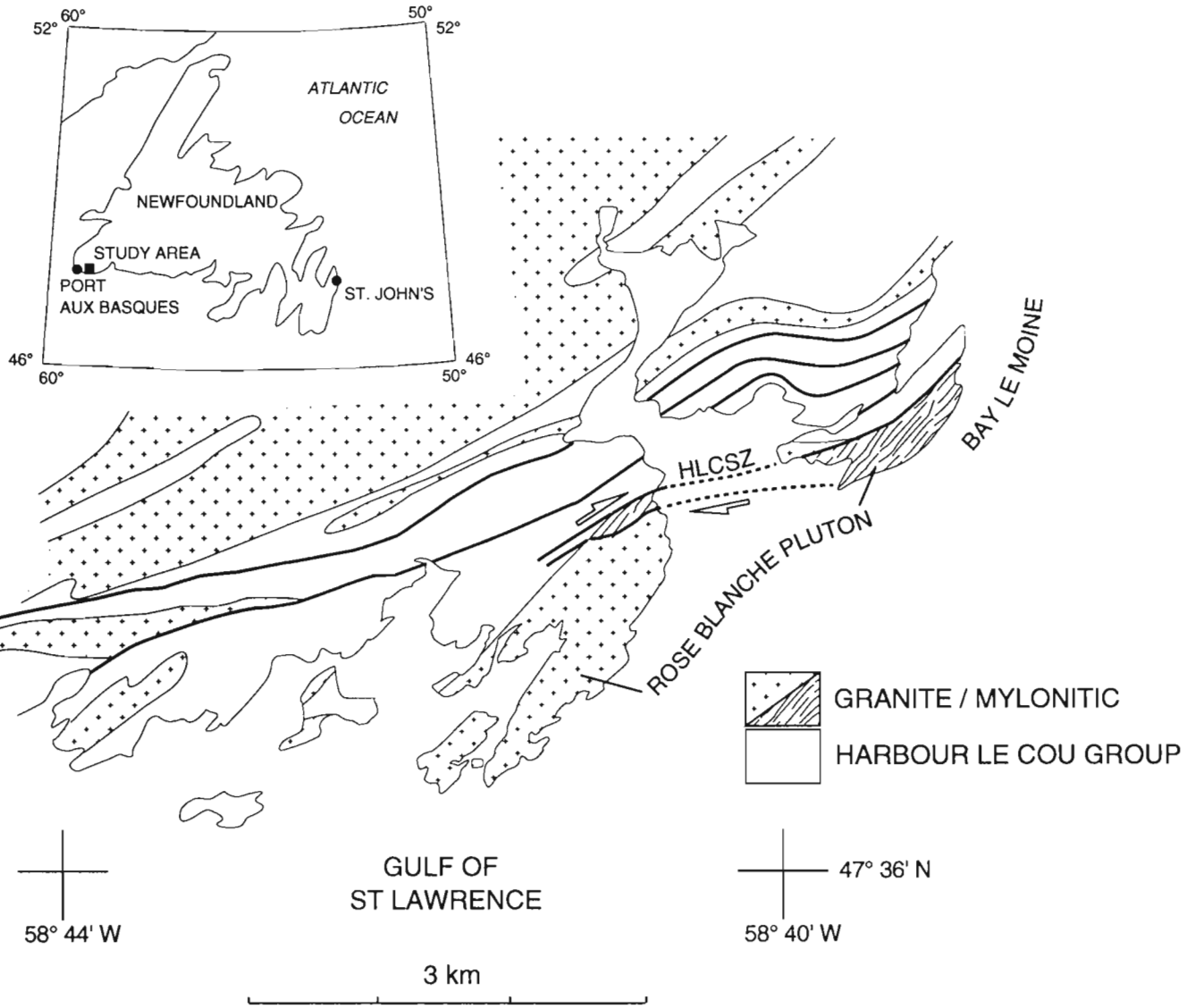

Figure 1. Location map of the Rose Blanche area.

early-D_3

A penetrative mineral shape preferred orientation foliation is present throughout the Rose Blanche pluton. The foliation strikes northeast and dips gently to moderately to the northwest (Fig. 2c, 3b). The dip of the foliation becomes slightly steeper approaching the Harbour le Cou shear zone on the northern margin of the pluton, where the granite has been mylonitized. Within this foliation, a weak lineation defined by elongate quartz can be measured in some outcrops, and trends north-northeast to northeast (Fig. 2c, 3a). These penetrative stretching lineations are highly discordant with respect to L_2, but are also overprinted locally by shearing related to D_3 (see below). As north-northeast-south-southwest to northeast-southwest stretching is kinematically compatible with D_3 regional transpression, we tentatively interpret the stretching lineation and associated foliation in the pluton as early-D_3, and will refer to them herein as the early-D_3 fabrics, and as the S_3 foliation and the L_3 stretching lineation.

Thin section observations of the early-D_3 fabrics indicate that a small amount of solid-state strain has affected the pluton over its entire outcrop area. Strain is recorded by the elongate shapes of quartz aggregates, which typically have aspect ratios of about 4:1 observed in thin sections cut parallel to the lineation and perpendicular to the foliation. Varying degrees of dynamic recrystallization of quartz have accompanied strain. Highly embayed quartz-quartz grain boundaries indicate that grain boundary migration was probably the

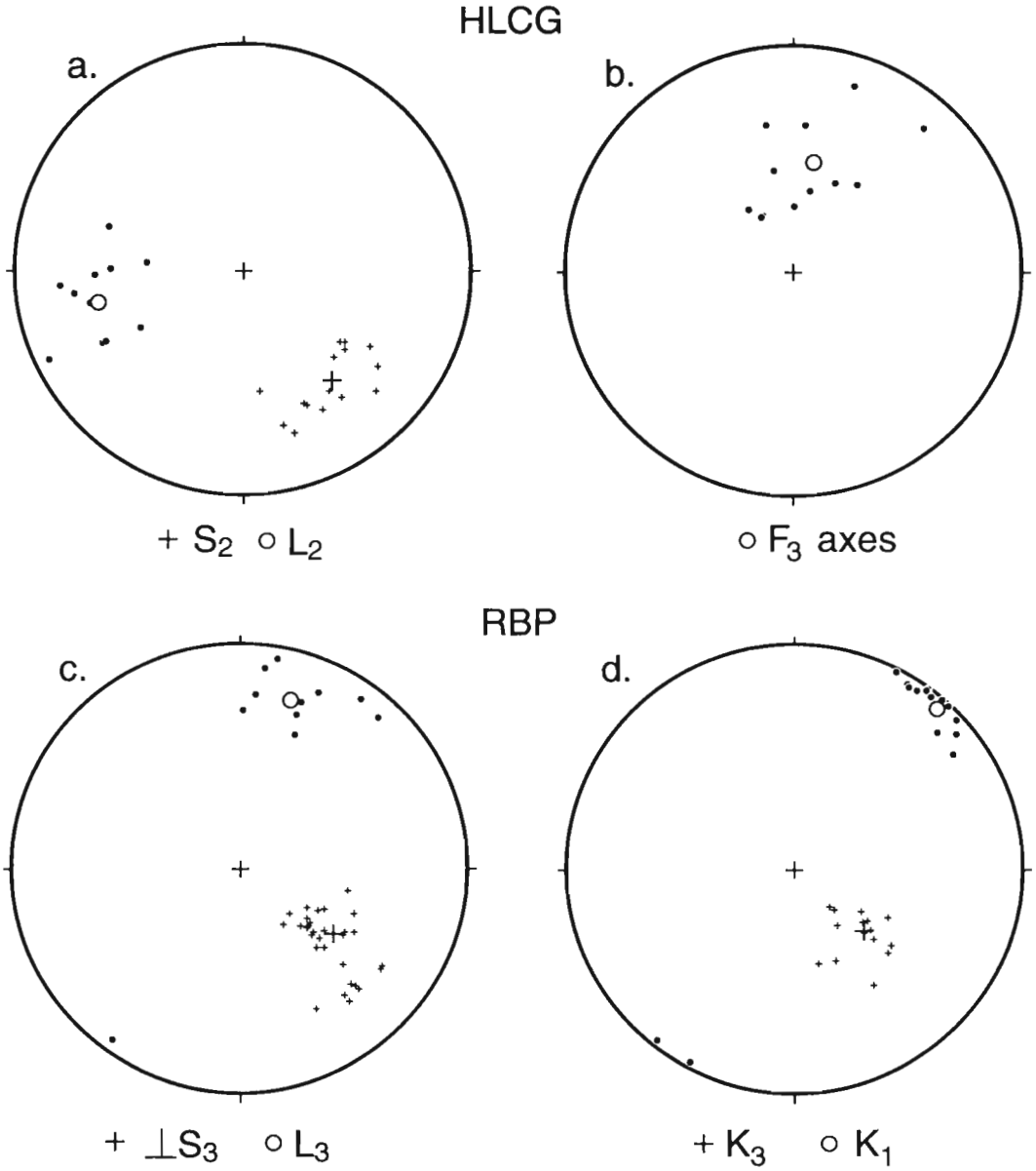

Figure 2. Equal-area lower-hemisphere plots of important structural and magnetic fabric elements. HLCG: Harbour le Cou Group, RBP: Rose Blanche pluton.

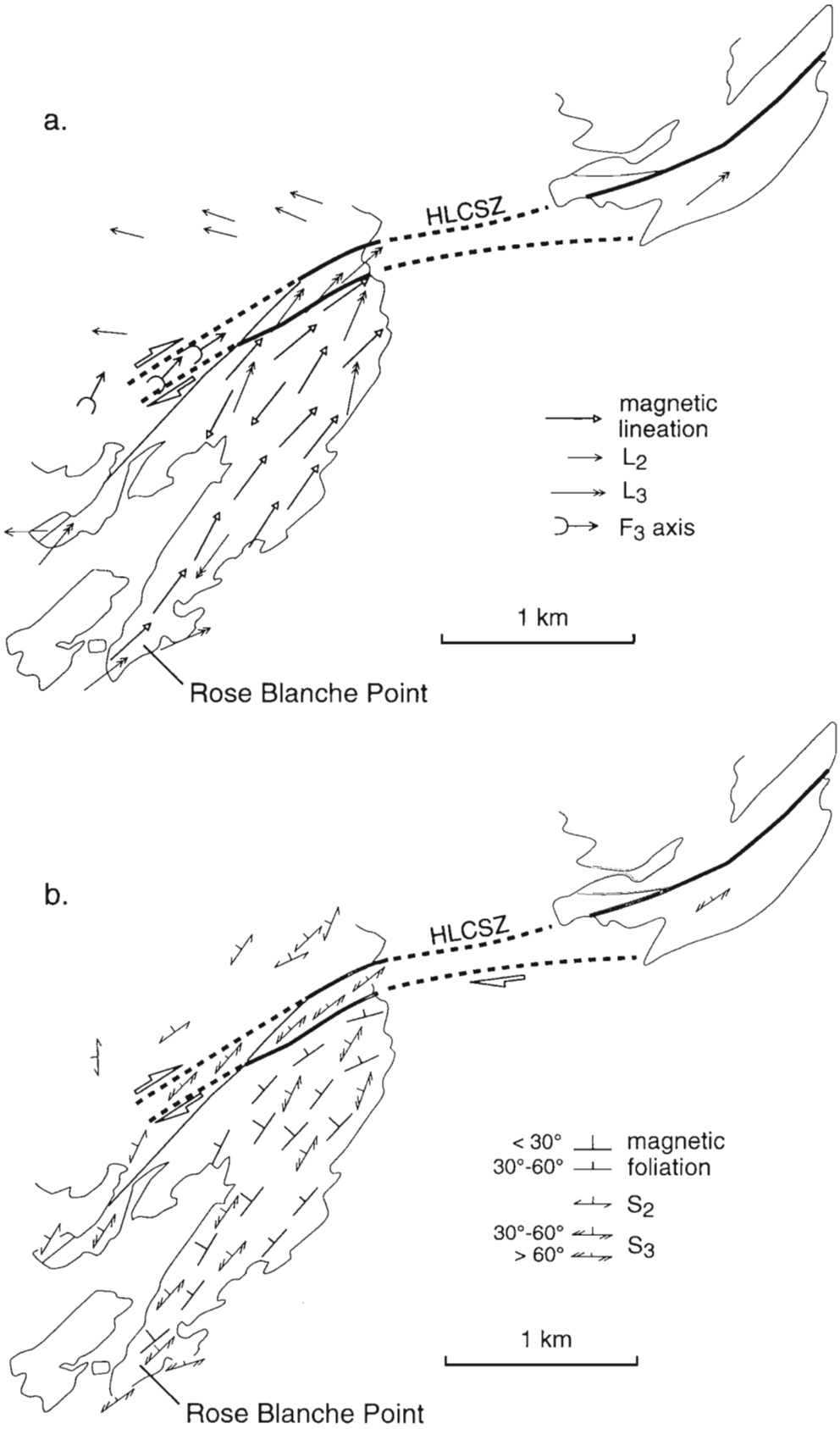

Figure 3. Simplified structural maps of the study area. For geology refer to Figure 1. HLCSZ: Harbour le Cou shear zone.

dominant recrystallization mechanism. This suggests that the quartz recrystallized under relatively high temperature conditions, a conclusion supported by the homogeneous distribution of strain throughout the pluton, which can be qualitatively determined by observation of the relative intensity of the fabric from outcrop to outcrop. These observations of recrystallization textures and mesoscopic structure indicate that the early-D_3 fabric was acquired following crystallization of the granite but before the pluton had cooled to temperatures where quartz dominantly deforms by solution transfer mechanisms (≈greenschist facies conditions).

Anisotropy of magnetic susceptibility analysis

Anisotropy of magnetic susceptibility analysis was carried out to indirectly determine the mineral shape preferred orientation, in order to verify our field measurements of the early-D_3 fabrics. Many previous studies of anisotropy of magnetic susceptibility fabrics in various rock types have shown that in most cases, the K_3 principal direction of the anisotropy of magnetic susceptibility ellipsoid (hardest magnetization direction) is perpendicular to the mineral foliation, while the K_1 principal direction (easiest magnetization direction) is parallel to the mineral or stretching lineation. Hence, the plane perpendicular to K_3 is referred to as the *magnetic foliation*, and K_1 is referred to as the *magnetic lineation* (Rochette et al., in press). Three 22.5 mm diameter drill cores were collected at each of 15 evenly spaced sampling sites within the weakly deformed part of the pluton. Two samples of 19 mm length were cut from each core and anisotropy of magnetic susceptibility measurements were carried out using a Kappabridge KLY-2 a.c. bridge (field strength 300 A m^{-1}, operating frequency 920 Hz) at the Department of Geology, University of Ottawa.

Magnetic susceptibility

In the general case, the magnetic susceptibility of a rock will be due to two components (Rochette, 1987): a matrix component made up of paramagnetic ferrosilicates and diamagnetic minerals (quartz, feldspar); and a component corresponding to disseminated ferromagnetic (s.l.) minerals (e.g. magnetite, hematite). The intrinsic susceptibility of ferromagnetic minerals is about 2 to 6 orders of magnitude greater than that of paramagnetic minerals (Borradaile, 1988), while the susceptibility of the diamagnetic minerals of the matrix is negligible. However, where the magnetic susceptibility of the rock is weak ($<10^{-3}$ SI), it may be dominated by the paramagnetic ferrosilicates (Rochette, 1987). For rocks where the *anisotropy* of the magnetic susceptibility is also dominated by paramagnetic minerals, the anisotropy parameter ($P = K_1 / K_3$) should not exceed 1.35 (Rochette, 1987). As pointed out by Benn et al. (in press), the presence of disseminated ferromagnetic minerals in the rock will also give rise to wide variations in both susceptibility and in anisotropy parameter at the outcrop scale.

A plot of the anisotropy parameter (P) vs. susceptibility (K) for each sample is presented in Figure 4a. Also indicated is the field for anisotropies and susceptibilities for rocks where the susceptibility would be due solely to ≤10% modal biotite ($K \approx 1300 \times 10^{-6}$). All samples fall within this field. The low values of anisotropy parameter and the very small variations in K indicate that both the susceptibility and the anisotropy of magnetic susceptibility are probably due to biotite.

In Figure 4b, we present a plot of anisotropy parameter versus the shape parameter for the susceptibility ellipsoid ($T = 2(\ln K_2 - \ln K_3)/(\ln K_1 - \ln K_3) - 1$) (Borradaile, 1988). For perfectly oblate ellipsoids T = 1, while T = -1 for perfectly prolate ellipsoids. The shape parameter is controlled by both the intrinsic anisotropy of magnetic susceptibility of biotite (almost perfectly oblate), and by the intensity and the symmetry of the biotite preferred orientation. During noncoaxial laminar flow, platy minerals such as biotite tend to align themselves in a zone about the finite stretching direction; the magnetic lineation (K_1 principal direction) will in this case correspond to the zone axis and to the X-direction of the finite strain ellipsoid (Bouchez et al., 1990). An increase in the flattening component of strain would result in a stronger orientation of biotite plates within the foliation plane, and thus a higher (positive) value of "T". In previous studies of the variations of shapes of anisotropy of magnetic

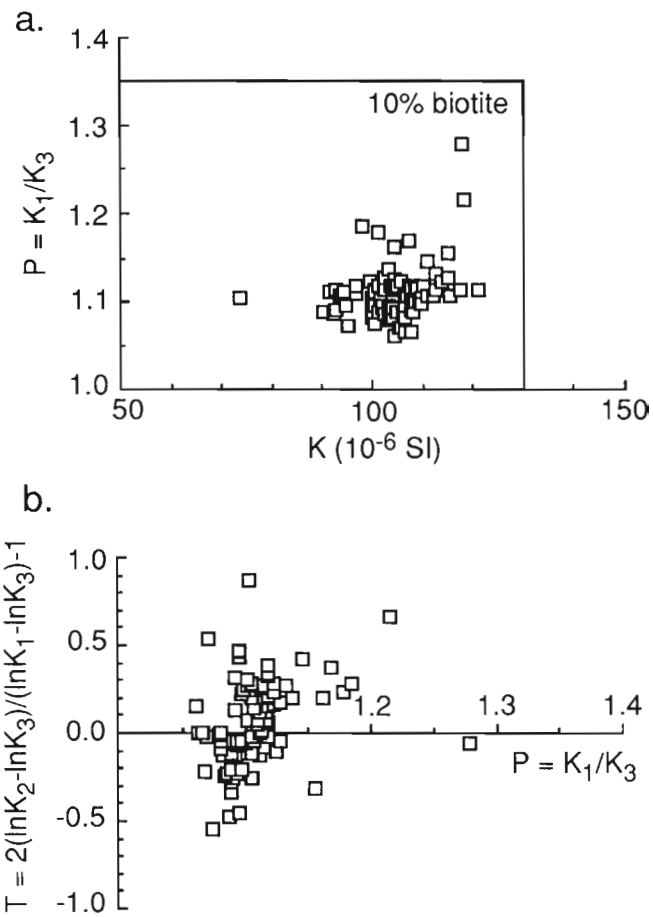

Figure 4. Plots of AMS fabric parameters for all samples collected within the Rose Blanche pluton. See discussion in text.

susceptibility ellipsoids within syntectonic granites, it has been shown that ellipsoids tend to be linear to planar-linear ($-1 \leq T \leq 0$) towards the interior of the plutons where textural evidence indicates the fabric is essentially due to magmatic flow, and more flattened towards the margins ($T > 0$) where the rock has undergone more solid-state strain (Guillet et al., 1983; Gleizes et al., 1991). Mesoscopically, this translates into a more intensely developed biotite foliation near pluton margins. Our samples show a moderate variation in ellipsoid shapes, most having $-0.5 \leq T \leq 0.5$. A map of the distribution of site-average values of the shape parameter is given in Figure 5. There is no relationship between locations of the sampling sites and proximity of the Rose Blanche pluton margin, nor does the ellipsoid shape become particularly flattened near the Harbour le Cou shear zone. The anisotropy of magnetic susceptibility data indicate that the biotite preferred orientations within the pluton record a relatively homogeneous distribution of weak ductile strain throughout the pluton, supporting our qualitative interpretation based on the intensity of the foliation observed in outcrop.

Directional data

Equal-area plots of the magnetic lineations and the poles to the magnetic foliations are presented in Figure 2d. These measurements correspond to the major and minor principal axes of the site average anisotropy of magnetic susceptibility ellipsoids calculated using the method of Jélinek (1978). Average poles to magnetic foliations are tightly grouped, and agree well with the poles to the measured mineral foliation. Average magnetic lineations form a tight cluster with an average subhorizontal northeast-southwest orientation, and are close to the measured stretching lineations within the pluton, though magnetic lineations tend to be slightly more easterly trending. The nature of this obliquity is intriguing, but it may be only apparent. Magnetic lineations represent the average petrofabric of all biotites contained in about 50 cm^3 of rock from an outcrop. The stretching lineations in the Rose Blanche pluton are relatively weak, and the accuracy of field measurements may not be as reliable as the anisotropy of magnetic susceptibility measurements.

Another interpretation of the obliquity between stretching and magnetic lineations in the pluton would involve an interference between two generations of structural fabrics, i.e. a refolding of the early-D_3 foliation by F_3. Aubourg et al. (1991) documented magnetic lineations nonparallel to stretching lineations in their study of weakly deformed black shales in the western Alps, and attributed this to the refolding of an older mica foliation. They interpreted the magnetic lineation as being parallel to the fold hinge lines, which would represent the rotation axis of the micas. It is unlikely that the magnetic lineations in the Rose Blanche pluton would represent F_3 fold axes because: 1) in thin sections cut perpendicular to the magnetic lineation, kinking of biotites, which would be expected if the rock were shortened

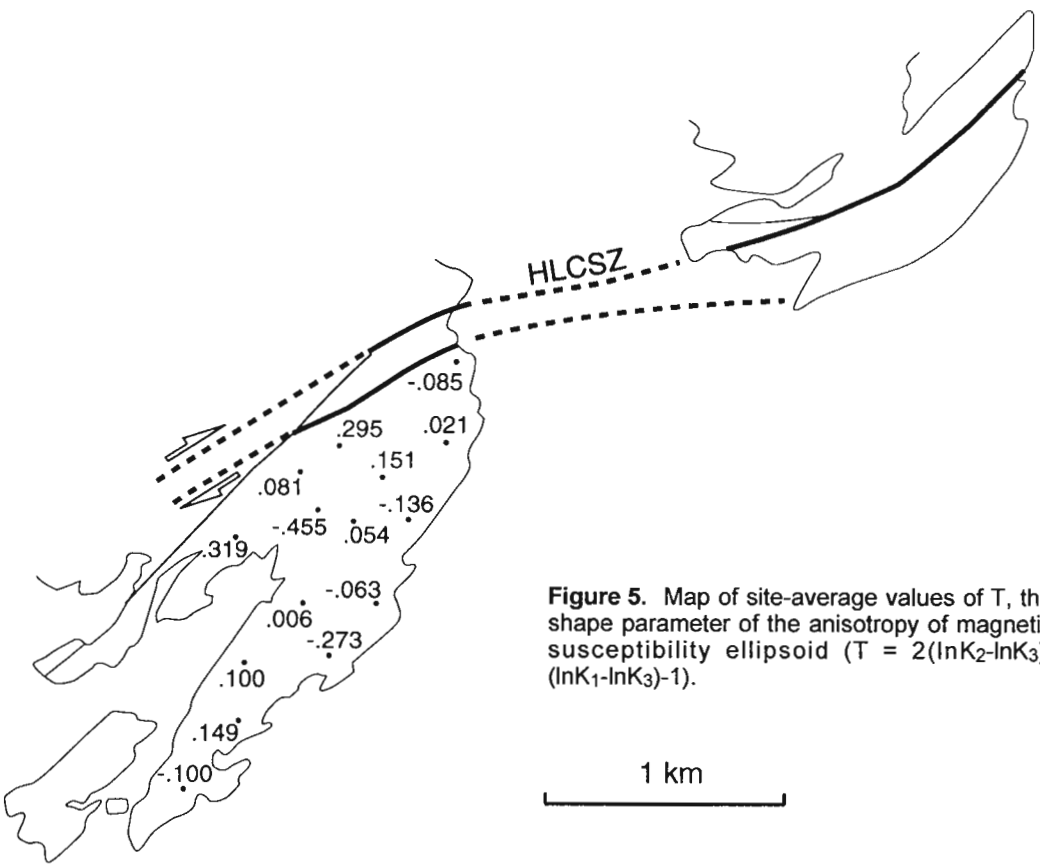

Figure 5. Map of site-average values of T, the shape parameter of the anisotropy of magnetic susceptibility ellipsoid ($T = 2(\ln K_2 - \ln K_3)/(\ln K_1 - \ln K_3) - 1$).

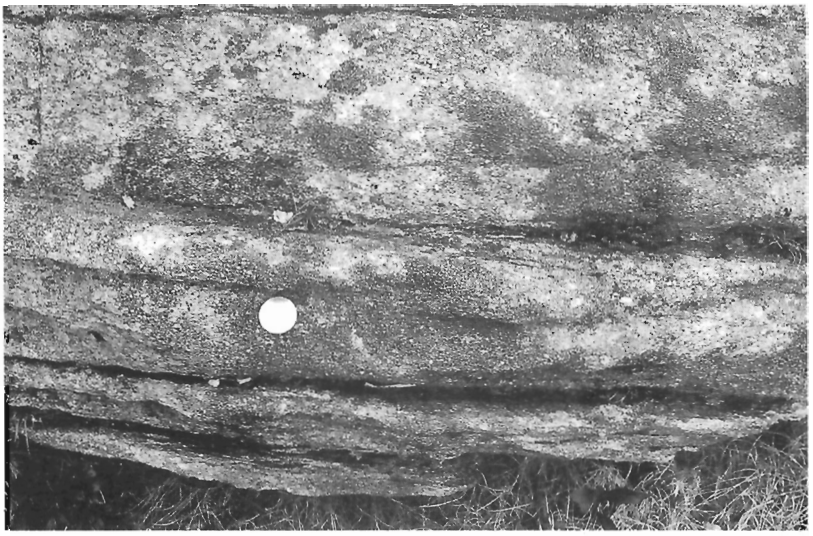

Figure 6.

Brittle-ductile D_3 shear zones within the S_3 foliation plane (Rose Blanche pluton). Shear zones are parallel to the long dimension of the photo. Diameter of coin is 2.6 cm.

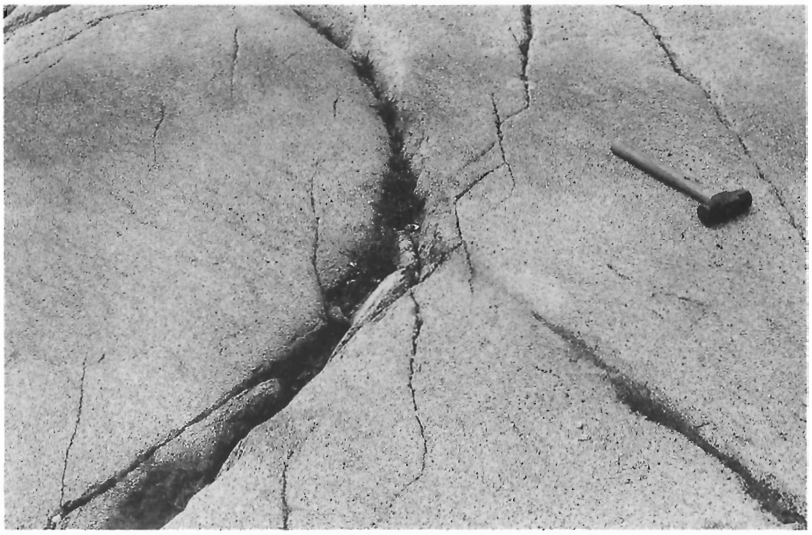

Figure 7.

Brittle-ductile D_3 shears in the Rose Blanche pluton, near the southern extremity of Rose Blanche Point (Fig. 3). The hammer is oriented about north-south, with the head to the north.

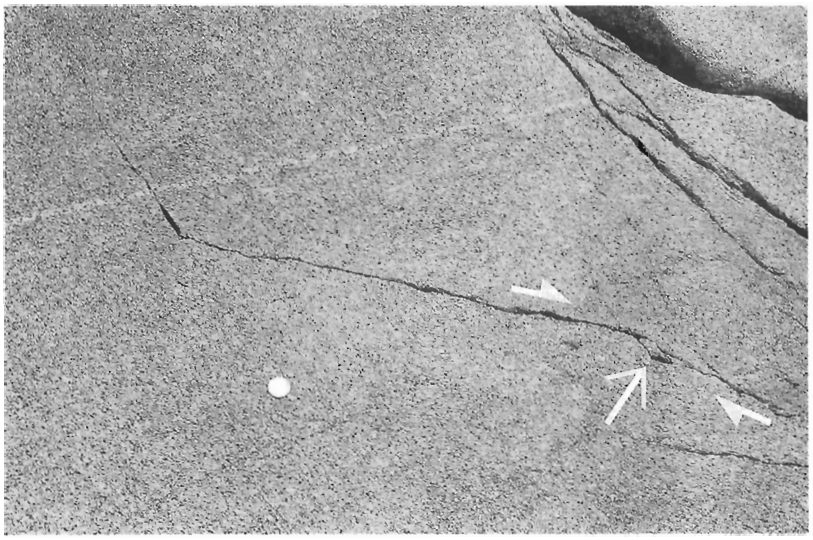

Figure 8.

Close-up view of brittle-ductile D_3 shears, same location as in Figure 7. The long dimension of the photo is oriented about north-south. The full arrow indicates a dextral pull-apart structure.

perpendicular to a pre-existing foliation, is very rare, and 2) poles to the magnetic foliation are tightly grouped and parallel to poles to the mineral foliation, and do not define a girdle as would be expected if the biotite foliation were folded. We therefore interpret the magnetic fabrics as recording a northeast to north-northeast early-D_3 shearing.

late-D_3

Several families of structures in the Rose Blanche pluton record ductile and brittle-ductile D_3 shearing, concentrated on the northern margin of the pluton and on Rose Blanche Point (Fig. 3). Ductile D_3 shear zones trend about 070° and dip steeply to the northwest. D_3 shearing on the northern margin of the pluton is concentrated within the mylonitic Harbour le Cou shear zone. On Rose Blanche Point, S-C fabrics are developed within shear zones up to several metres wide, though no true mylonites (in the sense of Hanmer, 1987) have been observed. The presence of these latter shear zones suggests that a larger ductile feature may be present to the south of the exposed pluton. S-C obliquities and gently northeastward-plunging lineations within these shear zones indicate a dominantly dextral strike-slip sense of movement associated with a small extensional component.

Two main families of brittle-ductile D_3 shears have been observed, concentrated mostly near the southern exposures on Rose Blanche Point. One family trends about 070° and dips steeply northwest, parallel to the ductile D_3 shear zones, while another family trends north to northeast, within the plane of the early-D_3 mineral foliation (Fig. 6). These small shear zones vary in thickness from a few millimetres (more brittle) to 10 cm (more ductile). The two families of shears can be seen to link up, where the 070° shears join terminations of the north-northeast-trending shears (Fig. 7). The formation of small pull-aparts at the junction of shears belonging to the two families testifies to the dextral movement on them (Fig. 8). Striations can be observed on the surfaces of narrower brittle-ductile shears; on the foliation-parallel shears striations plunge north-northeast, while on the east-northeast shears striations are subhorizontal or plunge gently to the east. These two families of late shears are thus kinematically congruent with the early-D_3 penetrative fabrics and with D_3 recorded within the Harbour le Cou shear zone.

SUMMARY

L_2 stretching lineations in the Harbour le Cou Group and in thin sheets of Rose Blanche granite within these rocks record bulk shearing, probably associated with D_2, which was transverse to the orogenic belt (van Staal et al., 1992b). Within the Rose Blanche pluton, low-intensity but very penetrative foliations and stretching lineations, which are corroborated by well defined magnetic fabrics, are tentatively attributed to early-D_3. These L_3 lineations within the pluton trend north-northeast to northeast, and record a principal stretch which is kinematically compatible with D_3 regional transpression. The homogeneous distribution of early-D_3 strain throughout the pluton as reflected in the nature of both the mesoscopic fabrics and the magnetic fabrics, along with the relatively high temperature recrystallization textures observed in quartz, indicate that the early-D_3 deformation affected the pluton before appreciable cooling, probably soon after emplacement and full crystallization. Our study suggests that the emplacement of the Rose Blanche Granite suite took place close to the transition between the orogen-transverse (D_2) and the orogen-parallel (D_3) kinematic frameworks.

At lower temperatures, ductile shear zones developed within the pluton in response to D_3. Deformation continued as the pluton cooled further into brittle-ductile conditions resulting in brittle-ductile shearing both parallel to the ductile shear zones, and also within the pre-existing plane of anisotropy defined by the early-D_3 mineral foliation in the pluton. Both the ductile and brittle-ductile shear zones within the pluton are dextral. Thus the shearing movement on foliation-parallel brittle-ductile D_3 shears appears to be kinematically congruent with the penetrative early-D_3 deformation in the pluton. This suggests that the different generations of structures within the pluton record progressive D_3 deformation synchronous with progressive cooling of the pluton.

CONCLUSIONS

This paper shows that a structural and anisotropy of magnetic susceptibility study of syntectonic plutons and their wall rocks can add to the understanding of the structural and tectonic evolution of a region. The structural, microstructural, and anisotropy of magnetic susceptibility study presented here shows that orogen-parallel stretching lineations, compatible with regional D_3 transpression, were imparted into a probably fully crystallized but still relatively hot Rose Blanche pluton. This is consistent with field structural evidence suggesting that the pluton had intruded during the latest stages of D_2 (van Staal et al., 1992a, b; Lin et al., 1993). D_3 ductile and brittle-ductile shearing of the pluton was synchronous with its progressive cooling. Precise isotopic dating of the crystallization and/or cooling ages of the pluton may provide tight constraint on the absolute timing of the transition between D_2 and D_3 and onset of D_3 in the Rose Blanche area.

ACKNOWLEDGMENTS

C. Lee is thanked for assistance and discussion in the field. This work was dominantly supported by an NSERC operating grant to K. Benn.

REFERENCES

Aubourg, Ch., Rochette, P., and Vialon, P.
1991: Subtle stretching lineation revealed by magnetic fabric of Callovian-Oxfordian black shales (French Alps); Tectonophysics, v. 185, p. 211-223.

Benn, K., Rochette, P., Bouchez, J.-L., and Hattori, K.
in press: Magnetic susceptibility, magnetic mineralogy and magnetic fabrics vs. structural fabrics in a late Archean granitoid-gneiss belt; Precambrian Research.

Borradaile, G.J.
1988: Magnetic susceptibility, petrofabrics and strain; Tectonophysics, v. 156, p. 1-20.

Bouchez, J.-L., Gleizes, G., Djouadi, T., and Rochette, P.
1990: Microstructure and magnetic susceptibility applied to emplacement kinematics of granites: the example of the Foix pluton (French Pyrenees); Tectonophysics, v. 184, p. 157-171.

Brown, P.A.
1976: Geology of the Rose Blanche map area (110/11); Newfoundland Department of Mines and Energy, Mineral Development Division, Report 76-5, 16 p.

Carr, S.D.
1992: Tectonic setting and U-Pb geochronology of the early Tertiary Ladybird leucogranite suite, Thor-Odin-Pinnacles area, southern Omineca Belt, British Columbia; Tectonics, v. 11, p. 258-278.

Chappell, B.W. and White, A.J.R.
1974: Two contrasting granite types; Pacific Geology, v. 8, p. 173-174.

Gapais, D.
1989: Shear structures within deformed granites: Mechanical and thermal indicators; Geology, v. 17, p. 1144-1147.

Gleizes, G., Leblanc, D., and Bouchez, J.-L.
1991: Le pluton granitique de Bassiès (Pyrénées ariégeoises): zonation, structure et mise en place; Comptes Rendus à l'Académie des Sciences, v. 312, p. 755-762.

Guillet, P., Bouchez, J.-L., and Wagner, J.-J.
1983: Anisotropy of magnetic susceptibility and magmatic structures in the Guérande granite massif (France); Tectonics, v. 2, p. 419-429.

Hanmer, S.
1987: Textural map units in quartzo-feldspathic mylonitic rocks; Canadian Journal of Earth Sciences, v. 24, p. 2065-2073.

Jelinek, V.
1978: Statistical processing of anisotropy of magnetic susceptibility measured on groups of specimens; Studia geophysica et Geodetica, v. 22, p. 50-62.

Jover, O. and Bouchez, J.-L.
1986: Mise en place syntectonique des granitoïdes de l'ouest du Massif Central français; Comptes Rendus à l'Académie des Sciences, v. 303, p. 969-974.

LeFort, P.
1981: Manaslu Leucogranite: A collision signature of the Himalaya and a model for its genesis and emplacement: Journal of Geophysical Research, v. 86, p. 10545-10568.

Lin, S., van Staal, C.R., and Lee, C.
1993: The Harbour Le Cou Group and its correlation with the Bay du Nord Group, southwestern Newfoundland; in Current Research, Part D; Geological Survey of Canada, Paper 93-1D.

Maniar, P.D. and Piccoli, P.M.
1989: Tectonic discrimination of granitoids; Geological Society of America Bulletin, v. 101, p. 635-643.

Paterson, S.R. and Tobisch, O.T.
1988: Using pluton ages to date regional deformations: problems with commonly used criteria; Geology, v. 16, p. 1108-1111.

Paterson, S.R., Vernon, R.H., and Tobisch, O.T.
1989: A review of criteria for the identification of magmatic and tectonic foliations in granitoids; Journal of Structural Geology, v. 11, p. 349-363.

Rochette, P.
1987: Magnetic susceptibility of the rock matrix related to magnetic fabric studies; Journal of Structural Geology, v. 9, p. 1015-1020.

Rochette, P., Jackson, M., and Aubourg, C.
in press: Rock magnetism and the interpretation of anisotropy of magnetic susceptibility; Reviews of Geophysics.

van Staal, C.R., Winchester, J.A., Brown, M., and Burgess, J.L.
1992a: A reconnaissance geotraverse through southwestern Newfoundland; in Current Research, Part D; Geological Survey of Canada, Paper 92-1D, p. 133-143.

van Staal, C.R., Burgess, J.L., Hall, L., Lee, C., Lin, S., and Schofield, D.
1992b: Geology of the Port aux Basques-Rose Blanche area (NTS 11-O/10 & 11-O/11); in Report of Activities 1992; Newfoundland Department of Mines and Energy, Geological Survey Branch. Government of Newfoundland and Labrador.

Geological Survey of Canada Project 730044

Application of FIELDLOG software to structural analysis in the Bathurst mining camp, New Brunswick[1]

J.A. de Roo[2], C.R. van Staal[3], and B. Brodaric[3]

de Roo, J.A., van Staal, C.R., and Brodaric, B., 1993: Application of FIELDLOG software to structural analysis in the Bathurst mining camp, New Brunswick; in Current Research, Part D; Geological Survey of Canada, Paper 93-1D, p. 83-92.

Abstract: This paper presents results of structural mapping of the Bathurst mining camp in the Appalachians of New Brunswick. The study area comprises Middle-Late Ordovician volcanogenic rocks (the Tetagouche and Fournier groups) and older turbiditic rocks (Miramichi Group). These units are exposed as pods of weakly deformed rocks that are encased in mostly steeply dipping mylonites, phyllites, and schists. The overall structure is complex as a result of multiple folding, kinking, and cleavage generation (the D_1-D_4 deformation events).

Structural data were recorded by means of customized software (FIELDLOG) and then exported to AUTOCAD and standard stereographic software. This enabled us to compute maps of the Bathurst camp, plot D_1-D_4 structural elements such as foliations and lineations separately, and extract stereograms. The result expands our understanding of the small-scale deformations to the regional scale and confirms that the major folds of the area are D_4 structures.

Résumé : On présente, dans cet article, les résultats de la cartographie structurale de la région du camp minier de Bathurst dans les Appalaches du Nouveau-Brunswick. La région à l'étude comprend des roches d'origine volcanique, datant de l'intervalle s'étendant de l'Ordovicien moyen à tardif (groupes de Tetagouche et de Fournier), et des roches turbiditiques plus anciennes (Groupe de Miramichi). Ces unités affleurent sous forme de masses minéralisées allongées, composées de roches faiblement déformées contenues dans des mylonites, des phyllites et des schistes accusant le plus souvent un fort pendage. La structure d'ensemble a été rendue complexe par des épisodes multiples de formation de plis, de flexures répétées, et de clivages (épisodes de déformation D_1 à D_4).

On a enregistré les données structurales au moyen d'un logiciel spécifique (FIELDLOG), puis on les a transférées dans le logiciel AUTOCAD et le logiciel stéréographique normalisé. On a ainsi pu dresser des cartes du camp minier de Bathurst au moyen de calculs, de représenter séparément les éléments structuraux D_1 à D_4 comme les foliations et linéations, et de produire des stéréogrammes. Les résultats permettent une meilleure compréhension, à l'échelle régionale, des déformations de petite échelle et confirment que les grands plis de la région sont des structures D_4.

[1] Contribution to Canada-New Brunswick Cooperation Agreement on Mineral Development 1990-1995, a subsidiary agreement under the Economic and Regional Development Agreement. Project funded by the Geological Survey of Canada.

[2] Quebec Geoscience Centre, Sainte-Foy

[3] Continental Geoscience Division

INTRODUCTION

The study area is located near Bathurst in northern New Brunswick (Fig. 1) and is of economic and tectonic importance. In economic terms it is known as the Bathurst mining camp, producing gold and base metals from several stratabound massive sulphide deposits (McAllister, 1960; Boyle, 1965; Franklin et al., 1981; Davies et al., 1983). In tectonic terms it is a window exposing the inner parts of the Appalachian Orogen, known as the Gander and Dunnage zones (Williams, 1979) or Central Mobile Belt (Williams, 1964; van der Pluijm and van Staal, 1988).

This report is part of a federal-provincial geological mapping project of several years, covering the Bathurst camp on a 1:20 000 scale. Mapping data presented here were recorded digitally on site using standard software (AUTOCAD v. 11) and customized software (FIELDLOG v. 2.83a; Brodaric, 1992). The FIELDLOG program can be run on a portable computer using an independent power base, and it was designed to tabulate mapping data on a geographic basis for export to spatial analysis or design programs such as SPANS or AUTOCAD. Because of complex and polyphase deformation in the Bathurst camp we used a customized version of FIELDLOG for analysis of structural data in stereographic projection (see Fig. 2) and in plan view. For the latter purpose, we used AUTOCAD to compute maps of the Bathurst camp and plot trends of foliations (S_1, S_2, etc.) and lineations (L_1, L_2, etc.) separately or in combination. Over 5000 digitized readings were processed. The result expands our understanding of small-scale tectonic overprinting relationships to the regional scale (see Fig. 3).

GEOLOGY OF THE BATHURST CAMP

The Bathurst area constitutes the northern part of the Miramichi Highlands, a belt of pre-Silurian rocks extending across New Brunswick (Ruitenberg et al., 1977; Fyffe, 1982; van Staal and Fyffe, 1991). The northern Miramichi

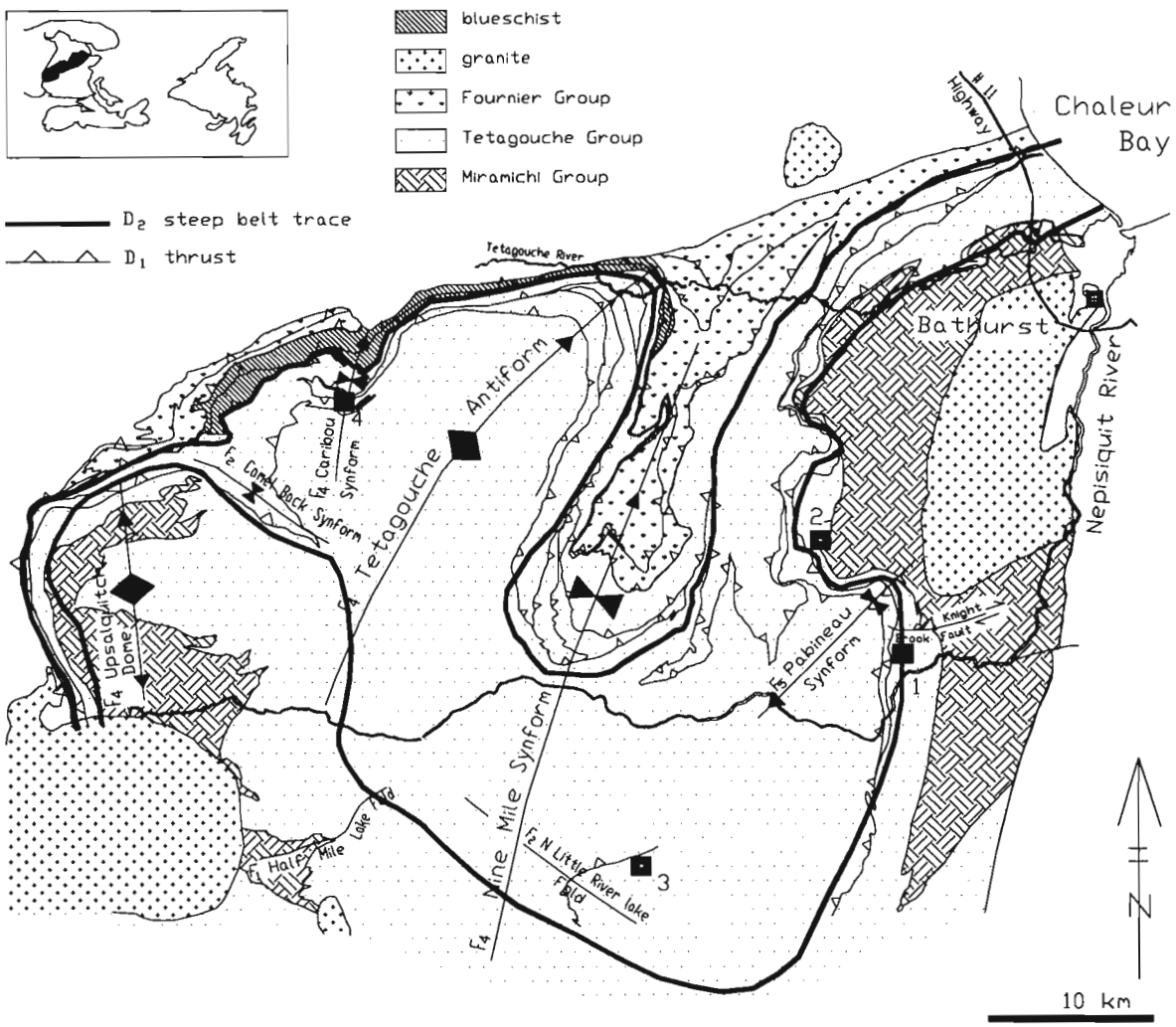

Figure 1. AUTOCAD map of main structural features of the northeastern Miramichi Highlands at Bathurst, New Brunswick (compilation of 1:20 000 scale mapping; inset shows location of Miramichi Highlands). Mines: 1= Brunswick #6; 2= Brunswick #12; 3= Heath Steele Mines; 4= Caribou.

Highlands include quartzose turbidites (Miramichi Group: van Staal and Fyffe, 1991), bimodal volcanic and sedimentary rocks (Tetagouche Group: Skinner, 1974; van Staal, 1987) and ophiolitic rocks (Fournier Group: van Staal and Langton, 1990). These units are separated from overlying Carboniferous and Siluro-Devonian sedimentary and metavolcanic rocks by a set of disconformities and by a major shear zone (the Rocky Brook - Millstream (RBM) Fault: Davies, 1979; Fyffe, 1982; van Staal and Williams, 1988). North of the Rocky Brook - Millstream Fault the Tetagouche and Fournier groups constitute the Elmtree-Belledune Inlier (van Staal and Langton, 1990), which is not discussed here. The fault zone separating the inlier from the main body of pre-Silurian rocks is marked by a belt of Silurian rocks (the Nigadoo River Synclinorium; Walker et al., 1991).

The Miramichi Group mainly consists of quartz sandstones and shales of Early Ordovician, and possibly older, age (Fyffe et al., 1983), supposedly representing a submarine fan setting (Rice and van Staal, 1992). The Tetagouche Group mainly consists of a Middle Ordovician package of felsic epiclastic, volcaniclastic, and volcanic rocks. Also present are: polychrome shale, jasper, iron-formation, ore-bearing sulphides, alkalic and tholeiitic pillow basalts, tuffaceous sandstones, and dark shales. This package is underlain by conglomerates, and calcarenites and is overlain by feldspathic wackes and black shales (van Staal and Langton, 1990). Overall, the rocks of the Tetagouche Group presumably record deposition in a back-arc rift to a Korean-type passive margin (van Staal et al., 1991). The Fournier Group is also Middle Ordovician and includes tholeiitic, alkalic and intermediate basalts, lithic wackes, arkoses, conglomerates and black shales. These rocks probably formed in the ensimatic part of a back-arc oceanic setting (van Staal et al., 1991; Rice and van Staal, 1992).

The pre-Silurian rocks are host to plutonic bodies of porphyritic granite and metagabbro. They are consanguinous with the volcanogenic rocks and thus appear to have been emplaced prior to regional deformation and metamorphism (van Staal and Fyffe, 1991; van Staal et al., 1991). Regionally the metamorphism was of greenschist facies (van Staal, 1985). The contact between the Tetagouche Group and the Fournier Group is marked by tectonic mélange and a 70 km long, narrow belt of blueschist facies metamorphism (Trzcienski et al., 1984; van Staal et al., 1990; Fig. 1). After and during the main deformation and metamorphism, the rock complex was intruded by a second generation of bimodal plutons, stocks and dykes (Fyffe et al., 1981).

DEFORMATION

The pre-Silurian rocks were penetratively and multiply deformed and record a heterogeneous strain distribution (Helmstaedt, 1970, 1971; Davis, 1972; Skinner, 1974; McBride, 1976; Saif et al., 1978; van Staal and Williams, 1984; Irrinki, 1986; van Staal, 1986, 1987; Moreton and Williams, 1986; van Staal et al., 1988; de Roo and Williams, 1990; de Roo et al., 1990, 1991; de Roo and van Staal, 1991, 1992). We have identified five generations of small-scale structures on the basis of overprinting relationships, structural style and orientation. We attribute the structures to four deformation events (D_1-D_4), each of which affected the Miramichi Group, Tetagouche Group, and Fournier Group rocks to a comparable extent. Both the Fournier and Tetagouche Group include black shales of Caradocian age and both are disconformably overlain by Carboniferous rocks that are not penetratively deformed. Hence the small-scale structures described here formed between the Caradocian and Carboniferous.

Early structures (D_1 and D_2): transposition

The earliest deformation (D_1) comprises F_1 folds and an axial planar cleavage or schistosity (S_1). S_1 is mostly parallel to the compositional layering (S_0). F_1 folds are noncylindrical, isoclinal, or even rootless, which supports a model explaining the parallelism of S_0 and S_1 by rotation of S_0 into S_1 during F_1 transposition folding (Helmstaedt, 1971; van Staal and Williams, 1984; Irrinki, 1986; van Staal, 1987; de Roo et al., 1990, 1991). The noncylindrical F_1 folds and transposition are associated with D_1 shear zones. The latter show a mylonitic lineation (L_1) defined by porphyroclasts of feldspar and quartz, attenuated pillows, lapilli and agglomerate fragments, and by a preferred grain shape fabric (van Staal, 1987; de Roo and Williams, 1990).

S_1 is overprinted by a differentiated crenulation cleavage (S_2) that is axial planar to F_2 folds marking highly differential strain (Helmstaedt, 1970, 1971; Saif et al., 1978; van Staal and Williams, 1984; Irrinki, 1986; de Roo et al., 1990, 1991). Locally the F_2 folds of S_1 are monoclinal crenulations resembling S/C-fabrics. Elsewhere S_2 envelops tight to isoclinal F_2 folds, indicating partial F_2 transposition of S_1 into S_2. As a result of post-D_2 deformation, the orientations of S_1, L_1, S_2 and L_2 vary, although moderate to steep attitudes predominate (Fig. 2).

Late structures (D_3 and D_4): kink folding

Recumbent folds and moderately dipping kink bands are exposed across the Bathurst area. Locally the principal foliation they deform is a crenulation cleavage that has been identified as S_2 on the basis of style and correlation of overprinting relationships (van Staal and Williams, 1984; de Roo et al., 1990; de Roo and van Staal, 1991). The recumbent folding (F_3) explains why S_2 shows opposing dip directions in neighbouring outcrops. F_3 folds are spaced and mostly open, but locally tight. Some are accompanied by F_3 crenulations and an axial planar cleavage (S_3). In steeply dipping phyllonites the F_3 folds are mostly of chevron style, or turn from box-like folds into conjugate pairs of kinks with a semi-horizontal bisectrix plane. The change in style from folds to kinks is explained by the fact that the phyllonites provide a strong layering anisotropy. This favours kinking over folding as a process of layer-parallel shortening (Paterson and Weiss, 1966). Some F_3 kinks are marked by an S_3 foliation of superposed, microscopic kinks. This kink-cleavage can be seen in chevrons but may also be

present in one of the conjugate pair of kinks, irrespective of its asymmetry. Hence S_3 can have three possible orientations, although a horizontal one predominates (Fig. 2).

The kinks and S_3 cleavage have been overprinted by two sets of kink-like folds (F_4 and F_5) with vertical axial planar cleavages (S_4 and S_5; de Roo and van Staal, 1991). Because of their similarity in style and conjugate attitude (Fig. 2), we group both sets of structures in one deformation event (D_4). Like S_3, S_4 and S_5 either consist of a crenulation cleavage or of microkink arrays. S_5 has an overall northeasterly strike (de Roo et al., 1990). S_4 has an overall northwesterly strike (Fig. 2) but is also superposed on asymmetrical kinks and can therefore occur in three possible orientations, like S_3.

Large scale structures

Correlation between neighbouring outcrops of readings of D_1-D_4 structural elements (cleavages, fold axes, and lineations) resulted in form surfaces or trends being established for each structural element computed (Fig. 3). The form surfaces represent about 5 000 readings stored in a digital databank, although earlier, hand-drawn maps were also consulted. Comparison of the form surfaces with fold asymmetry patterns and stratigraphy allowed the identification of large-scale folds (Fig. 1). This procedure has restricted applicability to the D_3 and D_4 events because they include conjugate sets of small-scale structures. There is also a bias resulting from localized data collection. To illustrate this, readings of D_x structures (e.g., S_2) were drawn as very small symbols on the appropriate S_x map (S_2 in this case) so as to appear as clutter representing the raw data distribution. Also, the digital data correlation was made interpretatively on a one-to-one basis by switching scales of observation, rather than by plotting statistical averages of groups of readings. The latter procedure is pointless because of the complex, noncylindrical folding.

The maps of Figure 3 present a complex structure created by multiple folding. The three-dimensional exposure provided by the mines of the Bathurst camp has allowed a reconstruction of relevant parts of this structure. Detailed mapping at the Brunswick #6 and #12 mines (Fig. 1) has shown that the local geometry is dominated by F_2 folds. Most have steeply dipping axial planes with shallowly plunging L_2 intersection lineations (van Staal and Williams, 1984). The fold pattern reveals a complex geometry of attenuated and overturned domes and basins. These were explained as overturned F_1 structures that were F_2 upright folded (van Staal and Williams, 1984). Because S_1 is mostly parallel to S_0, the overturned F_1 folds have been explained by progressive thrusting along the D_1 shear zones referred to above (van Staal and Williams, 1984; van Staal, 1987). This model is supported by repetition of chronostratigraphically dated rock units in the direction of younging, i.e., normal to the strike of S_2 (van Staal et al., 1988). The direction of thrusting is poorly constrained because of complex post-D_1 deformation.

Overturned F_1 folds are also present at Heath Steele Mines (Fig. 1). At this mine S_2 and S_1 form surfaces are oblique to one another, whereas S_0 and S_1 are generally parallel, indicating macroscopic F_1 transposition of S_0 (de Roo et al., 1990, 1991). A similar geometry has been mapped west of the mine, where a major F_1 fold (the Half Mile Lake Fold; de Roo and van Staal, 1991) is transected by the S_2 form surface (Fig. 1, 3a, b). When followed back eastward along strike, S_2 is axial planar to a major F_2 fold (the North Little River Lake Fold; de Roo et al., 1990). Parasitic F_2 folds on the northern

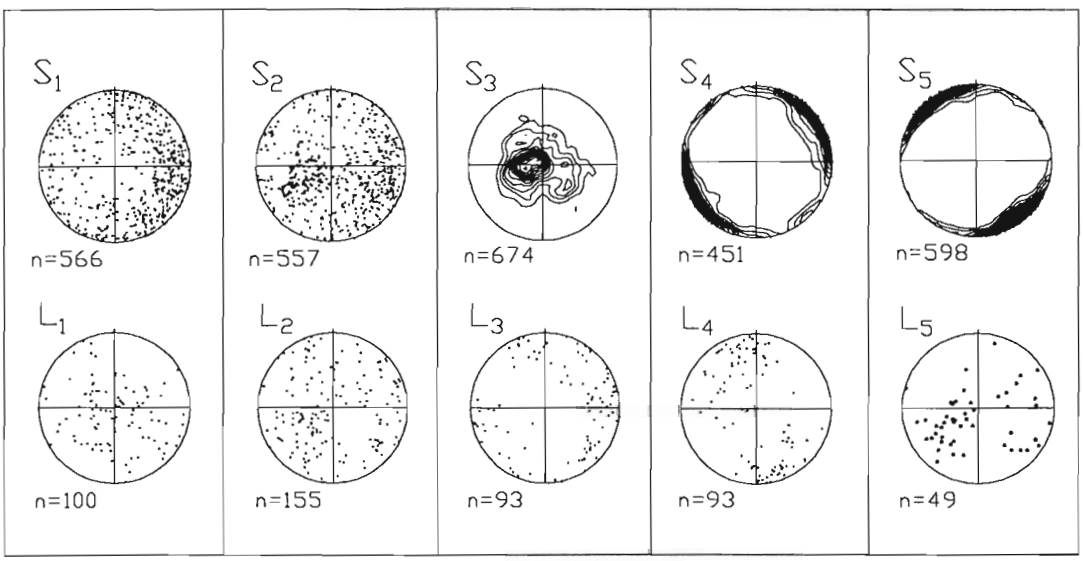

Figure 2. Stereographic lower hemisphere of equal area plots of linear elements (L_x; fold axes and intersection lineations) and poles to cleavages (S_x) from the area shown in Figure 1. The plots were extracted from the FIELDLOG databank using SpheriStat 1987 software. The L_1 plot includes readings of the extension lineation in D_1 mylonites.

limb of this fold show an S-asymmetry, whereas parasitic F_2 folds on its southwestern limb show a Z-asymmetry. The parasitic Z-folds grade into transposition folds marking a zone of high D_2 strain. Rocks in this zone are mylonites or phyllonites with a strong, subvertical S_2 foliation and moderately to gently plunging F_2 fold axes and mineral lineations (de Roo et al., 1990). This zone of high D_2 strain represents the "steep belts" of recent literature (van Staal, 1987; de Roo et al., 1990). Like the small-scale counterpart described by de Roo et al. (1990) the major D_2 steep belts are marked by heterogeneously distributed D_2 strain and grade laterally into less deformed rocks. Hence they have an irregular strain profile and are not discrete faults.

The structure of the Brunswick #6 and #12 mines shows similar features as the D_2 steep belt at Heath Steele Mines: (1) D_1 shear zones are parallel to S_2, which is an F_2 transposition foliation; (2) the main layering is steeply dipping and includes phyllonitic rocks with mostly shallowly plunging linear elements (van Staal and Williams, 1984). Rocks with these structures form a continuous belt (the "Brunswick Horizon") that has been traced along strike of S_2

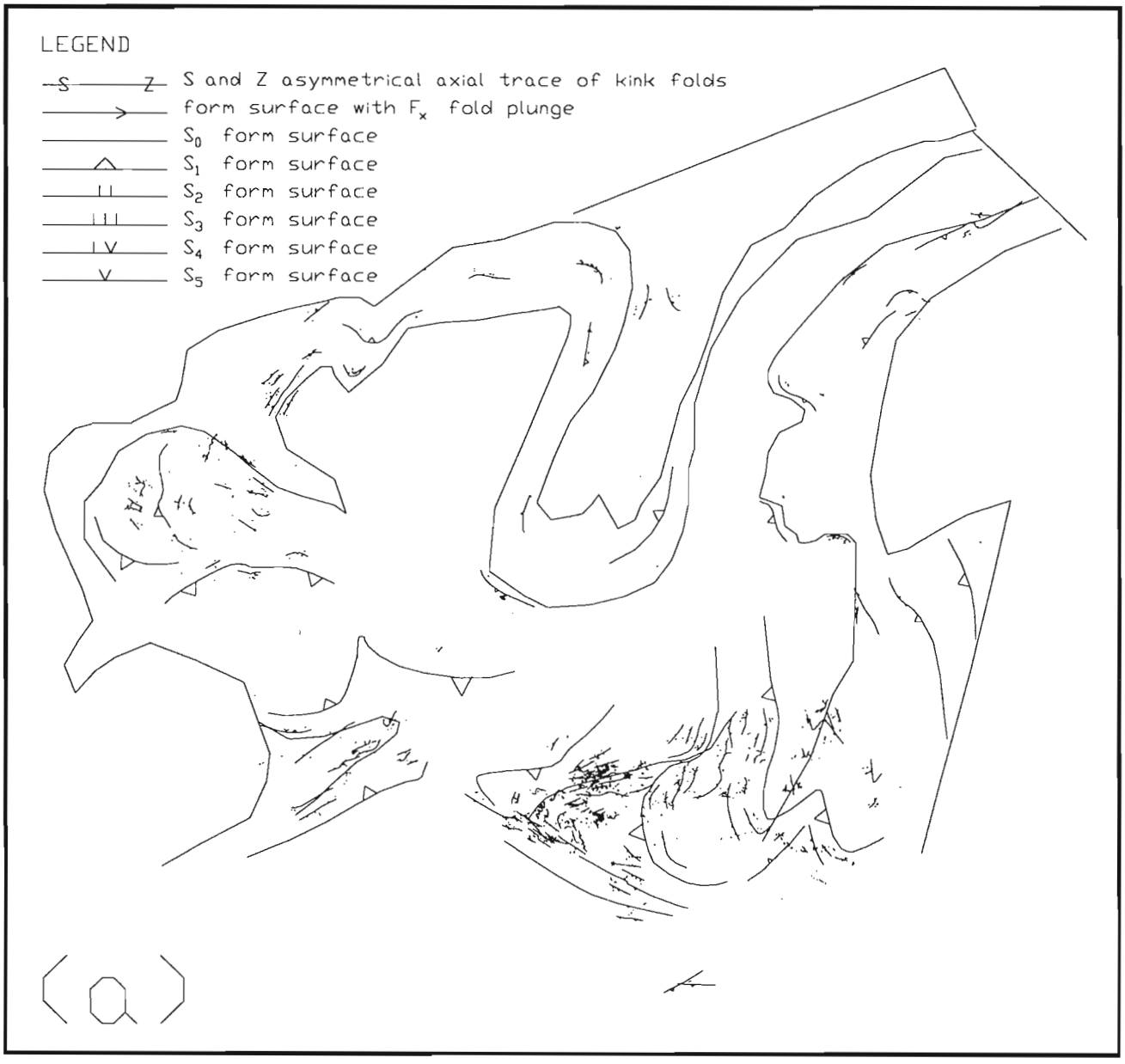

Figure 3. (a-e) Structural form surface (trend) maps of the Bathurst area, as compiled from digital mapping of the orientation of the compositional layering (S_0), cleavages, fold axes, intersection lineations, and fold asymmetry (same area as Fig. 1). Shown are: **(a)** S_1; **(b)** S_2; **(c)** S_3; **(d)** S_4; **(e)** S_5. A legend is shown in (a); note that the larger these symbols, the more interpretative they are.

toward the north and south. South of the railway tracks leading to Heath Steele Mines this belt disappears under a relatively thick glacial till cover, but form surface mapping (Fig. 3a, b) indicates that its strike extension along S_2 matches up with the southeastern tip of the zone of high D_2 strain exposed at Heath Steele Mines. Hence the latter zone is regarded as a continuation of the Brunswick Horizon so that both form part of one major D_2 steep belt. This continuation may well be less apparent in detail if the most intensely D_2 deformed parts of the D_2 steep belts occur en echelon.

A second zone of high D_2 strain with similar features is present to the north. Rocks with D_2 steep belt features have been mapped along strike of S_2 from Caribou mine (Fig. 1) eastward to the Millstream River near the coast, where it incorporates F_2 folded D_1 shear zones (van Staal et al., 1988). This second D_2 steep belt is also marked by phyllonitic rocks with a steeply dipping principal foliation (S_2) and mostly moderately to gently plunging L_2 linear elements, and it includes the blueschists. van Staal et al. (1990) have argued that the belt of blueschists developed during D_1 thrusting as a former suture zone separating the Tetagouche and Fournier groups. Its present structure indicates that the blueschist belt is now incorporated in the D_2 steep belt.

Despite the geometrical complexity produced by F_1/F_2 fold interference, most of the F_2 folds recognizable in the steep belts have an S-asymmetry. Outside the steep belts the strike of S_1 varies from S_2 mainly in an anticlockwise direction (compare Fig. 3a with 3b).

Figure 3b.

Figure 3c. and Figure 3d.

In the Upsalquitch Lake area the main foliations (S_1 and S_2) are shallow-dipping on average, but their form surfaces reveal that they have been warped into an open dome by later deformation (Helmstaedt, 1971). The dome is an F_4 structure (the F_4 Upsalquitch Dome in Fig. 1) overprinting S_3, as is shown by the deflection of S_3 form surfaces (Fig. 3c). Outside the F_4 dome S_3 shows a northeasterly strike trend, which we attribute to F_5 upright folding (compare Fig. 3c and 3e).

The D_2 steep belts have been deformed into a pair of giant vertical folds (the Tetagouche Fold and Nine Mile Fold; Fig. 1). In the hinge of the latter S_0 dips north (van Staal, 1986). Also, sedimentary features (crossbedding, flute casts, pillows) to either side of the northern steep belt indicate an overall stratigraphic younging to the north (van Staal et al., 1988). Hence the Tetagouche Fold and Nine Mile Fold probably are a northerly plunging antiform and synform, respectively (van Staal, 1986, 1987).

The steep belts are also deformed by conjugate pairs of vertical, post-S_3 kinks that have a constant angular relationship to the main foliation (S_2), no matter what the orientation of this foliation is. At Caribou mine, Davis (1972) explained this relationship by macroscopic folding after the small-scale kinking. As noted by van Staal (1986), his arguments can be extended to small-scale kinks situated across the Tetagouche Antiform and Nine Mile Synform. Hence we refer to these giant folds as D_{4b} structures, and to the kinks as D_{4a} structures. For consistency we classify the F_4 Upsalquitch Dome as a D_{4b} structure.

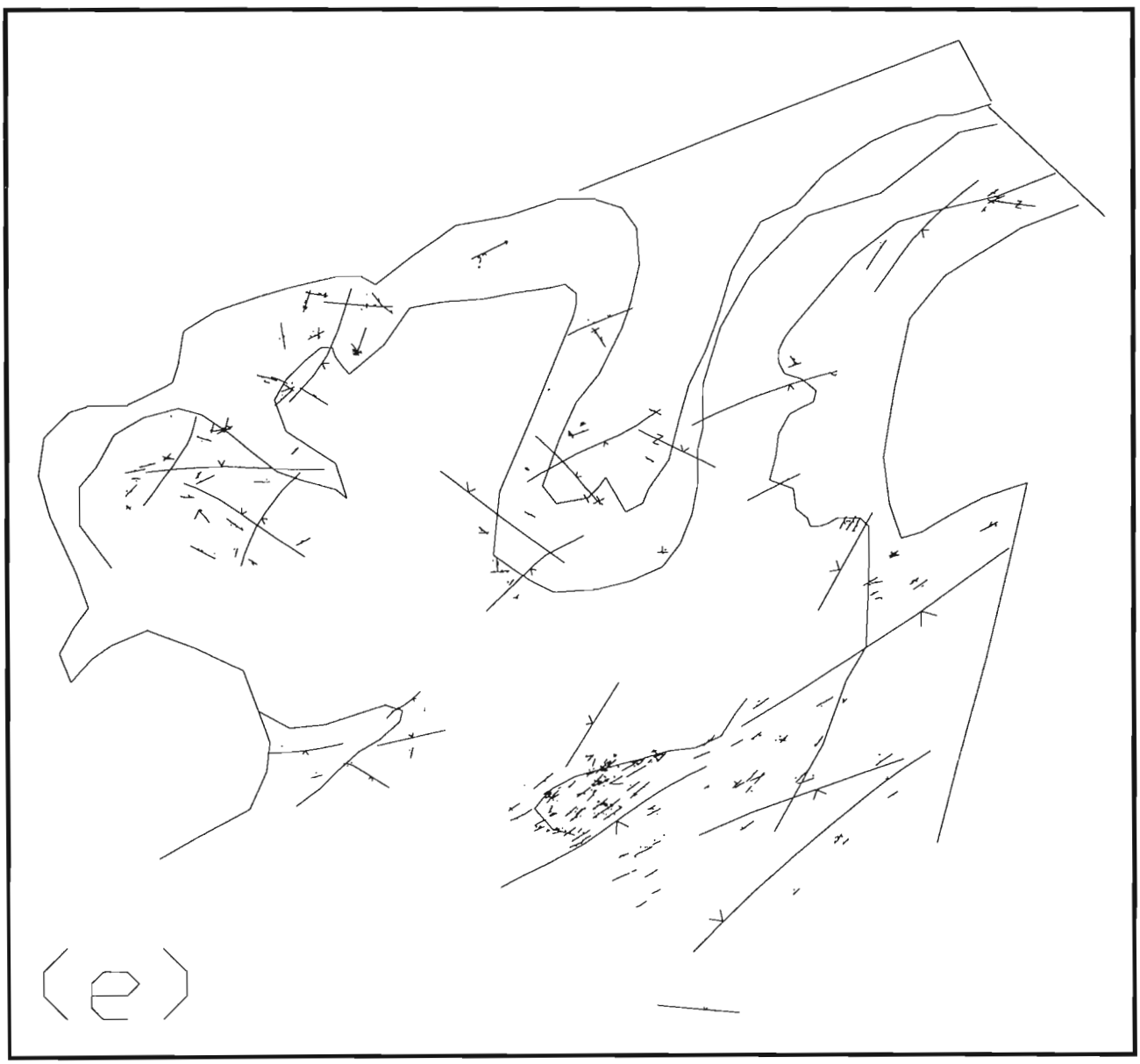

Figure 3e.

Although S_4 and S_5 form a conjugate pair on average (Fig. 2), S_5 cuts all other structures, striking mainly east to northeasterly (Fig. 3e). S_5 is axial planar to the Pabineau Synform (Fig. 1). S_3 changes orientation across this synform, whereas S_4 is parallel to its short limb (Fig. 3c, d). Hence the Pabineau Synform is interpreted as an F_5 structure. There are also F_5 kink folds that turn along strike into easterly striking joints and small faults. They may show both dip-slip and strike-slip, but easterly striking faults in the Brunswick mines area show a dextral offset in excess of 100 m, like the Knights Brook Fault (Fig. 1). The F_4 Caribou Synform is also dextrally offset by an easterly trending fault, illustrating the regional nature of the dextral slip.

We relate the dextral movements to activity on subsidiary splays of the Rocky Brook - Millstream Fault for three reasons: (1) Structural and age relationships indicate that, like S_5, the Rocky Brook - Millstream Fault formed late in the local tectonic history and is part of a regional system of dextral faults (Fyffe, 1982; Bourque et al., 1985; Malo and Béland, 1985, 1989; van Staal and Williams, 1988). (2) Near Bathurst the Rocky Brook - Millstream Fault is marked by the Nigadoo River Synclinorium, a belt of Silurian rocks intersected by accessory fault splays showing dip-slip as well as strike-slip (Walker et al., 1991). This geometry supports a splayed faulting model. (3) The synclinorium is obliquely transected by its principal cleavage and associated folds at an angle that befits a model of dextral transpression (van Staal, 1988; van Staal and Fyffe, 1991). The synclinorium strikes parallel to S_5 form surfaces in the pre-Silurian rocks.

ACKNOWLEDGMENTS

This paper is a contribution to the Canada-New Brunswick Mineral Development Agreement 1990-1995. We gratefully acknowledge financial support under this Agreement. We owe much to the Bathurst team of the New Brunswick Department of Natural Resources for putting up with us for so long. We thank Alain Tremblay for reviewing the manuscript.

REFERENCES

Bourque, P.A., Laurent, R., and St-Julien, P.
1985: Acadian wrench faulting in southern Gaspé Peninsula, Quebec Appalachians; Geological Association of Canada-Mineralogical Association of Canada, Program with Abstracts 10, p. A6.

Boyle, R.W.
1965: Origin of the Bathurst - Newcastle sulfide deposits, New Brunswick; Economic Geology, v. 60, p. 1529-1532.

Brodaric, B.
1992: Fieldlog (version 2.83a); Continental Geosciences Division, Geological Survey of Canada, Ottawa, Manual, 86 p.

Davies, J.L.
1979: Geological map of northern New Brunswick; New Brunswick Department of Natural Resources, Mineral Resources Branch, Fredericton, Map NR-3.

Davies, J.L., Fyffe, L.R., and McAllister, A.L.
1983: Geology and massive sulphides of the Bathurst area, New Brunswick; in Field trip guidebook to stratabound sulphide deposits, Bathurst area, N.B., Canada and west-central New England, U.S.A., (ed.) D.F. Sangster; Geological Survey of Canada, Miscellaneous Report 36, p. 1-30.

Davis, G.H.
1972: Deformational history of the Caribou strata-bound sulfide deposit, Bathurst, New Brunswick, Canada; Economic Geology, v. 67, p. 634-655.

de Roo, J.A. and Williams, P.F.
1990: Dynamic recrystallization and solution transfer in mylonitic rocks of the Tetagouche Group, northern New Brunswick, Canada; Geological Society of America Bulletin, v. 102, p. 1544-1554.

de Roo, J.A. and van Staal, C.R.
1991: The structure of the Half Mile Lake region, Bathurst Camp, New Brunswick; in Current Research, Part D; Geological Survey of Canada, Paper 91-1D, p. 179-186.
1992: Structural studies of the Bathurst region, Canadian Appalachians; Geological Association of Canada-Mineralogical Association of Canada, Abstracts, v. 17, p. A25.

de Roo, J.A., Moreton, C., Williams, P.F., and van Staal, C.R.
1990: The structure of the Heath Steele Mines region, Bathurst Camp, New Brunswick; Atlantic Geology, v. 26, p. 27-41.

de Roo, J.A., Williams, P.F., and Moreton, C.
1991: Structure and evolution of the Heath Steele base metal sulfide orebodies, Bathurst Camp, New Brunswick, Canada; Economic Geology, v. 86, p. 927-943.

Franklin, J.M., Lydon, J.W., and Sangster, D.F.
1981: Volcanic-associated massive sulphide deposits; Economic Geology 75th Anniversary Volume, p. 485-627.

Fyffe, L.R.
1982: Taconian and Acadian structural trends in central and northern New Brunswick; in Major structural zones and faults of the northern Appalachians, eds. P. St-Julien and J. Béland; Geological Association of Canada, Ottawa, Special Paper 24, p. 117-129.

Fyffe, L.R., Forbes, W.H., and Riva, J.
1983: Graptolites from the Benton area of west-central New Brunswick and their regional significance; Maritime Sediments and Atlantic Geology, v. 19, p. 117-125.

Fyffe, L.R., Pajari, G.E.Jr., and Cherry, M.E.
1981: The Acadian plutonic rocks of New Brunswick; Maritime Sediments and Atlantic Geology, v. 17, p. 23-36.

Helmstaedt, H.
1970: Geology of map area O-6; head of Middle River and Wildcat Brook (Northern New Brunswick); New Brunswick Department of Natural Resources, Mineral Resources Branch, Fredericton, Report of map series 70-1, 17 p.
1971: Structural geology of Portage Lakes area, Bathurst - Newcastle district, New Brunswick; Geological Survey of Canada, Paper 70-28, 52 p.

Irrinki, R.R.
1986: Geology of Big Bald Mountain map area (NTS 21 0/1), New Brunswick; Mineral Resources Division, Department of Forests, Mines and Energy, New Brunswick, Fredericton, Map Report 86-2, 55 p.

Malo, M. and Béland, J.
1985: Évolution structurale du segment oriental de l'anticlinorium d'Aroostook-Percé, Gaspésie, Québec; Geological Association of Canada-Mineralogical Association of Canada, Program with Abstracts 10, p. A37.
1989: Acadian strike-slip tectonics in the Gaspé region, Quebec Appalachians; Canadian Journal of Earth Sciences, v. 26, p. 1764-1777.

McAllister, A.L.
1960: Massive sulphide deposits in New Brunswick; Canadian Institute of Mining and Metallurgy Bulletin, v. 53, no. 574, p. 88-98.

McBride, D.E.
1976: The structure and stratigraphy of the B-zone, Heath Steele Mines, Newcastle, New Brunswick; Ph.D. thesis, University of New Brunswick, Fredericton, New Brunswick, 227 p.

Moreton, C. and Williams, P.F.
1986: Structural and stratigraphic relationships at the B-zone orebody, Heath Steele Mines, Newcastle, New Brunswick; in Current Research, Part B; Geological Survey of Canada, Paper 86-1B, p. 57-64.

Paterson, M.S. and Weiss, L.E.
1966: Experimental deformation and folding of phyllite; Geological Society of America Bulletin, v. 77, p. 343-374.

Rice, R.J. and van Staal, C.R.
1992: Sedimentological studies in the Ordovician Miramichi, Tetagouche and Fournier groups in the Bathurst camp and the Belledune-Elmtree Inlier, northern New Brunswick; in Current Research, Part D; Geological Survey of Canada, Paper 92-1D, p. 257-264.

Ruitenberg, A.A., Fyffe, L.R., McCutcheon, S.R., St. Peter, C.J., Irrinki, R.R., and Venugopal, D.V.
1977: Evolution of pre-Carboniferous tectonostratigraphic zones in the New Brunswick Appalachians; Geoscience Canada, v. 4, p. 171-181.

Saif, S.I., McAllister, A.L., and Murphy, W.L.
1978: Geology of the Key Anacon Mine area, Bathurst, New Brunswick; Canadian Mining and Metallurgy Bulletin, v. 71, no. 791, p. 161-168.

Skinner, R.
1974: Geology of Tetagouche Lakes, Bathurst, and Nepisiguit Falls map-areas, New Brunswick; Geological Survey of Canada, Memoir 371, 133 p.

Trzcienski, W.E. Jr., Carmichael, D.M., and Helmstaedt, H.
1984: Zoned sodic amphibole: petrologic indicator of changing pressure and temperature during tectonism in the Bathurst area, New Brunswick, Canada; Contributions to Mineralogy and Petrology, v. 85, p. 311-320.

van Staal, C.R.
1985: Structure and metamorphism of the Brunswick Mines area, Bathurst, New Brunswick, Canada; Ph.D. thesis, University of New Brunswick, Fredericton, New Brunswick, 484 p.
1986: Preliminary results of structural investigations in the Bathurst Camp of northern New Brunswick; in Current Research, Part A; Geological Survey of Canada, Paper 86-1A, p. 193-204.
1987: Tectonic setting of the Tetagouche Group in northern New Brunswick: implications for plate tectonic models of the northern Appalachians; Canadian Journal of Earth Sciences, v. 24, p. 1329-1351.
1988: A new look at the structural history of the Silurian Chaleur Group in northern New Brunswick: evidence for a complex polyphase deformation history and dextral shear associated with F_3 folding; Maritime Sediments and Atlantic Geology, v. 24 (AGS Conference Abstracts), p. 216-217.

van Staal, C.R. and Fyffe, L.R.
1991: Dunnage and Gander Zones, New Brunswick: Canadian Appalachian region; New Brunswick Department of Natural Resources and Energy, Mineral Resources Branch, Fredericton, Geoscience Report 91-2, 39 p.

van Staal, C.R. and Langton, J.P.
1990: Geology of Ordovician massive sulphide deposits and their host rocks in northern New Brunswick; in Mineral Deposits of New Brunswick and Nova Scotia, (ed.) D.R. Boyle; Geological Survey of Canada, Open File 2157, p. 1-21.

van Staal, C.R. and Williams, P.F.
1984: Structure, origin and concentration of the Brunswick 12 and 6 orebodies; Economic Geology, v. 79, p. 1669-1692.
1988: Collision along an irregular margin: a regional plate tectonic interpretation of the Canadian Appalachians: discussion; Canadian Journal of Earth Sciences, v. 25, p. 1912-1916.

van Staal, C.R., Ravenhurst, C.E., Winchester, J.A., Roddick, J.C., and Langton, J.P.
1990: Post-Taconic blueschist suture in the northern Appalachians of northern New Brunswick, Canada; Geology, v. 18, p. 1073-1077.

van Staal, C.R., Winchester, J.A., and Bédard, J.H.
1991: Geochemical variations in Middle Ordovician volcanic rocks of the northern Miramichi Highlands and their tectonic significance; Canadian Journal of Earth Sciences, v. 28, p. 1031-1049.

van Staal, C.R., Winchester, J., and Cullen, R.
1988: Evidence for D_1-related thrusting and folding in the Bathurst-Millstream River area, New Brunswick; in Current Research, Part B; Geological Survey of Canada, Paper 88-1B, p. 135-148.

van der Pluijm, B.A. and van Staal, C.R.
1988: Characteristics and evolution of the Central Mobile Belt, Canadian Appalachians; Journal of Geology, v. 96, p. 535-547.

Walker, J., Gower, S., and McCutcheon, S.R.
1991: Antinouri-Nicholas Project, Gloucester and Restigouche Counties, northern New Brunswick; (C-NBCAMD), p. 87-99.

Williams, H.
1964: The Appalachians in northeastern Newfoundland – a two sided symmetrical system; American Journal of Science, v. 262, p. 1137-1158.
1979: Appalachian Orogen in Canada; Canadian Journal of Earth Sciences, v. 16, p. 792-807.

Geological Survey of Canada Project 900038

A search for neotectonic features in the Passamaquoddy Bay region, southwestern New Brunswick

K.B.S. Burke[1] and P. Stringer[1]
Geophysics Division

Burke, K.B.S. and Stringer, P., 1993: A search for neotectonic features in the Passamaquoddy Bay region, southwestern New Brunswick; in Current Research, Part D; Geological Survey of Canada, Paper 93-1D, p. 93-102.

Abstract: The Passamaquoddy Bay region of southwestern New Brunswick is an area of moderate seismicity. Northwest- and north-northwest- trending faults, which displace the Ministers Island diabase dyke of early Jurassic age on the north side of Passamaquoddy Bay, represent the latest known tectonic movements. No evidence was found of disturbed Quaternary sediments at these faults. Glacial striations checked at twenty-four locations show no postglacial displacement. Marine seismic profiling indicated no disturbance of Quaternary sediments associated with faults in Passamaquoddy Bay, although a northerly alignment of pockmarks and the presence of "plumose" structures represent potentially neotectonic features. Continuity of the Ministers Island dyke across the Oak Bay Fault in the St. Croix River, and its sinistral offset in Big Bay, were confirmed by marine magnetic profiling. The study suggests that the search for neotectonic features is probably of limited value in seismic hazard assessment in zones such as the Passamaquoddy Bay region.

Résumé : La région de la baie Passamaquoddy, dans le sud-ouest du Nouveau-Brunswick, est une zone de sismicité moyenne. Des failles d'orientation nord-ouest et nord-nord-ouest, qui décalent le dyke de diabase de Ministers Island, datant du début du Jurassique, du côté nord de la baie Passamaquoddy, correspondent aux mouvements tectoniques connus les plus récents. On n'a trouvé aucun indice de la présence de sédiments quaternaires dérangés à l'emplacement de ces failles. Les stries glaciaires examinées à 24 endroits ne témoignent d'aucun déplacement post-glaciaire. Les profils sismiques marins n'ont révélé aucun dérangement des sédiments quaternaires qui soit associé à des failles survenues dans la baie Passamaquoddy, mais un alignement nord de petits trous glaciaires et la présence de structures «plumeuses» pourraient s'avérer des éléments néotectoniques. La continuité du dyke de Ministers Island de part et d'autre de la faille d'Oak Bay dans la rivière St. Croix, et son déplacement horizontal sénestre dans la baie Big, ont été confirmés par des profils magnétiques marins. L'étude semble indiquer que la recherche de d'éléments néotectoniques n'a probablement qu'une valeur limitée du point de vue de l'évaluation des risques sismiques dans des zones telles que la région de la baie Passamaquoddy.

[1] Geology Department, University of New Brunswick, P.O. Box 4400, Fredericton, New Brunswick E3B 5A3

INTRODUCTION

Although assessment of seismic hazard in eastern Canada is based on methods that allow the incorporation of geological and geophysical data (e.g. Basham et al., 1985), seismic hazard estimates are still largely based on rather short and often incomplete historical records of earthquakes. One reason for this shortcoming is the lack of detailed neotectonic information in many areas of enhanced seismicity. In order to address this problem, a multi-disciplinary group MAGNEC - "Multi-Agency Group for Neotectonics in Eastern Canada" - was formed in 1986, with participation by scientists from the federal government, provincial governments, crown corporations, and several universities in eastern Canada (Adams et al., 1988). Three localities were selected for detailed neotectonic studies: Prince Edward County, Ontario; Charlevoix County, Quebec; and Passamaquoddy Bay, New Brunswick. The Passamaquoddy Bay region (Fig. 1) was chosen as an example of a zone of moderate seismicity with an unknown potential for a large earthquake. Three earthquakes of magnitude 5 or larger have occurred in the last 185 years.

The basic objective of the study has been to identify neotectonic features in the Passamaquoddy Bay region. Since previous mapping has indicated that some of the northwest- and north-northwest-trending faults apparently displace a diabase dyke of early Jurassic age on land to the north of Passamaquoddy Bay (Stringer and Burke, 1985), faults in the region were compiled (Fig. 2). Detailed magnetic traverses were made in areas of dyke offset to confirm post-early Jurassic fault activity, and a search was made for offset glacial striations and displacement of Holocene and Pleistocene sediments adjacent to faults. Marine seismic and magnetic surveys (Fader, 1989) extended the search for neotectonic features into the Holocene and Pleistocene sediments beneath Passamaquoddy Bay.

Regional geology

The area around Passamaquoddy Bay is underlain by Silurian to Lower Jurassic rocks; faults trend predominantly either northeast or northwest to north-northwest (Fig. 2).

The Silurian rocks in the northwest and southeast corners of Figure 2 include mainly volcanic and sedimentary strata that are steeply inclined with northeasterly strike (Ruitenberg, 1968).

The Eastport Formation, regarded as Lower Devonian (Gedinnian) in age based on ostracode faunas (Pickerill and Pajari, 1976), comprises redbeds and volcanic strata; volcanics in the lower part of the stratigraphic sequence (northeast corner of Figure 2) have been dated as Silurian (Dadd et al., 1989). The Eastport strata mostly dip moderately to gently westward.

The extensive granitic and gabbroic intrusions are mainly Lower Devonian in age (Dgr and Dga in Fig. 2). Abbott (1986) indicated a Silurian to Lower Devonian age for the gabbroic intrusions in Maine (SDga), and Bevier (1989) reported a preliminary U-Pb zircon Silurian date (430 ± 3 Ma) for the Utopia granite (Sgr).

The Upper Devonian rocks of the Perry Formation consist of red sandstone, siltstone, and conglomerate beds which are gently inclined or horizontal; the sediments rest unconformably upon the Eastport Formation and the granitic and gabbroic intrusions. Three basaltic lava units are present within the Perry Formation near St. Andrews (Fig. 2).

The early Jurassic Ministers Island diabase dyke intrudes the Eastport and Perry formations on the north side of Passamaquoddy Bay and also the granitic intrusions in Maine (Fig. 2); the dyke shows apparent fault offsets. The dyke is 3.5-15 m thick, and dips steeply (75-90°) north-northwest.

The region has been heavily glaciated, and is mostly covered by a heavy overburden of Pleistocene till and glacial gravels (Alcock and Perry, 1945; Alcock and MacKenzie, 1946); at several places on the coast, well-bedded Holocene sands and clays are exposed. Deformed glacial deposits at two localities north and west of Passamaquoddy Bay probably originated due to melting of buried ice masses (Kumarapeli, 1990). Glacial striations are common on coastal outcrops.

Faults trend northeast on the southeast side of Passamaquoddy Bay in the vicinity of Deer Island (Fig. 2), and show normal or high-angle reverse dip-slip displacement of Perry Formation beds against older rocks.

Faults on the north and west sides of Passamaquoddy Bay predominantly trend northwest to north-northwest, and include the major north-northwest-trending Oak Bay Fault. Displacement on the northwest- and north-northwest-

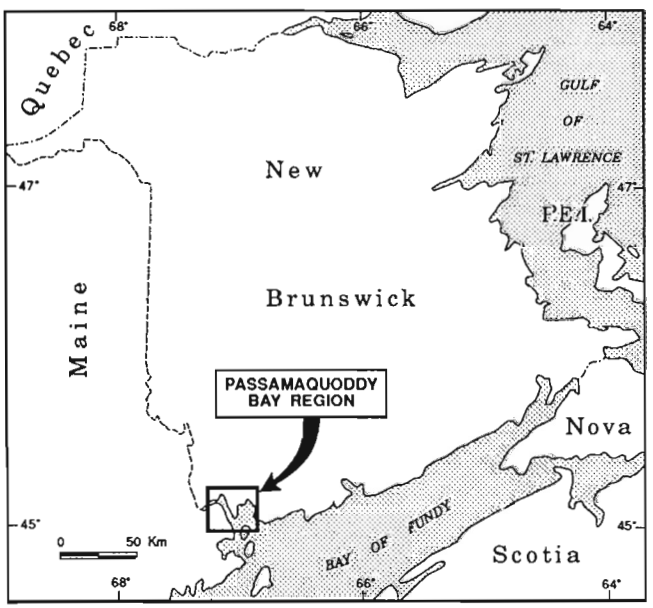

Figure 1. Location map of the Passamaquoddy Bay region.

trending faults is mainly strike slip, and predominantly sinistral (Hay, 1967). The Oak Bay Fault has been mapped by Gates (1989) as a zone of subparallel faults about 1 km wide at Oak Bay (Fig. 2). A fault near the Maine coast proposed by Amos (1958, p. 87), shown in Figure 2 as a northwest-trending splay off the main Oak Bay Fault, 5 km northwest of St. Andrews, shows sinistral offset of the Perry Formation (Stringer et al., 1991).

The age of faulting in southwestern New Brunswick is mainly Paleozoic. Movement on the northeast-trending faults occurred during both Devonian and Carboniferous times (Leger and Williams, 1986, p. 117). Sinistral strike-slip movement on the north-northwest-trending Oak Bay Fault (Cumming, 1966, Fig. 3) occurred in Middle Devonian (3 km displacement) and post-Upper Devonian (1 km) times (Stringer and Burke, 1985). Local offsets of the Ministers Island dyke indicate that movement on some of the northwest- and north-northwest-trending faults occurred in post-Lower Jurassic time.

Seismicity of the region

Barosh (1981) listed more than fifty local earthquakes reported since 1870 in the Passamaquoddy Bay region and stated that an average of seven earthquakes a year in the magnitude M_c range from 1 to 3.2 had been recorded since

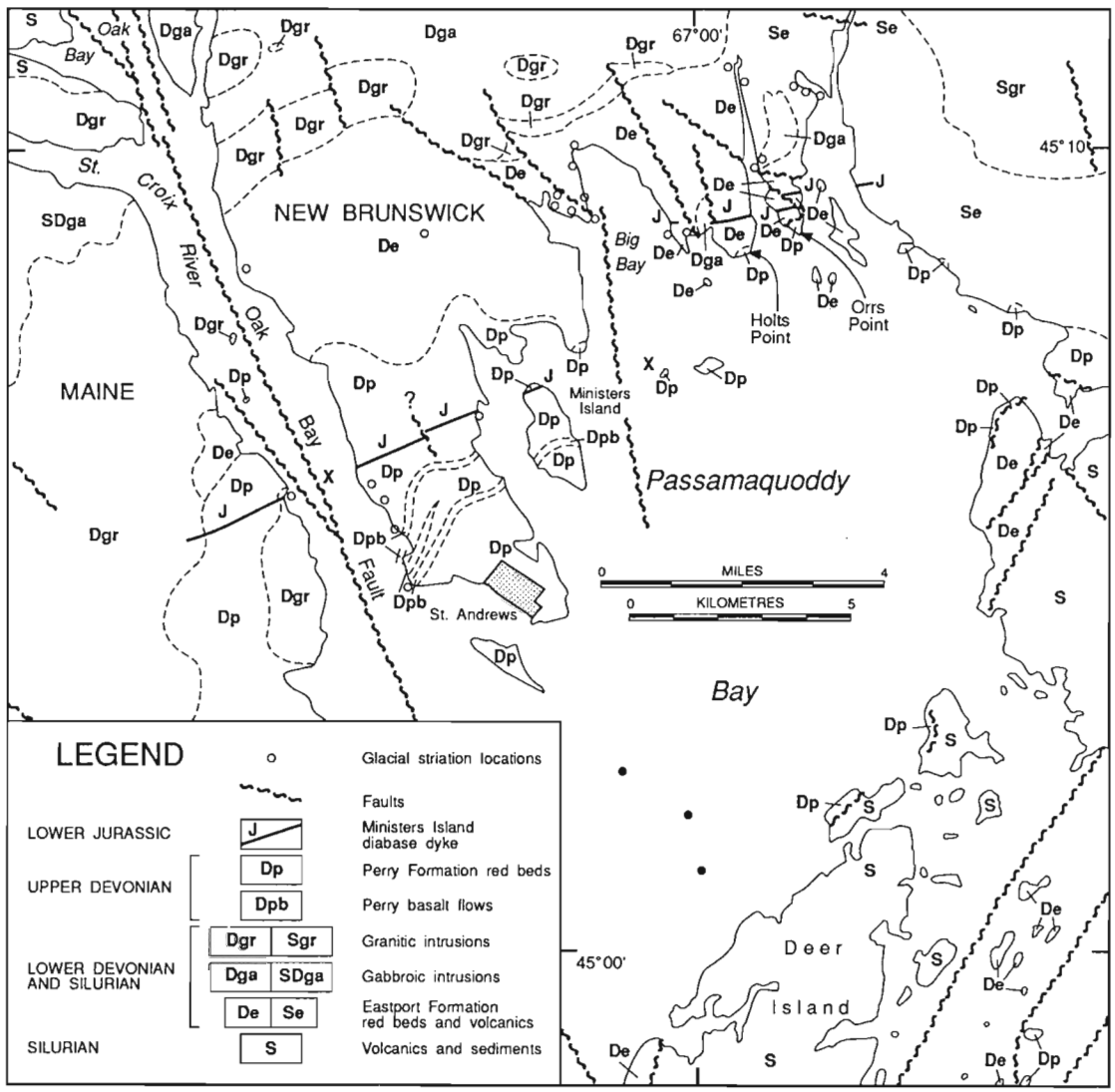

Figure 2. Outline map of the bedrock geology showing faults in the Passamaquoddy Bay region, southwestern New Brunswick and eastern Maine (compiled mainly from Alcock and Perry, 1945; Alcock and MacKenzie, 1946; Alcock, 1948; Cumming, 1966; Hay, 1967; Ruitenberg, 1968; Stringer and Burke, 1985; Abbott, 1986; Fay, 1988; Gates, 1989; Stringer et al., 1991). Solid circles in southern Passamaquoddy Bay mark offshore drill holes in Perry Formation at the bedrock surface (International Passamaquoddy Engineering Board, 1959, Plates 2-2, 2-4). "X" marks offshore locations of the Ministers Island dyke based on magnetic profiles. Glacial striations at the locations shown were checked for offset.

the installation of a network of three seismographs in southeastern Maine in 1975. Foley et al. (1984) suggested that the historical record of the last 111 years shows frequent earthquakes, as well as evidence of sporadic episodes of stronger seismicity. A re-evaluation of the four largest pre-1982 earthquakes, listed in the catalogue of Smith (1962) for Maine and New Brunswick, has shown that three of these events were located in the Passamaquoddy Bay region (Leblanc and Burke, 1985); the earthquakes occurred on May 17, 1817, October 22, 1869, and March 21, 1904, with felt area magnitudes (M_{bLg}) of 4.5-5, 5.7, and 5.9 respectively. A fault plane solution for a smaller event in Passamaquoddy Bay, the January 19, 1984, magnitude M_n = 3.8 earthquake (Foley et al., 1985, Table 2), indicates a thrust fault striking west-northwest, but the solution is poorly constrained.

Explanations for the enhanced seismicity of the Passamaquoddy Bay region have centred on two themes: a high rate of local subsidence and correlation with known faults. Evidence for a relatively high rate of subsidence is discussed in detail by Anderson et al. (1989). The positions of uplifted glaciomarine deltas, the accretion of salt marshes, the differential erosion of coastal archeological sites, and the drowning of historical coastal works, all point to an anomalous downwarping of the region, which has occurred at different rates over the last 14 000 years. Gates (1989) proposed that a weak and fractured crust, with a long history of faulting and subsidence (from Devonian times), was responsible for the concentration of subsidence and earthquake activity.

Analysis of data from repeated levelling surveys in eastern Maine indicated an anomalously high rate of subsidence in the Passamaquoddy Bay region; Tyler and Ladd (1980) concluded that the subsidence rate was 9 mm/a in the Eastport area. Reilinger (1987) questioned the validity of this result, which he believed could be explained by large systematic errors in the 1942 levelling survey included in the Tyler and Ladd analysis. Re-analysis of the levelling data, omitting the 1942 survey results, yielded a contemporary subsidence rate of 1-2 mm/a, consistent with the longer-term postglacial downwarping rates obtained along the Maine coast. This lower rate of subsidence was confirmed by the analysis of tide-gauge data from Eastport (Reilinger, 1987). Nevertheless, Tyler (1989) argued that random and systematic errors would only account for 4 mm/a of the anomalous subsidence and the remaining 5 mm/a would seem to be caused by more rapid crustal deformation.

An apparent association of epicentres with the Oak Bay Fault at a regional scale has been noted (Rast et al., 1979, Fig. 1; Barosh, 1981). However, examination of splay fault traces on land failed to find any evidence of Pleistocene-Holocene movement (Newman, 1979). The continuity of the Ministers Island dyke across the trace of the Oak Bay Fault in the St. Croix River (Stringer and Burke, 1985), and the lack of disturbance in Quaternary sediments over fault traces in the St. Croix River shown by marine seismic profiling (Kelley et al., 1989), also suggest that this fault does not play a major role in present day seismicity. However, it is possible that other faults elsewhere in the region may be active, and one goal of the present study was to locate them.

POTENTIALLY NEOTECTONIC FEATURES ON LAND

Offset of the Ministers Island dyke on northwest- and north-northwest-trending faults

A projected approximately 200 m sinistral offset of the Ministers Island dyke on land north of Orrs Point (Fig. 2), which coincides with a tentative northwest-trending fault mapped by Van Wagoner and Fay (1988, Fig. 2), has been interpreted as strike-slip fault displacement of the dyke (Stringer and Burke, 1985). Fault displacements of the dyke would represent the youngest geologically recognizable fault activity in the region, and neotectonic movements may be concentrated along such faults.

Table 1. Magnetic susceptibility measurements

Rock unit	Number of readings	Magnetic susceptibility (S.I. units)	
		Range	Mean (S.D.)
Ministers Island dyke	70	1.44×10^{-2} - 3.12×10^{-2}	$2.38 \pm 0.04 \times 10^{-2}$
Perry Formation sediments	53	5.03×10^{-5} - 2.58×10^{-3}	$7.51 \pm 5.15 \times 10^{-4}$
Eastport Formation rhyolitic flows	35	2.16×10^{-3} - 9.59×10^{-3}	$5.76 \pm 0.21 \times 10^{-3}$

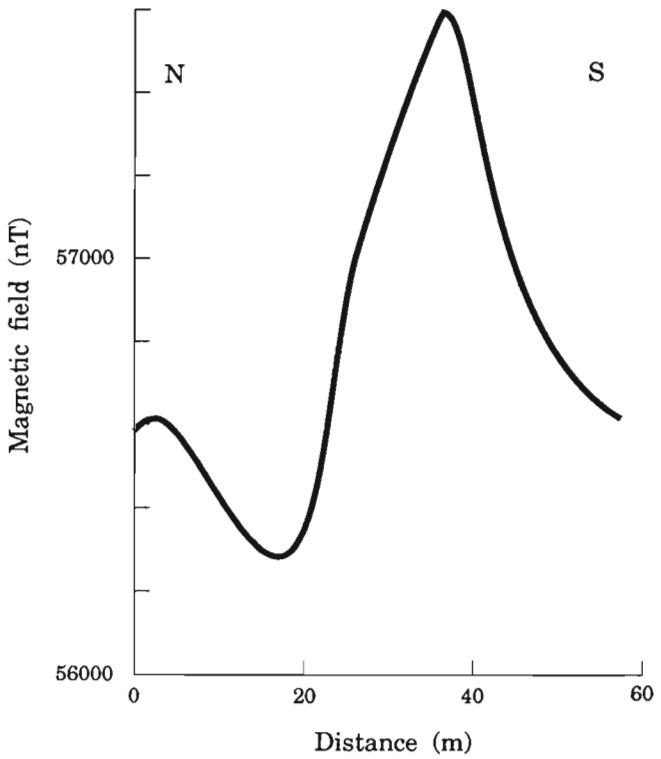

Figure 3. Magnetic profile over the Ministers Island dyke intruded into Perry Formation sandstone, northeast shore of Ministers Island, N.B. The dyke is 12 m wide.

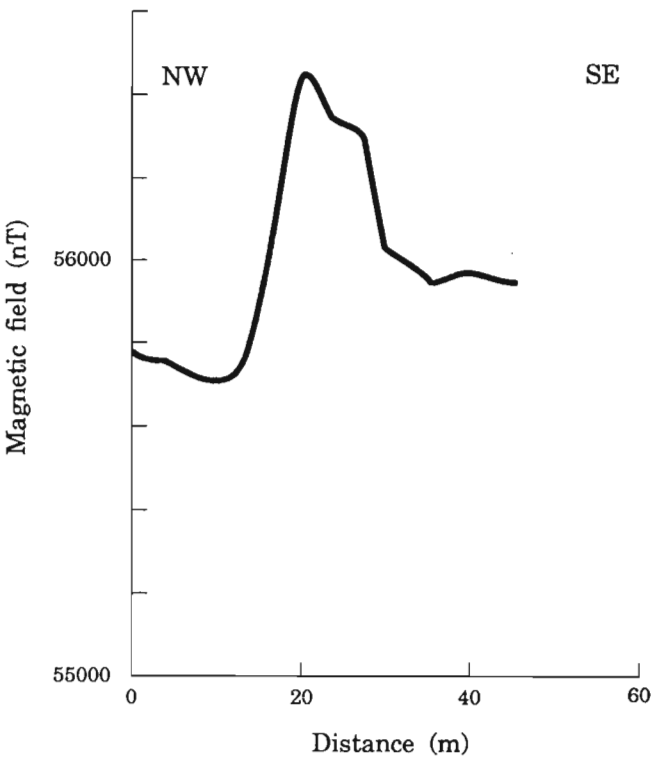

Figure 4. Magnetic profile over the Ministers Island dyke intruded into Eastport Formation rhyolite, west side of Holts Point, N.B. The dyke is 4 m wide at the nearest outcrop.

At coastal exposures of the Ministers Island dyke and country rocks, in situ magnetic susceptibility values for the various rock types were obtained (Table 1). The contrast in susceptibility between the dyke and the Perry Formation sediments of almost two orders of magnitude leads to a strong and characteristic magnetic anomaly, as shown in Figure 3. A reduction in contrast in susceptibility between the dyke and the rhyolitic units of the Eastport Formation to less than one order of magnitude decreases the amplitude of the anomaly (Fig. 4), and together with a decrease in width of the dyke makes the anomaly a smaller target to map (see also Stringer and Burke, 1985, Fig. 5).

The Ministers Island dyke north of Orrs Point, which has been located in subsurface from ground magnetometer traverses at 1 m or 2 m spacings (Fig. 5), intrudes rhyolitic rocks of the Eastport Formation. Thus, anomalies in the magnetic traverses, compared with those of the dyke where it intrudes Perry Formation redbeds (e.g. Fig. 3), are smaller in both amplitude and width. The distribution of the anomaly peaks (Fig. 5) clearly confirms the termination of the dyke inland from both sides of the peninsula. The slightly irregular

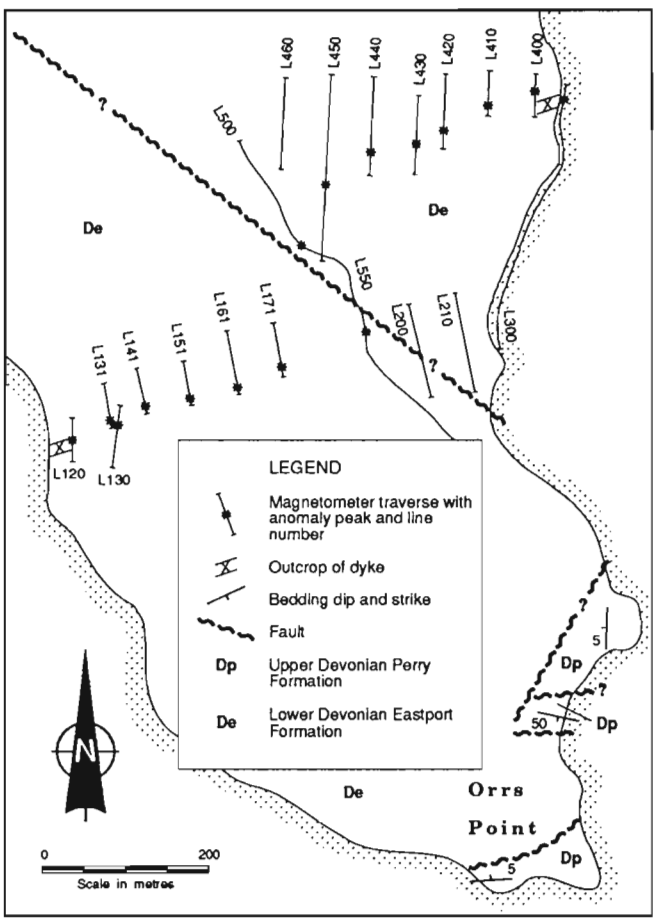

Figure 5. Outline geological map showing the position of the Ministers Island dyke on Orrs Point, N.B., interpreted from magnetic traverses.

trend of the dyke based on the anomaly peaks suggests that other faults with minor sinistral and dextral offsets are present.

A minor approximately 12 m dextral offset of the Ministers Island dyke on a north-northwest-trending strike-slip fault has been mapped west of Orrs Point, on the west shore of the Bocabec River (Fig. 6), 1 km north of Holts Point. The dyke, about 4 m wide, intrudes gently dipping, red silty sandstone beds of the Eastport Formation, and also intrudes a northerly-trending older diabase dyke. The fault plane, strike 154°, dip 85° eastward, is exposed for a short distance in brecciated sediments. Magnetometer traverses indicate that the Ministers Island dyke terminates seaward at its northern outcrop, and landward at its southern outcrop (inset map, Fig. 6). The contact of the dyke with the Eastport sandstone strikes 075° and dips 85°S; however, columns in the dyke formed by crude columnar jointing plunge 0°-2° southward, suggesting that the overall dip of the dyke at this location is subvertical. The fault offset of the dyke is therefore strike slip. The highly fractured appearance of the dyke, not seen at outcrops of the dyke elsewhere, supports offset of the dyke by faulting.

Intrusion of the Ministers Island dyke appears to postdate all displacement on the Oak Bay Fault (Stringer and Burke, 1985); the dyke maintains an 060° trend across both the fault and the north-northwest-trending splay in the St. Croix River between New Brunswick and Maine (Fig. 2). The continuity of the dyke across the faults has been confirmed by an offshore magnetic profile (Fig. 7); the anomaly is located on trend with the land outcrops. The north-northwest-trending fault offshore in Big Bay (Fig. 2) likewise predates intrusion of the Ministers Island dyke, as indicated by marine magnetic profiling (see below).

Glacial striations

The offsets of the Ministers Island dyke suggest that the youngest fault movements have occurred on the north side of Passamaquoddy Bay. Accordingly, a search was made for fault displacements of glacial striations similar to those recorded 80 km to the east at Saint John, ascribed to postglacial tectonic stresses by Matthew (1894) and to

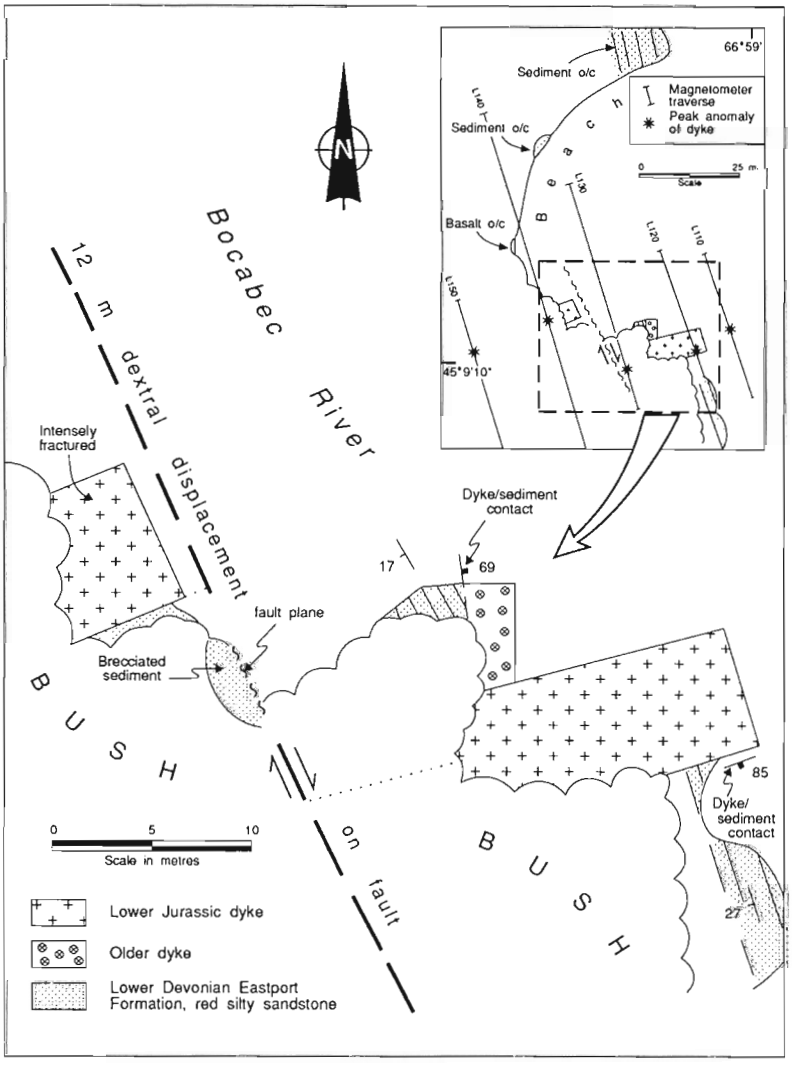

Figure 6. Geological sketch map showing offset of the Ministers Island dyke by faulting, west bank of the Bocabec River, 1 km north of Holts Point, N.B. Inset map shows detailed magnetic traverse lines; "o/c" indicates outcrop. (See Fig. 2 for location of Holts Point).

differential rates of glacitectonic loading and unloading by Broster and Burke (1990). However, no offsets were found at twenty-four widespread locations (Fig. 2).

MARINE GEOPHYSICAL SURVEY

Because the geological and geophysical surveys on land did not reveal any neotectonic features, the investigation was extended to the offshore area of Passamaquoddy Bay. The marine vessel M.V. Navicula of the Atlantic Geoscience Centre was used to run seismic profiling, sidescan sonar and magnetometer measurements along the tracks shown in Figure 8. Marine magnetic measurements were taken at 10 second intervals (i.e. about 21 m apart). Further information on instrumentation and survey procedure is included in the cruise report by Fader (1989).

The main purpose of the marine seismic investigation was to detect any disturbance in the Quaternary sediments that could be associated with active faulting. The bedrock surface was represented on most of the seismic profiles as swarms of hyperbolic echoes and only rarely was there penetration into the rocks below. Therefore the positions of faults were mostly inferred from the presence of bedrock scarps. No disturbed sediments were noted in association with any of the bedrock scarps, or over the projected positions of fault traces from land, and it is quite possible that the scarps have a nontectonic, probably glacial, origin.

Depth to seafloor, depth to bedrock, and total magnetic field maps, prepared from the seismic and magnetic profiling data, are shown in Figures 9, 10, and 11. Local depressions to the east of Ministers Island (Fig. 9) were identified as

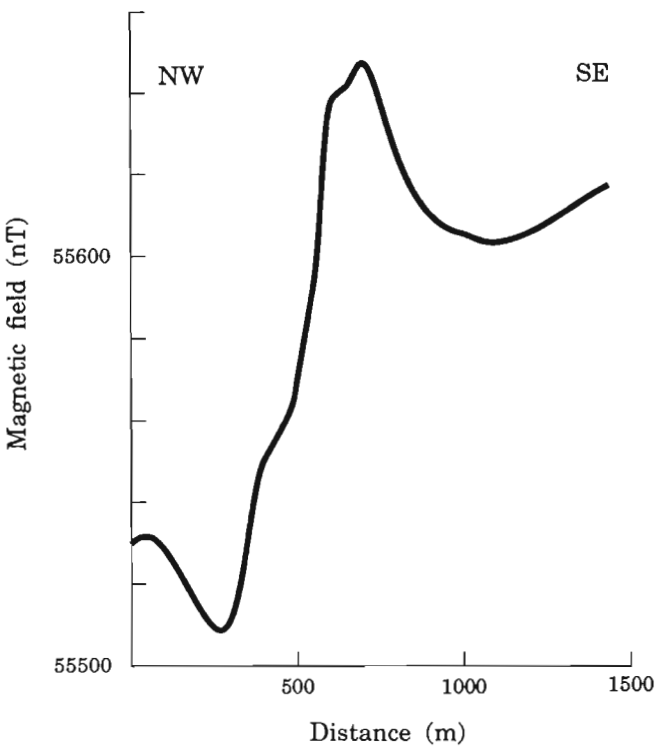

Figure 7. Marine magnetic profile over the Ministers Island dyke intruded into Perry Formation sandstone, St. Croix River, N.B. (Note the change in both vertical and horizontal scales compared with the magnetic profiles in Fig. 3 and 4). Offshore location of the profile is shown in Figure 2.

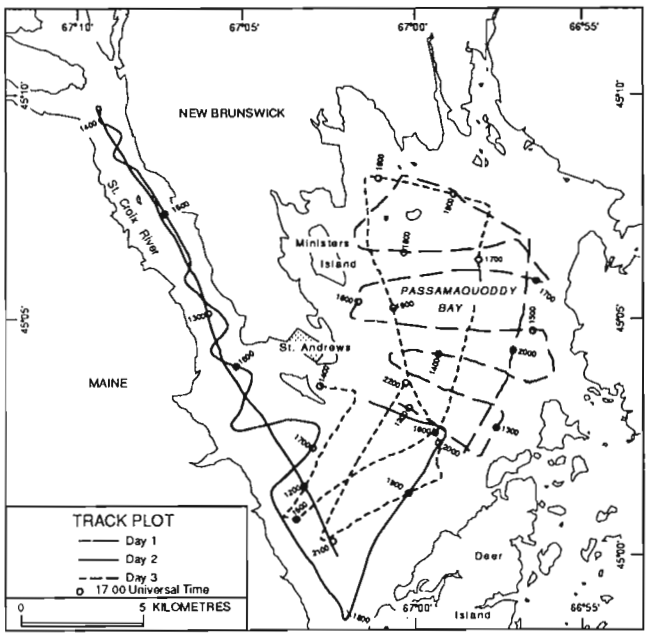

Figure 8. Plot of tracks in Passamaquoddy Bay of the June 28-July 1, 1988, marine geophysical survey.

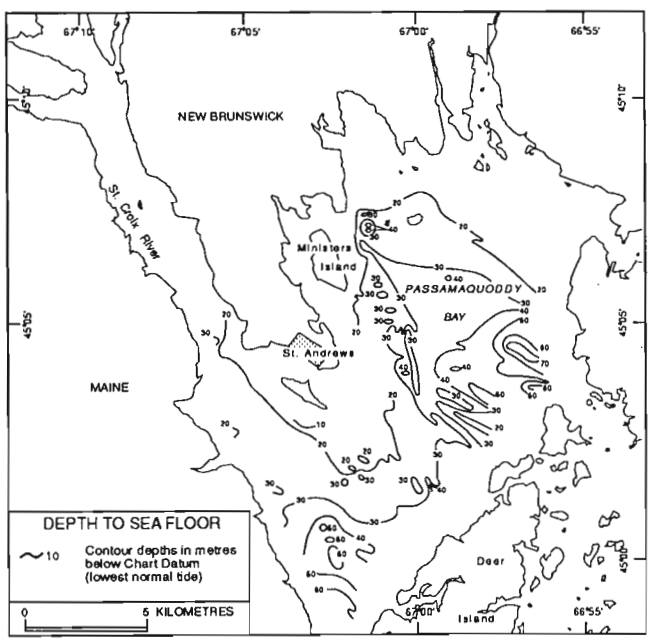

Figure 9. Depth to seafloor in Passamaquoddy Bay.

pockmarks by Fader (1989, Fig. 2), caused by the venting of gas from the Perry Formation. Because the pockmarks have a preferred northerly alignment (Pecore and Fader, 1990), the release of gas might be associated with an active fault (Fader, 1989, p. 6). Support for this hypothesis of active faulting is given by the identification of "plumose" structures on sidescan sonar displays at five locations along the northerly trend; similar features in the Great Lakes have been associated with active subbottom faults (Fader, 1989).

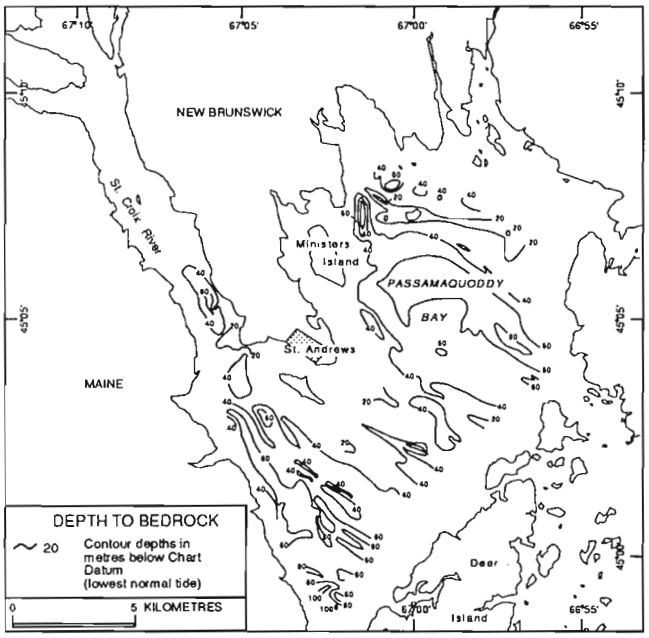

Figure 10. Depth to bedrock in Passamaquoddy Bay.

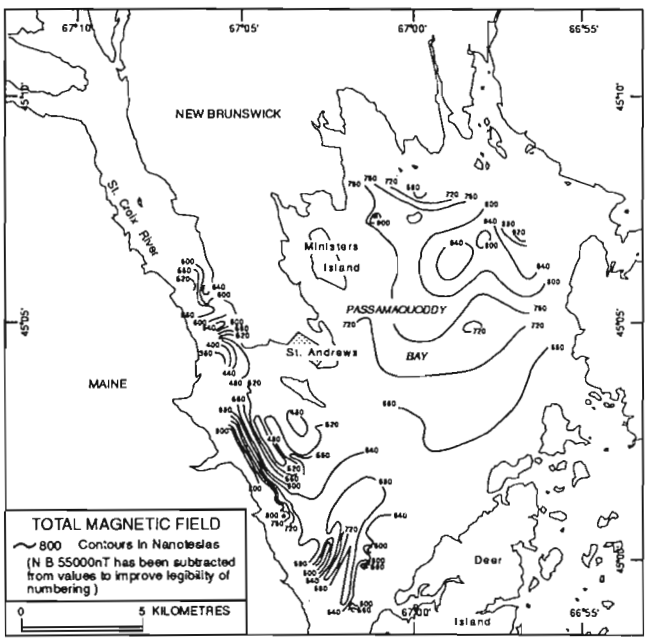

Figure 11. Total magnetic field in Passamaquoddy Bay.

The main trend of lows and highs on the bedrock surface in Passamaquoddy Bay is northwest (Fig. 10). A linear bedrock surface low with a more northerly trend is present northeast of Ministers Island; this low may be the expression of a fault, herein named the Big Bay Fault. It coincides with the series of small pockmark depressions in the seafloor (Fig. 9). The fault's continuation to the south (Fig. 2), based on further pockmark depressions (Fig. 9), is tentative because there is no depression in the bedrock surface (Fig. 10).

Contours of the total magnetic field (Fig. 11) correlate with the known bedrock geology (Fig. 2). Along the southwest side of Passamaquoddy Bay in Maine, where Perry Formation basalt outcrops (Abbott, 1986; Gates, 1989), the contour gradients are steep and there are several intense magnetic highs. This pattern is cut off to the northeast, probably by the Oak Bay fault zone, and the contours develop a more open, low gradient pattern associated with increased thickness of the Perry Formation sediments. In northeastern Passamaquoddy Bay, the broad magnetic high is probably caused by a mafic unit in the underlying Eastport Formation. The swing in the contours to a northerly direction, east of Ministers Island, may be an expression of the Big Bay Fault.

The Ministers Island dyke shows a sinistral offset of about 3000 m in Passamaquoddy Bay, from east of Ministers Island to Big Bay (Fig. 2). The offset was attributed either to faulting or to en echelon offset in the original intrusion of the dyke

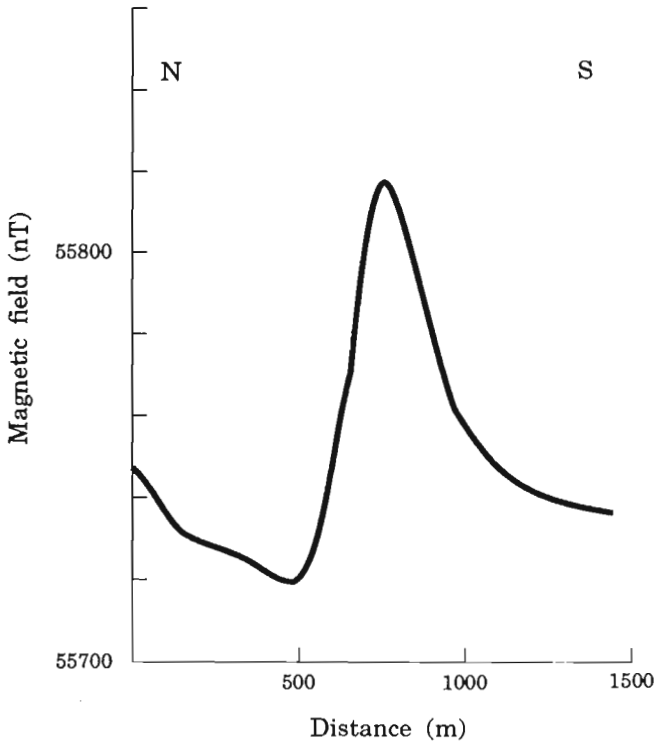

Figure 12. Marine magnetic profile over the Ministers Island dyke intruded into Perry Formation sandstone, 2 km east of Ministers Island, N.B. (Note the change in both vertical and horizontal scales compared with the magnetic profiles in Fig. 3 and 4). Offshore location of the profile is shown in Figure 2.

(Stringer and Burke, 1985). The Ministers Island dyke is represented offshore in northern Passamaquoddy Bay by a small magnetic high, located 2 km east-northeast of Ministers Island (Fig. 11); a north-south magnetic profile across the high (Fig. 12) is similar to other profiles across the Ministers Island dyke (Fig. 3, 4, 7). The high is situated about 500 m east of the Big Bay Fault; the trend of the Ministers Island dyke apparently is continuous from Ministers Island to the high, and is not displaced by the fault. The total magnetic field map (Fig. 11) indicates that the Ministers Island dyke does not continue farther to the east-northeast beyond the small magnetic high, confirming the apparent sinistral offset of the dyke to the eastern shore of Big Bay (Fig. 2). However, the offset cannot be attributed to the Big Bay Fault.

NEOTECTONIC IMPLICATIONS

The study has found little evidence for neotectonic features which can be associated with earthquake activity in the Passamaquoddy Bay region. The alignment of pockmarks and the "plumose" structures revealed by the marine geophysical profiling in the northwest part of Passamaquoddy Bay are the best candidates, and even these might have other explanations. For example, the alignment of pockmarks might be explained by the presence of a long-dormant fault zone, which provides an easier path for the migration of gas from the bedrock sediments, rather than an active fault with accompanying outgassing. The "plumose" structures may be caused by normal seafloor slumping unrelated to active faulting. A microearthquake survey with accurate positioning of hypocentres is needed to establish a direct link of this seafloor area with enhanced seismicity.

On land, no evidence of neotectonic activity was found. The northwest- and north-northwest-trending faults that displace the Ministers Island dyke show no evidence of disturbance of Quaternary deposits. Observed glacial striations do not show offset.

The lack of neotectonic features in a region that has been subjected to magnitude 5 and greater earthquakes is not unusual in the northern Appalachians. A thorough study of the epicentral region of the January 9, 1982, Miramichi earthquake and subsequent aftershocks in central New Brunswick, immediately after the events, only found a "thrust joint" ground break with 25 mm displacement of limited extent, a few minor cracks and a stress-relief buckle, with no evidence of a major surface break (Basham and Adams, 1984). Therefore, because the last earthquake of significant size in the Passamaquoddy Bay region was the magnitude 5.9 event in 1904, it is possible that similar neotectonic features associated with this event have long since been obliterated by normal weathering processes. It is interesting to note that cracking of the earth was reported at the time of an earthquake in the Passamaquoddy Bay area in 1851; Burke et al. (1987) quote an account from the February 5, 1851 *Saint Andrews Standard* which states "A friend at CampoBello [*sic*] informs that the shock was felt on that Island and in the vicinity of Friar's Head [22 km south-southeast of St. Andrews], an opening in the earth an inch in width and extending about half a mile in length was caused by this convulsion of nature". A search in the vicinity of Friar Head during the present study did not reveal any remaining trace of this crack.

We conclude that the search for neotectonic features will probably be of limited assistance in assessing the seismic hazard in zones of moderate seismicity such as the Passamaquoddy Bay region. Perhaps a more fruitful approach to understanding the seismicity of such regions would be a study of the microseismicity and the fault mechanisms of appropriate events recorded by permanent networks.

ACKNOWLEDGMENTS

We thank John Adams, Geophysics Division, Geological Survey of Canada, for his help and advice as Scientific Liaison Officer for the project and for providing funds in support of the marine geophysical survey. Gordon Fader, Atlantic Geoscience Centre, and his technical staff, together with Captain Neil Langille and crew of the M.V. Navicula, contributed to the offshore investigation. We gratefully acknowledge the assistance of NSERC Scholarship summer students: Craig Hickey mainly with field surveys, Chris Hawkes with the 1:50 000 geological map compilation and the marine geophysical surveys, and John Currie with computer processing of the magnetic data. David Pirie and Angel Gomez laser-drafted the figures, and Diane Tabor typed the manuscript.

REFERENCES

Abbott, R.N., Jr.
1986: Preliminary report on the bedrock geology of the Devils Head, Robbinston, and Red Beach 7.5-minute quadrangles, Maine; Maine Geological Survey, Open File No. 86-73, 36 p.

Adams, J., Bowlby, J.R., Wallach, J., and White, O.
1988: MAGNEC - A new initiative for the study of neotectonics in eastern Canada; Program with Abstracts, Geological Association of Canada-Mineralogical Association of Canada, v. 13, p. A1.

Alcock, F.J.
1948: Campobello, New Brunswick; Geological Survey of Canada, Map 964A.

Alcock, F.J. and MacKenzie, G.S.
1946: Preliminary map, St. Stephen, Charlotte Co., New Brunswick; Geological Survey of Canada, Map 46-2.

Alcock, F.J. and Perry, S.C.
1945: Preliminary map, St. George, Charlotte Co., New Brunswick; Geological Survey of Canada, Paper 45-1.

Amos, D.H.
1958: Geology and petrology of the Calais and Robbinston quadrangles, Maine; Ph.D. thesis, University of Illinois, Urbana, Illinois, 232 p.

Anderson, W.A., Borns, H.W. Jr., Kelley, J.T., and Thompson, W.B.
1989: Neotectonic activity in coastal Maine; in Neotectonics of Maine, studies in seismicity, crustal warping, and sea-level change, (ed.) W.A. Anderson and H.W. Borns, Jr.; Maine Geological Survey, Bulletin 40, p. 1-10.

Barosh, P.J.
1981: Seismicity and tectonics of the Passamaquoddy Bay area, Maine and New Brunswick; Abstracts with Programs, Geological Society of America, v. 13, p. 122.

Basham, P.W. and Adams, J.
1984: The Miramichi, New Brunswick earthquakes: near-surface thrust faulting in the northern Appalachians; Geoscience Canada, v. 11, p. 115-121.

Basham, P.W., Weichert, D.H., Anglin, F.M., and Berry, M.J.
1985: New probabilistic strong ground motion maps of Canada; Seismological Society of America Bulletin, v. 75, p. 563-595.

Bevier, M.L.
1989: Preliminary U-Pb geochronologic results for igneous and metamorphic rocks, New Brunswick; in Project summaries for 1989, (ed.) S.A. Abbott; New Brunswick Department of Natural Resources and Energy, Information Circular 89-2, p. 190-194.

Broster, B.E. and Burke, K.B.S.
1990: Glacigenic postglacial faulting at Saint John, New Brunswick; Atlantic Geology, v. 26, p. 125-138.

Burke, K.B.S., Slauenwhite, S., and Biddiscombe, P.
1987: Historical seismicity of the Passamaquoddy Bay region of New Brunswick for the period 1811 to 1900; Contract Report 23222-6-3421101-ST, 93 p.

Cumming, L.M.
1966: Geology of the Passamaquoddy Bay region, Charlotte County, New Brunswick; Geological Survey of Canada, Paper 65-29, 36 p.

Dadd, K.A., Van Wagoner, N.A., Baldwin, D.K., and McNeil, W.
1989: Cyclic, bimodal volcanism in a Siluro-Devonian continental volcanic zone: the Eastport Formation, southwestern New Brunswick; Atlantic Geology, v. 25, p. 156-157.

Fader, G.B.J.
1989: Cruise Report 88-018(C), Phase 4, 88-018(C), Phase 5, M.V. Navicula, Passamaquoddy Bay and Bay of Fundy; Atlantic Geoscience Centre, Geological Survey of Canada, Bedford Institute of Oceanography, Dartmouth, Nova Scotia, 20 p.

Fay, V.K.
1988: Lower Devonian volcanic and sedimentary rocks of the Eastport Formation, southwest New Brunswick; M.Sc. thesis, University of New Brunswick, Fredericton, New Brunswick, 155 p.

Foley, J.E., Doll, C., Filipkowski, F., and Lorsbach, G.
1985: Seismicity of the northeastern United States; Northeastern U.S. Seismic Network Bulletin No. 34, Weston Observatory, Boston College, Boston, Massachusetts.

Foley, J.E., Ebel, J.E., and Kafka, A.L.
1984: Recent and historic seismicity of southeastern Maine; Canadian Geophysical Union, Eleventh Annual Meeting, Canadian Meteorological and Oceanographic Society, Eighteenth Annual Congress, Joint Programme with Abstracts, p. 65-66.

Gates, O.
1989: The geology and geophysics of the Passamaquoddy Bay area, Maine and New Brunswick, and their bearing on local subsidence; in Neotectonics of Maine, studies in seismicity, crustal warping, and sea-level change, (ed.) W.A. Anderson and H.W. Borns, Jr.; Maine Geological Survey, Bulletin 40, p. 11-24.

Hay, P.W.
1967: Sedimentary and volcanic rocks of the St. Andrews-St. George area, Charlotte County, New Brunswick; Mineral Resources Branch, Department of Natural Resources, New Brunswick, Map Series 67-1.

International Passamaquoddy Engineering Board
1959: Investigation of the International Passamaquoddy Tidal Power Project; Report to the International Joint Commission, Appendix 2, Geology, Foundations and Materials; Ottawa, Ontario, and Washington, D.C., 112 p.

Kelley, J.T., Belknap, D.F., Shipp, R.C., and Miller, S.B.
1989: An investigation of neotectonic activity in coastal Maine by seismic reflection methods; in Neotectonics of Maine, studies in seismicity, crustal warping, and sea-level change, (ed.) W.A. Anderson and H.W. Borns, Jr.; Maine Geological Survey, Bulletin 40, p. 157-204.

Kumarapeli, S.
1990: Deformed glacial deposits of Passamaquoddy Bay area, New Brunswick: products of seismic shaking? MAGNEC/AMNEC Research Report, Contribution No. 90-01, Atomic Energy Control Board, Ottawa, Ontario, 63 p.

Leblanc, G. and Burke, K.B.S.
1985: Re-evaluation of the 1817, 1855, 1869 and 1904 Maine-New Brunswick area earthquakes; Earthquake Notes, v. 56, p. 107-123.

Leger, A. and Williams, P.F.
1986: Transcurrent faulting history of southern New Brunswick; in Current Research, Part B; Geological Survey of Canada, Paper 86-1B, p. 111-120.

Matthew, G.F.
1894: Movements of the earth's crust at St. John, N.B., in post-glacial times; Bulletin of the Natural History Society of New Brunswick, v. 3, no. 12, p. 34-42.

Newman, W.A.
1979: The possibility of Pleistocene-Holocene movement along the Oak Bay Fault on the Maine-New Brunswick border; Maine Geological Survey, Open File 79-20, 7 p.

Pecore, S.S. and Fader, G.B.J.
1990: Surficial geology, pockmarks, and associated neotectonic features of Passamaquoddy Bay, New Brunswick, Canada; Geological Survey of Canada, Open File 2213, 45 p.

Pickerill, R.K. and Pajari, G.E., Jr.
1976: The Eastport Formation (Lower Devonian) in the northern Passamaquoddy Bay area, southwest New Brunswick; Canadian Journal of Earth Sciences, v. 13, p. 266-270.

Rast, N., Burke, K.B.S., and Rast, D.
1979: The earthquakes of Atlantic Canada and their relationship to structure; Geoscience Canada, v. 6, p. 173-180.

Reilinger, R.
1987: Reanalysis of crustal warping in Maine; Geology, v. 15, p. 958-961.

Ruitenberg, A.A.
1968: Geology and mineral deposits, Passamaquoddy Bay area; Mineral Resources Branch, Department of Natural Resources, New Brunswick, Report of Investigation No. 7, 47 p.

Smith, W.E.T.
1962: Earthquakes of Eastern Canada and adjacent areas 1534-1927; Publication of the Dominion Observatory, Ottawa, Canada, v. XXVI, p. 271-301.

Stringer, P. and Burke, K.B.S.
1985: Structure in southwest New Brunswick, Excursion 9; in "Fredericton 85" field excursions, Volume III, (ed.) R.K. Pickerill, C.K. Mawer, and L.R. Fyffe; Geological Association of Canada-Mineralogical Association of Canada, p. 1-34.

Stringer, P., Burke, K.B.S., and Dunn, T.
1991: Stratigraphy, structure and associated igneous rocks of the Upper Devonian Perry Formation in the St Andrews area, southwest New Brunswick, and adjacent coastal Maine; in Geology of the coastal lithotectonic block and neighbouring terranes, eastern Maine and southern New Brunswick, (ed.) A. Ludman; New England Intercollegiate Geological Conference, 83rd Annual Meeting, Wm. C. Brown, Dubuque, Iowa, p. 222-264.

Tyler, D.
1989: Geodetic evidence of current crustal motion in Maine; in Neotectonics of Maine, studies in seismicity, crustal warping, and sea-level change, (ed.) W.A. Anderson and H.W. Borns, Jr.; Maine Geological Survey, Bulletin 40, p. 205-208.

Tyler, D. and Ladd, J.W.
1980: Vertical crustal movement in Maine; Maine Geological Survey, Open File Report 80-34, 53 p.

Van Wagoner, N.A. and Fay, V.K.
1988: Stratigraphy and volcanology of a portion of the Lower Devonian volcanic rocks of southwestern New Brunswick; in Current Research, Part B; Geological Survey of Canada, Paper 88-1B, p. 67-78.

EMR Research Agreement 49-04-89

Compressional deformation and extensional denudation of Early Silurian volcanic overlap assemblages in western Cape Breton Island, Nova Scotia[1]

G. Lynch, C. Tremblay, and H. Rose[2]
Quebec Geoscience Centre, Sainte-Foy

Lynch, G., Tremblay, C., and Rose, H., 1993: Compressional deformation and extensional denudation of Early Silurian volcanic overlap assemblages in western Cape Breton Island, Nova Scotia; in Current Research, Part D; Geological Survey of Canada, Paper 93-1D, p. 103-110.

Abstract: Early Silurian pyroclastic rocks, calk-alkaline volcanic units, and associated coarse siliciclastic rocks in western Cape Breton Island occur as part of a vast Appalachian overlap assemblage deposited unconformably on accreted terranes. Acadian faulting and deformation of the assemblages occurred within a regime of reverse-oblique shear, resulting in the imbrication of basement and cover sequences across thick mylonite zones, and the juxtaposition of high grade and low grade metamorphic domains.

A major low-angle extensional fault complex in the southwestern Cape Breton Highlands consists of thick shallow-dipping mylonite overprinted by cataclastic horizons and chloritic breccias. The shear zone crosscuts and transports low grade volcanic rocks of the Upper Devonian Fisset Brook Formation in its hanging wall to the south and west, and juxtaposes them against exhumed medium to high grade metamorphic rocks in the footwall, including rocks of the overlap assemblage and mylonitic gneiss.

Résumé : Des roches pyroclastiques, des unités volcaniques calco-alcalines et des roches silicoclastiques à grain grossier associées, datées du Silurien précoce, et situées dans l'ouest de l'île du Cap-Breton, font partie d'un vaste assemblage appalachien de recouvrement qui s'est accumulé en discordance sur des terranes d'accrétion. Les failles et la déformation des assemblages ont eu lieu pendant l'Acadien dans un régime de cisaillement inverse-oblique, qui a causé l'imbrication du socle et des séquences de couverture à travers d'épaisses zones mylonitiques, et la juxtaposition de domaines métamorphiques intensément et faiblement métamorphisés.

Un important complexe à failles de distension peu inclinées situé dans le sud-ouest des hautes-terres du Cap-Breton se compose d'épaisses mylonites à faible pendage, auxquelles se superposent des horizons cataclastiques et des brèches chloriteuses. La zone de cisaillement recoupe et transporte des roches volcaniques faiblement métamorphisées de la Formation de Fisset Brook (Dévonien supérieur) au niveau de son toit au sud et à l'ouest, et les juxtapose au niveau du mur à des roches moyennement à intensément métamorphisées exhumées, notamment à des roches de l'assemblage de recouvrement et du gneiss mylonitique.

[1] Contribution to Canada-Nova Scotia Cooperation Agreement on Mineral Development 1990-1992, a subsidiary agreement under the Economic and Regional Development Agreement. Project funded by the Geological Survey of Canada.

[2] Department of Geology, University of Vermont, Burlington, VT 05405 U.S.A.

INTRODUCTION

Early Silurian calc-alkalic pyroclastic deposits and associated clastic rocks are regionally distributed across a wide portion of the Canadian Appalachians (Williams, 1979; Barr and Jamieson, 1991), occurring as a tectonic overlap assemblage (Williams, 1979; Chandler et al., 1987; O'Brien et al., 1991) deposited unconformably upon various Ordovician or older terranes providing an upper limit on the age of accretion. Characteristics and contact relations of the overlap assemblage are particularly well exposed and documented in southwestern Newfoundland where a stratovolcano association deposited under marine and nonmarine conditions above a major unconformity is reported (O'Brien et al., 1991). Features of the overlap assemblage are characteristic of volcanic rocks in Cape Breton Island (Lynch and Tremblay, 1992), of known or presumed Early Silurian age which comprise the Aspy Terrane of Barr and Raeside (1989). Volcanological and geochemical aspects of the rocks argue that volcanic activity was subduction-related (Jamieson et al., 1990; Barr and Jamieson, 1991), however subduction-diagnostic lithologies such as blueschists, ultramafic rocks, or trench mélange of similar age have not been found.

This paper reports on the lithology, contact relations, and deformation of Early Silurian volcanic rocks and correlated units from Cape Breton Island in the Mabou, Ainslie, and Middle River areas (Fig. 1). Arguments are presented for expansion of the volcanic field to include pyroclastic deposits in these areas previously thought to be Devonian in age (Barr and Jamieson, 1991). Features of a complex deformation history are highlighted as well, and significant new shear zones are identified of both compressional and extensional origin. New developments in Cape Breton tectonics include the identification of major low-angle brittle-ductile extensional faulting in the southwestern Highlands (Lynch and Tremblay, 1992; Lynch, 1992). Further details on the timing, field relations, and the regional extent of such faulting is presented.

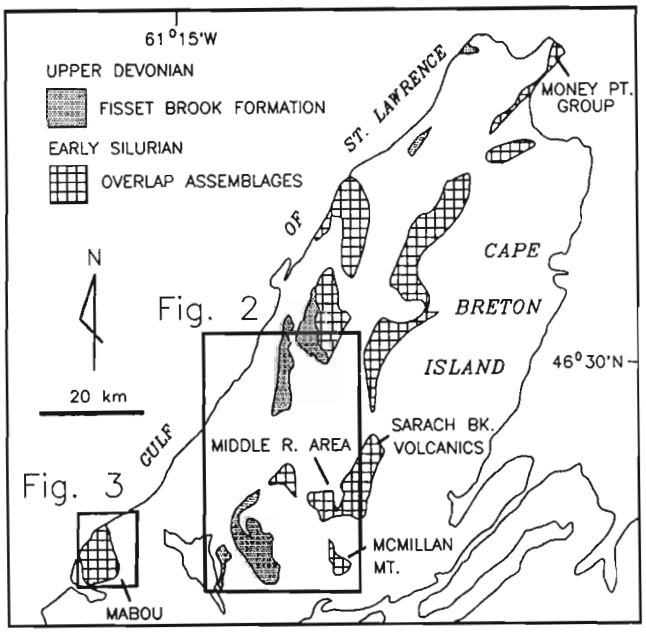

Figure 1. Location map and distribution of Early Silurian and Upper Devonian volcanic rocks in the Cape Breton Highlands.

EARLY SILURIAN OVERLAP ASSEMBLAGES

The Money Point Group (Macdonald and Smith, 1980) and Sarach Brook Metamorphic Suite (Barr and Jamieson, 1991) are well preserved and accurately dated sequences of Early Silurian volcanic rocks of Cape Breton Island (Fig. 1). The geology of these is briefly reviewed for comparison with pyroclastic rocks of the MacMillan Mountain volcanic unit which is reported as being Devonian in age (Jamieson and Doucet, 1983; Barr and Jamieson, 1991), and with a large unit of pyroclastic rocks from the Mabou area which has been correlated with the Upper Devonian Fisset Brook Formation (Barr and Macdonald, 1989; Barr and Jamieson, 1991). Details of the internal stratigraphy from the widely scattered sites are complex and variable, as is typical for explosive pyroclastic fields. However characteristic rock types are found in all areas demonstrating a compatible volcanic environment, distinct from the bimodal basalt-rhyolite and redbed assemblage typical of the Upper Devonian Fisset Brook Formation (Blanchard et al., 1984).

Sarach Brook Metamorphic Suite

The Sarach Brook Metamorphic Suite (Barr et al., 1987; Barr and Jamieson, 1991) is a well bedded succession consisting of fine grained to aphanitic basalt, porphyritic andesite, lapilli and bomb felsic pyroclastics, crystal tuff, epiclastic sandstone, quartz-rich wacke, conglomerate, and black slate. Zircon from felsic crystal tuff has been dated by the U-Pb method, indicating a crystallization date of 433 +7/-4 Ma (Dunning et al., 1990). Well preserved portions show only moderate degrees of metamorphism, however high grade gneiss and metamorphic units thought to be equivalent to the Sarach Brook volcanic rocks (Jamieson, 1981; Jamieson and Doucet, 1983), have been obliquely thrust over the low grade members towards the east-southeast along a thick zone of greenschist-grade mylonite during Acadian deformation (Horne, in press).

Conglomerate in the higher grade rocks from the western portion of the Sarach Brook Metamorphic Suite are highly strained and have been affected by upper greenschist grade (biotite) metamorphism. Moderately sorted, well rounded clasts up to 5 cm in diameter are dominated by granitic clasts and epidotized diorite. Detrital feldspar and vitreous blue quartz clasts are abundant in some layers where the rock is arkosic in composition. A sharp contact was observed between the conglomerate and a large body of medium- to coarse-grained foliated diorite; the age of the diorite is unknown, but the contact is possibly an unconformity assuming that the diorite clasts from the conglomerate were derived from the adjacent diorite pluton. The conglomerate near the contact is approximately 4-10 m thick, and progresses upwards to a thick succession of chloritic metawacke containing dispersed quartz or feldspar pebbles.

Money Point Group

The Money Point Group (MacDonald and Smith, 1980) of Northern Cape Breton Island has been dated at 427.5 ± 4 Ma by the U-Pb method with zircon extracted from a metarhyolite (Keppie et al., 1992). Metamorphism is variable, but well preserved sections show clear primary bedding between units of tuff, basalt, andesite, rhyolite, and sedimentary rocks. Tuffaceous and pyroclastic units include fine grained (ash ?) tuffs, crystal tuffs, and a wide variety of coarse lithic tuffs dominated by lapilli and bombs of andesite and basalt as well as occasional pumice. Interbedded metasedimentary rocks include phyllite, schist, quartzite, quartz-pebble conglomerate, and calc-silicate rocks. Quartzites are gradational to wackes which are more feldspathic. Clasts of quartzite or polycrystalline quartz in the conglomerates are up to 5 cm in length, and individual beds are up to 5 m thick. The conglomerates occur near the top of the group (MacDonald and Smith, 1980). The basal contact of the Money Point Group has not been identified; however immediately to the south, high grade rocks of the Cheticamp Lake Metamorphic Suite which are thought to be equivalent to the Money Point Group (Barr and Jamieson, 1991), have a basal conglomerate containing clasts of quartzite and granitic gneiss deposited unconformably upon the Proterozoic McMillan Flowage Formation of the Bras d'Or terrane (Lin et al., 1991). The contact relationship and correlation suggest that the Money Point Group was deposited unconformably upon the Bras d'Or terrane.

MacMillan Mountain volcanic unit

In the southern Cape Breton Highlands the MacMillan Mountain volcanic unit (Fig. 1, 2) consists of relatively fresh, weakly deformed mafic, intermediate, and felsic volcanic and pyroclastic rocks, with associated sedimentary lithologies. Based on the similarities and distinctiveness of the volcanic assemblages Jamieson (1981) originally correlated the MacMillan Mountain volcanic unit with the Sarach Brook

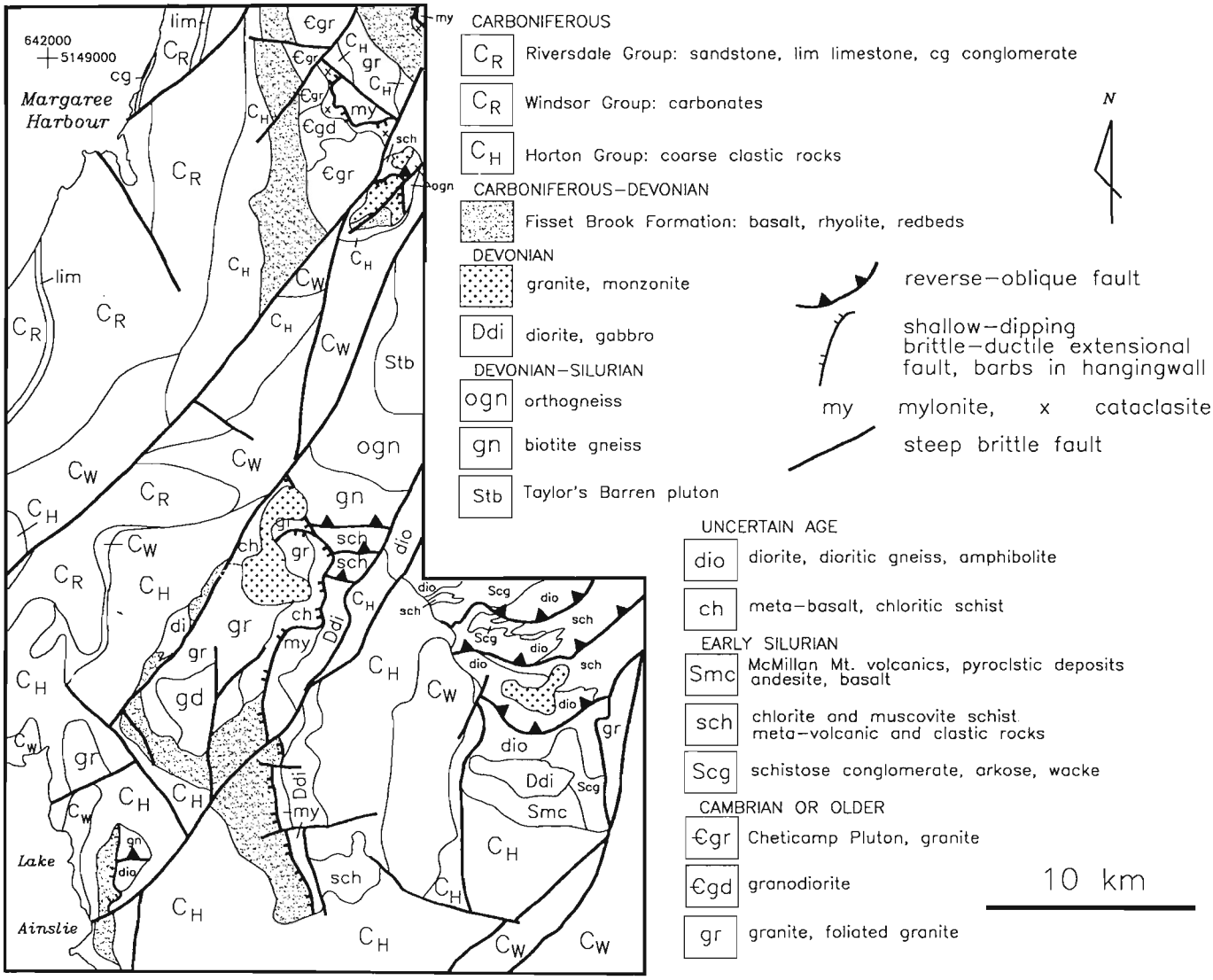

Figure 2. Geological map of the southwestern Cape Breton Highlands.

Metamorphic Suite. Collectively these were referred to as the Crowdis Mountain volcanics (Jamieson, 1981). However, age dating by the Rb-Sr method produced an apparent age of 384 ± 10 Ma for the MacMillan Mountain volcanic unit, leading Jamieson and Doucet (1983) and others (Barr and Jamieson, 1991) to conclude that the unit is Devonian in age. But as suggested by Horne (in press) Rb-Sr ages are unreliable when estimating crystallization ages for rocks in the Cape Breton Highlands. With further mapping we concur with Jamieson's (1981) initial correlations.

In the MacMillan Mountain unit, dark green to brick red andesite is common, with local trachytic varieties. Basalt is closely associated with andesite and may be amygdular. Basalt and andesite form thick crudely bedded blocky flows with vitrophyre along contacts. Rhyolite is fine grained to aphanitic, with occasional spherulites. Pyroclastic deposits are highly variable but typically well bedded. Laminated ash-flow tuffs and crystal tuffs are common. Welded lapilli tuff forms distinctive light coloured horizons containing pumice fragments. Sedimentary rocks include siltstone, coarse sand arkose, and lithic-arkose. Pebble conglomerate with quartzite, granite, quartz, and feldspar clasts occurs along the northeast limit of the MacMillan Mountain volcanic unit immediately adjacent to foliated granite of uncertain age and diorite of the Kathy Road Dioritic Suite (560 Ma, Dunning et al., 1990). The exact nature of the contact is unknown, but the local rock assemblage suggests the possibility of an unconformity.

Mabou Highlands Metamorphic Suite

In the Mabou area of the southwestern Cape Breton Highlands (Fig. 1, 3), Barr and Jamieson (1991) correlate medium to high grade metavolcanic rocks of the Mabou Highlands Metamorphic Suite with those of the Sarach Brook Metamorphic Suite on the basis of similar lithologies and metamorphic histories. They exclude from this grouping low grade pyroclastic rocks occurring along the western margin of the Mabou Highlands. This low grade assemblage was designated to be Devonian and tentatively correlated with the Upper Devonian Fisset Brook Formation (Blanchard et al., 1984; Barr and Macdonald, 1989; Barr and Jamieson, 1991). However this correlation is inconsistent with the types of lithology, volcanic facies, and environment, and ignores the presence of Silurian fossiliferous dolomitic limestone (Phinney, 1956; Barr and Macdonald, 1989) intercalated with shale, arenite, and andesite along the western Mabou Highlands. Therefore we argue that despite the lack of intense

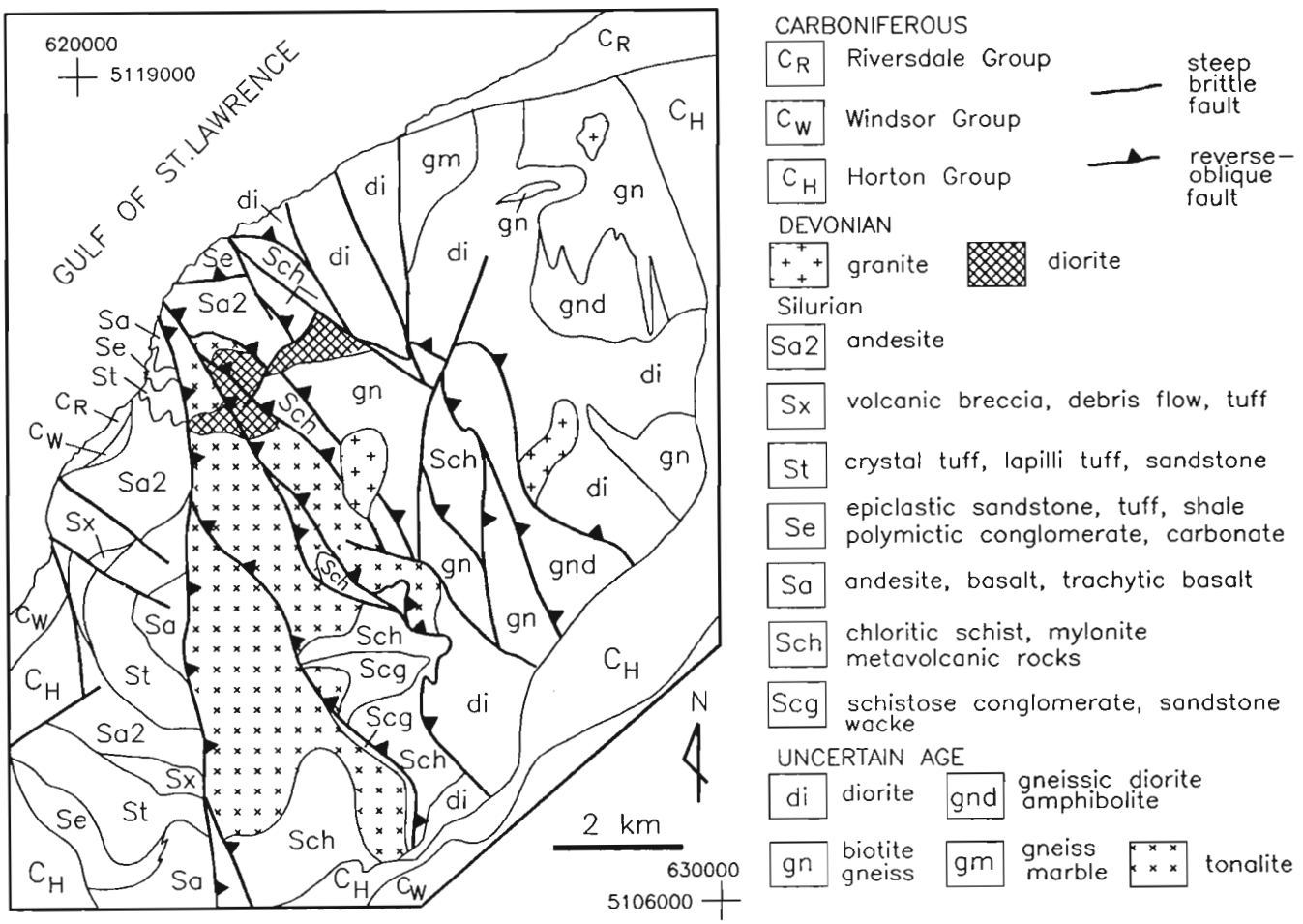

Figure 3. Geological map of the Mabou Highlands.

metamorphism, the pyroclastic nature of the rocks and the presence of Silurian fauna clearly place the low grade unit along the western Mabou Highlands within the Early Silurian overlap assemblage.

The low grade volcanics are locally chloritized and epidotized, and may contain an associated foliation. The unit is mylonitized and fault-bounded to the east. Voluminous crystal tuff is widespread, is well bedded to laminated, and contains greater than 50% plagioclase crystals. Welded and nonwelded lapilli tuff and volcanic breccia of andesitic composition are interbedded with finer grained tuffs. Ash and mud supported volcanic debris-flow breccias contain large angular fragments of epidotized volcanic tuff, andesite, and rare tonalite. Andesitic volcanic flow breccias also occur. Less abundant volcanic rock types are trachytic andesite, vesicular basalt, rhyolite, and pumiceous rhyolite. Interbedded sedimentary rocks are generally subordinate to the volcanic rocks. Siltstone, arenite, and arkose occur. Fossiliferous dolomitic limestone is interbedded with a sandstone-dominated sequence containing thin andesite flows.

To the east within an imbricate fault system (Fig. 3), the higher grade volcanic rocks range from greenschist to amphibolite grade. Plagioclase-rich crystal tuff and thinly bedded varicoloured ash-flow tuffs occur locally. Andesite flows and autobrecciated flows are abundant, as well as basalt. Poorly sorted, volcanic debris-flow breccia contains angular matrix-supported clasts up to 40 cm long of rhyolite, tuff, and other volcanic rocks. Lapilli tuff of various compositions is widespread. Thin beds of grey-white limestone occur between epiclastic sandstone beds and black carbonaceous phyllite or schist. A thick unit of strongly deformed polymictic conglomerate contains well rounded clasts up to 1 m long of granite, tonalite, syenite, granitic gneiss, limestone, as well as multicoloured volcanic clasts of andesite, basalt, rhyolite, and tuff. An unconformity was observed along a granite body of unknown age and of limited surface extent; the unconformity features a thin (50 cm thick) moderately to steeply dipping bed of foliated well sorted quartz-feldspar pebble conglomerate containing well-rounded quartz, feldspar, and granite clasts, resting directly on the granite body. The conglomerate passes rapidly upwards into thinly bedded multicoloured tuff 5 m thick, followed by interbedded black carbonaceous schist and light coloured limestone. Plutonic rocks of unknown age form the basement to the volcanic sequence.

STRUCTURE

Early Silurian volcanic rocks in the western Cape Breton Highlands have been affected by at least three major penetrative deformation events (Lynch and Tremblay, 1992). The events are defined by 1) an early stage of imbricate thrusting and isoclinal folding (D_1), followed by 2) a phase of reverse-oblique faulting and upright folding (D_2), and 3) a late stage of low-angle extensional faulting (D_3). The effects of D_1 and D_3 above are relatively restricted or localized, whereas the structures associated with D_2 are widespread. The three deformation episodes were referred to as being of Acadian age (Lynch and Tremblay, 1992), but the distinctive character and distribution of each phase warrants further subdivision. The early thrusting (D_1) in the western Cape Breton Highlands is probably pre-Acadian since D_1 thrusts are truncated by D_2 reverse faults and overprinted by syn-D_2 metamorphic isograds associated with Acadian high grade metamorphism (Lynch and Tremblay, 1992). The D_3 extensional faulting is post-Acadian since low-angle detachment faults crosscut the Upper Devonian rocks of the Fisset Brook Formation. Gneissic rocks are affected by D_2 and D_3, older fabrics in the gneisses are not addressed in this presentation.

D_1

Polyphase folding is recorded in stratified tuff, shale, and carbonate sequences within the northwestern Mabou Highlands. Steeply-dipping to upright, moderately northwest-southeast plunging isoclinal folds (D_1) are overprinted by upright tight north-trending folds (D_2), producing hook interference patterns. An axial-planar cleavage is associated with both phases of folding. The isoclinal folds occur adjacent to discrete thrusts which have repeated portions of the stratigraphy including slivers of granitic basement rocks.

On Sugarloaf Mountain in the northeast sector of Figure 2, isoclinal folds (D_1) in chloritic schist (metabasalt) are overprinted by upright tight northwest-trending folds and associated axial-planar foliation linked to D_2 deformation. Although D_1 appears to be widely distributed, the effects of D_1 on regional map patterns is difficult to establish due to overprinting phases of deformation. However, large-scale imbrication of stratigraphy during D_1 faulting was documented in the Cheticamp River area by Lynch and Tremblay (1992).

Reverse-oblique shear, D_2

Reverse-oblique shear zones occur in the Cape Breton Highlands, resulting from intense deformation linked to the Acadian orogeny (Lin and Williams, 1992; Lynch, 1992; Lynch and Tremblay, 1992). The shear zones are typified by steeply-dipping mylonites of variable thicknesses containing mineral and stretching lineations ranging in orientations from down-dip to horizontal. Deformation developed within a regime of reverse-oblique shear, with faults accommodating strike-slip and reverse components of movement. Typically the shear zones juxtapose high grade rocks metamorphosed at middle crustal levels in Acadian time (Plint and Jamieson, 1989; Reynolds et al., 1989; Keppie et al., 1992) against low grade rocks from upper crustal levels. Telescoping of amphibolite, and greenschist grade domains is observed across these faults. Biotite is common along many shear planes, but metamorphic assemblages are quite varied and may contain among others staurolite, muscovite, garnet, lineated kyanite, amphiboles, or greenschist to lower greenschist metamorphic minerals. Mineral lineations associated with primary mineral growth are well developed. Lineations due to mineral trails developed during grain size reduction also occur. Augen of quartzofeldspathic lenses

locally form complex shapes suggesting rotation during non-coaxial shear. Asymmetric intrafolial folds also provide information on shear sense within the mylonites. Pegmatite or granitic dykes are widely associated with the reverse-oblique shear zones, and display synkinematic relationships to deformation by crosscutting the shear zones and being flattened within them.

The Sarach Brook shear zone (Jamieson, 1981; Horne, in press) is a steeply-dipping greenschist grade mylonite zone which forms the northwest boundary to low grade volcanic rocks of the Sarach Brook Metamorphic Suite. Medium to high grade rocks were obliquely thrust along the shear zone towards the southeast over the low grade volcanic assemblage. The intrusion of syntectonic granitic dykes along the fault indicates an Early Devonian (Acadian) age for deformation (Horne, in press). Reverse and sinistral components of movement were reported (Horne, in press). To the south, similar relationships are found where high grade kyanite-bearing gneiss and amphibolite have moved upwards along thick, east-striking amphibole-bearing mylonite, and are juxtaposed against upper greenschist and locally staurolite-bearing assemblages of the Sarach Brook Metamorphic Suite. The latter are limited further to the south by mylonites which accommodated reverse movement and uplift of metamorphosed lithologies towards the south over low grade, fine grained diorite and rocks of the McMillan Mountain volcanic suite. The northeast-trending assemblage of low grade Silurian pyroclastic rocks define a low grade front in the footwall of the high grade overthrust system. Steeply-plunging lineations, pressure shadows, rotated augens, and C-S fabrics indicate reverse motion along the mylonites.

In the Mabou area (Fig. 3) abundant and thick steeply-dipping mylonite zones occur. These include a significant volume of mylonitized plutonic and gneissic rocks previously mapped as metarhyolite (Barr and Macdonald, 1989). The shear zones define moderately to steeply-dipping faults which strike north to northwest. The map pattern in the Mabou area outlines a northward-tapering imbricate stack bounded to the west by a relatively straight, north-striking mylonitic fault (Fig. 3). Lineations plunge to the north along mylonite zones. Shear sense indicators (winged inclusions and C-S fabrics) indicate combined dextral-reverse motion transporting blocks upwards and towards the south. A decrease in metamorphic grade is observed from east to west as major mylonite zones are crossed; from amphibolitic gneiss, to greenschist and biotite-bearing schistose metavolcanic and pyroclastic rocks, to lower greenschist volcanic, pyroclastic and clastic assemblages in the west. Small to outcrop scale polyclinal, disharmonic intrafolal box folds within laminated mylonite occur between planar strands of mylonite within shear zones. Larger scale folded mylonitic shear zones are detached along and were apparently transported by adjacent mylonitic faults.

Extensional faulting D_3

A thick, low-angle, mylonitic to cataclastic, extensional shear zone occurs in the southwestern Cape Breton Highlands. It can be traced north-south for approximately 50 km from near Cheticamp to east of Lake Ainslie (Fig. 3). The quality of exposure is variable and the shear zone outcrops discontinuously. Unconformably overlying units and younger faults also limit its exposure. The shear zone consists of flat-lying to shallow-dipping mylonitic gneiss and schist, cataclasite, and chloritic breccia. A consistent temporal evolution of fault-rock types is observed from early ductile fabrics, to brittle-ductile, to late cataclasis. Age constraints on faulting are provided by the Upper Devonian to Carboniferous Fisset Brook Formation (Blanchard et al., 1984) which is locally crosscut by the shear zone, and by the unconformably overlying Visean Windsor Group. Tournaisian coarse clastic rocks of the Horton Group also lie in angular unconformity with the mylonitic rocks. But it is postulated that debris flows of the Horton Group may be associated with brittle low-angle faulting. Rocks of the Fisset Brook Formation and underlying units occur in the hanging wall of the fault zone. Footwall rocks consist of medium to high grade rocks of the Cape Breton Highlands which were unroofed during extension. Shear sense indicators suggest a west to southwest tectonic transport of the upper plate.

Mylonitic gneiss consists of thinly layered to laminated quartzofeldspathic biotite gneiss derived from various plutonic rocks including granite, granodiorite, and diorite. Stretching and mineral lineations plunge moderately from south to west. Axes to small-scale sheath folds parallel the stretching lineations. Complex fold interference patterns are observed including eye folds, hook folds, and croissant folds. The mylonitic gneiss is up to 1000 m in thickness along some portions of the shear zone, but more typically is 100-300 m thick. Overprinting the mylonitic gneiss and other lithologies are mylonites in which feldspar segregations do not define the principal foliation, but rather occur as augen and have been affected by intense grain-size reduction and muscovite growth. A wide range of textures are associated with the mylonites; quartz-feldspar segregations with pressure shadows, micaceous shear bands, augen feldspar, C-S fabrics, en echelon extensional shear bands, and late tension gashes formed perpendicular to mineral lineations and mineral trails. Slickensides and quartz-fibre growths also parallel penetrative mineral lineation, and locally accompanied syntectonic hematization of the shear bands. Mafic mylonitized rocks are intensely chloritized, and contain associated epidote and calcite giving the rocks a dark green appearance which greatly contrasts with the light coloured muscovite-rich mylonites. A well exposed section along Turner Brook provides a clear view of relationships between the shear zone and the Fisset Brook Formation; fresh nonmetamorphosed vesicular basalt interbedded with redbed siltstone and minor conglomerate pass abruptly downwards into weakly chloritized and mildly foliated vesicular basalt and redbeds, which grade into well developed moderately-dipping chloritic mylonite. The exposure shows that relatively young fresh units of the Fisset Brook Formation are affected by at least lower greenschist mylonitization. In the vicinity of the Margaree River, granite correlated with the Upper Devonian Salmon Pool Pluton (Jamieson et al., 1987) has been affected by low-angle shearing. Transport of younger low grade rocks above older high grade rocks suggests that the shear zone was

formed during tectonic extension, and that it likely accommodated considerable vertical and lateral translation of units in order to juxtapose these contrasting lithologies.

Cataclastic zones form broad domains and irregular map units (Fig. 2). The zones contain a weak flat-lying foliation, or more typically no fabric. Cataclastic faults also occur as thin horizons (50 cm) along the mylonitic foliation. Cataclasite either directly overprints mylonite or is found within some regions of the hanging wall. Breccia is quite variable, and may have coarse angular fragments, or fault surfaces may be dominated by pea-sized clasts. Microbreccia was also found in some areas rendering protoliths difficult to map. Matrix to the breccia is chloritic, and may locally contain hematite and goethite. Slickenside striations may occur along fault planes, as well as quartz-fibres. Low-angle brittle faults occur in the Fisset Brook Formation in the proximity of shallow-dipping mylonites, and have been observed in the overlying Horton Group where associated outcrop-scale detached folds were found.

CONCLUSIONS

The Early Silurian volcanic field has been expanded to include pyroclastic sequences in the Mabou and Middle River areas previously thought to be of Devonian age. The correlations are based principally on lithological similarities, but the occurrence of fossiliferous Silurian carbonates in the Mabou sequence and the overprint of Acadian deformation provide further arguments. The abundance of conglomerate containing granitic and plutonic clasts, as well as a basal unconformity observed locally indicate that the Early Silurian assemblages were deposited unconformably on continental crust, likely as part of an Early Silurian overlap assemblage.

A major Acadian reverse-oblique shear zone and imbricate fault stack is now recognized in the Mabou area and is linked to a similar fault system in the Middle River area. Thick mylonite zones and telescoping of metamorphic domains are characteristic features. Significant low-angle extensional brittle-ductile shear has been mapped along strike from north to south for approximately 45 km. Extension postdates the Upper Devonian Fisset Brook Formation, which was transported as the upper plate down over exhumed high grade older schist and gneiss.

ACKNOWLEDGMENTS

We would like to thank Renaud Delisle for his assistance and excellence during fieldwork. A field trip and introduction to Carboniferous stratigraphy in the region by Peter Giles proved to be both tremendously useful and informative. We also thank Alain Tremblay for a thorough review of the manuscript.

REFERENCES

Barr, S.M. and Jamieson, R.A.
1991: Tectonic setting and regional correlation of Ordovician-Silurian rocks of the Aspy terrane, Cape Breton Island, Nova Scotia; Canadian Journal of Earth Sciences, v. 28, p. 1769-1779.

Barr, S.M. and Macdonald, A.S.
1989: Geology of the Mabou Highlands, western Cape Breton Island, Nova Scotia; Nova Scotia Department of Mines and Energy, Paper 89-2.

Barr, S.M. and Raeside, R.P.
1989: Tectono-stratigraphic divisions of Cape Breton Island, Nova Scotia; Geology, v. 17, p. 822-825.

Barr, S.M., Raeside, R.P., White, C.E., and Yaowanoiyothin, W.
1987: Geology of northeastern and central Cape Breton Highlands, Nova Scotia; in Current Research, Part A; Geological Survey of Canada, Paper 87-1A, p. 199-207.

Blanchard, M.-C., Jamieson, R.A., and More, E.B.
1984: Late Devonian – Early Carboniferous volcanism in western Cape Breton Island, Nova Scotia; Canadian Journal of Earth Sciences, v. 21, p. 762-774.

Chandler, F.W., Loveridge, D., and Currie, K.L.
1987: The age of the Springdale Group, western Newfoundland, and correlative rocks – evidence for a Llandovery overlap assemblage in the Canadian Appalachians; Transactions of the Royal Society (Edinburgh) in Earth Sciences, v. 78, p. 41-49.

Dunning, G.R., Barr, S.M., Raeside, R.P., and Jamieson, R.A.
1990: U-Pb zircon, titanite, and monazite ages in the Bras d'Or and Aspy terranes of Cape Breton Island, Nova Scotia: implications for magmatic and metamorphic history; Geological Society of America, Bulletin, v. 102, p. 322-330.

Horne, R.J.
in press: Report on the Geology of south-central Cape Breton Highlands Cape Breton Island, Nova Scotia; Nova Scotia Department of Natural Resources, Paper.

Jamieson, R.A.
1981: The geology of the Crowdis Mountain volcanics, southern Cape Breton Highlands; in Current Research, Part C; Geological Survey of Canada, Paper 91-1C, p. 77-81.

Jamieson, R.A. and Doucet, P.
1983: The Middle River – Crowdis Mountain area, southern Cape Breton Highlands; in Current Research, Part A; Geological Survey of Canada, Paper 83-1A, p. 269-275.

Jamieson, R.A., Tallman, P.C., Plint, H.E., and Connors, K.A.
1990: Regional geological setting of pre-Carboniferous mineral deposits in the western Cape Breton Highlands, Nova Scotia; in Mineral Deposit Studies in Nova Scotia, Volume 1, (ed.) A.L. Sangster; Geological Survey of Canada, Paper 90-8, p. 77-99.

Jamieson, R.A., Tallman, P., Marcotte, J.A., Plint, H.E., and Connors, K.A.
1987: Geology of the west-central Cape Breton Highlands, Nova Scotia; Geological Survey of Canada, Paper 87-13.

Keppie, J.D., Dallmeyer, R.D., and Krogh, T.E.
1992: U-Pb and $^{40}Ar/^{39}Ar$ mineral ages from Cape North northern Cape Breton Island: implications for accretion of the Avalon composite terrane; Canadian Journal of Earth Sciences, v. 29, p. 277-295.

Lin, S. and Williams, P.F.
1992: Ductile faulting in northeast Cape Breton Highlands, Nova Scotia: Late Silurian thrusting and Late Devonian Transpression; Geological Association of Canada-Mineralogical Association of Canada, Abstracts Volume, v. 17, p. A67.

Lin, S., Williams, P.F., and Raeside, R.P.
1991: The discovery of a conglomerate at the base of the Cheticamp Lake Metamorphic Suite and its implication for the geological interpretation of Cape Breton Island, Nova Scotia; Nova Scotia Department of Natural Resources, Report 91-5, p. 50.

Lynch, J.V.G.
1992: Extensional collapse of the Appalachian Orogen: evidence from the Cape Breton Highlands; Geological Association of Canada-Mineralogical Association of Canada, Abstracts Volume, v. 17, p. A69.

Lynch, J.V.G. and Tremblay, C.
1992: Imbricate thrusting, reverse-oblique shear, and ductile extensional shear in the Acadian Orogen, central Cape Breton Highlands, Nova Scotia; in Current Research, Part D; Geological Survey of Canada, Paper 92-1D, p. 91-100.

Macdonald, A.S. and Smith, P.K.
1980: Geology of Cape North area, northern Cape Breton Island, Nova Scotia; Nova Scotia Department of Mines and Energy, Paper 80-1, 60 p.

O'Brien, B.H., O'Brien, S.J., and Dunning, G.R.
1991: Silurian cover, Late Precambrian-Early Ordovician basement, and the chronology of Silurian orogenesis in the Hermitage flexure (Newfoundland Appalachians); American Journal of Science, v. 291, p. 760-799.

Phinney, W.C.
1956: Structural relationships around the southern extension of the Mabou Highlands, Inverness County, Cape Breton Island, Nova Scotia; M.Sc. thesis, Massachusettes Institute of Technology, Cambridge, Massachusettes.

Plint, H.E. and Jamieson, R.A.
1989: Microstructure, metamorphism, and tectonics of the western Cape Breton Highlands, Nova Scotia; Journal of Metamorphic Geology, v. 7, p. 407-424.

Reynolds, P.H., Jamieson, R.A., Barr, S.M., and Raeside, R.P.
1989: A $^{40}Ar/^{39}Ar$ study of the Cape Breton Highlands, Nova Scotia: thermal histories and tectonic implications; Canadian Journal of Earth Sciences, v. 26, p. 2081-2091.

Williams, H.
1979: Appalachian Orogen in Canada; Canadian Journal of Earth Sciences, v. 16, p. 792-807.

Geological Survey of Canada Project 920001-AL

Preliminary study on diagenesis and mineralization of the Jubilee Pb-Zn deposit, Nova Scotia

S. Paradis, M. Savard, and F. Fallara[1]
Quebec Geoscience Centre, Sainte-Foy

Paradis, S., Savard, M., and Fallara, F., 1993: Preliminary study on diagenesis and mineralization of the Jubilee Pb-Zn deposit, Nova Scotia; in Current Research, Part D; Geological Survey of Canada, Paper 93-1D, p. 111-119.

Abstract: The Jubilee stratabound Zn-Pb deposit in Cape Breton Island is hosted by brecciated Carboniferous limestone of the Lower Windsor Group. The base of the Windsor Group consists of limestone cyanobacterial laminites of the Macumber Formation overlain by limestone-evaporite interbeds and a massive anhydrite cap of the Carrolls Corner Formation equivalent.

Mineralization consists of pyrite, sphalerite, and galena, with minor amounts of marcasite, chalcopyrite, and barite, occurring as cavity and breccia fillings, veins, limestone replacement, and disseminations. A spatial relationship is observed between the mineralized breccia and the steeply-dipping Jubilee Fault, which crosscuts the Windsor Group. Carbonates are the principal gangue mineral. Mineral paragenesis indicates that mineralization post-dated a fibrous brownish calcite cement, and mostly pre-dated coarse anhedral white calcite.

Résumé : Le gisement stratoïde de Pb-Zn de Jubilee dans l'île du Cap-Breton est logé dans les calcaires brèchiques d'âge carbonifère du Groupe de Windsor. La base du Groupe de Windsor est constituée d'un calcaire à laminites cyanobactériennes de la Formation de Macumber recouvert d'intercalations de calcaire et d'évaporite, le tout coiffé d'une épaisse séquence d'anhydrite massive de l'équivalent de la Formation de Carrolls Corner.

La minéralisation consiste principalement de pyrite, sphalérite et galène, et de petites quantités de marcasite, chalcopyrite et barytine. Elle se présente sous forme de remplissage de cavités et de brèches, de veines, de remplacement du calcaire et de cristaux disséminés. Une relation spatiale existe entre la brèche minéralisée et la faille abrupte de Jubilee qui recoupe les unités du Groupe de Windsor. Les carbonates sont les principaux minéraux de gangue. La paragenèse minérale indique que la minéralisation est postérieure au ciment de calcite brune fibreuse et est antérieure au ciment de calcite blanche grossière de forme allotriomorphique.

[1] Université Laval, Département de géologie, Sainte-Foy (Québec) G1K 7P4

INTRODUCTION

The Jubilee Pb-Zn deposit is located near Little Narrows on the Iona Peninsula, Cape Breton Island, Nova Scotia (Fig. 1). It is an unusual stratabound limestone-hosted Pb-Zn deposit because dolostone is conspicuously absent in the Jubilee carbonate lithologies. This contrasts markedly with most reported Mississippi Valley Type (MVT) Pb-Zn deposits which are hosted by dolostone.

The information presented in this paper follows the detailed geological study of Hein et al. (1988, in press) and Graves et al. (1990) on the Jubilee Pb-Zn deposit. It represents the first phase of a combined diagenetic and metallogenic study of the Jubilee deposit and is based mainly on detailed examination and sampling of drill cores from 25 drill holes from the Nova Scotia Department of Mines and Energy Core Storage Facility in Stellarton.

The aim of this study is to establish the paragenetic sequence by examining the relationship between mineralization and diagenetic processes such as cementation, dissolution, and stylolitization. In the first phase of the study, we identify the different carbonate, sulphide, and sulphate phases and their relative timing of which some of the results are presented here. In a subsequent study, we will characterize the various generations of carbonates with geochemical tracers, such as $\delta^{18}O$, $\delta^{13}C$, $^{87}Sr/^{86}Sr$, Mg, Sr, Fe, and Mn, to help in characterizing the different fluids that affected the Macumber Formation in the vicinity of the Jubilee deposit.

GEOLOGICAL SETTING

The Jubilee deposit is located in the Carboniferous River Denys sub-basin which forms part of the Maritimes basin (Ravenhurst et al., 1989). Thick accumulations of terrestrial and shallow-marine sediments were deposited in pull-apart basins related to post-Acadian rifting (Belt, 1968; Sheridan and Drake, 1968; Howie and Barss, 1975; Fralick and Schenk, 1981). The stratigraphic sequence in the Maritimes basin has been divided, in ascending order, into the Horton, Windsor, Canso-Riversdale-Cumberland, and Pictou groups (Bell, 1929; Ravenhurst et al., 1989). The Windsor Group is the main unit of interest in this paper because it contains the Jubilee Pb-Zn deposit, and other well known Pb-Zn and Ba occurrences and deposits, such as the Pb-Zn Gays River deposit (Ravenhurst et al., 1989).

The Windsor Group is composed of carbonates, evaporites and siltstones of Visean age (348-336 Ma) which conformably overlie rocks of the Horton Group of Frasnian (?) to Tournaisian age (360-350 Ma). Rocks of the Windsor Group represent a major marine transgression into a continental basin that is preceded and followed by continental sedimentation (Geldsetzer, 1977; Kirkham, 1978; Giles, 1981).

GEOLOGY OF THE JUBILEE DEPOSIT

Footwall rocks to the Jubilee deposit consist of continental clastic units of grey and red sandstone, siltstone, and conglomerate of the Horton Group. The Lower Windsor Group which consists predominantly of dark grey marine limestone of Macumber Formation is overlain by a thick sequence of anhydrite (Fig. 2). The contact between the Horton and Windsor groups is sharp and conformable. However, regionally extensive shearing and fault breccia forming a broad detachment zone with underlying strata and basement rocks occur along the Macumber Formation (Lynch and Giles, in press).

The detailed stratigraphic column of the Lower Windsor Group in the Jubilee area is, in ascending order: 1) limestone cyanobacterial laminites with oolites, peloids and oncolites, 2) limestone cyanobacterial laminites, 3) transitional interbedded limestone and sulphates (gypsum or anhydrite), and 4) a massive anhydrite sequence with rare interbeds of limestone and halite.

Mineralization occurs within brecciated limestone which is preferentially located within the transitional interbedded limestone-sulphates facies. However, the mineralized breccia also occurs in the cyanobacterial laminites facies and

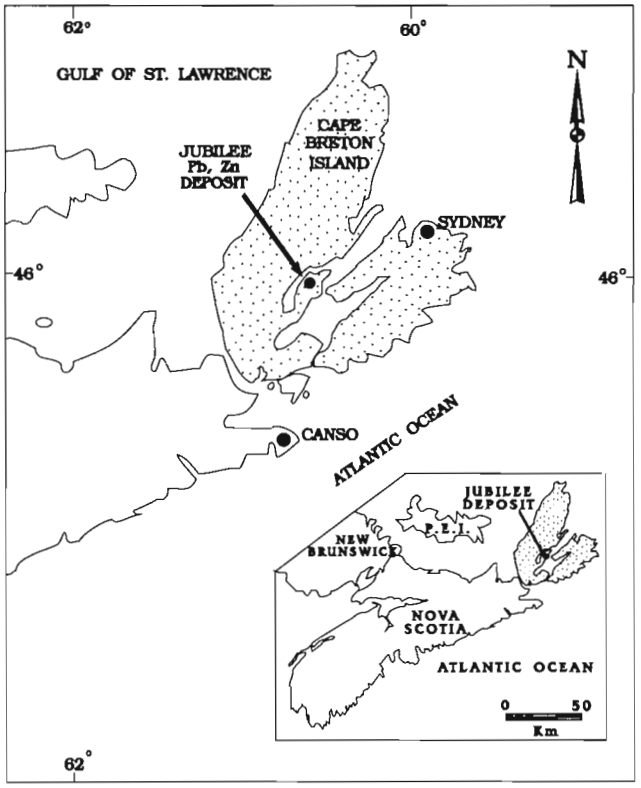

Figure 1. Location of the Jubilee Pb-Zn deposit within Cape Breton Island, Nova Scotia.

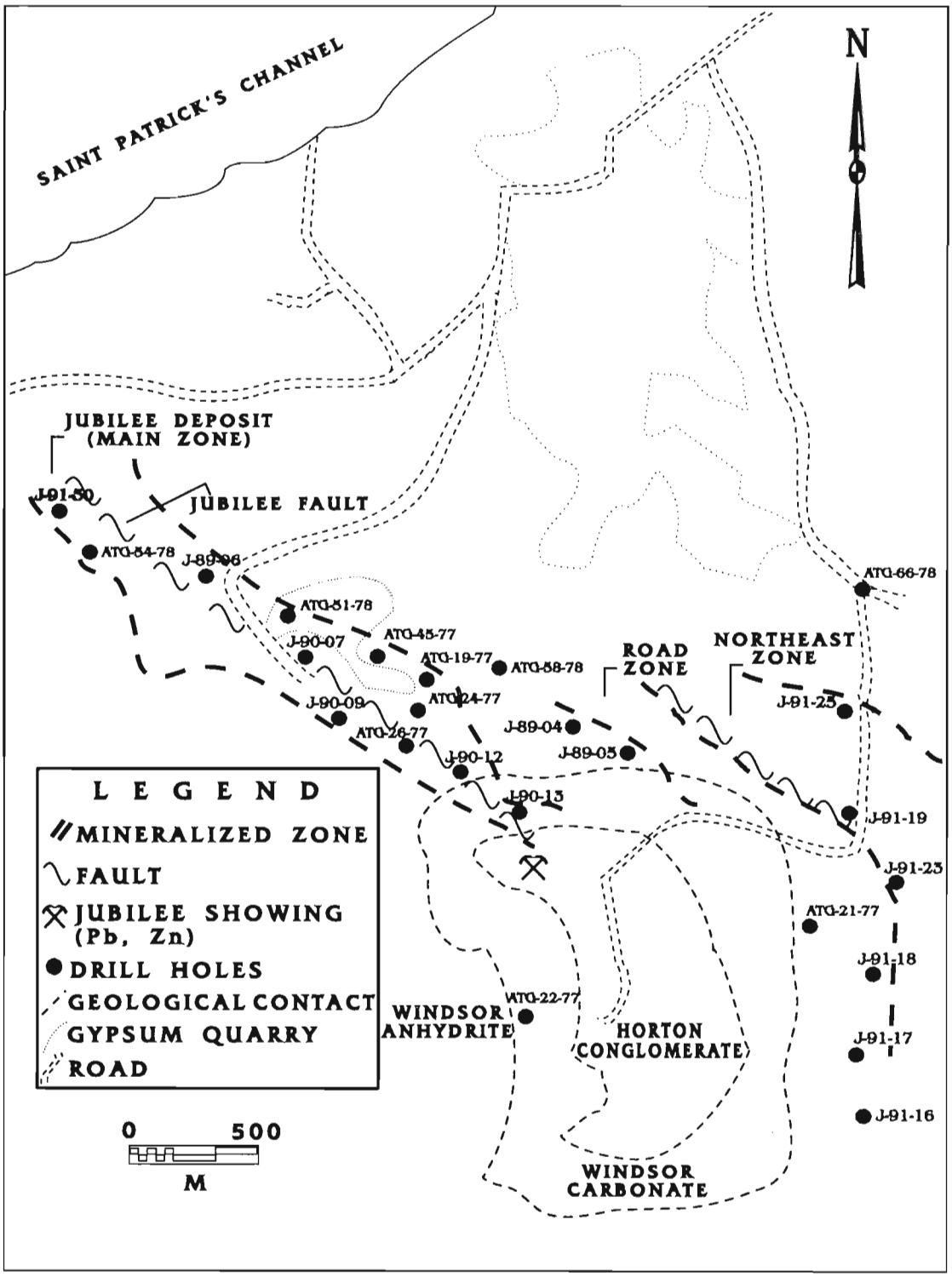

Figure 2. Geology of the Jubilee Pb-Zn deposit and drill hole location (modified from Graham, 1979). Locations of the J-90 drill holes are from Falconbridge Limited, Windsor, Nova Scotia.

continues upwards into the interbedded limestone-sulphates facies, or it may be entirely located within the cyanobacterial laminites facies. The breccia reaches a maximum thickness of 15 m and is thickest close to the Jubilee Fault (Graves et al., 1990).

Limestone cyanobacterial laminites

An oncolitic, oolitic, and peloid cyanobacterial laminites facies (Fig. 3) occurs at the base of the Lower Windsor Group, in contact with the underlying Horton Group. Its thickness varies from a few millimetres to about 1 cm. This facies is overlain by a limestone cyanobacterial laminites having no oolite and oncolite and which has thicknesses varying between 1 and 10 m. The laminated limestone is then overlain by another section of oncolitic, oolitic, and peloid cyanobacterial laminites. The passage between the different facies is gradational.

The laminated limestone is characterized by alternating parallel and horizontal bands of light colour limestone and dark organic-rich limestone. Graves et al. (1990) and Hein et al. (in press) describe this lithology. They noted the poor sorting, the rare presence of cross- and ripple-laminations, the inverse-to-normal grading, the absence of bioturbation, and the lack of bidirectional crossbedding, wave ripple marks, flaser structures or algal microfilaments. These features may be interpreted to suggest that the limestones are neither shallow marine nor algal in origin, but are probable deep-water resedimented carbonates deposited by sediment-gravity flows (Hein et al., 1988).

The depositional environment of the fine laminites at the base of Windsor Group has been debated by stratigraphers and sedimentologists; Schenk (1967) first interpreted these beds as being ancient analogues of modern supratidal stromatolitic facies whereas Giles and Boehner (1982) suggested that they are deep water fine cryptalgal or cyanobacterian laminites. More recently, Schenk (1990) proposed that they are deep water methane-related structures. Thus, although genetic processes and origin of this lithology are still disputed, most agree on a basinal environment of deposition.

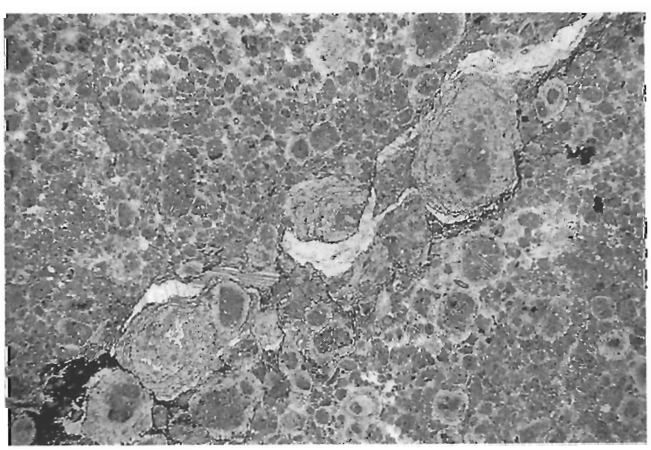

Figure 3. Stylolitized oncolitic and oolitic limestone. Long dimension of photo is 4.5 mm.

Interbedded limestone and sulphates

This unit overlies the limestone cyanobacterial laminites. The contact between the two units is gradational. It consists of parallel and horizontal bands of light and dark colour organic-rich laminated limestone interbedded with anhydrite or gypsum bands. The unit is highly strained, possibly due to compaction; it is brecciated and fractured and contains bedding-parallel stylolites and other dissolution features. Anhydrite or gypsum nodules are strongly boudinaged (Fig. 4).

Anhydrite

This lithology was not examined in detail in this study because it does not contain much lead-zinc mineralization. It consists of thick bands (tens of metres) of massive anhydrite interbedded with rare and thin bands (few tens of centimetres) of limestone-anhydrite. Stewart (1978) interpreted this facies as originating from deep-water brines.

Structure

The main structural feature in the Jubilee deposit area is a northwest elongated horst, called the "Jubilee dome" (Graves et al., 1990; Hein et al., in press). Conglomerate of The Horton Group is exposed in the core of the horst and is overlain by limestone of The Macumber Formation. The limestone is succeeded by a transitional unit of the Carrolls Corner Formation equivalent which consists of interbedded limestone and evaporite that is capped by a thick anhydrite unit. The margins of the horst are bounded by northwest-southeast normal faults called the Jubilee and Road faults. Lead and zinc mineralization occur in narrow zones parallel to these faults (see Fig. 2). Most of the drilling was done in the vicinity of the faults. Bed-thickness and facies changes occur within carbonates and clastic rocks in the vicinity of these faults, which suggest to Hein et al. (in press) that fault movement occurred during sedimentation of the Upper Horton Group and the carbonates of the Macumber Formation.

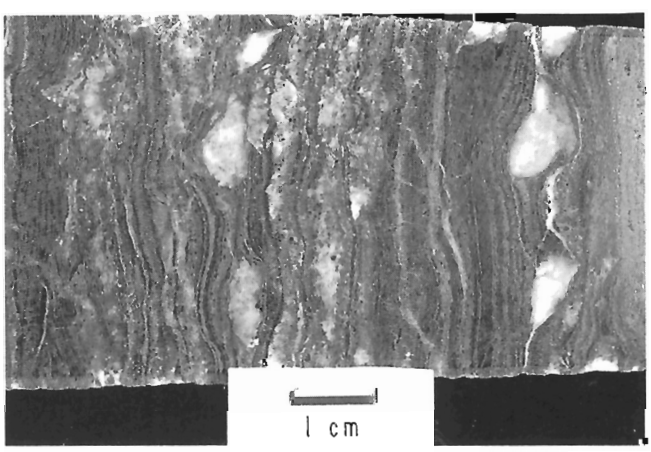

Figure 4. Polished rock slab of cyanobacterial laminites containing anhydrite nodules (in white) that are boudinaged and rotated.

PETROGRAPHIC TECHNIQUES

The study of the paragenetic sequence has been based upon twenty five polished thin sections which were examined under transmitted and reflected light microscope and in cathodoluminescence (CL) using a Nuclide Corporation, model ELM-2E instrument. Staining with Alizarin Red S and potassium ferrocyanide solutions using Dickson's (1965) method was used on ten rock slabs to distinguish calcite from dolomite phases and to quantify their iron content.

PARAGENESIS

The various carbonate lithologies of the Macumber Formation around the Jubilee deposit are exclusively composed of calcite with certain amounts of sulphide (pyrite, marcasite, sphalerite, galena, and chalcopyrite) and sulphate (barite, anhydrite, and gypsum) minerals. These mineral phases succeeded each other in the following order: (1) framboidal disseminated pyrite, (2) fractures, breccias, and dissolution features, (3) pore and fracture filling early fibrous brownish calcite, (4) pyrite and marcasite, (5) sphalerite, (6) galena, (7) chalcopyrite, (8) coarse-grained anhedral recrystallized white calcite, (9) barite, anhydrite, and gypsum. This paragenetic sequence is illustrated in Figure 5.

Carbonates

In the Jubilee deposit area, carbonates are exclusively composed of calcite. In hand specimens, staining tests show that calcite is poor in Fe^{++}. Massive dolomitization of limestones seems to be restricted to central Nova Scotia (Savard, 1991).

Sediments were strongly affected by recrystallization; they form aggregates of small granular subhedral pseudospar mosaic that in cathodoluminescence (CL) is uniformly dull to luminescent (Fig. 6a, b). In rare occurrences, component crystals are still non-luminescent.

The first cement to precipitate is a brownish (inclusion-rich) fibrous calcite (Fig. 7, 8). This cement always occurs in breccias where it replaces and coats recrystallized partly dissolved and stylolitized fragments. Fibres form isopach layers that are up to several millimetres thick which fill fractures and cavities. Low amplitude stylolites that are parallel to bedding were present before brecciation. Fracturing and brecciation have locally affected this generation of cement (Fig. 9), indicating that a first phase of fracturing and brecciation occurred before and is partly contemporaneous to precipitation of fibrous calcite. This generation of cement predated precipitation of the main mineralizing event, i.e., pyrite, sphalerite and galena. In cathodoluminescence, the fibrous calcite is mainly luminescent (Fig. 6b).

Small to coarse (up to 6 mm) anhedral, white (inclusion-free) crystals constitute the last calcite cement that precipitated (Fig. 10). It fills fractures, postdates fibrous calcite, and mineralization, but pre-dates barite and the last generation of stylolites (see Fig. 5). In cathodoluminescence, this cement is always dull to luminescent.

Liquid hydrocarbons and solid organic matter are frequently observed in zones of high porosity and of sulphide mineralization, and along stylolites. Hein et al. (in press) found hydrocarbon-bearing fluid inclusions and bitumen solid inclusions in sphalerite and barite crystals and noted their absence in post-mineralization anhedral white calcite. Thus, they concluded that hydrocarbon emplacement occurred during sphalerite crystallization and before the last calcite cement precipitation.

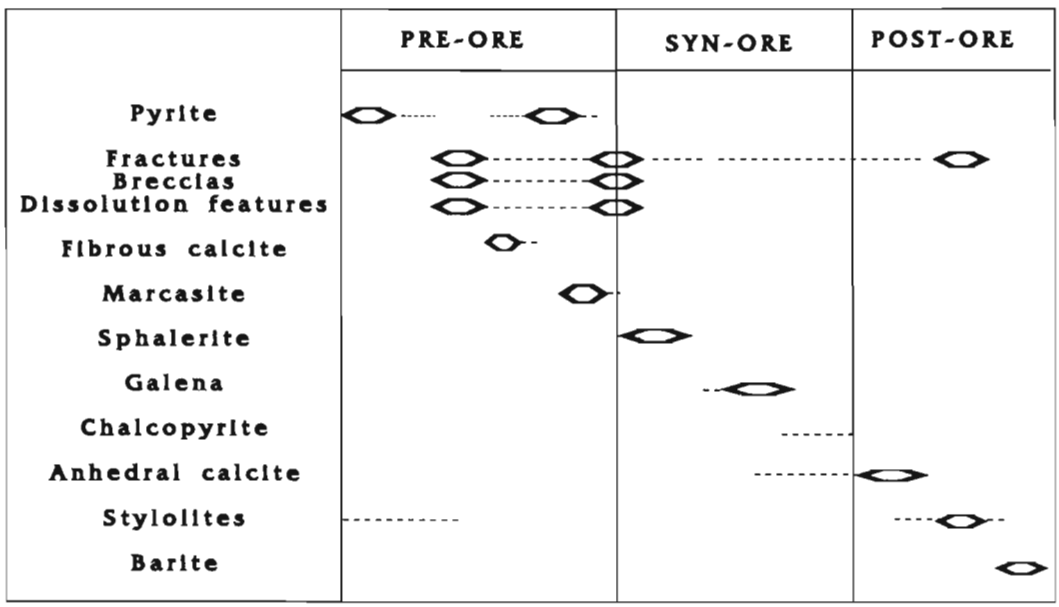

Figure 5. Paragenetic sequences at the Jubilee Pb-Zn deposit. The relative chronology refers to mineralization (pyrite, sphalerite, and galena).

Breccias

Non-mineralized and mineralized breccias occur within carbonates of the Lower Windsor Group. The most common non-mineralized breccia has been described by Hein et al. (1988) as a "rock-matrix breccia". It is composed of a chaotic, well-sorted mass of angular to sub-rounded centimetre-sized limestone fragments of the Macumber Formation in a fine grained matrix or in a medium to coarse fibrous calcite cement. Fragments are usually not recrystallized and their original laminated or oolitic textures can still be recognized. This breccia is clast-supported with some rotation of the fragments. According to Hein et al. (in press), individual clasts seem to have fallen into cavities created by dissolution of evaporitic interbeds; this breccia being interpreted as an evaporite solution breccia. However, remnants of the original anhydrite beds have not been observed.

The mineralized breccia consists mostly of recrystallized and corroded centimetre-scale limestone fragments of the Macumber Formation showing a mottled appearance in a mineralized calcite cement (Fig. 7). Rare fragments are unrecrystallized and their original laminated or oolitic textures can still be recognized. This breccia is composed of angular to subrounded limestone fragments, fibrous and anhedral recrystallized calcite, and sulphide minerals.

Sulphides

The stratabound mineralization of the Jubilee Pb-Zn deposit is hosted by limestone breccias of the Lower Windsor Group. It is predominantly discordant and occurs as disseminations, cavity and breccia fillings, veins, and replacement. Mineralization is epigenetic and related to areas of enhanced permeability, and shows a spatial relationship to the northwest-southeast faults.

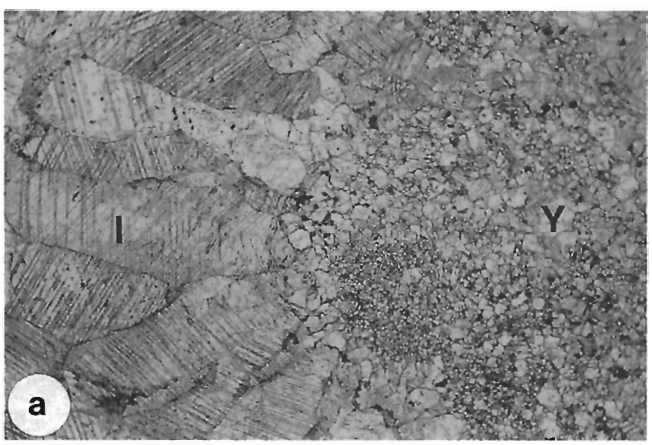

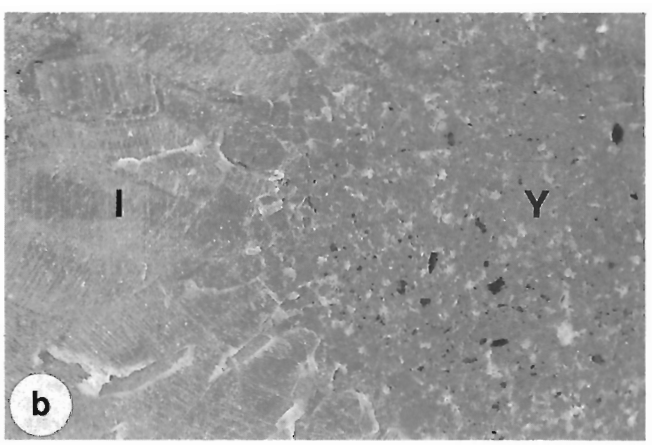

Figure 6. Photomicrographs of a polished thin section showing recrystallized coarse fibrous calcite (I) and neomorphozed marine substrate (Y). Components are uniformly dull to luminescent in cathodoluminescence. **(a)** Plane-polarized light. **(b)** Cathodoluminescence. Long dimension of photos is 4.5 mm.

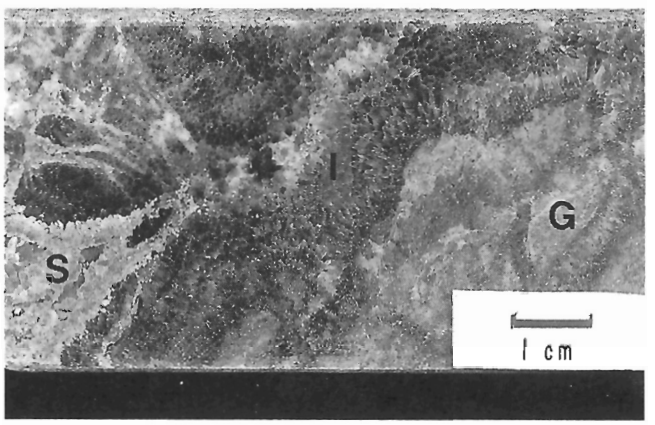

Figure 7. Polished rock slab of the mineralized breccia. Rounded limestone fragments (G) were mechanically detached and probably dissolved. Fibrous calcite cement (I) binds the fragments and is post-dated by sulphides (S). Note that the limestone fragments show no recognizable texture.

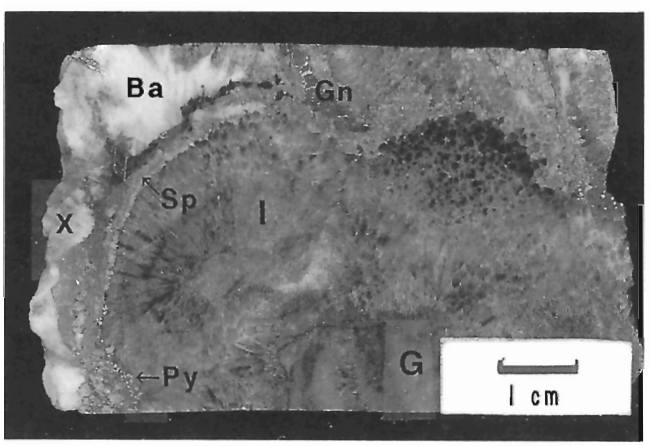

Figure 8. Polished rock slab of the mineralized breccia. The paragenesis is well illustrated with a succession of fibrous calcite (I) around recrystallized fragments (G), intergrowths of pyrite-marcasite (Py), sphalerite (Sp), galena (Gn), and barite (Ba), and late coarse anhydral calcite (X).

Sulphide minerals consist mainly of aggregates of pyrite-marcasite, sphalerite, and galena with minor chalcopyrite. The non-sulphide phases consist of calcite, barite, anhydrite, gypsum, and an unknown mineral. Hein et al. (in press) also noted some occurrences of fluorite in the drill cores.

The small spheroidal and anhedral pyrite crystals are the first pyrite to precipitate in the sediment. They occur as free grains in the limestone and along bedding planes. This pyrite is probably of diagenetic origin.

Pyrite and marcasite are the first sulphides to precipitate after the beginning of fracturing and brecciation and after precipitation of the fibrous calcite cement. A second episode of fracturing occurred after precipitation of pyrite and marcasite. Crystals form intimate intergrowths that are brecciated and fractured. Marcasite partly replaces euhedral pyrite crystals and displays the following textures: 1) delicate colloform intergrowths of pyrite-marcasite on vein and cavity walls, along stylolites and bedding planes, and around fragments, 2) radiating and arborescent growth of spheroidal and colloform textures that may form massive replacement zones (Fig. 11), and 3) anhedral to subhedral disseminated crystals along bedding planes and stylolites. In breccias, pyrite-marcasite colloform intergrowths fill interstices between fragments and in fragments, and they coat fragments that are in places cemented by fibrous calcite (Fig. 12). When extensive, the pyrite-marcasite mineralization forms massive replacement zones with relicts of limestone fragments (Fig. 13). Fine grained aggregates of anhedral to subhedral pyrite crystals sometimes envelop anhedral sphalerite crystals. In veins, pyrite-marcasite forms colloform lacework intergrowths covering the walls of the veins. Many of the veins are symmetrically banded with fibrous brownish calcite at the wall, followed inwards by pyrite-marcasite, sphalerite, galena, and calcite at the centre.

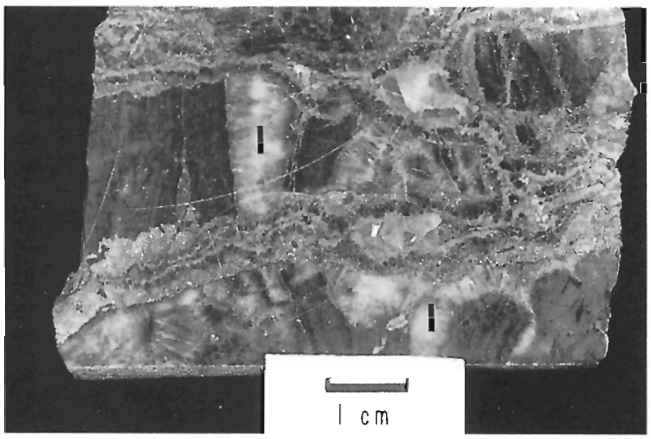

Figure 9. Polished rock slab of the mineralized breccia. Mineralized fractures crosscut non-mineralized breccia. Note the fibrous calcite (I) around fragments being crosscut by fractures.

Sphalerite is pale yellow to reddish brown. It is colloform with growth layers, and as disseminated anhedral to euhedral crystals growing on the periphery of cavities (that may be covered with fibrous calcite), limestone clasts, and pyrite crystals, and along stylolites and bedding planes. Disseminated sphalerite occurs as single or aggregates of anhedral to euhedral crystals that concentrate mainly along stylolites and bedding planes, and in the interstices between pyrite-marcasite crystals. The colloform sphalerite principally covers the cavity walls and the vein walls after pyrite-marcasite intergrowths. This sphalerite usually shows delicate growth bands of various colors.

Galena occurs as anhedral to euhedral crystals of various sizes. The crystals usually fill cracks and fractures in other sulphides. It also occurs in late calcite veins and around pyrite and sphalerite crystals as aggregates of anhedral to subhedral crystals. In rare occurrences, galena is present as inclusions in colloform sphalerite where it seems to be contemporaneous with the precipitation of sphalerite.

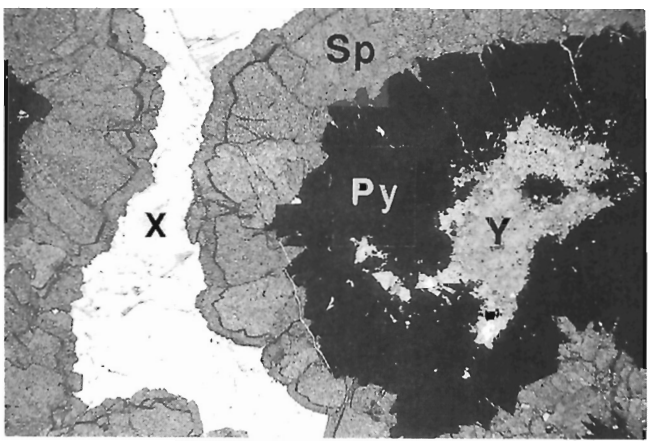

Figure 10. Late white calcite (X) fills pore spaces between sulphides. Note the paragenetic sequence: neomorphozed marine substrate (Y), pyrite (Py), and sphalerite (Sp). Long dimension of photo is 4.5 mm.

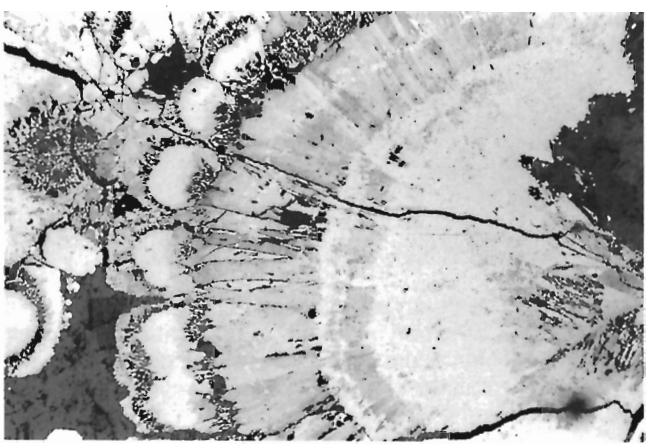

Figure 11. Radiating growth of spheroidal and colloform pyrite-marcasite textures. Long dimension of photo is 1.0 mm.

Chalcopyrite is a minor accessory in the Jubilee mineralization. It occurs mainly as inclusions in galena, sphalerite, pyrite and marcasite, as anhedral disseminated crystals around pyrite, and as infillings of cracks in brecciated pyrite crystals. The paragenetic position of chalcopyrite is uncertain but seems to be contemporaneous to galena precipitation or slightly after.

Barite is an accessory mineral that occurs as aggregates of lath-like crystals in post-sulphide cavities. Barite laths crosscut sphalerite crystals and the coarse anhedral white calcite.

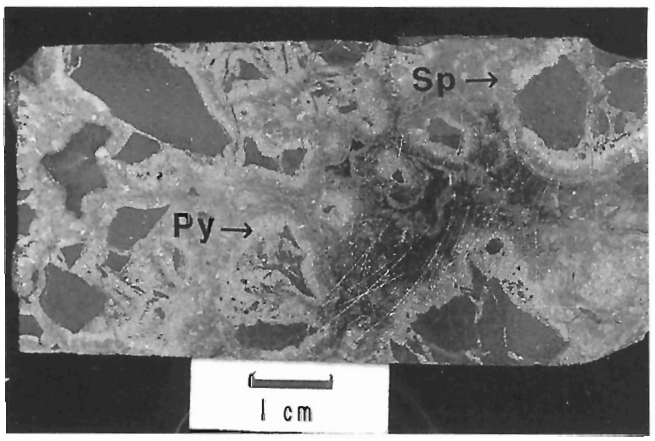

Figure 12. Polished rock slab of the mineralized breccia. Intergrowths of pyrite-marcasite (Py) followed by colloform sphalerite (Sp) surround angular limestone fragments; coarse anhedral calcite fills remaining pores.

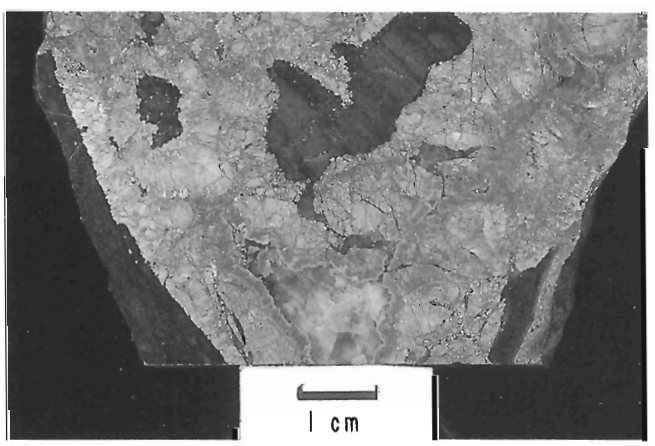

Figure 13. Polished rock slab of massive mineralization constituted of colloform intergrowths of pyrite-marcasite and colloform sphalerite forming bands growing on the periphery of pyrite-marcasite. Note floating remains of limestone cyanobacterial laminites.

DISCUSSION

Diagenetic features observed in the Jubilee area, such as fracturing, brecciation, partial dissolution, open space filling textures, late anhedral white calcite, and stylolites have also been recognized in other carbonates of the Antigonish, Mahone Bay, and Musquodoboit-Shubenacadie sub-basins in Nova Scotia (Savard, 1991). However, important differences also exist between the Jubilee area and the other sub-basins: (1) the early fibrous calcite cement that predated mineralization seems to be restricted to the Jubilee area; (2) dolomitization that is pervasive and pre-mineralization in carbonates of the Musquodoboit-Shubenacadie sub-basin and minor in the Mahone Bay and Antigonish sub-basins (Savard, 1992) is absent in the Jubilee area; and (3) there is a strong fault control on the limestone breccias and on the mineralization at Jubilee. This last observation is most important in consideration of any ore genetic model for the Jubilee deposit. The aim of this preliminary study is not to establish an ore genetic model for the Jubilee mineralization, but to evaluate the link between any diagenetic features and mineralization and to draw a paragenetic scenario into which the mineralizing event took place.

Several periods of brecciation affected the host rocks. The first major period post-dated the first stylolites during burial diagenesis, and continued with the onset of mineralization. Brecciation accompanied by dissolution of the limestone created large open spaces that were subsequently filled first by the fibrous calcite and secondly by pyrite and marcasite. The second important period of brecciation occurred after pyrite-marcasite precipitation. This brecciation was possibly synchronous to the precipitation of sphalerite and galena. A last phase of fracturing occurred after the precipitation of sulphides and is syn- to post-anhedral calcite. Recrystallization is extensive within the limestone fragments and the fibrous calcite cement. It may have been caused by the mineralizing fluid. Brecciation at Jubilee is likely due to faulting and dissolution. The mineralization is clearly epigenetic with a strong association to the faults, i.e., mineralization utilizes a secondary porosity produced by faulting and subsequent brecciation of the host rock. Fracturing and brecciation at Jubilee could well be associated to a more regional tectonic event, such as the extensive shearing and faulting of pre- to syn-Wesphalian age that affected the basal Carboniferous Windsor Group in western Cape Breton Island and central Nova Scotia (Lynch and Giles, in press).

According to Hein et al. (in press), most of the brecciation was caused by sulphate dissolution that predated sulphide mineralization and subsequent collapse of the remaining limestone in a unit originally made of laminated limestone interbedded with sulphates. However, as we mentioned previously no evidence for dissolution of pre-existing

anhydrite laminae was observed. Consequently, we suggest that brecciation has a tectonic origin or is the result of dissolution and collapse of limestone beds.

At this stage of the study, it is too early to speculate on the nature of the diagenetic processes that were involved. One must investigate if the early fibrous calcite as well as the limestone breccias are common to carbonates of the River Denys sub-basin and to other sub-basins or if they are only restricted to mineralized zones in the sub-basins. The answer to these questions may open new perspectives in mineral exploration.

ACKNOWLEDGMENTS

Scientists and technicians of the Nova Scotia Department of Mines and Energy are thanked for their support and availability. Robert Stewart of Falconbridge Limited in Windsor, Nova Scotia kindly provided a location map of drill holes J-90 and has given us access to their claims. We are grateful to G. Lynch for a thorough review of this paper.

REFERENCES

Bell, W.A.
1929: Horton-Windsor district Nova Scotia; Geological Survey of Canada, Memoir 155, 268 p.

Belt, E.S.
1968: Post-Acadian rifts and related facies, eastern Canada; in Studies of Appalachian geology Northern and Maritime, (ed.) E. Zen et al.; New York, Wiley Intersci., p. 95-113.

Dickson, J.A.D.
1965: A modified staining technique for carbonates in thin section; Nature, v. 205, p. 587.

Fralick, P.W. and Schenk, P.E.
1981: Mollasse deposition and basin evolution in a wrench tectonic setting: The late Paleozoic eastern Cumberland basin, Maritime Canada; Geological Association of Canada, Special Paper 23, p. 77-97.

Geldsetzer, H.H.J.
1977: The Windsor Group of Cape Breton Island, Nova Scotia; in Report of Activities, Part A; Geological Survey of Canada, Paper 77-1A, p. 425-428.

Giles, P.S.
1981: Major transgressive-regressive cycles in the Middle to Late Visean rocks of Nova Scotia; Department of Mines and Energy, Nova Scotia, Paper 81-2, 27 p.

Giles, P.S. and Boehner, R.C.
1982: Geological map of the Shubenacadie and Musquodoboit Basins, central Nova Scotia; Nova Scotia Department of Mines and Energy, Map 82-4, scale: 1:50 000.

Graham, R.A.F.
1979: The Iona Rear lead-zinc project, Nova Scotia, Review of Data; Report to Texasgulf Canada Ltd, May 1979, 3 enclosures, 12 p.

Graves, M.C., Hein, F.J., and Ruffman, A.
1990: The geology of the Jubilee zinc-lead deposit, Victoria County, Cape Breton Island, Nova Scotia supplementary data; Geological Survey of Canada, Open File 2279, 80 p.

Hein, F.J., Graves, M.C., and Ruffman, A.
1988: Geology of the Jubilee zinc-lead deposit, Victoria County, Cape Breton Island, Nova Scotia; Geological Survey of Canada, Open File 1891, 134 p.

Hein, F.J., Graves, M.C., and Ruffman, A.
in press: The Jubilee Zn-Pb deposit, Nova Scotia: the role of synsedimentary faults; in Mineral Deposit Studies in Nova Scotia, v. 2, (ed.) A.L. Sangster; Geological Survey of Canada, Paper 91-9.

Howie, R.D and Barss, M.S.
1975: Upper Paleozoic rocks of the Atlantic provinces, Gulf of St-Lawrence, and adjacent continental shelf; Geological Survey of Canada, Paper 74-30, p. 35-50.

Kirkham, R.V.
1978: Base metal and uranium distribution along the Windsor-Horton contact central Cape Breton Island, Nova Scotia; in Current Research, Part B; Geological Survey of Canada, Paper 78-1B, p. 121-135.

Lynch, G. and Giles P.
in press: The Ainslie detachment - field evidence of carboniferous low-angle extensional faulting, Nova Scotia; Geological Association of Canada Annual Meeting, Program with Abstracts.

Ravenhurst, C.E., Reynolds, P.H., Zentill, M., Krueger, H.W., and Blenkinsop, J.
1989: Formation of Carboniferous Pb-Zn and barite mineralization from basin-derived fluids, Nova Scotia, Canada; Economic Geology, v. 84, p. 1471-1488.

Savard, M.M.
1991: A preliminary report on the relationship between mineralization and carbonate diagenesis in the Gays River Formation, Nova Scotia; in Current Research, Part D; Geological Survey of Canada, Paper 91-1D, p. 147-156.

Savard, M.M.
1992: Diagenèse pré- et post-minéralisation: implications pour le dépôt de Gays River, Nouvelle-Écosse; dans Recherche en cours, Partie E; Commission géologique du Canada, Étude 92-1E, p. 289-298.

Schenk, P.E.
1967: The Macumber Formation of the Maritimes Provinces, Canada — a Mississippian analogue to recent strand-line carbonates of the Persian Gulf; Journal of Sedimentary Petrology, v. 37, p. 365-376.

Schenk, P.E.
1990: Deep-water, bacterial precipitated, peloidal laminite containing chemosynthetic, microbial mounds, Carboniferous, Atlantic Canada; Geological Association of Canada Annual Meeting, Program with Abstracts, p. A-117-118.

Sheridan, R.E. and Drake, C.L.
1968: Seaward extension of the Canadian Appalachians: Canadian Journal of Earth Sciences, v. 5, p. 337-374.

Stewart, E.B.
1978: A study of the lead-zinc mineralization at Jubilee, Victoria county, Nova Scotia; M.Sc. thesis, Acadia University, Nova Scotia, 190 p.

Geological Survey of Canada Project 920004SP

Nano-pore transport mechanism of tight shales from the Scotian Shelf, offshore Nova Scotia

T.J. Katsube
Mineral Resources Division

Katsube, T.J., 1993: Nano-pore transport mechanism of tight shales from the Scotian Shelf, offshore Nova Scotia; in Current Research, Part D; Geological Survey of Canada, Paper 93-1D, p. 121-127.

Abstract: Permeabilities and formation factors have been calculated using pore-size distribution data for nano-pores of shale samples from the Venture Gas Field, offshore Nova Scotia. The results indicate that, when using a tortuosity of unity and the porosity from all the nano-pores, the calculated permeabilities and formation factors differ from the experimentally measured values by a factor between 10 and 100. However, when using a tortuosity value obtained from the literature, of 3.3, and partial porosity values above the critical partial porosity of 0.39 %, the calculated and measured values agree within the accuracy of the experimental measurements. Partial porosity is the porosity of the pore-size ranges (e.g., 1.0 to 1.6 nm or 1.6 to 2.5 nm) constituting the pore-distribution of a sample. These results have significant implications for understanding the hydrocarbon expulsion mechanism of shales, and for describing the hydrocarbon generation, migration and accumulation history within sedimentary basins.

Résumé : On a calculé la perméabilité et les valeurs du facteur de formation à partir des données sur les distributions du diamètre des pores, relativement aux nanopores d'échantillons de shale provenant du champ gazéifère de Venture au large des côtes de la Nouvelle-Écosse. Les résultats indiquent que si l'on emploie une tortuosité de valeur égale à l'unité et la porosité de tous les nanopores, les perméabilités calculées et les valeurs du facteur de formation diffèrent des valeurs mesurées à la suite d'expériences d'un facteur de 10 à 100. Cependant, si l'on emploie une valeur de tortuosité égale à 3,3, telle qu'indiquée dans la documentation scientifique, et des valeurs de la porosité partielle supérieures à la porosité partielle critique qui est de 0,39 %, la relation entre les valeurs calculées et les valeurs mesurées s'améliore au point où les valeurs calculées de la perméabilité concordent presque avec les valeurs mesurées. La porosité partielle est la porosité dans la gamme de diamètres des pores (par ex., 1,0 à 1,6 nm ou 1,6 à 2,5 nm) représentant la distribution du diamètre des pores dans un échantillon. Ces résultats ont des implications importantes, en ce qu'ils aident à expliquer le mécanisme d'expulsion des hydrocarbures des shales, et à décrire la génèse, la migration et les étapes d'accumulation des hydrocarbures dans les bassins sédimentaires.

INTRODUCTION

The description of hydrocarbon generation, migration and accumulation history within sedimentary basins (Williamson, 1992) requires shale petrophysical data, especially on tight shales (Mudford and Best, 1989). The petrophysical properties of tight shales from the Venture Gas field, offshore Nova Scotia, have been measured in order to obtain representative information. The results have shown that the nano-pores, in the range of 3 to 16 nm, constitute the main pore throats (Katsube et al., 1990, 1991, 1992) or fluid flow paths in the tight shales (4500-5600 m depth). These shales have extremely low permeabilities, in the range of 10^{-22} to $2x10^{-20}$ m^2 (Katsube et al., 1991, 1992; Coyner et al., 1993). Also the nano-pores of these shales are characterized by a unimodal distribution of pores (Fig. 1) between 0.3 and 30 nm (Katsube, 1992), with mean pore-sizes or modes in the range of 4-12 nm.

In principle, the extremely small pores are expected to produce very low permeabilities. However, it is not known whether the calculated permeabilities using the pore-size distribution data (Katsube, 1992) would agree with the experimentally measured permeabilities (Coyner et al., 1993). This paper presents comparative results between experimental measurements of permeabilities and formation factor values with those calculated using the nano-pore data of 10 shale samples from the Venture Gas Field.

Permeability, k, is related to pore structure parameters by the following equation (Walsh and Brace, 1984):

$$k = (d^2\phi)/(b\tau^2), \quad (1)$$

where d, ϕ and τ are the pore-size, porosity and tortuosity, and b is a coefficient that is equal to 8 for circular pores and equal to 12 for sheetlike pores (Carman, 1948; Prasuhn, 1980). Similarly, the formation factor, F, is related to the pore structure parameters by the following equation (Winsauer et al., 1952):

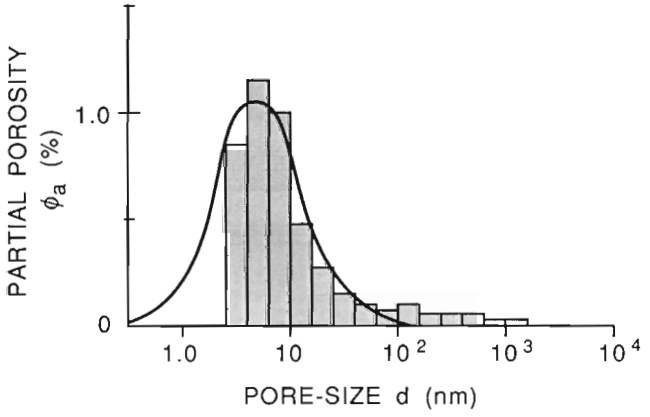

Figure 1. Unimodal distribution of nano-pores (0.3-30 nm) that characterize the shales from the Venture Gas Field, offshore Nova Scotia (from data in Katsube, 1992).

$$F = \tau^2/\phi. \quad (2)$$

The pore-size distribution is represented by the partial porosities, ϕ_a, for each pore-size range, as shown in Figure 1. Therefore, the nano-pore porosity, ϕ_{np}, is expressed as follows (Katsube, 1992):

$$\phi_{np} = \sum \phi_{ai} \quad (3)$$

for log(d) between $\log(d_{np}) - 3\sigma$ and $\log(d_{np}) + 3\sigma$,

where i is the number of the pore-size range or pore-size cell (Fig. 1), ϕ_{ai} is the partial porosity of the i-th pore-size range, and d_{np} and σ are the mean pore-size and standard deviation (logarithmic value) of the nano-pore distribution. In Figure 1, the horizontal axis represents the log of the pore-size (d), with 0.2 being the logarithmic width of the pore-size ranges.

By replacing ϕ with ϕ_{ai} in Equations (1) and (2), we can determine the permeability, k_i, and formation factor, F_i, of each pore-size range, with d_i being the geometric mean of the pore-size range:

$$k_i = (d_i^2 \phi_{ai})/(b\tau^2), \quad (1')$$

and

$$F_i = \tau^2/\phi_{ai}. \quad (2')$$

If it is assumed that each pore-size range represents pores that are parallel to each other, then the permeability, k_c, and formation factor, F_c, of the entire pore-size distribution is determined by accumulating the permeability and formation factor values of the pore-size ranges as follows:

$$k_c = \sum (k_i) = \sum (d_i^2 \phi_{ai})/(b\tau^2) \quad (4)$$

and

$$F_c = \{\sum (1/F_i)\}^{-1} = \{\sum (\phi_{ai}/\tau^2)\}^{-1}, \quad (5)$$

for log(d) between $[\log(d_{np}) - 3\sigma]$ and $[\log(d_{np}) + 3\sigma]$.

If we represent the partial accumulated permeability and accumulated formation factor starting from the smaller pore-sizes to a specific pore-size range of d_i by k_{ci} and F_{ci}, then from Equations (4) and (5) we obtain

$$k_{ci} = \sum (k_i) \quad (4')$$

and

$$F_{ci} = \{\Sigma\ (1/F_i)\}^{-1} \qquad (5')$$

for log(d) between $[\log(d_{np}) - 3\sigma]$ and $\log(d_i)$.

The partial porosity, ϕ_{ai}, is obtained from the following normal distribution equation (Katsube, 1992) when the nano-pore distribution characteristics (ϕ_{max}, d_{np} or ℓ_{np}, and σ) are known:

$$\phi_{ai}(\ell) = \phi_{max} \exp[-(\ell-\ell_{np})^2/(2\sigma^2)], \qquad (6)$$

where ℓ is a variable representing the log of pore-size d:

$$\ell = \log(d), \qquad (7)$$

ℓ_{np} is the log of the mean pore-size or mode of the nano-pores (d_{np}) and ϕ_{max} is the maximum nano-pore porosity. The mean pore-size and the mode are equal, since this equation represents a normal distribution curve and is symmetrical. In this paper, the permeability and formation factor for all 10 shale samples are calculated for the Venture Gas field samples, using Equations (4) to (6), and then the results are compared with actual measurements.

PETROPHYSICAL CHARACTERISTICS OF THE VENTURE SAMPLES

The nano-pore characteristics (Katsube, 1992) of the 10 shale samples from the Venture Gas field, offshore Nova Scotia, are listed in Table 1. These characteristics are represented by three parameters: maximum nano-pore porosity (ϕ_{max}), log of the nano-pore mode (d_{np}) which is also expressed by ℓ_{np}, and the standard deviation (σ). The standard deviation is represented by logarithmic values of the pore-size, as already explained (Katsube, 1992). While the nano-pore porosity (ϕ_{np}) is a characteristic of the sample, it can be derived from the other three parameters (Katsube, 1992), as indicated by Equations (3) and (6). The experimentally measured permeability (k_o) and formation factor (F_o) for these 10 shale samples are also listed in Table 1. The formation factor (F_o) data have been obtained from the literature (Katsube et al., 1990, 1991). The permeabilities listed in the table are the permeabilities (k_o) at zero pressure, and have been obtained from regression analysis of the permeability versus effective pressure data presented in Katsube et al. (1991) and Coyner et al. (1993), using Equation (6) in Katsube et al. (1991). This equation is an empirical equation representing the permeability as a function of effective pressure. The reduced major axis (Katsube and Agterberg, 1990) was used in the regression analysis when determining the k_o values listed in Table 1.

Table 1. Petrophysical characteristics of shale samples (Katsube et al., 1990,1991; Katsube, 1992; Coyner et al., 1993) from the Venture Gas Field, offshore Nova Scotia

Sample	k_o	F_o	ϕ_{np}	ϕ_{max}	d_{np}	ℓ_{np}	σ
V-1	14.1	541	5.53	1.07	4.41	0.644	0.412
V-2	140.	236	6.51	1.26	11.5	1.062	0.412
V-3	831.	268	6.97	0.983	5.61	0.749	0.566
V-4	56.2	452	10.2	1.56	3.51	0.545	0.520
V-5	31.6	1030	4.51	0.721	2.73	0.437	0.500
V-6	1.62	17600	1.53	0.386	5.88	0.769	0.316
V-7	16.2	433	5.84	1.13	5.58	0.746	0.412
V-8	61.7	305	8.37	1.62	6.82	0.834	0.412
V-9	3.8	1630	2.35	0.42	5.70	0.756	0.447
V-10	15.1	343	5.83	1.04	4.75	0.677	0.477
Units	10^{-21} m^2		%	%	nm		

k_o = Measured permeability.
F_o = Measured formation factor.
ϕ_{np} = Nano-pore porosity.
ϕ_{max} = Maximum partial porosity of the nano-pore distribution.
d_{np} = Mean pore-size or mode of the nano-pore distribution.
ℓ_{np} = $\log(d_{np})$.
σ = Standard deviation (expressed as log of the pore-size).

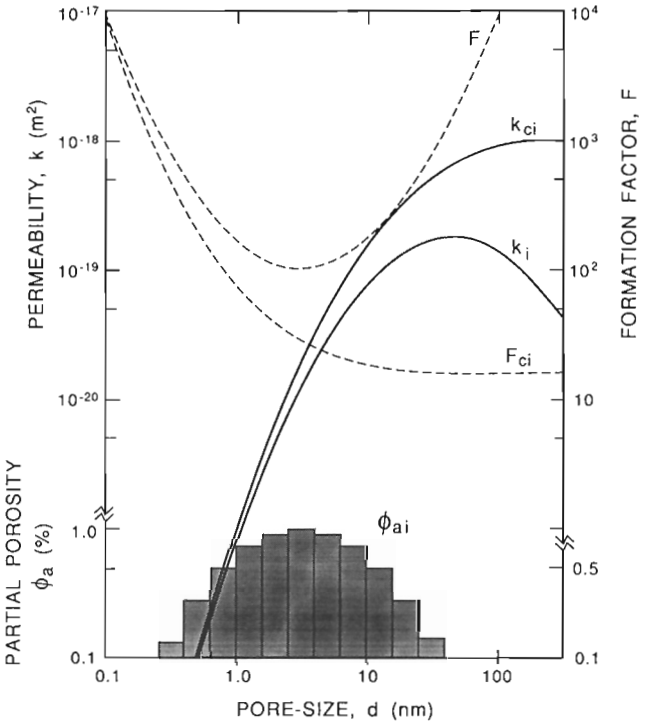

Figure 2. The nano-pore-size distribution of a fictitious sample representing a typical shale from the Venture Gas Field (Table 1), having nano-pore characteristics of ϕ_{max}=1.0 %, d_{np}=3.2 nm, σ=0.5, ϕ_{np}=6.2 %, τ = 1 and b=8. ϕ_{ai} represents the nano-pore partial porosity distribution. The curves k_i and k_{ci} represent the permeability of each pore-size range (Equation 1') and that of the partial accumulated permeability (Equation 4'). The curves F_i and F_{ci} represent the formation factor of each pore-size range (Equation 2') and that of the partial accumulated formation factor (Equation 5').

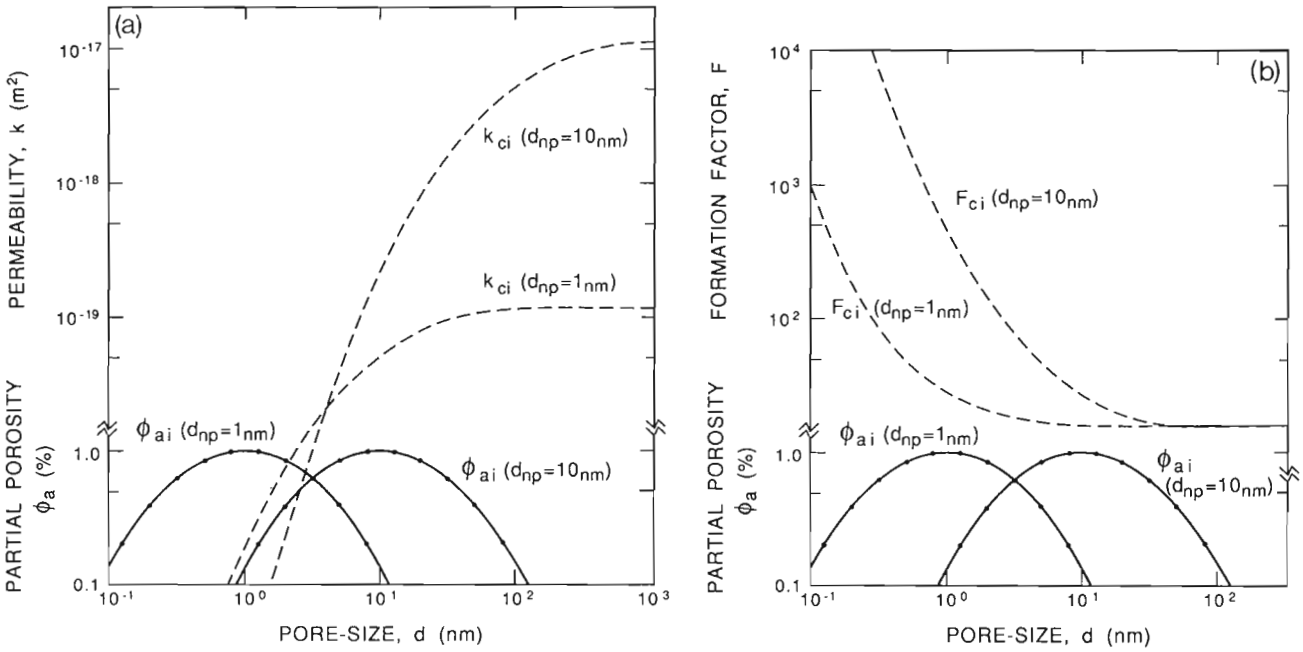

Figure 3. Effect of the variation of mean nano-pore-size (d_{np}) on permeability (k) and formation factor (F), for nano-pore distributions with characteristic of ϕ_{max}=1.0 %, σ=0.5 and τ=1 (b=8). ϕ_{ai} represents the nano-pore partial porosity distribution curves for two different mean nano-pore-sizes (d_{np}). **(a)** k_{ci} represents the partial accumulated permeability curves for d_{np}=1 nm and d_{np}=10 nm. **(b)** F_{ci} represents the partial accumulated formation factor curves for the same two pore-size distributions.

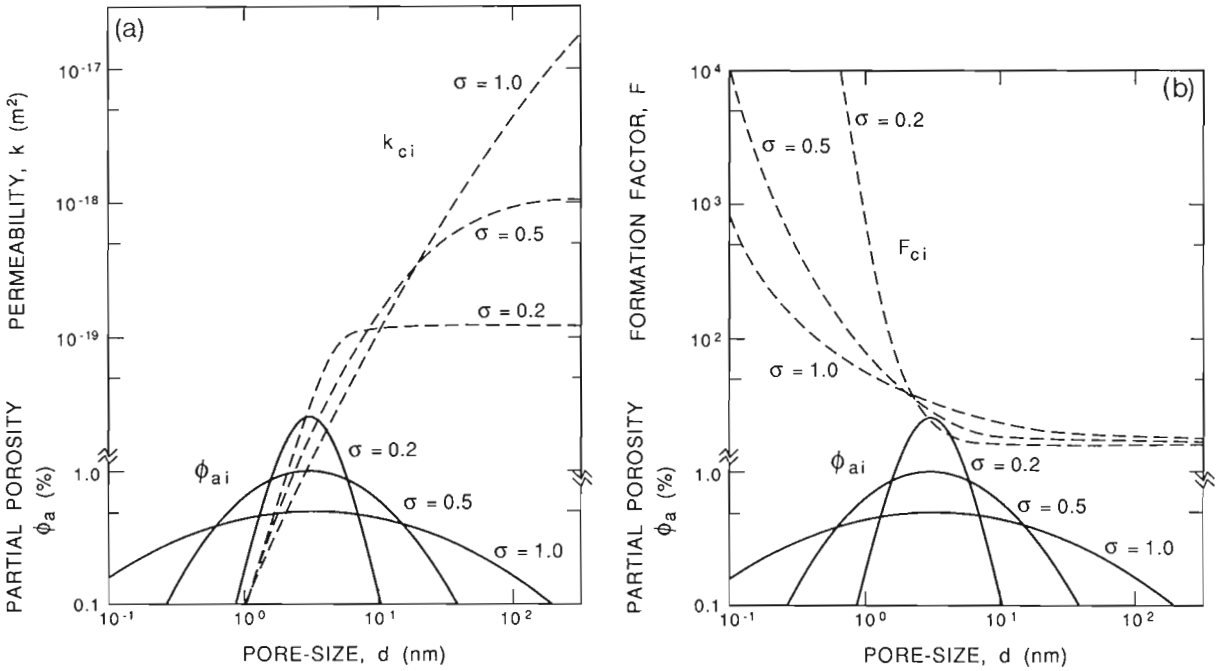

Figure 4. Effect of the variation of standard deviation (σ) on permeability (k) and formation factor (F), for nano-pore distributions with characteristic of d_{np}=3.2 nm, ϕ_{np}=6.2 % and τ=1 (b=8). ϕ_{ai} represents the nano-pore partial porosity distribution curves for three different standard deviations (σ). **(a)** k_{ci} represents the partial accumulated permeability curves for σ=0.1, 0.5 and 1.0. **(b)** F_{ci} represents the partial accumulated formation factor curves for the same three pore-size distributions.

k AND F DETERMINATION FROM NANO-PORE DISTRIBUTION

The pore-size distribution for a fictitious shale sample from the Venture Gas field and its permeability and formation factor curves determined by Equations (1′), (2′), (4′) and (5′) are displayed in Figure 2. This fictitious sample has been given the nano-pore characteristics defined by ϕ_{max}=1.0 %, d_{np}=3.2 nm, and σ=0.5, and are representative values of the shales in Table 1. The nano-pore porosity of such a sample is ϕ_{np}=6.2 %, a value representing a typical tight shale sample (Table 1). The tortuosity (τ) is assumed to be unity with the pore cross section being circular (b=8) for these calculations, unless stated otherwise. Note that the pore-size of the maximum permeability of the "k_i" curve is offset, by a factor of 10, from that (d_{np}) of ϕ_{ai} and "F_i".

In order to examine the effect of d_{np} on k and F, two (k_{ci} and F_{ci}) of the curves in Figure 2 have been calculated for two different pore-size distributions: one with d_{np}=1 nm, and other with d_{np}=10 nm. The other two parameters are identical for the two distributions: ϕ_{max}=1.0 % and σ=0.5. The results are shown in Figures 3a and b. While a change in d_{np} causes a change in the shape of the partial accumulated formation factor curves (F_{ci} in Fig. 3b), the accumulated formation factor (F_c) values are identical. In comparison, a change in d_{np} causes a significant change, not only in the partial accumulated permeability curves (k_{ci} in Fig. 3a), but also in the accumulated values of k_c. This difference between the effect of d_{np} on k and F is explained by k being a function of pore-size (d) whereas F is not, as can be seen by comparing Equations (4) and (5).

In order to examine the effect of σ on k and F, similar curves have been calculated for three different standard deviations: σ=0.2, 0.5 and 1.0. Two other parameters are identical for the three distributions: ϕ_{np}=6.2 % and d_{np}= 3.2 nm. Since ϕ_{np} is a function of ϕ_{max} and σ (Equations 3 and 6; and Katsube, 1992), ϕ_{max} varies according to the value of σ, for this case. The results are displayed in Figures 4a and b. Again, while the change in σ causes a change in the partial accumulated formation factor curves (F_{ci} in Fig. 4b), the accumulated values (F_c) are identical. In comparison, a change in σ causes a significant change, not only in the partial accumulated permeability curves (k_{ci} in Figure 4a), but also in the accumulated values of k_c. Similar to the case of Figure 3, the difference between the effect of σ on k and F is explained by k being a function of pore-size (d) whereas F is not (Equations 4 and 5). Although d_{np} is identical for the three different distributions, the partial porosities (ϕ_{ai}) for the different pore-sizes differ.

These results (Fig. 3, 4) show that under the condition of a constant nano-pore porosity (ϕ_{np}), variations in pore-size mode (d_{np}) and standard deviation (σ) will have a significant effect on the accumulated permeability (k_c), but not on the accumulated formation factor (F_c) values. These results also show that the accumulated permeability (k_c) and formation factor (F_c) values differ considerably from the experimentally measured ones (Table 1). The values of $1.1 \times 10^{-18} m^2$ and 16 for k_c and F_c in Figure 2 are about 70 times larger than k_o, and about 20 times smaller than F_o for sample V-10 (Table 1). Sample V-10 is taken as representative of the 10 samples for this comparison.

k AND F DETERMINATION FOR THE VENTURE SAMPLES

There are two methods to determine the accumulated permeability and formation factor values for the Venture samples. The first is to follow the same procedures as for the fictitious sample (Fig. 3, 4), using Equations (4) and (5). The second is to use the nano-pore-size distribution data for the Venture shale samples already in the literature (Katsube, 1992). The former procedure will be used in this case. The results of the accumulated permeability and formation factor determination using the first procedure are represented by k_{c1} and F_{c1}, and are listed in Tables 2a and b. These results are compared with the experimental measurements, k_o and F_o, in Figures 5a and b. They show that the calculated permeability values are about 10-100 times larger than the measured ones (k_o), and the calculated formation factor (F_{c1}) values are about 10-100 times smaller than the measured ones (F_o).

INTRODUCTION OF TORTUOSITY AND POROSITY LIMITS

All calculations, so far, have assumed tortuosity (τ) to be unity. Let us now consider tortuosity to be otherwise, and use τ = 3.3, a value obtained by Katsube et al. (1990, 1991). The calculated values of permeability and formation factor will now change by a factor of about 10, as indicated by Equations (4) and (5), since τ^2 = 10.9. The calculated values of permeability and formation factor using the new tortuosity value (τ = 3.3) are represented by k_{c2} and F_{c2}, and are listed in Tables 2a and b. The comparison with k_o is shown in Figure 5a, indicating a considerable improvement of correlation between the two parameters. A considerable improvement between F_o and F_{c2} is also seen (Table 2b). However, there are still considerable differences between measured and calculated values.

Katsube et al. (1992) have observed two critical nano-pore porosities in these shales. The nano-pores are thought to have a relatively good inter-connectivity with about 50 - 60 % contributing to flow of fluids at larger nano-pore porosities. However, as the nano-pore porosity (ϕ_{np}) decreases, there is a critical nano-pore porosity below which the relatively good inter-connectivity brakes down, with only a reduced portion of the pores contributing to the flow of fluids. This is the first critical nano-pore porosity. This leaves a larger portion of the nano-pores to become disconnected and end up as pocket or blind pores. As the nano-pore porosity (ϕ_{np}) continues to decrease, all nano-pores become disconnected. This is the second critical nano-pore porosity. Below this porosity, fluids may enter the rock through the pores

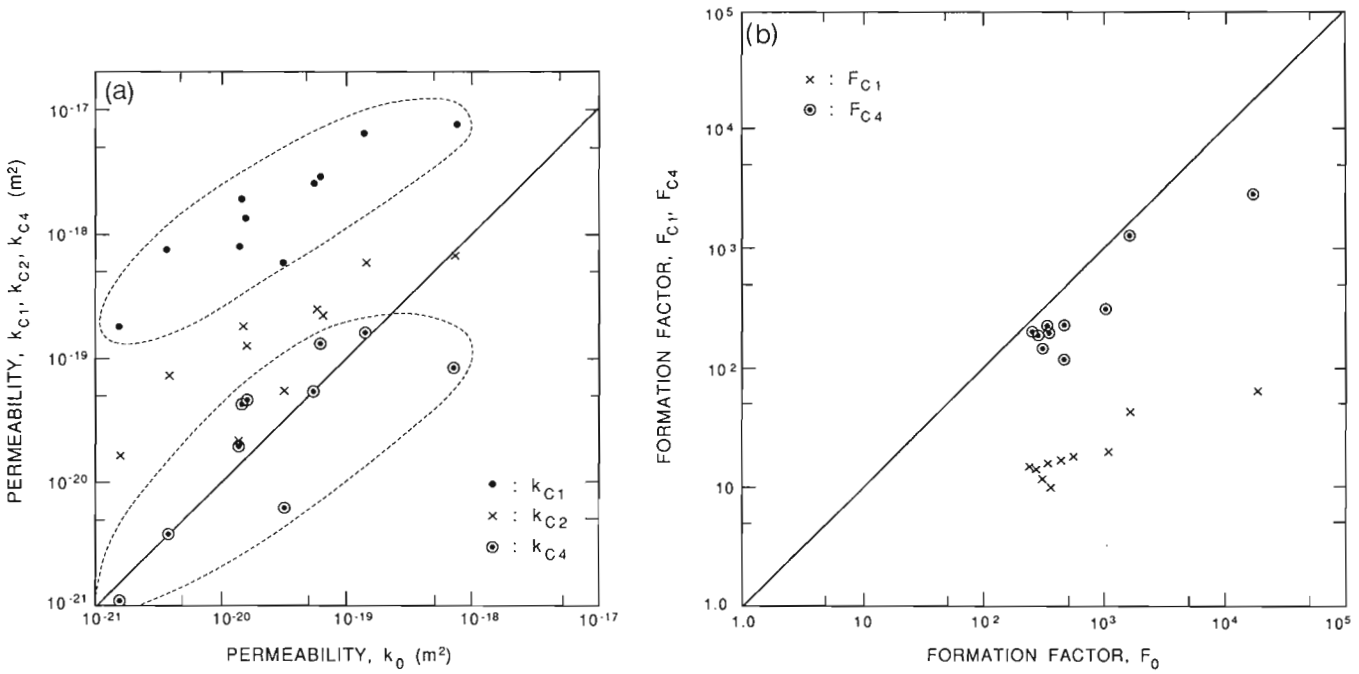

Figure 5. Calculated permeability and formation factor values verses the experimentally measured values (k_o and F_o). **(a)** k_{c1} and k_{c2} represent the calculated permeabilities for $\tau = 1$ and $\tau = 3.3$. k_{c4} represents the calculated permeabilities for $\tau = 3.3$ with partial porosities only above the critical partial porosity (ϕ_{acr}) of 0.39 %. **(b)** F_{c1} and F_{c4} represent the calculated formation factor values for $\tau = 1$, and $\tau = 3.3$ with partial porosities only above the critical partial porosity (ϕ_{acr}).

Table 2a. Measured permeabilities (Katsube et al., 1991; Coyner et al., 1993) and calculated permeabilities using the nano-pore data (Katsube, 1992) for the shale samples from the Venture Gas Field offshore Nova Scotia

Sample	k_o	k_{c1}	k_{c2}	k_{c3}	k_{c4}
V-1	14.1	810	74.4	230	21.2
V-2	140.	6500	597	1805	166
V-3	831.	7500	689	931	85.5
V-4	56.2	2700	248	613	56.2
V-5	31.6	600	55.1	70.8	6.50
V-6	1.62	190	17.4	12.0	1.10
V-7	16.2	1400	129	513	47.1
V-8	61.7	2900	266	1437	132
V-9	3.8	790	72.5	44.0	4.04
V-10	15.1	2000	184	484	44.4
Units		$x10^{-21}$ m^2			

k_o = Measured permeability.
k_{c1} = Calculated permeability, assuming $\tau = 1$, using all nano-pore porosity.
k_{c2} = k_{c1}/τ^2 ($\tau = 3.3$).
k_{c3} = Calculated permeability, assuming $\tau = 1$, using limited nano-pore porosity ($\phi_a > 0.39$ %).
k_{c4} = k_{c3}/τ^2 ($\tau = 3.3$).

Table 2b. Measured formation factor values (Katsube et al., 1990, 1991) and calculated formation factor values using the nano-pore data (Katsube, 1992) for the shale samples from the Venture Gas Field offshore Nova Scotia

Sample	F_o	F_{c1}	F_{c2}	F_{c3}	F_{c4}
V-1	541	18	196	20.8	227
V-2	236	15	163	18.1	197
V-3	268	14	152	17.0	185
V-4	452	9.8	107	10.7	116
V-5	1030	22	240	28.4	310
V-6	17600	65	708	270	2940
V-7	433	17	185	20.3	221
V-8	305	12	131	13.2	144
V-9	1630	43	468	122	1329
V-10	343	16	174	18.6	203

F_o = Measured formation-factor.
F_{c1} = Calculated formation-factor assuming $\tau = 1$, using all nano-pore porosity.
F_{c2} = $F_{c1}\tau^2$ ($\tau = 3.3$).
F_{c3} = Calculated formation-factor, assuming $\tau = 1$, using limited nano-pore porosity ($\phi_a > 0.39$ %).
F_{c4} = $F_{c3}\tau^2$ ($\tau = 3.3$).

connected to the surface of a sample, but will not flow from one end to the other. In other words, there are no flow paths below this porosity.

It seems reasonable to apply this critical porosity concept to the pore-size distribution of the nano-pores. That is, it is possible to consider a critical partial porosity (ϕ_{acr}) for each pore-size range, under which the flow pores become disconnected and do not serve any more as flow paths for that pore-size range. The question is what value will ϕ_{acr} take?. Since Sample V-6, which has the smallest nano-pore porosity (Table 1), is barely permeable ($k_o = 1.6 \times 10^{-21}$ m^2, Table 1), let us take its ϕ_{max} value as the critical partial porosity (ϕ_{acr}) for the pore-size ranges or for the pore-size cells. That is, ϕ_{acr}=0.39 %. The calculated permeability and formation factor using only partial porosities larger than ϕ_{acr} are represented by k_{c3} and F_{c3} and are listed in Tables 2a and b. The same parameters calculated with $\tau = 3.3$, are represented by k_{c4} and F_{c4}, and are also listed in Tables 2a and b. The relationship between these values and the k_o and F_o values are displayed in Figures 5a and b, showing a considerable improvement in the correlation. In fact, the k_{c4} values are in general agreement with those of k_o (Figure 5a). The F_{c4} values are smaller than those of F_o by a factor of only about 2 (Fig. 5b), a considerable improvement over the previous cases where the calculated and measured values differed by a factor of 10 - 100.

DISCUSSIONS AND CONCLUSIONS

Permeability and formation factor values have been calculated from pore-size distributions of nano-pores, assuming that each pore-size range constituting the distribution represents a tortuous flow path with a circular cross-section. In addition, these flow paths are considered to be parallel to each other. Conventional equations (Walsh and Brace, 1984; Winsauer et al., 1952) have been used for these calculations. These calculations have been used to analyze the relationship between permeability and formation factor with the pore-size distribution characteristics of the nano-pores, such as the effect of variations in nano-pore mode and standard deviation on permeability and formation factor. The results are displayed in Figures 2 to 4.

The calculated values have been compared with measured values. The results indicate that, when using a tortuosity of unity and the porosity of all nano-pores, the calculated permeabilities and formation factor values differ from the measured values by a factor of about 10 - 100. However, when using a tortuosity value of 3.3 (obtained from Katsube et al., 1991) and partial porosity values only above an assumed critical partial porosity of 0.39 %, the relationship between calculated and measured values improve considerably. In fact, the calculated permeabilities almost agree with the measured values.

ACKNOWLEDGMENTS

The author is grateful to M.E. Best (Pacific Geoscience Centre) for critically reviewing this paper, and for his directions given to this study. The author is also grateful to M. Williamson (Atlantic Geoscience Centre) for his support of this study.

REFERENCES

Carman, P.C.
1948: Some physical aspects of water flow in porous media; Discussions of Faraday Society, No.3, 72-77.

Coyner, K, Katsube, T.J., Best, M.E., and Williamson, M.
1993: Gas and water permeability of tight shales from the Venture Gas Field offshore Nova Scotia; in Current Research, Part D; Geological Survey of Canada, Paper 93-D.

Katsube, T.J.
1992: Statistical analysis of pore-size distribution data of tight shales from the Scotian Shelf: in Current Research, Part E; Geological Survey of Canada, Paper 92-1E, p. 365-372.

Katsube, T.J. and Agterberg, F.P.
1990: Use of statistical methods to extract significant information from scattered data in petrophysics: in Statistical Applications in the Earth Sciences, (ed.) F.P. Agterberg and G.F. Bonham-Carter; Geological Survey of Canada, Paper 89-9, p. 263-270.

Katsube, T.J., Murphy, T.B., Best, M.E., and Mudford, B.S.
1990: Pore structure characteristics of low permeability shales from deep formations; in Proceedings of the 1990 SCA (Society of Core Analysts) 4th Annual Technical Conference, August, 1990, Dallas, Texas, SCA-9010, p.1-21.

Katsube, T.J., Best, M.E., and Mudford, B.S.
1991: Petrophysical characteristics of shales from the Scotian shelf; Geophysics, v. 56, p. 1681-1689.

Katsube, T.J., Williamson, M., and Best, M.E.
1992: Shale pore structure evolution and its effect on permeability; in Symposium Volume III of the Thirty-Third Annual Symposium of the Society of Professional Well Log Analysts (SPWLA), The Society of Core Analysts Preprints, Oklahoma City, Oklahoma, June 15-17, 1992, Paper SCA-9214, 1-22.

Mudford, B.S. and Best, M.E.
1989: Venture Gas Field, offshore Nova Scotia; case study of overpressuring in region of low sedimentation rate; American Association of Petroleum Geologists Bulletin, v. 73, p. 1383-1396.

Prasuhn, A.L.
1980: Fundamentals of Fluid Mechanics; Prentice-Hall, Englewood Cliffs, New Jersey.

Walsh, J.B. and Brace, W.F.
1984: The effect of pressure on porosity and the transport properties of rocks; Journal of Geophysical Research, v. 89, p. 9425-9431.

Williamson, M.A.
1992: Hydrocarbon resource study of east coast frontier basins; past present and future (Abstract); in Current Activity Forum, Geological Survey of Canada, Program with Abstracts, v. 4.

Winsauer, W.O., Shearin, H.M., Masson, P.H., and Williams, M.
1952: Resistivity of brine-saturated sands in relation to pore-geometry; American Association of Petroleum Geologists Bulletin, v. 36, p. 253-277.

Geological Survey of Canada Project 870057

Gas and water permeability of tight shales from the Venture Gas Field, offshore Nova Scotia

K. Coyner[1], T.J. Katsube, M.E. Best[2], and M. Williamson[3]
Mineral Resources Division

Coyner, K., Katsube, T.J., Best, M.E., and Williamson, M., 1993: Gas and water permeability of tight shales from the Venture Gas Field, offshore Nova Scotia; in Current Research, Part D; Geological Survey of Canada, Paper 93-1D, p. 129-136.

Abstract: Quantitative models describing the hydrocarbon generation, migration and accumulation history of the Sable and Jeanne d'Arc basins (offshore eastern Canada) require, as input, extensive petrophysical information of shales. Various studies are being carried out to provide such petrophysical data. For an example, absolute permeability, as a function of confining pressure, has been measured on a suite of 10 tight shale samples from a depth of 4600-5600 m in the Venture Gas Field. Gas-water relative permeability for one of these samples has also been measured.

The results indicate that the permeabilities vary between 10^{-22} m^2 to 7.4 x 10^{-19} m^2 for effective confining pressures from 60 to 2.5 MPa, respectively. These are extremely small values. Preliminary results for relative permeability measurements, using nitrogen gas, for one of the samples indicate that the gas permeability is 1.9 x 10^{-20} m^2 to 2.0 x 10^{-20} m^2 at irreducible water saturation (31 to 39%), and is 4.5 x 10^{-21} m^2 at 76% water saturation.

Résumé : Les modèles quantitatifs décrivant la génèse, la migration et les étapes d'accumulation des hydrocarbures dans les bassins de Sable et de Jeanne d'Arc (régions extracôtières de l'est du Canada) exigent l'apport de vastes quantités d'information pétrophysique sur les shales. On procède actuellement à diverses études dans le but de rcueillir ces données pétrophysiques. On a par exemple mesuré la perméabilité absolue en fonction de la pression lithostatique sur une série de dix échantillons de shale peu perméable prélevés entre 4 600 et 5 600 m dans le champ gazéifère de Venture. On a aussi mesuré la perméabilité relative vis-à-vis du mélange gaz-eau de l'un de ces échantillons.

Les résultats indiquent que les perméabilités sont de l'ordre de 10^{-22} m^2 à 7,4 x 10^{-19} m^2 aux pressions lithostatiques effectives de 60 à 2,5 MPa. Ces valeurs sont extrêmement faibles. Les résultats préliminaires des mesures de la perméabilité relative, effectuées avec de l'azote gazeux sur l'un des échantillons, montrent que la perméabilité vis-à-vis du gaz est de (1,9 - 2,0) x 10^{-21} m^2 à un niveau irréductible de saturation en eau (31 à 39 %), et de 4,5 x 10^{-21} m^2 à un niveau de saturation en eau de 76 %.

[1] Verde GeoScience, R.R. #1 Box 117, Tunbridge, Vermont 05077
[2] Pacific Geoscience Centre, Sidney
[3] Atlantic Geoscience Centre, Dartmouth

INTRODUCTION

Efforts to develop quantitative models of the hydrocarbon generation, migration and accumulation histories of the Sable and Jeanne d'Arc basins, offshore eastern Canada, require extensive information on shale petrophysical properties. Although there is an abundance of such information for sandstones and carbonate rocks, there is almost no similar data for shales (Mudford and Best, 1989). Specific requirements include information on the effect of pressure on absolute and relative permeabilities, and on porosity of shales.

Various studies are being carried out to provide such petrophysical data. As part of these studies, absolute permeability as a function of confining pressure has been measured on a suite of 10 tight shale samples from a depth of 4600-5600 m in the Venture Gas Field offshore Nova Scotia. Gas-water relative permeability for one of these samples has also been measured. Permeability is routinely measured for core analysis of reservoir rocks by conventional techniques (American Petroleum Institute, 1956). However, permeability measurements for rocks with values below 10^{-15} m^2 are more difficult. Many shales have permeabilities below this value (Brace, 1980), particularly tight shales from deep zones (Mudford and Best, 1989; Luffel and Guidry, 1989; Katsube et al, 1991). Introduction of the transient decay method (Brace et al., 1968) has made such measurements possible, with a large data set of low permeabilities, in the 10^{-19} to 10^{-17} m^2 range, having been measured for crystalline rocks (Katsube and Kamineni, 1983; Katsube et al., 1985; Katsube and Walsh, 1987). Tight shale absolute permeabilities are about 10 to 100 times smaller than the minimum permeabilities found for crystalline rocks (Katsube et al., 1991). Shale relative permeability measurements are, therefore, considerably more difficult to make. The purpose of this paper is to provide information on extremely low absolute permeabilities and preliminary information on gas permeabilities for these tight shales.

The distribution of oil and gas in sedimentary basins is the result of the complex, dynamic interaction of chemical, physical and geological processes. The accuracy and predictive ability of hydrocarbon charge models for these sedimentary basins depend largely on the quantity and quality of the data available from the basins, and on the validity of the assumptions made during model development. A long term study is underway to develop such models for the Jeanne d'Arc Basin, offshore Newfoundland, and the Sable Basin, offshore Nova Scotia. The purpose is to determine hydrocarbon charge risk and uncertainty, and to provide quantitative information on the remaining resource endowment of the basins. The study consists of developing models, using modern modelling techniques (Welte and Yalcin, 1987; Ungerer et al., 1990) in conjunction with high quality database available for current and previous interpretations (Keen and Williams, 1990; Geological Survey of Canada's East Coast Basin atlas series; Bell, 1989; Cant, 1990).

The study consists of a series of linked models that account for:

1. The initial deposition, preservation and distribution of organic matter, its quality, type and volume (source potential).

Table 1. Sampling information on locations and depths (after Katsube et al., 1991).

Sample	Venture well (I.D.)	Depth (m)	Length (cm)	Direction
1	B-13	4693.40	10	H & V
2	"	4694.95	5	V
3	B-43	4916.36	4	V
4	"	4962.48	8	V
5	B-52	5122.35	6	V
6	"	5131.54	6	V
7	B-52	5271.59	5	V
8	"	5273.53	5	V
9	B-52	5553.65	6	V
10	"	5556.95	10	H & V

I.D. = well identification number

H = sample taken for measurement in horizontal direction

V = sample taken for measurement in vertical direction

Table 2. Lithological and petrofacies classification (after Katsube et al., in prep.).

Sample Number	Lithological Description	Petrofacies
1	Lithorenitic, shaly and sandy siltstone	Siltstone
2	Calcareous, fossiliferous and lithorenitic sandstone	Sandstone
3	Lithorenitic, shaly and sandy siltstone	Siltstone
4	Organic matter-rich, silty shale	Shale
5	Organic matter-rich, silty and sandy shale	Shale
6	Sandy, skeletal lime wackestone	Lime Wackestone
7	Lithorenitic, shaly and sandy siltstone	Siltstone
8	Shaly, lithorenitic sandstone	Sandstone
9	Interbedded sublithorenitic sandstone and silty shale.	Shale
10	Parallel laminated organic matter-rich, silty shale.	Shale

2. The subsidence, compaction, pore pressure, thermal maturity and generation history of the source rock system (primary migration).
3. The subsidence, compaction, thermal, pressure and diagenetic history of the aquifer system (secondary migration).
4. The geometrical and mechanical evolution of the major traps in the basin (entrapment).

Modelling of source rock and reservoir systems in this way requires extensive assumptions and information regarding specific rock properties, particularly their progressive evolution with basin subsidence and compaction. For example, information on porosity reduction in muds as they are compressed, heated, and in some cases over-pressured, is essential to accurately derive compaction corrected subsidence histories. Furthermore, an understanding of porosity/permeability relationships with depth, including permeability characteristics of tight shales, is required to model the sealing capacity of shales at depth and to numerically simulate formation pore pressure evolution through time. Comprehensive data regarding these properties is lacking in many areas, particularly the physical and chemical properties of shales. Therefore, the Geological Survey of Canada has designed a study to extend our basic knowledge of the physical properties of compacted and tight shales, both in their present-day and historical state.

METHOD OF PERMEABILITY DETERMINATION

Samples

The 10 shale samples have been obtained from depths between 4700 m and 5600 m in three wells located in the Venture Gas Field, offshore Nova Scotia (Katsube et al., 1991), as indicated in Table 1. The results of lithological and petrofacies classification (Katsube et al., in prep.) are listed in Table 2. Cylindrical plugs with a diameter of 25.4 mm (1 inch) were cored in the vertical direction from 101.6 mm (4 inch) split core samples, as described in Katsube et al. (1991). Such plugs were obtained from all 10 samples, and subsequently cut into discs with thicknesses of 5 to 8 mm for the permeability measurements.

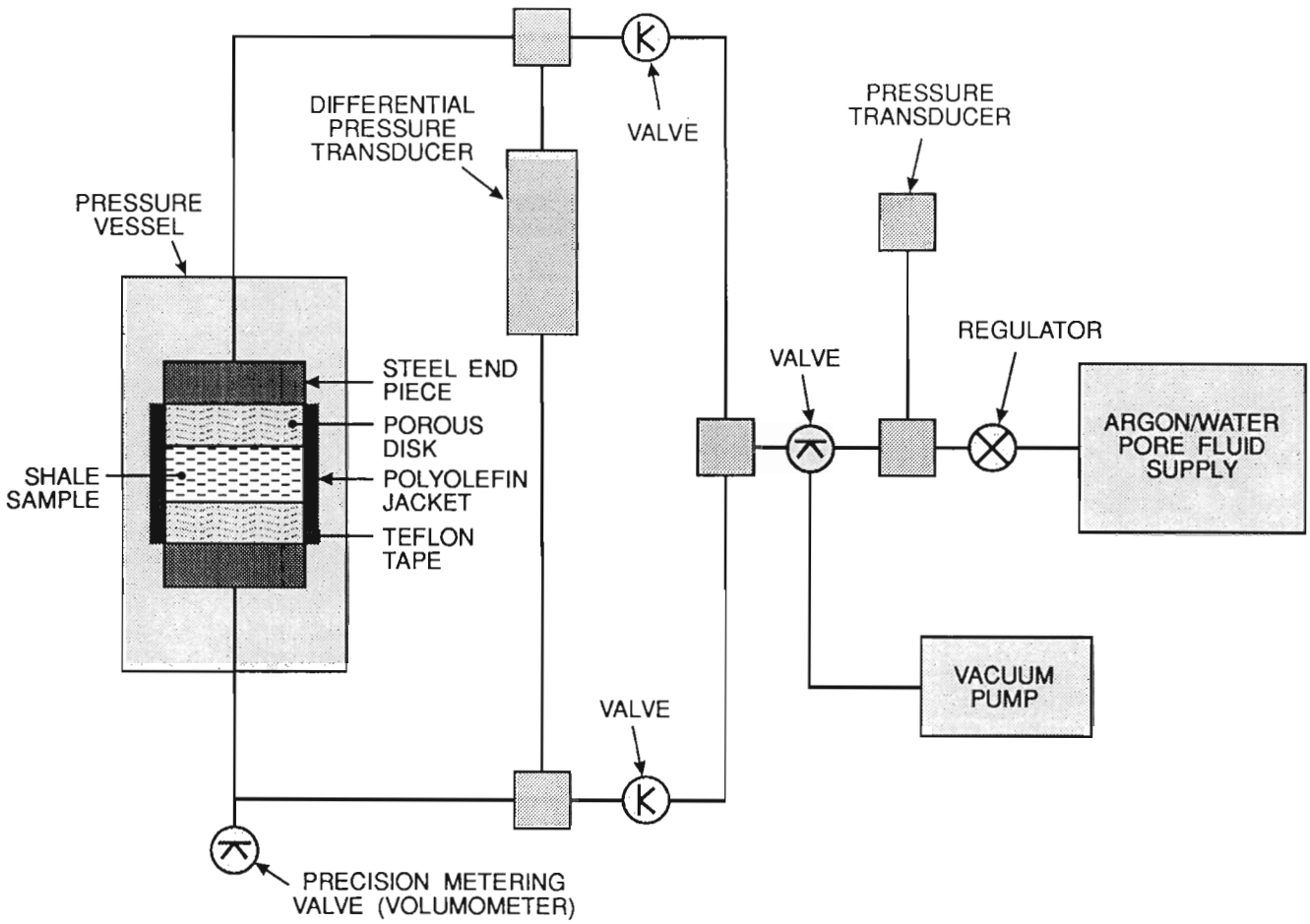

Figure 1. Schematic diagram of the experimental apparatus used for measuring permeability by the transient pulse decay (TPD) technique.

Method of Measurement

Sample permeabilities may be measured using either constant flow, constant head, or transient pulse decay (TPD) techniques. The first two follow directly from the application of Darcy's Law using steady state conditions and are more appropriate for samples with permeabilities in the order of 10^{-15} m^2 (1 mD) or greater. If permeabilities are lower, the flow rates are often too small for precise determination using typical laboratory apparatus for the first two techniques. Instead, the transient pulse decay technique, first introduced by Brace et al. (1968), has greater resolution for low permeability measurements. Consequently, the transient pulse decay technique is used to measure the permeabilities of these shale samples.

Brace et al. (1968) used the transient pulse decay technique, for the first time, to measure sub-micro Darcy permeabilities ($<10^{-18}$ m^2) of granite samples subjected to elevated confining and pore pressures. The experimental technique incorporates pore fluid access at both ends of a jacketed sample under pressure. A small pore pressure pulse is introduced at one end of the specimen. The quasi-exponential decay of this pressure pulse is recorded using pressure transducers as a function of time. The rate of decay is related to permeability, fluid viscosity, sample dimensions, fluid compressibility and pore fluid volume.

In the original work by Brace et al. (1968), the transient was analyzed as a pure exponential decay between two reservoirs with compressibilities equal to water, and the contribution of the pore fluid volume within the rock deemed

Table 3a. Permeability of water-saturated shale samples, Numbers 1-5, from the Venture Gas Field offshore Nova Scotia.

sample/ (Mes. No.)	Pressures (MPa)			Permeability (10^{-21} m^2)
	Confining	Pore	Effective	
1	12.5	10	2.5	8.5 ± 1
	15.0	10	5.0	4.7 ± 0.4
	20.0	10	10	1.7 ± 0.1
	50.0	10	40	0.7 ± 0.1
2	20.0	10	10	35.0 ± 6
	30.0	10	20	29.0 ± 3
	40.0	10	30	5.4 ± 0.6
3	12.8	10	2.8	737. ± 4
	15.0	10	5.0	437. ± 35
	17.5	10	7.5	350. ± 11
	20.0	10	10	296. ± 4
	25.0	10	15	148. ± 8.6
	30.0	10	20	34.7 ± 12.5
	35.0	10	25	14. ± 1.5
	40.0	10	30	6.2 ± 0.7
	45.0	10	35	3.2 ± 0.1
	50.0	10	40	0.9 ± 0.3
	55.0	10	55	1.2 ± 0.4
	60.0	10	50	0.8 ± 0.3
	70.0	10	60	0.3 ± 0.05
4	15.0	10	5.0	31.0 ± 2
	20.0	10	10	22.0 ± 2
	30.0	10	20	18.0 ± 2
	40.0	10	30	5.3 ± 0.6
	50.0	10	40	2.0 ± 0.4
5	20.0	10	10	20.0 ± 2
	30.0	10	20	13.0 ± 2
	40.0	10	30	8.2 ± 0.9

Table 3b. Permeability of water-saturated shale samples, Numbers 6-10, from the Venture Gas Field offshore Nova Scotia.

sample/ (Mes. No.)	Pressures (MPa)			Permeability (10^{-21} m^2)
	Confining	Pore	Effective	
6	13.5	10	3.5	2.1 ± 0.1
	15.0	10	5.0	0.8 ± 0.1
	20.0	10	10	0.54± 0.01
	22.5	10	12.5	0.31± 0.15
	25.0	10	15	0.27± 0.03
	30.0	10	10	0.29± 0.15
7	12.5	10	2.5	21. ±10.
	15.0	10	5.0	14. ± 7.
	17.5	10	7.5	11. ± 5.
	20.0	10	10	8. ± 4.
	25.0	10	15	4.3 ± 2.1
	30.0	10	20	3.0 ± 1.5
	35.0	10	25	1.4 ± 0.7
	40.0	10	30	1.3 ± 0.2
	45.0	10	35	0.88± 0.44
	50.0	10	40	0.88± 0.44
	55.0	10	45	0.64± 0.32
	60.0	10	50	0.43± 0.44
	65.0	10	55	0.41± 0.20
	70.0	10	60	0.33± 0.16
8	20.0	10	10	58.0 ± 4
	30.0	10	20	26.0 ± 4
	40.0	10	30	19.0 ± 2
	50.0	10	40	17.0 ± 2
	70.0	10	60	11.0 ± 1
9 - (1)*	20.0	10	10	2.0 ± 0.1
	30.0	10	20	1.2 ± 0.1
- (2)*	20.0	10	10	2.4 ± 0.1
	25.0	10	15	1.4 ± 0.1
	30.0	10	20	1.3 ± 0.1
	35.0	10	25	1.0 ± 0.1
	40.0	10	30	0.6 ± 0.1
	50.0	10	40	0.4 ± 0.1
10	12.5	10	2.5	16.0 ± 2
	15.0	10	5.0	9.4 ± 1
	20.0	10	10	4.2 ± 0.4
	50.0	10	40	0.9 ± 0.1
	70.0	10	60	0.1 ± 0.1

*: Measurement Number

negligible since porosities were small. Subsequent experimental developments (Coyner et al., 1979) indicated that reservoir compressibilities were approximately an order of magnitude greater than pure water because of compliancy in the pressure tubing, O-ring, and diaphragm-style pressure transducers. This enhanced compressibility was directly measured and could be accounted for in the calculations of permeability from transient pulse decay data. Theoretical and experimental efforts (Lin, 1977; Heard et al., 1979; Hsich et al., 1981; Neuzil et al., 1981) further defined these effects and established a better understanding of the technique. These developments allow the transient pulse decay technique (Brace et al., 1968) to be used, with sufficient accuracy, to measure the extremely low shale permeabilities (Katsube et al., 1991).

Experimental procedures

The samples were precisely dimensioned to within 0.002 cm, then vacuum-saturated with a 30 000 ppm NaCl brine solution for at least 48 hours prior to testing. Each sample was stacked between two porous discs, located between two stainless steel end plugs, and jacketed with elastomer tubing (Fig. 1). This assembly was placed into a 400 MPa (4 kB) pressure vessel with an arrangement that allowed pore fluid access to either end of the sample from outside of the pressure vessel through stainless steel pressure tubing, the end plugs, and the two porous discs. A schematic diagram of the experimental apparatus is shown in Figure 1. Pore fluid pressures and confining pressures were controlled through a series of valves and pumps. The absolute pore pressure was measured with a Data Instruments pressure transducer. The differential pore pressure across the sample ends was measured with a CEC 200 psi differential pressure transducer, and the confining pressure and absolute pore pressure were established and monitored with visual digital panel meter readouts. The output from the differential pressure transducers was recorded on a strip-chart recorder.

Permeabilities at different confining pressures and pore fluid pressures were measured with the transient pulse decay technique (Brace et al., 1968). After the confining and pore fluid pressures equilibrated, as determined by drift of the transducer readouts, a quasi-instantaneous pore pressure pulse was introduced at one end of the sample. The magnitude of the pulse was approximately 1 MPa (145 psi). The equilibrium of this pressure pulse through the sample was recorded as a function of time with the chart recorder output of the differential pressure transducer. Decay times were typically in the order of 1-3 hours. Each individual pulse decay was recorded on semi-log paper and the slope measured. The slopes were measured to within ± 10%. Permeabilities were then calculated from this slope.

EXPERIMENTAL RESULTS

The experimental results of absolute permeability for 100% water-saturation measured as a function of confining pressure are listed in Tables 3a and b for the 10 shale samples. The effective pressure range is from 2.5 to 60 MPa. Measured permeabilities range downward from a maximum of 7.4 x 10^{-19} m^2 (740 nD) for sample 3 at 2.8 MPa, to the minimum permeability value measured with the system of 10^{-22} m^2 (0.1 nD) for sample 10 at 60 MPa.

Table 4. Gas permeability at varied water content for Sample 10. The porosity (5.7%) used for water content calculations was obtained by vacuum drying at 105°C (see also Katsube et al., 1992).

Water Saturation (%)	Gas Absolute Permeability (k in $10x^{-21}$ m^2)	Relative Permeability (%)
31	19.0	100
39	20.0	106
46	12.0	57
55	10.0	44
76	4.5	10
100	2.9	0

The relative permeability to gas for partially saturations for sample 10 is listed in Table 4. These measurements were conducted at a constant confining pressure of 3.0 MPa and a constant pore pressure of 0.7 MPa. The porosity (5.7%) used for water content calculations was obtained by vacuum drying at 105°C (see also Katsube et al., 1992).

An example of a transient pulse decay curve from the permeability measurements is shown in Figure 2 for a sample with extremely low permeability (Sample 6). The horizontal and vertical axis represent time and differential pressure across the sample.

DISCUSSION

The permeability values obtained for these shales (see Tables 3a and b), in the range of 10^{-22} m^2 (0.1 nD) to 7.4 x 10^{-19} m^2 (740 nD), are within the range of shale permeabilities in the literature (Brace, 1980). The permeability values below 10^{-21} m^2 (1 nD) reached at the largest effective pressures in this study, are close to the lowest permeabilities reported for shales (Luffel and Guidry, 1989; Brace, 1980; Lin, 1978).

Since the samples were obtained from depths of 4600-5600 m, the corresponding effective overburden pressures are approximately 74 to 90 MPa, slightly higher than the maximum effective pressure used for the measurements. That is, assuming a bulk density of 2600 kg/m^3 (Katsube et al., 1991) for the shales and 1000 kg/m^3 for the water column using a normal hydrostatic pressure gradient. However, these shale samples are from over-pressured zones (Mudford and Best, 1989) offshore Nova Scotia, suggesting that the in-situ effective pressures are likely to be smaller than the corresponding effective overburden pressures stated above, and therefore the in-situ permeabilities are more likely to be within the range of these measured values.

The results of a petrophysical study consisting of permeability, porosity, formation-factor, and mercury porosimetry measurements by Katsube et al. (1991), suggest that the extremely low permeabilities ($<10^{-20}$ m^2) occur because the flow path consists of a network of very tortuous pores (true tortuosity = 3.3) with small diameters, in the order of 8 nm to 16 nm.

The relative permeability measurements in Table 4 provide the first published indication of how gas permeability varies with partial saturation in a tight shale. During normal diagenesis and compaction of shales both liquid and gas are expelled from the pore space. The liquid (brine) includes seawater entrapped during shale formation and diagenetic transformations of shale minerals,

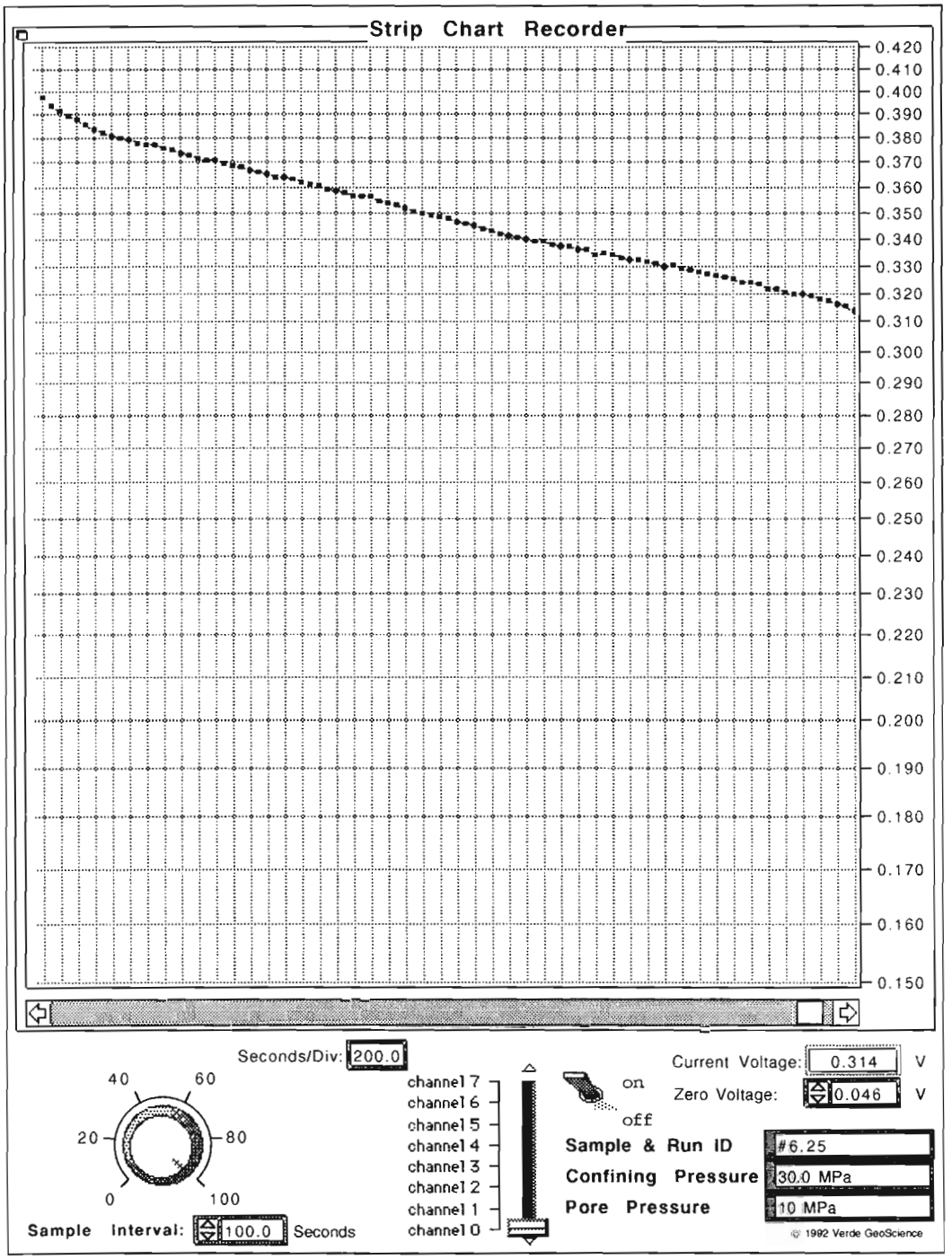

Figure 2. Example of the transient pulse decay curve from a permeability measurement for a sample with low permeability (Sample 6). The decay slope is 2.2 x 10^{-5}/sec. The horizontal and vertical axis represent time and differential pressure across the sample.

particularlythe montmorillonite to illite transformation. The gas, if it exists, is a result of the thermal maturation of organic kerogen. The organic gas (methane) is easily dissolved into the pore liquid early in the process. When gas production exceeds the capacity of the pore liquid to absorb it, either because of an insufficient source of additional pore fluid or kinetic effects, the partial vapour pressure of the gas is exceeded and a free gas phase develops within the pore space. Gas and fluid permeabilities are then determined by the percentage of gas accumulation and its location within the pore space.

The location of the gas within the pores was not determined in this study (e.g., NMR and/or CT imagery). A partially saturated shale sample was assumed to be in equilibrium with the pore fluid used for the permeability measurements. Nitrogen gas was used for the relative permeability measurements, as previously stated. The data indicate that at water saturations below irreducible water saturation (31 to 39%), the gas permeability increases rapidly with decreasing saturation. At lower water saturation, the water is likely to be concentrated in the smaller and poorly connected pores which do not contribute to permeability. Therefore, the nitrogen gas that was used to measure permeability relatively easily permeated the sample through the larger pores. At higher water saturations (above 39%) relative permeability decreases as the water fills the larger pores and blocks the gas. At 100% water saturation there is still some measurable permeability. This observation, which needs to be confirmed, can be partly explained by considering the diffusion of the nitrogen gas into the pore water.

CONCLUSIONS

Permeability measurements have been carried out on 10 shale samples from the Venture Gas Field offshore Nova Scotia. The results indicate that the permeabilities are in the order of 10^{-22} m^2 (0.1 nD) to 7.4 x 10^{-19} m^2 (740 nD) at effective confining pressures of 60 down to 2.5 MPa. Preliminary results for relative permeability measurements, using nitrogen gas, for one of the samples indicate that the gas permeability is (1.9 - 2.0) x 10^{-20} m^2 at irreducible water saturation (31 to 39%), and is 4.5 x 10^{-21} m^2 at 76% water saturation.

ACKNOWLEDGMENTS

Part of these measurements were performed at New England Research (White River Junction, Vermont). The authors are grateful to H.S. Salem (Atlantic Geoscience Centre, Dartmouth) for critically reviewing this paper.

REFERENCES

American Petroleum Institute
1956: Recommended practice for determining permeability of porous media: API Recommended Practice 27 (RP 27) Third Edition (1952), American Petroleum Institute, Washington, D.C. p. 27.

Bell, J.S.
1989: The stress regime of the Scotian Shelf offshore eastern Canada to 6 kilometres depth and implications for rock mechanics and hydrocarbon migration: Proceedings; Rock at great depth; Rock mechanics and rock physics at great depth; Berichte; Felsmechanik und Felsphysik in grosser Tiefe; v. 3. p. 1243-1265.

Brace, W.F.
1980: Permeability of crystalline and argillacious rocks; International Journal of Rock Mechanics and Mining Sciences and Geomechanics Abstracts, v. 17, p. 241-251.

Brace, W.F., Walsh, J.B., and Frangos, W.T.
1968: Permeability of granite under high pressure; Journal of Geophysical Research, v. 73, p. 2225-2236.

Cant, D.J. (co-ordinator)
1990: Scotian Shelf. Frontier Geoscience Project East Coast Basin Atlas Series; Geological Survey of Canada, Dartmouth, Nova Scotia.

Coyner, K.B., Walsh, J.B., and Brace, W.F.
1979: New Laboratory measurements of permeability and electrical resistivity of crystalline rocks; 1979 Fall Meeting of the American Geophysical Union, San Francisco, California.

Heard, H.C., Trimmer, D., Duba, A., and Bonner, B.
1979: Permeability of generic repository rocks at simulated in-situ conditions; Lawrence Livermore Laboratory, Livermore, California, Report UCRL-82609.

Hsieh, P.A., Tracy, J.V., Neuzil, C.E., Bredhoeft, J.D., and Silliman, S.E.
1981: A transient laboratory method for determining the hydraulic properties of tight rocks - I. Theory; International Journal of Rock Mechanics and Mining Sciences and Geomechanics Abstracts, 18, p. 245-252.

Katsube, T.J. and Kamineni, D.C.
1983: Effect of alteration on pore structure of crystalline rocks; Core samples from Atikokan, Ontario; Canadian Mineralogist, v. 21, p. 637-646.

Katsube, T.J. and Walsh, J.B.
1987: Effective aperture for fluid flow in microcracks; International Journal of Rock Mechanics and Mining Sciences and Geomechanics Abstracts, v. 24, p. 175-183.

Katsube, T.J., Best, M.E., and Mudford, B.S.
1991: Petrophysical characteristics of shales from the Scotian shelf; Geophysics, v. 56, p. 1681-1689.

Katsube, T.J., Percival, J.B., and Hume, J.P.
1985: Characterization of the rock mass by pore structure parameters; Atomic Energy of Canada Limited Technical Record, TR-299, p. 375-413.

Katsube, T.J., Scromeda, N., and Williamson, M.
1992: Effective porosity of tight shales from the Venture Gas Field, offshore Nova Scotia; in Current Research, Part D; Geological Survey of Canada, Paper 92-1D, p. 111-119.

Keen, M.J. and Williams, G.L.
1990: Geology of the Continental Margin of Eastern Canada, (ed.) M.J. Keen and G.L. Williams, Geological Survey of Canada, no 2. (also Geological Society of America, Geology of North America v. I-1, 853 p.).

Lin, W.
1977: Compressible fluid flow through rocks of variable permeability; Lawrence Livermore Laboratory, Livermore, California, Report UCRL-52304.
1978: Measuring the permeability of Eleana Argillite from Area 17, Nevada Test Site, using the transient method; Lawrence Livermore Laboratory, Livermore, California, Report UCRL-52604.

Luffel, D.L. and Guidry, F.K.
1989: Reservoir rock properties of Devonian shale from core and log analysis: The Society of Core Analysts, Annual Technical Conference Preprints, v. I, Aug. 2-3, Paper 8910.

Mudford, B.S. and Best, M.E.
1989: Venture Gas Field, offshore Nova Scotia; case study of overpressuring in region of low sedimentation rate; American Association of Petroleum Geologists Bulletin, v. 73, p. 1383-1396.

Neuzil, C.E., Colley, C., Silliman, S.E., Bredhoeft, J.D., and Hsieh, P.A.
1981: A transient laboratory method for determining the hydraulic properties of tight rocks - II. Application; International Journal of Rock Mechanics and Mining Sciences and Geomechanics Abstracts, v. 18, p. 253-258.

Ungerer, P., Burrus, J., Doligez, B., Chenet, P.Y., and Bessis, F.
1990: Basin evaluation by two-dimensional modelling of heat transfer, fluid flow, hydrocarbon generation, and migration; American Association of Petroleum Geolgists Bulletin, v. 74, p. 309-335.

Welte, D.H. and Yalcin, M.N.
1987: Formation and occurrence of petroleum in sedimentary basins as deduced from computer aided basin modelling; Petroleum geochemistry and exploration in the Afro-Asian region, Oil and Natural Gas Comm., Baroda, India. p. 17-23.

Geological Survey of Canada Project 870057

Magnetic susceptibility as a Quaternary correlation tool: examples from Hudson Strait sediment cores, eastern Canadian Arctic

W.F. Manley[1,2], B. MacLean, M.W. Kerwin[2], and J.T. Andrews[2]
Atlantic Geoscience Centre, Dartmouth

Manley, W.F., MacLean, B., Kerwin, M.W., and Andrews, J.T., 1993: Magnetic susceptibility as a Quaternary correlation tool: examples from Hudson Strait sediment cores, eastern Canadian Arctic; in Current Research, Part D; Geological Survey of Canada, Paper 93-1D, p. 137-145.

Abstract: Comparison of magnetic susceptibility (MS) variations among closely spaced sediment cores from the Hudson Strait region shows that magnetic susceptibility offers a simple and convincing means of stratigraphic correlation. Whole-core, volume magnetic susceptibility was measured on four cores collected from Hudson Strait and Hatton Basin during CSS Hudson cruise 92-028. Downcore variations exhibit peaks of 130-180 x 10^{-5} SI units rising above values of 50-100 x 10^{-5} SI units. These variations are compared with magnetic susceptibility signatures of nearby cores collected previously. With one exception, downcore MS variations are easily correlated between cores 0.1 to 26 km apart. Visual correlations commonly have a precision of 20 cm or better. These MS correlations document relative ages and stratigraphic positions among cores and permit comparison of chronological, sedimentological, and paleoenvironmental data to help reconstruct late Quaternary glacial and marine environments at the northeast margin of the Laurentide Ice Sheet.

Résumé : En comparant les variations de susceptibilité magnétique (SM) que montrent entre elles des carottes de sédiments très rapprochées provenant de la région du détroit d'Hudson, on constate que la SM est un moyen simple et convaincant d'établir des corrélations stratigraphiques. On a mesuré la SM du volume total de quatre carottes recueillies dans le détroit d'Hudson et dans le bassin de Hatton au cours de la croisière 92-028 du navire océanographique CSS Hudson. Les variations observées dans les carottes de haut en bas affichent des maxima de 130 à 180 x 10^{-5} unités SI dominant des valeurs de 50 à 100 x 10^{-5} unités SI. On compare ces variations aux signatures SM de carottes adjacentes recueillies antérieurement. À une exception près, les variations de SM observées de haut en bas se laissent facilement corréler entre des carottes distantes de 0,1 à 26 km les unes des autres. Les corrélations visuelles ont habituellement une précision d'au moins 20 cm. Ces corrélations des SM aident les chercheurs à mieux déterminer la position stratigraphique et l'âge relatifs des carottes, permettant la comparison des données chronologiques, sédimentologiques et paléoenvironnementales et contribuant ainsi à la reconstitution des milieux glaciaires et marins de la fin du Quaternaire sur la marge nord-est de l'inlandsis laurentidien.

[1] Center for Geochronological Research
[2] INSTAAR and Department of Geological Sciences, University of Colorado, Boulder, Colorado 80309-450

INTRODUCTION

Whole-core, volume magnetic susceptibility was measured on four sediment cores taken from Hudson Strait and Hatton Basin during cruise 92-028 of the **CSS Hudson** in September 1992. Magnetic susceptibility (MS), a measure of sediments' ability to hold an induced magnetic field, is an indicator of sediment density, texture, and mineralogy (Thompson and Oldfield, 1986; e.g., Andrews and Jennings, 1987; Andrews et al., 1991). The magnetic susceptibility signature of the cores can be used to ascertain sediment provenance in relation to late Quaternary glacial history. In the Hudson Strait region, this history included advances of the northeastern Laurentide Ice Sheet into Hudson Strait (Lauriol and Gray, 1987; Vilks et al., 1989; MacLean et al., 1991, in press; Manley and Kaufman, 1992; Laymon, 1992) and a postulated series of rapid late-glacial advances across the strait (Miller et al., 1988; Miller and Kaufman, 1990; Stravers et al., 1992). Magnetic susceptibility can also be used in a broader sense to help reconstruct late-glacial and postglacial environments and paleo-oceanographic conditions. Considerations of regional and temporal changes in magnetic susceptibility and their relation to glacial dynamics and paleoenvironments will be explored in later studies. This study reviews the magnetic susceptibility data collected during the 1992 cruise, presents nine new accelerator mass spectrometry (AMS) radiocarbon dates, and highlights the utility of magnetic susceptibility as a correlation tool.

Quaternary marine sediment was sampled in cores from four localities in the Hudson Strait region during Phase II of cruise 92-028 (Fig. 1, Table 1). Three of the localities lie in sediment basins within the strait, whereas the fourth lies in the Hatton Basin, 70 km seaward of the mouth of the strait. Earlier paleo-oceanographic studies within Hudson Strait (Vilks et al., 1989; MacLean et al.,1991, in press; MacLean and Vilks, 1992) and on the adjacent continental shelf (Josenhans et al., 1986; Praeg et al., 1986; Andrews et al., 1990), which interpreted geophysical survey data, foraminiferal assemblages, and depositional chronologies, indicated that these localities contain an important regional signal of late Quaternary glacial and postglacial events.

A Benthos piston corer was used to retrieve the sediment section at three of the localities (92-028-153, -155, and -158). Each piston core (e.g., 92-028-153P) is associated with a trigger weight core (e.g. 92-028-153T). Core 92-028-157G was collected with a Benthos gravity corer.

Table 1. Core locations

Core	Latitude	Longitude	Water depth (m)
84-035-014	60° 59.20' N	62° 27.30' W	605
90-023-045	60° 56.75' N	66° 08.25' W	845
90-023-064	61° 07.50' N	70° 34.60' W	196
90-023-107	61° 20.67' N	70° 37.77' W	182
92-028-153	61° 20.64' N	70° 37.73' W	184
92-028-155	61° 09.50' N	70° 34.20' W	196
92-028-157	60° 56.86' N	66° 07.86' W	860
92-028-158	61° 00.00' N	62° 55.57' W	622

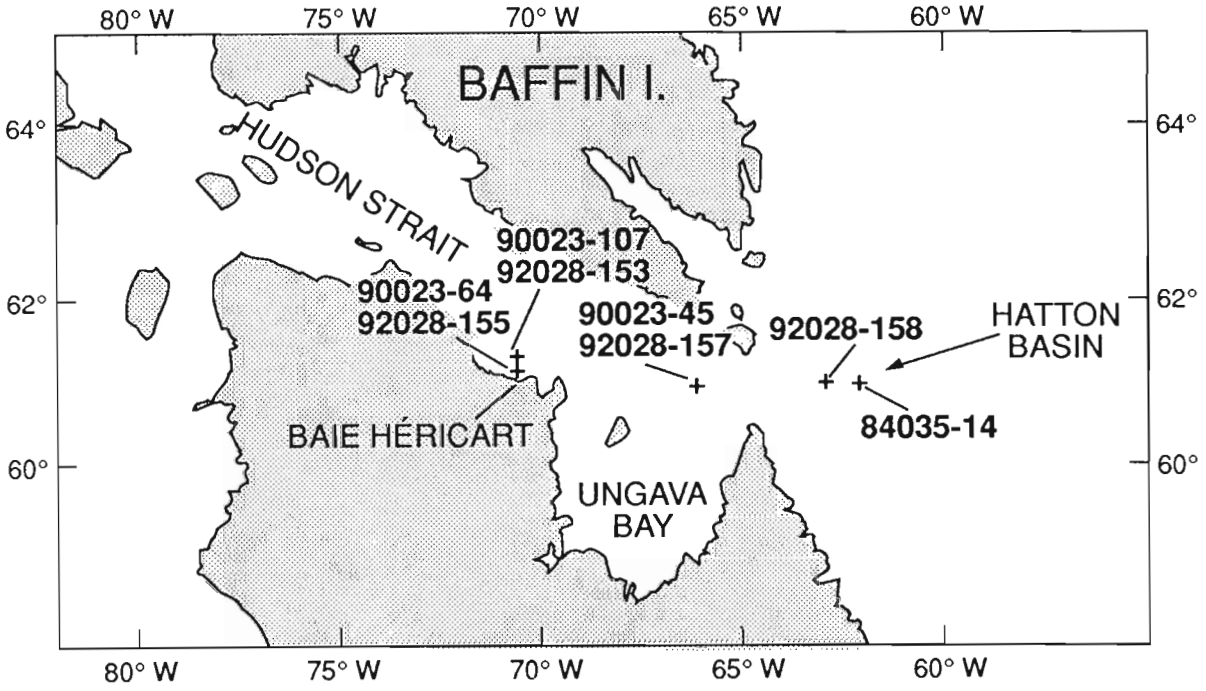

Figure 1. Map showing core site locations.

Three of the cores sites were selected to coincide closely (<4 km) with sites occupied in 1990 (cruise 90-023); MacLean et al., 1991), for two reasons: a) to retrieve sediments from lower in the section than was possible with the large-diameter AGC corer used in 1990; and b) to recover the upper part of the section that was by-passed (blown away) and unsampled by the large corer in 1990. The lower section will be used to obtain more complete chrono- and bio-stratigraphic data relating to depositional environments and the late-glacial history of the region; the uppermost section will provide information relating to postglacial conditions and proxy data relating to global change. Fortuitously, core-site reoccupation allowed us to test magnetic susceptibility as a correlation tool among closely spaced cores. The fourth core site from 1992 lies within 30 km of a core site occupied in 1984 (cruise 84-035).

STRATIGRAPHIC SETTING

High resolution seismic reflection profiles illustrate the late Quaternary setting of the three core localities within Hudson Strait (Fig. 2, 3, and 4). Core pairs 92-028-153/90-023-107 and 92-028-155/90-023-064 were taken near former

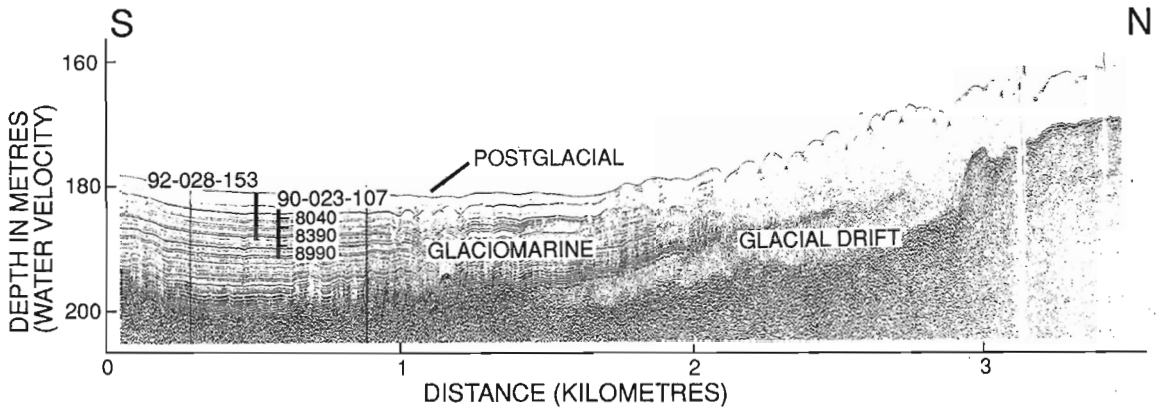

Figure 2. Huntec high resolution seismic reflection profile across core sites 92-028-153 and 90-023-107 in the Baie Héricart area of south-central Hudson Strait, illustrating acoustic stratigraphy and radiocarbon chronology (Modified from MacLean et al., in press).

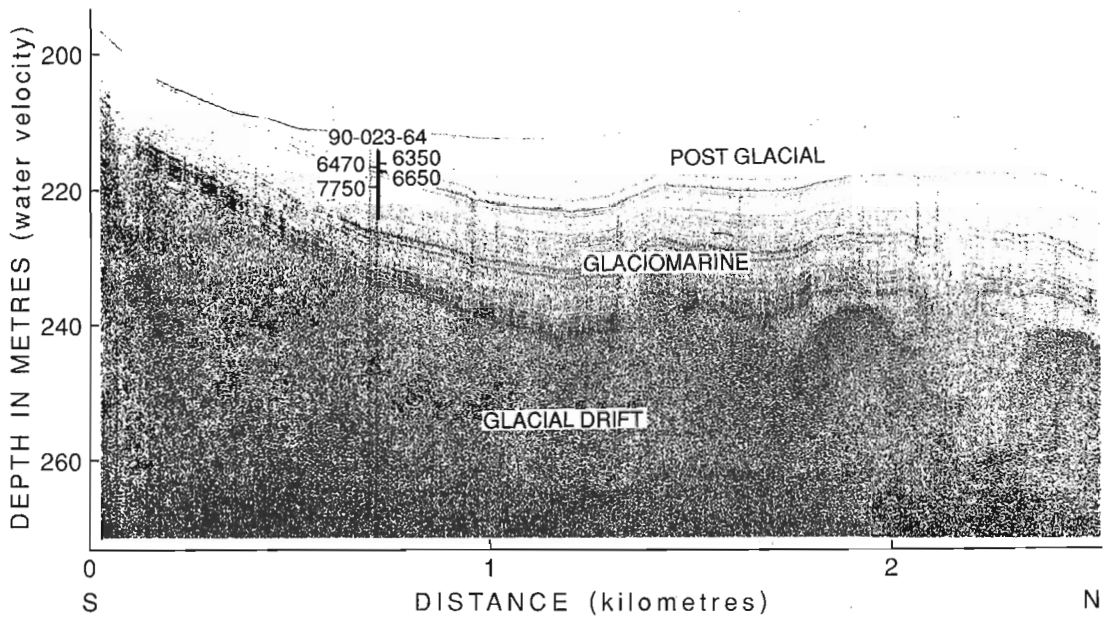

Figure 3. Huntec high resolution seismic reflection profile across core site 90-023-064 in the Baie Héricart area, illustrating acoustic stratigraphy and radiocarbon chronology. Core 92-028-155 was obtained in a similar geological setting 3.7 km to the north toward the northern margin of the basin.

ice-margin positions in the Baie Héricart area of south central Hudson Strait. Core pair 92-028-157/90-023-045 is from the eastern basin of the strait. Foraminiferal assemblages and the acoustically stratified character of the sediments indicate that proximal to distal glaciomarine deposits constitute much of the sediment section at these localities (Vilks et al., 1989; MacLean et al., in press). An overlying layer of generally acoustically transparent, postglacial sediment ranges in thickness from about 3 m at 92-028-153/90-023-107 (Fig.2) to about 8 m at 90-023-064 (Fig.3) and to perhaps as much as 14 m at 90-023-045 (Fig.4). Glaciomarine sediment makes up most of the section at 92-028-158 and 84-035-014 localities in the Hatton Basin (Evans, 1990).

METHODS

Magnetic susceptibility was measured onboard using a Bartington MS-1 meter and a 12.5-cm-diameter, 2.5-cm wide loop linked to a laptop computer. Measurements were made every 2.5 cm along the length of each core, except for intervals of 2.5-10 cm at core section breaks. Magnetic susceptibility data were available for interpretation usually within 24 hours of core retrieval. Replicate analyses of the trigger weight core at site 92-028-153 demonstrated an average difference in measurement between repeated measurements of 2% and maximum difference of 8%. The 1992 magnetic susceptibility data were compared to magnetic susceptibility measurements made on nearby cores taken during cruise 90-023 (Andrews et al., 1991) and cruise 84-035. Magnetic susceptibility measurements of the 90-023 and 84-035 cores followed the same methodology used in cruise 92-028, except for a sampling interval of 5 cm. Volume magnetic susceptibility is presented in 10^{-5} SI units (dimensionless) in Figures 5 to 8. Note that absolute magnetic susceptibility values of the 90-023 cores are 20-44% greater than those of the other cores (on average for correlative intervals), as expected given the larger diameter of the 90-023 cores (9.92 cm) as compared to the 6.69 cm diameter of the 92-028 and 84-035 cores.

Nine new AMS (accelerator mass spectometry) radiocarbon dates on marine bivalves and foraminifera are presented in Table 2 with three previously published dates, to illustrate an application of the magnetic susceptibility correlations and to facilitate tentative correlation between dated cores (see Discussion).

RESULTS

Magnetic susceptibility values in the four 92-028 cores vary from 10 to 220 x 10^{-5} SI units with average core values of 86-101 units. The magnetic susceptibility plots generally exhibit baselines with values of 50-100 units and well defined peaks rising to 130-180 units. Magnetic susceptibility values change downcore without single data point outliers. High magnetic susceptibility peaks in the cores may reflect delivery of sediment derived from glacial erosion of Precambrian granites and gneisses surrounding the strait (cf.,Stravers, 1986; Andrews and Stravers, in press). High magnetic susceptibility may also reflect possible

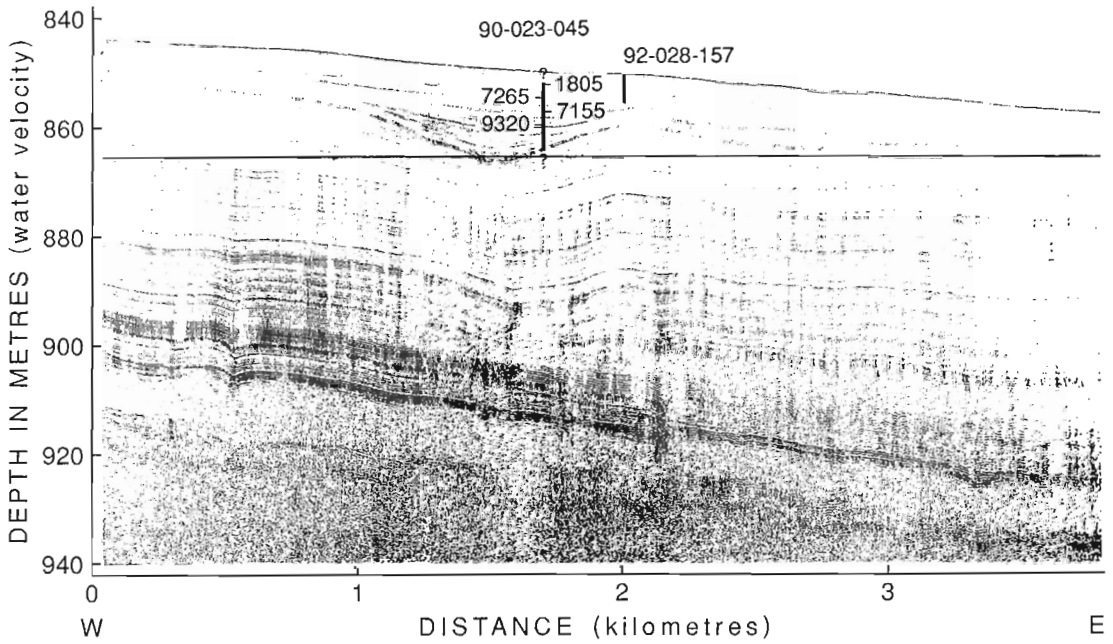

Figure 4. Huntec high resolution seismic reflection profile across core sites 92-028-157 and 90-023-045 in the large basin north of Ungava Bay in eastern Hudson Strait illustrating acoustic stratigraphy and radiocarbon chronology. Placement of the top of core 90-023-045 on the seismic profile is uncertain. (Modified from McLean et al., 1991).

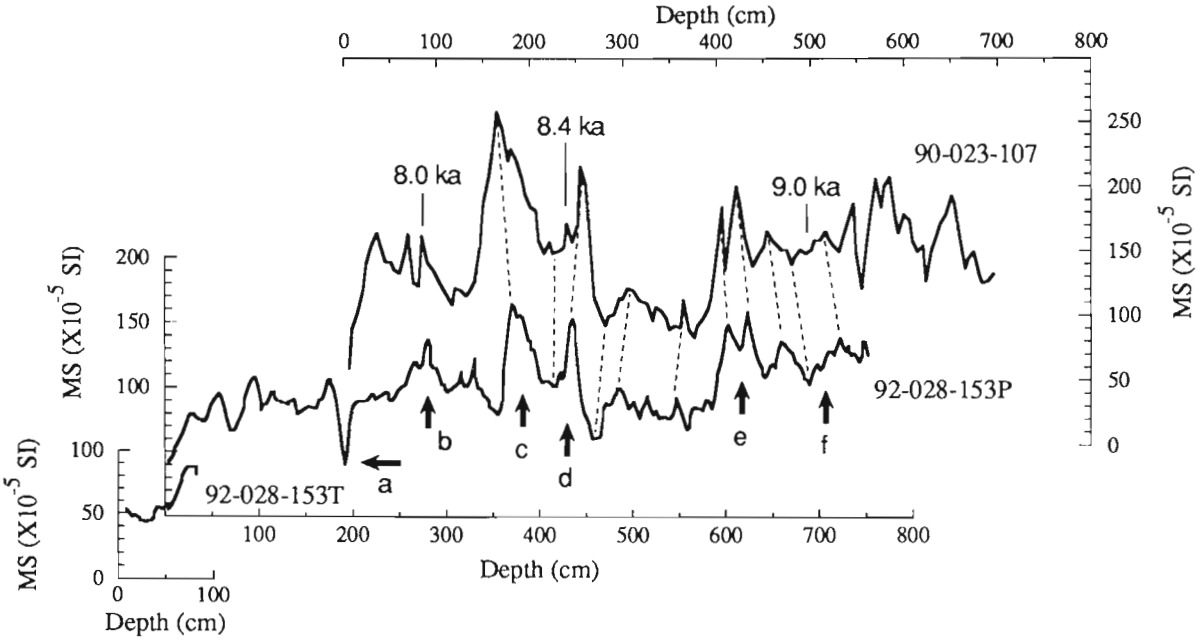

Figure 5. Magnetic susceptibility of cores 92-028-153P (a piston core), 92-028-153T (the trigger weight core), and 90-023-107 from the Baie Héricart area. Site 90-023-107 lies close (about 0.1 km) to site 92-028-153 (Fig. 2). Also shown are accelerator mass spectrometry radiocarbon dates (Table 2). Plots are offset along depth, and visually estimated tie lines are shown to facilitate magnetic susceptibility correlation. Arrows illustrate tentative correlations to cores in Figure 6.

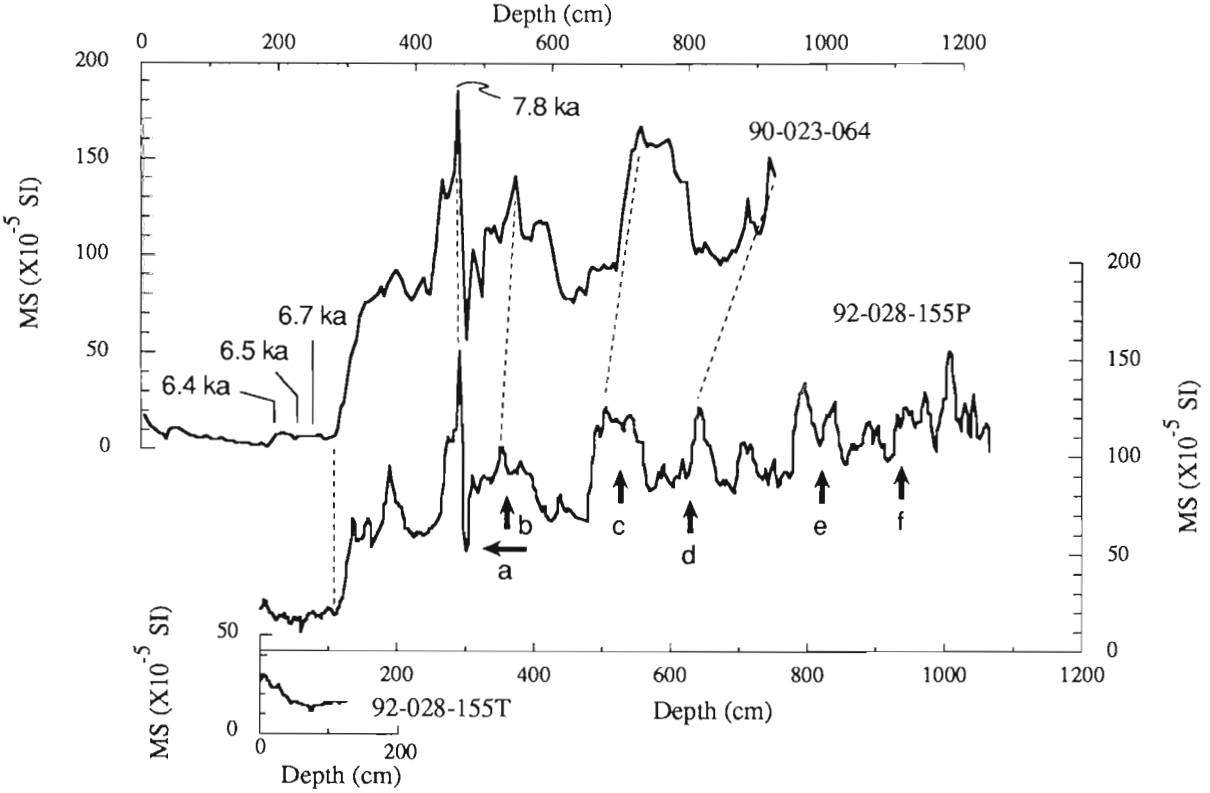

Figure 6. Magnetic susceptibility profiles of cores 92-028-155P, 92-028-155T, and 90-023-064 from the Baie Héricart area. Site 90-023-064 lies 3.7 km from site 92-028-155. Also shown are tie lines and accelerator mass spectrometry radiocarbon dates. These cores were taken about 21 km from the cores shown in Figure 5. Arrows illustrate tentative correlations to cores shown in Figure 5.

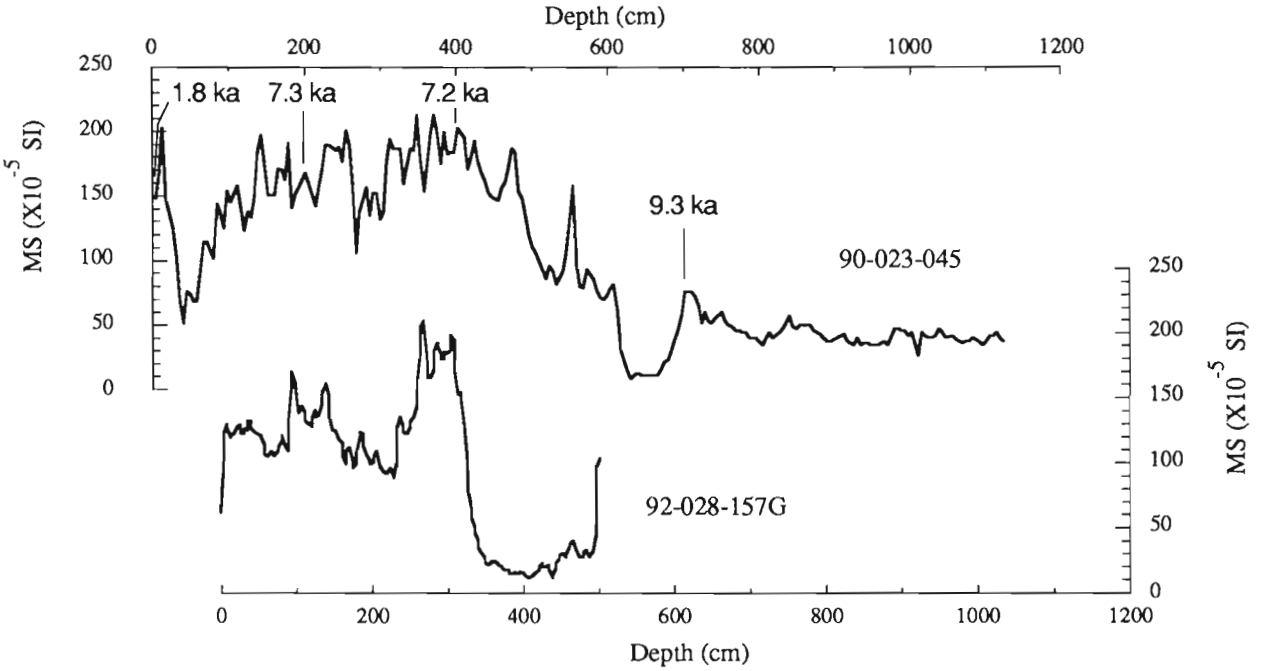

Figure 7. Magnetic susceptibility profiles of cores 92-028-157G (a gravity core) and 90-023-045 from eastern Hudson Strait. Site 90-023-045 lies about 0.4 km from site 92-028-157 (Fig. 4). Also shown are accelerator mass spectrometry radiocarbon dates.

Table 2. Radiocarbon dates for sediment cores from the Hudson Strait region

Core	Reference	Laboratory number	Reported radiocarbon age (^{14}C yr BP)[a]	Corrected radiocarbon age (yr BP)[b]	Depth (cm)	Material[c]
84-035-014	Evans (1990)	AA-4255	9355 ± 70	8945 ± 70	200-205	F b
90-023-045	this study	AA-8961	2215 ± 55	1805 ± 55	2-4	F b
90-023-045	this study	AA-8962	7675 ± 115	7265 ± 115	198-200	F b
90-023-045	this study	AA-8963	7565 ± 60	7155 ± 60	398-399	F p/b
90-023-045	this study	AA-8964	9730 ± 70	9320 ± 70	695-705	F p/b
90-023-064	this study	TO-2459	6760 ± 70	6350 ± 70	195	B
90-023-064	this study	TO-2460	6880 ± 70	6470 ± 70	225	B
90-023-064	this study	TO-2462	7060 ± 70	6650 ± 70	250	B
90-023-064	this study	TO-3263	8160 ± 150	7750 ± 150	460-462	F b
90-023-107	MacLean et al. (in press)	TO-2471	8450 ± 70	8040 ± 70	80-82	B
90-023-107	MacLean et al. (in press)	TO-2472	8800 ± 70	8390 ± 70	236	B
90-023-107	this study	TO-3274	9400 ± 190	8990 ± 190	497-499	F b

[a] The Univ. of Arizona (AA) and Univ. of Toronto (TO) have reported these dates relative to $\delta^{13}C = -25‰$ with an error term of one standard deviation.

[b] Reported ages have been corrected for the marine reservoir effect by subtracting 410 yr. Note that some studies in the Hudson Strait region (e.g., Vilks et al., 1989; MacLean et al., in press) have presented radiocarbon dates on bivalves and foraminifera with a marine reservoir correction of 410 yr, whereas others (e.g., Miller et al., 1988; Andrews et al., 1990) have presented dates with a reservoir correction of 450 yr.

[c] Abbreviations are: F b, benthic foraminifera; F p/b, mixed assemblage of planktonic and benthic foraminifera; B, marine bivalve.

concentration of a surface lag of such material due to current winnowing at the sea floor. Conversely, low magnetic susceptibility excursions may record pulses of high carbonate sedimen- tation derived from glacial erosion of Paleozoic limestone and dolostone on the floors of Hudson Strait, Hudson Bay, and Foxe Basin (cf., Andrews et al., 1990; Andrews and Tedesco, in press).

Comparison of the 92-028 cores with cores taken during previous cruises shows that magnetic susceptibility offers a rapid and convincing means of stratigraphic correlation (Fig. 5 to 8). For example, magnetic susceptibility variations from core 92-028-153P closely mirror those in core 90-023-107, taken about 0.1 km away (Fig. 5). Most major and minor peaks are identifiable on both records. Correlation between the two cores commonly has a precision of 20 cm or less at any given level, and many peaks and troughs can be directly correlated. A close match exists also for cores 92-028-155P and 90-023-064 (Fig. 6), even though they were taken from sites 3.7 km apart. Correlation is less certain for cores 92-028-157G and 90-023-045 (separated by about 0.4 km; Fig. 7). However, cores 92-028-158P and 84-035-014 clearly can be correlated despite a separation of 25.9 km (Fig. 8). Magnetic susceptibility can also be used to correlate between piston cores and trigger weight cores.

DISCUSSION

The magnetic susceptibility correlations document relative stratigraphic positions between cores, and have several applications, including evaluation of core recovery and establishment of a relative chronology. For example, comparison of 92-028-153P (a piston core) with 92-028-153T (the corresponding trigger weight core) suggests that the piston core missed only about 50 cm of the uppermost sediment section, or that the uppermost section was compressed in the piston core (Fig.5). Also, the magnetic susceptibility data show that core 92-028-153P sampled the upper 200 cm of sediment section that was not recovered (bypassed) by core 90-023-107 due to recovery problems with the large diameter AGC corer during the 1990 cruise. Furthermore, although 92-028-153P is slightly longer than 90-023-107, the magnetic susceptibility data indicate that the former lacks the lowermost 150 cm of section represented in the latter; the base of 90-023-107, therefore, should be older than the base of 92-028-153P.

Importantly, the magnetic susceptibility correlations can be used to quickly transfer downcore chronology from a dated core to an undated one. For instance, available radiocarbon dates in core 90-023-107 (Table 2; Fig. 5) can be readily

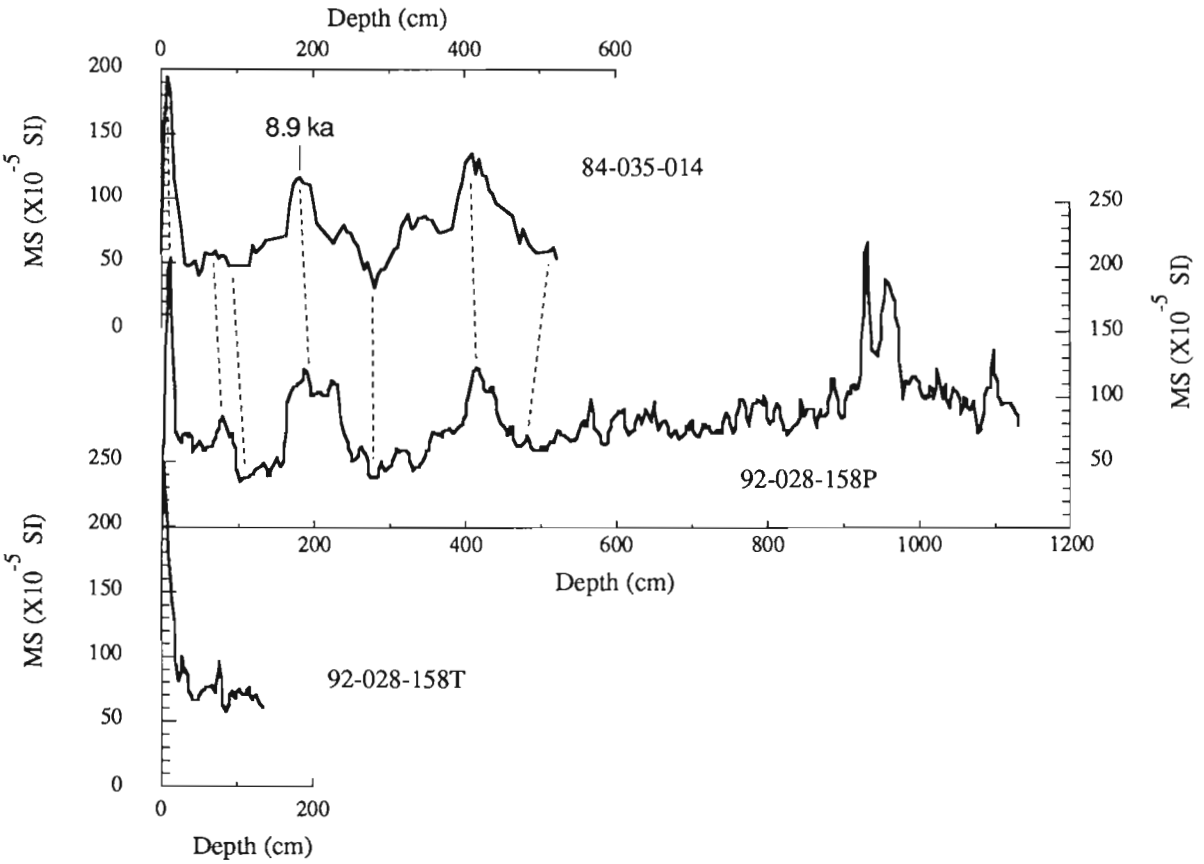

Figure 8. Magnetic susceptibility profiles of cores 92-028-158P, 92-028-158T, and 84-035-014 from Hatton Basin, east of the mouth of Hudson Strait. Also shown are tie lines and an accelerator mass spectrometry radiocarbon date. Site 84-035-014 lies 25.9 km from site 92-028-158.

correlated to levels in core 92-028-153P, assuming that the magnetic susceptibility changes are not time-transgressive over short distances. This indicates that sediment at a depth of about 420 cm in core 92-028-153P probably has an age of about 8.4 ka (thousands of years before present), and that the base of the core dates to about 9.0 - 9.2 ka.

Additional applications, including documentation of local stratigraphic variation and analysis of relative deposition rates, are illustrated by another pair of cores from south central Hudson Strait (Fig.6). The magnetic susceptibility plots indicate that core 92-028-155P lacks an interval correlative with the upper ca. 180 cm of low-magnetic susceptibility sediment at the top of core 90-023-064. Because 92-028-155P correlates well with its trigger weight counterpart, imperfect recovery of the uppermost section at the core site is unlikely, as is differential sediment compaction within the core. Instead, the comparison suggests that low-magnetic susceptibility sediment (postglacial sediment) thins over the span of 3.7 km from the 90-023-064 site to the 92-028-155P site – an observation supported by acoustic profile data. Also, correlations downcore suggest that glaciomarine sedimentation rates were slightly higher at the 90-023-064 site than at the 92-028-155P site. Note also that 92-028-155P captured about 4.5 m more section at its base than did 90-023-064.

Cores 92-028-157G and 90-023-045, about 0.4 km apart from the eastern basin of Hudson Strait, offer an example of uncertain magnetic susceptibility correlation (Fig. 7). The interval of unusually low magnetic susceptibility sediment near the base of 92-028-157G might correlate with the low magnetic susceptibility interval in core 90-023-045 at a depth of 610-690 cm. However, because the large diameter AGC corer used in 1990 may have by-passed the uppermost few metres of section at the core site, and because the gravity corer used in 1992 probably recovered the uppermost section at the site, the low magnetic susceptibility interval in core 92-028-157G may instead correlate with the low magnetic susceptibility pulse near the top of 90-023-045 (at a depth of 20-70 cm). Readily traceable reflectors in the seismic profile across the core sites (Fig. 4) indicate that variable local stratigraphy is unlikely. This hypothesis will be tested by comparison of other rock magnetic and mineralogical parameters, biostratigraphic markers and radiocarbon dates.

Cores 92-028-158P and 84-035-014 illustrate magnetic susceptibility correlation between sites in the Hatton Basin (Figs. 1, 8). Although there is some variation in detail, correlative stratigraphy is immediately apparent despite a separation of about 26 km. Also, the data show that core 92-028-158P contains about 6.4 m of section at its base that was not recovered in 84-035-014. Good correlation with the trigger weight core (92-028-158T) implies that both piston cores (92-028-158P and 84-035-014) captured the uppermost sediment section at each site.

Magnetic susceptibility correlation over long distances among the 1992 cores or among the 1990 cores will be tested later in concert with radiocarbon chronologies, biostratigraphic markers, lithostratigraphic changes, and statistical sequence analysis. However, preliminary visual correlation among cores from the Baie Héricart area (Figs. 5, 6), with additional constraints provided by radiocarbon chronologies (Table 2), suggests that core pairs 92-028-153/ 90-023-107 and 92-028-155/90-023-064 can be inter-correlated over the span of about 21 km that separates them. Tentative correlations are shown by arrows in Figures 5 and 6. For example, the level dated in core 90-023-107 at 8.4 ka (depth of 236 cm) may correlate with a depth of 890 cm in core 90-023-064 (430 cm below a date of 7.8 ka). Also, the level dated in core 90-023-107 at 9.0 ka (depth of 497-499 cm) may correlate with a depth of about 920 cm in core 92-028-155P.

The most important immediate use of the magnetic susceptibility data is to evaluate the success of meeting coring objectives in areas close to previously cored localities; i.e., the magnetic susceptibility correlations provide rapid assessment of the recovery of targeted stratigraphy - much more quickly, easily, and economically than could be assessed with other correlation methods. For example, the magnetic susceptibility data indicate that the uppermost sediment section near core 90-023-107, which was lost during the 1990 operation, was successfully recovered in 1992 as intended. Also, the correlations show that the 1992 cruise was more successful than the 1990 cruise near core site 90-023-064 in retrieving samples from lower in the sediment section, which should be a focus of investigations to reconstruct late-glacial and postglacial events. Similarly, the magnetic susceptibility correlations demonstrate that the 1992 cruise achieved its goal of obtaining a significantly longer record than was previously available of paleo-oceanographic conditions in Hatton Basin. Core 92- 028-158 appears to double the length of the high resolution record of late-glacial events apparent in core 84-035-014 (Evans, 1990).

Thus, magnetic susceptibility can be used to quickly determine relative stratigraphic positions and relative ages among closely spaced sediment cores. The magnetic susceptibility correlations permit analysis of core recovery, local stratigraphic variation, relative rates of deposition, downcore depositional histories (via transfer of radiocarbon chronologies) and completion of coring objectives. In this way, the magnetic susceptibility correlations can quickly guide other types of analyses by presenting testable hypotheses and tentative age assignments, and will help to reconstruct glacial and postglacial environments at the northeastern margin of the Laurentide Ice Sheet.

ACKNOWLEDGMENTS

We thank Captain F. H. Berchem, officers, and crew of **CSS Hudson**, A. Boyce, L. Johnson, R. Murphy, and K. Wagner of AGC, and M. Uyesugi of Geoforce for their excellent cooperation and support during Cruise 92-028. N. Weiner and W. Briggs (INSTAAR) conducted the magnetic susceptibility analyses during the 1990 cruise. N. Weiner and B. Deonarine (AGC) sampled and identified foraminifera for radiocarbon dates. We are grateful to G. Miller (INSTAAR)

and C.F.M. Lewis (AGC) for review of the manuscript. This study was partially funded by NSF grants EAR-9005179 and DPP-9122811.

REFERENCES

Andrews, J.T. and Jennings, A.E.
1987: Influence of sediment source and type on the magnetic susceptibility of fiord and shelf deposits, Baffin Island and Baffin Bay, N.W.T.; Canadian Journal of Earth Sciences, v. 24, p. 1386-1401.

Andrews, J.T. and Stravers, J.A.
in press: Magnetic susceptibility of late Quaternary marine sediments, Frobisher Bay, N.W.T.: An indicator of changes in provenance and processes; submitted to Quaternary Science Reviews.

Andrews, J.T. and Tedesco, K.
in press: Detrital carbonate-rich sediments, northwestern Labrador Sea: Implications for ice-sheet dynamics and iceberg rafting (Heinrich) events in the North Atlantic; Geology.

Andrews, J.T., Evans, L.W., Williams, K.M., Briggs, W.M., Jull, A.J.T., Erlenkeuser, H., and Hardy, I.
1990: Cryosphere/ocean interactions at the margin of the Laurentide ice sheet during the Younger Dryas Chron: SE Baffin Shelf, Northwest Territories; Paleoceanography, v.5, p. 921-935.

Andrews, J.T., Briggs, W.M., and Weiner, N.
1991: Rock and paleomagnetic studies of cored sediments during Hudson Cruise HU90-023 in Frobisher Bay, Ungava Bay, and Hudson Strait, Northwest Territories; in Current Research, Part E; Geological Survey of Canada, Paper 91-1E, p. 317-320.

Evans, L.W.
1990: Late Quaternary stratigraphy of the Hatton and Resolution Basins, southeast Baffin Island shelf, N.W.T., Canada; M.Sc. thesis; University of Colorado, Boulder, Colorado, 189 p.

Josenhans, H.W., Zevenhuizen, J., and Klassen, R.A.
1986: The Quaternary geology of the Labrador Shelf; Canadian Journal of Earth Sciences, v. 23, p. 1190 - 1213.

Lauriol, B. and Gray, J.T.
1987: The decay and disappearance of the Late Wisconsin ice sheet in the Ungava Peninsula, northern Quebec, Canada; Arctic and Alpine Research, v. 19, p. 109-126.

Laymon, C.A.
1992: Glacial geology of western Hudson Strait, Canada, with reference to Laurentide Ice Sheet dynamics; Geological Society of America Bulletin, v. 104, p. 1169-1177.

MacLean, B. and Vilks, G.
1992: New seismo-, bio, and chrono-stratigraphic data on Quaternary sediments in Hudson Strait and Ungava Bay; 22nd Arctic Workshop, University of Colorado, Boulder, Colorado, March, 1992, Program and Abstracts, p.95-97.

MacLean, B., Vilks, G., Aitken, A., Allen, V., Briggs, W., Bruneau, D., Doiron, A., Escamilla, M., Hardy, I., Miner, J., Mode, W., Powell, R., Retelle, M., Stravers, J., Taylor, A., and Weiner, N.
1991: Investigations of the Quaternary geology of Hudson Strait and Ungava Bay, Northwest Territories; in Current Research, Part E; Geological Survey of Canada, Paper 91-1E, p. 305-315.

MacLean, B., Vilks, G., and Deonarine, B.
in press: Depositional environments and history of late Quaternary sediments in Hudson Strait and Ungava Bay: further evidence from seismic and biostratigraphic data; Géographie Physique et Quaternaire.

Manley, W.F. and Kaufman, D.S.
1992: Late-glacial patterns of ice flow, glaciomarine sedimentation, and sea-level change near Lake Harbour, southernmost Baffin Island; 22nd Arctic Workshop, University of Colorado, Boulder, Colorado, Program and Abstracts, p. 98-100.

Miller, G.H. and Kaufman, D.S.
1990: Rapid fluctuations of the Laurentide ice sheet at the mouth of Hudson Strait: new evidence for ocean/ice-sheet interactions as a control on the Younger Dryas; Paleoceanography, v. 5, p.907-919.

Miller, G.H., Hearty, P.J., and Stravers, J.A.
1988: Ice-sheet dynamics and glacial history of southeasternmost Baffin Island and outermost Hudson Strait; Quaternary Research, v. 30, p. 116-136.

Praeg, D.B., MacLean, B., Hardy, I.A., Mudie, P.J.
1986: Quaternary geology of the southeast Baffin Island continental shelf; Geological Survey of Canada, Paper 85-14, 38 p.

Stravers, J.A.
1986: Glacial geology of outer Meta Incognita Peninsula, southern Baffin Island, Arctic Canada; Ph.D. dissertation, University of Colorado, Boulder, Colorado, 231 p.

Stravers, J.A., Miller, G.H., and Kaufman, D.S.
1992: Late glacial ice margins and deglacial chronology for Hudson Strait, eastern Canadian Arctic; Canadian Journal of Earth Sciences, v. 29, p. 1000-1017.

Thompson, R. and Oldfield, F.
1986: Environmental Magnetism; Allen & Unwin, Winchester, Mass., 219 p.

Vilks, G., MacLean, B., Deonarine, B., Currie, C.G., and Moran, K.
1989: Late Quaternary paleoceanography and sedimentary environments in Hudson Strait; Géographie Physique et Quaternaire, v. 43, p. 161-178.

Geological Survey of Canada Projects 760015 and 830045

Structural elements of the Magdalen Basin, Gulf of St. Lawrence, from seismic reflection data

P. Durling and F. Marillier
Atlantic Geoscience Centre, Dartmouth

Durling, P. and Marillier, F., 1993: Structural elements of the Magdalen Basin, Gulf of St. Lawrence, from seismic reflection data; in Current Research, Part D; Geological Survey of Canada, Paper 93-1D, p. 147-154.

Abstract: Maps of structural features, depth to basement, and depth to base Windsor Group show that the Late Devonian-Permian Magdalen Basin is more than 12 km deep, and the earliest sediments, the Horton Group, were deposited in numerous half-grabens. These grabens are bounded by faults that are generally parallel to pre-existing basement structures. These are offshore extensions of faults mapped in New Brunswick and Gaspésie. Near the deepest part of the basin, a unit of highly deformed rocks underlies strata affected by intense salt activity. A two stage development is interpreted for the Magdalen Basin. A Late Devonian-Early Carboniferous crustal extensional phase is indicated by the widespread distribution of the Horton Group half-grabens, followed by a crustal subsidence phase involving Windsor Group (Visean) and younger strata. A post-Windsor Group transpressional phase may have contributed to regional subsidence through crustal loading.

Résumé : Les cartes des éléments structuraux, de la profondeur du socle, et de la profondeur de la base du Groupe de Windsor montrent que la profondeur du bassin de la Madeleine (Dévonien tardif au Permien) est supérieure à 12 km, et que les sédiments les plus anciens, soit le Groupe de Horton, se sont accumulés dans de nombreux demi-grabens. Ces grabens sont bordés par des failles généralement parallèles à des structures pré-existantes du socle. Celles-ci forment le prolongement en mer de failles cartographiées au Nouveau Brunswick et en Gaspésie. Dans la région où le bassin atteint sa plus grande profondeur, une unité de roches très déformées est sous-jacente à des couches sédimentaires perturbées par des mouvements intenses salifères. Le dévelopement du bassin de la Madeleine s'est effectué en deux étapes. La large répartition des demi-grabens du Groupe de Horton témoigne d'une phase de distension crustale survenue entre le Dévonien tardif et le Carbonifère précoce; elle a été suivie d'une phase de subsidence crustale impliquant le Groupe de Windsor (Viséen) et les couches plus récentes. Une phase de transpression postérieure au Groupe de Winsdor a pu contribuer à la subsidence régionale par chargement de la croûte.

INTRODUCTION

The Magdalen Basin in the Gulf of St. Lawrence is the largest of several basins comprising the Maritimes Basin (Fig. 1), which developed from mid-Devonian to Permian time following the Acadian orogeny. The origin of this successor basin is still being debated, and our knowledge of its tectonic history remains sketchy. Nearly three quarters of the Maritimes Basin underlies the Gulf of St. Lawrence, yet most of the present geological knowledge base was gathered almost entirely from onshore areas which may not adequately represent the geology of the entire basin. A systematic study of the structural and stratigraphic data offshore is therefore an essential component of any synthesis addressing the tectonics of the whole basin.

In this paper we present a selection of preliminary results from a compilation and interpretation of seismic reflection profiles acquired in the Magdalen Basin, mainly by the oil industry. These data show the main faults and associated rift basins, and are used to help recognize the main tectonic events affecting the history of the Magdalen Basin. This work is a follow up of a previous study in the western part of the basin (Durling and Marillier, 1990).

STRATIGRAPHY AND SEISMIC DATA

The sediments of the Magdalen Basin are subdivided into the continental redbeds of the Horton Group (Middle Devonian to Early Visean), the mainly marine evaporite deposits of the Windsor Group (Middle Visean to Early Namurian), and the continental rocks of the Mabou, Cumberland, and Pictou groups (Namurian to Permian) (Ryan et al., 1991). The Early Carboniferous strata are locally associated with volcanism, with some of the youngest volcanics occurring in the Windsor Group in the Magdalen Islands (Barr et al., 1985).

The approximately 30 000 km of seismic reflection profiles used in this study (Fig. 2) come from industry data publicly released (5 to 6 seconds of two-way travel time or TWT) and from a deep seismic reflection survey (16 to 19 s TWT) in the Gulf of St. Lawrence (Marillier et al., 1989). The seismic reflection data were acquired between 1968 and 1986 and range widely in quality.

We systematically mapped two seismic horizons in the Magdalen Basin, the top of pre-Acadian basement (base of the Horton Group) and the base of the Windsor Group. Stratigraphy was controlled where possible by ties to wells (Fig. 3). In order to display the mapped horizons digitally, the

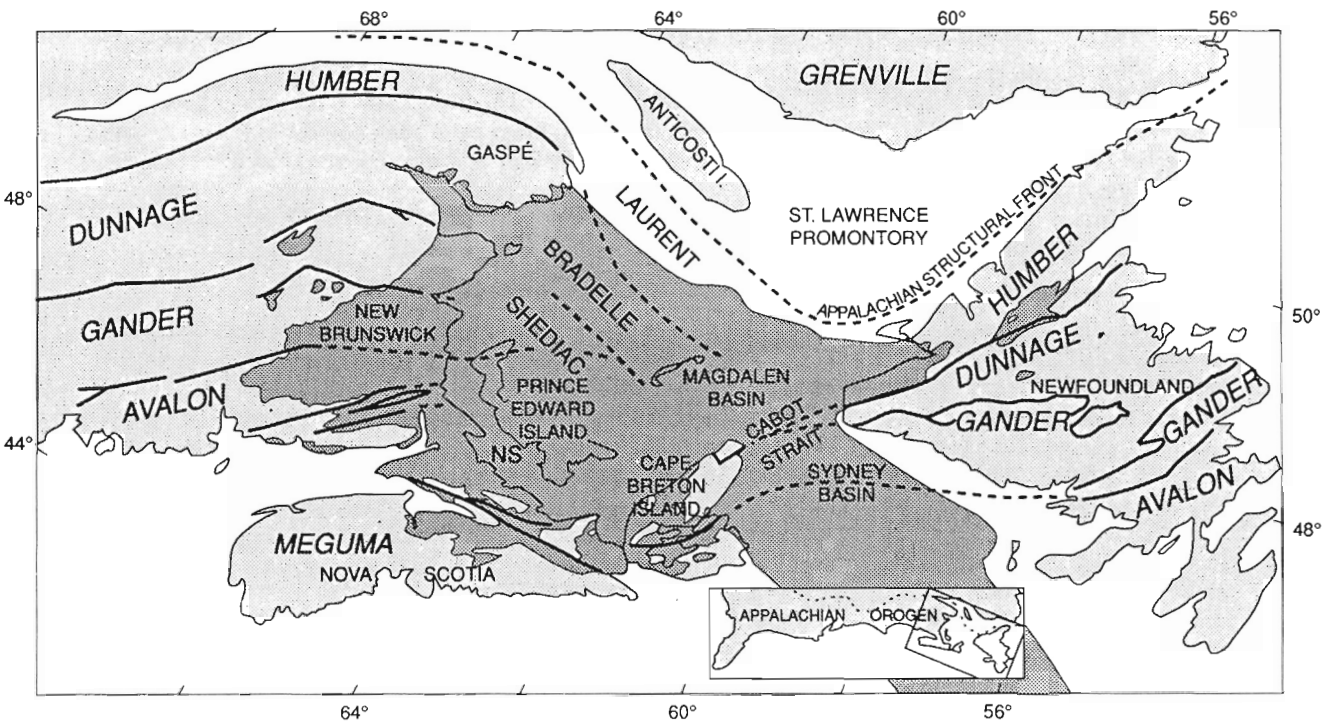

Figure 1. Location map with main geological elements in the northern Appalachians with tectonostratigraphic zones on land and upper crustal blocks offshore. The stippled area denotes the Maritimes Basin. NS – Northumberland Strait.

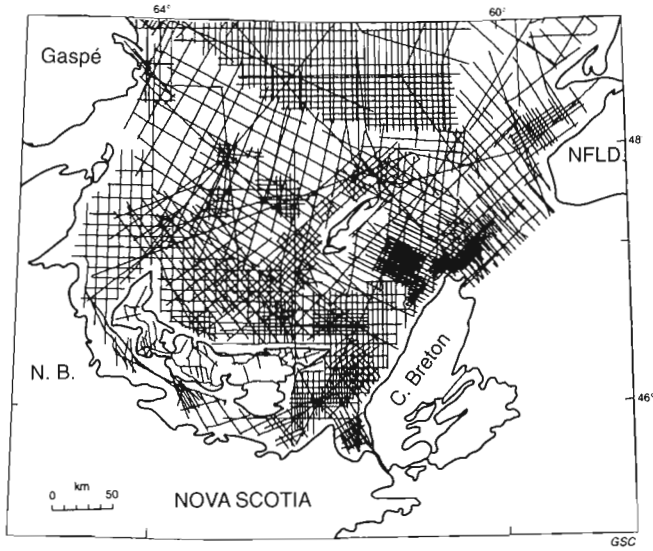

Figure 2.

Seismic reflection profiles in the Gulf of St. Lawrence.

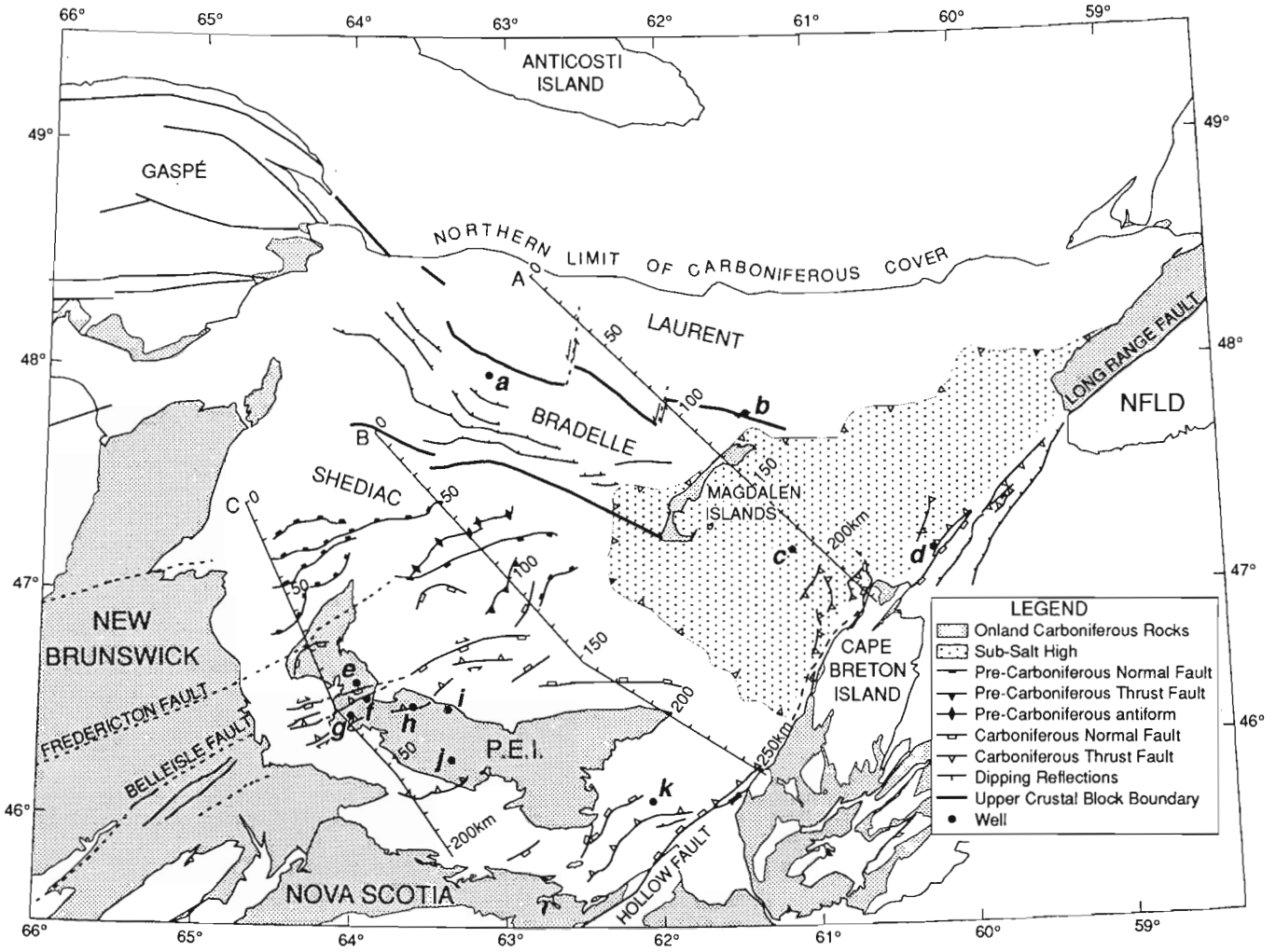

Figure 3. Major structural elements in the Magdalen Basin. This figure only shows the main features, many details have been removed for sake of clarity. Note the offshore continuation of faults in New Brunswick and Gaspésie. A, B, and C - cross-sections shown in Figure 4. Lower case letters refer to wells used in this study: a-Bradelle L-49, b-Brion Island No. 1, c-Cap Rouge F-52, d-St. Paul P-91, e-Porthill No. 1, f-McDougall No. 1, g-Wellington No. 1, h-Irishtown No. 1, i-Greengables No. 1, j-Tyrone No. 1, and k-Northumberland Strait F-25.

seismic data were digitized at inflection points on each horizon, interpolated at an interval of 1 km and subjected to gridding and contouring programs. Two-way travel times were converted to depth using an average velocity function computed from 43 seismic refraction profiles distributed over the entire basin.

STRUCTURAL ELEMENTS OF THE MAGDALEN BASIN

Major faults affecting basement or the immediately overlying sediments were mapped throughout the Magdalen Basin (Fig. 3). The fault systems in the Bradelle and Shediac upper crustal blocks (Durling and Marillier, 1990) are parallel to the major faults and gravity and magnetic anomalies in Gaspésie and in New Brunswick respectively. Apparent normal and reverse movements are interpreted along the faults, and strike-slip motion is inferred where flower structures are recognized (Reading, 1980). However, strike-slip faults are typically difficult to recognize on seismic profiles, and therefore it is possible that they are under represented in Figures 3 and 4. The contrasting trends of the faults in the two basement blocks (northwest-southeast in Bradelle, northeast-southwest in Shediac) suggest that the blocks underwent different tectonic histories. The boundary between them represents a major break in the upper crust (Durling and Marillier, 1990) and may correspond to the proposed "Canso Fault" (Barr and Reaside, 1986; McCutcheon and Robinson, 1987; Stockmal et al., 1990).

In the Shediac block, northeast-striking faults display throws of up to 7 km (Fig. 4c). Several of these faults controlled the deposition of Horton Group sediments in half-graben subbasins. There is also evidence for half-graben development in the Bradelle block. In the vicinity of Prince Edward Island reflection patterns typical of positive flower structures are interpreted as faults affecting Horton and Windsor Group strata. Such structures are characteristic of transpressional strike-slip environments (Reading, 1980). These subbasins and the style of deformation extend towards New Brunswick, where similar movements with comparable amplitude are inferred (Webb, 1963); to the northeast, Horton Group subbasins shallow and deformation diminishes (Fig. 4b). Transpression does not appear to have significantly changed the overall geometry of the Horton subbasins, and their present elongated shape is probably not much different from their original shape.

East of the Magdalen Islands, features characteristic of the Bradelle and Shediac basement blocks cannot be mapped either because the seismic data do not show any basement features or because basement is too deep to be observed on the seismic sections, i.e. it is located beyond 6 seconds two-way travel time. In a triangular area between the Magdalen Islands, Cape Breton Island, and the southwestern tip of Newfoundland, Windsor and younger sediments are underlain by a unit termed the sub-salt high (Fig. 3). This unit is roughly dome shaped; a cross-section of the sub-salt high is shown in Figure 4a.

The sub-salt high has a complex structure revealed by generally poorly defined seismic reflections with highly variable dips in many places. However, the geometry of some

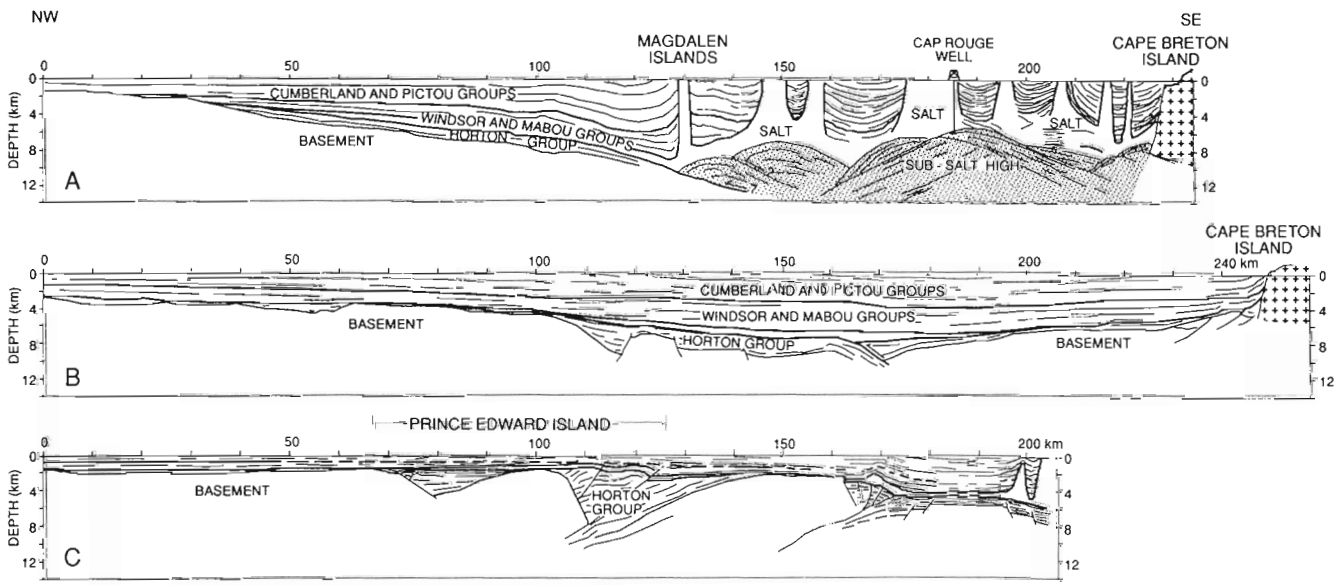

Figure 4. Cross-sections through the Magdalen Basin based on seismic profiles converted to depth. Vertical exaggeration is approximately X 1.8. Several different tectonic styles are illustrated in this figure: formation of salt diapiric structures possibly associated with movements in the sub-salt high (**A**), deposition of Horton Group sediments coeval with basement faulting and formation of half-graben subbasins (**B** and **C**); flat sedimentary bedding of the Windsor and younger groups indicating general crustal subsidence (**B**), and finally positive flower structures suggesting transpressional movements (**C**).

reflections suggest the presence of thrust faults (Fig. 4a). Windsor Group salt above the rugged top of the sub-salt high is intensely deformed and displays penetrative diapiric structures of considerable height and width. In areas outside the sub-salt high, salt generally occurs as bedded salt or is gently deformed into pillows, suggesting that intense salt diapirism and the formation of the sub-salt high are related. In places near the edge of the sub-salt high, the attitude of the Horton Group beds suggest that they may extend beneath this structure. The nature of the rocks within the sub-salt high cannot be inferred from seismic data. The Cap Rouge well reached the top of the sub-salt high and samples taken at the well bottom, beneath a section of Horton Group rocks, were interpreted as volcanics of Mississippian age (Shell Canada Limited, 1973) or Pre-Cambrian age (Canadian Stratigraphic Service Limited, Shell-Amoco Cap Rouge F-52, Log No. E-70). If the volcanics are Mississippian, they are probably associated with an extensional phase prior to the development of the high.

In the Cabot Strait, between Newfoundland and Cape Breton Island, the sediments are thinner than in the central part of the basin, and a complex northeast-striking fault system affects both basement and sediments. The faults are interpreted as offshore extensions of faults in southwest Newfoundland and particularly the Long Range Fault. This fault was active during deposition of the Anguille (Horton) Group through to post-Westphalian times (Knight, 1983) with possible strike-slip movement. However, east-west faults truncating the northeast striking features, and therefore postdating them, have also been observed in this area (G. Langdon, pers. comm., 1992). Along the coast of western Cape Breton Island a series of faults with the same northeast strike are observed (Fig. 3, 4a, and 4b). We interpret them as the offshore extension of the Hollow Fault. More work is still necessary because of the complexity of the structure in this area.

NEW MAPS OF DEPTH TO BASEMENT AND DEPTH TO BASE WINDSOR GROUP

The depth to basement map (Fig. 5) shows the base of the Horton Group which in most places lies on metamorphic basement of the Acadian Orogen. Metamorphic basement rocks were drilled in the Porthill No. 1 and the Northumberland Strait F-25 wells (for location see Fig. 3), and they typically correspond to areas on the seismic reflection profiles that displayed chaotic reflections, steeply dipping reflections or no reflections (acoustic basement) beneath the Carboniferous strata. The sediment-basement interface commonly corresponds to a change in reflection character rather than a distinct reflection, and therefore it is occasionally

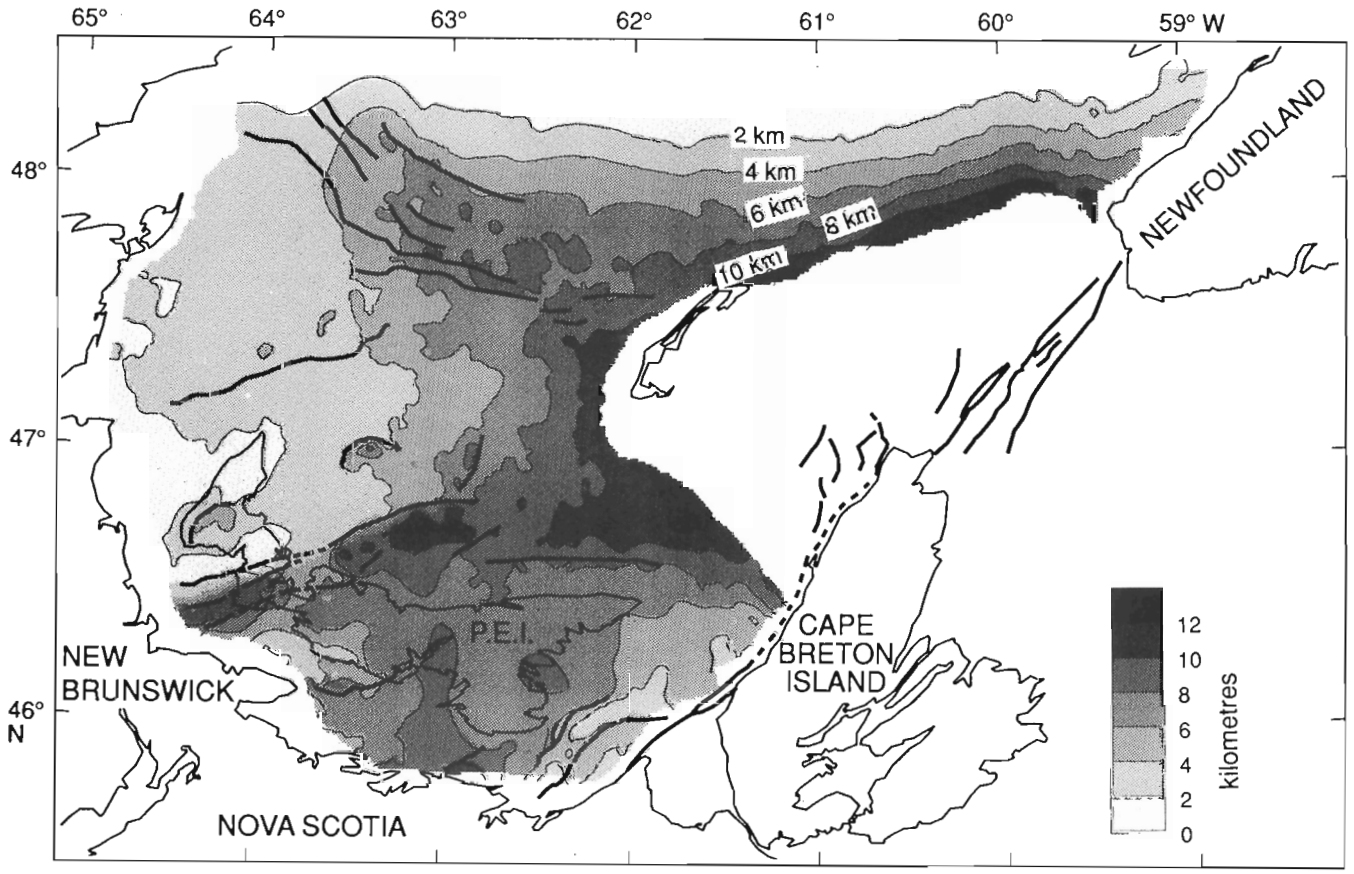

Figure 5. Depth to pre-Horton Group basement map in the Magdalen Basin. Major faults affecting basement are shown, emphasizing the X pattern they form.

difficult to locate accurately. In a few places, reflections indicating sedimentary stratification beneath reflections typical of Horton Group strata are observed. These reflections were interpreted as older sediments and, for consistency, were not differentiated from the metamorphic basement.

This new depth to basement map reveals considerably more details than previously published maps (Wade et al., 1977; Bell and Howie, 1990). Basement generally coincides with the base of the Horton Group while the base Windsor Group map (Fig. 6) generally indicates the top of the Horton Group. Thus, comparison of the two maps gives an indication of the distribution of the Horton Group subbasins, most of which are bounded by faults as shown in Figure 3 (see also Durling and Marillier, 1990). Widespread distribution of Horton Group subbasins in the Magdalen Basin is suggested, indicating that these basins developed during regional extension. The long axis of the main Horton Group subbasins and their bounding faults are more or less parallel to the branches of a prominent X-pattern which is outlined by the depth contours and centred near the Magdalen Islands. Transtensional rift environments commonly develop synthetic and antithetic strike-slip faults at specific angles to each other (see e.g. Sylvester, 1988), and the X-pattern displayed in the depth to basement map resembles the fault patterns observed in strike-slip regimes. However, the branches of the 'X' are parallel to the trends of the structures in the Bradelle and Shediac upper crustal blocks (Fig. 3), and since both dip-slip and strike-slip faults commonly develop parallel to structural grain, orthogonal and transtensional rift models may explain these observations equally well. Strike- slip faults are recognized along the Belleisle Fault and in the Cabot Strait area but several other basins occur where strike- slip faults are not recognized.

The base of the Windsor Group is represented by a distinctive, high amplitude continuous reflection on the seismic profiles that corresponds to the base of a regional marine evaporite unit. This unit is present over most of the Magdalen Basin but is absent northwest of the Belleisle Fault on the extension of the New Brunswick platform. In this area the base Windsor Group depth map (Fig. 6) corresponds to the top of a sequence of rocks that we interpreted as Horton Group on the basis of seismic character.

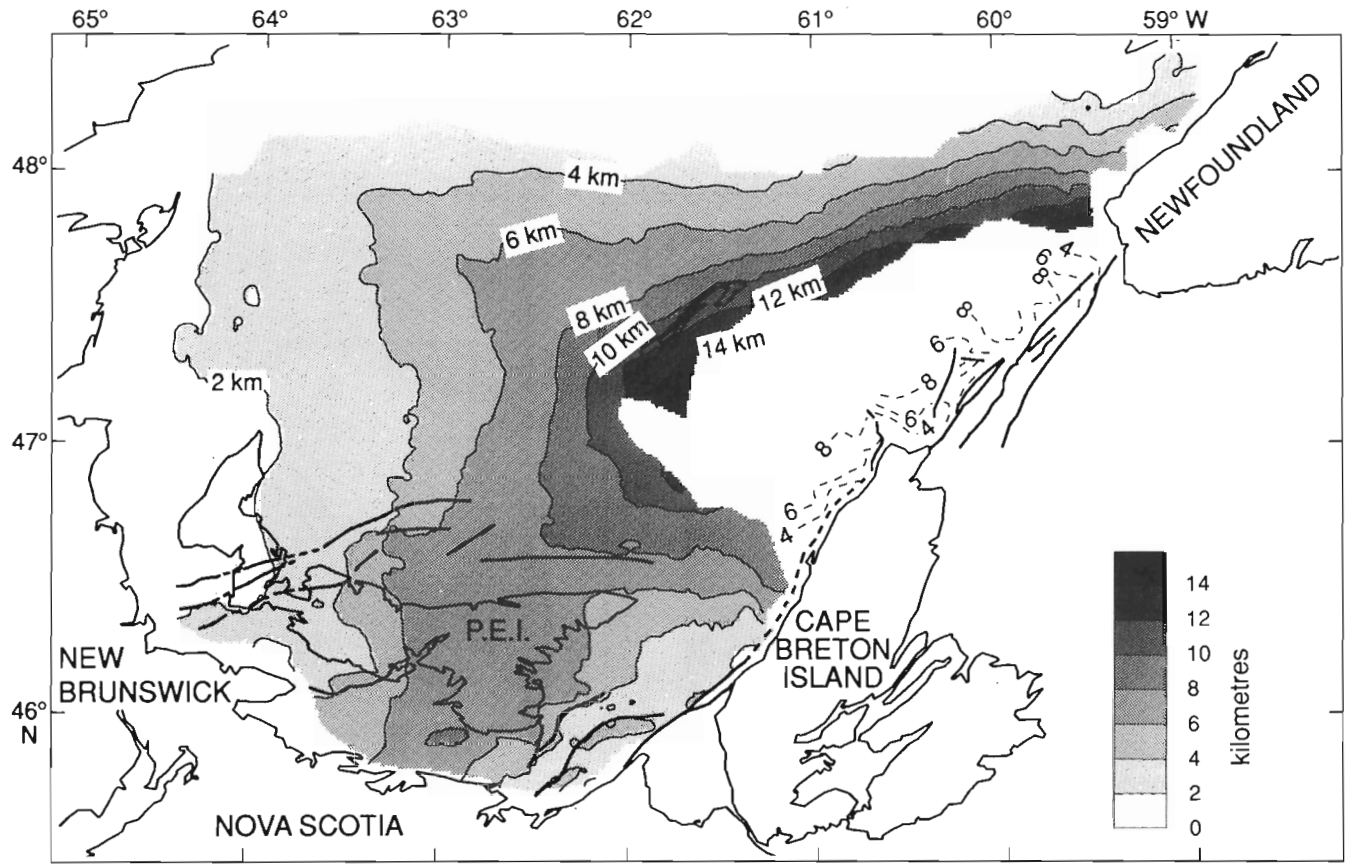

Figure 6. Depth to base Windsor Group map in the Magdalen Basin. Major faults affecting the Windsor Group are shown. The smoothness of the depth contours emphasizes the general subsidence of the entire area. Dashed contours represent approximate depth.

The depth to base Windsor Group map (Fig. 6) deepens like the basement towards the sub-salt high, peripheral to which a strong gradient occurs. The map shows depths of 12 km adjacent to the sub-salt high and demonstrates that the thickest accumulation of sediments in the Magdalen basin occurred after deposition of the Horton Group. This is illustrated in Figure 4B, where Horton Group rocks, deposited locally in deep grabens and half-grabens and elsewhere as a thin veneer, are overlain by much thicker younger Carboniferous and Permian strata. Howie and Barss (1975) suggested the inverse, where the Horton Group was deposited regionally as a thick sequence of rocks, locally interrupted by basement horsts. The fact that the base Windsor Group is much smoother than basement and the absence of evidence for steeply dipping extensional faults within these strata indicates that the rifting phase associated with Horton Group deposition was essentially over by the time the Windsor Group was deposited. The rocks from the Horton Group are interpreted as syn-rift sediments whereas Windsor Group and younger rocks correspond to a post-rift phase.

The base Windsor Group horizon dips toward the sub-salt high the same way a blanket suspended by its corners would dip toward a weight placed on the blanket. However, transpression along the offshore extension of the Belleisle Fault and in the Cabot Strait between Cape Breton and Newfoundland (G. Langdon, pers. comm., 1992) indicates a basin inversion phase postdating Windsor Group deposition. These observations may be interpreted in the context of a regional post-Windsor Group transpressional regime, whereby the sub-salt high underthrust the Windsor Group sediments, and its load contributed to regional subsidence. A post-Windsor Group thrust model may be used to explain the presence of Mississippian or older volcanics occurring on a high. The deformations indicated by our data may be related to Late Carboniferous thrust faulting documented along the south coast of New Brunswick (Nance, 1987).

CONCLUSION

The history of the Magdalen Basin appears to be related to a Late Devonian-Early Carboniferous extensional phase, associated with the formation of Horton Group subbasins and related volcanics, and a post-rift thermal subsidence phase. Subsidence may have been controlled, inpart, by crustal loading through transpressional tectonics.

Models invoking large strike-slip displacements and the development of pull-apart basins are an attractive way to accommodate both extensional and compressional structures in a sedimentary basin (i.e. Bradley, 1982). However, our data suggests that strike-slip tectonics is not a necessary (although it is a possible) mechanism to produce the distribution and orientation of the Horton Group grabens and half-grabens observed. The presence of inverted Horton Group basins and large deformed areas like the sub-salt high are structural complications that may hold the key to a better understanding of the sequence of events that controlled the development of the Magdalen Basin.

ACKNOWLEDGMENTS

We thank Bill Kay, and especially Claudia Currie for their assistance while digitizing the seismic horizons. The use of Art Jackson's software to condition the digital data is gratefully acknowledged. Gridding and contouring programs of the Potential Field Group, Atlantic Geoscience Centre, were used to produce the digital maps. The figures were drafted by K. Hale. The manuscript was substantially improved by the critical reviews provided by P.S. Giles and D.J.W. Piper.

REFERENCES

Barr, S.M. and Raeside, R.P.
1986: Pre-Carboniferous subdivisions of Cape Breton Island, Nova Scotia; Maritime Sediments and Atlantic Geology, v. 22, p. 252-263.

Barr, S.M., Brisbois, D., and MacDonald, A.S.
1985: Carboniferous volcanic rocks of the Magdalen Islands, Gulf of St. Lawrence; Canadian Journal of Earth Sciences, v. 22, p. 1679-1688.

Bell, J.S. and Howie, R.D.
1990: Paleozoic geology; Chapter 4 in Geology of the Continental Margin of Eastern Canada, (ed.) M.J. Keen and G.L. Williams; Geological Survey of Canada, Geology of Canada, no. 2, p. 141-165.

Bradley, D.C.
1982: Subsidence in Late Paleozoic basins in the northern Appalachians; Tectonics, v. 1, p. 107-123.

Durling, P. and Marillier, F.
1990: Structural trends and basement rock subdivisions in the western Gulf of St. Lawrence, Northern Appalachians; Atlantic Geology, v. 26, p. 79-95.

Howie, R.D. and Barss, M.
1975: Upper Paleozoic Rocks of the Atlantic provinces, Gulf of St. Lawrence and adjacent continental shelf; in Offshore Geology of Eastern Canada, Vol. 2, Regional Geology, (ed.) W.J.M. Van der Linden and J.A. Wade; Geological Survey of Canada, Paper 74-30, v. 2, p. 35-50.

Knight, I.
1983: Geology of the Carboniferous Bay St. George subbasin, western Newfoundland; Mineral Development Division, Department of Mines and Energy, Government of Newfoundland and Labrador, Memoir 1, 358 p.

McCutcheon, S.R. and Robinson, P.T.
1987: Geological constraints on the genesis of the Maritimes basin, Atlantic Canada; in Sedimentary basins and basin-forming mechanisms, (ed.) C. Beaumont, and A.J. Tankard; Canadian Society of Petroleum Geologists, Memoir v. 12, p. 287-297.

Marillier, F., Keen, C.E., Stockmal, G.S., Quinlan, G., Williams, H., Colman-Sadd, S.P., and O'Brien, S.J.
1989: Crustal structure and surface zonation of the Canadian Appalachians: implications of deep seismic data; Canadian Journal of Earth Sciences, v. 26, p. 305-321.

Nance, R.D.
1987: Dextral transpression and Late Carboniferous sedimentation in the Fundy coastal zone of southern New Brunswick; in Sedimentary basins and basin-forming mechanisms, (ed.) C. Beaumont, and A.J. Tankard; Canadian Society of Petroleum Geologists, Memoir v. 12, p. 363-377.

Reading, H.G.
1980: Characteristics and recognition of strike-slip fault systems; in Sedimentation in Oblique-slip Mobile Zones, (ed.) P.F. Ballance and H.G. Reading; Special Publication of the International Association of Sedimentologists, v. 4, p. 7-26.

Ryan, R.J., Boehner, R.C., and Calder, J.H.
1991: Lithostratigraphic revisions of the upper Carboniferous to lower Permian strata in the Cumberland Basin, Nova Scotia and the regional implications of the Maritimes Basin in Atlantic Canada; Bulletin of Canadian Petroleum Geology, v. 4, p. 289-314.

Shell Canada Limited
1973: Cap Rouge F-52: Well History Report by Shell — Amoco; Canada Oil and Gas Lands Administration, Department of Energy Mines and Resources, Canada.

Stockmal, G.S., Colman-Sadd, S.P., Keen, C.E., Marillier, F., O'Brien, S.J., and Quinlan, G.M.
1990: Deep seismic structure and plate tectonic evolution of the Canadian Appalachians; Tectonics, v. 9, p. 45-62.

Sylvester, A.G.
1988: Strike-slip faults; Geological Society of America Bulletin, v. 100, p. 1666-1703.

Wade, J.A., Grant, A.C., Sanford, B.V., and Barss, M.S.
1977: Basement structure, Eastern Canada and adjacent areas; Geological Survey of Canada, Map 1400A.

Webb, G.W.
1963: Occurrence and exploration significance of strike-slip faults in southern New Brunswick, Canada; Bulletin of the American Association of Petroleum Geologists, v. 47, p. 1904-1927.

Geological Survey of Canada Projects 880032 and 920062

Étude structurale et métamorphique des roches cambro-ordoviciennes du groupe de Shickshock, Gaspésie septentrionale, Québec

G.E. Camiré, M. Malo[1], et A. Tremblay[1]
Centre géoscientifique de Québec, Sainte-Foy

Camiré, G.E., Malo, M., et Tremblay, A., 1993: Étude structurale et métamorphique des roches cambro-ordoviciennes du groupe de Shickshock, Gaspésie septentrionale, Québec; dans Recherches en cours, Partie D; Commission géologique du Canada, Étude 93-1D, p. 155-160.

Résumé : Situées en Gaspésie septentrionale (Québec), les roches cambro-ordoviciennes du groupe de Shickshock forment une unité structurale distincte à l'intérieur du domaine interne taconien de la chaîne appalachienne, où elles sont principalement confinées à la nappe du mont Logan. Les roches volcaniques mafiques et les roches sédimentaires du groupe de Shickshock ont été régionalement métamorphisées aux faciès des schistes verts et des amphibolites au cours de l'orogénèse taconienne à l'Ordovicien moyen. Le métamorphisme augmente du nord vers le sud, où apparaissent des paragénèses à muscovite+biotite ± grenat ±staurotide±sillimanite±chlorite dans les lits pélitiques. Les travaux préliminaires révèlent également que la linéation d'allongement contenue dans le plan de la schistosité principale (S_1), de direction générale est-nord-est-ouest-sud-ouest, est faiblement plongeante et sub-parallèle à la chaîne appalachienne. Ce trait particulier semble indiquer, à priori, que le métamorphisme régional a pu être associé à la mise en place de nappes dans un régime de déformation transpressive.

Abstract: The Cambro-Ordovician Shickshock Group, located in northern Gaspésie, is a distinct structural unit of the Taconian internal domain of the Appalachians, where it is mainly confined to the Logan Nappe. Mafic volcanic and sedimentary rocks of the Shickshock Group have been regionally metamorphosed to amphibolite and greenschist grades during the Taconian orogeny in the Middle Ordovician. Metamorphism increases from north to south, where newly recognized biotite+muscovite± garnet±staurolite±sillimanite parageneses have been locally observed in thin metapelitic beds. Preliminary work has also shown that the main shistosity (S_1), which strikes east-northeast-west-southwest, contains a gently plunging elongation lineation, more-or-less parallel to the Appalachian Belt. This suggests that regional metamorphism may have been related to the emplacement of nappes in a transpressive regime of deformation.

[1] INRS - Géoressources, 2700 rue Einstein, C.P. 7500, Sainte-Foy (Québec) G1V 4C7

INTRODUCTION

Les terrains cambro-ordoviciens de la péninsule gaspésienne appartiennent au supergroupe de Québec et sont subdivisés en trois domaines tectoniques qui sont, du nord-ouest au sud-est : le domaine des failles de chevauchement imbriquées, le domaine des nappes externes et le domaine des nappes internes (St-Julien et Hubert, 1975) (fig. 1). Ils ont été déformés au cours de l'orogénèse taconienne (Ordovicien moyen à tardif) et aussi, à un degré moindre au cours de l'orogénèse acadienne (Dévonien moyen à tardif). Le domaine interne taconien comprend la nappe du mont Albert (mont Albert et amphibolite du Diable) et celle du mont Logan, à laquelle sont confinées, en grande partie, les roches du groupe de Shickshock (Hadrynien? à Cambrien précoce?; Slivitzky et al., 1991).

Au sud, le groupe de Shickshock est limité par la faille de Shickshock-Sud qui le sépare des strates siluriennes du synclinorium de Gaspé-Connecticut Valley (fig. 1). La faille de Shickshock-Sud est interprétée comme une faille acadienne de décrochement dextre (Berger, 1985; Lebel, 1985), superposée à la ligne Baie Verte -Brompton (Malo et al., 1992), une importante suture continent-océan formée au cours de l'orogénèse taconienne (Williams et St-Julien, 1982). Cette suture aurait été réactivée par des failles de décrochement au cours de l'orogénèse acadienne dans cette partie de la Gaspésie (Malo et al., 1992). Au nord, on considère que les roches du groupe de Shickshock chevauchent les roches sédimentaires ordoviciennes des formations de l'Orignal et de Romieu (domaine des nappes externes) le long de la faille du lac Cascapédia (e.g. Beaudin, 1980; Slitvizky et al.,1991) (fig. 2) et qu'elles sont elles-mêmes chevauchées par la nappe ophiolitique du mont Albert (fig. 2) (e.g. Laurent, 1977; Gagnon et Jamieson, 1985).

Les roches volcaniques mafiques et les roches sédimentaires du groupe de Shickshock sont été régionalement métamorphisées aux faciès des schistes verts et des amphibolites au cours de l'orogénèse taconienne (e.g. Mattinson, 1964; St-Julien et al., 1990). Bien que leur degré de métamorphisme contraste nettement avec celui des roches siluriennes et ordoviciennes environnantes (St-Julien et al., 1990), les roches du groupe de Shickshock n'ont, jusqu'à présent, fait l'objet d'aucune étude métamorphique approfondie. Au cours de l'été 1992, des travaux visant à retracer l'évolution structurale et métamorphique des roches du groupe de Shickshock lors de l'orogénèse taconienne ont donc été entrepris. Pour ce faire, des coupes structurales de direction générale nord-ouest-sud-est recoupant le grain tectonique et un échantillonnage serré ont été effectués dans la partie centrale du groupe de Shickshock (fig. 3), le long des rivières du Cap-Chat et du Cap-Chat-Est, des ruisseaux Go-Ashore, Wilson, Aumay, Bascon, Bricault, Paris et Bouynot ainsi que le long du lac Matane.

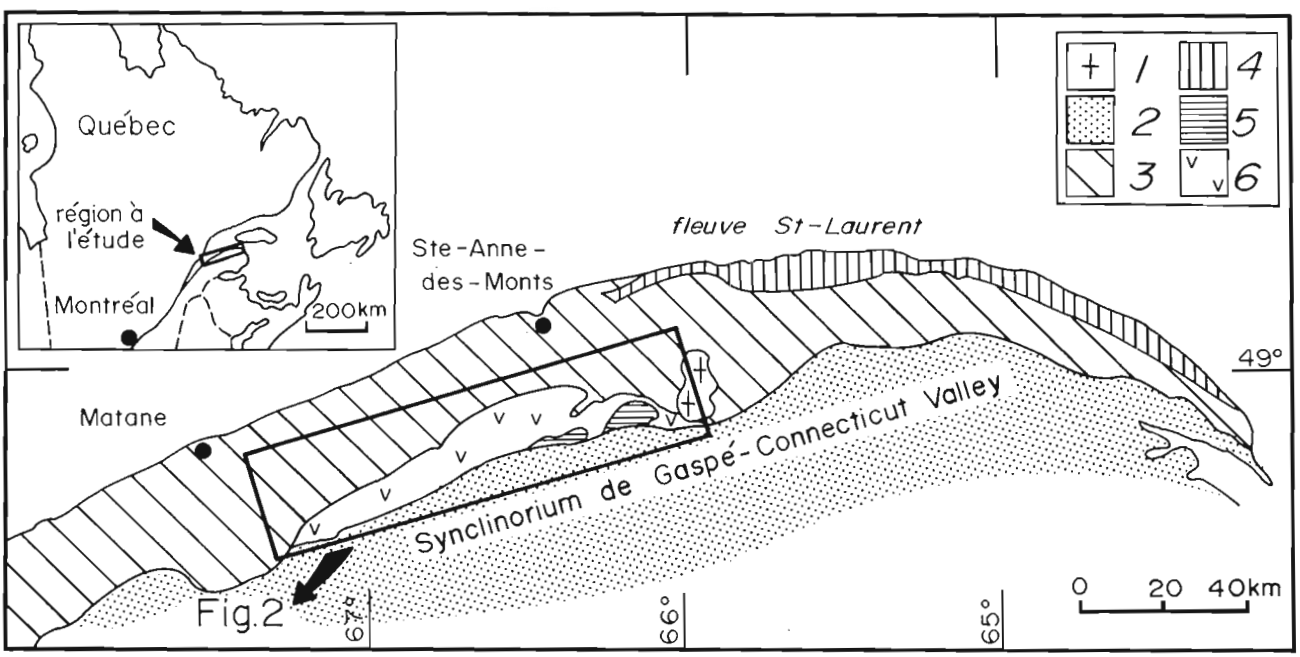

Figure 1. Carte géologique simplifiée des unités tectono-stratigraphiques de la Gaspésie septentrionale (modifiée de Slivitzky et al., 1991). Silurien et Dévonien: 1 = roches intrusives; 2 = roches sédimentaires et volcaniques du synclinorium de Gaspé - Connecticut Valley. Cambrien et Ordovicien: 3 = domaine des nappes externes (roches sédimentaires et mélanges); 4 = domaine des failles de chevauchement imbriquées (roches sédimentaires); domaine des nappes internes, 5 = nappe du mont Albert (roches ultramafiques du mont Albert et amphibolite du Diable), 6 = nappe du mont Logan (roches métavolcaniques et métasédimentaires du groupe de Shickshock).

TRAVAUX ANTÉRIEURS

Des cartes géologiques partielles du groupe de Shickshock ont été réalisées par Dresser et Dennis (1944), Osborne et Archambault (1948), MacGregor (1962, 1964), Girard (1967), Ollerenshaw (1967), Aumento (1969), Carrara (1972) et Beaudin (1980, 1984). Les travaux les plus détaillés demeurent ceux de Mattinson (1964), d'Ollerenshaw (1967) et de Beaudin (1980, 1984) qui subdivisèrent le groupe de Shickshock en unités lithologiques informelles. La limite sud du groupe de Shickshock, la faille de Shickshock-Sud, a également fait l'objet de levés structuraux récents par Lebel (1985) et Berger (1985). Une description succinte de la structure, de la pétrologie et de la géochimie des roches du groupe de Shickshock a été réalisée par St-Julien et al. (1990) et reprise par Slivitzky et al. (1991) dans le cadre de leur synthèse géologique du cambro-ordovicien du nord de la Gaspésie.

LITHOLOGIES DU GROUPE DE SHICKSHOCK

Le groupe de Shickshock est principalement constitué d'un empilement monotone de roches métavolcaniques mafiques, par endroits coussinées et amygdalaires, rarement bréchiformes ou tuffacées, et injectées de filons-couches métagabbroïques de quelques mètres d'épaisseur. La

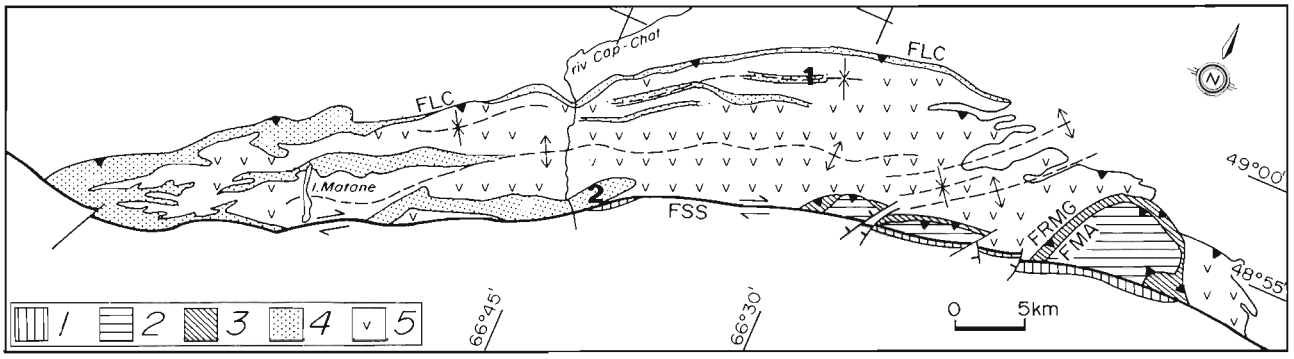

Figure 2. Carte géologique simplifiée illustrant la répartition des nappes constituant le domaine des nappes internes en Gaspésie septentrionale (modifiée de Slivitzky et al., 1991). 1 = brèche de Shickshock-Sud. Nappe du mont Albert: 2 = roches ultramafiques du mont Albert, et 3 = amphibolite du Diable. Nappe du mont Logan, groupe de Shickshock: 4 = roches métasédimentaires, et 5 = roches métavolcaniques. FLC = faille du lac Cascapédia; FMA = faille du mont Albert; FRMG = faille du ruisseau des Marches du Géant; FSS = faille de Shickshock-Sud. Les numéros en caractère gras correspondent à des localités décrites dans le texte.

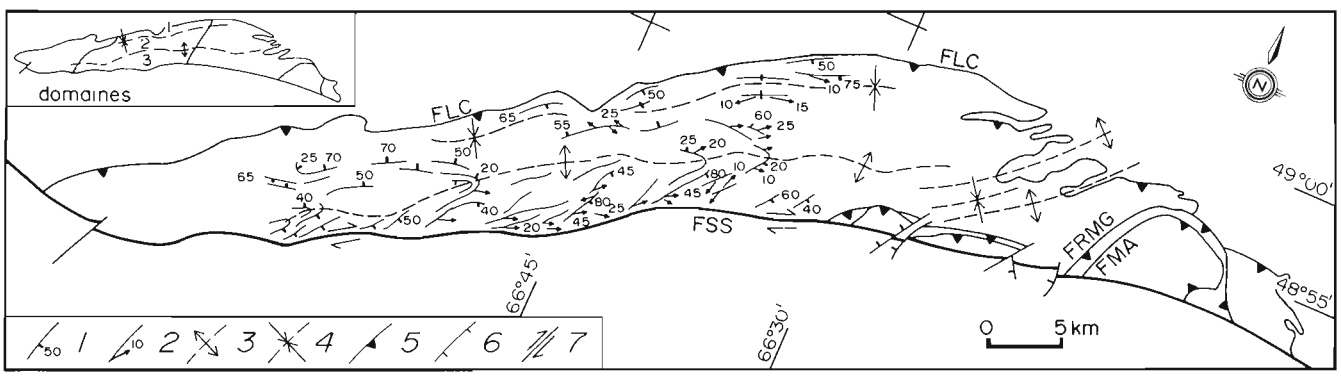

Figure 3. Trajectoires de la schistosité régionale S_1 et de la linéation d'allongement (d'étirement et minérale, L_1), groupe de Shickshock (nappe du mont Logan). À noter que seule la partie centrale du groupe de Shickshock a été couverte par le présent levé. 1 = trajectoire et pendage de la S_1; 2 = direction et pendage de la linéation L_1 contenue dans le plan S_1; 3 = antiforme; 4 = synforme; 5 = faille de chevauchement; 6 = faille normale; 7 = faille de décrochement dextre. FLC = faille du lac Cascapédia; FMA = faille du mont Albert; FRMG = faille du ruisseau des Marches du Géant; FSS = faille de Shickshock-Sud. La localisation des domaines structuraux (1, 2 et 3) et la zone couverte par le présent rapport sont indiquées sur la figure en cartouche. Les domaines sont délimités par les traces axiales des plis régionaux (synforme et antiforme) qui affectent le groupe de Shickshock.

séquence est intercalée de minces horizons de roches métasédimentaires (fig. 2): des métaarkoses, des métasiltstones, des métapélites et, par endroits, des métaconglomérats. La présence exceptionnelle de métacalcaires, le long du ruisseau Bascon, a de plus été rapportée par Mattinson (1964). Les roches métasédimentaires affleurent sporadiquement et elles ne constituent pas de bons horizons marqueurs. Les roches métasédimentaires, qui composent chacune des bandes apparaissant sur la figure 2, se présentent sous des aspects variés, autant par leurs compositions, leurs assemblages minéralogiques et leurs déformations internes que par leurs relations structurales avec les roches métavolcaniques environnantes. Les contacts entre les roches métavolcaniques et les métaarkoses et métasiltstones sont le plus souvent concordants. Cependant la plupart des horizons métapélitiques observés étaient juxtaposés aux roches métavolcaniques le long de zones de cisaillement syn- à tardimétamorphiques.

GÉOLOGIE STRUCTURALE

Quatre phases de plissement sont observées au sein des roches cambro-ordoviciennes de la Gaspésie septentrionale; les deux premières sont attribuées à l'orogénèse taconienne et les deux autres à l'orogénèse acadienne (e.g. Carrara et Fyson, 1973; Slivitzky et al., 1991). Les roches du groupe de Shickshock ont été affectées par au moins trois de ces phases de plissement.

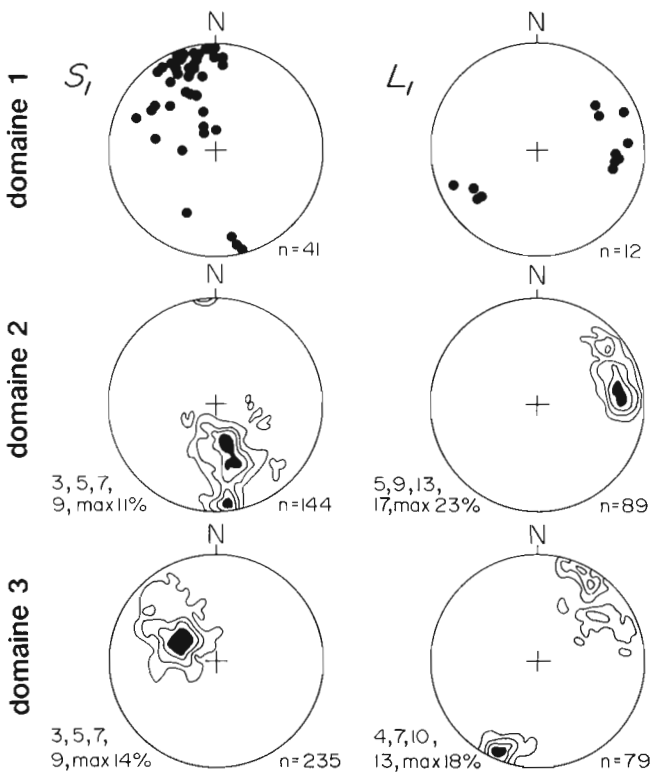

Figure 4. Projections stéréographiques des pôles de la schistosité régionale S_1 et de la linéation d'allongement (L_1) (projection équiaire, hémisphère inférieur). La localisation des domaines est indiquée sur la figure 3.

L'intensité de la déformation D_1 varie grandement au sein de la nappe du mont Logan, où des bandes de roches cisaillées (métasédimentaires et métavolcaniques) alternent avec d'épais horizons (quelques centaines de mètres) de roches moins déformées. La schistosité régionale, S_1, est une schistosité de flux définie par l'alignement des amphiboles et des chlorites dans les roches métavolcaniques, et par celui des micas, des minéraux opaques et plus rarement des rubans de quartz dans les roches métasédimentaires. De direction générale est-nord-est-ouest-sud-ouest, elle est inclinée plus ou moins fortement vers le nord ou vers le sud selon sa position à l'intérieur des structures synformes et antiformes tardives (acadiennes, P_3?) qui la reprennent (voir domaines 1, 2 et 3; fig. 3 et 4). À l'approche de la faille de Shickshock-Sud, la direction de la schistosité S_1 est nettement plus orientée vers le nord et le nord-est (fig. 3 et 4, domaine 3).

On observe par endroits un passage graduel entre la schistosité S_1 et une foliation mylonitique. L'observation de lames minces d'amphibolites mafiques a également révélé que la S_1 transpose localement une schistosité antérieure et qu'elle délimite des microlithons présentant des arcs polygonaux et des plis intrafoliaux. Étant donné que l'on ne connaît pas l'étendue de cette schistosité ante-S_1, on considère dans le cadre du présent rapport, que la schistosité régionale est une schistosité S_1, telle qu'observée sur le terrain, mais l'on note qu'elle pourrait être localement, sinon régionallement, une schistosité composite $S_{1\text{-}2}$.

L'un des éléments structuraux les plus significatifs est la présence d'une linéation d'allongement comprise dans le plan de la schistosité S_1. Il s'agit plus souvent d'une linéation minérale bien définie par l'alignement des amphiboles qu'une linéation d'étirement. Elle est aussi bien développée dans les métagabbros que dans les roches métavolcaniques et métasédimentaires. Oblique sur S_1, cette linéation d'allongement (L_1) plonge faiblement à modérément vers l'est et le nord-est ou vers le sud-ouest (fig. 3 et 4). Il est important de noter que sa direction est parallèle au grain structural de l'orogène dans ce segment des Appalaches.

Il y a peu de plis mégascopiques dans les roches du groupe de Shickshock et les relations angulaires entre S_1, L_1 et la phase de plissement P_1 sont peu connues à l'échelle régionale. Cependant, on a observé des plis P_1 d'ordre décimétrique dans un horizon métapélitique du domaine 1 (**1** sur fig. 2). Il s'agit de plis isoclinaux à charnières déracinées et à faible pendage vers l'est (axes EN080/20). La schistosité S_1 est de plan axial et l'allongement, parallèle à la charnière.

S_1 et L_1 sont affectées par un clivage de crénulation (S_2), localement conjugué, qui apparaît comme une froissement discret de la schistosité régionale. Cette crénulation est facilement observable sur les plans S_1, mais difficilement sur les coupes perpendiculaires, où elle fait un angle d'environ 45° avec S_1. La crénulation L_2 plonge faiblement à modérément vers le nord-nord-est ou l'est, mais aussi vers le sud. Seuls des plis ouverts à serrés d'ordre centimétrique associés

à cette crénulation ont été observés. À priori, il ne semble pas que le clivage de crénulation S_2 soit de plan axial aux plis régionaux (synforme et antiforme de la fig. 3 qui délimitent les domaines structuraux) qui affectent le groupe de Shickshock dans la région à l'étude, car l'orientation et le pendage de S_2 varient en fonction de sa position à l'intérieur de ces structures tardives (P_3) comme c'est le cas pour S_1 (voir aussi Carrara et Fyson (1972) pour relations entre P_2 et P_3).

MÉTAMORPHISME

Au sein du groupe de Shickshock, le métamorphisme augmente du nord-est vers le sud-ouest, du faciès des schistes verts à celui des amphibolites (e.g. Mattinson, 1964; St-Julien et al., 1990) et culmine aux abords de la faille de Shickshock-Sud.

Les observations en lame mince des roches métasédimentaires présentées ci-dessous sont restreintes à des échantillons provenant de la bande située la plus au sud, le long de la faille de Shickshock-Sud (**2** sur fig. 2). La plupart des minéraux ont une extinction roulante. Les textures sont hétérogranulaires à isogranulaires dans les métaarkoses et les métasiltstones. Les textures polygonales en mosaïque sont plutôt rares et n'ont été observées qu'aux abords immédiats de la faille de Shickshock-Sud. Les métapélites ont des textures grano-lépidoblastiques à porphyroblastiques. Elles comportent des assemblages à muscovite + biotite ± grenat ± staurotide ± sillimanite ± chlorite. La muscovite est le mica le plus abondant. La sillimanite est fibrolitique, rarement prismatique. Sa cristallisation semble syn- à tardi-S_1. Les grenats et les staurotides forment des blastes de moins de 1 mm et montrent localement de nombreuses inclusions hélicithiques de minéraux opaques et de quartz, exceptionnellement en spirale dans le grenat. Le grenat est syn- à post-S_1 et le staurotide, post-S_1. La tourmaline est commune, mais elle n'est présente qu'en faible proportion. Les métapélites de la bande sud ont donc atteint les champs de stabilité du staurotide et de la sillimanite, soit des températures d'au moins 550 °C et des pressions qui peuvent être comprises entre 2 et 8 kbar (grille de Spear et Cheney, 1989). Bien que les roches métasédimentaires aient subi les effets des plissements post-S_1, il n'y a pas d'indices de rétromorphose liée à ces phases de déformation. En effet, peu de réactions rétrogrades ont été observées dans les lames disponibles, mise à part la rétrogradation locale de biotite en chlorite.

Dans la partie sud de la zone étudiée, les amphibolites mafiques ont des textures nématoblastiques bien définies par l'allongement de hornblendes millimétriques. La proportion d'amphibole peut facilement dépasser 75 %. Certains horizons sont riches en épidote qui semble secondaire et qui se retrouve au voisinage de plagioclases passablement altérés. Le métamorphisme semble décroître de façon graduelle vers le nord, où des schistes à actinote + chlorite + épidote + plagioclase ± quartz ± opaques avec ou sans calcite secondaire peuvent être observés.

DISCUSSION ET CONCLUSIONS

La déformation et le métamorphisme des roches du groupe de Shickshock ont, jusqu'à ce jour, été principalement attribués à des mouvements compressifs et à des chevauchements d'âge taconien. L'allongement faiblement plongeant sur S_1 observé dans l'ensemble des roches du groupe de Shickshock est cependant inhabituel dans les Appalaches québéçoises et difficilement expliqué par des mouvements compressifs simples.

D'après St-Julien et al. (1990), la schistosité régionale (S_1), originellement sub-horizontale, serait parallèle à la surface axiale de plis couchés formés lors du déplacement précoce (D_1) de la nappe du mont Logan vers le nord ou le nord-nord-ouest. Dans un second temps (post-D_1), la nappe se serait déplacée horizontalement vers l'ouest ou le sud-ouest, produisant ainsi dans les phyllades sous-jacentes de la formation de l'Orignal 1) la linéation d'étirement et les textures S/C associées et, 2) superposés à la schistosité S_1, des plis en fourreau dont les charnières seraient parallèles à l'étirement. Ces premiers mouvements auraient été suivis d'une phase compressive nord-ouest-sud-est qui a produit des ondulations macroscopiques et le clivage de crénulation S_2. Il n'est pas clair si ces auteurs considèrent que les linéations d'étirement observées dans la formation de l'Orignal et les linéations d'allongement développées dans les roches du groupe de Shickshock ont été produites par la même phase de déformation. Les résultats obtenus, bien que préliminaires, indiquent toutefois que la linéation d'allongement présente dans les roaches du groupe de Shickshock n'est pas superposée à la schistosité S_1, mais qu'elle en est contemporaine.

Il y a peu de plis mégascopiques dans les roches du groupe de Shickshock et pas d'indices de plis couchés P_1. Si, tel que proposé par St-Julien et al. (1990), la schistosité S_1 est de plan axial à des plis couchés vers le nord-nord-ouest, il faut que la L_1 ait été parallèle aux charnières et originellement de direction nord-est-sud-ouest pour que les relations actuelles entre S_1 et L_1 puissent être expliquées. D'un autre côté, si la schistosité S_1 est reliée à la formation de plis d'entraînement et à du cisaillement associés à un premier mouvement de la nappe du mont Logan vers le nord-nord-ouest, on s'attendrait à ce que la L_1 soit actuellement fortement plongeante dans le plan de la S_1. En fait, l'origine de la S_1 est incertaine et il n'est pas évident qu'elle ait été une schistosité régionalement horizontale. Étant donné les relations entre S_1 et L_1, on croit qu'il est possible que ces structures tectoniques se soient développées de façon contemporaine dans un régime de déformation transpressive qui, à priori, expliquerait avantageusement l'épaississement crustal observé (faciès des amphibolites atteint dans la partie sud du groupe de Shickshock), l'allongement oblique et faiblement plongeant sur S_1 et les cisaillements syn-métamorphiques localisés.

Les travaux qui suivront au cours de l'année viseront à caractériser et à établir la relation entre le métamorphisme et la déformation des roches du groupe de Shickshock. Pour ce faire, il s'agira donc 1) d'établir la séquence des déformations syn- à tardi-métamorphiques, 2) d'identifier en lame mince les indicateurs cinématiques de la déformation, puisque ceux-ci sont difficilement observables sur le terrain, 3)

d'établir la séquence des réactions métamorphiques prograde et rétrogrades, 4) de quantifier les conditions PT du métamorphisme régional et 5) de replacer les résultats obtenus dans un contexte régional.

REMERCIEMENTS

Les auteurs remercient Greg Lynch (CGC) qui a aimablement revisé le manuscript et Isabelle Roy qui a assisté G.E. Camiré au cours des travaux de terrain.

RÉFÉRENCES

Aumento, F.
1969: Serpentine mineralogy of ultrabasic intrusions in Canada and on the mid-Atlantic Ridge; Geological Survey of Canada, Preliminary Report 69-53.

Beaudin, J.
1980: Région du mont Albert et du lac Cascapédia; Ministère de l'Énergie et des Ressources du Québec, DPV-705.
1984: Analyse structurale du groupe de Shickshock et de la péridotite alpine du mont Albert, Gaspésie; thèse de doctorat, Université Laval, Québec, Québec.

Berger, J.
1985: Analyse structurale de la faille de Shickshock Sud en Gaspésie occidentale, Québec; mémoire de maîtrise, Université de Montréal, Montréal, Québec.

Carrara, A.
1972: Structural geology of Lower Paleozoic rocks, Mount Albert area, Gaspé Peninsula, Québec; Ph.D. thesis, Ottawa University, Ottawa, Ontario.

Carrara, A. and Fyson, W.K.
1973: Taconic and Acadian folds in northern and western Gaspé Peninsula, Québec; Canadian Journal of Earth Sciences, v. 10, p. 498-509.

Dresser, J.A. et Dennis, T.
1944: Géologie du Québec; Ministère des Mines du Québec, RG-20.

Gagnon, Y. and Jamieson, R.A.
1985: Geology of the Mount Albert region, Gaspé Peninsula, Québec; in Current Research, Part A; Geological Survey of Canada, Paper 85-1A, p. 783-788.

Girard, P.
1967: Géologie de la région de mont Richardson; Ministère des Richesses naturelles du Québec; RP-563.

Laurent, R.
1977: Ophiolites from the northern Appalachians of Québec; in North American ophiolites, edited by R.G. Coleman and W.P. Irwin; Oregon Department of Geology and Mineral Industries, bulletin 95, p. 25-40.

Lebel, D.
1985: Analyse structurale de la déformation acadienne, principalement la faille de Shickshock Sud dans la région de Rimouski-Matapédia; mémoire de maîtrise, Université de Montréal, Montréal, Québec.

MacGregor, I.D.
1962: Geology, petrology and geochemistry of the Mount Albert and associated ultramafic bodies of central Gaspé, Québec; M.Sc. thesis, Queen's University, Kingston, Ontario.
1964: A study of the contact metamorphism aureole surrounding the Mount Albert ultramafic intrusion; Ph.D. thesis, Princeton University, Princeton, New Jersey.

Malo, M., Kirkwood, D., de Broucker, G., and St-Julien, P.
1992: A re-evaluation of the position of the Baie Verte-Brompton Line in the Québec Appalachians: the influence of Middle-Devonian strike-slip faulting in Gaspé Peninsula; Canadian Journal of Earth Sciences, v. 29, p. 1265-1273.

Mattinson, C.R.
1964: Région du mont Logan, comtés de Matane et de Gaspé-Nord; Ministère des Richesses naturelles du Québec, RG-118.

Ollerenshaw, N.C.
1967: Région de Cuoq-Langis, comtés de Matapédia et de Matane; Ministère des Richesses naturelles du Québec; RP-465.

Osborne, F.F. and Archambault, M.
1948: Chromiferous chromite chlorite from Mount Albert, Québec; Royal Society of Canada, Transactions XLII, Section IV, May 1948.

St-Julien, P. and Hubert, C.
1975: Evolution of the Taconian orogen in the Québec Appalachians; American Journal of Sciences, v.275-A, p.337-362.

St-Julien, P., Trzcienski, W.E. Jr., and Wilson, C.
1990: A structural, petrological and geochemical traverse of the Shickshock terrane, Gaspésie; New England Intercollegiate Geological Conference Guidebook for Field Trips in la Gaspésie, Québec, 82nd Annual Meeting, p. 248-284.

Slivitzky, A., St-Julien, P. et Lachambre, G.
1991: Synthèse géologique du Cambro-Ordovicien du nord de la Gaspésie; Ministère de l'Énergie et des Ressources du Québec, ET 88-14.

Spear, F.S. and Cheney, J.T.
1989: A petrogenetic grid for pelitic schists in the system SiO_2-Al_2O_3-FeO-MgO-K_2O-H_2O; Contributions to mineralogy and petrology, v.101, p.149-164.

Williams, H. and St-Julien, P.
1982: The Baie Verte-Brompton Line: early Paleozoic continent-ocean interface in the Canadian Appalachians; in Major structural zones and faults of the Northern Appalachians; edited by P. St-Julien and J. Béland; Geological Association of Canada, Special Publication 24, p. 177-207.

Projet 92001GP de la Commission géologique du Canada

Lithostratigraphy and paleoenvironmental evolution of the Upper Ordovician Trenton Group, southern Quebec

Denis Lavoie
Quebec Geoscience Centre, Sainte-Foy

Lavoie, D., 1993: Lithostratigraphy and paleoenvironmental evolution of the Upper Ordovician Trenton Group, southern Quebec; in Current Research, Part D; Geological Survey of Canada, Paper 93-1D, p. 161-172.

Abstract: The Trenton Group (Upper Ordovician) of southern Quebec is a threefold carbonate unit. Its lower part is made up of the laterally equivalent Ouareau, Fontaine, St-Alban and Pont-Rouge formations. These units overlie either unconformably or conformably the Black River Group; lithofacies indicate shallow subtidal deposition. The overlying Deschambault Formation represents carbonate ramp deposits. The upper part of the Trenton Group is made up of the Montréal and the Tétreauville formations in the southwestern part of the platform, and the correlatives Saint-Casimir and Grondines members of the Neuville Formation in the northeastern sector. These units represent progressively deeper outer shelf deposition. Sequence analysis shows that the Trenton Group records transgressive conditions following a sea level lowstand in the basin. Regional facies distribution indicates that the Trenton platform was dissected by extensional faults, tectonically-driven subsidence of the platform is responsible for the transgressive conditions.

Résumé : Le Groupe de Trenton (Ordovicien supérieur), sud du Québec est une unité tripartite à carbonates. Sa portion inférieure est constituée par les formations de Ouareau, de Fontaine, de St-Alban et de Pont-Rouge. Ces unités surmontent en discordance ou concordance le Groupe de Black River; elles témoignent d'une sédimentation infratidale en eau peu profonde. La formation sus-jacente de Deschambault montre des dépôts de rampe à roches carbonatées. La portion sommitale du groupe est constituée des formations de Montréal et de Tétreauville (secteur sud-ouest), directement corrélables avec les membres de Saint-Casimir et de Grondines (Formation de Neuville, secteur nord-est). Ces unités représentent des dépôts de plate-forme externe. L'analyse séquentielle montre que le Groupe de Trenton enregistre une transgression suivant un épisode de bas niveau marin. La répartition régionale des faciès indique que cette plate-forme était morcellée par des failles de distension; la subsidence tectonique de la plate-forme est responsable de la transgression.

INTRODUCTION

The gently southeast dipping 1500 to 3000 m Cambrian - Ordovician succession of the St. Lawrence Lowlands of southern Quebec records platformal sedimentation in a complete Wilson cycle, from opening of the Iapetus ocean in Late Precambrian time, up to its partial closure in Late Ordovician time (Globensky, 1987). Following this event (the Taconian orogeny), marine to subaerial siliciclastic sedimentation resumed in successor basins with, however, almost no preserved record of younger than latest Ordovician sedimentation.

Early mapping and study of the area resulted in a lithostratigraphic framework (Globensky, 1987) relying on the numerous paleontological and resulting biostratigraphic works. However, the sedimentology and diagenesis of most carbonate and siliciclastic units are poorly constrained, apart from some studies either on specific units (Hofmann, 1963; Young, 1964; Mehrtens, 1979; Bernstein, 1992; Lavoie, 1992) or oriented towards specific themes (B.E.I.C.I.P., 1975; INRS-Pétrole, 1975, 1976a, b; Bertrand and Héroux, 1981; Bertrand et al., 1983; Tassé et al., 1987; Héroux and Tassé, 1990). Facies distribution, sequence studies, carbonate diagenesis, and interplays between facies patterns and active tectonism still need to be fully documented and integrated before paleogeographic evolution of the Quebec segment of the northern margin of Iapetus ocean can be completely understood.

In that long term perspective, the 1991 field work mostly focused on regional facies distribution of the Upper Ordovician Deschambault Formation of the Trenton Group (Lavoie, 1992). The Deschambault facies are best interpreted in terms of a shallow water carbonate ramp, however, the regional survey also documented important facies and thicknesses changes over the entire Deschambault platform (Lavoie, 1992). These changes were related to synsedimentary extensional tectonism. The objectives of the 1992 field season (2 months) were 1) to complete the facies picture for the entire Trenton Group (Late Ordovician) of the St. Lawrence Lowlands platform and, 2) to document the effects of tectonism in the evolution of the Trenton platform.

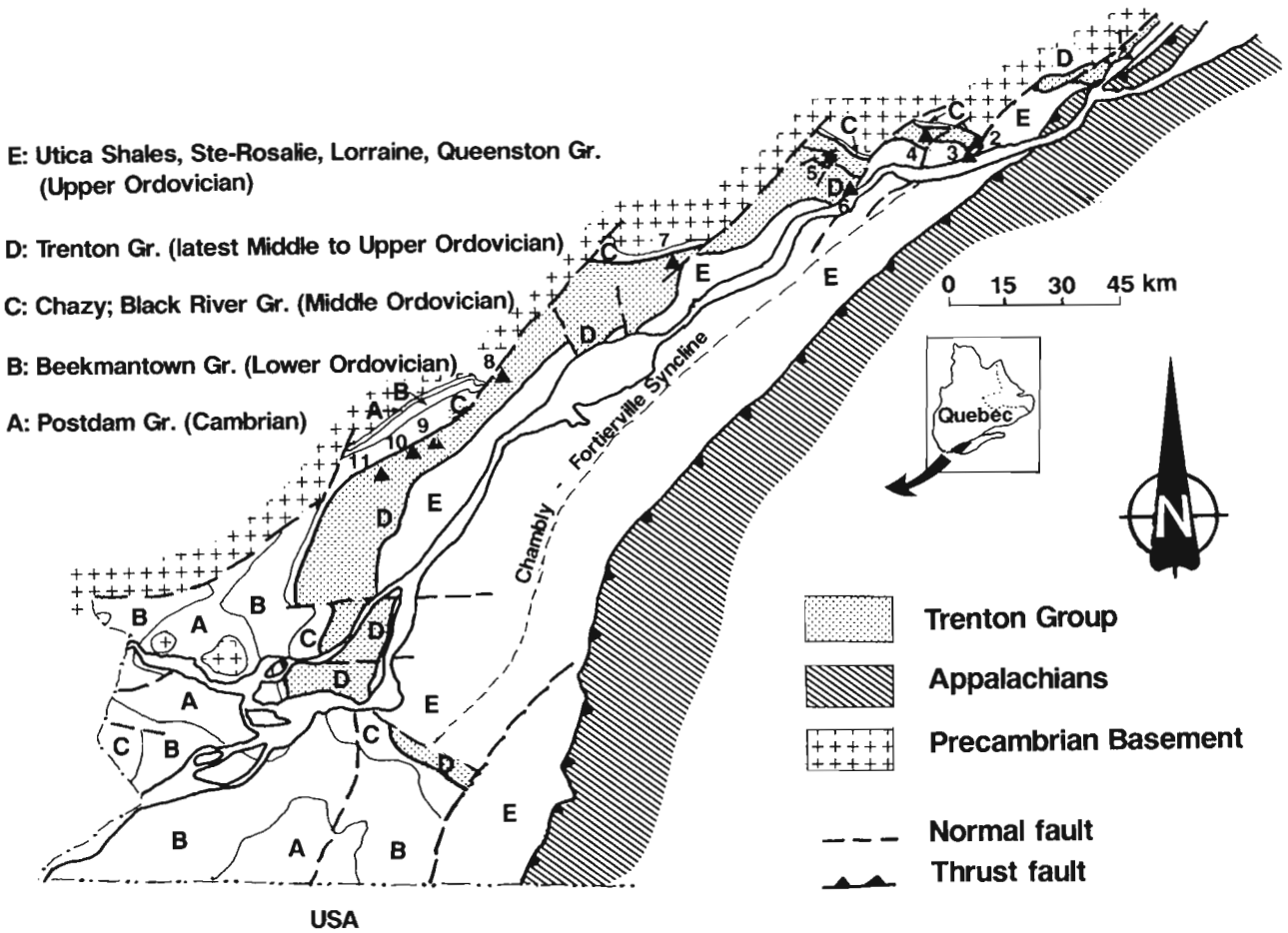

Figure 1. Simplified geological map of the St. Lawrence Lowlands with locations of the described sections. Sections 1: Montmorency River, 2: Neuville quarry, 3: St. Lawrence shore at Neuville, 4: Jacques Cartier River, 5: Sainte-Anne River, 6: St. Lawrence shore at Grondines, 7: Lard River, 8: Chicot River, 9: Assomption River, 10: Ouareau River, 11: Saint-Esprit River.

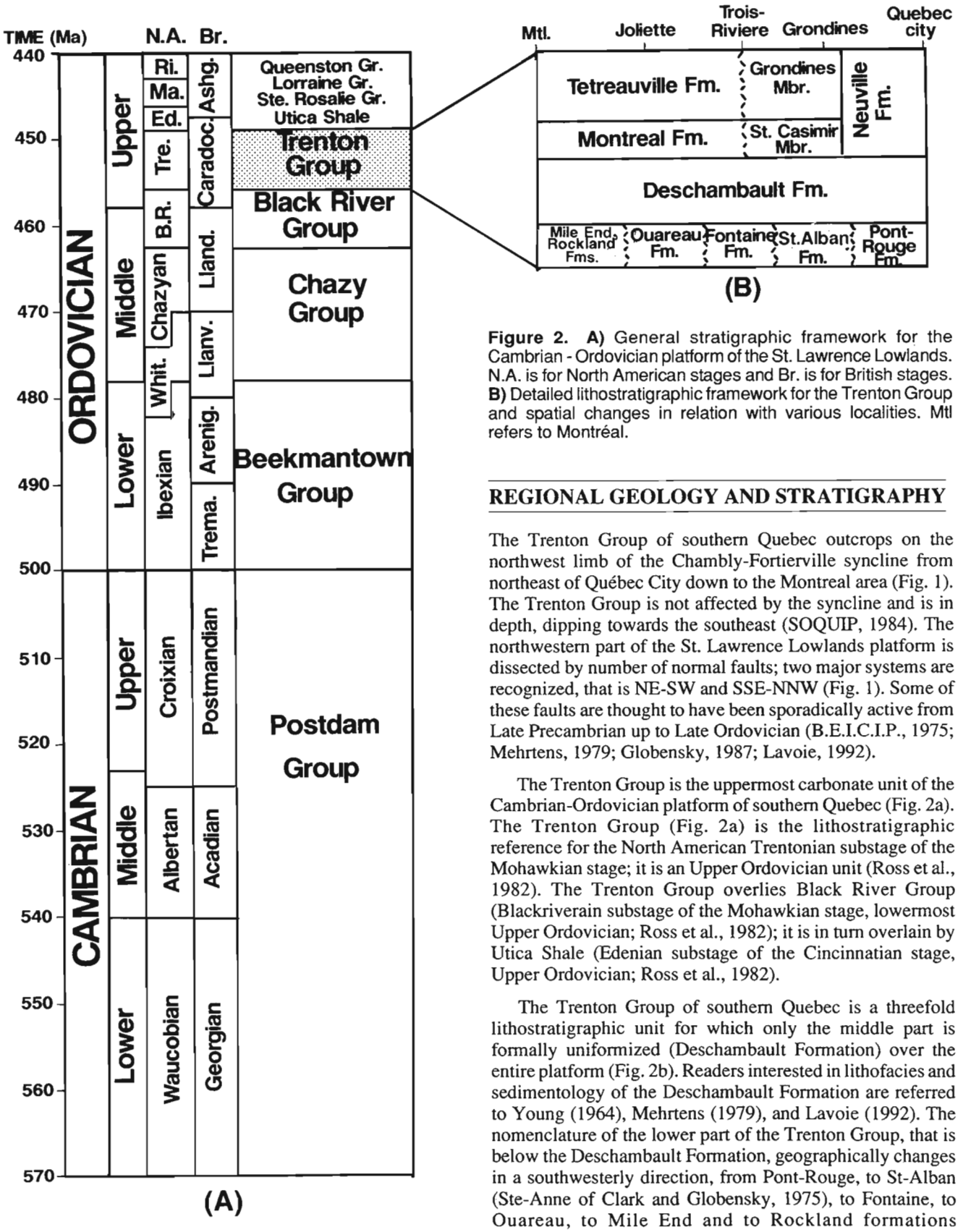

Figure 2. **A)** General stratigraphic framework for the Cambrian - Ordovician platform of the St. Lawrence Lowlands. N.A. is for North American stages and Br. is for British stages. **B)** Detailed lithostratigraphic framework for the Trenton Group and spatial changes in relation with various localities. Mtl refers to Montréal.

REGIONAL GEOLOGY AND STRATIGRAPHY

The Trenton Group of southern Quebec outcrops on the northwest limb of the Chambly-Fortierville syncline from northeast of Québec City down to the Montreal area (Fig. 1). The Trenton Group is not affected by the syncline and is in depth, dipping towards the southeast (SOQUIP, 1984). The northwestern part of the St. Lawrence Lowlands platform is dissected by number of normal faults; two major systems are recognized, that is NE-SW and SSE-NNW (Fig. 1). Some of these faults are thought to have been sporadically active from Late Precambrian up to Late Ordovician (B.E.I.C.I.P., 1975; Mehrtens, 1979; Globensky, 1987; Lavoie, 1992).

The Trenton Group is the uppermost carbonate unit of the Cambrian-Ordovician platform of southern Quebec (Fig. 2a). The Trenton Group (Fig. 2a) is the lithostratigraphic reference for the North American Trentonian substage of the Mohawkian stage; it is an Upper Ordovician unit (Ross et al., 1982). The Trenton Group overlies Black River Group (Blackriverain substage of the Mohawkian stage, lowermost Upper Ordovician; Ross et al., 1982); it is in turn overlain by Utica Shale (Edenian substage of the Cincinnatian stage, Upper Ordovician; Ross et al., 1982).

The Trenton Group of southern Quebec is a threefold lithostratigraphic unit for which only the middle part is formally uniformized (Deschambault Formation) over the entire platform (Fig. 2b). Readers interested in lithofacies and sedimentology of the Deschambault Formation are referred to Young (1964), Mehrtens (1979), and Lavoie (1992). The nomenclature of the lower part of the Trenton Group, that is below the Deschambault Formation, geographically changes in a southwesterly direction, from Pont-Rouge, to St-Alban (Ste-Anne of Clark and Globensky, 1975), to Fontaine, to Ouareau, to Mile End and to Rockland formations (Globensky, 1987; and Fig. 2b herein). The nomenclature of the upper part of the Trenton Group changes from Neuville

Formation (made up of the St-Casimir and Grondines members) in the northeastern sector of the platform, to the Montréal and Tétreauville formations (equivalent to the St-Casimir and Grondines members, respectively) in the southwestern part of it (Globensky, 1987; Fig. 2b herein).

THE LOWER PART OF TRENTON GROUP

The lower part of the Trenton Group is a thin 1.3 to 4.7 m thick carbonate interval (Fig. 3).

Nature of the lower and upper contacts

The various units constituting the lower part of the Trenton Group (see above) overlie either conformably or unconformably the upper unit of the Black River Group. From subsurface information, they unconformably overlie the Precambrian basement in the northeastern sector of the platform (Clark and Globensky, 1973). The conformable relationship is seldom seen (Fig. 3, section 10 and Fig. 4a), the lithological expression of the transition is subtle; the uppermost beds of the Black River Group and the lowermost beds of the Trenton Group are typified by bioclastic

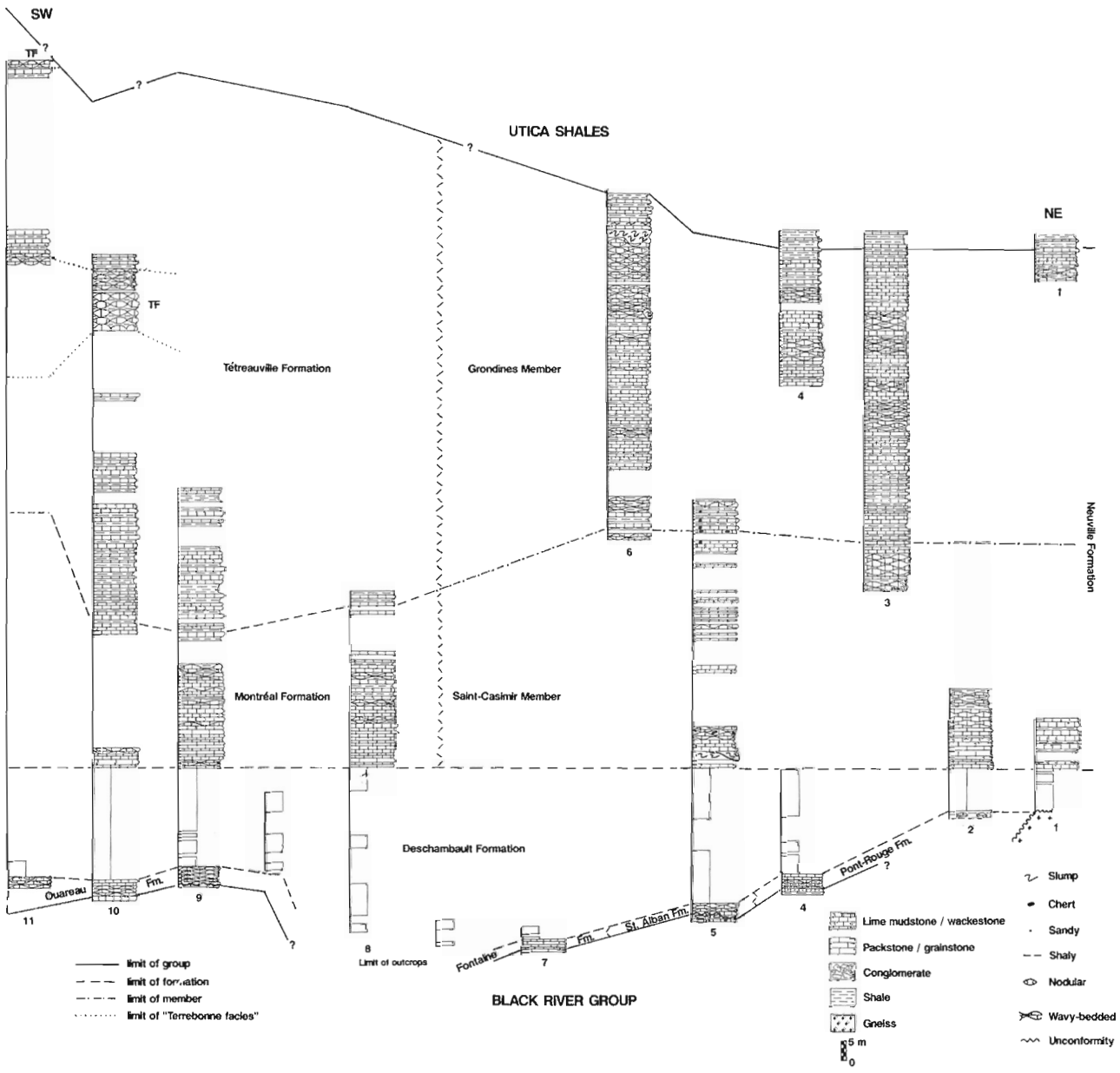

Figure 3. Lithostratigraphic correlations for the Trenton Group. The part of the sections that refers to the Deschambault Formation is described in Lavoie (1992). The contact between the Deschambault and Neuville/Montréal formations is used as datum line. Location of sections in Figure 1.

wackestones and packstones with, however, the packstones being more typical of the lower part of the Trenton. The transition is however, marked by a notable change of the faunal elements and given by appearance of typical Trenton fauna (Globensky, 1987). As such, the conformable contact between the Black River and Trenton groups is defined on biostratigraphic rather than lithostratigraphic grounds. Clark and Globensky (1976) clearly stressed that point but kept the unconventional lithostratigraphic framework proposed by Okulitch (1939).

Evidence for an unconformable relationship between the Black River and Trenton groups are noted at some of the localities where this contact is visible (Fig. 3, sections 5, 7 and 9). This unconformable relationship is best seen at the Sainte-Anne section (section 5) where the transition between Black River Group and St-Alban Formation of Trenton Group is marked by a karstic topography present at the top of Black River Group. Field evidence for subaerial exposure include: 1) collapse breccias (Fig. 4b), 2) rinnenkarrens (Fig. 4c) that are locally bored, 3) irregular topography of the uppermost Black River beds, and 4) small karst pits and enlarged joints connected to the exposure surface and filled

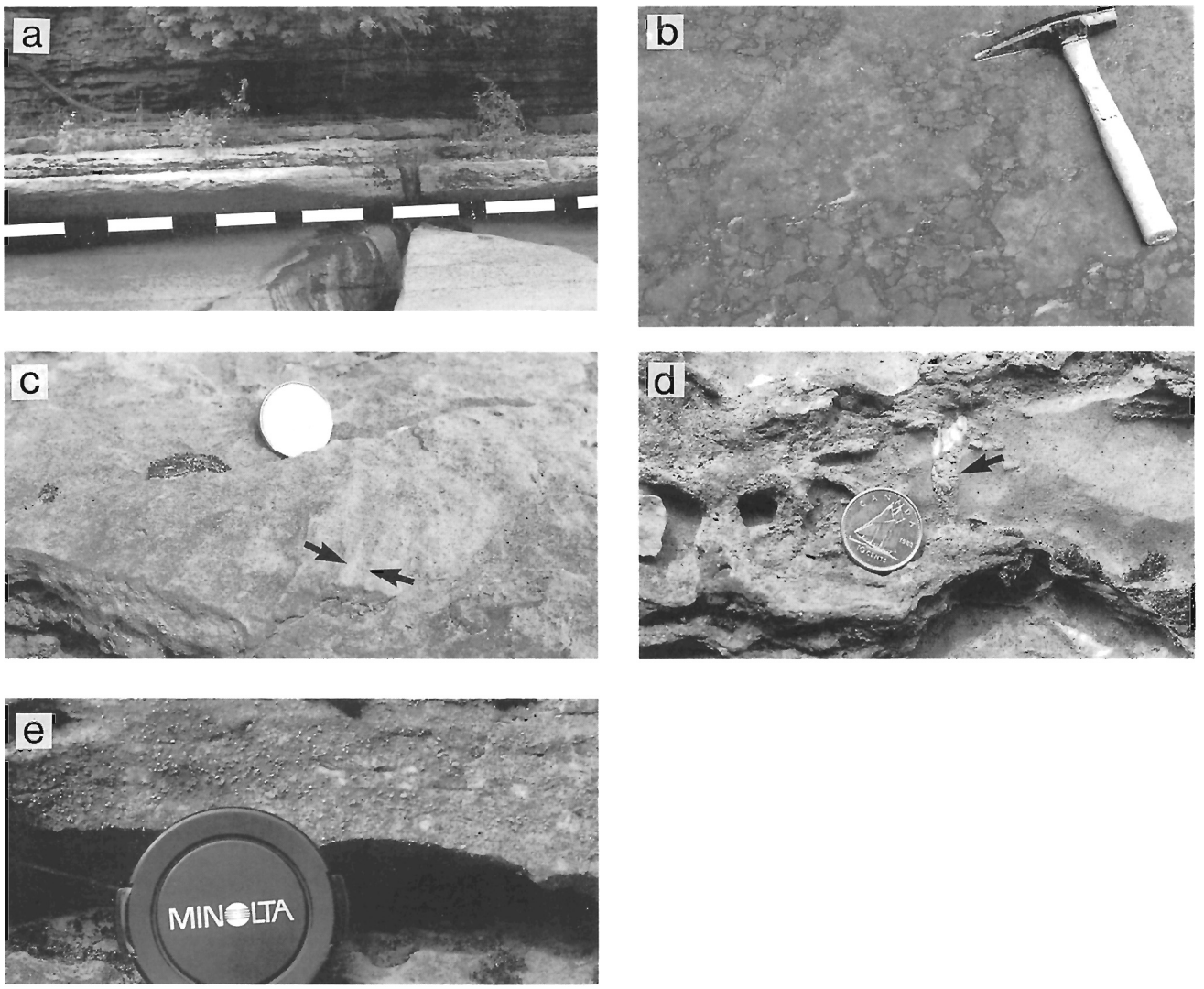

Figure 4. Contact between the Black River and Trenton groups. **a)** Conformable contact (outline in white) between the underlying wackestones of the Black River Group and the overlying wackestones/packstones of the Ouareau Formation (Trenton Group). Ouareau section. **b)** Plane-bedding view of a collapse breccia observed near the top of Black River Group. Note the puzzle-like texture of the breccia, the angularity and homogeneity of the clasts and the presence of irregularly-shaped remnants of non-brecciated limestones. Ste-Anne section. **c)** Plane-bedding view of steep-sided rinnenkarrens (one is outlined by arrows) occurring at the top of Black River Group. Ste-Anne section. **d)** Cross-section view of a small solution void filled with locally derived geopetal sediment. The remaining porosity is filled with blocky calcite. Ste-Anne section. **e)** Cross-section view of the lowermost bed of the St-Alban Formation made up of quartzose grainstone sediment. Ste-Anne section.

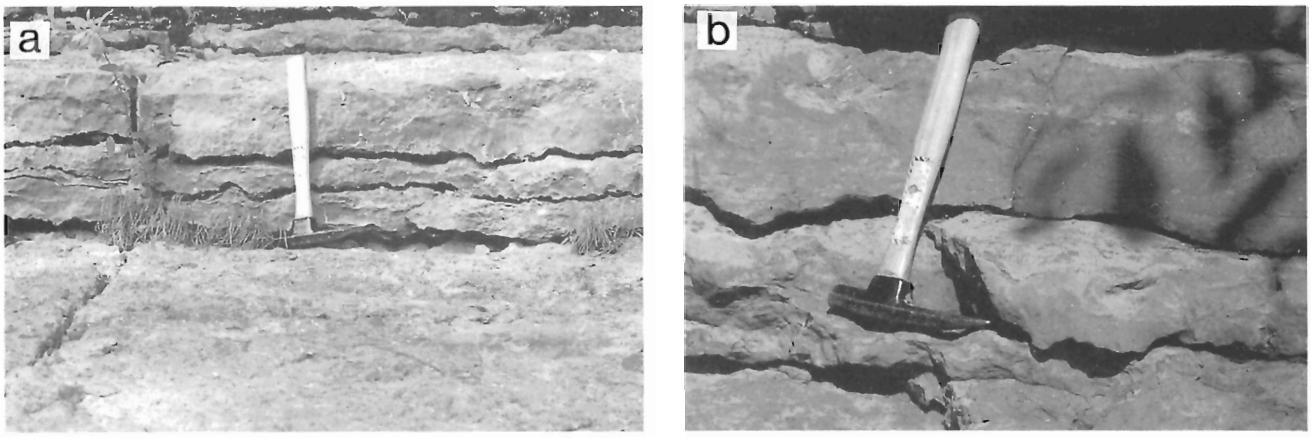

Figure 5. Lower part of the Trenton group. **a)** Wavy-bedded wackestones of the Pont-Rouge Formation with millimetre-sized limy shale partings. Jacques Cartier section. **b)** Wavy- and thickly-bedded wackestones of the Ouareau Formation. Shale is absent from this exposure. Ouareau section.

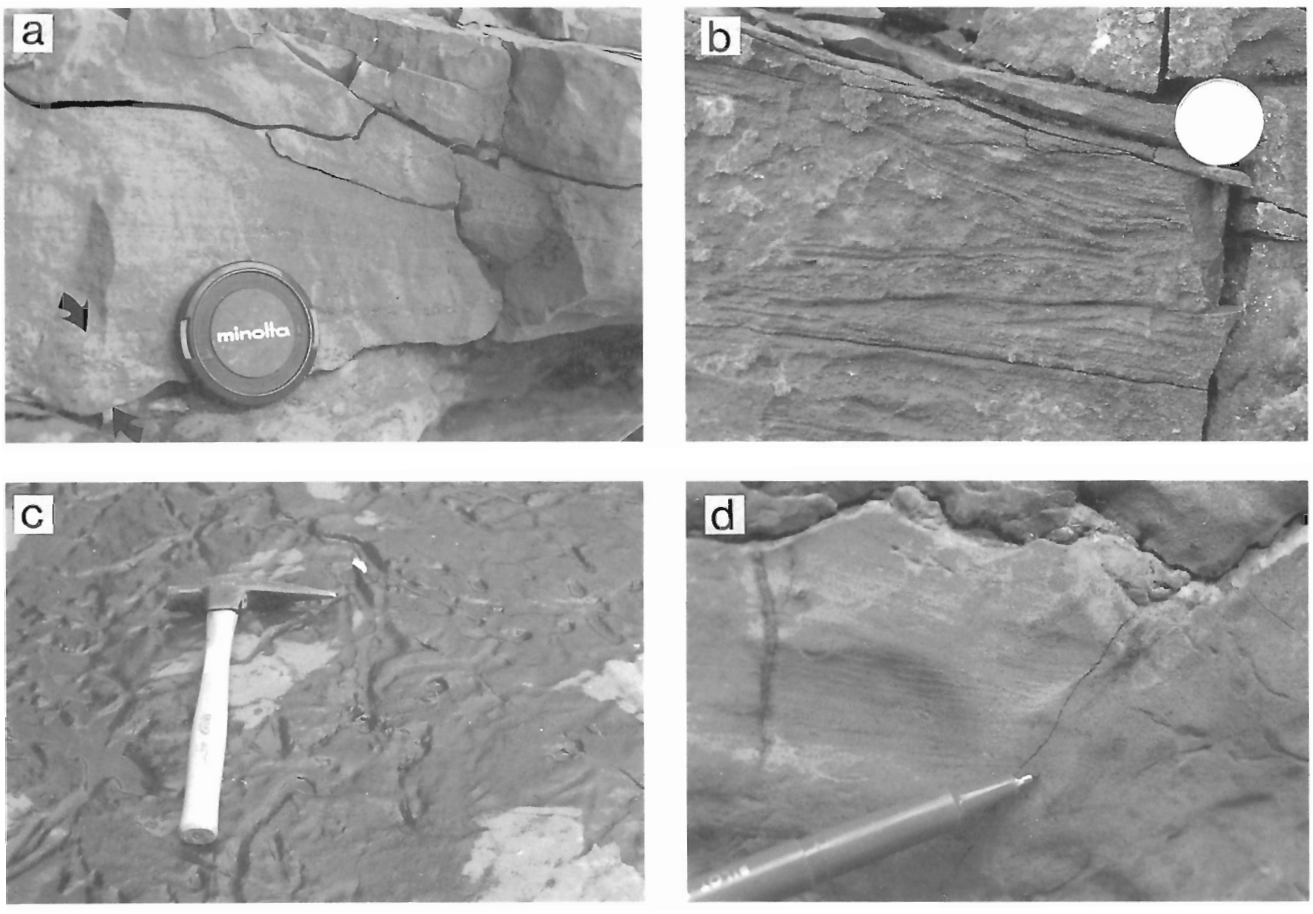

Figure 6. Lower part of the Trenton Group (Ouareau Formation), southwestern sector of the platform. **a)** Thickly bedded packstone with a centimetre-sized gravel lag at the bottom of the bed (outlined by arrows) overlain by parallel and trough cross-laminated sediment. Assomption section. **b)** Packstone with abundant internal parallel and cross-laminations. Saint-Esprit section. **c)** Plane-bedding view of the typical abundance of horizontal burrows observed in the Ouareau Formation. Assomption section. **d)** Cross-section view of the burrowed and mottled limestone with, in the left side of the photograph, preserved laminations in unburrowed sediment. Assomption section.

with geopetal sediment (Fig. 4d). The immediately overlying St-Alban bed is given by a 10 cm thick quartzoze, cross-laminated grainstone (Fig. 4e). Okulitch (1939) and Clark and Globensky (1975) disagreed on the nature of the transition at this locality; our new observations support Clark and Globensky's (1975) erosive hypothesis.

The upper contact of the lower units of the Trenton Group with the overlying Deschambault Formation is conformable to seldom disconformable. The nature of that contact is fully addressed in Lavoie (1992).

Lithofacies

The confused lithostratigraphic framework for the lower part of the Trenton Group (Fig. 2b) is in part reflected by some regional lithological variations. As a whole, the various units of the lower part of the Trenton Group are typically bioclastic wackestones and packstones generally occurring in wavy, thinly- to thickly-bedded horizons with some limy shale partings of variable thicknesses (Fig. 5a, b). Fauna is everywhere dominated by gastropods; red algae, brachiopods, crinoids and less commonly, corals are subordinate. However, distinct lithological variations are noted between units in the southwest (Ouareau Formation) and northeast localities (St-Alban and Pont-Rouge formations), with the unit in the central area (Fontaine Formation) sharing characteristics of both sectors.

The Ouareau Formation is characterized by an abundance of bioclastic packstones and grainstones, wackestones are less common. Limy shale occurs as millimetre-sized partings. The coarse grained carbonates commonly show evidence of important wave activity and reworking, such as gravel lag at bottom of beds (Fig. 6a), grading, imbrication of long axis of shelly material, parallel and planar cross-laminations, all of which occur in ripples and megaripples of variable amplitudes and wavelengths (Fig. 6b). The beds that are devoid of internal sedimentary structures are highly bioturbated mottled limestones (Fig. 6c, d); bioturbation is clearly associated with wave energy in the destruction of sedimentary structures.

The northeastern sector units (St-Alban and Pont-Rouge formations) are mostly characterized by bioclastic wackestones with less common packstones and lime mudstones (Fig. 5a). Grainstones are scarce and only seen as thin lenses in the wackestones. Internal sedimentary structures are few and given by parallel and cross-laminations (Fig. 7a). As for the southwestern unit, bioturbation is common. However, for the Pont-Rouge Formation, it is the site of preferential chertification of the limestones (Fig. 7b). Limy shale is ubiquitous and occur in millimetre- to centimetre-sized interbeds, the northeasternmost field exposure of the lower Trenton Group (Pont-Rouge Formation at Neuville quarry; Fig. 3, section 2 and Fig. 7c) shows that limy shale is the dominant rock type.

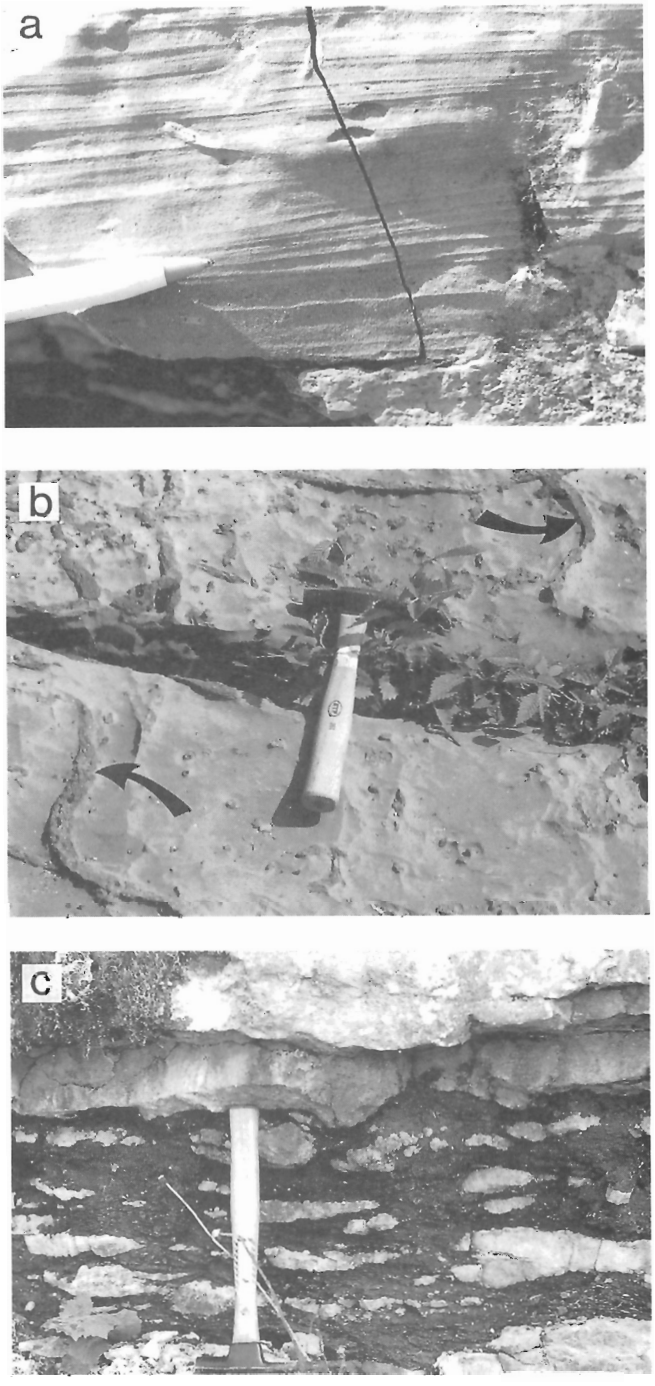

Figure 7. Lower part of Trenton Group, northeastern sector of the platform. a) Planar cross-laminations developed in fine grained wackestone of the St-Alban Formation. Ste-Anne section. b) Plane-bedding view of chertified burrows (arrows) in Pont-Rouge Formation. Jacques Cartier section. c) Cross-section view of nodular wackestones set in a dominant limy shale succession, Pont-Rouge Formation. The contact with the overlying crudely-bedded Deschambault Formation is at the lower end of the hammer. Neuville quarry section.

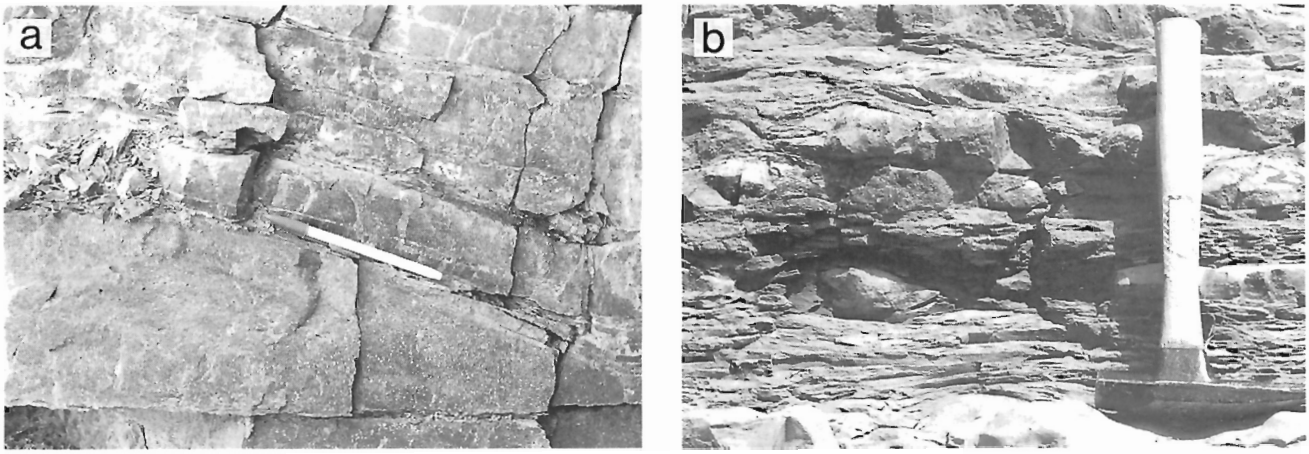

Figure 8. Lower and upper contacts of the upper part of the Trenton Group. **a)** Gradual transition from the Deschambault Formation given by the progressive disappearance of cross-bedded bioclastic grainstones of Deschambault-type, interbedded with dominantly thinly- and planar-bedded wackestone-lime mudstone succession, typical of the lower part of the upper Trenton. Neuville quarry section. **b)** Gradual transition with Utica Shales given by wavy-bedded lime mudstones occurring in a dominantly shale succession. Percentage and thickness of shales increase up-section to ultimately give way to a carbonate-free succession. Jacques Cartier section.

Preliminary paleoenvironmental interpretation

Litho- and biofacies data are strong advocates for shallow subtidal deposition of the various units of the lower part of the Trenton Group. These units locally conformably overlie the shallow subtidal (lagoonal; Globensky, 1987) deposits of the upper part of Black River Group with, as previously discussed, no major lithological break. At most localities, the lower part of Trenton Group unconformably overlies a sub-aerial exposure surface at the top of Black River Group; there the lower Trenton lithofacies are similar to the ones seen in the conformable transition and likely represent similar paleoenvironmental conditions. The units of the lower part of Trenton Group are conformably to locally disconformably overlain by the shallow water carbonate ramp deposits of the Deschambault Formation (Lavoie, 1992).

The most common lithofacies of the lower Trenton units are the bioclastic wackestones and packstones/grainstones. The latter dominate in the southwest sector of the study area; they are characterized by abundant wave induced structures indicative of reworking of sediment above fairweather wave base. They are regarded as sand shoals and bars developed on an agitated shallow water platform (Wilson, 1986). The lithofacies in the northeastern sector are generally finer grained and muddier, wackestones dominate the successions and limy shales are more abundant. The preservation of greater amount of level bottom muds in this area could be interpreted as resulting from deposition either in a slightly deeper subtidal setting or in a wave-surge protected area on the platform. The associated fauna in both area is similar. The southwestern sector fauna is reworked but para- autochthonous in origin; the fauna is dominated by shallow water inhabitants (gastropods and red algae).

THE UPPER PART OF TRENTON GROUP

The upper part of the Trenton Group is a 125 to 200 m thick twofold unit (Fig. 3). As presented above, the lithostratigraphic framework is made up of either one formation with two members (Neuville Formation with the Saint-Casimir Member and the overlying Grondines Member) in the northeastern sector or, for the southwestern part of the study area, two formations (Montréal and Tétreauville formations), that are directly correlative with the members of Neuville Formation (Fig. 2b, 3).

Nature of the lower and upper contacts

The contact with the underlying Deschambault Formation is partly addressed in Lavoie (1992). This contact is conformable and gradual over a few metres. The lower succession of the upper part of Trenton Group is everywhere made up of coarse grained, wavy-bedded and cross-stratified bioclastic packstones / grainstones of Deschambault type, interbedded with fine grained, planar- to wavy-bedded wackestones, lime mudstones and limy shales more typical of the remaining of the lower unit of the upper Trenton Group (Fig. 8a).

The contact with the overlying siliciclastic-dominated Utica Shales is also conformable and gradual over a few metres; the uppermost metres of the upper part of the Trenton Group are characterized by a rapid increase in the amount and thickness of fine grained siliciclastic beds heralding the shale-dominated Utica Group (Fig. 8b).

Lithofacies

Saint-Casimir Member (Neuville Formation) and Montréal Formation

This is the lower unit of the upper part of Trenton Group. Its thickness ranges from 35 to 60 m (Fig. 3). The dominant lithofacies is given by wavy-bedded, lime mudstones and wackestones (Fig. 9a) occurring in beds ranging from 5 to 20 cm thick (average = 12 cm). These carbonates show fairly abundant internal sedimentary structures such as grading, parallel laminations, planar to trough cross-laminations and less commonly hummocky cross-laminations. Bioclastic material is dominated by brachiopods, bryozoans and trilobites; bioturbation is common and produced by various horizontal-dwellers. These carbonates are interbedded with minor amounts of limy shales (2 to 10%) that occur in millimetre- to centimetre-sized horizons.

As previously discussed, the first few metres of the upper part of Trenton Group are characterized by interlayering of the above described fine grained limestones with coarse grained bioclastic limestones of Deschambault type (Fig. 8a). Higher upsection, packstones and grainstones only occur as centimetre-sized lenses in the lime mudstone / wackestone lithofacies. As a rule, the amount of coarse grained carbonate decreases upsection.

This interval in the upper part of Trenton Group is locally typified by important synsedimentary deformation structures, including truncated surfaces, slumps and dismembered beds (Fig. 9b, c).

Preliminary paleoenvironmental interpretation

The Saint-Casimir Member of Neuville Formation and Montreal Formation are preliminarily interpreted to represent relatively shallow outer shelf deposits, above the fairweather wave base. This interpretation relies on the predominantly fine grained nature of the sediment, the normal open marine fauna that is physically reworked and the nature of sedimentary structures observed (fairweather and storm waves induced) (Wilson, 1986). The onlapping of outer shelf facies over the Deschambault carbonate ramp deposits (Lavoie, 1992, his Fig. 2d) could support the presence of a gently sloping depositional environment, at least locally. This last observation could explain the presence of local synsedimentary deformation structures as could rapid sedimentation rates.

Grondines Member (Neuville Formation) and Tétreauville Formation

This is the upper unit of the upper part of the Trenton Group. Its thickness ranges from 70 to 130 m (Fig. 3). The dominant lithofacies is given by planar-bedded, lime mudstones and less commonly wackestones (Fig. 10a) occurring in beds ranging from 5 to 18 cm thick (average = 10 cm). Internal sedimentary structures are few and consist of fine parallel laminations and scarce hummocks. The limestones are interbedded with up to 50% of limy shales (average = 15%). For the best exposed sections, there is a cyclicity observed in

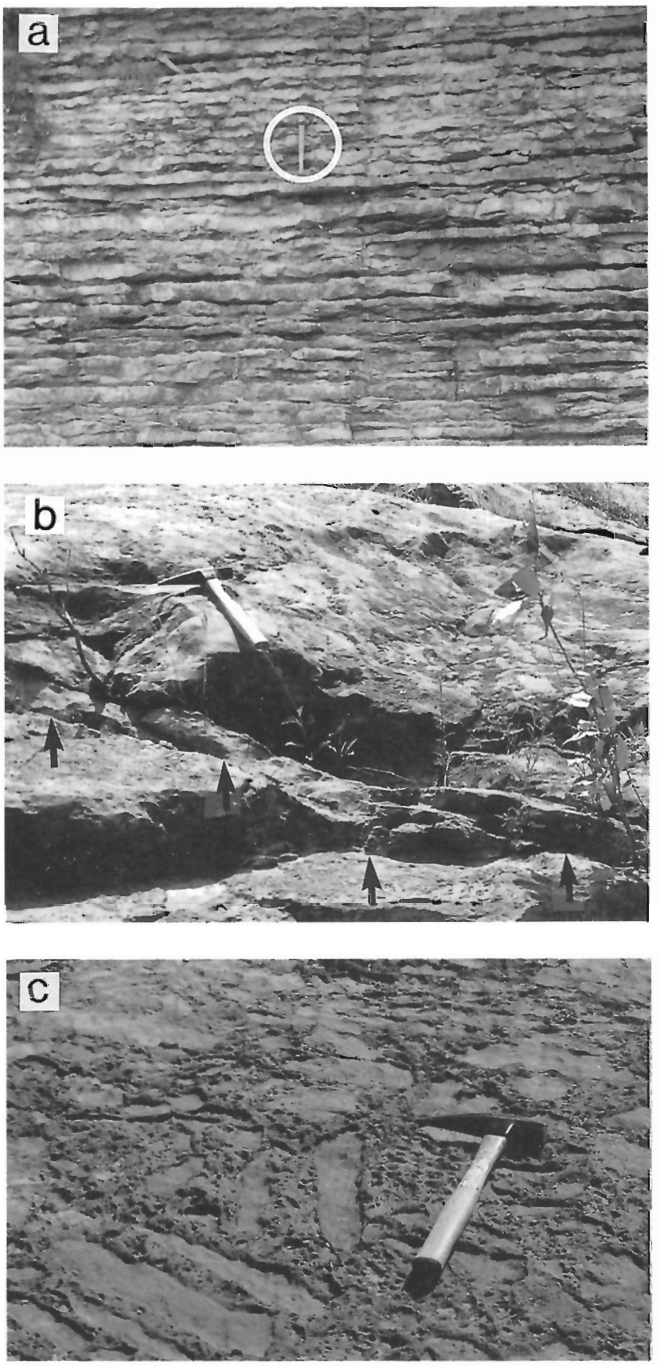

Figure 9. Montréal Formation and St-Casimir Member of Neuville Formation. **a)** Typical succession of wavy-bedded wackestones with few limy shale partings. Hammer (circled) for scale. Neuville shore section. **b)** Plane-bedding view of a truncated surface (outlined by arrows) at the base of a slumped horizon. Ste-Anne section. **c)** Dismembered carbonate beds from intense rotational synsedimentary deformation resulting in oligomict conglomerate with typical raft-shaped wackestone fragments. Ste-Anne section.

the limestone/shale succession, with each individual cycle (1 to 2 m thick) given by an upward increase in the percentage and thickness of limestone beds (Fig. 10a). Bioclastic material is either represented by in situ macrofauna, (bryozoans, brachiopods, pelecypods, among others) or by a fine ash of disarticulated and definitively reworked material, concentrated in bioclastic lenses observed in the fine grained limestones. Bioturbation is common and represented by small horizontal and vertical burrows.

In the southwestern part of the St. Lawrence Lowlands platform, a nodular to strongly wavy-bedded facies known as the "Terrebonne facies" (formerly the Terrebone Member of Clark, 1972) is observed at two stratigraphic intervals (Fig. 3). The nodular facies is predominantly given by bioclastic-rich grainstones and packstones with the nodules surrounded by various amount of limy shales (Fig. 10b). These coarse grained sediments are sometimes deposited as graded and laminated sediment in small-scale channels cutting through various carbonate lithologies. Nodular to wavy-bedded wackestones are also present. The transition from and to the planar-bedded, fine grained limestones of the Tétreauville Formation is gradual over a very few metres.

Synsedimentary deformation structures are locally developed (Fig. 10c) and were mostly observed in the northeastern part of the platform (Grondines Member).

Preliminary paleoenvironmental interpretation

The Grondines Member of Neuville Formation and Tétreauville Formation are preliminarily interpreted as relatively deep outer shelf deposits, well under the fairweather wave base but possibly over the storm wave base. This interpretation is supported by the uniformed sedimentation of fine grained material, the normal open marine fauna that is commonly preserved in life position, the local reworking and disarticulation of bioclastic material, likely from wanning flow currents of storm origin and the lack of well defined sedimentary structures besides some large

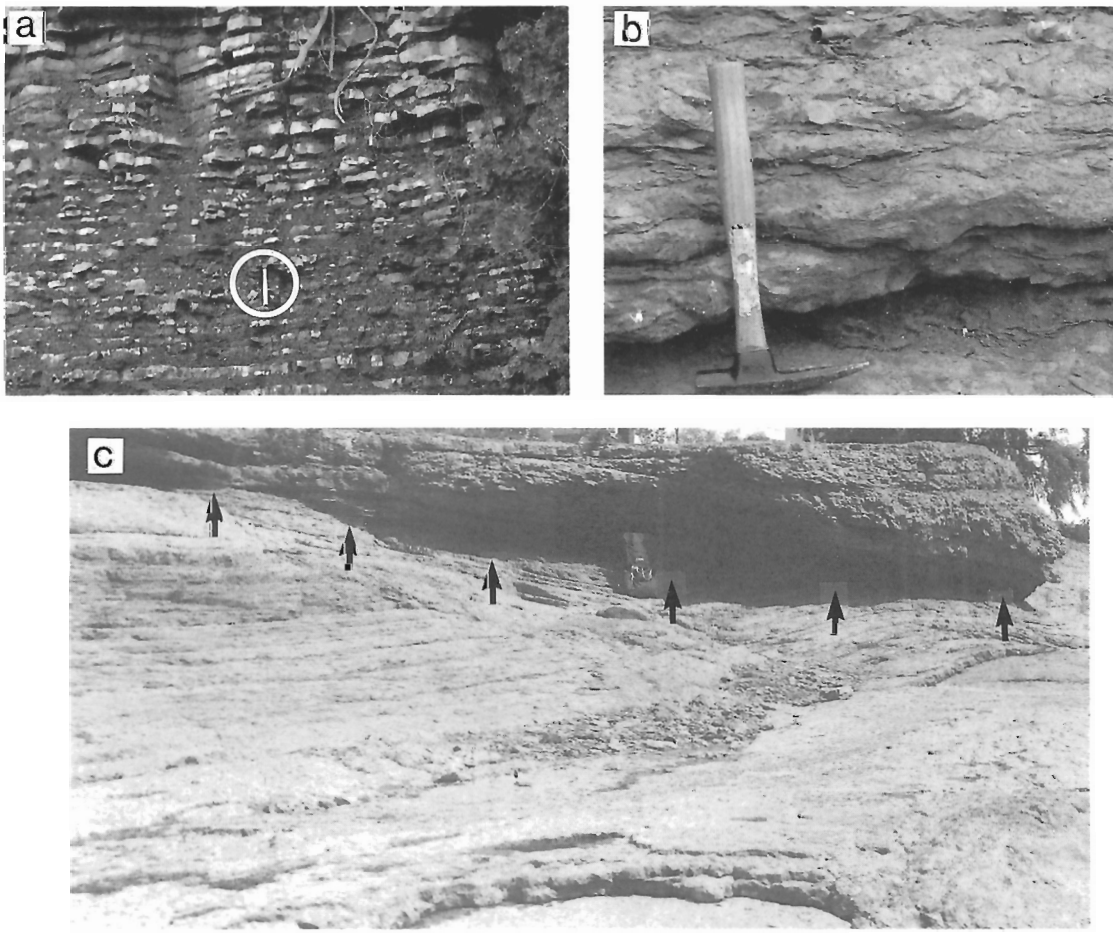

Figure 10. Tétreauville Formation and Grondines Member of Neuville Formation. **a)** Typical succession of planar-bedded wackestones and lime mudstones with abundant limy shale interbeds. Note the upward increase in thickness and abundance of carbonate beds. Hammer (circled) for scale. Grondines shore section. **b)** Nodular packstones surrounded by limy shales, "Terrebonne facies". Ouareau section. **c)** Truncated surface (outline by arrows) at the top of a intensely slumped horizon, over which a 2 metre- sized, well-bedded carbonate unit has slid. Packsac for scale. Grondines shore section.

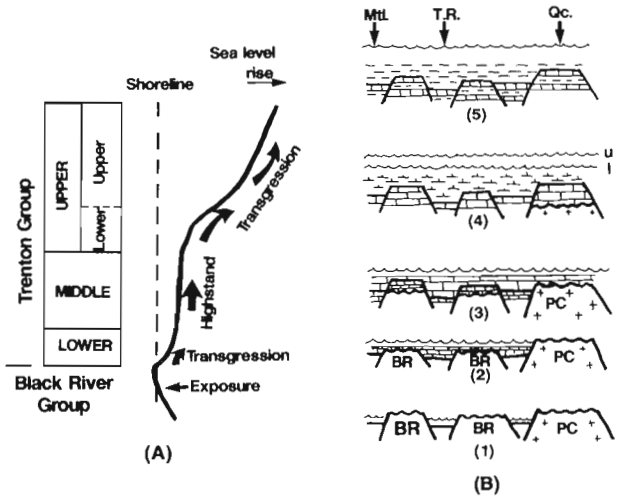

Figure 11. A) Sea level fluctuations recognized in the Trenton Group. The lower Trenton refers to the lower part of the Trenton Group (see text), the middle Trenton equals the Deschambault Formation, the lower part of the upper Trenton refers to Montréal Formation and Saint-Casimir Member whereas the upper part of the upper Trenton refers to Tétreauville Formation and Grondines Member. **B)** Proposed paleogeographic evolution of the latest Black River - earliest Utica time interval (see text for explanation). BR is Black River Group, PC is Precambrian basement, Mtl is Montréal, T.R. is Trois-Rivières and Qc is Québec City. Vertical scale for 11b is strongly exaggerated.

scale hummocky cross-stratifications (Wilson, 1986). The typical greater amount of limy shales in this interval of the upper part of Trenton Group is most likely related to an increase in subsidence rate of the platform and to the difficulty for the shallow subtidal carbonate factory to keep pace with rising sea level. The general upward increase in fine grained siliciclastic sedimentation heralds the overlying Utica Shales.

The Terrebonne facies could be interpreted either as a number of coarse-grained influx from the shallower part of the shelf into the more deeper outer shelf setting (Clark, 1972) or as resulting from seaward progradation of the shallower part of the outer shelf (e.g. Montréal Formation) following a pause or a decrease in the subsidence of the platform.

DISCUSSION

The Trenton Group of southern Quebec is a threefold lithostratigraphic unit with, 1) a lower part of very shallow subtidal and locally restricted carbonate sedimentation, 2) a middle part of shallow subtidal sedimentation on an open carbonate ramp, and 3) an upper part of initially shallow to ultimately deep outer shelf sedimentation. The Trenton commonly overlies a subaerial exposure surface at the top of Black River Group. Whether the relative sea level fall at the end of Black River sedimentation is of eustatic or tectonic origin is problematic. The Mohawkian Stage (englobing the Blackriverain and Trentonian Substages) is a period of relative eustatic sea level rise (Vail et al., 1977; Hallam, 1984). The tectonic scenario is supported by, 1) the local conformable transition between the two groups, 2) the proposed paleogeographic and paleotectonic evolution for the Trenton Group (see below), and 3) the tectonically active setting of the Quebec Reentrant for that time interval (Knight et al., 1991).

The vertical paleoenvironmental evolution of the Trenton is summarized in terms of relative sea level evolution in Figure 11a. This sea level evolution can be seen as resulting from a general transgressive event composed of an initial minor transgressive phase, a succeeding major sea level highstand phase followed by the resumption and acceleration of the transgressive event. A similar paleoenvironmental evolution for the Trenton Group was proposed from rock thin sections and organic matter studies (Bertrand and Héroux, 1981).

It is still unclear whether the sea level rise recorded in the Trenton results from eustasy, tectonism or even from a combination of the two end-members. The published eustatic sea level curves for Late Ordovician time suggest worldwide sea level rise for that time interval (Vail et al., 1977; Hallam, 1984). Some, however, also argues for local and regional tectonic overprints. The latest are demonstrated by 1) the likely tectonically-driven sea level fall at the end of Black River time, 2) the important thickness and regional facies changes in Deschambault Formation (Lavoie, 1992), and 3) the active tectonic environment in which the carbonate platform of the Quebec Reentrant evolved in that time interval (Knight et al., 1991).

The Late Ordovician carbonate sedimentation in the Quebec Reentrant was synchronous with the tectonic emplacement of allochthons on the carbonate shelf at the St. Lawrence Promontory (Knight et al., 1991). Flyschoid sedimentation heralding the westward migration of Taconian allochthons started in middle Middle Ordovician time on the continental slope facies in the Quebec Reentrant (Bernstein et al., 1992). The initiation of accretion at the continental margin occurs almost synchronously with the end of Trenton sedimentation in southern Quebec as expressed by the sedimentation of the overlying syn-orogenic flysch (Sainte-Rosalie Group; Globensky, 1987).

CONCLUSIONS

The following general statements are drawn from this field study and are used as working hypothesis in the ongoing research.

The Trenton Group is a threefold lithostratigraphic interpreted to represent progressively deeper sedimentary conditions on a carbonate platform. Figure 11b summarizes the proposed paleogeographic and paleotectonic evolution for the Trenton Group of southern Quebec. It is shown that the Trenton platform was likely dissected by extensional faults delineating separate tectonic blocks that were subsiding at different rates. The local and regional variability (fault controlled?) of the sedimentary history of the basin is

clear for the lower part of the Trenton (this study) and for the middle part of it (Lavoie, 1992). An alternative explanation would be that the Trenton platform in its earliest stage of development, was typified by geographic highs and lows, likely following the migration of a peripheral bulge on the Quebec Reentrant continental margin at the end of the Middle Ordovician (Knight et al., 1991). However, the same tectonic event would have resulted in faulting of the platform leading to the first scenario.

In latest Black River time (Fig. 11b (1)), subaerial exposure was synchronous with local continued sedimentation for the Black River Group in the southern part of the platform is suggested as well as subaerial exposure of precambrian basement in the northern segment of the platform. In earliest Trenton time (Fig. 11b (2)); shallow water sedimentation, locally protected, was occurring over the entire platform in the south, but the Precambrian basement was still subearially exposed in the north. In middle Trenton time (Fig. 11b (3)); shallow to locally deep water, highstand carbonate ramp sedimentation was established over the entire platform. In late Trenton time (Fig. 11b (4)); the acceleration of tectonic subsidence of the platform resulted in deep to deeper outer shelf mixed sedimentation. Finally, in earliest Utica time (Fig. 11b (5)), the final drowning of the carbonate platform occurred, synchronous with syn-orogenic flyschoid sedimentation.

ACKNOWLEDGMENTS

The author is indebted to E. Asselin and to P. Gervais for an invaluable and patient field assistance. Critical reading of the manuscript was assured by R. Bertrand of CGQ, his help is acknowledged.

REFERENCES

B.E.I.C.I.P. (Bureau d'Études Industrielles et de Coopération Technique de l'Institut Français du Pétrole)
1975: Étude sédimentologique du Cambro-Ordovicien des Basses-Terres du Saint-Laurent; Ministère des Richesses Naturelles du Québec, DP-375.

Bernstein, L.
1992: The Lower Ordovician Beekmantown Group, Quebec and Ontario; Ph.D. thesis, Université de Montréal, Montréal.

Bernstein, L., James, N.P., and Lavoie, D.
1992: Cambro-Ordovician stratigraphy in the Quebec Reentrant, Grosses-Roches - Les méchins area, Gaspésie, Québec; in Current Research, Part E; Geological Survey of Canada, Paper 92-1E, p. 381-392.

Bertrand, R. and Héroux, Y.
1981: Carbone organique: indicateur potentiel de paléoenvironments; deux exemples; Canadian Journal of Earth Sciences, v. 18, p. 1838-1849.

Bertrand, R., Humbert, L., Achab, A., Calise, G., Chagnon, A., Héroux, Y., and Globensky, Y.
1983: Recristallisation des calcaires micritiques en fonction de la maturation thermique dans les Basses-Terres du Saint-Laurent du Québec; Canadian Journal of Earth Sciences, v. 20, p. 66-85.

Clark, T.H.
1972: Région de Montréal / Montréal area; Ministère des Richesses naturelles du Québec, RG 152.

Clark, T.H. and Globensky, Y.
1973: Portneuf et parties de St-Raymond et de Lyster; Ministère des Richesses Naturelles du Québec, RG 148.
1975: Région de Grondines / Grondines area; Ministère des Richesses naturelles du Québec, RG 154.
1976: Région de Laurentides (moitié est) et de Rawdon (partie sud-est) / Laurentides (east half) and Rawdon (southeast part) map-areas; Ministère des Richesses naturelles du Québec, RG 157.

Globensky, Y.
1987: Géologie des Basses-Terres du Saint-Laurent; Ministère de l'Énergie et des Ressources du Québec, MM 85-02.

Hallam, A.
1984: Pre-Quaternary sea level changes; Annual Review of Earth and Planetary Sciences, v. 12, p. 205-243.

Héroux, Y. and Tassé, N.
1990: Organic-matter alteration in an early Paleozoic basin: Zonation around mineral showings compared to that around intrusions, St. Lawrence Lowlands, Quebec, Canada; Geological Society of America Bulletin, v. 102, p. 877-888.

Hofmann, H.J.
1963: Ordovician Chazy Group in southern Quebec; Bulletin of American Association of Petroleum Geologists, v. 47, p. 270-301.

INRS-Pétrole
1975: Stratigraphie et potentiel pétrolier du sondage Husky Gentilly No. 1; Ministère de l'Énergie et des Ressources du Québec, DP-0322.
1976a: Forage Bald Mountain St-Roch No. 1; Ministère de l'Énergie et des Ressources du Québec, DPV-0367.
1976b: Etude des Groupes de Lorraine, d'Utica et de Trenton, Basses-Terres du Saint-Laurent; Ministère de l'Énergie et des Ressources du Québec, DP-0375.

Knight, I., James, N.P., and Lane, T.E.
1991: The Ordovician St. George Unconformity, northern Appalachians: The relationship of plate convergence at the St. Lawrence Promontory to the Sauk/Tippecanoe sequence boundary; Bulletin of the Geological Society of America, v. 103, p. 1200-1225.

Lavoie, D.
1992: The Middle Ordovician (Caradocian) Deschambault Formation, St. Lawrence Lowlands, southern Quebec: a shallow water carbonate ramp on a drowning platform; in Current Research, Part D; Geological Survey of Canada, Paper 92-1D, p. 223-234.

Mehrtens, C.J.
1979: A paleoenvironmental reconstruction of a shelf margin, the Caradoc (Middle Ordovician) of southern Quebec; Ph.D. thesis, The University of Chicago, Chicago.

Okulitch, V.J.
1939: The Black River Group in the region between Montreal and Quebec; American Journal of Sciences, v. 237, p. 81-93.

Ross, R.J., and 27 others
1982: The Ordovician System in the United States: correlation chart and explanatory notes; International Union of Geological Sciences, Publication No. 12, 73 p.

SOQUIP (Société Québécoise d'Initiatives Pétrolières)
1984: Carte structurale du Trenton Autochtone; Ministère de l'Énergie et des Ressources du Québec, DP 84-31B.

Tassé, N., Schrijver, K., Héroux, Y., and Chagnon, A.
1987: Étude gitologique et évaluation du potentiel minéral des Basses-Terres du Saint-Laurent; Ministère de l'Énergie et des Ressources du Québec, MB 87-46.

Vail, P.R., Mitchum, R.M., Todd, R.G., and Widmier, J.M.
1977: Seismic stratigraphy and global sea level changes from seismic stratigraphy; in Stratigraphic interpretation of seismic data, (ed.) C.E. Payton; American Association of Petroleum Geologists, Memoir 26, p. 49-212.

Wilson, J.L.
1986: Carbonate Facies in Geologic History; Springer-Verlag, New York, Heidelberg, Berlin, 471 p.

Young, F.G.
1964: Petrology of the Deschambault Formation, Trenton Group, St. Lawrence Lowlands of Quebec; M.Sc. thesis, McGill University, Montréal.

Geological Survey of Canada Project 920001 ML

Comparison of three electromagnetic techniques to determine conductivity of overburden in northeastern Ontario[1]

G.J. Palacky
Mineral Resources Division

Palacky, G.J., 1993: Comparison of three electromagnetic techniques to determine conductivity of overburden in northeastern Ontario; in Current Research, Part D; Geological Survey of Canada, Paper 93-1D, p. 173-182.

Abstract: During the 1992 field season, conductivities were measured with the Geonics EM-31 instrument at 22 borehole sites. The results have been compared with conductivity estimates based on horizontal-loop electromagnetic (HLEM) and helicopter electromagnetic (HEM) data. Conductivities obtained with the three techniques were similar in areas of homogenous overburden. In areas of complex Quaternary stratigraphy, EM-31 data reflected mostly the conductivity of the near-surface layer and were in good agreement with conductivities of the first layer determined by inversion of HLEM data. Apparent conductivities calculated from HEM data reflect the average conductivity of Quaternary sediments, except for areas of shallow overburden, where they become smaller because of the effect of the resistive bedrock. Analysis of the data shows that caution should be exercised when interpreting Quaternary geology from apparent conductivity maps, particularly in areas of thin or complex overburden. Instead of maps, use should be made of conductivity sections, which can also be produced from HEM data.

Résumé : Au cours de la période de prospection de 1992, on a mesuré les conductivités à l'aide de l'appareil Geonics EM-31 a 22 emplacements de trous de sondage. On a comparé les résultats aux valeurs estimées de la conductivité établies à partir de l'interprétation des levés électromagnétiques avec bobines horizontales (HLEM) et des levés électromagnétiques héliportés (HEM). Les conductivités mesurées par ces trois techniques étaient semblables dans les zones où les terrains de couverture sont homogènes. Dans les secteurs où la stratigraphie quaternaire est complexe, les données EM-31 reflétaient principalement la conductivité de la couche de subsurface et concordaient bien avec les conductivités de la couche supérieure, telles que déterminées par inversion des données HLEM. Les conductivités apparentes calculées à partie des données HEM reflètent la conductivité moyenne des sédiments quaternaires, sauf dans les secteurs de terrains de couverture peu épais, où elles diminuent en raison de l'influence du substratum rocheux, dont la résistivité est élevée. L'analyse des données montre qu'il faut interpréter avec prudence la géologie quaternaire d'après les cartes de la conductivité apparente, surtout dans les secteurs où les terrains de couverture sont minces ou de nature complexe. Au lieu de cartes, on devrait employer les profils de conductivité, que l'on peut aussi établir à partir des données HEM.

[1] Contribution to Canada-Ontario Subsidiary Agreement on Northern Ontario Development (1991-1995), a subsidiary agreement under the Economic and Regional Development Agreement. Project funded by the Geological Survey of Canada.

INTRODUCTION

During the last decade, maps of apparent conductivity have become standard products of airborne electromagnetic (AEM) surveys. Such maps have successfully been used in mineral exploration and other applications (Palacky and West, 1991). Since 1985, the Geological Survey of Canada has been investigating the possibility of using apparent conductivity maps and conductivity sections for mapping of Quaternary sediments (Palacky et al., 1992a). An extensive program has been funded under the Canada-Ontario Mineral Development Agreement (1985-1990). Results of ground electromagnetic (EM) surveys have been used to locate boreholes for overburden investigations in the Kapuskasing-Timmins area (Palacky et al., 1992c, d). By correlating the results of ground EM measurements and drilling, Palacky and Stephens (1990) have found that clay, till, and sand have distinct conductivities in a given area. The average conductivity of sand was 4.3 mS/m, till 8.9 mS/m, and clay 21.6 mS/m (milliSiemens per metre). This finding means that if conductivities of the three sediment types can be accurately measured in the field, such information could be used in Quaternary geological mapping.

A problem, which has not been studied in detail, is whether maps of apparent conductivity resulting from AEM surveys can be used for such purpose. No systematic comparison has ever been attempted of conductivity estimates based on ground and airborne EM data. While similar conductivity patterns can be seen in maps compiled from various types of AEM measurements, the actual conductivity values depend on the AEM system used in the survey and on the interpretation model. Over the same area, time-domain and helicopter AEM surveys will yield different conductivity values.

In interpretation of AEM data, conductivities are calculated using a selected model at all survey points along the flight lines. The distance between such points depends on the aircraft speed and data sampling interval. In recent surveys, this interval has been 10 times per second, corresponding a ground distance of 5 to 15 m. As the line spacing of AEM surveys is typically 200 m, the density of reliable conductivity determinations will always be much higher in the flight direction. To obtain a conductivity map, conductivities are interpolated between the lines and gridded.

The model most often used in conductivity calculations is a homogenous half-space. In most regions of Canada, Quaternary stratigraphy is rather complex, and clay, silt, till, and sand are often found in the same borehole. In such conditions, the interpretation model becomes inadequate and the estimated conductivities do not reflect the true conductivity of various overburden layers. The calculated value is therefore called apparent conductivity.

Ground conductivity can also be interpreted from the results of ground EM measurements or resistivity soundings. While the latter method provides the most accurate data on conductivities in a layered medium, it is slower and more expensive than EM techniques. Conductivity can be measured in situ using specifically designed EM instruments (Geonics EM-31 and EM-34) or it can be interpreted from the results of other types of ground EM surveys. Unless the ground is electrically homogenous (which is seldom the case), conductivity determinations will vary with ground penetration, which depends on the equipment used and on the survey parameters, particularly the frequency and transmitter-receiver separation.

Palacky et al. (1992b) described the use of several geophysical methods at the Val Gagné test site, where 20 to 50 m of conductive, mostly homogenous clay overlie resistive bedrock. Geonics EM-31 and EM-34 conductivity measurements, horizontal-loop EM (HLEM) surveys and resistivity sounding yielded similar conductivity values. After evaluation of the results it was concluded that the four methods would be equally suitable for conductivity mapping. It was found later that overburden elsewhere in northeastern Ontario is usually electrically inhomogeneous and that the site is not typical of the area. The routine ground EM coverage along the drilling transects was carried out with the multifrequency APEX MaxMin I system, which allows a great flexibility in interpretation of conductivity of horizontal layers.

After evaluation of existing data from extensive ground and airborne EM surveys in northeastern Ontario (Palacky and Stephens, 1991; Smith, 1992), it was decided to make a new comparison of three techniques (Geonics EM-31, HLEM, and helicopter AEM) at various drilling sites that would be more representative of Quaternary geology in northeastern Ontario. The immediate need for such investigation was prompted by the necessity to compile overburden conductivity maps in the Blake River Syncline area, north of Kirkland Lake. The time-domain AEM survey was flown in April-May 1992 and was funded by the Northern Ontario Development Agreement (NODA).

In June 1992, ground conductivities were measured with the Geonics EM-31 instrument at 22 borehole sites in northeastern Ontario. The data have been correlated with conductivities interpreted from helicopter AEM (HEM) and HLEM surveys. Figure 1 gives the location of the boreholes and of two transects surveyed with an HEM system (Kapuskasing and Smooth Rock Falls).

GEOLOGY

Most of northeastern Ontario is covered by Quaternary sediments, whose thickness can reach 60 m. Overburden studies are an integral part of drift prospecting which is an important mineral exploration technique widely used in the area (DiLabio and Coker, 1989). Smith (1992) described the results of a project whose aim was to link previously unknown Quaternary stratigraphy in the area north of the Timmins mining camp with that established from abundant exposures in the Moose River basin. Using funding provided by the Canada-Ontario Mineral Development Agreement (1985-1990), 70 boreholes were drilled using Rotasonic equipment in 1987-1988. Stratigraphic interpretation of the results has indicated a sequence of at least four and probably

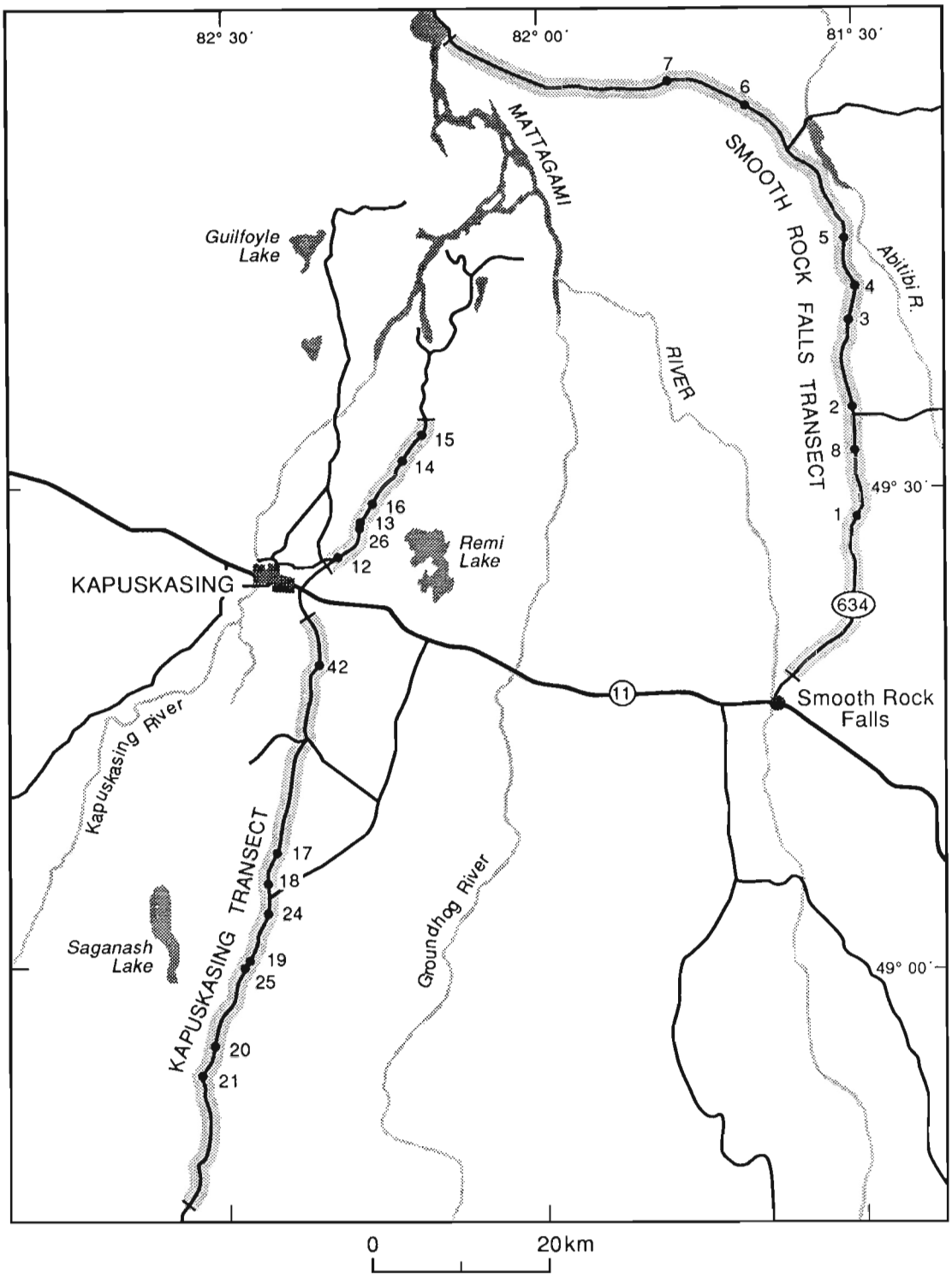

Figure 1. Location of Kapuskasing and Smooth Rock Falls transects in northeastern Ontario. HEM surveys were flown along the shaded lines. Detailed ground investigations were carried out in the vicinity of boreholes whose location is depicted by dots with numbers.

Table 1. Location (township, latitude and longitude) and simplified Quaternary log (drill core log) of boreholes (BH) along the Smooth Rock Falls transect

BH	Township	Latitude	Longitude	Drill Core Log
7	Sheldon	49°55.22'	81°47.62'	over 32 m sand
6	Pinard	49°53.58'	81°39.66'	0-6 m till, 6-82 m sand/silt
5	Avon	49°45.27'	81°30.61'	0-5 m clay/silt, 5-16 m sand, 16-18 m clay/silt, 18-34 m till
4	Homuth	49°42.27'	81°29.87'	0-12 m sand, 12-35 m mostly till
3	Homuth	49°40.55'	81°30.50'	0-2 m clay/silt, 2-10 m sand, 10-32 m mostly till, 32-38 m sand
2	Adanac	49°34.56'	81°30.42'	0-14 m sand/till, 14-36 m clay/silt, 36-44 m till
8	Adanac	49°32.17'	81°30.38'	0-7 m till, 7-32 m clay/silt, 32-39 m till
1	Adanac	49°28.00'	81°30.50'	0-7 m till/silt, 7-37 m clay/silt, 37-40 m till

Table 2. Location (township, latitude and longitude) and simplified Quaternary log (drill core log) of boreholes (BH) along the Kapuskasing transect

BH	Township	Latitude	Longitude	Drill Core Log
15	Gurney	49°33.50'	82°11.00'	0-2 m till, 2-9 m clay/silt
14	Gurney	49°31.87'	82°13.10'	0-2 m till, 2-12 m clay
16	Gurney	49°29.00'	82°15.95'	0-7 m sand, 7-16 m clay/silt, 16-25 m till, minor sand
13	Teetzel	49°27.88'	82°16.95'	0-3 m clay/silt, 3-30 m mostly till, minor sand
26	Teetzel	49°27.83'	82°17.00'	0-3 m clay/silt, 3-30 m mostly till, minor clay and sand
12	O'Brien	49°25.34'	82°19.87'	0-2 m clay/silt, 2-19 m sand, 19-29 m till, minor sand
42	Swanson	49°15.22'	82°22.63'	0-33 m clay, 33-35 m sand
17	Casselman	49°06.10'	82°25.88'	0-19 m clay/silt, 19-34 m sand
18	Casselman	49°05.00'	82°26.06'	0-3 m till, 3-8 m clay/silt, 8-23 m sand, 23-35 m till
24	Casselman	49°03.78'	82°26.08'	0-6 m clay/silt, 6-9 m sand
19	Fenton	49°00.20'	82°28.25'	0-2 m clay, 2-4 m till, 4-15 m sand, 15-29 m till, 29-35 m sand
25	Fenton	49°00.11'	82°28.42'	0-5 m clay, 5-12 m sand, 12-24 m till
20	Seaton	48°55.28'	82°31.08'	0-15 m clay, 15-23 m till
21	Seaton	48°53.55'	82°32.09'	0-5 m clay, 5-22 m sand, 22-26 m till/silt

five till units. In many boreholes, sand and/or glaciolacustrine clay were intersected. In her memoir, Smith (1992) lists the drilling results in detail.

In Tables 1 and 2, a summary is given of Quaternary lithology intersected in selected boreholes located along the Smooth Rock Falls and Kapuskasing HEM transects. The same sites were used for correlation of various types of conductivity determinations. Listed are, in sequence, the borehole number, the name of the township in which the borehole is located, latitude and longitude of the site, and simplified borehole lithology. As the purpose of the study was to establish a correlation between Quaternary lithology and conductivity, references to stratigraphy have been omitted. Layers thinner than 1 m were not listed and sequences consisting of alternating sediments are not discriminated (e.g., clay and silt sequence is denominated clay/silt).

FIELD TECHNIQUES

During the 1992 field survey, the geographic coordinates of all borehole sites were determined with a GPS (Global Positioning System) Pathfinder unit. The manufacturer, Sumav Corporation, claims accuracy of 15 m, but because of "Selective Availability" (a US military euphemism for degrading the GPS signal for other users), the actual precision was reduced to about 50 m. The latitudes and longitudes listed in Table 1 are given to one hundredth of a minute (approximately 18 m).

The Geonics EM-31 instrument measures ground conductivity at low induction numbers (McNeill, 1990). Two small horizontal coils are placed 3.66 m apart at the ends of a rigid boom. The operating frequency is 9.8 kHz and the effective depth of penetration is approximately 6 m. The instrument is operated by one person and conductivity readings can be carried out quickly. During the field work, at least ten readings were taken near the borehole; the stations were spaced 10 m along a profile centred on the borehole. The results listed in the second column of Tables 3 and 4 (EM-31 – σ_a) are the average values of all readings taken (in mS/m).

Helicopter EM (HEM) surveys were carried out in 1987 along the Kapuskasing and Smooth Rock Falls transects. The contractor, Aerodat Limited, used a multicoil, multi-frequency EM system. The receivers and transmitters were mounted in a bird whose terrain clearance was maintained at approximately 30 m. Two pairs of vertical coaxial coils were operated at frequencies 935 and 4531 Hz, two horizontal coplanar coils at 4175 and 32 000 Hz. The transmitter-receiver separation is approximately 7 m. The system was described in detail by Palacky and West (1991). Conductivity or conductance can be calculated from the field data assuming a certain interpretation model. In this study, the model was a 200 m thick horizontal layer which is equivalent to homogenous half-space. The assumption of a layer unrealistically thick to approximate overburden most likely resulted in underestimating overburden conductivity at many locations. For comparisons in this study, use was made only of apparent conductivities calculated from the horizontal coplanar responses. Apparent conductivities listed in Tables 3 and 4 (HEM) are for the frequency of 4175 Hz (σ_{lf}) and 32 kHz (σ_{hf}). Because of different depth penetration, it was expected that estimates based on the low-frequency response would be lower than those derived from high-frequency data.

Table 3. Conductivities at selected boreholes (BH) along the Smooth Rock Falls transect: Column 2 - values measured in the field with the Geonics EM-31 instrument (σ_a), 3 and 4 - values interpreted from helicopter EM (HEM) data measured at the frequency of 4175 Hz (σ_{lf}) and 32 kHz (σ_{hf}), 5 - apparent conductivity σ_a, 6 to 8 - first, second and third layer conductivities (σ_1, σ_2, σ_3), 9 to 11 corresponding layer thicknesses (z_1, z_2, z_3). The last seven values were obtained by inversion of horizontal-loop EM (HLEM) data

BH	EM-31	HEM	HEM	HLEM	HLEM	HLEM	HLEM	HLEM	HLEM	HLEM
	σ_a	σ_{lf}	σ_{hf}	σ_a	σ_1	σ_2	σ_3	z_1	z_2	z_3
#	mS/m	mS/m	mS/m	mS/m	mS/m	mS/m	mS/m	m	m	m
7	5.2	4	5	2.4	4.1	0.1*		52		
6	11.5	9	10	10.2	9.7	0.1*		71		
5	7.2	6	7	6.1	18.8	2.8	14.3	5	15	34
4	11.8	5	9	5.1	3.1	10.5	0.1*	13	35	
3	6.8	5	7	4.1	16.6	5.0	8.0	2	10	38
2	11.5	9	14	8.6	3.0	20.0	7.7	15	36	45
8	19.8	14	16	12.9	2.9	18.2	6.5	7	32	39
1	19.1	10	14	13.4	6.1	23.3	0.1*	7	37	

Horizontal-loop EM (HLEM) measurements were carried with the APEX MaxMin I instrument. The primary EM field is generated by a horizontal coil; the EM response is measured by means of another horizontal coil which is sensitive to changes in emf of the secondary magnetic field. The recorded parameters are in-phase and quadrature components at 8 frequencies (110, 220, 440, 880, 1760, 3520, 7040, and 14 080 Hz). Detailed description of the system can be found in Frischknecht et al. (1991). In the surveys described here, the coil separation was 100 m. The results of all HLEM measurements in the Kapuskasing-Timmins area were released as a GSC Open File (Palacky and Stephens, 1991).

In-phase and quadrature readings must be processed in order to obtain estimates of ground conductivity. Interpretation can be made by matching the measured values to phasor diagrams (manually, or by computer), or by data inversion. In northeastern Ontario, use was made of EMIX-MM software (Interpex, 1988). This inversion program is based on ridge regression described by Inman (1975). Examples of field data processed with the software were published by Palacky (1991).

In Tables 3 and 4, conductivities are listed which were calculated specifically for this study using two models: a) Homogeneous half-space: result - apparent conductivity σ_a; b) Two or three horizontal layers: the outputs are conductivities of the first, second and third layer (σ_1, σ_2, σ_3, respectively), and their respective thicknesses (z_1, z_2, z_3). Bedrock conductivity values are indicated by asterisk and fixed at 0.1 mS/m.

DISCUSSION OF RESULTS

Two-layer situations

Unless the ground is homogenous, different estimates of apparent conductivity are obtained with the three EM techniques under consideration. In this section, two-layer situations (overburden, bedrock) are analyzed using examples from the Kapuskasing and Smooth Rock Falls transects.

Table 4. Conductivities at selected boreholes (BH) along the Kapuskasing transect: Column 2 - values measured in the field with the Geonics EM-31 instrument (σ_a), 3 and 4 - values interpreted from helicopter EM (HEM) data measured at the frequency of 4175 Hz (σ_{lf}) and 32 kHz (σ_{hf}), 5 - apparent conductivity σ_a, 6 and 7 - first and second layer conductivities (σ_1, σ_2), 8 and 9 corresponding layer thicknesses (z_1, z_2). The last five values were obtained by inversion of horizontal-loop EM (HLEM) data

BH	EM-31	HEM	HEM	HLEM	HLEM	HLEM	HLEM	HLEM
	σ_a	σ_{lf}	σ_{hf}	σ_a	σ_1	σ_2	z_1	z_2
#	mS/m	mS/m	mS/m	mS/m	mS/m	mS/m	m	m
15	11.2	1.5	2	1.3	12.5	0.1*	9	
14	18.4	3	8	7.3	18.1	0.1*	12	
16	12.4	4	7	6.1	15.2	5.1	12	24
13	19.4	2.5	5	5.2	35.0	4.7	3	36
26	17.5	2.5	5	5.2	26.0	4.8	3	25
12	21.5	5	9	7.4	28.3	6.2	3	30
42	26.4	17	19	17.8	24.0	0.1*	35	
17	31.5	16	21	20.0	29.4	1.8	20	34
18	25.5	7	10	10.9	28.4	2.1	9	34
24	25.8	8	11	12.2	29.4	1.4	6	10
19	20.7	6	10	8.5	21.5	7.8	2	40
25	22.9	5	9	7.7	25.0	6.2	5	25
20	23.0	9	14	12.6	23.7	4.8	15	21
21	23.8	6	10	8.4	23.2	5.6	7	27

Only one borehole (7, Smooth Rock Falls transect) was located in an area where overburden is deep and homogenous. Over 32 m of sand were intersected before the drilling was terminated. Conductivity measured with the EM-31 instrument was 5.2 mS/m. Apparent conductivities determined by interpretation of HEM data were 4 mS/m for the low frequency and 5 mS/m for 32 kHz. Inversion of HLEM data yielded 2.4 mS/m for the homogenous half-space model and 4.1 mS/m for the first layer assuming a two-layer model (Table 3). The HLEM method, which has the deepest penetration, was more affected by the underlying resistive bedrock than other techniques; therefore σ_a was lower than σ_1. All other values were within the range found by Palacky and Stephens (1990) for sand in the area (4.3 ± 1.3 mS/m).

At borehole 42 (Kapuskasing transect), 33 m of clay were intersected. If the clay layer were thicker than the penetration of all techniques, the estimated conductivities would be very close. EM-31 measurements indicated a value of 26.4 mS/m, HEM survey 17 and 19 mS/m (for low and high frequency, respectively), inversion of HLEM data resulted in apparent conductivity estimate of 17.8 mS/m and first-layer conductivity of 24.0 mS/m. The most reliable clay conductivity estimates were obtained from HLEM inversion using a two-layer model and EM-31 surveys. Palacky and Stephens (1990) found a conductivity range of 21.6 ± 3.2 mS/m for clay in the survey area. Apparent conductivities determined from HEM and HLEM surveys were affected by the underlying resistive bedrock.

There are three other situations in which inversion of HLEM data indicated overburden consisting of one layer: borehole 6 on the Smooth Rock transect, and boreholes 14 and 15 on the Kapuskasing transect. At borehole 6, a 6 m thick till layer was underlain by 76 m of sand and silt. All conductivity estimates were close, ranging from 9.7 to 11.5 mS/m, thus indicating that all techniques perceived the overburden as homogenous and thick.

At boreholes 14 and 15, conductivity estimates based on different techniques varied. The thin overburden (9 to 12 m) is formed by clay under a 2 m thick veneer of till. As expected, the EM-31 results and σ_1 were close (18.4 and 18.1 mS/m, respectively, at borehole 14; 11.2 and 12.5 mS/m at borehole 15). Apparent conductivities determined by interpretation of HEM and HLEM data were much lower (between 1.5 and 8 mS/m). The conductivity estimates were affected by the resistive bedrock because of the much greater depth penetration of the two techniques.

The last two examples demonstrate that σ_a determined from HEM data in area of shallow overburden are not representative of overburden conductivity.

Kapuskasing transect

At the remaining 12 boreholes along the Kapuskasing transect, overburden could be approximated by two layers (three-layer model). According to the results of HLEM data inversion, the most conductive layer was at the top. This finding is consistent with geology - with the exception of borehole 16, clay and/or silt form the uppermost layer in the area. The first layer conductivity (Table 4) was fairly consistent, ranging from 21.5 to 35.0 mS/m (mean 24.5 mS/m for 11 boreholes). The EM-31 conductivity determinations varied between 17.5 and 31.5 mS/m (mean 21.0 mS/m). These values are close to the mean conductivity of clay (21.6 mS/m) found by Palacky and Stephens (1990). The conductivity of the second layer varied significantly; it was low (from 1.4 to 2.1 mS/m) at boreholes 17, 18, and 24, where the layer is composed mostly of sand. At the remaining boreholes, till predominates and the average conductivity was 5.0 mS/m.

The mean conductivity determined from HEM data at 11 boreholes was 6.1 and 9.5 mS/m (low and high frequency data, respectively). The average apparent conductivity estimated by inversion of HLEM data (homogenous half-space model) was 8.9 mS/m. The analysis shows that the low-frequency HEM data are mostly affected by the second layer, which is generally much thicker, than by the more conductive first layer (see columns z_1 and z_2 in Table 4). Poor correlation between HEM and EM-31 conductivities is caused by a difference in depth penetration of the two systems in a geologically complex area.

The highest apparent HEM conductivities along the Kapuskasing transect were estimated at boreholes 17 and 42, where thick clay layers were intersected. The lowest σ_a values were estimated at boreholes 14 and 15, where the overburden layer is thin. It would be extremely difficult to correctly determine Quaternary lithology at other locations from HEM conductivity patterns.

Smooth Rock Falls transect

The most complex overburden conditions were found along the Smooth Rock Falls transect. Logs from six boreholes located along the transect are depicted in Figure 2. HLEM data could best be interpreted using a four-layer model, although the three-layer model was used at two locations. Conductivities (in mS/m) obtained by constrained inversion with fixed layer thicknesses are indicated in the illustration. The conductivity distribution varies along the transect. In its northern part (boreholes 3, 4, and 5), a till layer 17 to 21 m thick is overlain by sand. Locally, at boreholes 3 and 5, there is a thin (less than 5 m) clay layer, and HLEM data can be interpreted with a four-layer model (the first and third layers are conductive, the second layer and basement are resistive). Conductivity of sand varied between 2.8 and 5.0 mS/m, that of till from 8.0 to 14.3 mS/m. Apparent conductivities remained low and within a narrow range, from 4.1 to 6.1 mS/m, indicating that the thin clay layer had an almost negligible effect on HLEM data.

Apparent conductivities estimated from HEM data (Table 3) were almost identical at the low frequency - 4175 Hz (between 5 and 6 mS/m) and somewhat higher at the high frequency - 32 kHz (between 7 and 9 mS/m). Conductivities measured with the EM-31 instrument were low at boreholes 3 and 5 (6.8 and 7.2 mS/m, respectively), but higher at borehole 4 (11.8 mS/m). The measurements are not consistent with the drilling results and the inversion of HLEM data; it

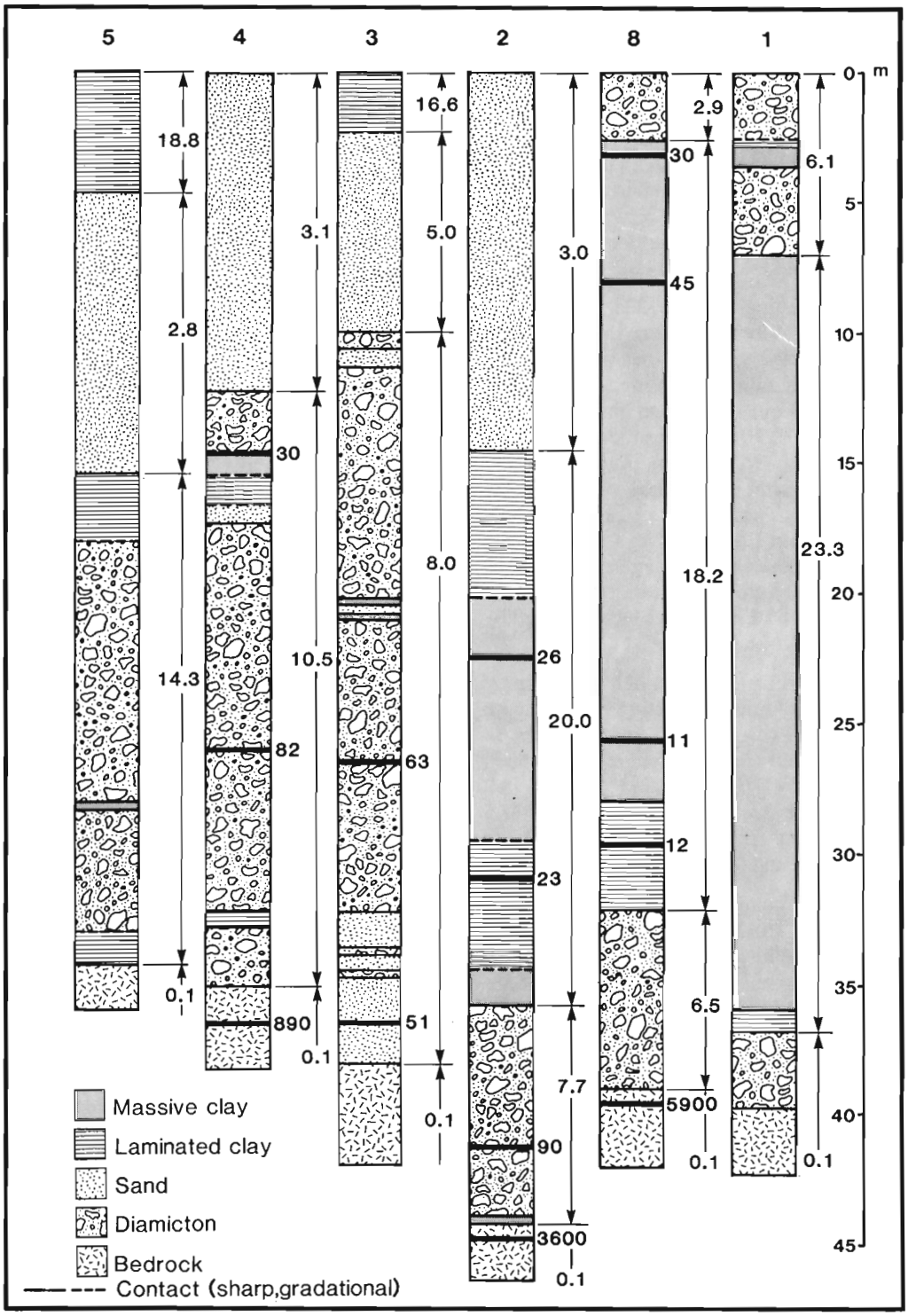

Figure 2. Drill logs of six holes along the Smooth Rock Falls transect. Numbers between arrows indicate conductivities determined by inversion of HLEM data. Resistivities determined in laboratory on drill core samples are written next to thick horizontal lines which indicate the sample origin. Drill log information courtesy of S.L. Smith (pers. comm., 1992).

was expected that readings at boreholes 3 and 5 would be higher than at borehole 4, where no clay was intersected by drilling.

At boreholes 1, 2, and 8, conductive clay is overlain by more resistive sediments - sand in borehole 2 and till in boreholes 1 and 8. The respective conductivities of the first layer determined by inversion of HLEM data were 3.0, 6.1, and 2.9 mS/m. At all three boreholes, EM-31 conductivities were much higher, 11.5, 19.1, and 19.8 mS/m, respectively. Apparently, the readings were affected by the underlying clay whose mean conductivity from HLEM data inversion was over 20 mS/m. Apparent conductivity estimates from HEM data ranged from 9 to 14 mS/m for low-frequency data and between 14 and 16 mS/m for high-frequency data. There was a good agreement between these estimates and HLEM apparent conductivity.

In situ conductivity determinations were complemented by laboratory resistivity measurements on drill core samples (Katsube, pers. comm., 1992). The samples were 8-9.5 cm in diameter and 10-25 cm in length. To preserve their natural water content, they were sealed in plastic shortly after their recovery from the borehole. The laboratory measurement technique was described by Katsube et al. (1973). In Figure 2, the setting of the samples and their resistivities are indicated in the drill log (the measured values are shown rather than their inverse, conductivity). Seven clay samples were analyzed from boreholes 2, 4, and 8. Their average resistivity was 25.3 Ω•m, corresponding to conductivity of 39.5 mS/m. This value is significantly higher than any estimate based on interpretation of EM data. No explanation can be given at present for the discrepancy. The variation of resistivity along the clay sequence in borehole 8 is of interest. Three till samples were analyzed from boreholes 2, 3, and 4. Their average resistivity was 78.3 Ω•m. The corresponding conductivity (12.8 mS/m) is close to the values determined by inversion of HLEM data.

Perhaps the most significant finding based on conductivity correlations along the Smooth Rock Falls transect is that apparent conductivities estimated from HEM surveys could be used to distinguish the southern, predominantly clayey portion from the till-rich segment in the north without expensive ground follow-up. Distinct Quaternary environments can be identified by analyzing inverted HLEM data, but not by interpretation of EM-31 measurements.

CONCLUSIONS

Conductivities determined in situ by different EM techniques are identical only in areas of thick and homogenous overburden. In more complex areas, measured or interpreted conductivity depends on the system and the interpretation technique used. Geonics EM-31 measurements are affected only by the conductivity distribution in the upper 5 to 10 m. In most situations investigated, EM-31 conductivities were close to values determined for the near-surface layer by inversion of HLEM data, but there were significant exceptions to this finding.

Airborne EM methods are potentially useful for mapping of Quaternary sediments and maps of apparent conductivity have been used for this purpose. The analysis made in this paper suggests that interpretation of such maps must be approached with caution. Apparent conductivities calculated from HEM are influenced by the conductivities of all layers, including resistive bedrock, to a depth of 30 to 50 m. At all locations, conductivities determined from 4175 Hz data were lower than from 32 kHz data; this fact is consistent with dependence of depth penetration on frequency. In areas of thin overburden, apparent conductivity is much less than expected for a given sediment type. In areas of complex layering, maps of apparent conductivity do not yield sufficiently diagnostic information for Quaternary mapping. Much better results can be obtained by interpretation of conductivity sections calculated from HEM data, as described by Palacky et al. (1992b).

Surveys with the Geonics EM-31 instrument may give values widely differing from HEM apparent conductivities thus rendering the technique apparently unsuitable for ground follow-up. However, EM-31 measurements may still yield useful results under certain conditions. If the measured conductivity is much higher than σ_a estimated from HEM surveys, most likely a near surface clay layer overlies till or sand. If EM-31 measurements yield a much lower conductivity than HEM, clay should be expected in the Quaternary sequence even if it is not evident on the surface. However, ground follow-up with a multifrequency HLEM system would yield more accurate results.

ACKNOWLEDGMENTS

The 1992 field work was funded by the Northern Ontario Development Agreement, 1991-1995. In the data analysis use was made of data previously acquired using funding by the Canada-Ontario Mineral Development Agreement, 1985-1990. The author was assisted in the field by E. Coderre, a student at the University of Ottawa. Dr. T.J. Katsube and J. Hume of the Mineral Resources Division measured resistivities of drill core samples. Drilling data were provided by S.L. Smith of Environment Canada. Dr. P. Keating of the Geophysics Division reviewed the manuscript. S.J. Davis of the Mineral Resources Division drafted the figures.

REFERENCES

DiLabio, R.N.W. and Coker, W.B. (ed.)
1989: Drift prospecting; Geological Survey of Canada, Paper 89-20, 169 p.

Frischknecht, F.C., Labson, V.F., Spies, B.R., and Anderson, W.L.
1991: Profiling methods using small sources; in Electromagnetic Methods in Applied Geophysics, v. 2 - Applications, (ed.) M.N. Nabighian; Investigations in Geophysics 3, Society of Exploration Geophysicists, p. 105-270.

Inman, J.R.
1975: Resistivity inversion with ridge regression; Geophysics, v. 40, p. 798-817.

Interpex Limited
1988: EMIX-MM - User's Manual; Interpex Ltd., Golden, Colorado.

Katsube, T.J., Ahrens, R.H., and Collett, L.S.
1973: Electrical nonlinear phenomena in rocks; Geophysics, v. 38, p. 106-124.
McNeill, J.D.
1990: Use of electromagnetic methods for groundwater studies; in Geotechnical and Environmental Geophysics, v. 1 - Review and Tutorial, (ed.) S.H. Ward; Investigations in Geophysics 5, Society of Exploration Geophysicists, p. 191-218.
Palacky, G.J.
1991: Application of the multifrequency horizontal-loop EM method in overburden investigations; Geophysical Prospecting, v. 39, p. 1061-1082.
Palacky, G.J. and Stephens, L.E.
1990: Mapping of Quaternary sediments in northeastern Ontario using ground electromagnetic methods; Geophysics, v. 55, p. 1595-1604.
1991: Results of multifrequency horizontal-loop electromagnetic measurements along transects in northeastern Ontario; Geological Survey of Canada, Open File 2343.
Palacky, G.J. and West, G.F.
1991: Airborne electromagnetic methods; in Electromagnetic Methods in Applied Geophysics, v. 2 - Applications, (ed.) M.N. Nabighian; Investigations in Geophysics 3, Society of Exploration Geophysicists, p. 811-877.
Palacky, G.J., Holladay, J.S., and Walker, P.
1992a: Inversion of helicopter electromagnets data along the Kapuskasing transect, Ontario; in Current Research, Part E; Geological Survey of Canada, Paper 92-1E, p. 177-184.
Palacky, G.J., Mwenifumbo, J., and Stephens, L.E.
1992b: Geophysical studies at the Val Gagné test site, Ontario; in Current Research, Part E; Geological Survey of Canada, Paper 92-1E, p. 185-193.
Palacky, G.J., Smith, S.L., and Stephens, L.E.
1992c: Quaternary investigations in Geary, Thorburn, and Wilhelmina Townships, Ontario; in Current Research, Part E; Geological Survey of Canada, Paper 92-1E, p. 201-206.
Palacky, G.J., Smith, S.L., and Stephens, L.E.
1992d: Use of ground electromagnetic measurements to locate sites for overburden drilling near Smoky Falls, Ontario; in Current Research, Part E; Geological Survey of Canada, Paper 92-1E, p. 195-200.
Smith, S.L.
1992: Quaternary stratigraphic drilling transect, Timmins to the Moose River Basin, Ontario; Geological Survey of Canada Bulletin 415, 94 p.

Geological Survey of Canada Project 850058

Observations on the gold deposits of Eastern Hebei Province, China

K.H. Poulsen[1] and J.K. Mortensen[2]

Poulsen, K.H. and Mortensen, J.K., 1993: Observations on the gold deposits of Eastern Hebei Province, China; in Current Research, Part D; Geological Survey of Canada, Paper 93-1D, p. 183-190.

Abstract: Hundreds of gold occurrences in Eastern Hebei Province are hosted mainly by Precambrian gneisses of North China Platform and to a lesser degree by Mesozoic granitoid rocks. The Jinchangyu deposit, of mesothermal quartz vein type, and the Yu Erya deposit, of both gold porphyry and quartz vein types are the largest examples in each of the respective categories. These and other gold deposits in North China platform are metallogenically related to Mesozoic peraluminous continental felsic magmatism and locally to belts of Mo enrichment.

Résumé : Dans l'est de la Province d'Hebei, des centaines de venues aurifères sont principalement contenues dans des gneiss précambriens de la Plate-forme de Chine septentrionale, et dans une moindre mesure, dans des roches granitoïdes d'âge mésozoïque. Le gisement de Jinchangyu, du type filonien quartzeux mésothermal, et le gisement de Yu Erya, à la fois du type porphyrique aurifère et du type filonien quartzeux aurifère, sont les plus vastes dans l'une et l'autre catégories. Ces gisements et d'autres gisements aurifères de la Plate-forme de Chine septentrionale sont métallogéniquement apparentés au magmatisme continental à caractère felsique hyperalumineux qui s'est manifesté au Mésozoïque et, par endroits, à des zones d'enrichissement en Mo.

[1] Mineral Resources Division
[2] Continental Geoscience Division

INTRODUCTION

The authors conducted three weeks of field work in 1992 in Eastern Hebei Province, People's Republic of China for the purpose of completing the examination of a cross-section of major types of gold deposits in North China Platform. The field work was conducted in collaboration with the Shenyang Institute of Geology and Mineral Resources and the Eastern Hebei Bureau of Geology and Mineral Resources under the terms of the Canada-China Extended Memorandum of Understanding (1990-1993).

Iron production from Precambrian banded iron-formations notwithstanding, Eastern Hebei Uplift is noted mainly as a gold-producing region containing 197 deposits that extend along the axis of the uplift. Most of these are small (less than 1 tonne gold) but three in the central part of the gold belt are significant: Jinchangyu (70 t), Yu Erya (40 t) and Huajian-Niuxinshan (6 t). Most of our field work was focussed on Jinchangyu and Yu Erya because they are commonly cited as type examples of Chinese gold deposits. It is perhaps noteworthy that the Eastern Hebei gold belt projects eastward into Liaoning Province where major quartz molybdenite veins and molybdenite skarns are located approximately 100 km east-northeast of Taozhanzi (Huang et al., 1990). Molybdenite and base metal deposits are nonetheless rare in Eastern Hebei although we had the opportunity to briefly examine a few small-scale examples. In particular, a zoned, intrusion-related Mesozoic polymetallic vein system in the Taozhanzi area was examined. It includes small galena-sphalerite-carbonate veins (Taozhanzi), chalcopyrite-pyrite-carbonate veins (Majiagou, Donggou) as well as a fault-controlled epithermal gold deposit (Waitaoshan) at the contact between Jurassic volcanics and Precambrian gneiss.

We also examined the stratabound Gaobanhe pyrite-Pb-Zn deposit, hosted by Middle Proterozoic carbonate rocks and mined mainly for pyrite used in sulphuric acid production.

EASTERN HEBEI UPLIFT

The geology of the Eastern Hebei (Jidong) Uplift conforms in major characteristics to the Western Liaoning (Liaoxi) and Eastern Shandong (Jiaodong) uplifts described in our previous studies (Poulsen et al., 1990).

The Eastern Hebei uplift (Fig. 1) is cored by medium to high grade orthogneiss, amphibolite and paragneiss which Chinese geologists have divided into stratigraphic formations but which are better viewed as lithological assemblages. The Jinchangyu assemblage is composed predominantly of metatonalite, locally orthopyroxene-bearing, with lesser intercalated massive to gneissic amphibolite containing local lenses of banded iron-formation. The Taipingzhai and Malanyu assemblages are both composed mainly of orthopyroxene-bearing orthogneiss and lesser metatrondhjemite, biotite-rich metatexite and paragneiss as well as minor metamorphosed banded iron-formation. The only distinction between the Taipingzhai and Malanyu assemblages seems to be the upper amphibolite facies metamorphism of the former by contrast with the granulite facies of the latter. The presence of convincing examples of banded iron-formation in both amphibolite and paragneiss suggests that at least some of the metamorphic rocks in the uplift are of supracrustal origin and perhaps represent poorly preserved remnants of Precambrian granite-greenstone and metasedimentary-gneissic terranes. The most reliable radiometric ages for the metamorphic rocks (Pidgeon, 1980; Jahn and Zhang, 1984) suggest a large component of Late Archean (circa 2.5 to 2.6 Ga plutonism) but some authors (Sun et al.,1989; Jahn and Zhang, 1984) have suggested that Early Proterozoic metamorphism also affected the rocks of this region.

Non-metamorphosed Middle to Upper Proterozoic and minor lower Paleozoic sedimentary sequences overlie the metamorphic rocks with angular unconformity on the flanks of the basement uplift (Fig. 1). The Proterozoic sequence has an aggregate thickness of 9500 m (Wang, 1986) and is divisible in ascending order into 11 formations that define the Changchengian (Great Wall), Jixian and Qingbaikouan groups. Facies variations in this quartzite, shale and dolomitic limestone sequence are independent of location with respect to the uplift. These Proterozoic rocks and overlying lower Paleozoic limestone (<2 km thick) dip gently to moderately away from, but are absent in, the core of the uplift suggesting a substantial amount of crustal unroofing during uplift.

Mesozoic volcanic and continental sedimentary rocks, mainly of Jurassic age, occur primarily in basins developed unconformably on the Middle to upper Proterozoic sedimentary rocks on the flanks of the uplift (Fig. 1). The volcanic rocks are composed mainly of andesitic and dacitic tuff and breccia and local flow-banded rhyolite. Only within small inliers in the core of the uplift in the Jinchangyu area do volcanic rocks of this type lie directly on Precambrian gneiss, without intervening Proterozoic-Paleozoic strata.

Mesozoic (Yanshanian) granitoid rocks comprise a major component of the Eastern Hebei Uplift. A prominent chain of intrusions extends eastward along the axis of the uplift from Malanyu through Jinchangyu where it broadens into a wider zone of irregular granitoid distribution (Fig. 1). The intrusions are hosted by both Precambrian gneiss and unmetamorphosed Proterozoic sedimentary strata. They are composed of biotite granite, granodiorite and quartz monzonite but locally contain a substantial proportion of diorite. Primary muscovite was noted in several of the granitic bodies and garnetiferous leucocratic pods were observed in the Qingshankou granite near Jinchangyu. This evidence, together with available geochemical data, suggest that many of the Mesozoic granites are peraluminous in composition.

Numerous east-, northeast-, and northwest-trending faults of Yanshanian age are present within the uplift. Most extensive is the east-west Xifengkou-Qinglong Fault that is parallel to the axis of the uplift and defines the northern margin of its basement core. The northeast faults such as those through Jinchangyu, Yu Erya and Gaobanhe have a profound local control on the distribution of rock units and are

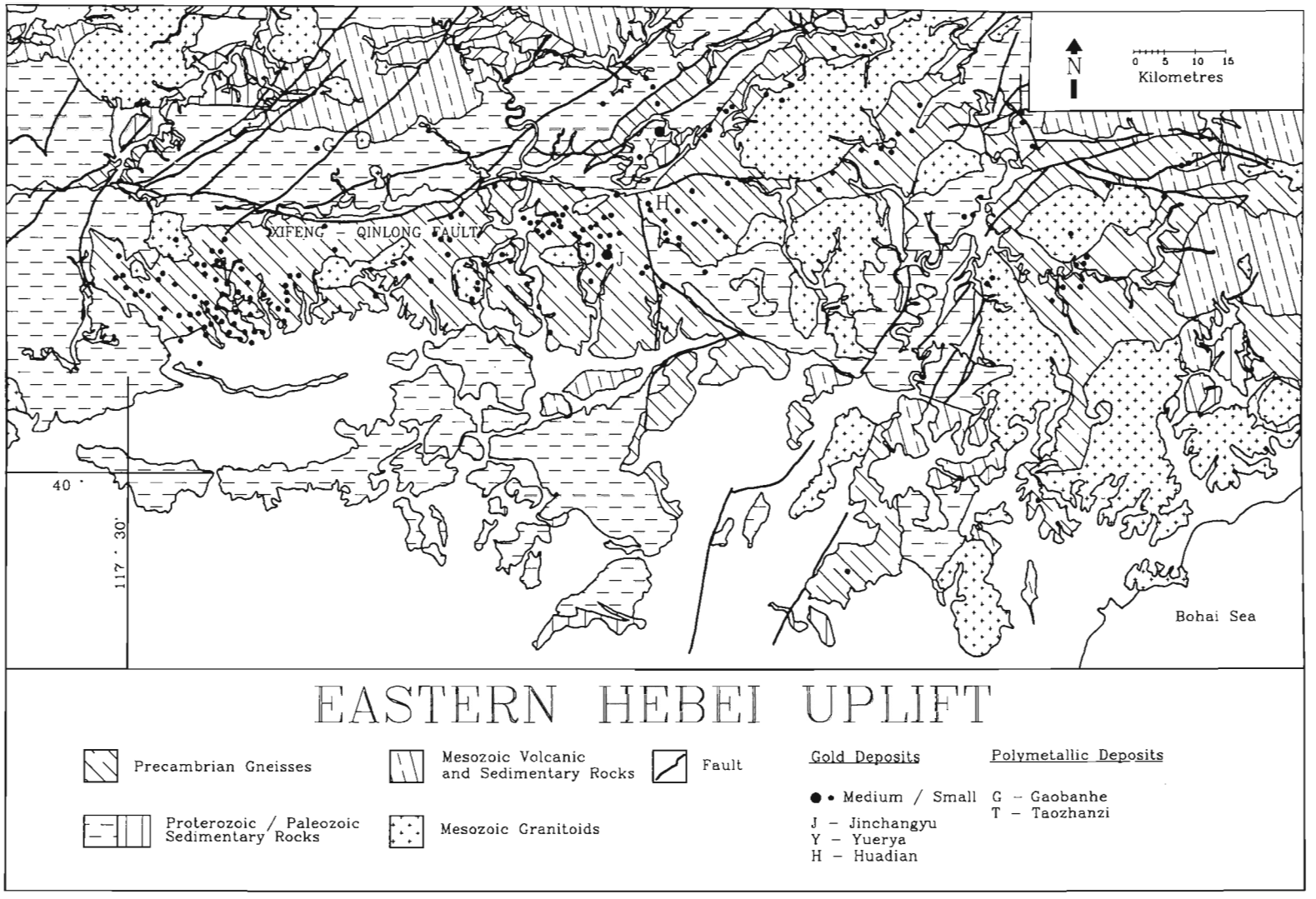

Figure 1. Geological sketch map showing the locations of gold deposits in Eastern Hebei Province (unpublished data, Yu Runlin). The locations of the major gold deposits at Jinchangyu (J), Yu Erya (Y) and Huadian (H); the Taozhanzi (T) polymetallic district and the Gaobanhe (G) Pb-Zn-pyrite deposit are shown for reference.

commonly loci of gold ±base metal orebodies. The northwest faults appear to be the youngest and least extensive structures and at Jinchangyu and Yu Erya post-date gold deposition.

JINCHANGYU GOLD DEPOSIT

Jinchangyu is the largest of eleven gold deposits distributed around the Mesozoic Qinshankou granite within the gneissic Precambrian core of the Eastern Hebei Uplift (Fig. 2). The Qinshankou intrusion is composed mainly of pink equigranular leucogranite and biotite granite that locally contains coarse primary muscovite and metre-diameter leucocratic garnetiferous orbicular patches. The main granodiorite phase is itself cut locally by fine grained quartz feldspar porphyry dykes that are also abundant in the adjacent gneisses.

The Precambrian host rocks at Jinchangyu are composed mainly of amphibolite and tonalite of the Jinchangyu assemblage. Massive varieties of both, as well as banded intercalations of the two, are common. Narrow lenses of banded iron-formation occur within the amphibolite northwest of the mine. Gneissic banding in these upper amphibolite facies metamorphic rocks dips 55-75 degrees to the northwest except in the vicinity of younger faults where it was observed to attain subhorizontal attitudes.

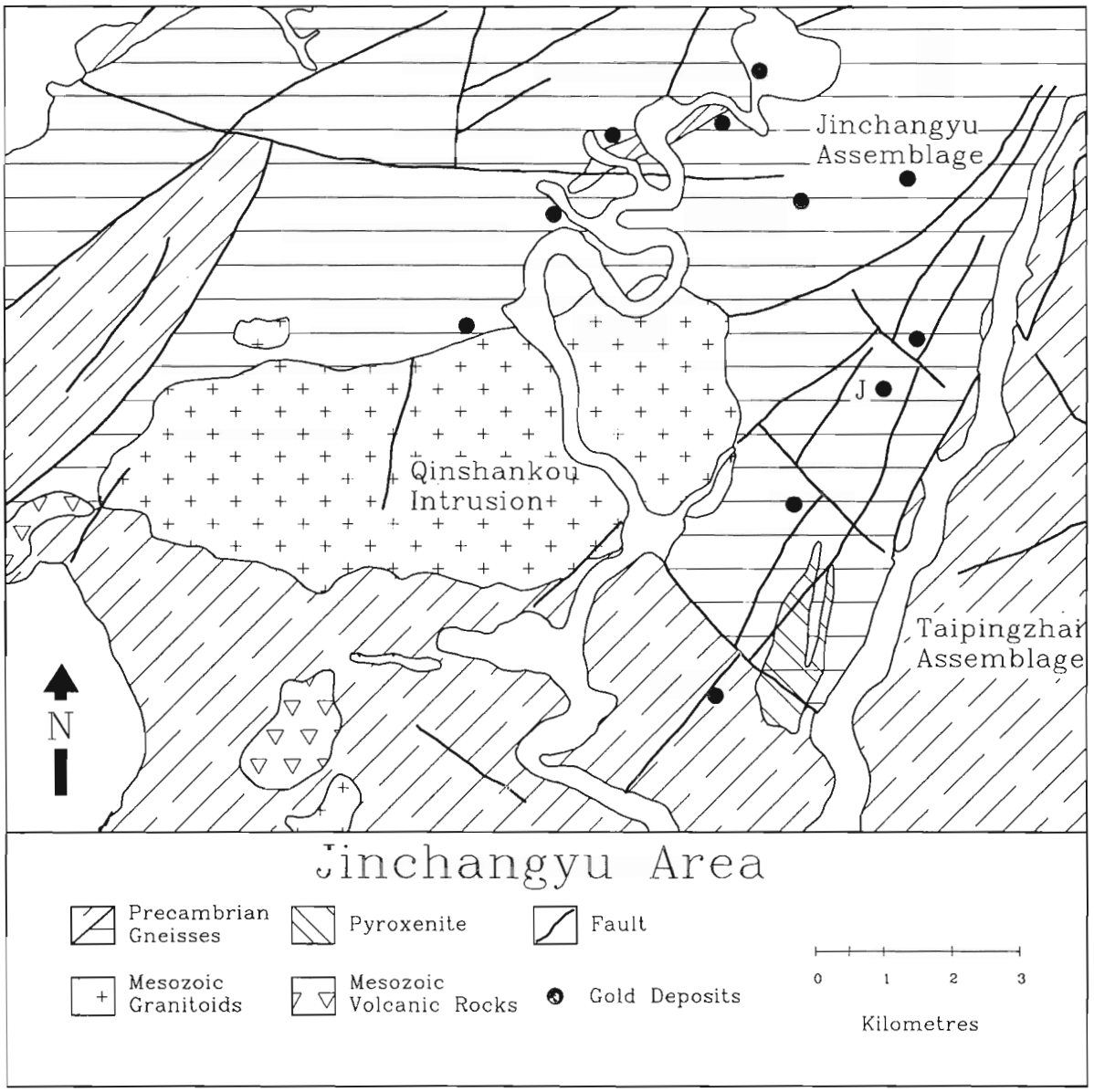

Figure 2. Geological map of the area surrounding the Qinshankou granite showing the distribution of gold deposits including the Jinchangyu mine (J). The location of the Jinchangyu area is shown in Figure 1. (unpublished data, Yu Runlin)

The main loci of gold mineralization at Jinchangyu are northeast-striking retrograde shear zones in which chlorite and sericite schist, developed in the Precambrian gneiss, contain contorted and irregular veins of quartz, albite and dolomite. Pyrite is widely disseminated in these zones and low grade gold (1-3 g/t) accompanies the alteration. At several localities the hydrothermal alteration was also observed to be superposed on pink to brick red fine grained felsic dykes of the type observed to cut the Qinshankou intrusion. Swarms of these dykes containing distinctive 2-3 mm quartz and feldspar phenocrysts occur throughout the mine area and appear to coincide with foliated fault zones and in several cases were noted to be moderately deformed along millimetre to centimetre spaced slip surfaces. Where the dykes occur near ore zones, they too are laced by stockworks and arrays of shallow-dipping quartz-albite veinlets around which the intervening dyke remnants are mineralized with 2-5 cm pyrite crystals. Away from ore zones, where dykes have not been superposed by significant veining and visible alteration, they were also noted to contain oval to irregular aggregates of fine grained pyrite (magmatic segregations?) that reportedly contain no gold.

The main sources of gold ore in the Jinchangyu Mine are 1-20 m thick quartz veins that occur in the central parts of the hydrothermally altered zones. The veins were observed to clearly cut both hydrothermally altered Precambrian rocks and porphyry dykes. At many localities the discordances between the quartz veins and foliated country rocks were observed; the quartz veins typically have a steep dip whereas the host rocks possess a shallow schistosity into which ramifying protrusions of vein quartz extend outward from the otherwise discordant vein (Fig. 3). The veins are locally massive, commonly ribboned and near their contacts with altered wallrocks commonly contain subhorizontal slab-shaped inclusions of intensely altered and pyritized host rocks. These slab-shaped inclusions locally result in a breccia-vein appearance. Apart from the pyrite contained in the wallrock slabs and in thin wallrock ribbons parallel with vein margins, the essential characteristic of ore-grade (10 g/t) quartz veins is the presence of discontinuous centimetre-wide seams of fine grained pyrite that locally impart a crude banding to the veins. Although pyrite is the predominant sulphide mineral at Jinchangyu, molybdenite is a common constituent of the ore and the highest gold grades in the deposit coincide with geochemical enrichments of both Mo and Bi (Yu et al., 1989).

Figure 3. Cross-sectional view of the steep contact of the No. 2-5 quartz vein (right hand side) and altered Precambrian gneiss at Jinchangyu. Note the subhorizontal protrusions of quartz parallel to foliation in the gneiss. 023 Level Jinchangyu mine. GSC 1992-251-B

The youngest rocks observed at the Jinchangyu deposit are fine grained mafic dykes (lamprophyre in mine terminology). These dykes have undisturbed chilled contacts against foliated country rocks and only rarely are fractured and cut by late-stage calcite veinlets. Locally the dykes were observed to contain spherical 5 mm diameter ocelli or amygdules composed mainly of calcite. The dykes cut both felsic porphyry dykes and hydrothermally altered and veined country rocks.

YU ERYA GOLD DEPOSIT

Yu Erya is located 40 km northeast of Jinchangyu within the Mesozoic Yu Erya intrusion (Fig. 4). The granodiorite intrusion cuts steep northwest-dipping dolomititic limestone of the Gaoyuzhang Formation of the Jixian Group and many apophyses of the intrusion, particularly along bedding planes, result in its irregular outlines. Near the contacts with the intrusion, the limestone sequence is variably fractured and visibly altered to serpentine marble and minor skarn. The intrusion is 2.5 km long parallel to bedding and 700 m across at its widest. Exploration drilling has established an overall southeast plunge for the body (Fig. 4).

The Yu Erya mine is divided into three sectors: north, central and south on the basis of the types of ore found in each. As currently mined, the main sources of ore in all sectors are remarkably persistent narrow high grade quartz-pyrite veins, 100 to 300 m long, that dip 15 to 75 degrees northwest. The veins are typically 10 cm thick and reportedly grade 100s of grams/tonne gold (dilution leads to an average mine grade of 11 g/t Au). They are coincident with brittle faults along one vein margin where the grades attain their highest values in pyritic gouge (Fig. 5). Some veins were observed to occur along the margins of a diorite dyke that cuts the granodiorite and, at one locality, the relationship was observed to be that of diorite intruded along the vein and of shearing of their mutual contact.

The veins are composed primarily of quartz and approximately 30% pyrite; chalcopyrite was noted only in the few veins that occur in limestone in the north sector. Apart from the quartz-pyrite veins, 98 % of which occur within the granodiorite, a few pyrrhotite-pyrite "veins", parallel to bedding in the limestones have provided high grade ore in the north sector of the mine. We observed small-scale as well as stope-scale examples of this type of ore and concluded that it is actually a sulphide replacement type of mineralization in which delicate bedded laminae are faithfully replaced by sulphides.

The central sector of the mine is of considerable significance because of two unique attributes. First, it is the site of a central core of "yellow-pink granite" (Fig. 4b) that can visually be distinguished from surrounding "grey-white granite" (Yu et al., 1989). We observed variations between the two granite types at the scale of large hand-specimens and conclude that, rather than representing different intrusive phases (Yu et al., 1989), these variations are the products of hydrothermal alteration. The yellow-pink altered variety is the result of sericitization and the development of potassic feldspar whereas the grey-white variety commonly shows the effects of propylitic alteration. The other related attribute of the central zone is that, in addition to the thicker quartz-pyrite veins of the type described above, it contains millimetre- to centimetre-thick quartz-pyrite veinlets and abundant disseminated pyrite in the altered granitoid host rock away from the larger veins. The thicker quartz veins represent the main source of ore in this sector as well but, because of the presence of these intervening auriferous veinlets and disseminations (1 to 3 g/t Au), wallrock dilution is not as severe as elsewhere in the mine, stopes are wider and mining

Figure 5. Cross-sectional view of a quartz-pyrite vein at Yu Erya. The hammer is underlain by granodiorite and dark coloured gouge occupies the footwall contact of the vein (above hammer head) whereas the contact between vein quartz and the granodiorite at the hangingwall contact is sharp (upper left). New No. 1 Zone, 500 m level Yu Erya mine. GSC 1992-251H

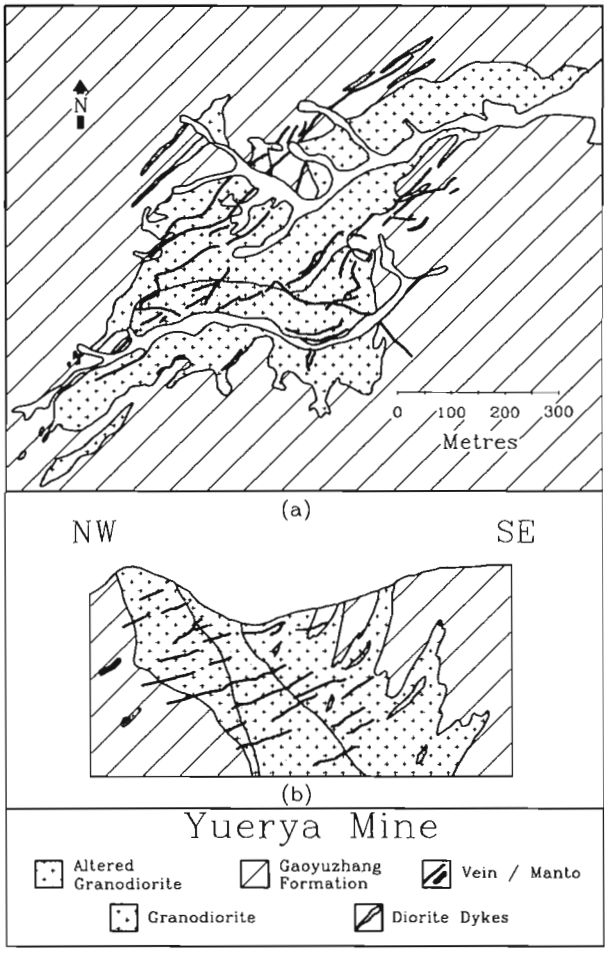

Figure 4. **a)** Geological map of the Yu Erya Mine (unpublished data provided by Yu Runlin). **b)** Schematic cross-section of the Yu Erya mine (adapted from Yu et al., 1989).

is more profitable. The surface expression of the central disseminated and veinlet zone is a 300 m-wide and up to 100 m deep oxidized cap that is currently being mined by villagers independent of the underground mining operation; processing of the oxidized material is achieved by rudimentary heap leaching.

DISCUSSION

Based on comparisons of mineralogy, fluid inclusion data, Pb isotope data on vein galena, light stable isotope (S,O,H) compositions of veins and altered rocks, as well as empirical spatial associations, Yu and Jia (1989) have argued that there is little genetic difference between Yu Erya and Jinchangyu types of mineralization. They noted the existence of low salinity fluid inclusions with homogenization temperatures in vein quartz as high as 370°C at Jinchangyu and placed this deposit in the mesothermal category. They suggested that observed linear arrays of Pb isotopic data ($^{207}Pb/^{204}Pb$ vs $^{206}Pb/^{204}Pb$) from both deposits are consistent with mixing of Precambrian and Mesozoic sources of lead and offered estimated mineralization ages of 133 Ma for Jinchangyu and 135-200 Ma for Yu Erya types of deposits. Their light stable isotope data were interpreted to reflect predominantly magmatic fluids with minor contributions from meteoric water. These authors therefore concluded that both Jinchangyu and Yu Erya types of deposits are related genetically to Mesozoic magmatism.

Yu et al. (1989) proposed different interpretations from similar data (fluid inclusions, Pb, S, C, H isotopes) as well as a data set of gold abundances of rocks in the Eastern Hebei area. They concluded that the Jinchangyu and Yu Erya type deposits had a multistage ore genesis that began in the Precambrian. They also suggested that amphibolites of the Jinchangyu assemblage are particularly enriched in gold and

therefore represent source beds that were formed as a result of Precambrian metamorphism and that the present deposits are simply the products of Mesozoic (Yanshanian) remobilization.

Sun et al. (1989) extended the concept of multistage genesis of the gold ores back to the initial formation of the amphibolites as gold-enriched basalts in a Late Archean volcano-sedimentary megacycle. They suggested a major period of gold introduction into shear zones by reaction of fluids with the gold-enriched strata in the Early Proterozoic followed by a period of remobilization, mainly in the Hercynian (Yu Erya) and to a lesser degree in the Yanshanian.

We note with interest that the conflicting interpretations of the Jinchangyu and Yu Erya deposits are based mainly on interpretation of analytical data from the deposits rather than on field relationships. The central controversy concerns the age of the deposits – Precambrian or Mesozoic? Our observations of unambiguous cross-cutting relationships suggest that there is little doubt that both are wholly Mesozoic. Samples collected during the course of our field work will be dated isotopically to place more precise constraints on the age of mineralization. Perhaps a more relevant metallogenic question in Eastern Hebei, however, is what the exact relationship between the gold deposits and plutonism really is.

Of the two, Yu Erya is, in our opinion, a clear example of an intrusion-related gold deposit of both porphyry and non-porphyry affinities (Sillitoe, 1991). Clearly the deposit is composed in large part of quartz-pyrite veins that are superimposed on the granodioritic host and to a lesser extent adjacent limestones. The presence of an independent potassically altered core with disseminated and stockwork styles of mineralization is nonetheless reminiscent of porphyry style gold mineralization and the observed auriferous pyrite-pyrrhotite replacements in adjacent dolomitic limestone have the characteristics of mantos. If one considers the potentially large volumes of low grade disseminated and stockwork mineralization at Yu Erya and the potential for discovery of additional manto-style mineralization distal to the intrusion, the geological reserves of gold in this deposit are certainly much larger than indicated by the current economic reserves of vein-type ore. From a North American perspective, this deposit would likely be evaluated as a large tonnage bulk minable resource. From a general perspective, the co-existence of both vein- and porphyry-styles of mineralization at Yu Erya is also of interest. As presently interpreted the vein-ores are said to be fault-controlled and post-magmatic (Yu et al., 1989) and the coincidence of veins and brittle faults is well-established. Apart from this relationship, however, the veins have many attributes of extensional veins filled with a single stage of pyrite and quartz. The veins are laterally persistent with little change in thickness or shape over tens of metres and locally have one wall in sharp contact with unsheared granitoid. Shearing is common, however, along at least one margin of most veins but this could merely represent a post-vein reactivation that results in ubiquitous pyritic gouge. If this were the case, the possibility exists that the veins at Yu Erya were more intimately related to the cooling history of the host intrusion, perhaps representing the inward retrograde collapse of a large hydrothermal system. The granitoid rock mass and porphyry system at Yu Erya appears to be tilted northward (Fig. 4b) by a lesser amount than the dolomitic limestones but by a similar amount as Jurassic strata that outcrop several kilometres to the north. Restoration of this tilt suggests that the quartz-pyrite veins could have formed with subhorizontal attitudes.

The relationship of the Jinchangyu deposit to granitic magmatism is less clearly defined than at Yu Erya. The distribution of gold deposits, including Jinchangyu, peripheral to the Qinshankou intrusion and the relationships among quartz veins and Mesozoic felsic dykes suggest possible spatial and temporal relationships to magmatism. The anomalous Mo-Bi composition of the ore also suggests a granitoid association but the direct genetic links are obscure. Of some significance is the fact that among the deposits that we have examined in North China Platform (Poulsen et al., 1990; this paper), Jinchangyu is the most "mesothermal" is its characteristics. It possesses the highest Au:Ag ratio (3:1), the most extensive alteration consisting of chlorite-carbonate-albite, the most ductile style of deformation (schist versus cataclasite and gouge) and ores that consist mainly of thick ribboned quartz veins. One possible explanation is that the granite-related mineralization in North China Platform formed over depth ranges spanning several kilometres and that continued uplift coincident with mineralization has served to telescope different depth zones into a common erosional level.

Our examination of the deposits of Eastern Hebei has highlighted what appears to be a recurrent theme for North China Platform gold deposits – spatial and genetic relationships with mildly peraluminous continental granitoid magmatism. None of the regions that we have examined contain significant examples of related base metal deposits but there is a weak association at the regional scale with Mo-(W) vein and Mo skarn deposits. This is at variance with the metallogenic association of gold with alkalic and calc-alkalic porphyry copper systems in the accreted terranes of the Canadian Cordillera. The continental setting of gold encountered in North China Platform coincides more closely with those parts of ancestral North America east of the Rocky Mountain Trench and suggests that the attributes of the Chinese deposits may form useful guidelines for gold exploration in central and eastern Yukon and in northeastern British Columbia.

ACKNOWLEDGMENTS

Mr. Lin Baoqin of the Shenyang Institute of Geology and Mineral Resources and Mr. Yu Runlin of the No. 2 Geological Team of Eastern Hebei Province made the logistic arrangements, made geological maps and supporting documentation available to us and led our 1992 field work. Mr. Zhang Lidong served capably as our interpreter and also took an active part in the field work. Mr. Qi Xueyi, Chief of the Geological Division, Jinchangyu mine and Mr. Yang Qui

Li, Chief Geologist, Yu Erya Mine, gave freely of their time and experience to show us the major features at the respective mines. F. Robert reviewed the manuscript.

REFERENCES

Huang Dianhao, Dong Qunying, and Gan Zhixian
1991: Molybdenum deposits of China; in Mineral Deposits of China, Volume 1; (ed.) The Editorial Committee of the Mineral Deposits of China; Geological Publishing House, Beijing, China, p. 288-355.

Jahn Borming and Zhang Zhongqing
1984: Radiometric ages (Rb-Sr, Sm-Nd, U-Pb) and REE geochemistry of Archean granulite gneisses from Eastern Hebei Province, China; in Archean Geochemistry, (ed.) A. Kroner, G.N. Hanson and A.M. Goodwin; Springer Verlag, p. 204-234.

Pidgeon, R.T.
1980: 2480 Ma old zircons from granulite facies rocks from east Hebei Province, North China Platform; Geological Reviews, v. 26, p. 198-207.

Poulsen, K.H., Taylor, B.E., Robert, F. and Mortensen, J.K.
1990: Observations on gold deposits in North China Platform; in Current Research, Part A; Geological Survey of Canada, Paper 90-1A, p. 33-44.

Sillitoe, R.
1991: Intrusion-related gold deposits; in Gold Metallogeny and Exploration, (ed.) R.P. Foster; Blackie, Glasgow and London, p. 165-209.

Sun Dazhong, Wang Kuiyuan, Wang Junlian, Yang Chunliang, and Zhao Fuming
1989: Studies on auriferous rock series of Archaean in Eastern Hebei; in Contributions to the Project of Regional Metallogenetic Conditions of Main Gold Deposit Types in China II. Eastern Hebei Province, (ed.) Shenyang Institute of Geology and Mineral Resources; Geological Publishing House, Beijing, p. 49-98.

Wang Hongzhen
1986: The Proterozoic; in The Geology of China, (ed.) Yang Zunyi, Cheng Yuqi and Wang Hongzhen; Oxford Monographs on Geology and Geophysics No. 3, p. 31-49.

Yu Changtao and Jia Bin
1989: Study on the genesis of major types of gold deposits and its mechanism of formation in Eastern Hebei; in Contributions to the Project of Regional Metallogenetic Conditions of Main Gold Deposit Types in China II. Eastern Hebei Province, (ed.) Shenyang Institute of Geology and Mineral Resources; Geological Publishing House, Beijing, p. 1-48.

Yu Runlin, Li Wenlai, Gu Shouzhi, Li Jiliang, Wang Fuzhan, Zhao Wenhao, Liu Sheng, and Zhang Haixiang
1989: Metallogenetic conditions of major gold ore type and ore-searching orientation in Eastern Hebei; in Contributions to the Project of Regional Metallogenetic Conditions of Main Gold Deposit Types in China II. Eastern Hebei Province, (ed.) Shenyang Institute of Geology and Mineral Resources; Geological Publishing House, Beijing, p. 99-146.

Geological Survey of Canada Project 900019

MILES laser microprobe. Part 1: system description

Bruce E. Taylor and Georges Beaudoin
Mineral Resources Division

Taylor, B.E. and Beaudoin, G., 1993: MILES laser microprobe. Part 1: system description; in Current Research, Part D; Geological Survey of Canada, Paper 93-1D, p. 191-198.

Abstract: High-spatial resolution stable isotope analysis is required for the solution of many problems in earth sciences. Here, we describe the development of the MILES laser microprobe which permits, at present, the sulphur isotope analysis of very small powder samples and of single reaction craters on sulphide surfaces. Samples are reacted with pure fluorine under a small-diameter CO_2 laser beam, monitored via a camera system. Incoporation of a safe method for the production and disposal of pure fluorine, and a variable temperature cryogenic trap distinguish this system, and contribute to its success. MILES is used in conjunction with a high-sensitivity isotope ratio mass spectrometer to produce results with an accuracy and precision equal, or superior, to conventional methods. Further development of MILES will include the capability to analyze silicate and carbonate minerals for stable isotopes.

Résumé : L'analyse à grande résolution spatiale des isotopes stables peut fournir la solution à plusieurs problèmes scientifiques dans le domaine des sciences de la Terre. On décrit, dans le présent article, le développement de la microsonde laser MILES qui permet, au moment présent, l'analyse isotopique du soufre dans de petits échantillons de poudre ou d'un simple cratère à la surface d'un grain de sulfure. Les échantillons réagissent avec du fluor pur sous un faisceau d'énergie émis par un laser au CO_2, et la réaction est observée au moyen d'une caméra. Le recours à une méthode sécuritaire de production et d'élimination du fluor pur, et l'utilisation d'un piège cryogénique à température variable, rendent ce système efficace tout en lui conférant son originalité. MILES est opéré conjointement avec un spectromètre de masse à sensibilité élevée, ce qui permet l'obtention de résultats avec une précision et une exactitude égales ou supérieures à celles obtenues par des méthodes classiques. Les développements futurs de la microsonde laser MILES permettront l'analyse des isotopes stables des silicates et des carbonates.

INTRODUCTION

For more than two decades, earth science has benefitted from high-spatial resolution X-ray analysis of minerals using the electron microprobe. In contrast, stable isotope geochemistry has, until recently, not had the benefit of similar technology, and conventional analysis typically requires the use of tedious mineral separation. High-spatial resolution isotopic analysis is essential to investigate the isotopic compositions and homogeneity of adjacent mineral grains in a rock. The equilibrium distribution of stable isotopes between adjacent minerals is a function of temperature (e.g., O'Neil, 1986). Previously, isotopic homogeneity among minerals on the order of several cubic centimetres in a rock had to be assumed, even though evidence has existed for isotopic zonation within minerals in altered rocks and in hydrothermal deposits.

Two recent technological advances show promise for high-spatial resolution stable isotope analysis: Secondary Ion Mass Spectrometry (SIMS, or ion microprobe) and the laser microprobe coupled to an isotope ratio mass spectrometer. In general, the ion microprobe offers high spatial resolution (10-20 μm) but with large uncertainties, whereas laser extraction techniques facilitate analysis of slightly larger domains (100-200 μm) at precisions approaching conventional techniques.

The ion microprobe has been used to demonstrate lead and sulphur isotope zoning in galena crystals from a Mississippi Valley-type lead-zinc deposit (Deloule et al., 1986), to analyze sulphide inclusions in diamonds (Chaussidon et al., 1989), and to document up to 40 permil fractionations between sulphide grains in mineralized sedimentary rocks (Eldridge et al., 1989; McKibben and Eldridge, 1989). However, cost, and large uncertainties (1-2 permil; 1σ) and matrix-related correction factors (e.g., up to 60 permil; Chaussidon and Lorand, 1990) curtail the use of the ion microprobe for stable isotope analysis.

Early applications of the laser microprobe concentrated on the collection and isotopic analysis of rare gases (Megrue, 1967; Muller et al., 1977). Subsequently, Franchi et al. (1986), Jones et al. (1986) and Sharp and O'Neil (1988) demonstrated the extraction of O, C, S, and N from selected minerals for stable isotope analysis. Successful developments in oxygen isotope analysis of refractory silicate and oxide minerals by Sharp (1990, 1992), and promising results for carbonates (Smalley et al., 1989; Dickson et al., 1990) have accelerated active research in this area, although a number of experimental problems are yet to be resolved (see Powell and Kyser, 1991).

Sulphur isotopic analysis using laser microprobes has utilized two different extraction methods: O_2 was used to combust sulphide sulphur to SO_2 by Crowe et al. (1990) and Kelley and Fallick (1990), whereas Rumble et al. (1991a, b) reported results of fluorination of sulphide minerals with BrF_5 or F_2. The precision and accuracy of sulphur isotope ratios determined via the SO_2 technique are compromised by mineral- and instrument-dependent fractionations as large as 8 permil (Kelley and Fallick, 1990). Reported precisions are 0.25 permil (1σ; Kelley and Fallick, 1990) and 0.15 to 0.43 permil (1σ; Crowe et al., 1990), for spatial resolutions on the order of 250-300 μm. Precision of $\delta^{34}S$ on SF_6 has been reported at 0.32 to 0.65 permil using BrF_5 (Rumble et al., 1991a), and 0.13 to 0.3 permil using F_2 (Rumble et al., 1991b), after purification using a gas chromatographic column with He carrier gas (Puchelt et al., 1971). This purification procedure is time consuming and may limit the minimum sample size which can be processed.

MILES (Micro-Isotopic Laser Extraction System) has been under development for several years in the Stable Isotope Laboratory of the Geological Survey of Canada. In this paper, we document the construction of a portion of this system designed for the fluorination of sulphide powders and single reaction craters using F_2. In conjunction with a Finnigan MAT-252 isotope ratio mass spectrometer, MILES has demonstrated superior performance in the sulphur isotope analysis of minerals with respect to sample size, spatial resolution, and preparation time (see Beaudoin and Taylor, 1993).

INSTRUMENTATION

Laser selection

Early attempts to apply laser techonology in micro-extraction systems for stable isotope geochemistry concentrated primarily on Nd-YAG lasers, which are characterized by a short wavelength (1.09 μm) and typically high power levels (particularly when utilized in a pulse mode). In 1988-89, B.E. Taylor had the opportunity to test the interaction (in air) of selected silicate, oxide, sulphide, and carbonate minerals with a variety of lasers. These included (with wavelengths and assisting companies in parentheses): Ar (476-514 nm; Spectraphysics), CO_2 (10.6 μm; Mellos-Griot), and Nd-YAG (1.06 μm; Coherent). The CO_2 laser proved the most generally applicable to heat the minerals tested to high temperatures (many to their melting points). This conclusion was in line with the expectation that the 10.6 μm wave length would be particularly well absorbed by metal-oxygen bonds (J.R. O'Neil, pers. comm., 1988; Sharp, 1990). Indeed, difficulty in heating some colourless silicate minerals with a Nd-YAG laser beam noted by some researchers (Sharp, pers. comm., 1990; Elsenheimer and Valley, 1992) is due to poor absorbance at 1.06 μm. Transition metal-bearing (e.g., Fe^{2+}) minerals exhibit much higher absorbance at 1.06 μm (Powell and Kyser, 1991). In further contrast to the CO_2 laser, the interaction of a Nd-YAG laser beam with clear minerals may also ablate the sample by fragmentation rather than by melting.

The spatial domain affected by the laser beam is a function of the laser, the mineral, and the duration, temperature, and nature of the extraction process used. The diameter (D) of the smallest spot of concentrated energy in the laser beam, known as the Airy disk, is approximated by:

$$D = 2.44 \lambda (F/A) \quad (1)$$

where λ is the wavelength of the laser source, F is the focal length, and A is the lense aperture. Depending on the beam delivery system, the Airy disk can contain as much as 84% of the laser energy. The remaining energy decreases rapidly outward from the central spot, appearing as a series of rings (e.g., Machewirth, 1988). For lasers using the fundamental TEM_{00} mode (as is the case in MILES), the power distribution across the focus spot is thought to be Gaussian. The diameter (D) of a focus spot containing 86.5% of the power (Airy disk) is given by:

$$D = 1.27\,\lambda\,(F/A) \qquad (2)$$

For this situation, moderately large differences in minimum and maxium optical path length (up to λ/2) can be tolerated with minimal reduction in energy of the focus spot. When this difference is less than λ/4, the lense system is said to be diffraction limited (Machewirth, 1988). For most systems presently in use in geological applications, the practical, minimum diameter of the focus spot of a CO_2 laser is about 40-50 μm.

MILES

Vacuum system

The general lay-out of vacuum system is shown in Figure 1. Vacuum is supplied by a 170 l/s corrosive series turbo-molecular pump (Balzers, TPH 170) and roughing pump (Balzers, DUO 1.5) charged with fluorinated pump fluids (Kryotox oil). This vacuum pump combination provides rapid pump-down, and long-term reliability in the event that corrosive gases (e.g., F_2, HF) should inadvertently be pumped directly, prior to neutralization. Low and high vacuum in the main manifold are monitored by a Granville-Phillips convectron gauge (series 275, analog readout) and an HPS (SensaVac™ series 421) cold cathode ionization gauge, respectively. These gauges provide trip-levels for valve control in future development. The routine background pressure in the manifold is on the order of 3×10^{-6} Torr when degassing the line and sample chamber over night. Background pressures in the extraction section of the vacuum line are well below 1×10^{-3} Torr (i.e., below scale on the HPS SensaVac™ series 315 pirani gauge and Hastings thermocouple-type vacuum gauge).

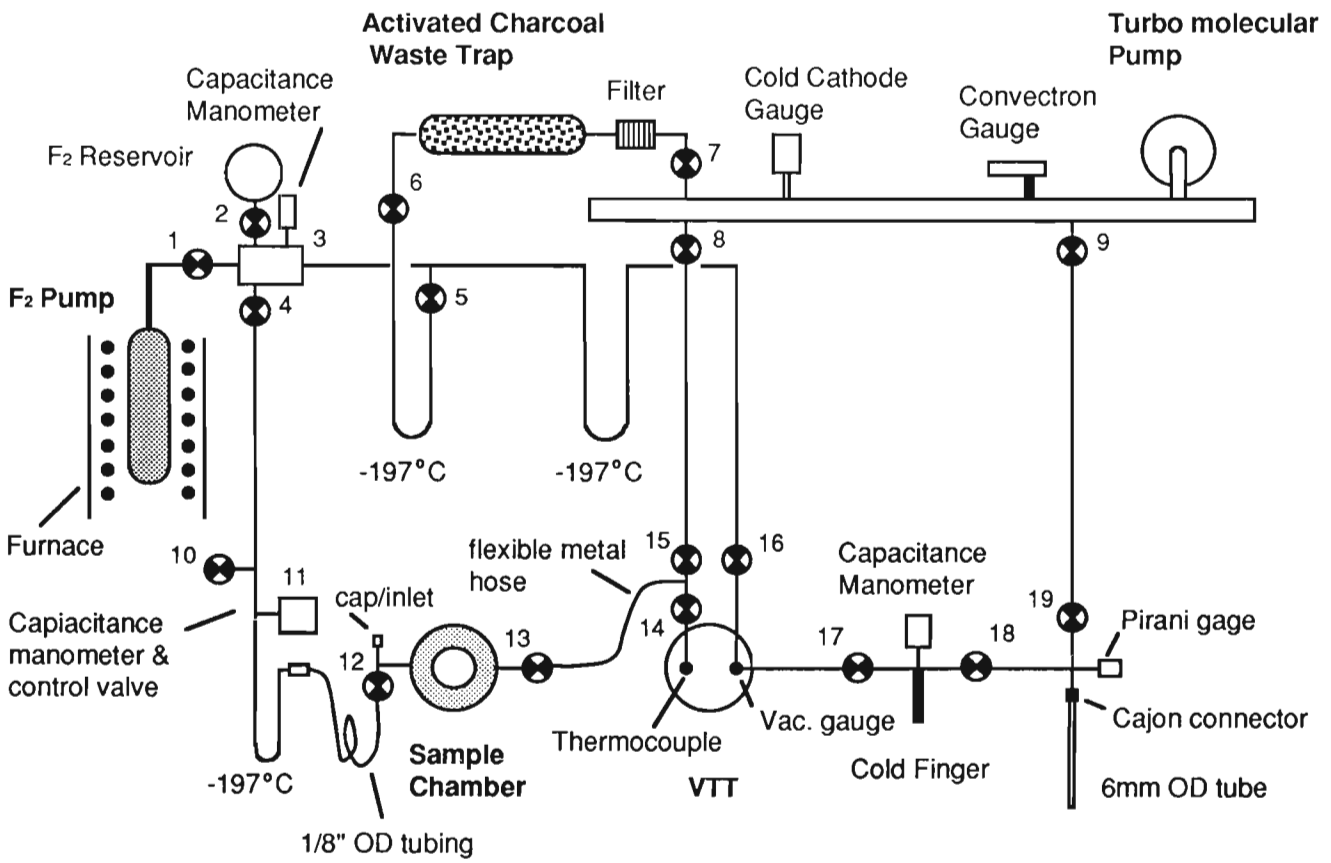

Figure 1. Schematic lay-out of MILES. All tubing is of stainless steel, connected by welding, stainless steel Swagelock™ fittings, or Conflat™ min-flanges.

The vacuum line is constructed of type 316 stainless steel tubing throughout, in either 1/2, 3/8, or 1/4 in. OD. Valves for all but the F_2 containment system are Nupro bellows-type high vacuum valves fitted with Kel-F stem tips. Valves connecting the vacuum system to the manifold are pneumatic (valves 8 and 9, Fig. 1), whereas the majority of operator-controlled valves are 1/4 in., toggle type. Unless otherwise indicated, all connections are made with Swagelock™ stainless steel ferrules.

Sample chamber

An exploded view of the small-volume sample chamber is shown in Figure 2. The chamber permits direct, vertical observation of the samples during reaction via a 2 in. OD, ThF_4-coated ZnSe window. This window has a very high transmissivity of the CO_2 laser beam, and is considerably more robust than BaF_2 windows used in other CO_2 laser systems (e.g., Sharp, 1990), which are fragile and have been known to fail due to thermal shock. The light amber colour of the ZnSe window does not interfere with the sample visibility and offers a considerable safety factor over BaF_2 with respect to containing the F_2. Both the window and the bottom of the stage are vacuum sealed with Kal-Rez O-rings. The bottom of the stage serves as a sample tray, and is removable in order to permit easy access and flexibility for future developments. The sample tray is drilled with twenty-one 1/4 in. OD by 0.5 in. deep holes which accommodate nickel crucibles which are drilled with 0.125 X 0.25 in. holes (Fig. 2). The crucibles are machined to facilitate ready evacuation. As needed, the crucibles can be individually cleaned, loaded, and stored with samples in a drying oven prior to use. Samples for in situ analysis (which may include slices up to nearly 2 in. diameter and of required thickness) are placed directly on the sample tray. Heating of the sample chamber during pump-down and pre-fluorination is accomplished by wrapping with a heating tape. The reagent inlet valve (12; Fig. 1) is connected to the sample chamber via a Swagelock "T" on one end of which is fitted an end cap which can be opened to release vacuum.

The sample chamber is supported by a cantilevered bracket (Fig. 3) attached to three mechanical translation stages: one manually controlled in the Z-direction, and two others, orthogonally mounted with linear actuators (Newport model 850 series) and operated by computer-control (Newport PMC300 motion controller system). This arrangement provides for a full 2 in. translation of the sample chamber, in either the X- or Y-direction. A joy stick provides convenient control of stage motion, in both slow and fast modes. The chamber is sealed by two valves, and is connected to the vacuum line by means of a 1/4 in. OD Cajon flexible metal hose. This provides for ease of movement of the stage without compromising the level of high vacuum.

Laser, beam delivery system, and optical system

A Synrad 30W, RF-excited, sealed CO_2 laser (Model C48-2-115) is vertically mounted (12; Fig. 3) behind an Olympus (model SZH) zoom (7.5X to 64X) stereo microscope with a 1X objective (1; Fig. 3). As a precaution because of the (space-efficient) vertical mounting, the laser is water cooled by a small fountain pump, reservoir, and fan-cooled heat exchanger. The laser beam exits the front of the laser with an approximate diameter of 0.25 in., and is delivered to a beam expander/collector lens system via three turning mirrors. The beam is directed to the sample via a final turning mirror (3; Fig. 3). The diameter of the focus spot (see equation 1) was estimated from the bottom of a reaction crater in pyrite, viewed in section, to be 40 μm. However, the minimum diameter of reaction craters produced (in air) on olivine wafers is of the order of 80 μm, probably because of the power distribution previously described. Reaction craters are larger in pyrite in an F_2 atmosphere (ca. 130 μm).

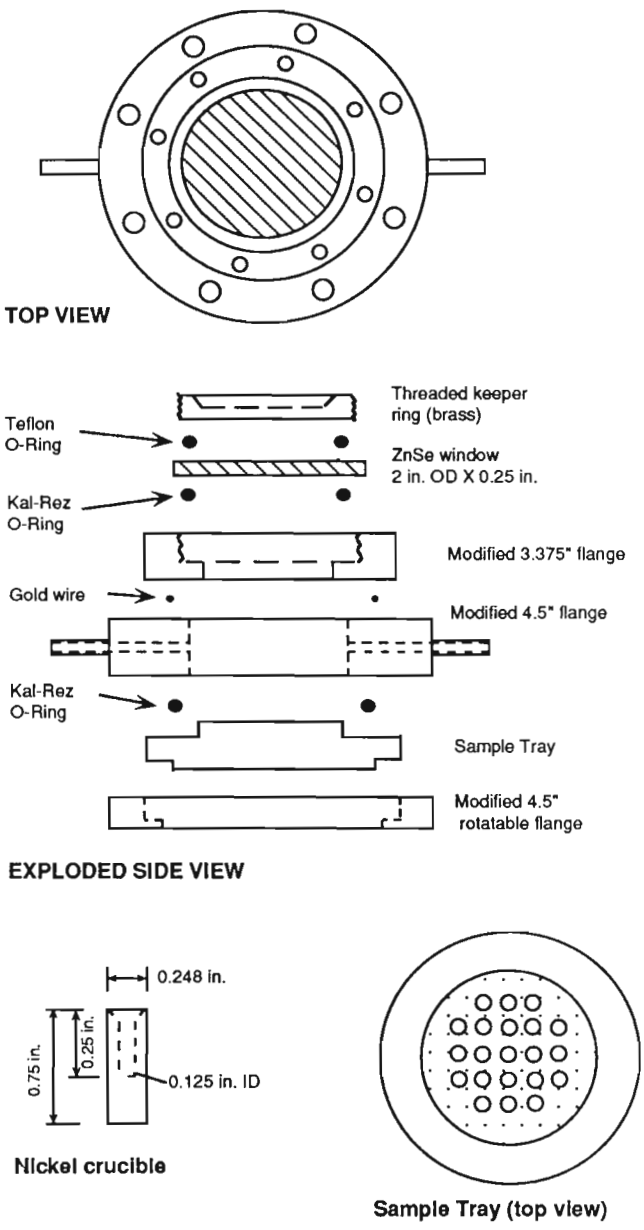

Figure 2. Exploded schematic diagram of small-volume, multi-sample chamber.

Control of both laser power and irradiation time are needed in order to optimize *in situ* reactions, and power control is needed for longer, sustained reaction of powders. We use a Synrad power controller (model CA-48-B) in conjunction with a Wavetek 2MHz (model 20) function generator to control both the power and duration of a pulse (or continuous beam). The temperature of reaction is limited, for the most part, by the melting points of the reacting minerals and by the melting/boiling points of the fluoride reaction products (e.g., PbF_2 from galena). Abrupt reaction crater walls suggest that thermal gradients may be very high. Friegelson et al. (1988) measured temperature gradients on the order of 100°C/0.3 mm from the laser contact point (1025°C) to the growth interface of oxide fibers.

During the reaction, the sample is viewed on a black and white 12 3/4" Panasonic video monitor (WV-5410) via a Cohu (model 4812-5000) camera mounted on the Olympus microscope (9; Fig. 3). The turning mirror (3; Fig. 3) is partially visible in the optical path only when viewed at low magnification; high magnification is normally used. In early tests, we found a co-axial He-Ne aiming laser to be unnecessary, and its reflection disturbingly high. From a test shot, the video screen can be marked to show the target point of the CO_2 laser beam.

Fluorine generation and clean-up

High purity (>99.7%) F_2 is produced by the thermal decomposition of K_2NiF_6(KF) according to the reaction (Asprey, 1976):

$$2[K_2NiF_6 \cdot KF]_{(s)} = 2\,K_3NiF_{6\,(s)} + F_{2\,(g)} \qquad (3)$$

The reaction proceeds to the right above about 250°C, and to the left below 250°C (but at low pressures, the absorption of F_2 is not 100%). Approximatley 850 g of K_2NiF_6(KF) is stored in a 300 cm^3 Hoke monel sample cylinder welded to a Nupro valve (SS-6UG-TWIN) with stellite stem tip. This fluoride salt is extremely hygroscopic, and the monel vessel was loaded in a glove box under a dry N_2 atmosphere. In order to avoid expulsion of some of the salt into the vacuum line during the initial evacuation, a fine monel screen filter was fashioned for the neck of the monel vessel and its mini-flange connector fitting.

The F_2 pump is operated as follows: with valves 2, 3, and 4 (Fig. 1) closed, valve 1 is opened, and the set-point of the temperature controller for the tube furnace which heats the pump is raised to a temperature to generate sufficient F_2 pressure in the system. With continued use, the temperature of the F_2 pump must be raised to higher levels to generate F_2. Slow heating of the F_2 pump, while continuously monitoring the pressure on a Setra capacitance manometer (model 280E), avoids dangerously high pressures. When the desired pressure of F_2 has been produced, valve 1 is closed and the temperature controller reset to 225°C. The furnace is rail-mounted such that, if required, it can be lowered to rapidly cool the F_2 pump. In order to avoid having to produce F_2 every day, a reservoir (see Fig. 1) is used to store F_2. Residual F_2 may be largely resorbed as described above.

As described by Asprey (1976), it is necessary to thermally "cycle" the F_2 pump several times before use, followed by pumping away of residual gases (probably mostly N_2, O_2) after resorbtion of the fluorine. We found that, despite our best efforts to avoid contamination, whether by moisture or, probably, carbon (see below), a period of poor performance was encountered after of several months. Rejuvenation of the F_2 pump under 6 atm. of commercial

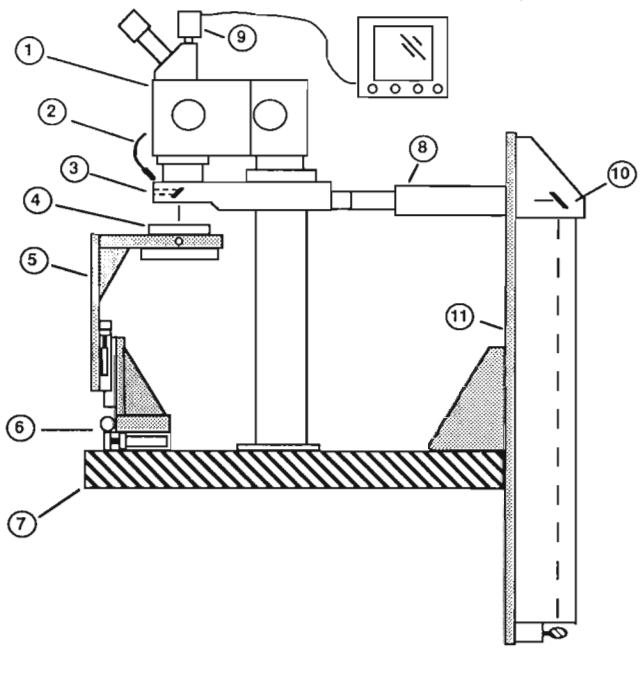

SIDE VIEW

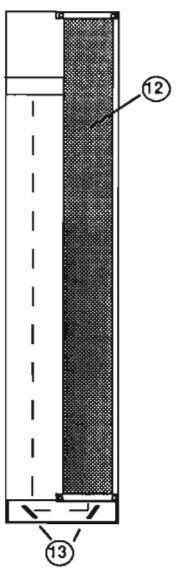

BACK VIEW (OF LASER)

Figure 3.

Schematic diagram of MILES laser and optical system: microscope (1), fiber optic illumination (2), sample stage (4), stage bracket (5), motorized translation stage (6), optical table (7), beam delivery system (8, 3), camera/monitor (9), mirrors (10, 13), laser mounting bracket (11), and CO_2 laser (12).

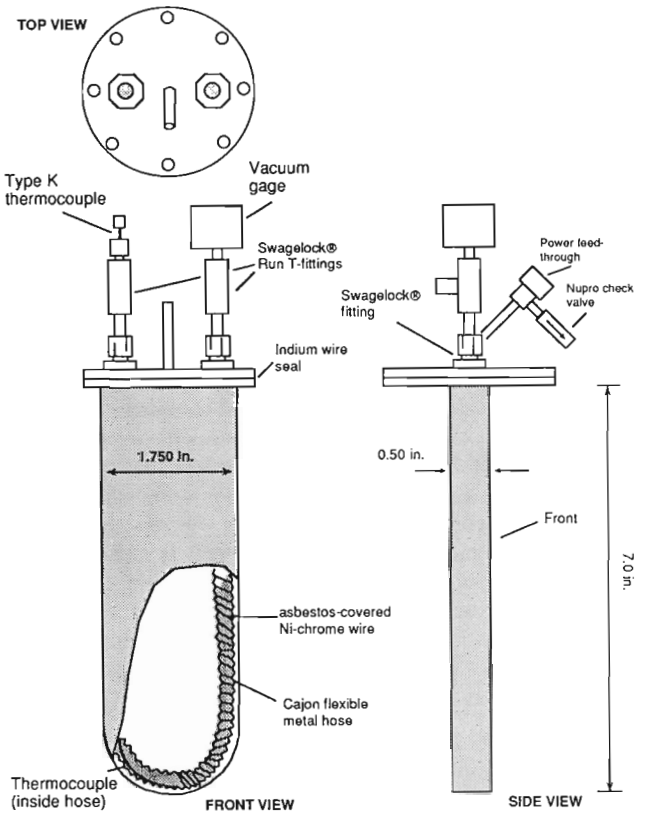

Figure 4. Schematic diagram of variable temperature cryogenic trap.

grade (ca. 97%) F_2 has resulted in much improved performance over that of the commercially-prepared K_2NiF_6(KF). The cyclinder of commercial grade F_2 is stored away from the laboratory in a wheel-mounted, custom cylinder cabinet (Matheson), and only brought to the laser/mass spectrometer lab for recharging the F_2 pump when required. Thus, the F_2 pump permits the safe, in-lab production of high-purity F_2 under low, controlled pressures, without the need for high-pressure F_2 cylinders in the near vicinity.

Once generated, F_2 is transferred to the sample chamber by means of an MKS flow controller valve (type 248) and capacitance manometer (type 107B). This system permits accurate control over the quantity of F_2 used for each reaction, ensuring control over an important experimental variable. As shown in Figure 1, the F_2 is passed through a trap at -197°C as an additional precaution against impurities (chiefly fluorocarbons). The F_2 source is connected to the sample chamber by means of a coiled length of 1/8 in. OD stainless steel tubing which provides sufficient flexibility for movement of the X-Y stage, while minimizing the volume of the line containing F_2.

Residual F_2 which is not resorbed by the F_2 pump at the end of each day, and excess F_2 from each reaction, are converted to inert CF_4 by passing over an activated charcoal trap, according to:

$$C_{(solid)} + 2\,F_{2\,(gas)} \rightarrow CF_{4\,(gas)} \qquad (4)$$

This reaction is extremely exothermic, and care must be taken to pass only small quantities at a time over the charcoal. This condition is routinely satisfied in day-to-day operation. Cold traps between the charcoal waste trap and the extraction line prohibit the back-diffusion of CF_4 and other fluorocarbons (see Fig. 1).

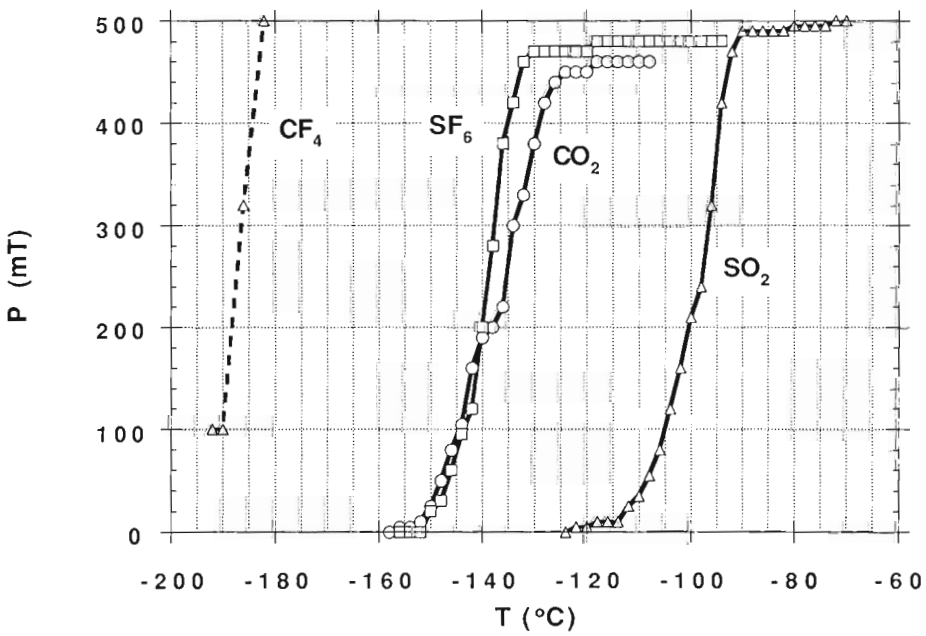

Figure 5.

Fractional distillation curves for pure CF_4, SF_6, CO_2, and SO_2, empirically determined for a prototype variable temperature cryogenic trap.

Sample purification

Although SF_6 is an ideal gas for mass spectrometry due to its inert chemical nature, monoisotopic composition of fluorine, and ready ionization to SF_5+ (Rees, 1978), isobaric interferences at mass 131 ($S^{36}F_5$+) are common. Large interferences at mass 131 lead to innacurate measurements of $^{34}S/^{32}S$ (Rumble et al., 1991b). In order to avoid time-consuming gas chromatographic separation, and to facilitate the analysis of very small samples (e.g., 0.1-0.2 μmole SF_6), we have incorporated a variable temperature cryogenic trap (VTT) to purify the SF_6.

Our VTT (Fig. 4), with attached thermocouple and vacuum gauge, is a modification of a design by Des Marais (1978). Principal improvements are: (1) a reduction in sheath-to-tubing distance which decreases response time; (2) internal placement of the thermocouple which allows for replacement in case of malfunction, (3) a removable sheath and Cajon flexible hose in case of malfunction of either hose or heater wire, and (4) a safety check-valve to prevent high internal pressures due to O_2 should an atmospheric leak in the sheath occur. This trap, when immersed in liquid nitrogen and the heater wire is connected to a variable transformer, is capable of temperature control to within 1°C, and permits the fractional distillation of pure components of gas mixtures (e.g., Des Marais, 1978). The temperatures are measured by a sheathed Cr-Al (type K) thermocouple whose tip touches the inner wall of the flexible tube, at the bottom of the trap. Shown in Figure 5 are distillation curves empirically-determined for pure CF_4, SF_6, CO_2, and SO_2. These curves (and the temperatures cited below) will vary slightly for each trap constructed owing to a number of factors, including exact placement of the sheathed thermocouple tip.

After reaction between a sulphide powder and F_2, the SF_6 and any other products (e.g., CF_4, HF, fluorocarbons) are condensed into the trap at -197°C, and the excess F_2 pumped away through the charcoal waste trap. The VTT is then slowly warmed to -178°C and the non-condensible gases pumped away. The trap is slowly warmed again to -139°C, and the SF_6 is collected and sealed in a 6 mm OD cracker tube for isotopic analysis. For single reaction craters, the sample of SF_6 is considerably smaller (by up to two orders of magnitude), and is harvested from the trap between ca. -162 and -158°C. With this technique, the $\delta^{36}S$ values are substantially reduced (0 to 150 permil). The small variations in these values do not correlate with any variations in $\delta^{34}S$ (Beaudoin and Taylor, 1993). The principal interference at mass 131, a fluorocarbon (C_3F_5+; Hoering, 1990), appears to have a finite vapour pressure over a range of temperatures. This behavior suggests that it condenses as a liquid rather than a solid, and that fractional distillation of SF_6 from the VTT minimizes, but cannot entirely avoid, this impurity. In any case, the results noted below, and described in more detail in Beaudoin and Taylor (1993), serve to illustrate the efficacy of the VTT in purification of SF_6 to a level adequate for accurate and precise determination of $^{34}S/^{32}S$ ratios in minerals.

ANALYSIS OF SULPHIDE MINERALS

MILES permits the fluorination, purification, and collection of SF_6 produced from either a single reaction crater, or from a small powder sample within 20-30 minutes. Beaudoin and Taylor (1993) demonstrate that the $\delta^{34}S$ of pyrite, galena, and sphalerite powders weighing <1.0 to 5.0 mg. can be routinely analyzed with a precision of <0.11 permil, and with an accuracy equal to conventional, large-sample analyses. This facilitates the analysis of single grains, or drilled micro-samples, which could not otherwise be accomplished with conventional techniques.

The exciting possiblities for isotopic research utilizing single reaction craters of ca. 125 μm diameter in pyrite, which yield 0.1 to 0.2 μmole SF_6, are within reach. Beaudoin and Taylor (1993) note that preliminary data on pyrite indicate a precision on $\delta^{34}S$ single crater analyses similar to that for powders. These are the most precise results, and the smallest sample domains, yet reported for sulphides. Moreover, matrix-dependent fractionations are not, as yet, indicated for single craters, and this should ensure high accuracy as well.

CONCLUSIONS AND FUTURE RESEARCH

We have described a CO_2 laser microprobe system for isotopic analysis of sulphide minerals that boasts the highest precision and smallest sample size yet reported for sulphides. The capability of safely producing pure F_2, in particular, and the innovative sample purification incorporated in MILES contribute to its success. Further developments are aimed at including the capability for isotopic analysis of silicates, oxides, and carbonates with similar precision and on similar scales.

ACKNOWLEDGMENTS

MILES has been developed over the last several years, but only with fabrication of critical components and the delivery of the Finnigan MAT 252 mass spectrometer could it be completed and tested. We are indebted to many. B.E. Taylor was made aware of Asprey's invention of the F_2 pump by G.P. Landis (USGS) a number of years ago. It is from Landis' early large-scale fluorination line that the idea for a charcoal waste trap was derived. Prof. Dr. S. Hoernes (Bonn) offered much useful advice on the operation of the F_2 pump. D. Des Marais (NASA) kindly provided heating wire for the variable temperature trap, and an early prototype trap from which we have developed an improved version. We thank D. Rumble (Carnegie Inst.) for informing us that the Ozark Mahoning Co. manufactures K_2NiF_6(KF). Discussion with him, and comparison with the laser system at the Geophysical Lab, Washington, D.C. during the preparation of this report was very informative. Many of the components of the vacuum system were carefully fabricated by S. Banszky, K. Lalonde,

and R. Forconi in the GSC Instrument Shop. The laser/optical system was designed in collaboration with, and supplied by, J. Lapp (Lapp Enterprises). Finally, G. Beaudoin acknowledges the support of a Visiting Fellowship in Canadian Goverment Laboratories at the Geological Survey of Canada.

REFERENCES

Asprey, L.B.
1976: The preparation of very pure fluorine gas; Journal of Fluorine Chemistry, v. 7, p. 359-361.

Beaudoin, G. and Taylor, B.E.
1993: MILES laser microprobe. Part 2: Preliminary assessment of precision and accuracy of sulphur isotope analysis; in Current Research, Part D; Geological Survey of Canada, Paper 93-1D.

Chaussidon, M. and Lorand, J.-P.
1990: Sulphur isotope composition of orogenic spinel lherzolite massifs from Ariege (North-Eastern Pyrenees, France): An ion microprobe study; Geo-chimica et Cosmochimica Acta, v. 54, p. 2835-2846.

Chaussidon, M., Albarède, F., and Sheppard, S.M.F.
1989: Sulphur isotope variations in the mantle from ion microprobe analysis of micro-sulphide inclusions; Earth and Planetary Sciences Letters, v. 92, p. 144-156.

Crowe, D.E., Valley, J.W., and Baker, K.L.
1990: Micro-analysis of sulfur isotope ratios and zonation by laser microprobe; Geochimica et Cosmochimica Acta, v. 54, p. 2075-2092.

Deloule, E., Allègre, C.J., Doe, B.
1986: Lead and sulphur isotope microstratigraphy in galena crystals from Mississippi-valley type deposits; Economic Geology, v. 81, p. 1307-1321.

Des Marais, D.J.
1978: Variable-temperature cryogenic trap for the separation of gas mixtures; Analytical Chemistry, v. 50, p. 1405-1406.

Dickson, J.A.D., Smalley, P.C., Raheim, A., and Stijfhoorn, D.E.
1990: Intracrystalline carbon and oxygen isotope variations in calcite revealed by laser microsampling; Geology, v. 18, p. 809-811.

Eldridge, C.S., Compston, W., Williams, I.S., and Walshe, J.L.
1989: Sulfur isotope analysis on the SHRIMP ion microprobe; United States Geological Survey Bulletin 1890, p. 163-174.

Elsenheimer, D. and Valley, J.W.
1992: In situ oxygen isotope analysis of feldspar and quartz by Nd:YAG laser microprobe; Chemical Geology (Isotope Geoscience Section), v. 101.

Franchi, I.A., Wright, I.P., Gibson, E.K., Jr., and Pillinger, C.T.
1986: The laser microprobe: A technique for extracting carbon, nitrogen, and oxygen from solid samples for isotopic measurements; Journal of Geophys-ical Research, v. 91, no. B4, p. D514-524.

Friegelson, R.S., Gazit, D., Fork, D.K., and Geballe, T.H.
1988: Superconducting Bi-Ca-Sr-Cu-O fibers grown by the laser-heated pedestal growth; Science, v. 240, p. 1642-1645.

Hoering, T.C.
1990: Development of the sulfur hexafluoride method for sulfur isotope analysis; Annual Report of the Director of the Geophysical Laboratory, Carnegie Institute of Washington, 1989-1990, p. 128-131.

Jones, L.M., Taylor, A.R., Winter, D.L., Hunt, S.P., and Keen, G.W.
1986: The use of the laser microprobe for preparation in stable isotope mass spectroscopy (abstract); Terra Congita, v. 6, p. 263.

Kelley, S.P. and Fallick, A.E.
1990: High precision spatially resolved analysis of $\delta^{34}S$ in sulfides using a laser extraction technique; Geochimica et Cosmochimica Acta, v. 54, p. 883-888.

Machewirth, J.P.
1988: Diffraction limited lenses for laser applications; The Photonics Design and Applications Handbook; Laurin Pub. Co., Pittsfield, Massachusetts, p. H246.

McKibben, M.A. and Eldridge, C.S.
1989: Sulfur isotopic variations among minerals and aqueous species in the Salton Sea geothermal system: A SHRIMP ion microprobe and conventional study of active ore genesis in a sediment-hosted environment; American Journal of Science, v. 289, p. 661-707.

Megrue, G.H.
1967: Isotopic analysis of rare gases with a laser microprobe; Science, v. 157, p. 1555-1556.

Muller, H.W., Plieninger, T., James, O.B., and Schaeffer, O.A.
1977: Laser probe ^{39}Ar-^{40}Ar dating of materials from the consortium breccia 73215; Proceedings of the Lunar Science Conference, v. 8, p. 2551-2565.

O'Neil, J.R.
1986: Theoretical and experimental aspects of isotopic fractionation; in Reviews in Mineralogy, (ed.) J.W. Valley, H.P. Taylor, Jr., and J.R. O'Neil; Mineralogical Society of America, v. 16, p. 1-40.

Powell, M.D. and Kyser, T.K.
1991: Analysis of $\delta^{13}C$ and $\delta^{18}O$ in calcite, dolomite, rhodochrosite and siderite using a laser extraction system; Chemical Geology (Isotope Geoscience Section), v. 94, p. 55-66.

Puchelt, H., Sabels, B.R., and Hoering, T.C.
1971: Preparation of sulfur hexafluoride for isotope geochemical analysis; Geo-chimica et Cosmochimica Acta, v. 35, p. 625-628.

Rees, C.E.
1978: Sulfur isotope measurements using SO_2 and SF_6: Geochimica et Cosmochim-ica Acta, v. 42, p. 383-389.

Rumble, D., Hoering, T.C., and Palin, J.M.
1991a: Microanalysis for $\delta^{34}S$ in sulfide minerals with laser fluorination (abstract); EOS, v. 72, p. 292.

Rumble, D., Palin, J.M, and Hoering, T.C.
1991b: Microanalysis of sulfur isotope ratios with laser fluorination using fluorine gas (abstract); Geological Society of America, Abstracts with Programs, v. 23, p. A412.

Sharp, Z.D.
1990: A laser-based microanalytical method for the in situ determination of oxy-gen isotope ratios in silicates and oxides; Geochimica et Cosmochimica Acta, v. 545, p. 1353-1357.
1992: In situ laser microprobe techniques for stable isotope analysis; Chemical Geology (Isotope Geoscience Section), v. 101, p. 3-19.

Sharp, Z.D. and O'Neil, J.R.
1988: A laser-based carbon reduction technique for oxygen isotope analysis of microsamples of silicates and oxides (abstract); Geological Society of America, Abstracts with Program, v. 20, p. A280.

Smalley, P.C., Stijfhoorn, D.E., Raheim, A. Johansen, H., and Dickson, J.A.D.
1989: The laser microprobe and its application to the study of C and O isotopes in calcite and aragonite; Sedimentary Geology, v. 65, p. 211-221.

Geological Survey of Canada Project 85-0013

MILES laser microprobe. Part 2: preliminary assessment of precision and accuracy of sulphur isotope analysis

Georges Beaudoin and Bruce E. Taylor
Mineral Resources Division

Beaudoin, G. and Taylor, B.E., 1993: MILES laser microprobe. Part 2: preliminary assessment of precision and accuracy of sulphur isotope analysis; in Current Research, Part D; Geological Survey of Canada, Paper 93-1D, p. 199-204.

Abstract: The precision of sulphur isotope analyses using the MILES laser microprobe ranges from 0.05 to 0.11‰ for powders of pyrite, galena, and sphalerite. The precision obtained using MILES is better than that obtained by conventional, large-sample SO_2 methods. MILES $\delta^{34}S$ values are independent of sample size and fluorine pressure. Preliminary data indicate that the accuracy of these analyses is good. No matrix-dependent or instrumental sulphur isotope effects are produced.

Résumé : La précision des analyses isotopiques du soufre effectuées à l'aide de la microsonde laser MILES varie de 0.05 à 0.11‰ pour des poudres de pyrite, de galène, et de sphalerite. La précision obtenue à l'aide de MILES est supérieure à celle obtenue à l'aide des techniques conventionnelles au SO_2 pour de gros échantillons. Les valeurs de $\delta^{34}S$ obtenues à l'aide de MILES sont indépendantes de la quantité d'échantillon utilisée et de la pression de fluor. Des données préliminaires indiquent que l'exactitude des analyses est bonne. Nous n'observons aucun effet isotopique associé à la composition de l'échantillon ou à l'instrument.

INTRODUCTION

Two methods are currently being developed for high spatial resolution sulphur isotope analysis of geological material. The first method is Secondary Ion Mass Spectrometry (SIMS). SIMS utilizes an O^- ion beam to produce positively charged secondary ions from a mineral surface, which are analyzed in a mass spectrometer to determine the sulphur isotope ratios. This method yields sulphur isotope ratios with a precision of 1-2‰ (Eldridge et al., 1987; Chaussidon and Lorand, 1990), which is significantly below the precision (0.2‰) of conventional combustion techniques. In addition, large instrumental sulphur isotope fractionations (up to 65‰; Eldridge et al., 1987; Chaussidon and Lorand, 1990), which are mineral-specific and vary with the chemical composition of the sulphide (Chaussidon and Lorand, 1990), must be accounted for. The spatial resolution of SIMS exceeds other methods, the domain sampled ranging from 20 to 60 μm in diameter.

The laser microprobe is the other method currently developed to obtain samples with high spatial resolution; "samples are" of the order of 2 x $10^{-3}mm^3$ (MILES) to 20 x $10^{-3}mm^3$ (Kelly and Fallick, 1990). In laser microprobes, a laser beam provides the energy to react a small domain of a mineral surface or a powder. Two different analytical techniques are being developed for sulphur isotope ratio analysis. In the first, the laser-SO_2 technique, sulphides are reacted with O_2 to produce $SO_{2(g)}$ for mass spectrometry (Crowe et al., 1990; Kelly and Fallick, 1990). The laser-SO_2 technique yields a mineral-dependent precision ranging from 0.1 to 0.5‰ for $\delta^{34}S$ (Crowe et al., 1990; Kelly and Fallick, 1990), which is comparable to conventional, large-sample SO_2 combustion techniques for which precision is commonly on the order of 0.2‰. The laser-SO_2 technique, however, also has instrumental sulphur isotope fractionations (up to 6‰) which are mineral-specific, and vary with the chemical composition, the laser operating conditions (Crowe et al., 1990), and the roughness of the mineral surface (Huston, pers. comm., 1992).

In the second technique, the laser-SF_6 technique, sulphides are reacted with fluorine to produce SF_6 for mass spectrometry (Rumble et al., 1991; this study). SF_6 is chemically inert, non-polar, and hydrophobic. These characteristics of SF_6 compare favourably with SO_2 which is polar, sensitive to moisture, and has a tendency to adsorb on the surfaces of the equipment. Another advantage of SF_6 over SO_2 is that the reagent F_2 has only one isotope (^{19}F), compared to three for O_2 (^{16}O, ^{17}O, ^{18}O), so that the sulphur isotopic composition of a sample of SF_6 can be measured directly without the need for correcting for isotopic composition of oxygen (Rees, 1978).

In this paper we report analytical results that permit a preliminary assessment of the precision and accuracy of $\delta^{34}S$ values from sulphide powders using MILES (Micro-Isotopic Laser Extraction System; Taylor and Beaudoin, 1993). In a forthcoming report, we will demonstrate the precision and accuracy of MILES for high spatial resolution sulphur isotope analysis.

ANALYTICAL METHOD

A small sample of sulphide powder, containing less than 30 μm S, is loaded into a Ni crucible and placed into a chamber that is brought to high vacuum (10^{-6} Torr). The reagent $F_{2(g)}$ is generated according to the reversible reaction (Asprey, 1976):

$$2\,[K_2NiF_6{\cdot}KF]_{(s)} = 2\,K_3NiF_{6\,(s)} + F_{2(g)} \qquad (1)$$

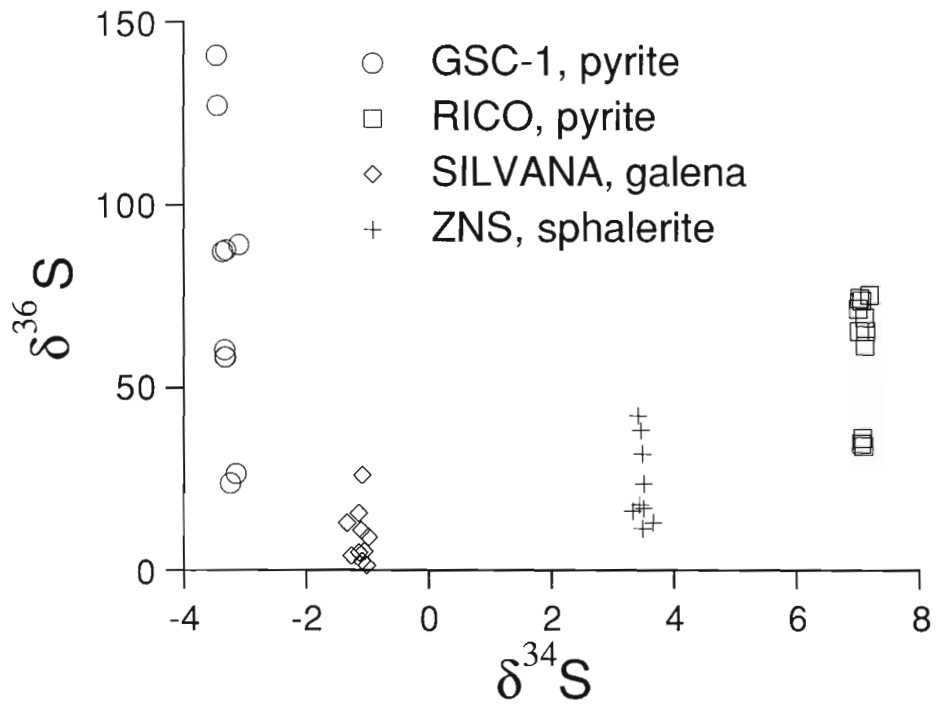

Figure 1.

Independence of $\delta^{34}S$ relative to $\delta^{36}S$ for the samples analyzed.

An aliquot of $F_{2(g)}$ is transferred into the sample chamber.

The laser energy is absorbed by the sulphide powder causing it to melt. The reaction proceeds at, or near, the onset of melting according to a reaction such as

$$7.5\ F_{2(g)} + FeS_{2(s)} = FeF_{3(s)} + 2\ SF_{6(g)} \quad (2)$$

The energy for the reaction is provided by a 30 W radio-frequency excited CO_2 laser beam with a 10.6 μm wavelength. For powders, a 4.5 KHz pulse is continuously produced by a frequency generator, and power control is provided by a 5 KHz variable duty cycle pulse generator. During the reaction, the laser power is slowly increased to maximum. This is necessary to prevent sputtering of the sulphide powder, which is observed when a high power laser beam is aimed suddenly on the sample. The sample is moved under the laser beam until the sulphide powder has been consumed. $SF_{6(g)}$ is transferred into a variable temperature cryogenic trap (Taylor and Beaudoin, 1993) and condensed below approximately -160°C. Excess F_2 is not condensed and is pumped through an activated charcoal trap where the strongly exothermic reaction

$$2\ F_{2(g)} + C_{(s)} = CF_{4(g)} \quad (3)$$

Table 1. Comparison of $^{34}S_{CDT}(SO_2)$ with MILES $^{34}S(SF_6)$ values for pyrite, galena, and sphalerite

Sample	Min.	$\delta^{34}S_{CDT}(SO_2)$			MILES $\delta^{34}S(SF_6)$[1]			$\Delta_{SO2\text{-}SF6}$	()[2]
		x[3]	s	n	x	s	n		
1. GSC-1	Pyrite	-10.09	0.13	3	-3.31	0.11	10	-6.78	(0.17)
2. RICO	Pyrite	0.19	0.21	4	7.07	0.05	11	-6.88	(0.22)
3. SILVANA	Galena	-7.84	0.15	9	-1.12	0.10	10	-6.72	(0.18)
4. ZNS	Sphalerite	-3.12	0.15	5	3.48	0.10	9	-6.60	(0.18)

1. $\delta^{34}S$ values relative to uncalibrated reference gas (see text). 2. Uncertainty = $(s_i^2+s_j^2)^{0.5}$.
3. x: average; s: standard deviation (1σ); n: number of measurements.

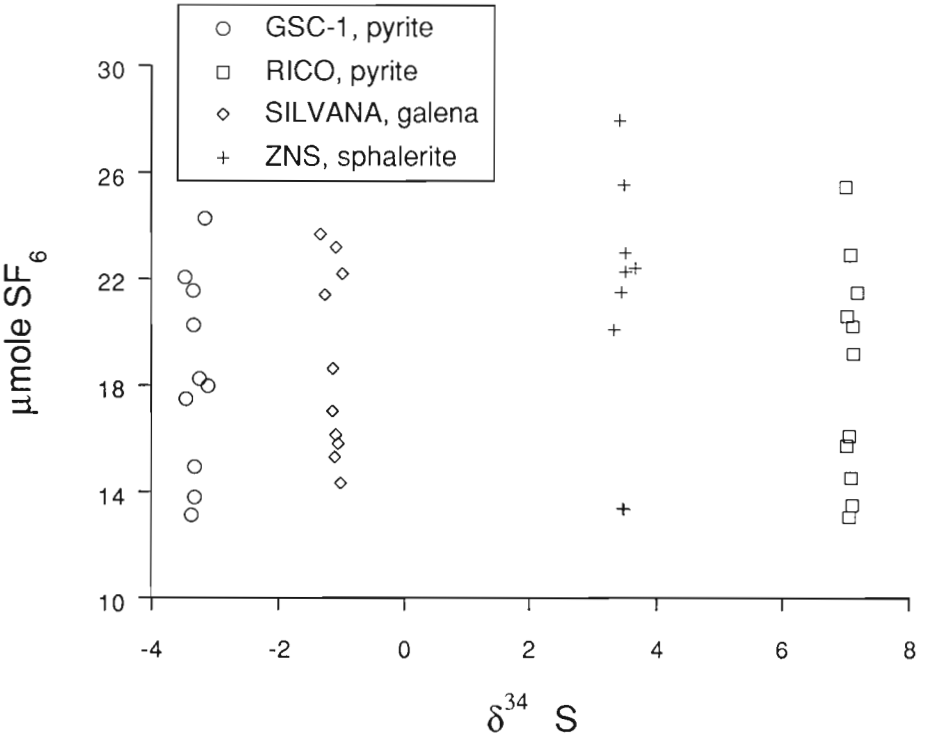

Figure 2.

Independence of $\delta^{34}S$ relative to sample size, measured in μm SF_6 extracted from a sample.

neutralizes the excess F_2. The condensed sample of SF_6 is purified by cryogenic distillation. The purified sample SF_6 is stored in a Pyrex cracker-tube pending its introduction into a Finnigan MAT 252 mass spectrometer for sulphur isotope analysis.

EXPERIMENTAL

Fluorine pressure

We determined empirically the molar ratio of F_2 to sample sulphur necessary to obtain complete reaction of a powdered sulphide. A minimum molar F_2/S ratio of 4.5 is necessary for complete reaction of mono- and di-sulphides, and compares well with the theoretical stoichiometric molar F_2/S ratio of 3.8 for pyrite, and of 4 for galena and sphalerite. To avoid experiments at limiting conditions, a molar F_2/S ratio of 6 is routinely used.

Cryogenic distillation

Product SF_6 commonly contains impurities that produce isobaric interferences, particularly at mass 131. For example, $^{12}C_3F_5$+ has a mass of 131 and its presence prevents accurate determination of $\delta^{36}S$ (Hoering, 1990). Traditionally, SF_6 purification has been accomplished by reacting SF_6 with NaOH followed by gas chromatography (Puchelt et al., 1971). This method is time consuming and has potential for memory effect.

A cryogenic variable temperature trap (Taylor and Beaudoin, 1993) is used on MILES to purify SF_6. SF_6 sublimates slowly at -160°C from the cryogenic variable temperature trap. Because some impurities have sublimation temperatures similar to that of SF_6, or because they have a high vapour pressure at the temperature of sublimation of SF_6, some impurities, presumably fluorocarbon compounds, cannot be completely separated from SF_6. A small isobaric interference at mass 131 prevents accurate determination of $\delta^{36}S$ values. The $\delta^{34}S$ values are, however, constant for a given sample for a range of $\delta^{36}S$ values that represent isobaric interference by trace amounts of impurities (Fig. 1). The presence of impurities at the concentrations attained by cryogenic distillation does not prevent determination of $\delta^{34}S$ values. The cryogenic distillation permits rapid (15 minutes) purification of small SF_6 samples (to 0.1 μm SF_6).

Table 2. Comparison of per mil fractionation between each pair of sulphides for the conventional SO_2 and MILES SF_6 techniques

Mineral pair[1] (i-j)	SO2		SF_6	
	Δ_{i-j}	$()^2$	Δ_{i-j}	$()^2$
2-1	10.28	(0.25)	10.38	(0.12)
2-3	8.03	(0.26)	8.19	(0.11)
2-4	3.31	(0.26)	3.59	(0.11)
3-1	2.25	(0.20)	2.19	(0.15)
4-1	6.97	(0.20)	6.79	(0.15)
4-3	4.72	(0.21)	4.60	(0.14)

1. Mineral number indexed in Table 1. 2. Uncertainty = $(s_i^2+s_j^2)^{0.5}$.

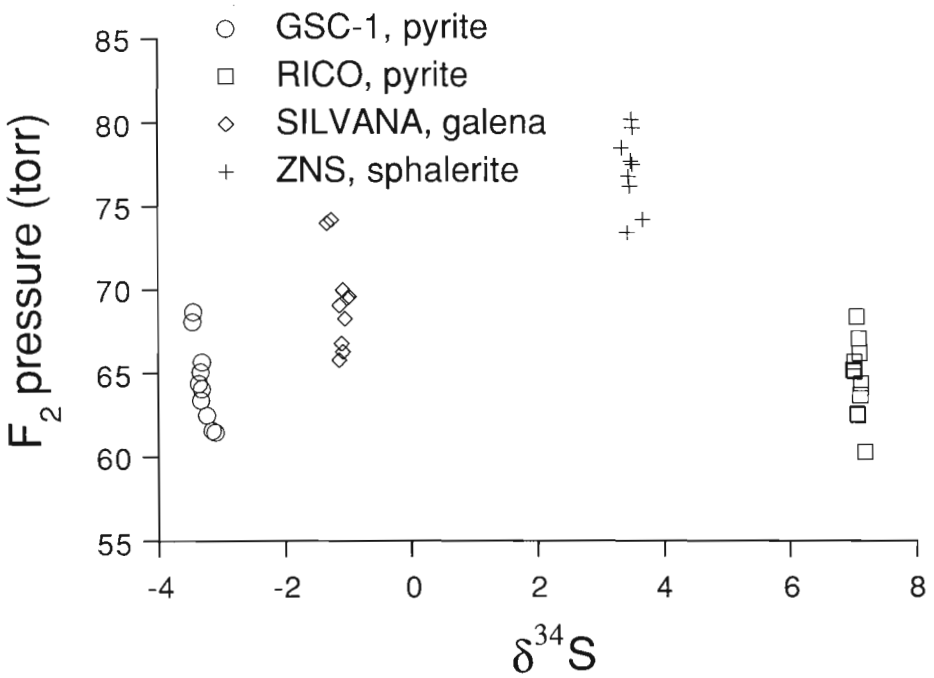

Figure 3.

Independence of $\delta^{34}S$ relative to the F_2 pressure in the sample chamber during reaction.

Precision and accuracy of MILES $\delta^{34}S$ values

Sulphur isotopic compositions are commonly reported using the standard δ-notation:

$$\delta^{34}S = [(^{34}S/^{32}S)_A / (^{34}S/^{32}S)_B - 1]\ 1000 \quad (4)$$

where A is the unknown and B is the reference SF_6. The precision of a sulphur isotope analysis is commonly estimated by replicate analysis of an isotopically homogeneous sample, and ranges from 0.05 to 0.11‰ for powders of pyrite, galena, and sphalerite analyzed using MILES (Table 1). The precision comprises analytical uncertainties associated with both the extraction process and mass spectrometry. The analytical uncertainty associated with mass spectrometry is commonly below 0.01‰, and is only a minor component of the total uncertainty. Therefore, most of the analytical uncertainty is ascribed to the extraction process. The precision obtained for the Rico pyrite (0.05‰, Table 1) is better than that obtained for the other samples analyzed, thus indicating sulphur isotopic heterogeneities in the other sulphides. We consider that the Rico pyrite reflects the real precision of the MILES laser microprobe for sulphide samples.

The SF_6 yield for each reaction ranges from 94.5 to 112.3% (Appendix). The samples analyzed contained 13.1 to 28.0 μm S and the pressure of F_2 during reaction ranged from 61.5 to 78.2 Torr (Appendix). There is no variation of $\delta^{34}S$ with either sample size (Fig. 2) or pressure of F_2 (Fig. 3). Preliminary data have been obtained from single craters formed on a polished surface of a pyrite crystal. The craters typically have a diameter and a depth of 130 μm, and produce approximately 0.2 μm SF_6, two orders of magnitude less SF_6 than from the powders. Our preliminary data indicate that a precision similar to that attained with powders will be obtained in the near future from single craters formed from sulphides in a rock slab, and will demonstrate the ability of MILES for high spatial resolution sampling and stable isotope analysis of geological material.

We are in the process of calibrating our SF_6 reference gas against Cañon Diablo Troilite (CDT). Therefore, we report the uncalibrated $\delta^{34}S$ values of our samples relative to our working standard. Although, the accuracy of MILES $\delta^{34}S$ values cannot be formally examined at this point, it can be estimated by computing the per mil fractionation between the MILES $\delta^{34}S$ value of a sample from its SO_2-conventional $\delta^{34}S_{CDT}$ value ($\Delta_{SO2\text{-}SF6}$). The $\Delta_{SO2\text{-}SF6}$ calculated from different samples are identical within uncertainty (Table 1). Another approach is to calculate the per mil fractionation between each of the samples ($\Delta_{x\text{-}y}$). The $\Delta_{x\text{-}y}$ values, similarly computed from $\delta^{34}S_{CDT}(SO_2)$ and MILES $\delta^{34}S$ (SF_6) values for each pair of sulphides, are identical within uncertainty (Table 2). These results indicate that MILES $\delta^{34}S$ data are accurate, independent of the sulphide matrix and, for pyrite at least, independent of the $\delta^{34}S_{CDT}$ of the sample.

ACKNOWLEDGMENTS

G. Beaudoin acknowledges the Geological Survey of Canada for a Visiting Fellowship in Canadian Government Laboratories.

REFERENCES

Asprey, L.B.
1976: The preparation of very pure fluorine gas; Journal of Fluorine Chemistry, v. 7, p. 359-361.

Chaussidon, M. and Lorand, J.-P.
1990: Sulphur isotope composition of orogenic spinel lherzolite massifs from Ariege (North-Eastern Pyrenees, France): An ion microprobe study; Geochimica et Cosmochimica Acta, v. 54, p. 2835-2846.

Crowe, D.E., Valley, J.W., and Baker, K.L.
1990: Micro-analysis of sulfur-isotope ratios and zonation by laser microprobe; Geochimica et Cosmochimica Acta, v. 54, p. 2075-2092.

Eldridge, C.S., Compston, W., Williams, I.S., Walshe, J.L., and Both, R.A.
1987: In situ microanalysis for $^{34}S/^{32}S$ ratios using the ion microprobe SHRIMP; International Journal of Mass Spectrometry and Ion Processes, v. 76, p. 65-83.

Hoering, T.C.
1990: Development of the sulfur hexafluoride method for sulfur isotope analysis. Annual Report of the Director, Geophysical Laboratory, Carnegie Institution, 1989-1990, p. 128-131.

Kelley, S.P. and Fallik, A.E.
1990: High precision spatially resolved analysis of $\delta^{34}S$ in sulphides using a laser extraction technique; Geochimica et Cosmochimica Acta, v. 54, p. 883-888.

Puchelt, H., Sabrels, B.R., and Hoering, T.C.
1971: Preparation of sulfur hexafluoride for isotope geochemical analysis; Geochimica et Cosmochimica Acta, v. 35, p. 626-628.

Rees, C.E.
1978: Sulphur isotope measurements using SO_2 and SF_6; Geochimica et Cosmochimica Acta, v. 42, p. 383-389.

Rumble, D., Palin, J.M., and Hoering, T.C.
1991: Laser fluorination of sulfide minerals with F_2 gas; Annual Report of the Director, Geophysical Laboratory, Carnegie Institution of Washington, 1990-1991, no. 2250, p. 30-34.

Taylor, B.E. and Beaudoin, G.
1993: MILES laser microprobe. Part 1: system description; in Current Research, Part D; Geological Survey of Canada, Paper 93-1D.

Geological Survey of Canada Project 850013

Appendix
Extraction and isotopic data using MILES

Run#	mg	p F2 (torr)	um SF_6	YIELD (%)	$\delta^{34}S$	$\delta^{36}S$
GSC-1, pyrite						
M18-1	0.99	62.50	18.25	110.5	-3.24	24.0
M18-2	1.25	68.10	22.08	106.0	-3.46	141.0
M18-3	0.82	65.70	13.81	101.0	-3.32	87.8
M18-4	1.06	61.50	17.98	101.7	-3.11	89.3
M18-5	1.03	68.70	17.49	101.9	-3.45	127.4
M18-6	0.72	64.40	13.14	109.5	-3.37	87.4
M18-7	1.36	61.60	24.29	107.1	-3.15	26.6
M18-10	0.86	64.10	14.95	104.3	-3.32	58.5
M18-11	1.24	63.40	20.27	98.1	-3.33	58.6
M18-12	1.22	65.10	21.57	106.1	-3.34	60.5
RICO, pyrite						
M19-1	1.08	63.70	20.21	112.3	7.11	61.6
M19-2	1.19	65.10	20.60	103.9	7.02	74.7
M19-3	0.84	66.20	13.50	96.4	7.10	69.4
M19-4	0.90	65.70	15.74	104.9	7.02	65.5
M19-5	1.11	64.40	19.18	103.7	7.12	65.6
M19-6	1.42	65.20	25.44	107.5	7.00	71.8
M19-7	0.94	62.60	16.10	102.8	7.06	73.9
M19-8	1.30	60.30	21.48	99.1	7.18	75.6
M19-10	1.37	62.50	22.90	100.3	7.07	36.2
M19-11	0.76	68.40	13.05	103.0	7.06	34.7
M19-12	0.83	67.10	14.53	105.0	7.09	34.0
SILVANA, galena						
M22-6	5.06	66.30	23.20	109.7	-1.09	26.2
M22-7	3.84	65.80	17.04	106.2	-1.15	15.9
M22-12	3.40	66.80	15.32	107.8	-1.11	11.1
M22-13	3.48	68.30	15.83	108.8	-1.06	5.3
M22-14	3.28	69.50	14.35	104.7	-1.01	1.6
M22-15	4.72	69.10	18.64	94.5	-1.14	5.0
M22-16	5.06	69.60	22.21	105.0	-0.99	9.3
M22-17	4.92	74.20	21.42	104.2	-1.27	4.2
M22-18	3.56	70.00	16.16	108.6	-1.09	2.7
M22-20	5.38	74.00	23.69	105.3	-1.34	13.1
ZNS, sphalerite						
M23-2	2.68	73.40	27.95	101.6	3.42	42.3
M23-5	2.40	77.70	25.53	103.7	3.48	31.8
M23-7	1.26	76.20	13.38	103.5	3.46	38.3
M23-8	1.90	78.50	20.09	103.1	3.33	16.4
M23-9	2.16	74.20	22.41	101.2	3.66	13.1
M23-11	1.23	80.20	13.35	105.8	3.49	11.5
M23-12	1.96	76.80	21.51	107.0	3.44	18.0
M23-13	2.18	77.50	22.29	99.7	3.51	17.0
M23-14	2.09	79.70	22.99	107.2	3.51	23.8

National gravity survey program of the Geological Survey of Canada, 1992-93

D.B. Hearty and R.A. Gibb
Geophysics Division

Hearty, D.B. and Gibb, R.A., 1993: National gravity survey program of the Geological Survey of Canada, 1992-93; in Current Research, Part D, Geological Survey of Canada, Paper 93-1D, p. 205-207.

Abstract: In 1992, five gravity surveys were completed under the national gravity survey program; two were reconnaissance surveys located in the Yukon Territory and Northwest Territories and the Arctic, one was a local gravity survey over a target in the Northwest Territories, one was an ice cap survey on Baffin Island, and one was a traverse along Lithoprobe seismic profiles in central Alberta. More than 4000 new gravity stations were added to the National Gravity Data Base and two Open File gravity maps were produced as a result of these surveys. In addition, absolute gravity measurements were made at several sites across Canada and at one site in the United States. Airborne gravity tests were conducted over Lake Ontario in collaboration with Sander Geophysics Ltd.

Résumé : En 1992, des cinq levés gravimétriques complétés dans le cadre du programme national de levés gravimétriques, deux étaient des levés de reconnaissance réalisés au Yukon et dans les Territoires du Nord-Ouest et dans l'Arctique, un était un levé gravimétrique local effectué au-dessus d'une cible située dans les Territoires du Nord-Ouest, un autre était un levé de la calotte glaciaire dans l'île de Baffin, et le dernier était une ligne transversale de levé suivant les profils sismiques Lithoprobe dans le centre de l'Alberta. On a ajouté plus de 4 000 nouvelles stations gravimétriques à la Base nationale de données gravimétriques, et publié deux cartes gravimétriques dans la série des Dossiers publics, à la suite de ces levés. En outre, des mesures gravimétriques absolues ont été réalisées en plusieurs endroits du territoire canadien et en un endroit des États-Unis. On a également réalisé des essais gravimétriques aéroportés au-dessus du lac Ontario en collaboration avec la société Sander Geophysics Ltd.

INTRODUCTION

In 1992-93, the national gravity mapping program comprised two reconnaissance surveys and three local surveys over geological targets. Significant progress towards completion of regional gravity coverage of Canada's landmass and waters was made in the Northwest Territories and in the Arctic. Two local surveys were completed in response to requests from the Mineral Resources Division and the Lithoprobe project and one was part of a research project by the Glaciology Division to monitor elevation changes on polar ice caps. Absolute measurements were made nationally and internationally to support a variety of programs and research studies.

Details of these surveys and highlights from the gravity standards program, gravity map production and developments in airborne gravity are given below.

NORTHWEST TERRITORIES

The Geophysics Division, the Pacific Geoscience Centre and the Mapping and Charting Establishment of the Department of National Defence and the US Defense Mapping Agency (DMA), in a major co-operative effort, completed the regional gravity survey of the southwest corner of the Northwest Territories in the period May 31 to July 28, 1992. Approximately 1760 gravity observations, with a spacing of 10-12 km covering eighteen 1:250 000 map sheets, were collected in year two of a three year survey program. A rapid-static surveying technique using dual frequency Ashtech XII GPS receivers with P-code capability in differential mode was used to obtain vertical and horizontal positioning for most gravity observation sites. A geodetic quality control network was established with approximate 100 km baseline lengths to supplement existing and sparse geodetic control in the area and to support the differential GPS positioning. The costs of this survey were shared by GSC and DMA in the ratio of 1:3. The collected gravity data will contribute to the National Gravity Mapping Program, to studies of resource potential and geological structure in the Northwest Territories and to a better determination of the geoid for the surveying industry.

ARCTIC CHANNELS

During March 1992, a gravity and bathymetry survey was conducted on the frozen ice surface east and north of Corwallis Island, in Wellington and Queens channels and Penny Strait. The survey, part of the National Gravity Mapping Program, was carried out by the Geophysics Division in co-operation with the Canadian Hydrographic Service and Polar Continental Shelf Project (PCSP). A total of 430 gravity stations with corresponding bathymetry was established at a 6 km grid spacing using portable GPS receivers (TANS Pathfinder model) in differential mode.

PENNY ICE CAP, BAFFIN ISLAND

In early May, the Geophysics Division in collaboration with Terrain Sciences Division, Memorial University, PCSP and the Science Institute of the Northwest Territories established sixteen gravity sites on the top of the Penny Ice Cap. Four sites were reoccupations of sites established in 1966 when an ice cap monitoring program was initiated to measure the growth and shrinkage of glaciers and ice caps as a measure of climatic change. Four LaCoste and Romberg gravity meters were used to conduct 66 gravity ties between ice cap stations and Iqaluit or Pangnirtung. Horizontal positioning was determined by GPS using Trimble Pathfinder and Basic model receivers.

DIANNE LAKE, NORTHWEST TERRITORIES

In July, a local gravity survey was conducted by the Geophysics Division over a mineral prospect located about 200 km northwest of Yellowknife at Dianne Lake in response to a request from the Mineral Resources Division. Seventy gravity stations were established; 47 on a 50 metre grid, 19 at various intervals along the lake shore and 4 near the Mar prospect about 2 km north of Dianne Lake. Horizontal positions were either chained for the grid locations or scaled from 1:50 000 NTS maps and vertical positions were either levelled or derived from altimeter measurements based on diamond drill hole (S-11) for control.

CENTRAL ALBERTA

In response to a request from the Continental Geoscience Division, gravity profiles were observed by the Geophysics Division along Lithoprobe seismic lines between Entwistle and Provost, Alberta. A total of 1040 gravity stations was established at 200 m and 500 m intervals along nine profile lines having a total length of approximately 512 km. Horizontal and vertical positions were established under contract using traditional survey techniques and GPS at 50 km intervals for control. A Scintrex CG-3 AUTOGRAV gravity meter was used for all gravity measurements and a LaCoste and Romberg gravity meter was used at every tenth site for additional control. The Scintrex gravity meter proved to be ideal for this type of survey and a significant improvement in production was realized with no loss in accuracy.

GRAVITY STANDARDS

The Canadian Gravity Standardization Net(CGSN) consists of some 2000 reference sites which provide datum for all relative gravity surveys that comprise the National Gravity Mapping Program and for geophysical exploration industry surveys. To ensure the integrity of this network all sites are inspected on a regular basis. During the summer approximately 200 gravity control stations were inspected in southern Quebec, Alberta, southern Manitoba and

northwestern Ontario. Stations were categorized according to national standards, descriptions were recompiled and corresponding data bases were updated. Two calibration surveys from Ottawa to Inuvik provided updated scale factors for eight gravity meters and an evaluation over almost the entire gravity range for Canada.

Several absolute stations were revisited or established across Canada for gravimeter calibration lines, to provide datum control for CGSN, to support Cascadia subduction zone studies and VLBI/GPS networks. New stations were established at Collingwood, Ontario, Albert Head, Heber Gorge and John Hart Lake in British Columbia and La Ronge, Saskatchewan. Repeat measurements were made at Orangeville, Gananoque, and Algonquin Radio Observatory in Ontario and Victoria, Myra Falls, Strathcona Dam and Penticton(3) in British Columbia. In addition, a measurement was made at International Falls, Minnesota as part of the international comparison studies for the International Absolute Gravity Base Network (IAGBN).

GRAVITY DATA BASE AND MAP PRODUCTION

The National Gravity Data Base contains in excess of 700 000 data points corresponding to a variety of land, ice and offshore measurements for the Canadian landmass, lakes and adjacent offshore areas. This year more than 4000 data points from regional or site specific surveys contributed by Geophysics Division and other agencies, were added to the digital holdings. These data are available through the Geophysical Data Centre in digital, gridded, profile or map form.

Thirty-four Bouguer anomaly and fourteen free air anomaly maps in the National Earth Science Series (NESS) (scale 1:1 000 000) are available through the GSC publications office. Eighteen new maps are currently in preparation and are scheduled for release before the end of March 1993.

Two Bouguer gravity maps were produced at a scale of 1:1 000 000; GSC Open File 2425, Bouguer Gravity Anomaly, Northern Baffin Island and GSC Open File 2525, Bouguer Gravity Anomaly, Yukon Territory.

AIRBORNE GRAVITY

In collaboration with Sander Geophysics, the Geophysics Division conducted airborne gravity tests over Lake Ontario. Gravity data were collected using the Division's LaCoste and Romberg dynamic gravimeter (SL-1) installed in a Cessna 402 aircraft and navigation was obtained using Trimble-4000 GPS receivers in differential mode. Vertical control was provided by a radar altimeter and a barometric altimeter aboard the aircraft. A negative anomaly about 60 km wide and 40 mGal in amplitude, chosen as a target for the tests, was resolved to within ±5 mGal. Efforts are continuing to improve gravimeter performance, especially during aircraft turns, to decrease the weight of the instrumentation for optimum use in a small aircraft, and to implement improvements to GPS technology as it becomes available.

Geological Survey of Canada Projects 860065, 860066, 860068, 860071, 860072

Aeromagnetic survey program of the Geological Survey of Canada, 1992-93

R. Dumont, P.E. Stone, F. Kiss, F. Dostaler,
K. Anderson, D. Jobin, D.J. Teskey, and R.A. Gibb
Geophysics Division

Dumont, R., Stone, P.E., Kiss, F., Dostaler, F., Anderson, K., Jobin, D., Teskey, D.J., and Gibb, R.A., 1993: Aeromagnetic survey program of the Geological Survey of Canada, 1992-93; in Current Research, Part D; Geological Survey of Canada, Paper 93-1D, p. 209-212.

Abstract: During 1992-93, the GSC collected 208 111 line kilometres of aeromagnetic data. Of these, 85 118 line kilometres were flown in Alberta and British Columbia during the third phase of a three year cost-sharing joint government-industry survey. In Saskatchewan and Manitoba, 53 360 line kilometres were flown in the second phase of a four year cost-sharing joint government-industry survey. A 28 600 line kilometre survey was flown over the polar margin off Axel Heiberg Island as a joint IAR/DREP/GSC project. The remaining data were collected under federal-provincial Mineral Development Agreement programs. In southeastern Alberta 33 940 line kilometres of aeromagnetic data were collected. In Ontario, 7093 line kilometres were flown in a combined electromagnetic-magnetic survey. In Saskatchewan and Manitoba 24 800 line kilometres of aeromagnetic gradiometer and VLF-EM surveys were compiled. In Nova Scotia and New Brunswick compilation of 17 707 line kilometres of gradiometer data was completed and published. The GSC aeromagnetic section also has acted as scientific authority for the third phase of a CIDA-sponsored aeromagnetic survey of Zimbabwe.

Résumé : En 1992-1993, la CGC a recueillie des données aéromagnétiques sur 208 111 kilomètres linéaires. De ce total, 85 118 kilomètres de levés aéroportés ont été réalisés en Alberta et en Colombie-Britannique lors de la troisième phase d'un projet de levé de trois ans dont le gouvernement fédéral et l'industrie se partagent les coûts. En Saskatchewan et au Manitoba, 53 360 kilomètres de levés aéroportés ont été réalisés lors de la seconde phase d'un projet de levé de quatre ans dont le gouvernement fédéral, le gouvernement provincial et l'industrie se partagent les coûts. Un levé de 28 600 kilomètres a été réalisé au-dessus de la marge polaire au large de l'île Axel Heiberg dans le cadre d'un projet conjoint entrepris par l'IRA, le CRDP et la CGC. On a recueilli les données restantes dans le cadre d'ententes fédérales-provinciales sur l'exploitation minérale. Dans la partie sud de l'Alberta, 33 940 kilomètres de levés aéromagnétiques ont été effectués. En Ontario, 7 093 kilomètres de levés aéromagnétiques et électro-magnétiques ont été réalisés. La compilation et la publication de données de gradiomètre vertical et de données électromagnétiques recueillies à très basse fréquence (EM-VLF) ont été complétées; ces données correspondent à un levé de 24 800 kilomètres réalisé au Manitoba et en Saskatchewan et à deux levés réalisés au Nouveau-Brunswick et en Nouvelle-Écosse totalisant 17 707 kilomètre linéaires. La CGC, en vertu d'une entente conclue avec l'Agence canadienne de développement international (ACDI), a continué d'agir à titre d'autorité scientifique et technique pour la compilation des données de la troisième phase d'un levé aéromagnétique effectué pour le compte de cette agence au Zimbabwe.

INTRODUCTION

The aeromagnetic survey program of the Geological Survey of Canada continued in 1992-93 with activity in eight existing projects – Alberta-British Columbia, Saskatchewan-Manitoba, the Polar Continental Margin, Zimbabwe and in gradiometer surveys in Saskatchewan, Manitoba, New Brunswick and Nova Scotia. New projects funded under federal-provincial Mineral Development Agreements were started in Ontario and in Alberta. Survey activity for 1992 is shown in Figure 1 and summarized in Table 1.

ALBERTA-BRITISH COLUMBIA

Phase three of this project was flown in the summer and fall of 1992 for a consortium of oil companies and the GSC on a cost-sharing basis (Teskey et al., 1991, 1992). The completion of this project is expected in the spring of 1993. The survey data will contribute to the Alberta Lithoprobe transect and to understanding the deep structure beneath the western Cordillera, important for oil exploration. Data from phase three will be released to the public in 1998.

SOUTHERN ALBERTA

The Cypress Hills, Alberta Mineral Development Agreement total field aeromagnetic survey was flown in the fall of 1992. The survey will assist in the exploration for kimberlites and mapping of the Precambrian basement. The publication of these data is planned for the second quarter of 1993.

SASKATCHEWAN-MANITOBA

The second phase of a four year cost-sharing industry-province-GSC survey was flown in Saskatchewan and Manitoba in the summer of 1992. The survey meets the dual objective of mapping the Precambrian basement and exploration for kimberlites (Teskey et al., 1992). Publication of the Saskatchewan survey data is planned for 1995 and publication of the Manitoba data for spring of 1993.

ZIMBABWE

The compilation of the third phase of this CIDA-sponsored survey was completed and final delivery of digital data and colour maps was completed in the summer of 1992. Data from all three phases were adjusted to the same level and merged to produce a series of six thematic maps at 1:1 000 000 scale covering the country.

AXEL HEIBERG

The GSC participated in a joint venture survey northwest of Axel Heiberg Island with the Defence Research Establishment Pacific (DREP) and the Institute of Aerospace Research (IAR) who carried out the field survey. Data collection for this survey will be completed in 1993, after which the data and maps will be released on Open File. Preliminary analysis of the 1991 data collected under this program has provided new insights into the structure of the polar continental Margin northwest of Axel Heiberg Island (Forsyth et al., in press).

AEROMAGNETIC GRADIOMETER SURVEYS

The compilation of the survey data flown in 1991 in New Brunswick and Nova Scotia has been completed. The digital data and colour maps were published in 1992. The compilation of the survey data for Manitoba (Talbot Lake area) flown in 1991 and Saskatchewan (Grassberry River area) flown in 1992 is in the final stage. Publication is planned for the first quarter of 1993 for both projects.

AEROMAGNETIC AND ELECTROMAGNETIC SURVEY TIME DOMAIN

The Blake River Syncline aeromagnetic-electromagnetic survey at Kirkland Lake, Ontario was flown in April 1992. The data and maps from this survey will be published in the first quarter of 1993.

Table 1. Aeromagnetic Surveys 1992-93

SURVEY	TYPE	LINE KM	LINE SPACING	ALTITUDE
Alberta/B.C. Phase III 1992-93	Aeromagnetic Total Field	85118	1.6 km	3813 m ASL 1830 m ASL 2135 m ASL
Saskatchewan Phase II 1992-93 (Quill Lake area)	Aeromagnetic Total Field	38300	800 m	150 m MTC
Manitoba Phase II 1992-93 (Dauphin area)	Aeromagnetic Total Field	15260	800 m	150 m MTC
Southern Alberta 1992-93 (Cypress Hills area)	Aeromagnetic Total Field	33940	800 m	150 m MTC
Ontario 1992-93 (Blake River area)	Aeromagnetic Time Domain EM	7093	200 m	120 m MTC
Axel Heiberg 1992-93	Aeromagnetic Total Field	28600	4 km	300 m ASL
ASL - Above Sea Level MTC - Mean Terrain Clearance				

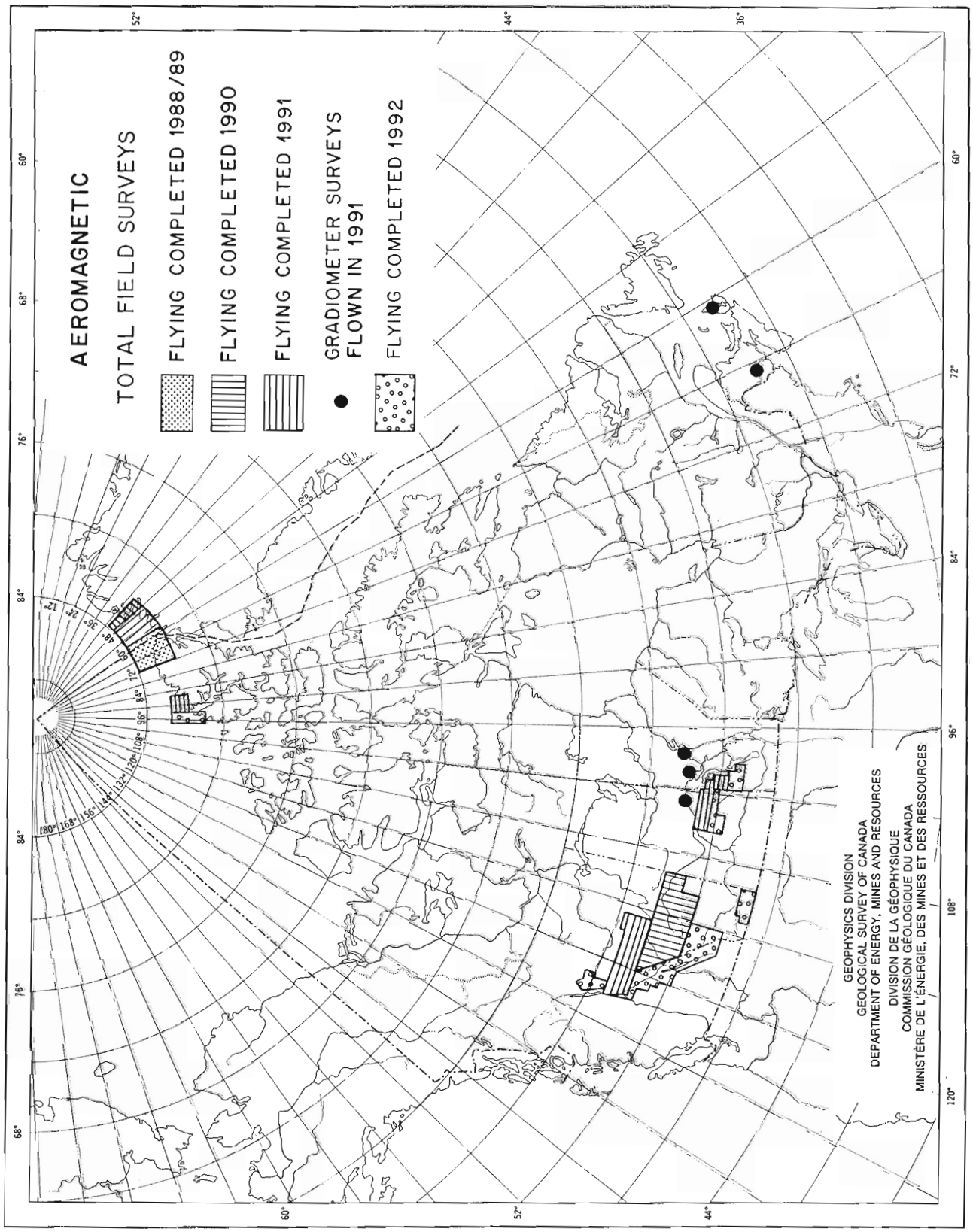

Figure 1. Aeromagnetic surveys in progress, 1992-93.

LEVELLING OF THE NATIONAL AEROMAGNETIC DATABASE

The GSC has undertaken to compile all of the total field aeromagnetic data covering Manitoba and Saskatchewan into a contiguous grid, sampled at 200 m. Using the existing 812.8 m levelled grid as a reference datum, profile data of adjacent surveys were levelled and gridded. High sensitivity detailed total field surveys have also been levelled to the same datum.

REFERENCES

Teskey, D.J., Tod, J., Stone, P.E., Ready, E.E., Knappers, W.A., Kiss, F., Dostaler, F., and Gibb, R.A.
1991: Aeromagnetic survey program of the Geological Survey of Canada 1990-91; in Current Research, Part D; Geological Survey of Canada, Paper 91-1D, p. 45-48.

Teskey, D.J., Stone, P.E., Kiss, F., Dostaler, F., Anderson, K., Tod, J., Knappers, W., Jobin, D., and Gibb, R.A.
1992: Aeromagnetic survey program of the Geological Survey of Canada, 1991-92; in Current Research, Part D; Geological Survey of Canada, Paper 92-1D, p. 73-76.

Forsyth, D.A., Okulitch, A.V., Marcotte, D., Nelson, J.B., Teskey, D.J., and Williamson, M.C.
In press: New aeromagnetic data from the Arctic margin near Nansen Sound: Canadian Journal of Earth Sciences.

Geological Survey of Canada Projects 850058, 900003, 900022, 900033, 900034, 910028, 910029, 910031, 910032, 920024, 920055

AUTHOR INDEX

NOTE TO CONTRIBUTORS

Submissions to the Discussion section of Current Research are welcome from both the staff of the Geological Survey of Canada and from the public. Discussions are limited to 6 double-spaced typewritten pages (about 1500 words) and are subject to review by the Chief Scientific Editor. Discussions are restricted to the scientific content of Geological Survey reports. General discussions concerning sector or government policy will not be accepted. All manuscripts must be computer word-processed on an IBM compatible system and must be submitted with a diskette using WordPerfect 5.0 or 5.1. Illustrations will be accepted only if, in the opinion of the editor, they are considered essential. In any case no redrafting will be undertaken and reproducible copy must accompany the original submissions. Discussion is limited to recent reports (not more than 2 years old) and may be in either English or French. Every effort is made to include both Discussion and Reply in the same issue. Current Research is published in January and July. Submissions should be sent to the Chief Scientific Editor, Geological Survey of Canada, 601 Booth Street, Ottawa, Canada, K1A 0E8.

AVIS AUX AUTEURS D'ARTICLES

Nous encourageons tant le personnel de la Commission géologique que le grand public à nous faire parvenir des articles destinés à la section discussion de la publication Recherches en cours. Le texte doit comprendre au plus six pages dactylographiées à double interligne (environ 1500 mots), texte qui peut faire l'objet d'un réexamen par le rédacteur scientifique en chef. Les discussions doivent se limiter au contenu scientifique des rapports de la Commission géologique. Les discussions générales sur le Secteur ou les politiques gouvernementales ne seront pas acceptées. Le texte doit être soumis à un traitement de texte informatisé par un système IBM compatible et enregistré sur disquette WordPerfect 5.0 ou 5.1. Les illustrations ne seront acceptées que dans la mesure où, selon l'opinion du rédacteur, elles seront considérées comme essentielles. Aucune retouche ne sera faite au texte et dans tous les cas, une copie qui puisse être reproduite doit accompagner le texte original. Les discussions en français ou en anglais doivent se limiter aux rapports récents (au plus de 2 ans). On s'efforcera de faire coïncider les articles destinés aux rubriques discussions et réponses dans le même numéro. La publication Recherches en cours paraît en janvier et en juillet. Les articles doivent être envoyés au rédacteur en chef scientifique, Commission géologique du Canada, 601, rue Booth, Ottawa, Canada, K1A 0E8.

Geological Survey of Canada Current Research, is now released twice a year, in January and in July. The four parts published in January 1993 (Paper 93-1, parts A to D) are listed below and can be purchased separately.

Recherches en cours, une publication de la Commission géologique du Canada, est publiée maintenant deux fois par année, en janvier et en juillet. Les quatre parties publiées en janvier 1993 (Étude 93-1, parties A à D) sont énumérées ci-dessous et vendues séparément.

Part A: Cordillera and Pacific Margin
Partie A : Cordillère et marge du Pacifique

Part B: Interior Plains and Arctic Canada
Partie B : Plaines intérieures et région arctique du Canada

Part C: Canadian Shield
Partie C : Bouclier canadien

Part D: Eastern Canada and national and general programs
Partie D : Est du Canada et programmes nationaux et généraux